Stimuli-Responsive Multifunctional Poly(ethylene glycol) Copolymers

Dissertation

zur Erlangung des Grades

"Doktor der Naturwissenschaften"

im Promotionsfach Chemie

am Fachbereich Chemie, Pharmazie und Geowissenschaften
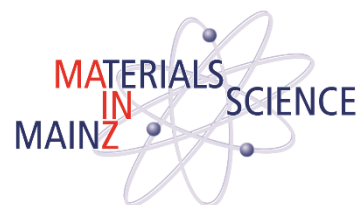
der Johannes Gutenberg-Universität

in Mainz

Jana Herzberger

geboren in Mainz

Mainz, Oktober 2016

██████████████████████

████████████████████████████

████████████████████████████

Tag der mündlichen Prüfung: ███████████

Die jetzt als Dissertation vorgelegte Arbeit wurde im Zeitraum von September 2013 bis Oktober 2016 am Institut für Organische Chemie der Johannes Gutenberg-Universität Mainz im Arbeitskreis von Prof. Dr. Holger Frey angefertigt.

Hiermit versichere ich gemäß § 10 Abs. 3d der Promotionsordnung vom 24.07.2007

a) Ich habe die jetzt als Dissertation vorgelegte Arbeit selbst angefertigt und alle benutzten Hilfsmittel (Literatur, Apparaturen, Material) in der Arbeit angegeben.

b) Ich habe oder hatte die jetzt als Dissertation vorgelegte Arbeit nicht als Prüfungsarbeit für eine staatliche oder andere wissenschaftliche Prüfung eingereicht.

c) Ich hatte weder die jetzt als Dissertation eingereichte Arbeit noch Teile davon bei einer anderen Fakultät bzw. einem anderen Fachbereich als Dissertation eingereicht.

"Etwas Gescheiteres kann einer doch nicht treiben in dieser schönen Welt, als zu spielen"

Henrik Ibsen

Table of Contents

Motivation and Objective

Poly(ethylene glycol) (PEG), also known as poly(ethylene oxide) (PEO) in case of higher molecular weights, belongs to a group of aliphatic polyethers and consists of ethylene glycol repeat units with a hydroxyl group at both termini. In contrast to polyoxymethylene (POM) or polytetrahydrofuran (PTHF), PEG possesses excellent solubility not only in organic solvents but also in water. Moreover, PEG's high chain-flexibility, chemical inertness together with its biocompatibility render it valuable for a range of applications.[1] In everyday products, PEG and its derivatives are used as soft components in polyurethane foams, e.g. mattresses or car seats, as stabilizers/surfactants in edibles, e.g. ice cream and as solvents/surfactants in a variety of body care products, e.g. shampoos or body lotion.[2] A more sophisticated application is the covalent attachment of PEG chains to proteins and peptides to increase blood circulation, which is known as PEGylation and has become a multi-billion-dollar market.[3]

However, the inherently low backbone functionality of PEG is the limiting factor for certain applications and many researchers are seeking strategies for improvement.[4, 5] As an illustrative example, consider the possibility of attaching several active molecules to one PEG chain; this dramatically increase its loading capacity while maintaining its water-solubility. Consequently, these multifunctional PEGs might serve as scaffolds for polymer-supported catalysis, but are also promising candidates for biomedical applications. In particular, an active drug, a target moiety and a label might be tethered to one single PEG chain.

Not only is the introduction of "active" functional groups of high interest, distributing multiple pendent groups along the polyether backbone is important for tailoring physical and chemical properties. For example, PEG's water solubility and crystallinity can be tuned

by incorporating several methyl groups into the polymer backbone by copolymerization of ethylene oxide (EO) with propylene oxide (PO).[6] Such modified PEGs exhibit a thermoresponsive character, meaning that at a specific temperature (<100 °C), a reversible coil-to-globule transition occurs and PEG precipitates.[7] Thermoresponsive materials are of interest for surface functionalization e.g. cell sheet engineering.[8] Additionally, PEG-*b*-PPO block copolymers consisting of a hydrophilic PEG block and a rather hydrophobic PPO block represent nonionic surfactants.

Besides simple methyl groups, many other interesting moieties are imaginable to be incorporate into PEG. In particular, by careful choice of functionality, smart, multi-stimuli responsive PEGs can be prepared.

To address the need of increasing the functionality of PEG and to tailor its properties, this thesis describes the synthesis of novel epoxide monomers and their utility in preparing multifunctional PEGs (*mf*-PEGs). Substituted epoxides are (i) copolymerized with EO to yield statistical copolymers or (ii) polymerized with methoxyPEG (mPEG) as a macroinitiator to obtain block copolymers (Scheme 1).

Multifunctional PEG
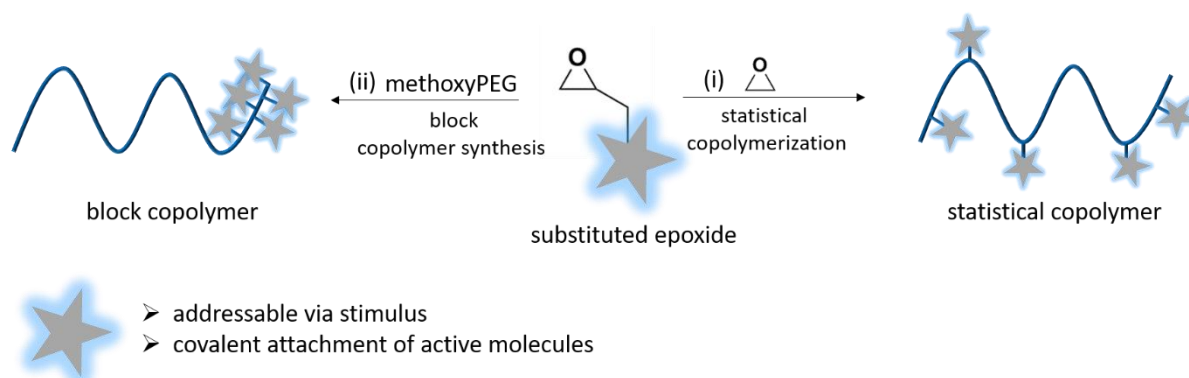
Scheme 1. Strategy to prepare multifunctional PEG by (co)polymerization of substituted epoxides.

Specifically, this thesis addresses the following questions:

1) *Can we prepare stimuli-responsive PEGs with tailored epoxide monomers via anionic ring opening polymerization (AROP)?*

Monomers based on glycidyl amine and glycidyl ether derivatives are explored for their use in anionic ring opening (co)polymerization (AROP) with ethylene oxide (EO). The main focus is the design of epoxide building blocks bearing pendent groups which i) do not interfere with the polymerization reaction and ii) offer PEG responsivity (to pH, temperature or oxidation agent) or possible post-polymerization modification. With the aim of achieving "smart" PEGs, first a thioether-functional epoxide is designed to realize oxidation-sensitive PEG. Intriguingly, thioether-functional PEG block copolymers form micelles in water, which then transform into unimers induced by an oxidation agent. These structures are promising candidates as nanocarriers for anti-inflammatory treatment (Chapter 2). Additionally, pH- and thermo-responsive PEGs are prepared by incorporation of tertiary amino-groups. The influence of glycidyl amine derivatives bearing hydrophobic alkyl chains on PEG's water-solubility are investigated on the nano- and macroscale with regard to temperature and pH changes (Chapter 3.2).

2) *Can we expand the limited range of functional epoxide monomers by utilizing monomer-activated AROP?*

Monomer-activated AROP has been studied as a mild polymerization alternative for sensitive epoxides in this thesis. It is utilized to generate nitrile- and alkyne functional PEGs from (co)polymerization of epicyanohydrin (EPICH) (Chapter 3.4) or glycidyl propargyl ether (GPgE) (Chapter 4) with EO, respectively. Both monomers are not polymerizable by conventional oxyanionic ROP because of the harsh reaction conditions. Nitrile-functional PEG gives access to amino, amide and carboxyl-functional PEG via facile post-

polymerization modification and alkyne-functional PEG represents a versatile scaffold to decorate PEG via quantitative click reaction.

3) *What kind of polymer structure is obtained by statistical copolymerization of ethylene oxide with such functional epoxides?*

New insights regarding the copolymer (micro)structure explains bulk thermal properties and behavior in aqueous solution. First, ^{13}C triad analysis is conducted to gain information about the comonomer distribution of all synthesized *mf*-PEGs. For a better understanding, the copolymerization of ethylene oxide and (i) glycidyl amines (Chapter 3.2) or (ii) glycidyl ethers (Chapters 2 and 4) is monitored *in-situ* by ^{1}H NMR spectroscopy to quantify reactivity ratios of the comonomers. This technique is further utilized to investigate differences in the reactivity behavior of EO and glycidyl ethers under conventional oxyanionic ROP and monomer-activated AROP conditions (Chapter 5).

References

[1] Herzberger, J.; Niederer, K.; Pohlit, H.; Seiwert, J.; Worm, M.; Wurm, F. R.; Frey, H., Polymerization of Ethylene Oxide, Propylene Oxide, and Other Alkylene Oxides: Synthesis, Novel Polymer Architectures, and Bioconjugation, *Chem. Rev.* **2016**, *116*, 2170–2243.

[2] Dingels, C.; Schömer, M.; Frey, H., Die vielen Gesichter des Poly(ethylenglykol)s, *Chem. unserer Zeit.* **2011**, *45*, 338–349.

[3] Pasut, G.; Veronese, F. M., State of the Art in PEGylation: The Great Versatility Achieved after Forty Years of Research, *J. Control. Release.* **2012**, *161*, 461–472.

[4] Obermeier, B.; Wurm, F.; Mangold, C.; Frey, H., Multifunctional Poly(ethylene glycol)s, *Angew. Chem. Int. Ed.* **2011**, *50*, 7988–7997.

[5] Mangold, C.; Wurm, F.; Frey, H., Functional PEG-based Polymers with Reactive Groups via Anionic ROP of Tailor-made Epoxides, *Polym. Chem.* **2012**, *3*, 1714–1721.

[6] Hamaide, T.; Goux, A.; Llauro, M.-F.; Spitz, R.; Guyot, A., *Stat*-Poly(ethylene oxide-*co*-propylene oxide). Synthesis, NMR Characterization and Crystallinity Studies. Correlation with Monte Carlo Simulation, *Angew. Makromol. Chemie.* **1996**, *237*, 55–77.

[7] Louai, A.; Sarazin, D.; Polle, G.; François, J.; Moreaux, F., Properties of Ethylene Oxide-Propylene Oxide Statistical Copolymers in Aqueous Solution, *Polymer.* **1991**, *32*, 703–712.

[8] Cole, M. A.; Voelcker, N. H.; Thissen, H.; Griesser, H. J., Stimuli-responsive Interfaces and Systems for the Control of Protein–Surface and Cell–Surface Interactions, *Biomaterials.* **2009**, *30*, 1827–1850.

Zusammenfassung

Im Rahmen dieser Arbeit wurden neuartige multifunktionelle Poly(ethylenglykol)e (*mf*-PEG) durch die Copolymerisation von Ethylenoxid mit unterschiedlichen, funktionellen Epoxidmonomere hergestellt. Mit dem gezielten Einbau eines geringen Anteils an Epoxidbausteinen können die Eigenschaften von PEG maßgeschneidert werden. Mittels tertiärer amino- oder thioetherfunktioneller Epoxide wurde *mf*-PEG erhalten, welches auf Oxidationsreagenzien, Temperatur- oder pH-Wert-Änderungen mit einer definierten Eigenschaftsänderung reagiert, also responsive Charakteristika besitzt. Weiterhin konnte mit dem Einbau eines nitrilhaltigen Epoxids PEG mit mehreren primären Amin-, Carboxyl- oder Amidgruppen durch polymeranaloge Modifikation hergestellt werden. Durch die Copolymerisation eines alkinhaltiges Epoxids mit Ethylenoxid wurde multifunktionelles PEG erhalten, welches durch Click-Chemie mit verschiedenen Bausteinen versehen werden kann. Abbildung 1 zeigt die verwendeten zentralen Epoxidmonomere im Überblick, zusammen mit möglichen Anwendungsbeispielen bzw. deren besonderen Eigenschaften.

Abbildung 1. Übersicht der verwendeten Epoxidmonomere zur Darstellung multifunktioneller PEGs.

Im einführenden **Kapitel 1** werden die besonderen Eigenschaften von PEG näher beleuchtet. Weiterhin beschreibt dieses Kapitel die im Rahmen dieser Arbeit verwendeten Syntheserouten. Hierbei werden die klassische oxyanionische ringöffnende Polymerisation (AROP) und eine Alternativmethode, die monomeraktivierte AROP erläutert. Das Kapitel schließt mit einer Übersicht von multifunktionellen PEGs und deren Eigenschaften. In diesem Zusammenhang wird auf das Reaktionsverhalten substituierter Epoxide bei der statistischen Copolymerisation mit Ethylenoxid (EO) eingegangen.

Kapitel 2 beschreibt die Synthese von thioetherfunktionellen PEGs ausgehend von einem neuen Epoxidmonomer, 2-(Mehtlythio)ethylglycidylether (MTEGE). Das Besondere dieser Strukturen ist ihre Adressierbarkeit mittels Oxidationsreagenzien:

Thioetherfunktionelle Blockcopolymere bilden in wässriger Lösung definierte Mizellen. Bei Zugabe eines Oxidationsmittels wird das hydrophobe Thioethersegment zu einem hydrophilen Sulfoxid oxidiert. Durch diesen Prozess werden hydrophile, vollständig wasserlösliche Polymere erhalten, und die Mizellen lösen sich auf. Dieses Verhalten wurde mittels NMR Spektroskopie, Lichtstreuung, Trübungsmessungen und Fluoreszenzspektroskopie im Detail untersucht. Zelltests zeigen eine hohe Verträglichkeit der Thioether-PEGs und deren oxidierten Spezies. Die gezielte Adressierbarkeit und Auflösung von Mizellstrukturen durch Oxidation ist für die Behandlung von Entzündungsherden im Körper von Interesse. Hierbei kann ein Wirkstoff in der Polymermizelle eingeschlossen werden. Im Idealfall wird dieser zum Entzündungsherd transportiert und dort durch Oxidation mit körpereigenen Oxidationsreagenzien gezielt freigesetzt. Abschließend wurden positiv geladene Sulfoniumstrukturen ausgehend von thioetherfunktionellen PEGs in einer click-artigen Reaktion hergestellt.

Kapitel 3 behandelt aminofunktionelle Polyether. Zunächst wird eine kurze Einleitung zu deren Synthese gegeben. Hierbei werden Strategien zur Darstellung primärer, sekundärer und tertiärer Amine beleuchtet. Dieser Abschnitt (**3.1**) ist aus einem veröffentlichten, umfassenden Übersichtsartikel entnommen und wurde von der Autorin dieser Dissertation geschrieben (Herzberger, J.; Niederer, K.; Pohlit, H.; Seiwert, J.; Worm, M.; Wurm, F. R.; Frey, H. *Chemical Reviews*, **2016**, *116*, 2170−2243 "Polymerization of Ethylene Oxide, Propylene Oxide, and Other Alkylene Oxides: Synthesis, Novel Polymer Architectures, and Bioconjugation").

Im **Unterkapitel 3.2** wird die Synthese von tertiären aminofunktionellen PEGs ausgehend von Glycidylaminen beschrieben. Hierfür wurden drei aminofunktionelle Epoxidmonomere synthetisiert: *N,N*-Di(*n*-butyl)glycidylether (DButGA), *N,N*-Di(*n*-hexyl)glycidylether (DHexGA) und *N,N*-Di(*n*-octyl)glycidylether (DOctGA). Diese

wurden mit Ethylenoxid copolymerisiert um statistische Copolymere zu erhalten und ausgehend von mPEG wurden Blockcopolymere hergestellt. Mittels ^{1}H NMR Kinetikstudien konnte gezeigt werden, dass die statistische Copolymerisation zu gradientenartigen Strukturen führt, wobei EO bevorzugt eingebaut wird. Ferner wurde das Verhalten der hergestellten aminofunktionellen PEGs in wässriger Lösung untersucht und der Einfluss von Temperatur- und pH-Wert im Detail betrachtet. Hierbei gaben Trübungsmessungen Aufschluss über das Verhalten dieser Strukturen auf makroskopischer Ebene, wobei Elektronenspinresonanz (EPR) Spektroskopie eingesetzt wurde, um eine Aussage zu den Phasenübergängen auf der Nanometerskala zu erhalten. Zusätzlich wurde mittels Lichtstreuung die Größe der gebildeten Aggregate bestimmt. Trübungspunkte konnten mit einem Gehalt von weniger als 15 mol% Glycidylamin zwischen 21 °C und 93 °C präzise eingestellt werden und mittels pH-Wert manipuliert werden.

Im **Unterkapitel 3.3** wurden aminofunktionelle Polyetherstrukturen (PEG-*co*-PDButGA) quaternisiert und somit positiv geladen. Die Quaternisierung erfolgte mittels Benzylbromid oder Methyliodid, wodurch die resultierenden Polyelektrolyte eine extrem hohe Glasübergangstemperatur (T_g) aufwiesen (zwischen 6 °C und 83 °C). Durch einen Anionenaustausch mit einem „weichen" Anion, Bis(trifluoromethylsulfonyl)imide (TFSI), wurden polyionische Flüssigkeiten erhalten. Im Gegensatz zu den Polyelektrolyten mit Halogenid-Gegenion, sind diese nun wasserunlöslich, gut löslich in THF und zeigen niedrigere T_gs im Bereich von -33 °C bis 18 °C. Dieses Kapitel ist in Zusammenarbeit mit Prof. Daniel Taton, Laboratoire de Chimie des Polymères Organiques, Université de Bordeaux, IPB-ENSCBP, Pessac Cedex, Frankreich, im Rahmen eines Forschungsaufenthaltes entstanden.

Im **Unterkapitel 3.4** wird Epicyanohydrin (EPICH) als Epoxidmonomer vorgestellt. Dieses erscheint auf den ersten Blick eher außergewöhnlich, da die Nitrilgruppe in

Nachbarschaft zum Epoxidring zu einem starken Elektronenzug führt. Hierdurch ist EPICH nicht über herkömmliche oxyanionische ringöffnende Polymerisation polymerisierbar, jedoch ermöglicht die milde monomeraktivierte AROP eine erfolgreiche Polymerisation. Copolymere von EO und EPICH dienen zur weiteren Funktionalisierung, insbesondere um Polyether mit primären Amin-, Carboxyl- und Amidgruppen zu erhalten. Amin- und carboxylfunktionalisierte PEGs sind aufgrund ihres Polyelektrolyt-Charakters von Interesse. Weiterhin können über diese Gruppen bioaktive Moleküle kovalent an das Polymer angebracht werden.

Im **Kapitel 4** werden alkinfunktionelle PEGs vorgestellt. Diese wurden durch die Copolymerisation von Glycidylpropargylether (GpgE) mit EO erhalten. Für eine erfolgreiche Synthese wurde die milde monomeraktivierte AROP verwendet. Hierdurch konnte eine zeitaufwendige „Schützung" der Alkingruppe umgangen werden. In der herkömmlichen oxyanionischen Polymerisation würde das Alkinproton zu Nebenreaktionen und unerwünschte Vernetzung führen. Über ¹H NMR Kinetikstudien konnte gezeigt werden, dass unter diesen Bedingungen GPgE deutlich langsamer polymerisiert als EO. Auf das Verhalten von Glycidylethern unter monomeraktivierten Bedingungen wird im nächsten Kapitel genauer eingegangen. Die hergestellten alkinfunktionellen Polymere wurden über kupferkatalysierte Click-Chemie mit α-Mannose versehen. Solche zuckerfunktionalisierten PEGs sind für Wechselwirkungsstudien mit Lektinen von Interesse. Zusammenfassend bieten alkinfunktionelle PEGs eine vielseitige Plattform zur Konjugation interessanter Bausteine.

Im letzten Kapitel, **Kapitel 5**, wird die Copolymerisation von EO mit Glycidylethern und der Einbau der Monomere in das Polymerrückgrat näher untersucht. Hierbei wurde die Copolymerisation von Ethoxyethylglycidylether (EEGE) und EO unter (i) herkömmlichen oxyanionischen und (ii) monomeraktivierten Bedingungen im NMR Röhrchen untersucht.

Kinetikstudien zeigten, dass das Reaktionsverhalten der beiden Monomere stark von den gewählten Polymerisationsbedingungen abhängt. Während bei der herkömmlichen oxyanionischen Polymerisation EEGE und EO gleich schnell reagieren ($r_{EO} \approx r_{EEGE}$), ist bei der monomeraktivierten AROP erstaunlicherweise EO stark bevorzugt ($r_{EO} = 8.0$ und $r_{EEGE} = 0.125$). Somit kann mit der Wahl der Reaktionsbedingungen die Verteilung der Monomere im Polymer beeinflusst und gesteuert werden, um beispielsweise in einem Schritt Block-Copolymer ähnliche Strukturen zu erhalten. Die Ergebnisse dieses Kapitels wurden in Zusammenarbeit mit Daniel Leibig erarbeitet.

Im **Anhang A1.** werden weitere Polymerisationsstrategien vorgestellt, die zum Erlangen hoher Molekulargewichte bei der Polymerisation substituierter Epoxide, eingesetzt werden können. Dieser Abschnitt ist aus einem veröffentlichten Übersichtsartikel entnommen und wurde von der Autorin dieser Dissertation geschrieben (Herzberger, J.; Niederer, K.; Pohlit, H.; Seiwert, J.; Worm, M.; Wurm, F. R.; Frey, H.*Chemical Reviews*, **2016**, *116*, 2170−2243 "Polymerization of Ethylene Oxide, Propylene Oxide, and Other Alkylene Oxides: Synthesis, Novel Polymer Architectures, and Bioconjugation").

In **A2.** wird thioetherfunktionelles, hochverzweigtes Polyglycerol vorgestellt. Durch die gezielte Copolymerisation von MTEGE und Glycidol werden hochverzweigte Strukturen erhalten, welche orthogonal funktionalisiert werden können. Während ausschließlich die Hydroxylgruppen mit Isocyanaten zu Urethanen reagieren, können die Thioether anschließend unter sauren Bedingungen mit Epoxiden zu Sulfoniumstrukturen umgesetzt werden. Dieses Kapitel zeigt die Ergebnisse, welche in einer Zusammenarbeit mit Dr. Jan Seiwert erhalten wurden.

Im **Anhang A3.** werden nitrilhaltige Poly(tetrahydrofurane) (PTHF) vorgestellt. Diese wurden ausgehend von Cyanoethylenoxid (CEO) und THF hergestellt. Analog zu EPICH ermöglicht die polymeranaloge Modifikation von CEO die Darstellung von amin- und

carboxylfunktionellem PTHF. Dieses Kapitel ist das Ergebnis einer Zusammenarbeit mit Dr. Eva-Maria Christ.

Anhang A4. In Zusammenarbeit mit dem Institut für Anorganische Chemie wurden catecholinitiierte PEGs als Liganden für Ni@γ-Fe$_2$O$_3$ Superpartikel eingesetzt. Hierbei ermöglicht PEG eine universelle Dispergierbarkeit der Partikel in wässriger Lösung.

Abstract

This thesis addresses the need for novel epoxide building blocks that allow for the synthesis of well-defined multifunctional PEGs. The introduction of only a few pendent groups along the polyether backbone can have a strong impact on the properties of PEG. Temperature, pH or redox-responsive PEG is prepared with tertiary amino- or thioether functional epoxides, respectively. Furthermore, synthetic strategies are provided to prepare multifunctional PEGs which are then suitable for post-polymerization modification without the need of protecting group chemistry. An overview of the epoxides introduced and utilized is illustrated in Scheme 1, and properties/possible applications are briefly listed.
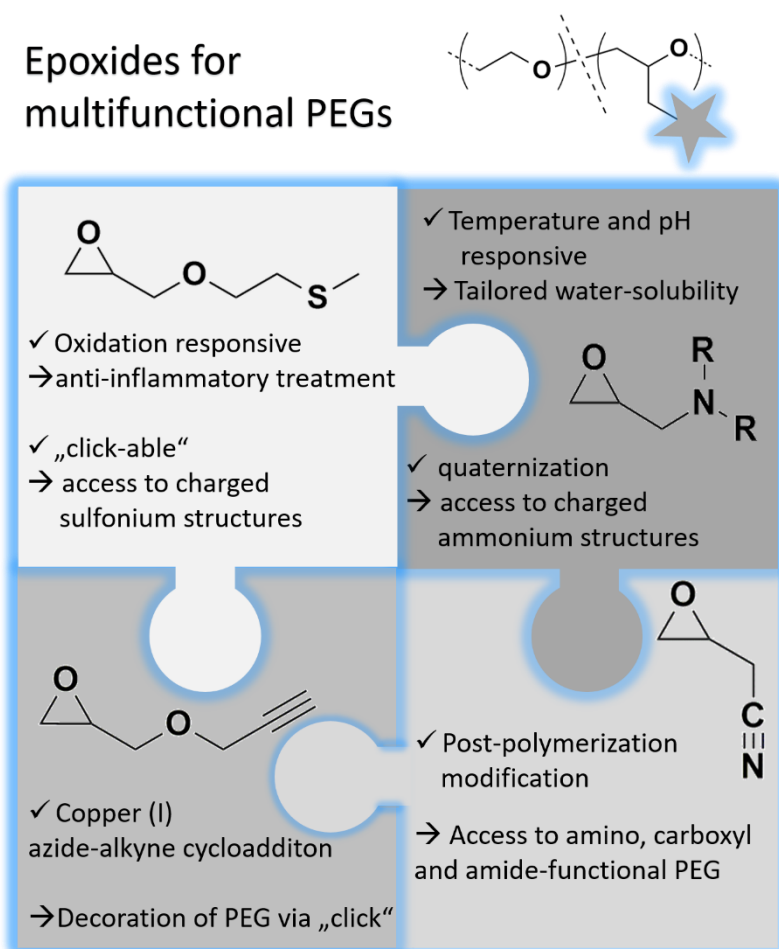
Scheme 1. Overview of utilized substituted epoxide monomers to prepare *mf*-PEG.

Chapter 1 provides a brief background of PEG's outstanding property profiles as well as the synthetic concepts and polymerization methods, required to understand the following chapters. Classical oxyanionic ring opening polymerization (AROP) and monomer-activated AROP are explained. After understanding the properties of PEG and the applied synthetic concepts, the need for additional functionality is highlighted. In this context, the chapter provides an overview of so-called "smart" and multifunctional PEGs (*mf*-PEGs) and concludes with a list of reactivity ratios determined for the copolymerization of EO and substituted epoxides under AROP conditions.

In **Chapter 2** the synthesis of thioether-functional PEGs is demonstrated. Random and block copolymers are prepared, capitalizing on the copolymerization of the novel 2-(methylthio)ethyl glycidyl ether (MTEGE) and EO or homopolymerization of MTEGE starting from a PEG macroinitiator. Their most intriguing feature is oxidation-responsiveness: mPEG-*b*-PMTEGE block copolymers form defined micelles in water and treatment with an oxidation agent leads to oxidation of the hydrophobic thioether to hydrophilic sulfoxide units. Subsequently, disassembly of the micelles to unimers takes place. Their response to oxidative agents is studied via NMR, light scattering, turbidity and fluorescence spectroscopy. Release studies with Nile Red illustrate their potential as oxidation-responsive nanocarriers. High cell viability render applications in the biomedical field possible. Due to their oxidation-response and biocompatibility, these structures might be suitable candidates for anti-inflammatory treatment. The versatility of thioether-functional PEG is further demonstrated by synthesizing sulfonium-functional materials by treating thioether-functional PEG with (i) alkyl halides and (ii) epoxides under acidic conditions.

Chapter 3 is introduced by a short overview of synthetic strategies to prepare amino-functional PEGs with the main focus on the direct copolymerization of nitrogen containing

functional epoxide monomers. Glycidyl amine derivatives are discussed as a suitable monomer class for AROP. This section (**Chapter 3.1**) was published as a part of *Chemical Reviews*, **2016**, *116*, 2170−2243 "Polymerization of Ethylene Oxide, Propylene Oxide, and Other Alkylene Oxides: Synthesis, Novel Polymer Architectures, and Bioconjugation" and was contributed by the author of this thesis. In **Chapter 3.2**, glycidyl amines bearing hydrophobic alkyl chains are presented for synthesis of tertiary amino-functional PEGs. Three different glycidyl amine derivatives, namely *N,N*-di(*n*-butyl) glycidyl amine (DButGA), *N,N*-di(*n*-hexyl) glycidyl amine (DHexGA) and *N,N*-di(*n*-octyl) glycidyl amine (DOctGA) are synthesized and (co)polymerized statistically with EO or initiated with methoxyPEG to yield block copolymers. Online ^{1}H NMR kinetic studies reveal a gradient like structure for the statistical copolymers. In a complementary study, the behavior of tertiary-functional PEGs in water is investigated on the nano- (continuous wave-electron paramagnetic resonance (CW-EPR) spectroscopy, light scattering) and macroscale (turbidity). Their response to temperature and pH-changes highlights their multi-stimuli responsive character. Cloud point temperatures are tunable from 21 to 93 °C with comonomer ratios < 15 mol%, while fully water-soluble structures are maintained at slightly acidic pH. In **Chapter 3.3,** polyelectrolytes are generated by quaternization of the tertiary amine moieties in diblock, triblock and gradient copolymers based on *N,N*-di(*n*-butyl)amino functional PEGs. Quaternization with methyl iodide or benzyl bromide produces water-soluble polymers, which exhibit high glass transition temperatures (T_gs of 6 °C to 83 °C). Anion exchange with bis(trifluoromethylsulfonyl)imide (TFSI) leads to a switch in properties: Polymers are water-insoluble but THF-soluble and possess T_gs in the range of -33 °C to 18 °C, despite their charged nature. This work was performed in collaboration with Prof. Daniel Taton, Laboratoire de Chimie des Polymères Organiques, Université de Bordeaux, IPB-ENSCBP, Pessac Cedex, France.

In **Chapter 3.4**, a rather unusual nitrile containing monomer, epicyanohydrin (EPICH), is used in a simple strategy to prepare primary amino-functional PEG. The strong electron withdrawing effect of the nitrile group requires mild polymerization conditions, realized by monomer activation with a Lewis acid. Most important, the EPICH monomer gives access to carboxyl, amide- and primary amino-functional PEG via facile post-polymerization modification. These structures represent positively and negatively charged PEG polyelectrolytes and also offer potential to tether pharmaceutically active compounds to PEG.

Chapter 4 illustrates alkyne-functional PEGs as a platform for click-functionalization via copper(I) catalyzed azide-alkyne cycloaddition (CuAAC). Direct copolymerization of EO with glycidyl propargyl ether (GPgE), without protection of the propargyl moiety, serve to introduce multiple alkyne moieties along the backbone. The key for a successful polymerization is mild reaction conditions, as realized by the monomer-activated AROP. Surprisingly, ^{1}H NMR kinetic studies revealed that EO reacts much faster than GPgE with reactivity ratios of $r_{EO} = 14.8$ and $r_{GPgE} = 0.076$, leading to block-like structures. PEG based glycopolymers are prepared by decorating the alkyne units with mannopyranosyl azide. Additionally, mannose-functionalized PGPgE homopolymer is prepared. Overall, alkyne-functional PEGs provide a platform for conjugation of bioactive molecules, dyes or other functional moieties.

The copolymerization differences of glycidyl ethers via conventional oxyanionic ROP and monomer-activated AROP with an aluminum Lewis acid are elucidated in **Chapter 5.** Copolymerization of ethoxy ethyl glycidyl ether (EEGE), a model glycidyl ether, with EO is monitored *in situ* via ^{1}H NMR spectroscopy. Unexpectedly, while conventional oxyanionic AROP leads to random copolymers with $r_{EO} \approx r_{EEGE}$, monomer activation produces tapered structures, with EO rich segments close to the initiator and EEGE rich

segments close to the terminus ($r_{EO} = 8.00$ and $r_{EEGE} = 0.125$). These results demonstrate that tailored copolymer structures can be realized in a one-pot synthesis by simple choice of initiator system. The results presented in this chapter were obtained in collaboration with Daniel Leibig.

In **Appendix A1.** alternative polymerization techniques to prepare PEG and high molecular weight derivatives are described, ranging from initiation with metal-free phosphazene bases or *N*-heterocyclic carbenes (NHC) to the use of heterogeneous double metal cyanide (DMC) catalysts. This chapter is a part of a published review article, Herzberger, J.; Niederer, K.; Pohlit, H.; Seiwert, J.; Worm, M.; Wurm, F. R.; Frey, H. *Chemical Reviews*, **2016**, *116*, 2170−2243 "Polymerization of Ethylene Oxide, Propylene Oxide, and Other Alkylene Oxides: Synthesis, Novel Polymer Architectures, and Bioconjugation", and was contributed by the author of this thesis.

A2. Thioether-functional hyperbranched polyglycidol (*hb*-PG) is presented. Polymers are synthesized from glycidol and MTEGE and give access to orthogonal functionalization of *hb*-PG. In particular, the hydroxyl groups react exclusively with isocyanates and form urethane linkages, while the thioether moieties are modified with epoxides leading to charged sulfonium moieties. The result presented in this chapter are of a collaborative effort with Dr. Jan Seiwert.

Inspired by epicyanohydrin and the use of nitrile groups as precursors for amines or carboxylic acids, in **A3.** nitrile-functional polyTHF is described, starting from cyano ethylene oxide (CEO) and THF, prepared via cationic copolymerization. This chapter is the result of a collaborative effort with Dr. Eva-Maria Christ.

A4. In collaborative work with the Institute of Inorganic Chemistry, catechol-initiated PEGs are applied as ligands for inorganic Ni@γ-Fe$_2$O$_3$ superparticles to render them water dispersible.

Graphical Abstract

Chapter 2.1:

Oxidation-Responsive and "Clickable" Poly(ethylene glycol) via Copolymerization of 2-(Methylthio)ethyl Glycidyl Ether
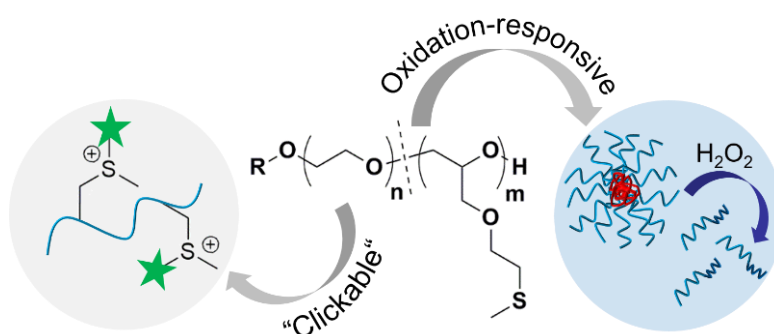
Chapter 3.2:

Stimuli-Responsive Tertiary Amine-Functional PEGs Based on *N,N*-Dialkyl Glycidyl Amines
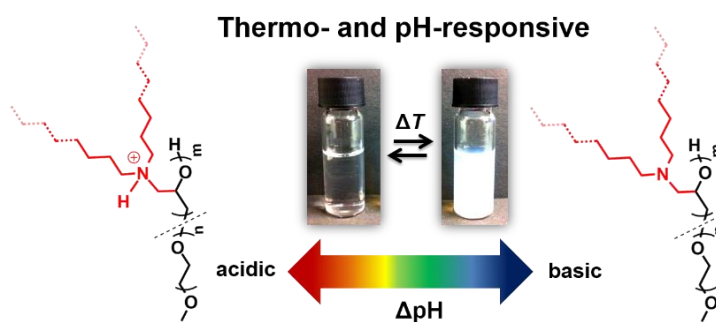
Chapter 3.3:

Structure-Property Study of Novel Copolyethers Based on PEG with Pendant Quaternary Ammoniums Obtained by Post-Polymerization Modification of Poly(glycidyl amine) Precursors
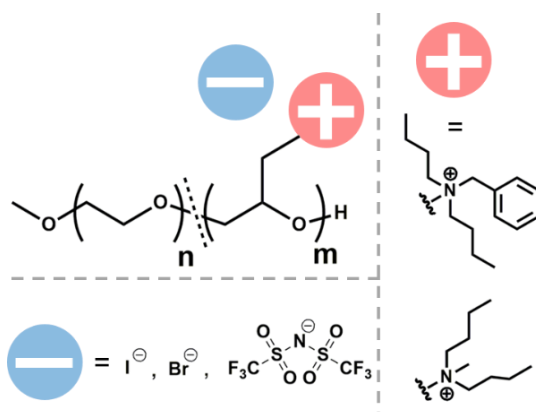
Chapter 3.4:

Epicyanohydrin: Polymerization by Monomer Activation gives Access to Nitrile, Amino and Carboxyl-Functional Poly(ethylene glycol)
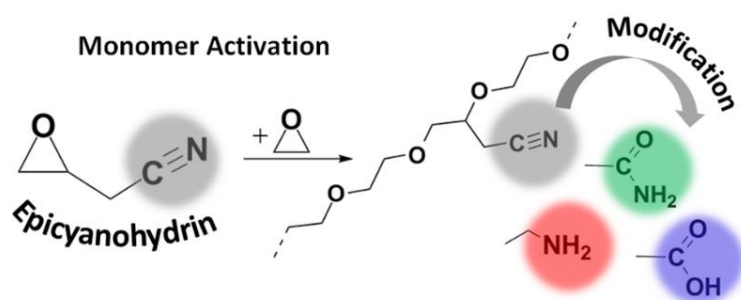
Chapter 4.1:

"Clickable PEG" via Anionic Copolymerization of Ethylene Oxide and Glycidyl Propargyl
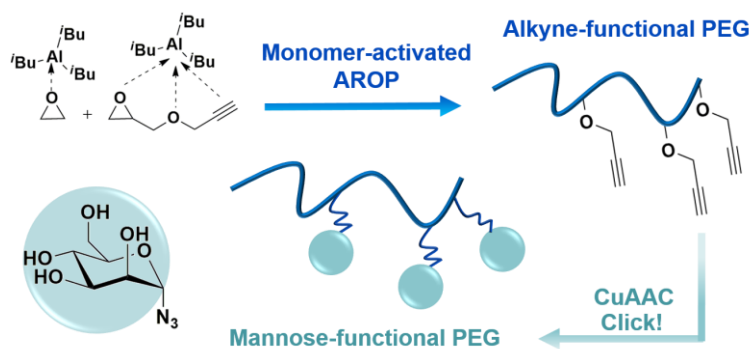
Ether

Chapter 5.1:

Conventional Oxyanionic versus Monomer-Activated Anionic Copolymerization of

Ethylene Oxide with Glycidyl Ethers: Striking Differences in Reactivity Ratios
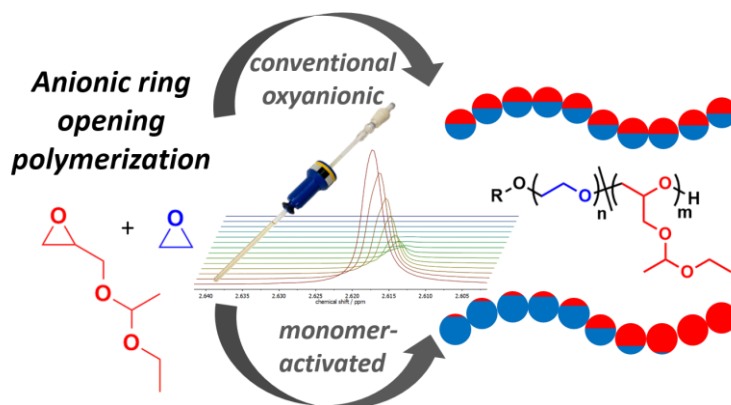
1 Introduction

In this chapter, an introduction to poly(ethylene glycol) (PEGs) and its exceptional property profile is given, and synthetic strategies to prepare well-defined PEGs are presented.

1.1 Properties and Applications of PEG

Poly(ethylene glycol) (PEG) belongs to the class of aliphatic polyethers and consists of ethylene glycol repeat units and one hydroxyl group at each chain end. Note that PEG with higher molecular weights is also called poly(ethylene oxide) (PEO), which refers to its origin, the ethylene oxide (EO) monomer. In contrast to other aliphatic polyethers such as polyoxymethylene (POM) or polytetrahydrofuran (PTHF), PEG shows excellent solubility in both organic solvents and water.[1] The origin of PEG the outstanding water solubility of PEG is still not fully understood. However, many experimental and theoretical studies suggest that the high aqueopus solubility arises from two factors (i) conformational behavior in aqueous solution with a preferred *trans-gauche-trans* (helical like) conformation[2] and (ii) the distance of oxygen atoms in the repeat units (CH_2CH_2O). Both allows for beneficial hydrogen bonding interactions with water molecules and the formation of an organized water structure around the polymer chain (Figure 1).[3, 4]
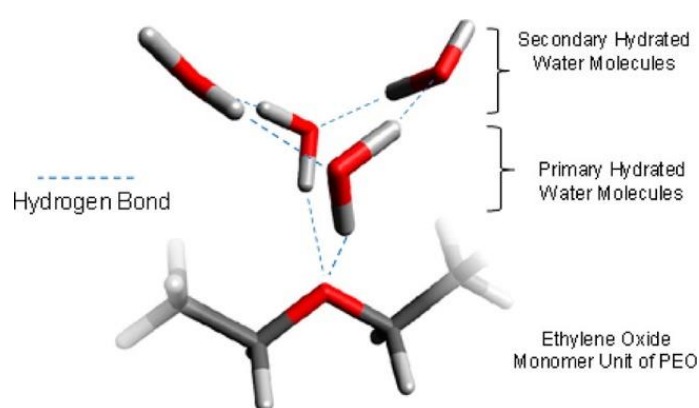
Figure 1. Schematic illustration of a hydrated ethylene oxide unit of PEG at the hydration number of $m_{EO} = 4$ at $T < 30$ °C. Adapted with permission from Shikata, T; Okuzono, M; Sugimoto, N. *Macromolecules*, 2013, *46*, 1956-1961.[4] Copyright 2013 American Chemical Society.

However, when an aqueous solution of PEG is heated, at a certain temperature this "water-cage" becomes entropically disfavored and a polymer coil-to-globule transition takes place. Consequently, PEG precipitates and a turbid solution results. This phenomenon is referred to as lower critical solution temperature (LCST), which is around 100 °C for PEG with sufficiently high molecular weights.[2] It should be mentioned, that the LCST reflects the lowest point of the miscibility gap in the phase diagram and depends on both the molecular weight and the concentration of the polymer solution. Mostly, researchers report cloud point temperatures of a given system and do not determine the exact LCST. Possibilities to tune and adjust PEG's cloud point temperature are discussed in the introductory section "multifunctional PEGs".

In addition to PEG's outstanding aqueous solubility, it possesses low immunogenicity and toxicity, which render it highly valuable for biomedical applications in general.[5] In the context of pharmaceuticals, "PEGylation", defined as the covalent attachment of PEG chains to bioactive substances has attracted immense attention and protein PEGylation has become a billion-dollar-market.[6] Unfortunately, PEG is not biodegradable, but if applied in the body, PEGs with molecular weights below 30,000 $g \cdot mol^{-1}$ can be easily cleared by the kidneys and no accumulation in the liver is observed.

Regarding its bulk properties: PEG is a flexible, semi-crystalline polymer with a glass transition temperature (T_g) in the range of -50 °C to -60 °C and a melting temperature reaching 66 °C with high molecular weight around 10,000 g·mol⁻¹.[7] In particular, PEGs with molecular weights around 600 g·mol⁻¹ are still liquids at room temperature and are used as solvents and wetting agents in body lotions. PEG with 1000 g·mol⁻¹ appears waxy at room temperature, and solid material is obtained starting with molecular weights around 2000 g·mol⁻¹ (Figure 2).
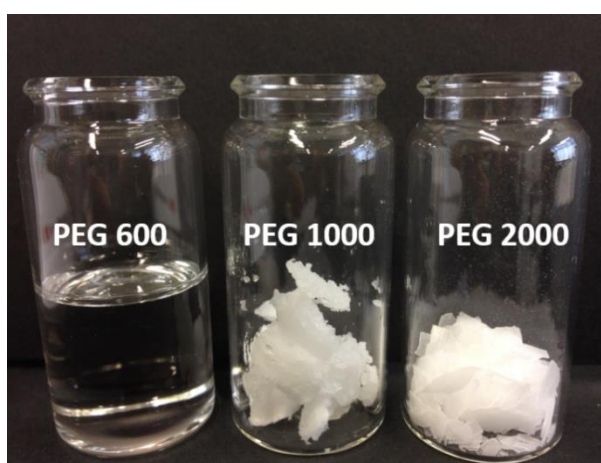
Figure 2. PEG with different molecular weights (600 g·mol⁻¹, 1000 g·mol⁻¹and 2000 g·mol⁻¹). Polymers were purchased from Merck (600 g·mol⁻¹) and Fluka (1000 g·mol⁻¹ and 2000 g·mol⁻¹), respectively.

The peculiar property profile of PEG renders it attractive for numerous applications ranging from commodity products to highly sophisticated pharmaceuticals. For example, PEG derivatives are applied as nonionic surfactants in edibles and cosmetics.[8] Polyether polyols based on propylene oxide (PO) and ethylene oxide (EO) serve as soft segments in polyurethane foams.[9] In the context of energy storage devices, PEG is one of the most important solid polymer electrolytes for lithium ion batteries.[10] Regarding pharmaceuticals, PEG chains can be covalently attached to therapeutic peptides or proteins to enhance blood

circulation times dramatically.[6, 11] Note that Dingels et al. provided a great overview of PEG's diversity and applications (article in German language).[8]

1.2 Polymerization Techniques

Various reviews cover the different synthetic strategies to prepare PEG and its derivatives.[12–15] In the following, only a short overview is given to describe the synthetic concepts required to understand the next chapters. PEG can be prepared employing different polymerization types, e.g. cationic, catalytic or anionic ring opening polymerization of ethylene oxide (EO). From these synthetic methods, the anionic ring opening polymerization (AROP) of EO is the most common route, being cost-effective, while leading to well-defined polymers due to its living character. In this thesis, classical AROP initiated with metal alkoxides and a slightly modified monomer-activated technique have been applied, which will be explained in the following section. Other polymerization strategies are explained in Appendix A1.

1.2.1 Anionic Ring Opening Polymerization (AROP)

The oxyanionic ring opening polymerization of EO dates back to 1863, first mentioned by Wurtz[16] and revisited by Staudinger and Schweitzer.[17] In 1940, Flory showed that the base initiated polymerization of EO leads to polymers with a Poisson distribution.[18] The high ring strain of EO (~114 kJ/mol) renders a nucleophilic ring-opening via S_N2 mechanism possible.[19] To obtain narrow molecular weight distributions, water traces have to be removed and the polymerization should be performed in vacuum or in inert atmosphere to minimize the risk of impurities. Suitable initiators are strong nucleophiles, such as alkali metal alkoxides, hydrides, alkyls, aryls, hydroxides, and amides. Polymerization can be either conducted in bulk (solvent free) or in a polar but aprotic solvent, such as THF, DMSO

or 1,4-dioxane. While the absence of irreversible side reactions is indispensable for a living process, reversible termination is allowed when $k_{reversible\ termination} \gg k_{propagation}$. This prerequisite is valid for the AROP of ethylene oxide. Partial deprotonation of an alcohol is sufficient to initiate and conduct the polymerization, due to a fast proton exchange ($k_{proton\ exchange} \gg k_{propagation}$) and all polymer chains grow simultaneously (Scheme 1).
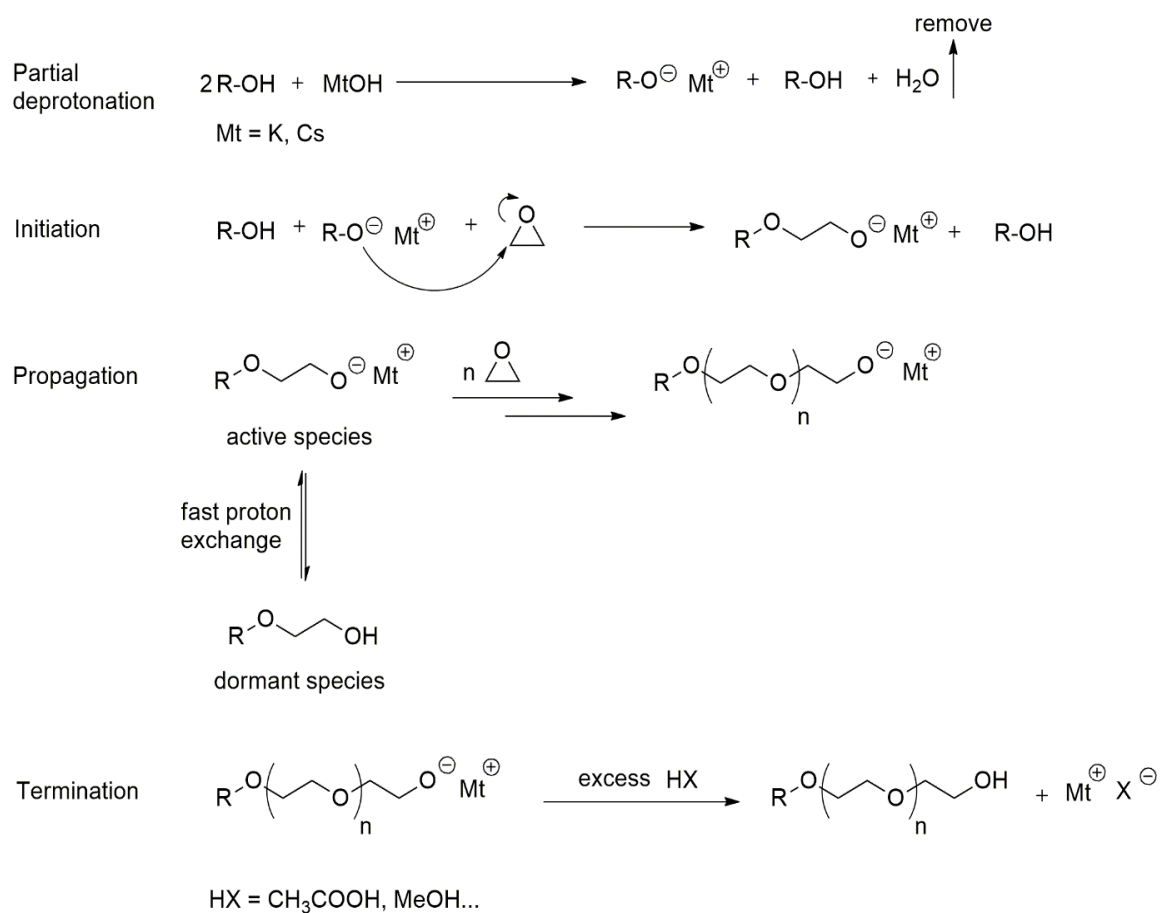
Scheme 1. Mechanism of the anionic ring opening polymerization (AROP) of ethylene oxide (EO).

In solution, the growing chain end might consist of the alkoxide and counterion as free ions, ion pair, or aggregates can be present (Scheme 2).

aggregate $\qquad$ ion pair $\qquad$ free ions

$$\left[\sim O^{\ominus} Mt^{\oplus} \right]_n \xrightarrow{K_{aggregation}} \sim O^{\ominus} Mt^{\oplus} \xrightarrow{K_{dissociation}} \sim O^{\ominus} + Mt^{\oplus}$$
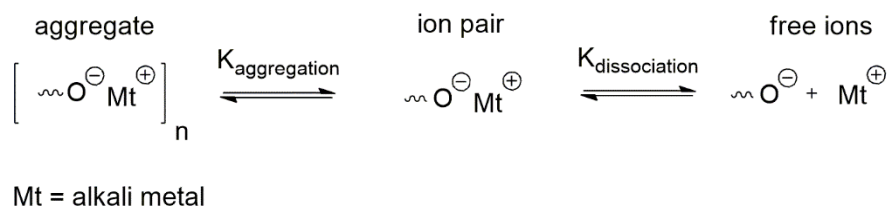
Mt = alkali metal

Scheme 2. Conformation of active chain end in solution: Aggregated chains (left), ion pairs (middle) and free ions (right).

In general, bulky and "soft" alkali metals such as potassium and cesium show low tendency to aggregate and are the most suitable counterions. In contrast, "hard" lithium ions form strong aggregates with the "hard" oxygen anion of the alkoxide initiator and impede polymerization. However, the polymerization kinetics are quite complex and are described in more detail elsewhere.[12]

Addition of a protic/acidic solvent terminates the anionic polymerization. α-ω-Bifunctional PEGs can be prepared by choice of a functional initiator and terminating agent.[20] In summary, the characteristics of living AROP are (i) strong bases as initiators (ii) well-defined polymers possessing Poisson distribution (iii) access to mono or bi-functional structures by choice of initiator and terminating agent.

1.2.2 Activated Monomer Strategy

The activated monomer technique is suitable to increase molecular weights of polyethers based on mono-substituted epoxides or to polymerize either (i) sensitive or (ii) unreactive epoxides. The following section is a contribution by the author of this thesis that was published as a part of *Chemical Reviews*, **2016**, *116*, 2170−2243 (Special Issue: Frontiers in Macromolecular and Supramolecular Science), titled: "Polymerization of Ethylene Oxide, Propylene Oxide, and Other Alkylene Oxides: Synthesis, Novel Polymer Architectures, and Bioconjugation".

In this section we give an overview of the "activated monomer mechanism" for the polymerization of epoxide monomers, developed by Carlotti and Deffieux, which represents a major breakthrough for many functional epoxides.[13, 21] In 2013, Carlotti et al. published a detailed review regarding polyether syntheses based on such activated or metal-free anionic ring-opening polymerizations of epoxides.[14] The "controlled" high speed anionic polymerization of PO by the monomer-activation technique was introduced in 2004.[21] Remarkably, this represents the first method that permits to obtain high molecular weight PPO (M_n up to 170,000 g/mol).[21] Inspired by the work of Inoue and co-workers[22–26] and Braune and Okuda,[27] monomer activation results from the interaction of a Lewis acid with the epoxide ring, reducing the electron density in the epoxide ring, thereby facilitating subsequent ring-opening. The initiation proceeds through formation of an "ate complex" between the Lewis acid (catalyst) and a weak nucleophile (initiating species), as illustrated in Scheme 3. Chain growth results exclusively in head-to-tail (H-T) linkages with no appearance of H-H or T-T junctions, and for racemic epoxides an atactic microstructure is obtained, indicating a coordination type mechanism.[21, 28]

The first initiating systems of this type were based on alkali metal alkoxides with trialkyl-aluminum species, resulting in an enhanced polymerization rate and little occurrence of transfer reactions compared to conventional AROP.[21] Improved initiator systems are based on organic salts, containing non-coordinating cations such as tetraalkyl ammonium halides or phosphonium salts combined with triisobutylaluminum as a catalyst, which fully suppress transfer reactions.[21, 28–32] However, besides the desired initiation *via* the respective halide anion, concurrent ring opening *via* hydride or *iso*-butyl groups is reported, which may lower molecular weights and lead to a fraction of ill-defined chain ends (Scheme 3e).[32, 33]

Suitable solvents for the activated monomer approach are aprotic and should preferably possess no complexing oxygen atoms. For example, THF complexes the aluminum

compound and thereby impedes activation of the epoxides. A suitable alternative solvent for THF is 2-methyltetrahydrofuran (MeTHF).[34] Further, the use of cyclohexane, toluene, dichloromethane, chlorobenzene[35] and fluorinated benzene was reported in literature.[21, 28, 32, 33, 36, 37]
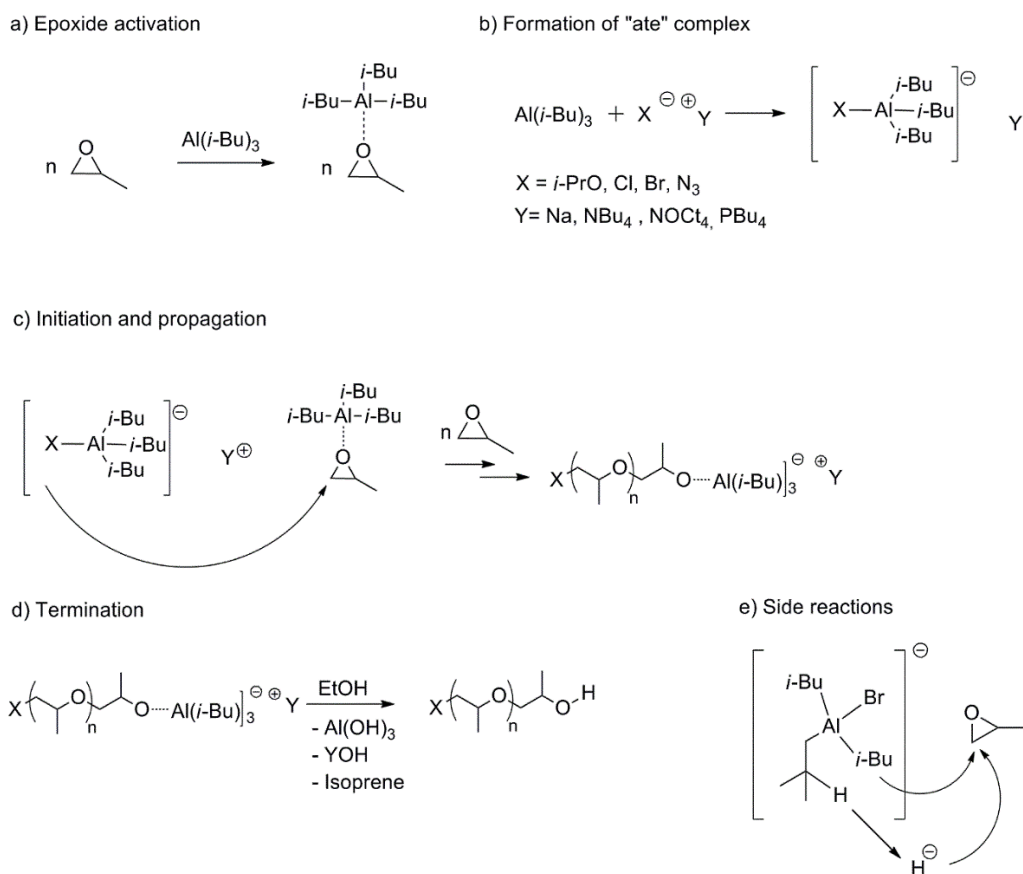
Scheme 3. Reaction mechanism of the "activated monomer" technique, exemplified for the polymerization of propylene oxide (PO).[21, 28, 32]

Note that the ratio of Lewis acid (catalyst) to the actual initiator has to exceed unity to ensure the formation of the "ate"-complex and simultaneously implement an activation of the epoxide ring, resulting in successful polymerization. Monomers with strong coordination capability require higher amounts of the catalyst to overcome strong interactions with the Lewis acid (Scheme 4). However, low ratios are preferred, to ensure narrow molecular weight distributions.[21, 28]
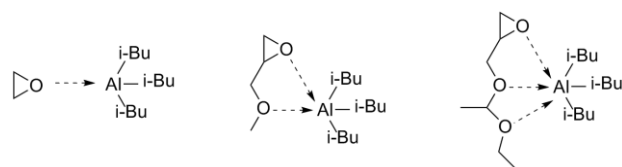
Scheme 4. Complexation of triisobutylaluminum by oxygen atoms. Interaction of triisobutylaluminum with EO, GME and EEGE (from left to right).

Strong activation of the epoxide ring brings about several advantages: (i) polymerizations can be carried out under mild reaction conditions (low temperatures, -30°C to room temperature) and (ii) with weak nucleophilic "ate" complexes as initiator and propagating species. Consequently, molecular weight limiting transfer-to-monomer reactions are suppressed, and high molecular weight polyethers are accessible, while the molecular weight distribution remains narrow. Additionally, polymerization rates are dramatically increased and the reactions can be carried out in hydrocarbon solvents (Figure 3).[21, 28, 36, 38]
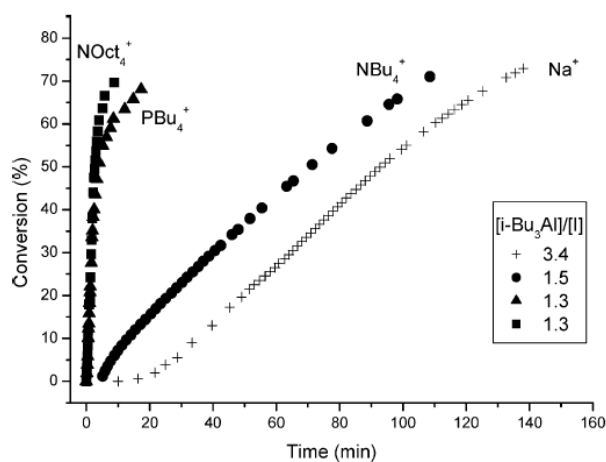
Figure 3. Conversion plotted versus time for PO polymerization initiated by *i*-PrONa, NBu₄Cl, NOct₄Br and PBu₄Cl in cyclohexane with the respective Lewis acid to initiator ratio and degrees of polymerization around 170-192. Adapted with permission from Labbé A, Carlotti S, Billouard C, Desbois P, Deffieux A, *Macromolecules* 40: 7842-7847 (2007).[28] Copyright 2007 American Chemical Society.

Within less than 2 hours, PPO samples with remarkably high molecular weights of 170,000 g·mol^{-1} and rather low PDI = 1.34 were accessible.[21, 28] Note that the use of conventional alkali metal initiators restricts the molecular weight of PPO to about 6000 g·mol^{-1},[39] and even the use of soft counterions such as cesium or the addition of crown ethers still limits the molecular weight to about 15,000 g·mol^{-1}.[40, 41] Further, the authors demonstrated the applicability of this method by preparing a number of high molecular weight polyethers such as high molecular weight PEEGE (up to 85,000 g·mol^{-1}),[37] PEG (up to 36,000 g·mol^{-1}) and PPO-PEG copolymers.[36] The fascinating synthetic options created by this method permitted to study the molecular weight dependence of the viscoelastic properties of linear polyglycerol (*lin*PG) in the entire molecular weight range of 1 kg·mol^{-1} to 100 kg·mol^{-1}. Detailed rheological features of *lin*PG and its permethylated analogue (*lin*PG-OMe) were reported, demonstrating the effect of a hydrogen bonding network from non-entangled to well-entangled chains.[42]

In general, the strong activation of the epoxide ring enables to polymerize a broad family of less reactive and sterically hindered epoxides, such as epoxides bearing hydrophobic alkyl chains (1,2-butene oxide, 1,2-hexene oxide, 1,2-octadecene oxide) and glycidyl methyl ether.[43–47] In addition, with the controlled polymerization of epichlorohydrin (ECH), Carlotti and co-workers demonstrated the high tolerance of this method towards functional groups. Interaction of the active species with the chloromethyl function was not observed, and homopolymers of PECH with molecular weights up to 80,000 g·mol^{-1} and PDIs below 1.25 were realized.[48] This strategy gives access to a library of novel polymers, based on post-polymerization modification of the chloride groups of PECH. Lynd and co-workers presented hydrolytically degradable PEG by copolymerizing ECH with EO. The copolymers were treated with potassium *tert*-butoxide to obtain poly(methylene ethylene oxide) units, leading to degradation at slightly acidic pH.[49] Also starting from PECH, Meyer et al. prepared poly(glycidyl amine).[50] Recently, Baker et al. reported the synthesis of a

polyether-based poly(ionic liquid) by derivatizing the chlorides of PECH with 1-butylimidazol, followed by anion exchange with lithium bis(trifluoromethane-sulfonyl)imide.[51] The modified polymers showed conductivities of 10^{-5} S cm^{-1} at 30 °C and 10^{-3} S cm^{-1} at 90 °C. Other challenging epoxides such as glycidyl methacrylate, fluorinated epoxides, allyl glycidyl ether and epicyanohydrin[35] were also successfully polymerized.[32, 33, 45, 46, 52]

In 2010, Carlotti and coworkers demonstrated that the activation of ethylene oxide even enables lithium salts to polymerize epoxides. In particular, this strategy permits the synthesis of PS-*b*-PEO and PI-*b*-PEO block copolymers in a one-pot reaction.[53] Further, the monomer activation with a Lewis acid can be combined with initiation *via* phosphazene alkoxides. Molecular weights of PPO up to 80,000 g·mol^{-1} were obtained in this case. However, a certain extent of transfer reactions yielding unsaturated chain ends was still observed.[38]

Recently, Babu and Muralidharan expanded the „activated monomer approach" towards the activation of the epoxide ring via Zn(II), Cd(II) or Cu(II) complexes of 2,5-bis(*N*-(2,6-diisopropylphenyl) iminomethyl)pyrrole.[54] The authors demonstrated successful polymerization of various phosphate based epoxides in THF at 70 °C by using tetrabutylammonium bromide as the actual initiator (Scheme 5).
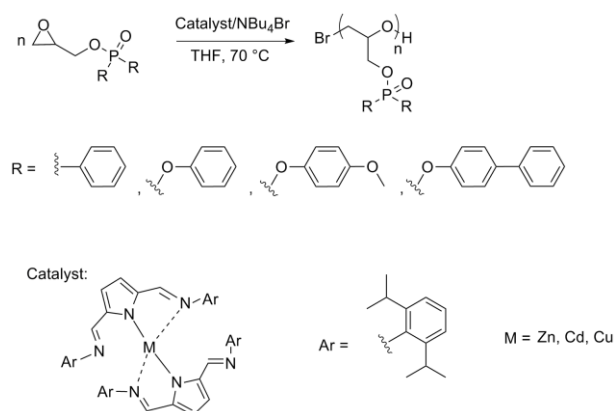
Scheme 5. Synthesis of phosphate-containing linear polyethers based on monomer activation.[54]

Very recently, Roos and Carlotti demonstrated the use of Grignard reagents as deprotonating agents for PO polymerization.[34] The authors deprotonated 1-butanol with various Grignard reagents and observed successful polymerization of PO in the presence of triisobutylaluminum as an activator. Molecular weights ranged from 2,500 to 10,000 g·mol^{-1}, while PDIs remained moderate (1.20-1.37). The formation of allylic end groups was completely suppressed; however initiation via various species was detected. MALDI-ToF measurements revealed initiation by (i) 30 % desired alkoxide magnesium halide (RO$^-$ $^+$MgX), (ii) 20 % hydride initiation from triisobutylaluminum (H$^-$ $^+$MgX) and (iii) 50 % halide initiation from the alkoxide magnesium halide (X$^-$ $^+$MgOR), as illustrated in Scheme 6.
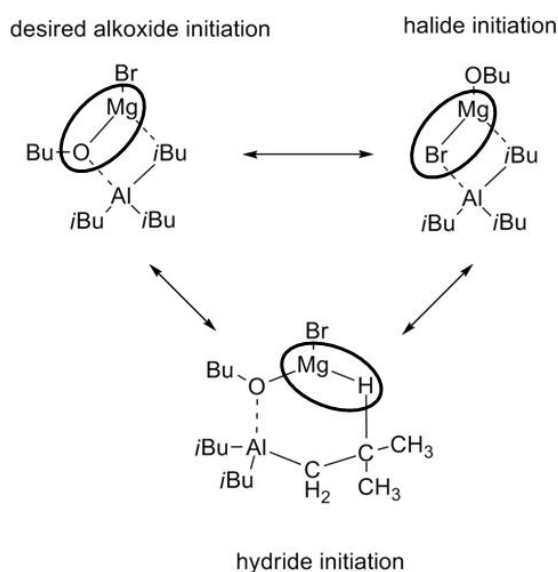
Scheme 6. Proposed initiation species for Grignard/alcohol/triisobutylaluminum system.[34]

Despite its fundamental advantages, the "activated monomer technique" also bears some challenges. To obtain low PDIs, the catalyst to initiator ratio has to be kept at a minimum and needs to be adjusted for each monomer system with respect to the targeted molecular weight. Further, removal of the residual initiator counterions, i.e., the tetraalkyl ammonium salts is often difficult and time-consuming. Simple precipitation of the polymer often leads

to unsatisfactory results. Column chromatography or long term dialysis can be performed, albeit with reduction of the polymer yield.[45] More hydrophobic polyethers, such as PEEGE, can also be purified by consecutive washing with saturated $NaHCO_3$ solution, NaCl solution (10 %) and water.[42]

Direct calculation of the absolute M_n via ^{1}H NMR spectroscopy using ^{1}H NMR signals of the initiator is generally not possible for the activated monomer approach, given the nature of the initiator species (bromide, chloride, azide). In literature, molecular weights are determined by SEC measurements (refractive index signal or UV signal). However, molecular weights analyzed by a general SEC set-up are not absolute values. Alternatively, end-group functionalization or absolute methods, such as static light scattering, have to be performed. Even though the formation of unsaturated end-groups can be mainly suppressed, undesired initiation by hydride or *iso*-butyl groups was also reported (Scheme 3e).[28, 32]

In summary, the "activated monomer mechanism" has become a well-established alternative to the conventional AROP within the last decade and is a crucial method, both to prepare high molecular weight polyethers and to polymerize a broad family of epoxides bearing functional groups to generate novel functional polyethers.

1.3 Multifunctional PEGs (*mf* PEGs)

PEG's properties are specifically tailored by distributing functionalities or pendent groups along the polyether backbone by copolymerization of ethylene oxide with monosubstituted epoxides. The simplest example is the statistical copolymerization of EO with propylene oxide (PO). The introduction of an "innocent" methyl group allows for adjusting or fully suppressing the crystallinity of PEG and tailoring its solubility in aqueous solution.[55–57]

In 2011, Obermeier *et al.* published a comprehensive review regarding *mf*- PEGs, giving synthetic guidelines and possible applications. Mangold et al. further highlighted potential

functional epoxides suitable for AROP.[58] Recent advances have been discussed in a review published elsewhere.[15] Here, only a brief overview is provided with the main focus on epoxide monomers leading to stimuli-responsive PEG. Note that in-chain modification via polycondensation/addition or copolymerization of EO with other strained rings bearing heteroatoms is not discussed in this thesis.

1.3.1 Anionic Ring Opening Polymerization of Monosubstituted Epoxides

Before the properties and possible applications of *mf*-PEGs are discussed, a short overview on their polymerization and related challenges is given. First, it should be mentioned that epoxides bearing substituents in α- and β-position or large, sterically hindered groups directly at the oxirane ring are not suitable for AROP. However, oxiranes bearing alkyl groups, such as propylene oxide (PO) and butylene oxide (BO) are polymerizable, but their reactivity decreases with increasing alkyl chain length.[59] Additionally, various derivatives of epichlorohydrin or glyicdol can be utilized. An overview of various epoxide monomers is illustrated in Scheme 11 in the next section.

In general, the ring-opening of monosubstituted epoxides can proceed at two different positions of the oxirane ring, which leads to a different polymer structure (head-to-tail, head-to-head or tail-to-tail), as shown in Scheme 7. Due to steric reasons, AROP of monosubstituted epoxides mainly results in regioregular head-to-tail connections.[60]

Mt = alkali metal
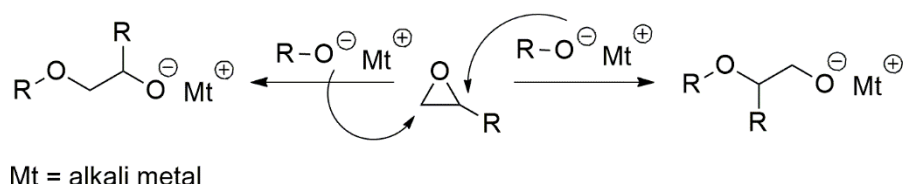
Scheme 7. Anionic ring opening of substituted epoxides: attack at the methylene position (left) or methine position (right).

In contrast to ethylene oxide, inherent side reactions can occur when substituted epoxides are polymerized. For example, during the polymerization of PO, proton abstraction by the growing chain end/initiator leads to a transfer of the negative charge to a monomer and the simultaneously formation of a double bond with subsequent generation of a new initiating species (Scheme 8). Consequently, targeted molecular weights decrease and full end group functionalization is lost. This is the reason why molecular weights of PPO in the base initiates AROP are limited to 6,000-15,000 $g \cdot mol^{-1}$. Note that the molecular weight limit varies with the counterion employed (e.g. Cs versus K).[12, 61, 62] Strong complexing agents, such as cryptands or crown ethers can be added to facilitate dissociation of the growing chain end and counterion. Therefore, the polymerization is accelerated, lower polymerization temperatures are necessary and transfer reactions are minimized.[14, 63]
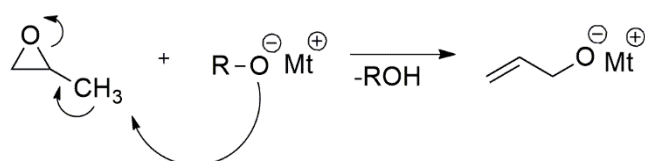
Scheme 8. Proton abstraction by strong base (initiator or active chain end), leading to double bond formation and generation of a new initiating species.

This described side reaction is a general problem of substituted epoxides. For example, the molecular weight of poly(ethoxy ethyl glycidyl ether) (PEEGE) homopolymer is limited to ~30,000 $g \cdot mol^{-1}$ in the base initiated AROP.[64] In addition, formation of carbonyl groups was reported for the polymerization of glycidyl phenyl ether (Scheme 9).[65]
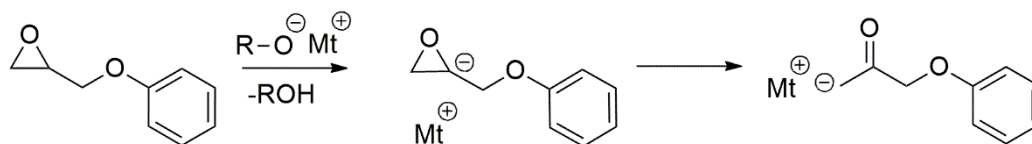
Scheme 9. Chain transfer to glycidyl phenyl ether with formation of carbonyl groups.[65]

To lower or suppress the described side reactions, other initiating systems or polymerization techniques can be applied. For example, the use of double metal cyanide (DMC) catalysts (see Appendix A1) or posphazene bases as deprotonation agent (see Appendix A1). Further, activation of the epoxide ring with a Lewis acid allows for polymerization under mild reaction conditions. The latter is often called "activated monomer technique", as explained in the previous section.

1.3.2 Monomer Synthesis and Properties of *mf*PEGs

In general, a facile and low cost synthesis is crucial for the future applicability of substituted epoxides as monomers. Herein, two major strategies are applied (i) oxidation of allylic structures or (ii) conversion of epichlorohydrin with (a) alcohols to yield glycidyl ethers or (b) amines to glycidyl amines under basic conditions. Additionally, (iii) ethoxy ethyl glycidyl ether (EEGE) is generally synthesized from glycidol and ethyl vinyl ether in analogy to a literature procedure[66] (Scheme 10).

(i)
mCPBA

a) glycidyl ethers
b) glycidyl amines

(ii)
HO-FG, NaOH
-NaCl

HN-R / R, NaOH
-NaCl
R > methyl

(iii)
, (H⁺)

FG = functional group
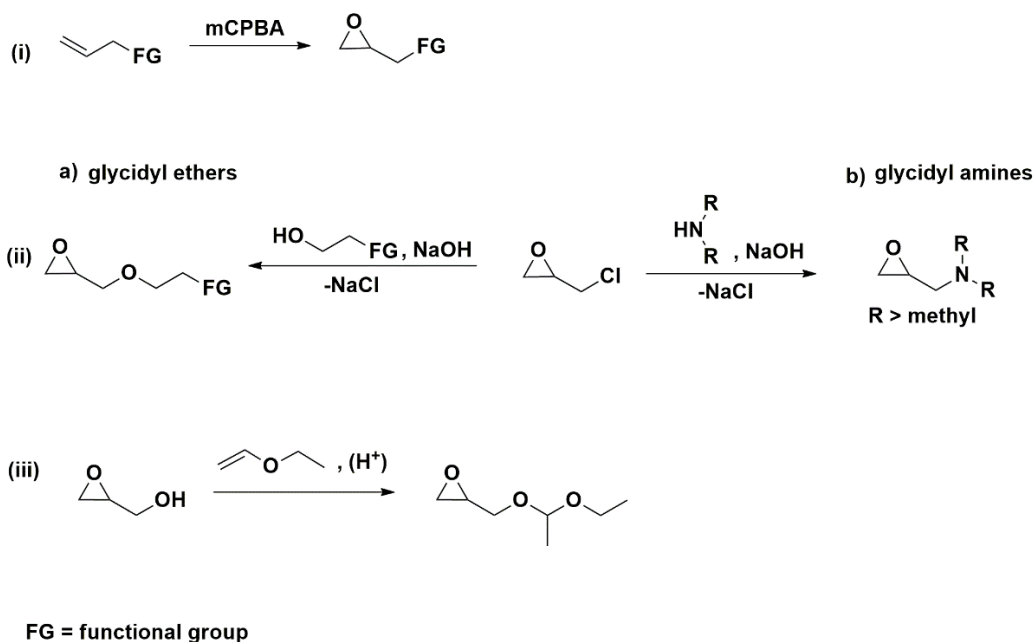
Scheme 10. Synthetic strategies for substituted epoxides, suitable as monomeric building blocks in AROP.

One major challenge is the design of epoxides bearing useful functional/pendent groups, while the functional groups do not interfere with the successive polymerization. Often times, protecting group chemistry is indispensable, e.g. protic groups need to be protected. A selection of suitable epoxide monomers is illustrated in Scheme 11, together with resulting properties or possible applications. Monomers highlighted with a red asterisk were studied in this thesis.
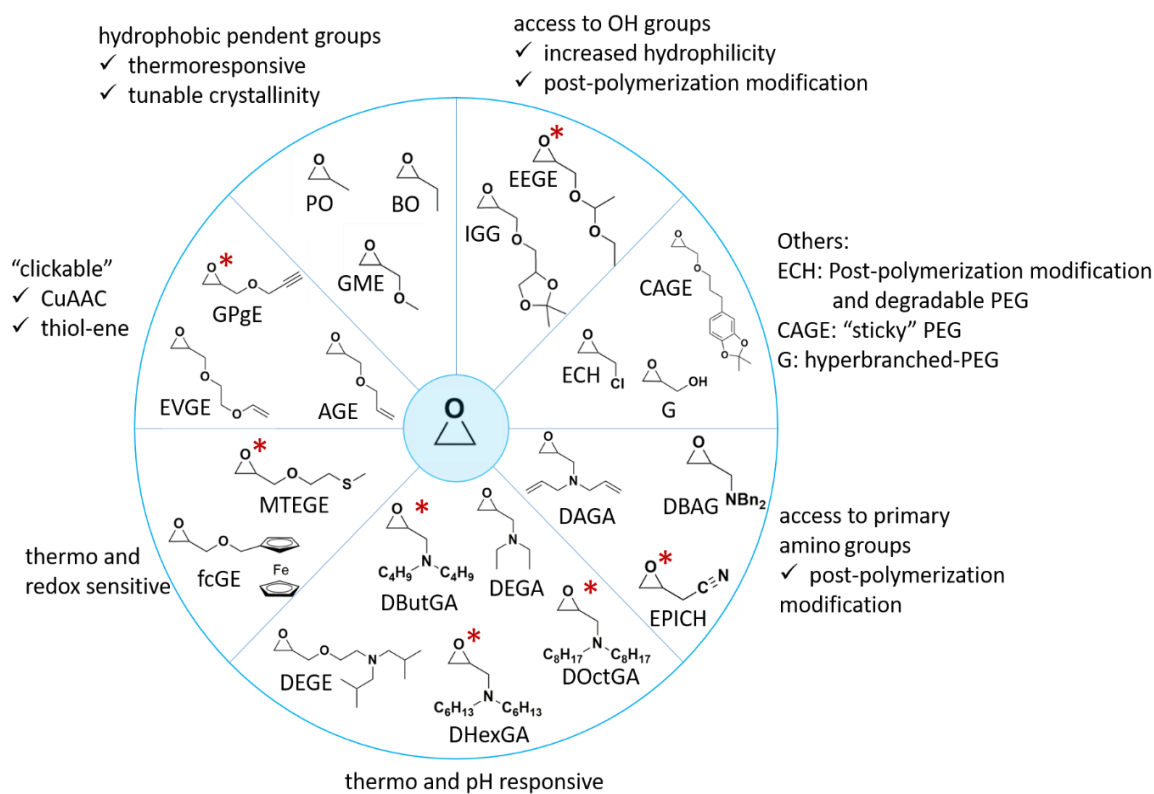
Scheme 11. Overview of substituted epoxides, which have been copolymerized with EO to yield *mf*-PEGs with listed "specialties" of each monomer group.

1.3.2.1 Thermoresponsive PEG

Thermoresponsive polymers are suitable for surface functionalization, which is important for cell tissue engineering[67] or on-demand drug delivery.[68] In particular PEG's high biocompatibility renders it promising as a thermoresponsive material for biomedical applications. The incorporation of hydrophobic moieties into PEG leads to a decrease of both the number of water molecules bound to the PEG backbone and their configurational entropy. The latter results in a large entropy gain associated with the release of water molecules, and therefore in an entropy-driven coil collapse upon heating. Consequently, distributing hydrophobic moieties along the PEG backbone allows for tailoring its solubility in aqueous solution and leads to a lowered LCST. Suitable monomers range from

alkylene oxides, such as propylene oxide (PO)[56] and butylene oxide (BO)[69] to glycidyl ethers bearing hydrophobic substituents. In 2011, Mangold et al. studied various thermoresponsive *mf*-PEGs based on glycidyl ether comonomers and showed that the cloud point temperature of PEG can be adjusted between 9 °C-82 °C.[70] Further, Müller et al. demonstrated that poly(ethylene glycol)-*co*-poly(glycidyl methyl ether) (PEG-*co*-PGME) with GME ratios of 42-100 mol% show cloud point temperatures in the range of 55-98 °C.[45] In this context, it should be mentioned that the distribution of the hydrophobic groups in the copolymer chain is crucial for their properties. For example, block copolymers with a short hydrophobic block can self-assemble to defined micelles. If the same amount of hydrophobic units is randomly distributed, a strong decrease in the cloud point temperature might occur, however, ordered solution structures are absent.

1.3.2.2 pH and thermoresponsive PEG

If an additional pH responsiveness is desired, for instance amino groups can be incorporated into PEG based polymers. Recently, Su and Jiang published a comprehensive review on multi-stimuli responsive amine-containing polyethers.[71] In particular tertiary alkyl amines can be directly introduced via copolymerization of either (i) glycidyl amine derivatives[72, 73] or (ii) glycidyl ethers bearing an additional amino group in the side chain, such as *N,N*-diisopropyl ethanolamine glycidyl ether (DEGE).[74] At slightly basic pH values, the nitrogen is deprotonated and the tertiary amino moiety possesses hydrophobic character. Consequently, a strong impact of the hydrophobic amino groups on the cloud point temperature is observed. In contrast, at pH values below the pK_a, the amine group is protonated and the polymer is fully water-soluble. Also, primary amino groups provide a pH responsiveness.[75] Challenges and possibilities related to the introduction of amino groups into PEG are discussed in more detail in Chapter 3.

1.3.2.3 Redox and thermoresponsive PEG

Copolymerization of EO with ferrocenyl glycidyl ether (fcGE) leads to thermo- and redox responsive PEG. Tonhauser et al. showed that with the incorporation of 2.8-10.6 mol% fcGE, the cloud point of PEG can be adjusted from 7 °C to 82 °C.[76] In addition to the thermoresponsiveness, oxidation to charged ferrocenium-PEGs leads to fully water-soluble structures. In follow-up work, Alkan et al. presented triple-responsive PEGs, based on copolymers of EO and vinyl ferrocenyl glycidyl ether (VfcGE): VfcGE leads to thermoresponsiveness, due to its hydrophobicity, to a redox-responsiveness thanks to the (Fe(II)/Fe(III) pair) and gives access to thiol-ene functionalization, which was used to introduce a pH responsive amine group. [75]

1.3.2.4 Clickable PEGs

PEGs bearing clickable units give access to a variety of functionalization possibilities at ambient conditions and the loading capacity of PEG can be greatly increased. The most prominent example is the commercially available allyl glycidyl ether (AGE), which can be functionalized after polymerization via thiol-ene click or hydrosilylation.[77, 78] A disadvantage of AGE is the rearrangement of the allylic double bonds to vinyl groups and also the occurrence of crosslinking during thiol-ene click reaction. As an alternative, ethoxy vinyl glycidyl ether (EVGE) can be applied.[79, 80] In case of EVGE, no rearrangement takes place, and the vinyl ether moiety is stable under click conditions. EVGE can be further functionalized with an alcohol moiety similar to the synthesis of EEGE to achieve acid sensitive acetal units, which give access to acid-triggered release of a payload.

1.3.2.5 Hydroxyl-functional PEG

The most prominent comonomer to increase the hydrophilicity of PEG and to provide hydroxyl groups along the polyether backbone is ethoxyethyl glycidyl ether (EEGE). EEGE was first described by Fitton et al.[66] and in 1994 Taton et al. showed the successful homopolymerization of EEGE under AROP conditions.[81] After polymerization, the protecting group can be easily cleaved under acidic conditions, releasing hydroxyl groups. EEGE has gained considerable attention, e.g. leading to biocompatible linear poly(glycerol) after deprotection.[82] Li and Chau demonstrated the versatility of PEG-*co*-linPG by post-polymerization modifications starting from the hydroxyl group.[83] In follow up work, Chau and co-workers applied PEG-*co*-linPG as polymeric drug carrier of cisplatin. In contrast to neat PEG, a four times higher loading capacity was achieved.[84]

Alternatively, allyl glycidyl ether or *tert*-butyl glycidyl ether can be applied as comonomers to release one hydroxyl group after removal of the protecting group. Deprotection is achieved via palladium catalyst or trifluoroacetic acid, respectively.[85] If two vicinal hydroxyl groups are desired, 1,2-isopropylidene glyceryl glycidyl ether (IGG) can be copolymerized with ethylene oxide, yielding protected P(EG-*co*-IGG).[86] Intriguingly, after deprotection of the IGG units, molecules bearing aldehyde or ketone functionality can be attached and subsequently released under acidic conditions.

1.3.3 Monomer Distribution in *mf*-PEGs

Understanding the monomer distribution in *mf*-PEGs is important to predict and explain the properties of the resulting copolymers. In particular, statistical copolymerization can lead to different copolymer structures, e.g. random, gradient, tapered or block structures, depending on the relative reactivity of the comonomers and the applied reaction conditions

(e.g. temperature, solvent, counterion, etc.).[87] In particular, copolymers with different monomer composition possess different properties, as it is discussed in detail in Chapter 2, 3.2 and 5. Taking a look at monosubstituted epoxide monomers, alkylene oxides (Figure 4), glycidyl ethers (Figure 6) and glycidyl amines (Figure 7) possess different electronic and steric properties and consequently different reactivity behaviors are expected, when they are copolymerized with EO. Various techniques can be employed to assess the comonomer distribution or the respective reactivity ratios of the comonomers, which is explained in detail elsewhere (see also Chapter 5).[15] In particular, *in-situ* monitoring of the copolymerization by IR,[88–91], Raman,[92, 93] UV[94, 95] and NMR spectroscopy is instrumental to determine reactivity ratios in a single experiment. In recent years, noninvasive, online ^{1}H and ^{13}C NMR spectroscopy have gained much attention to monitor epoxide copolymerizations in sealed NMR tubes.[96–98]

In the following, general trends for each monomer class are described, referring to the copolymerization with EO. Table 1 lists reported reactivity ratios and non-quantitative observations, obtained by ^{13}C triad analysis or bulk thermal properties. Note that the determined reactivity ratios can vary, depending on the analysis or calculation method applied, which has to be considered when absolute values are compared.

Alkylene Oxides
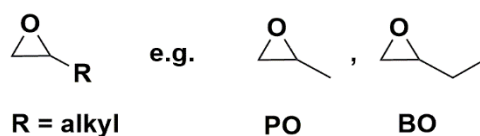
Figure 4. General structure of alkylene oxides, propylene oxide (PO) and butylene oxide (BO).

Alkylene oxides are monosubstituted oxiranes bearing an alkyl chain. Electronically, alkylene oxides do not strongly differ from EO. However, the steric bulk of the alkyl chain

leads to a strong steric effect, and generally EO possesses a higher reactivity in the copolymerization of alkylene oxides under base-initiated oxyanionic ROP conditions. The copolymerization of EO and PO is of industrial relevance and was therefore studied extensively by various groups. In 1991, Heatley and co-workers reinvestigated the reactivity ratios of EO and PO, which is shown in Table 1.[99] The authors reported reactivity ratios of $r_{EO} = 2.8$ and $r_{PO} = 0.25$, calculated by the least squares method. Notably, Carlotti, Deffieux and co-workers observed that applying the monomer-activated AROP, the reactivity of PO is further lowered.[36] It is proposed that the sterically demanding growing chain end ('ate' complex) impedes facile attachment of the larger PO compared to the small EO molecule (Figure 5).
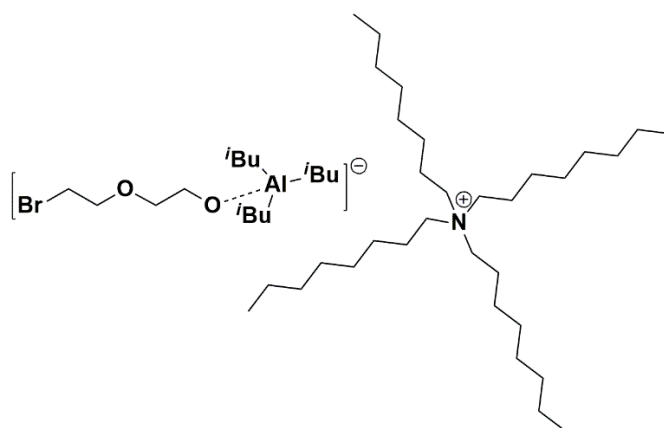
Figure 5. Proposed 'ate' complex in the monomer-activated AROP.[14]Exemplarily shown for a EO-based growing chain with tetra(*n*-octyl)bromide as initiator and triisobutylaluminum as Lewis acid.

Increasing the alkyl chain length from propyl to butyl (PO to BO), the reactivity of the respective monomer decreases in the copolymerization with EO, producing a stronger monomer compositional drift.[59] Allgaier and co-workers provided detailed ^{1}H NMR kinetic studies on the copolymerization of EO and BO, the reactivity ratios are listed in Table 1.[97]
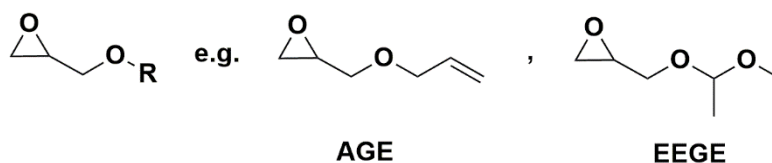
Figure 6. General structure of glycidyl ethers, allyl glycidyl ether (AGE) and ethoxyethyl glycidyl ether (EEGE).

Taking a look at glycidyl ethers, one would expect a lower reactivity when copolymerized with EO, due to their bulkiness in analogy to alkylene oxides. Surprisingly, for the base-initiated oxyanionic copolymerization of EO and glycidyl ethers, both monomers react similar and random structures are obtained, as reported repeatedly.[74, 78, 100] Even glycidyl ethers bearing extremely large substituents, e.g. catechol acetonide glycidyl ether (CAGE)[101] or 1,2-isopropylidene glyceryl glycidyl (IGG)[86] ether show reactivity ratios close to r = 1, when copolymerized with EO. These results can be explained by the presence of an additional oxygen atom in the monomer. In contrast to EO, glycidyl ethers can act as multidentate ligand for the respective counterion. This interaction and the increased Lewis basicity of glycidyl ethers, lowers their transition state energy of the ring opening, the latter being facilitated (Scheme 12).[80, 102]
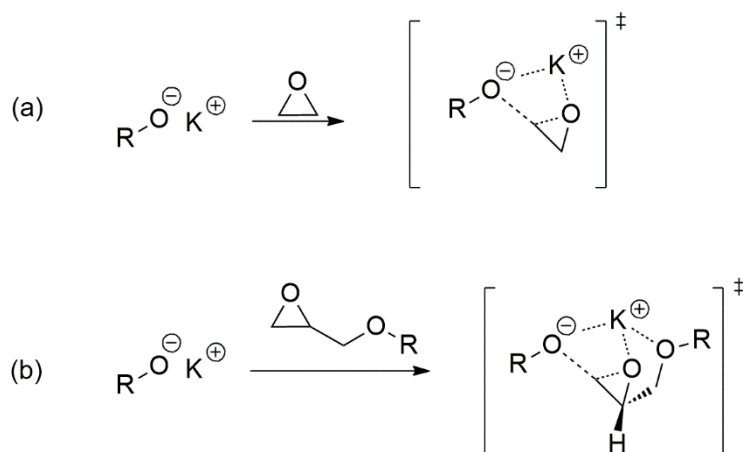
Scheme 12. Transition state structures proposed by Lynd and co-workers for the ring opening of (a) EO and (b) glycidyl ethers. DFT calculations revealed a lower transition state energy for the ring opening of the glycidyl ethers.[80]

The reactivity of glycidyl ethers copolymerized with ethylene oxide under monomer-activated AROP will be investigated in Chapter 4 and 5.

Glycidyl Amines
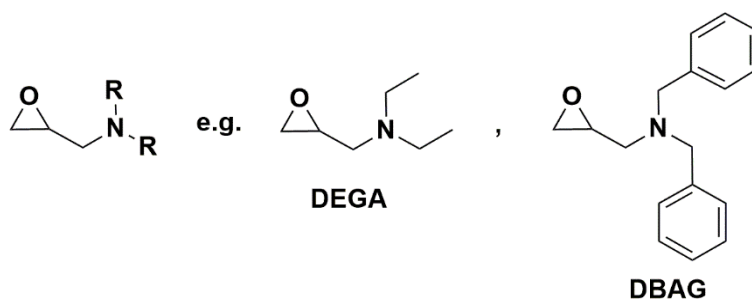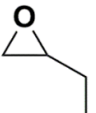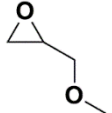
Figure 7. General structure of glycidyl amines, *N,N*-dietyhl glycidyl amine (DEGA) and *N,N*-dibenzyl amino glycidol (DBAG).

While the oxygen atom of glycidyl ethers facilitates the C-O bond cleavage and thereby their ring opening, similar effects are not observed for glycidyl amines. In the 1970ies in a very early work, Ponomarenko et al. studied the copolymerization of *N,N*-diethyl glycidyl amine (DEGA) with PO and observed a higher reactivity of PO.[102] These observations are

surprising, because the polar nitrogen atom was expected to facilitate ring opening, in analogy to glycidyl ethers. The authors proposed that the low reactivity of DEGA must result from a steric factor. Our group investigated the copolymerization of various glycidyl amine derivatives (*N,N*-Dibenzyl amino glycidol (DBAG),[96] *N,N*-diallyl glycidyl amine (DAGA),[103] DEGA)[72] with EO and observed the formation of gradient copolymers with preferred incorporation of EO. It can be assumed, that the substituents attached to the nitrogen atom shield the latter sufficiently, and no activating interaction with the counterion can takes place. In Chapter 3.2 we investigate how large alkyl chains on the nitrogen atom impacts reactivity of glycidyl amines.

Table 1. Comonomers, copolymerized with ethylene oxide, reactivity ratios and applied conditions and analysis. Rows highlighted in blue indicate reactivity ratios and monomer structures, which were investigated in this thesis.

Monomer	Reactivity ratios/ Copolymer structure	Conditions of AROP	Ref.	Analysis/ Calculation method
* PO	r_{EO}=2.8 r_{PO}=0.25	*Initiator:* potassium or sodium salt of 1-methoxy 2-propanolate *Solvent:* bulk conditions $T = 60\ °C$	99	Termination at low conversion ($< 10\%$), Calculated by least squares method
	r_{EO}=2.05 r_{PO}=0.013	*Initiator*: *i*-Bu$_3$Al/NOct$_4$Br *Solvent*: Toluene $T = 25\ °C$	36	Termination at low conversion ($< 10\%$), Calculated by Kelen-Tüdös
BO	r_{EO}=6.46 r_{BO}=0.148	*Initiator*: potassium 2(2-methoxyethoxy)ethanolate *Additive*: 18-crwon-6 *Solvent*: Toluene-d_8 $T = 10\ °C$	97	*In-situ* ^{1}H NMR, Calculated by least squares method
GME	Gradient, EO preferred	*Initiator*: *i*-Bu$_3$Al/NOct$_4$Br *Solvent*: Toluene $T = -15\ °C$ to RT	45	^{13}C triad analysis, bulk thermal properties

EEGE	r_{EO}= 1.20 r_{EEGE}= 0.76	*Initiator*: Potassium triethylene glycolate *Solvent*: THF/DMSO T = 60 °C	[100]	Termination at low conversion (< 10%), calculated by YBR method
	r_{EO}=1.05 r_{EEGE}=0.94	*Initiator*: Potassium 2-benzyloxyethonolate *Solvent*: DMSO-d_6 T = 40 °C	Chapter 5[105]	*In-situ* ^{1}H NMR, calculated in analogy to Lynd and co-workers[104]
	r_{EO}=1 r_{EEGE}=1	*Initiator*: 2-benzyloxyethoxide/K *Additive*: 18-crwon-6 *Solvent*: DMSO-d_6 T = 35 °C	Chapter 5[105]	*In-situ* ^{1}H NMR
	r_{EO}=8.0 r_{EEGE}=0.125	*Initiator*: *i*-Bu$_3$Al/NOct$_4$Br *Solvent*: Toluene-d_8 *Temperature*: -15 to RT	Chapter 5[105]	*In-situ* ^{1}H NMR, calculated in analogy to Lynd and co-workers,[104]
IGG	Random	*Initiator*: Cesium *N,N*-di(p-methoxybenzyl)-2-aminoethanolate *Solvent*: DMSO-d_6 T = 25 °C, 50 °C, 70 °C	[86]	*In-situ* ^{1}H NMR, ^{13}C triad analysis and bulk thermal properties
DEGE	r_{EO}=0.82 r_{DEGE}=1.28	*Initiator*: Potassium benzyl alcoholate *Solvent*: THF T = 45 °C	[74]	^{1}H NMR spectroscopy: monitoring initiation and first propagation step
MTEGE	r_{EO}=0.92 r_{MTEGE}=1.06	*Initiator*: Cesium 2-propoxyethonolate *Solvent*: DMSO-d_6 T = 40 °C	Chapter 2 [106]	*In-situ* ^{1}H NMR, calculated in analogy to Lynd and co-workers,[104] [13]C triad analysis and bulk thermal properties
fcGE	Random	*Initiator*: Cesium benzyl alcoholate *Solvent*: DMSO-d_6 T = 40 °C	[76]	*In-situ* ^{1}H NMR, ^{13}C triad analysis and bulk thermal properties

Structure		Reactivity ratios	Conditions	Ref.	Characterization
CAGE		r_{EO}=1.14 r_{MTEGE}=0.88	*Initiator*: 2-propoxyethoxide/Cs *Solvent*: DMSO-d_6/THF-d_8 mixture $T = 60$ °C	[101]	*In-situ* ^{1}H NMR
AGE		r_{EO}=0.54 r_{AGE}=1.31	*Initiator*: benzylalkoxide/K *Solvent*: THF $T = 45$ °C	[80]	^{1}H NMR spectroscopy: monitoring initiation and first propagation step
		Random	*Initiator*: 2-methoxyethoxide/Cs *Solvent*: DMSO-d_6 $T = 25$ °C, 40 °C	[78]	*In-situ* ^{1}H NMR, ^{13}C triad analysis, bulk thermal properties
EVGE		r_{EO}=0.32 r_{EVGE}=3.50	*Initiator*: benzylalkoxide/K *Solvent*: THF $T = 45$ °C	[80]	^{1}H NMR spectroscopy: monitoring initiation and first propagation step
		Random	*Initiator*: N,N-di(p-methoxy-benzyl)-2-amino ethoxide/Cs *Solvent*: THF $T = 90$ °C	[79]	^{13}C triad analysis, bulk thermal properties
GPgE		r_{EO}=14.8 r_{GPgE}=0.076	*Initiator*: i-Bu$_3$Al/NBu$_4$I *Solvent*: chlorobenze-d_5 $T = 0$-15 °C	Chapter 4	*In-situ* ^{1}H NMR, ^{13}C triad analysis and bulk thermal properties
	R= benzyl	Gradient, EO preferred	*Initiator*: 2-methoxyethoxide/Cs *Solvent*: DMSO-d_6 $T = 25$ °C, 50 °C, 60 °C, 70 °C	[96]	*In-situ* ^{1}H NMR, ^{13}C triad analysis, bulk thermal properties
	R= allyl	Gradient, EO preferred	*Initiator*: 2-benzyloxyethoxide/Cs *Solvent*: DMSO-d_6 $T = 40$ °C	[103]	*In-situ* ^{1}H NMR, ^{13}C triad analysis, bulk thermal properties

				72	*In-situ* ^{1}H NMR, ^{13}C triad analysis, bulk thermal properties
	R= ethyl	Gradient, EO preferred	*Initiator*: 2-benzyloxyethoxide/Cs *Solvent*: DMSO-d_6 $T = 40\ °C$	72	*In-situ* ^{1}H NMR, ^{13}C triad analysis, bulk thermal properties
	R= butyl	r_{EO}=1.84 r_{DButGA}=0.49	*Initiator*: Cesium 2-(methoxy)ethanolate *Solvent*: THF-d_8/DMSO-d_6 (5/1 mixture) $T = 80\ °C$	Chapter 3.2[107]	*In-situ* ^{1}H NMR, calculated by Fineman-Ross ^{13}C triad analysis, bulk thermal properties
	R= hexyl	Gradient, EO preferred	*Initiator*: Cesium 2-(methoxy)ethanolate *Solvent*: THF-d_8/DMSO-d_6 (5/1 mixture) $T = 80\ °C$	Chapter 3.2[107]	*In-situ* ^{1}H NMR, ^{13}C triad analysis, bulk thermal properties
	R= octyl	r_{EO}=1.78 r_{DOctGA}=0.42	*Initiator*: Cesium 2-(methoxy)ethanolate *Solvent*: THF-d_8/DMSO-d_6 (5/1 mixture) $T = 80\ °C$	Chapter 3.2[107]	*In-situ* ^{1}H NMR, calculated by Fineman-Ross analysis, ^{13}C triad analysis, bulk thermal properties
EPICH	Random		*Initiator*: i-Bu$_3$Al/NBu$_4$I *Solvent*: Chlorobenzene $T = $ -15 to room temperature	Chapter 3.4 [35]	^{13}C triad analysis, bulk thermal properties, backbone cleavage studies

*Several groups analyzed the copolymerization of EO and PO under conventional oxyanionic AROP conditions with varying initiator systems. A list of the different reactivity ratios, reported up to 1991 was given by Heatley and co-workers.[99]

1.4 References

[1] Israelachvili, J., The Different Faces of Poly(ethylene glycol), *PNAS.* **1997**, *94*, 8378–8379.

[2] Wada, R.; Fujimoto, K.; Kato, M., Why Is Poly(oxyethylene) Soluble in Water? Evidence from the Thermodynamic Profile of the Conformational Equilibria of 1,2-Dimethoxyethane and Dimethoxymethane Revealed by Raman Spectroscopy, *J. Phys. Chem. B.* **2014**, *118*, 12223–12231.

[3] Kjellander, R.; Florin, E., Water Structure and Changes in Thermal Stability of the System Poly(ethylene oxide)/Water, *J. Chem. Soc., Faraday Trans. 1.* **1981**, *77*, 2053.

[4] Shikata, T.; Okuzono, M.; Sugimoto, N., Temperature-Dependent Hydration/Dehydration Behavior of Poly(ethylene oxide)s in Aqueous Solution, *Macromolecules.* **2013**, 1956–1961.

[5] Fruijtier-Pölloth, C., Safety Assessment on Polyethylene Glycols (PEGs) and their Derivatives as Used in Cosmetic Products, *Toxicology.* **2005**, *214*, 1–38.

[6] Pasut, G.; Veronese, F. M., State of the Art in PEGylation: The Great Versatility Achieved after Forty Years of Research, *J. Control. Release.* **2012**, *161*, 461–472.

[7] Mandelkern, L.; Quinn, F. A.; Flory, P. J., Crystallization Kinetics in High Polymers. I. Bulk Polymers, *J. Appl. Phys.* **1954**, *25*, 830-839.

[8] Dingels, C.; Schömer, M.; Frey, H., Die vielen Gesichter des Poly(ethylenglykol)s, *Chem. unserer Zeit.* **2011**, *45*, 338–349.

[9] Engels, H.-W.; Pirkl, H.-G.; Albers, R.; Albach, R. W.; Krause, J.; Hoffmann, A.; Casselmann, H.; Dormish, J., Polyurethanes: Versatile Materials and Sustainable Problem Solvers for Today's Challenges, *Angew. Chem. Int. Ed.* **2013**, *52*, 9422–9441.

[10] Vallée, A.; Besner, S.; Prud'homme, J. Comparative Study of Poly(ethylene oxide) Electrolytes made with $LiN(CF_3SO_2)_2$, $LiCF_3SO_3$ and $LiClO_4$: Thermal Properties and Conductivity Behaviour, *Electrochim. Acta.* **1992**, *37*, 1579–1583.

[11] Veronese, F. M. Peptide and Protein PEGylation: A Review of Problems and Solutions, *Biomaterials.* **2001**, *22*, 405–417.

[12] Penczek, S.; Cypryk, M.; Duda, A.; Kubisa, P.; Slomkowski, S., Living Ring-Opening Polymerizations of Heterocyclic Monomers, *Prog. Polym. Sci.* **2007**, *32*, 247–282.

[13]   Deffieux, A.; Carlotti, S.; Barrère A., Anionic Ring-Opening Polymerization of Epoxides and Related Nucleophilic Polymerization Processes, *Polym. Sci. A Comprehensive Reference.* Elsevier, Amsterdam. **2012**, 117-140.

[14]   Brocas, A.-L.; Mantzaridis, C.; Tunc, D.; Carlotti, S., Polyether Synthesis: From Activated or Metal-Free Anionic Ring-Opening Polymerization of Epoxides to Functionalization, *Prog. Polym. Sci.* **2013**, 845–873.

[15]   Herzberger, J.; Niederer, K.; Pohlit, H.; Seiwert, J.; Worm, M.; Wurm, F. R.; Frey, H., Polymerization of Ethylene Oxide, Propylene Oxide, and Other Alkylene Oxides: Synthesis, Novel Polymer Architectures, and Bioconjugation, *Chem. Rev.* **2016**, *116*, 2170–2243.

[16]   Wurtz, C. A., Mémoire Sur L'oxyde D'éthylène Et Les Alcools Polyéthyléniques, *Ann. Chim. Phys.* **1863**, *69*, 317–354.

[17]   Staudinger, H.; Lohmann, H., Über hochpolymere Verbindungen. 81. Mitteilung. Über eukolloides Polyäthylenoxyd, *Justus Liebigs Ann. Chem.* **1933**, *505*, 41–51.

[18]   Flory, P. J., Molecular Size Distribution in Ethylene Oxide Polymers, *J. Am. Chem. Soc.* **1940**, *62*, 1561–1565.

[19]   Dudev, T; Lim, C., Ring Strain Energies from ab Initio Calculations, *J. Am. Chem. Soc.* **1998**, *120*, 4450–4458.

[20]   Thompson, M.S.; Vadala, T.P.; Vadala, M.L.; Lin, Y.; Riffle, J.S., Synthesis and Applications of Heterobifunctional Poly(ethylene oxide) Oligomers, *Polymer.* **2008**, *49*, 345–373.

[21]   Billouard, C.; Carlotti, S.; Desbois, P.; Deffieux, A., "Controlled" High-Speed Anionic Polymerization of Propylene Oxide Initiated by Alkali Metal Alkoxide/Trialkylaluminum Systems, *Macromolecules.* **2004**, *37*, 4038–4043.

[22]   Aida, T.; Inoue, S., Living Polymerization of Epoxides with Metalloporphyrin and Synthesis of Block Copolymers with Controlled Chain Lengths, *Macromolecules.* **1981**, *14*, 1162–1166.

[23]   Aida, T.; Mizuta, R.; Yoshida, Y.; Inoue, S., Polymerization of Epoxides Catalysed by Metalloporphine, *Die Makromolekulare Chemie.* **1981**, *182*, 1073–1079.

[24]   Sugimoto, H.; Kawamura, C.; Kuroki, M.; Aida, T.; Inoue, S., Lewis Acid-Assisted Anionic Ring-Opening Polymerization of Epoxide by the Aluminum Complexes of Porphyrin, Phthalocyanine, Tetraazaannulene, and Schiff Base as Initiators, *Macromolecules.* **1994**, *27*, 2013–2018.

[25]   Akatsuka, M.; Aida, T.; Inoue, S., High-Speed "Immortal" Polymerization of Epoxides Initiated with Aluminum Porphyrin. Acceleration of Propagation and Chain-Transfer Reactions by a Lewis Acid, *Macromolecules.* **1994**, *27*, 2820–2825.

[26]   Aida, T.; Inoue, S., Metalloporphyrins as Initiators for Living and Immortal Polymerizations, *Acc. Chem. Res.* **1996**, *29*, 39–48.

[27]   Braune, W.; Okuda, J., An Efficient Method for Controlled Propylene Oxide Polymerization: The Significance of Bimetallic Activation in Aluminum Lewis Acids, *Angew. Chem. Int. Ed.* **2003**, *42*, 64–68.

[28]   Labbé, A.; Carlotti, S.; Billouard, C.; Desbois, P.; Deffieux, A., Controlled High-Speed Anionic Polymerization of Propylene Oxide Initiated by Onium Salts in the Presence of Triisobutylaluminum, *Macromolecules.* **2007**, *40*, 7842–7847.

[29]   Deffieux, A.; Carlotti, S.; Desbois, P., New Perspectives in Living/Controlled Anionic Polymerization, *Macromol. Symp.* **2005**, *229*, 24–31.

[30]   Carlotti, S.; Desbois, P.; Billouard, C.; Deffieux, A., Reactivity Control in Anionic Polymerization of Ethylenic and Heterocyclic Monomers Through Formation of 'Ate' Complexes, *Polym. Int.* **2006**, *55*, 1126–1131.

[31]   Gervais, M.; Labbé, A.; Carlotti, S.; Deffieux, A., Direct Synthesis of α-Azido,ω-hydroxypolyethers by Monomer-Activated Anionic Polymerization, *Macromolecules.* **2009**, *42*, 2395–2400.

[32]   Sakakibara, K.; Nakano, K.; Nozaki, K., Regio-Controlled Ring-Opening Polymerization of Perfluoroalkyl-Substituted Epoxides, *Chem. Commun.* **2006**, 3334–3336.

[33]   Sakakibara, K.; Nakano, K.; Nozaki, K., Regioregular Polymerization of Fluorine-Containing Epoxides, *Macromolecules.* **2007**, *40*, 6136–6142.

[34]   K. Roos; S. Carlotti, Grignard-based Anionic Ring-Opening Polymerization of Propylene Oxide Activated by Triisobutylaluminum, *Eur. Polym. J.* **2015**, *70*, 240–246.

[35]   Herzberger, J.; Frey, H., Epicyanohydrin: Polymerization by Monomer Activation Gives Access to Nitrile-, Amino-, and Carboxyl-Functional Poly(ethylene glycol), *Macromolecules.* **2015**, *48*, 8144–8153.

[36]   Rejsek, V.; Sauvanier, D.; Billouard, C.; Desbois, P.; Deffieux, A.; Carlotti, S., Controlled Anionic Homo- and Copolymerization of Ethylene Oxide and Propylene Oxide by Monomer Activation, *Macromolecules.* **2007**, *40*, 6510–6514.

[37]   Gervais, M.; Brocas, A.-L.; Cendejas, G.; Deffieux, A.; Carlotti, S., Synthesis of Linear High Molar Mass Glycidol-Based Polymers by Monomer-Activated Anionic Polymerization, *Macromolecules.* **2010**, *43*, 1778–1784.

[38]   Brocas, A.-L.; Deffieux, A.; Le Malicot, N.; Carlotti, S., Combination of Phosphazene Base and Triisobutylaluminum for the Rapid Synthesis of Polyhydroxy Telechelic Poly(propylene oxide), *Polym. Chem.* **2012**, *3*, 1189–1195.

[39]   St. Pierre, L. E.; Price, C. C., The Room Temperature Polymerization of Propylene Oxide, *J. Am. Chem. Soc.* **1956**, *78*, 3432–3436.

[40]   Quirk, R. P.; Lizarraga, G. M., Anionic Synthesis of Well-defined, Poly[(styrene)-*block*-(propylene oxide)] Block Copolymers, *Macromol. Chem. Phys.* **2000**, *201*, 1395–1404.

[41]   Grobelny, Z.; Matlengiewicz, M.; Jurek, J.; Michalak, M.; Kwapulińska, D.; Swinarew, A.; Schab-Balcerzak, E., The Influence of Macrocyclic Ligands and Water on Propylene oxide Polymerization Initiated with Anhydrous Potassium Hydroxide in Tetrahydrofuran, *Eur. Polym. J.* **2013**, *49*, 3277–3288.

[42]   Osterwinter, C.; Schubert, C.; Tonhauser, C.; Wilms, D.; Frey, H.; Friedrich, C., Rheological Consequences of Hydrogen Bonding: Linear Viscoelastic Response of Linear Polyglycerol and Its Permethylated Analogues as a General Model for Hydroxyl-Functional Polymers, *Macromolecules.* **2015**, *48*, 119–130.

[43]   Brocas, A.-L.; Gervais, M.; Carlotti, S.; Pispas, S., Amphiphilic Diblock Copolymers based on Ethylene Oxide and Epoxides Bearing Aliphatic Side Chains, *Polym. Chem.* **2012**, *3*, 2148–2155.

[44]   Gervais, M.; Brocas, A.-L.; Deffieux, A.; Ibarboure, E.; Carlotti, S., Rapid and Controlled Synthesis of Hydrophobic Polyethers by Monomer Activation, *Pure Appl. Chem.* **2012**, *84*, 2103–2111.

[45]   Müller, S. S.; Moers, C.; Frey, H., A Challenging Comonomer Pair: Copolymerization of Ethylene Oxide and Glycidyl Methyl Ether to Thermoresponsive Polyethers, *Macromolecules.* **2014**, *47*, 5492–5500.

[46]   Labbé, A.; Brocas, A.-L.; Ibarboure, E.; Ishizone, T.; Hirao, A.; Deffieux, A.; Carlotti, S., Selective Ring-Opening Polymerization of Glycidyl Methacrylate: Toward the Synthesis of Cross-Linked (Co)polyethers with Thermoresponsive Properties, *Macromolecules.* **2011**, *44*, 6356–6364.

[47]   Labbé, A.; Carlotti, S.; Deffieux, A.; Hirao, A., Controlled Polymerization of Glycidyl Methyl Ether Initiated by Onium Salt/Triisobutylaluminum and Investigation of the Polymer LCST, *Macromol. Symp.* **2007**, *249-250*, 392–397.

[48]   Carlotti, S.; Labbé, A.; Rejsek, V.; Doutaz, S.; Gervais, M.; Deffieux, A., Living/Controlled Anionic Polymerization and Copolymerization of Epichlorohydrin with Tetraoctylammonium Bromide−Triisobutylaluminum Initiating Systems, *Macromolecules.* **2008**, *41*, 7058–7062.

[49]   Lundberg, P.; Lee, B. F.; van den Berg, S. A.; Pressly, E. D. ; Lee, A.; Hawker, C. J.; Lynd, N. A., Poly[(ethylene oxide)-*co*-(methylene ethylene oxide)]: A Hydrolytically Degradable Poly(ethylene oxide) Platform, *ACS Macro Lett.* **2012**, *1*, 1240–1243.

[50]   Meyer, J.; Keul, H.; Möller, M., Poly(glycidyl amine) and Copolymers with Glycidol and Glycidyl Amine Repeating Units: Synthesis and Characterization, *Macromolecules.* **2011**, *44*, 4082–4091.

[51]   Hu, H.; Yuan, W.; Lu, L.; Zhao, H.; Jia, Z.; Baker, G. L., Low Glass Transition Temperature Polymer Electrolyte Prepared from Ionic Liquid Grafted Polyethylene Oxide, *J. Polym. Sci. A Polym. Chem.* **2014**, *52*, 2104–2110.

[52]   Brocas, A.-L.; Cendejas, G.; Caillol, S.; Deffieux, A.; Carlotti, S., Controlled Synthesis of Polyepichlorohydrin with Pendant Cyclic Carbonate Functions for Isocyanate-free Polyurethane Networks, *J. Polym. Sci. A Polym. Chem.* **2011**, *49*, 2677–2684.

[53]   Rejsek, V.; Desbois, P.; Deffieux, A.; Carlotti, S., Polymerization of Ethylene Oxide Initiated by Lithium Derivatives via the Monomer-Activated Approach: Application to the Direct Synthesis of PS-*b*-PEO and PI-*b*-PEO Diblock Copolymers, *Polymer.* **2010**, *51*, 5674–5679.

[54]   Babu, H. V.; Muralidharan, K., Polyethers with Phosphate Pendant Groups by Monomer Activated Anionic Ring Opening Polymerization: Syntheses, Characterization and their Lithium-Ion Conductivities, *Polymer.* **2014**, *55*, 83–94.

[55]   Bailey, F. E.; Callard, R. W., Some Properties of Poly(ethylene oxide) in Aqueous Solution, *J. Appl. Polym. Sci.* **1959**, *1*, 56–62.

[56]   Louai, A.; Sarazin, D.; Polle, G.; François, J.; Moreaux, F., Properties of Ethylene Oxide-Propylene Oxide Statistical Copolymers in Aqueous Solution, *Polymer.* **1991**, *32*, 703–712.

[57]   Hamaide, T.; Goux, A.; Llauro, M.-F.; Spitz, R.; Guyot, A., *Stat*-Poly(ethylene oxide-*co*-propylene oxide). Synthesis, NMR Characterization and Crystallinity Studies. Correlation with Monte Carlo simulation, *Angew. Makromol. Chemie.* **1996**, *237*, 55–77.

[58]   Mangold, C.; Wurm, F.; Frey, H., Functional PEG-based Polymers with Reactive Groups via Anionic ROP of Tailor-made Epoxides, *Polym. Chem.* **2012**, *3*, 1714–1721.

[59]   Stolarzewicz, A.; Neugebauer, D., Influence of Substituent on the Polymerization of Oxiranes by Potassium Hydride, *Macromol. Chem. Phys.* **1999**, *200*, 2467–2470.

[60]   Chisholm, M. H.; Navarro-Llobet, D., NMR Assignments of Regioregular Poly(propylene oxide) at the Triad and Tetrad Level, *Macromolecules.* **2002**, *35*, 2389–2392.

[61]   Price, C. C.; Carmelite, D. D., Reactions of Epoxides in Dimethyl Sulfoxide Catalyzed by Potassium *t*-Butoxide, *J. Am. Chem. Soc.* **1966**, *88*, 4039–4044.

[62]   Charles C. Price, Polyethers, *Acc. Chem. Res.* **1974**, *7*, 294–301.

[63]   Allgaier, J.; Willbold, S.; Chang, T., Synthesis of Hydrophobic Poly(alkylene oxide)s and Amphiphilic Poly(alkylene oxide) Block Copolymers, *Macromolecules.* **2007**, *40*, 518–525.

[64]   Hans, M.; Keul, H.; Moeller, M., Chain Transfer Reactions Limit the Molecular Weight of Polyglycidol Prepared via Alkali Metal based Initiating Systems, *Polymer.* **2009**, *50*, 1103–1108.

[65]   Stolarzewicz, A., A New Chain Transfer Reaction in the Anionic Polymerization of 2,3-Epoxypropyl Phenyl Ether and Other Oxiranes, *Die Makromolekulare Chemie.* **1986**, *187*, 745–752.

[66]   Fitton, A. O.; Hill, J.; Jane, D. E.; Millar, R., Synthesis of Simple Oxetanes Carrying Reactive 2-Substituents, *Synthesis.* **1987**, *1987*, 1140–1142.

[67]   Cole, M. A.; Voelcker, N. H.; Thissen, H.; Griesser, H. J., Stimuli-Responsive Interfaces and Systems for the Control of Protein–Surface and Cell–Surface Interactions, *Biomaterials.* **2009**, *30*, 1827–1850.

[68]   Mura, S.; Nicolas, J.; Couvreur, P., Stimuli-Responsive Nanocarriers for Drug Delivery, *Nat Mater.* **2013**, *12*, 991–1003.

[69]   Yang, Y.-W.; Brine, G.; Yu, G-E.; Heatley, F.; Attwood, D.; Booth, C.; Malmsten, M., Association and Phase Behaviour of Statistical and Block Copolymers of Ethylene Oxide and Butylene Oxide in Water, *Polymer.* **1997**, *38*, 1659–1668.

[70]   Mangold, C.; Obermeier, B.; Wurm, F.; Frey, H., From an Epoxide Monomer Toolkit to Functional PEG Copolymers With Adjustable LCST Behavior, *Macromol. Rapid Commun.* **2011**, *32*, 1930–1934.

[71]   Su, Z.; Jiang ,X., Multi-Stimuli Responsive Amine-Containing Polyethers: Novel Building Blocks for Smart Assemblies, *Polymer.* **2016**, *93*, 221–239.

[72]   Reuss, V. S.; Werre, M.; Frey, H., Thermoresponsive Copolymers of Ethylene Oxide and *N,N*-Diethyl Glycidyl Amine: Polyether Polyelectrolytes and PEGylated Gold Nanoparticle Formation, *Macromol. Rapid Commun.* **2012**, *33*, 1556–1561.

[73]   Kurzbach, D.; Wilms, V. S.; Frey, H.; Hinderberger, D., Impact of Amino-Functionalization on the Response of Poly(ethylene glycol) (PEG) to External Stimuli, *ACS Macro Lett.* **2013**, *2*, 128–131.

[74]   Lee, A.; Lundberg, P.; Klinger, D.; Lee, B. F.; Hawker, C. J.; Lynd, N. A., Physiologically Relevant, pH-Responsive PEG-based Block and Statistical Copolymers with *N,N*-diisopropylamine Units, *Polym. Chem.* **2013**, 5735–5742.

[75]   Alkan, A.; Steinmetz, C.; Landfester, K.; Wurm, F. R., Triple-Stimuli-Responsive Ferrocene-Containing PEGs in Water and on the Surface, *ACS Appl. Mater. Interfaces.* **2015**, *7*, 26137–26144.

[76]   Tonhauser, C.; Alkan, A.; Schömer, M.; Dingels, C.; Ritz, S.; Mailänder, V.; Frey, H.; Wurm, F. R., Ferrocenyl Glycidyl Ether: A Versatile Ferrocene Monomer for Copolymerization with Ethylene Oxide to Water-Soluble, Thermoresponsive Copolymers, *Macromolecules.* **2013**, *46*, 647–655.

[77]   Koyama, Y.; Umehara, M.; Mizuno, A.; Itaba, M.; Yasukouchi, T.; Natsume, K.; Suginaka, A.; Watanabe, K., Synthesis of Novel Poly(ethylene glycol) Derivatives Having Pendant Amino Groups and Aggregating Behavior of Its Mixture with Fatty Acid in Water, *Bioconjugate Chem.* **1996**, *7*, 298–301.

[78]   Obermeier, B.; Frey, H., Poly(ethylene glycol-*co*-allyl glycidyl ether)s: A PEG-Based Modular Synthetic Platform for Multiple Bioconjugation, *Bioconjugate Chem.* **2011**, *22*, 436–444.

[79]   Mangold, C.; Dingels, C.; Obermeier, B.; Frey, H.; Wurm, F., PEG-based Multifunctional Polyethers with Highly Reactive Vinyl-Ether Side Chains for Click-Type Functionalization, *Macromolecules.* **2011**, *44*, 6326–6334.

[80]   Lee, B. F.; Wolffs, M.; Delaney, K. T.; Sprafke, J. K.; Leibfarth, F. A.; Hawker, C. J.; Lynd, N. A., Reactivity Ratios and Mechanistic Insight for Anionic Ring-Opening Copolymerization of Epoxides, *Macromolecules.* **2012**, *45*, 3722–3731.

[81]   Taton, D.; Le Borgne, A.; Sepulchre, M.; Spassky, N., Synthesis of Chiral and Racemic Functional Polymers from Glycidol and Thioglycidol, *Macromol. Chem. Phys.* **1994**, *195*, 139–148.

[82]   Thomas, A.; Müller, S. S.; Frey, H., Beyond Poly(ethylene glycol): Linear Polyglycerol as a Multifunctional Polyether for Biomedical and Pharmaceutical Applications, *Biomacromolecules.* **2014**, *15*, 1935–1954.

[83]   Li, Z.; Chau, Y., Synthesis of Linear Polyether Polyol Derivatives As New Materials for Bioconjugation, *Bioconjugate Chem.* **2009**, *20*, 780–789.

[84]   Zhou, P.; Li, Z.; Chau, Y., Synthesis, Characterization, and In Vivo Evaluation of Poly(ethylene oxide-*co*-glycidol)-Platinate Conjugate, *Eur. J. Pharm. Sci.* **2010**, *41*, 464–472.

[85]   Erberich, M.; Keul, H.; Möller, M., Polyglycidols with Two Orthogonal Protective Groups: Preparation, Selective Deprotection, and Functionalization, *Macromolecules.* **2007**, *40*, 3070–3079.

[86]   Mangold, C.; Wurm, F.; Obermeier, B.; Frey, H., "Functional Poly(ethylene glycol)": PEG-Based Random Copolymers with 1,2-Diol Side Chains and Terminal Amino Functionality, *Macromolecules.* **2010**, *43*, 8511–8518.

[87]   Mayo, F. R.; Lewis, F. M., Copolymerization. I. A Basis for Comparing the Behavior of Monomers in Copolymerization; The Copolymerization of Styrene and Methyl Methacrylate, *J. Am. Chem. Soc.* **1944**, *66*, 1594–1601.

[88]   Long, T. E.; Liu, H. Y.; Schell, B. A.; Teegarden, D. M.; Uerz, D. S., Determination of Solution Polymerization Kinetics by Near-Infrared Spectroscopy. Living Anionic Polymerization Processes, *Macromolecules.* **1993**, *26*, 6237–6242.

[89]   Pasquale, A. J.; Long, T. E., Real-Time Monitoring of the Stable Free Radical Polymerization of Styrene via in-Situ Mid-Infrared Spectroscopy, *Macromolecules.* **1999**, *32*, 7954–7957.

[90]   Fontoura, J. M. R.; Santos, A. F.; Silva, F. M.; Lenzi, M. K.; Lima, E. L.; Pinto, J. C., Monitoring and Control of Styrene Solution Polymerization using NIR Spectroscopy, *J. Appl. Polym. Sci.* **2003**, *90*, 1273–1289.

[91]   Shaikh, S.; Puskas, J. E.; Kaszas, G., A New High-throughput Approach to Measure Copolymerization Reactivity Ratios using Real-Time FTIR Monitoring, *J. Polym. Sci. A Polym. Chem.* **2004**, *42*, 4084–4100.

[92]   Wang, C.; Vickers, T. J.; Schlenoff, J. B.; Mann, C. K., *In Situ* Monitoring of Emulsion Polymerization Using Fiber-Optic Raman Spectroscopy, *Appl Spectrosc.* **1992**, *46*, 1729–1731.

[93]   van den Brink, M.; Pepers, M.; van Herk, A. M.; German, A. L., On-Line Monitoring and Composition Control of the Emulsion Copolymerization of VeoVA 9 and Butyl Acrylate by Raman Spectroscopy, *Polym. React. Eng.* **2001**, *9*, 101–133.

[94]   Alb, A. M.; Enohnyaket, P.; Drenski, M. F.; Head, A.; Reed, A. W.; Reed, W. F., Online Monitoring of Copolymerization Involving Comonomers of Similar Spectral Characteristics, *Macromolecules.* **2006**, *39*, 5705–5713.

[95]   Quinebèche, S.; Navarro, C.; Gnanou, Y.; Fontanille, M., In Situ mid-IR and UV–Visible Spectroscopies Applied to the Determination of Kinetic Parameters in the Anionic Copolymerization of Styrene and Isoprene, *Polymer.* **2009**, *50*, 1351–1357.

[96]   Obermeier, B.; Wurm, F.; Frey, H., Amino Functional Poly(ethylene glycol) Copolymers via Protected Amino Glycidol, *Macromolecules.* **2010**, *43*, 2244–2251.

[97]   Zhang, W.; Allgaier, J.; Zorn, R.; Willbold, S., Determination of the Compositional Profile for Tapered Copolymers of Ethylene Oxide and 1,2-Butylene Oxide by In-situ-NMR, *Macromolecules.* **2013**, *46*, 3931–3938.

[98]   Alkan, A.; Natalello, A.; Wagner, M.; Frey, H.; Wurm, F. R., Ferrocene-Containing Multifunctional Polyethers: Monomer Sequence Monitoring via Quantitative ^{13}C NMR Spectroscopy in Bulk, *Macromolecules.* **2014**, *47*, 2242–2249.

[99]   Heatley, F.; Yu, G.; Booth, C.; Blease, T. G., Determination of Reactivity Ratios For the Anionic Copolymerization of Ethylene Oxide and Propylene Oxide in Bulk, *Eur. Polym. J.* **1991**, *27*, 573–579.

[100]   Pang, X.; Jing, R.; Huang, J. Synthesis of Amphiphilic Macrocyclic Graft Copolymer Consisting of a Poly(ethylene oxide) Ring and Multi-poly(ε-caprolactone) Lateral Chains, *Polymer.* **2008**, *49*, 893–900.

[101]   Niederer, K.; Schüll, C.; Leibig, D.; Johann, T.; Frey, H., Catechol Acetonide Glycidyl Ether (CAGE): A Functional Epoxide Monomer for Linear and Hyperbranched Multi-Catechol Functional Polyether Architectures, *Macromolecules.* **2016**, *49*, 1655–1665.

[102]   Ponomarenko, V. A.; Khomutov, A. M.; Il'chenko, S. I.; Ignatenko, A. V., The Effect of Substituents of the Anionic Polymerization of α-Oxides, *Polym. Sci.USSR.* **1971**, *13*, 1735–1740.

[103] Reuss, V. S.; Obermeier, B.; Dingels, C.; Frey, H., *N,N*-Diallylglycidylamine: A Key Monomer for Amino-Functional Poly(ethylene glycol) Architectures, *Macromolecules.* **2012**, *45*, 4581–4589.

[104] Beckingham, B. S.; Sanoja, G. E.; Lynd, N. A., Simple and Accurate Determination of Reactivity Ratios Using a Nonterminal Model of Chain Copolymerization, *Macromolecules.* **2015**, *48*, 6922–6930.

[105] Herzberger, J.; Leibig, D.; Liermann, J. C.; Frey, H., Conventional Oxyanionic versus Monomer-Activated Anionic Copolymerization of Ethylene Oxide with Glycidyl Ethers: Striking Differences in Reactivity Ratios, *ACS Macro Lett.* **2016**, *5*, 1206-1211.

[106] Herzberger, J.; Fischer, K.; Leibig, D.; Bros, M.; Thiermann, R.; Frey, H., Oxidation-Responsive and "Clickable" Poly(ethylene glycol) via Copolymerization of 2-(Methylthio)ethyl Glycidyl Ether, *J. Am. Chem. Soc.* **2016**, *138*, 9212–9223.

[107] Herzberger, J.; Kurzbach, D.; Werre, M.; Fischer, K.; Hinderberger, D.; Frey, H., Stimuli-Responsive Tertiary Amine Functional PEGs Based on *N,N*-Dialkylglycidylamines, *Macromolecules.* **2014**, *47*, 7679–7690.

2 Thioether-functional

Poly(ethylene glycol) Copolymers

2.1 Oxidation-Responsive and "Clickable" Poly(ethylene glycol) via Copolymerization of 2-(Methylthio)ethyl Glycidyl Ether

Jana Herzberger[a,b], Karl Fischer[c], Daniel Leibig[a,b], Matthias Bros[d], Raphael Thiermann[e] Holger Frey[a,b]*

[a]Institute of Organic Chemistry, Johannes Gutenberg-University Mainz, Duesbergweg 10-14, 55128 Mainz, Germany

[b]Graduate School Materials Science in Mainz, Staudinger Weg 9, 55128 Mainz, Germany

[c]Institute of Physical Chemistry, Johannes Gutenberg-University Mainz, Duesbergweg 10-14, 55128 Mainz, Germany

[d]Department of Dermatology, University Medical Center of the Johannes Gutenberg-University, Langenbeckstrasse 1, 55131 Mainz, Germany

[e]Fraunhofer ICT-IMM, Carl-Zeiss-Str.18-20, 55129 Mainz, Germany

*E-Mail: hfrey@uni-mainz.de
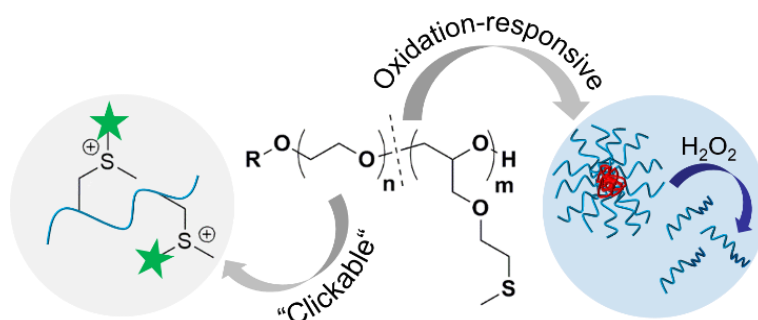
2.1.1 Abstract

Poly(ethylene glycol) (PEG) is a widely used biocompatible polymer. We describe a novel epoxide monomer with methyl-thioether moiety, 2-(methylthio)ethyl glycidyl ether (MTEGE), which enables the synthesis of well-defined thioether-functional poly(ethylene glycol). Random and block mPEG-*b*-PMTEGE copolymers ($M_w/M_n = 1.05\text{-}1.17$) were obtained via anionic ring opening polymerization (AROP) with molecular weights ranging from 5,600 to 12,000 g·mol^{-1}. The statistical copolymerization of MTEGE with ethylene oxide results in a random microstructure ($r_{EO} = 0.92 \pm 0.02$ and $r_{MTEGE} = 1.06 \pm 0.02$), which was confirmed by *in-situ* ^{1}H NMR kinetic studies. The random copolymers are thermoresponsive in aqueous solution, with a wide range of tunable transition temperatures of 88 °C to 28 °C. In contrast, mPEG-*b*-PMTEGE block copolymers formed well-defined micelles ($R_h \approx 9\text{-}15$ nm) in water, studied by detailed light scattering (DLS and SLS). Intriguingly, the thioether moieties of MTEGE can be selectively oxidized into sulfoxide units, leading to full disassembly of the micelles, as confirmed by detection of pure unimers (DLS and SLS). Oxidation-responsive release of encapsulated Nile Red demonstrates the potential of these micelles as redox-responsive nanocarriers. MTT assays showed only minor effects of the thioethers and their oxidized derivatives on the cellular metabolism of WEHI-164 and HEK-293T cell lines (1-1000 μg·mL^{-1}). Further, sulfonium PEG polyelectrolytes can be obtained via alkylation or alkoxylation of MTEGE, providing access to a large variety of functional groups at the charged sulfur atom.

2.1.2 Introduction

In recent years, there has been an emerging interest in aliphatic thioether-functional polymers.[1] At first glance, thioethers may seem rather unreactive and unspectacular, particularly compared to their thiol or disulfide analogues and thus have often been overlooked as a functional group by themselves. However, in contrast to regular ethers, the nature of sulfur provides the possibility to functionalize thioethers via oxidation, alkylation and alkoxylation[1–4] which can lead to interesting material properties. In the 1970ies, Ringsdorf and co-workers demonstrated that oxidized poly[2-(methylsulfinyl)ethyl acrylate] and –methacrylate can serve as polymeric resorption enhancing alternatives to low molecular weight DMSO.[5, 6] 30 years later, Hubbell, Tirelli and co-workers recognized the potential of polythioethers as redox-responsive nanocarriers for inflammation targeting.[7] In the oxidative milieu of inflamed tissue, hydrophobic thioethers are oxidized to more polar sulfoxides or sulfones, leading to a change in the hydrophobic/hydrophilic balance with disassembly of the nanostructure. This remarkable work inspired the design of various oxidation-responsive nanocarriers based on thioether-functional polymers.[8–19] Additionally, the nucleophilicity of sulfides allows for sulfonium salt formation with alkyl halides, similar to the quaternization of amines. Deming and co-workers demonstrated the suitability of thioether moieties as precursors for a variety of stable, water-soluble and highly functional polypeptide sulfonium derivatives, by click-type "quaternization" of poly(L-methionine).[3, 4, 20] Furthermore, their analogy to nitrogen-based polyelectrolytes inspired Long and co-workers to study sulfonium-functional PMMA derivatives as nonviral nucleic acid delivery agents.[21] Similar structures have also been investigated for siRNA complexation, confirming their high potential as drug delivery vehicle in biological environment.[22]

For biomedical applications, hydrophobic thioethers are often combined with poly(ethylene glycol) (PEG) as a hydrophilic block to provide aqueous solubility. PEG is a highly water-soluble, biocompatible polyether with low immunogenicity, antigenicity and toxicity.[23] However, for most of the strategies mentioned above, the nature of the thioether-block differs strongly from PEG or is based on step-growth polymerization,[17, 19] which are accompanied by broad molecular weight distributions.

Here, we present the synthesis of a novel epoxide building block, 2-(methylthio)ethyl glycidyl ether (MTEGE), which is broadly applicable to generate thioether functional PEGs via anionic ring opening polymerization (AROP) (Scheme 1).
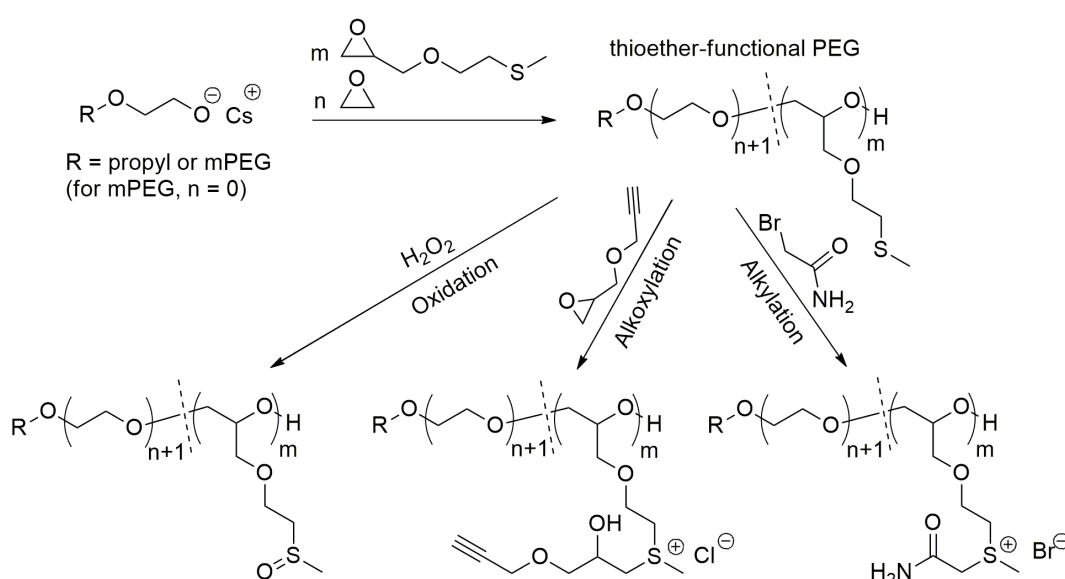
Scheme 1. Anionic ring opening (co)polymerization (AROP) of MTEGE with EO or with mPEG as macroinitiator, yielding random and block copolymers. Functionalization can be performed via oxidation, alkoxylation or alkylation.

We believe that MTEGE represents a useful alternative to episulfide/propylene sulfide, acrylate-based monomers or thiol-ene click chemistry, because it leads to well-defined polymers with a mere polyether backbone and *S*-methyl moieties as side chains. Most

important, AROP of epoxides is a well-established industrial process. To date, similar structures have only been reported by post-polymerization modification of polyepichlorohydrin with sodium alkanethiolates.[24] Additionally, we demonstrate the suitability of thioether-PEGs for (1) oxidation-responsive structures and (2) functional sulfonium-PEG polyelectrolytes (Scheme 1).

2.1.3 Experimental Part

Monomer synthesis. 2-(Methylthio)ethyl glycidyl ether was synthesized in analogy to *N,N*-diisopropylglycidylether.[25] 2-(Methylthio)ethanol (1 eq, 10 ml) was introduced to a round bottom flask and crushed sodium hydroxide pellets (1 eq, 4.6 g) were added. The mixture was cooled to 0 °C and epichlorohydrin (2 eq, 18 mL) was added dropwise, followed by vigorously stirring for 48 h. Afterwards, the mixture was placed in a centrifuge (15 min, 4500 rpm) and the organic phase was collected and dried over MgSO₄. The product was purified via fractionated vacuum distillation ($p = 0.006$ mbar, $T_b = 60$ °C). Repeated distillation resulted in yields of 50-60 %. ρ (23 °C) = 1.10 g·mL^{-1}. ^{1}H NMR (CDCL₃, 400 MHz, δ): 3.78 (dd, 1H, ring-C$H_{2,a}$O-, $J = 11.6$, 2.9 Hz); 3.77-3.58 ppm (m, 2H, -OCH_2CH₂); 3.40 (dd, 1H, ring-C$H_{2,a}$O-, $J = 11.6$, 5.9 Hz); 3.15 (ddt, 1H, CH_{ring}, $J = 5.7$, 4.1, 2.8 Hz), 2.79 (dd, 1H, C$H_{2b,ring}$, $J = 5.0$, 4.2 Hz); 2.69 (t, 2H, -CH_2S, $J = 6.7$ Hz); 2.61 (dd, 1H,C$H_{2a,ring}$, $J = 5.0$, 2.7 Hz); 2.14 (s, 3H, -CH_3,). ^{13}C NMR (CDCL₃, 100 MHz, δ): 71.73 (ring-CH₂O-), 70.79 (-OCH₂CH₂), 50.93 (CH$_{ring}$), 44.32 (CH$_{2,ring}$), 33.67 (-CH₂S), 16,19 (-CH₃).

FDMS *m/z*: [M$^+$] calc. for C₆H₁₂O₂S, 148.06; found, 148.2.

All information on additional reagents, methods and reaction conditions are detailed in the Supporting Information.

2.1.4 Results and Discussion

A. Monomer synthesis, (Co)polymerization of MTEGE with EO, Characterization and Thermal Properties.

Monomer synthesis. MTEGE was synthesized in a one-step procedure starting from epichlorohydrin and 2-(methylthio)ethanol (both commercially available) (Scheme 2), in analogy to the literature known *N,N*-diisopropyl ethanolamine glycidyl ether (DEGE).[25]
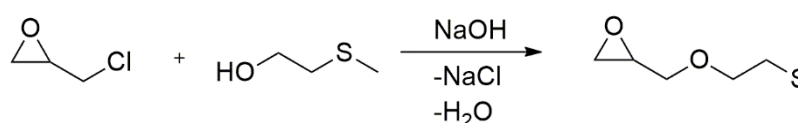
Scheme 2. Synthesis of the thioether functional epoxide monomer 2-(methylthio)ethyl glycidyl ether (MTEGE).

Purification was performed via repeated fractionated distillation under reduced pressure, lowering the overall yield to 50-60 %. However, unreacted reagents can be recollected. Note that column chromatography (silica and aluminum oxide) should be avoided due to occurring side reactions, most likely due to catalyzed ring-opening of the epoxide by the thioether unit. Detailed characterization by ^{1}H, ^{13}C and 2D NMR is given in the Supporting Information (Figure S1-S4).

PEG-ran-PMTEGE, mPEG-b-PMTEGE and PMTEGE (co)polymers. The thioether-functional epoxide MTEGE, can be polymerized via anionic ring opening polymerization (AROP) in a one-step procedure. Here, we synthesized multi-thioether functional PEG with random or block-type structures by either i) statistical copolymerization of MTEGE with EO (PEG-*ran*-PMTEGE) or ii) initiation of MTEGE with mPEG (mPEG-*b*-PMTEGE) (Scheme 1). Further, PMTEGE homopolymer was successfully prepared. All (co)polymers show monomodal distributions and narrow PDIs (1.05-1.17) with molecular weights in the

range of 5,000-12,000 $\text{g} \cdot \text{mol}^{-1}$(Figure 1, Table 1). The block copolymers show a clear shift to smaller elution volumes (higher molecular weights) with increasing MTEGE units, compared to the macroinitiator mPEG-5000 (Figure 1, right).

The molecular weights of the block copolymers were found to be slightly lower than anticipated (Table 1). Chain transfer to the monomer via proton abstraction can occur, which is a common side reaction for glycidyl ethers.[26] This leads to the formation of new initiating species, which generates homopolymer impurities and lowers the targeted molecular weight. However, side products were easily removed via precipitation of the block copolymers into diethyl ether (Figure S5). Note, that no double bonds were detected for the random copolymers and proton abstraction can be excluded. A slight discrepancy of the targeted comonomer content might be due to small differences in measuring liquid EO.
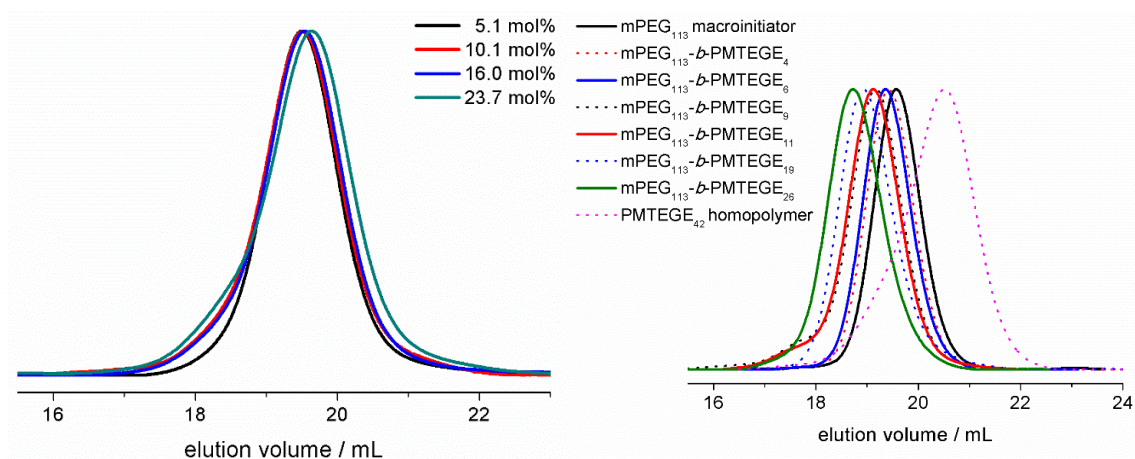

Figure 1. SEC elution traces (DMF, PEG standard, RI detection) of random PEG-*ran*-PMTEGE copolymers (left) and mPEG$_{113}$ macroinitiator, mPEG-*b*-PMTEGE block copolymers and PMTEGE homopolymer (right).

Number averaged molecular weights were determined from ^{1}H NMR spectra, referring all signals to the resonance of the initiator (Figure 2, S6 and S7). The slight discrepancy between M_n obtained by NMR and SEC is caused by the hydrophobic thioether side chains,

68

leading to a different hydrodynamic volume of PEG-PMTEGE (co)polymers compared to PEG (SEC in DMF, PEG standards). This trend is most distinct for the random PEG-*ran*-PMTEGE copolymers and is frequently observed for multi-functional PEGs.[27–29] EO/MTEGE ratios were also calculated from ^{1}H NMR spectra comparing the signal of the methyl group (-SCH_3) at 2.15 ppm to the polyether backbone signal at 3.4-3.8 ppm (Figure 2 and S7). Overall, ratios were varied from 3-24 mol%, yielding water-soluble polymers while preserving PEG's outstanding properties, and increasing its functionality (Table 1). The PMTEGE homopolymer is water-insoluble, but soluble in THF, benzene and DMSO. Detailed ^{1}H and ^{13}C NMR characterization of the block and homopolymers are shown in the Supporting Information (Figure S6-S8).

Table 1. Characterization data for the series of random PEG-*ran*-PMTEGE, mPEG-*b*-PMTEGE block copolymers, mPEG and PMTEGE homopolymer.

Sample[b]	MTEGE[a]	MTEGE[b]	M_n[b]/ g·mol^{-1}	M_n[c]/ g·mol^{-1}	PDI[c]	T_g/ °C	T_m/ °C	ΔH/ J·g^{-1}	T_c/ °C
mPEG$_{113}$	0	0	5000	4700	1.05	-53	64	186	---
PEG$_{150}$-*ran*-PMTEGE$_8$	5	5.1	7800	4900	1.06	-61	35	82	88
PEG$_{178}$-*ran*-PMTEGE$_{20}$	10	10.1	10,800	4900	1.15	-64	22	40	60
PEG$_{137}$-*ran*-PMTEGE$_{26}$	15	16.0	10,000	4700	1.15	-64	7	30	46
PEG$_{135}$-*ran*-PMTEGE$_{42}$	25	23.7	12,200	4560	1.17	-63	---	---	28
mPEG$_{113}$-*b*-MTEGE$_4$	4.2	3.4	5590	4980	1.08	-57	57	150	---
mPEG$_{113}$-*b*-MTEGE$_6$	5.0	5.0	5890	5130	1.08	-58	56	142	---
mPEG$_{113}$-*b*-PMTEGE$_9$	8.1	7.4	6330	5890	1.15	-58	55	125	---
mPEG$_{113}$-*b*-PMTEGE$_{11}$	9.6	8.9	6630	5820	1.09	-59	55	123	---
mPEG$_{113}$-*b*-PMTEGE$_{19}$	15.0	14.4	7810	5940	1.10	-61	53	109	---
mPEG$_{113}$-*b*-PMTEGE$_{26}$	20	18.7	8850	6840	1.09	-62	51	91	95
PMTEGE$_{42}$	100	100	6330	3300	1.14	-62	---	---	insoluble

[a] Targeted comonomer content
[b] Comonomer content determined via ^{1}H NMR spectroscopy
[c] Determined via SEC measurements (DMF, RI signal, PEG standard)
T_g: Glass transition temperature
T_m: Melting temperature
ΔH: Melting enthalpy
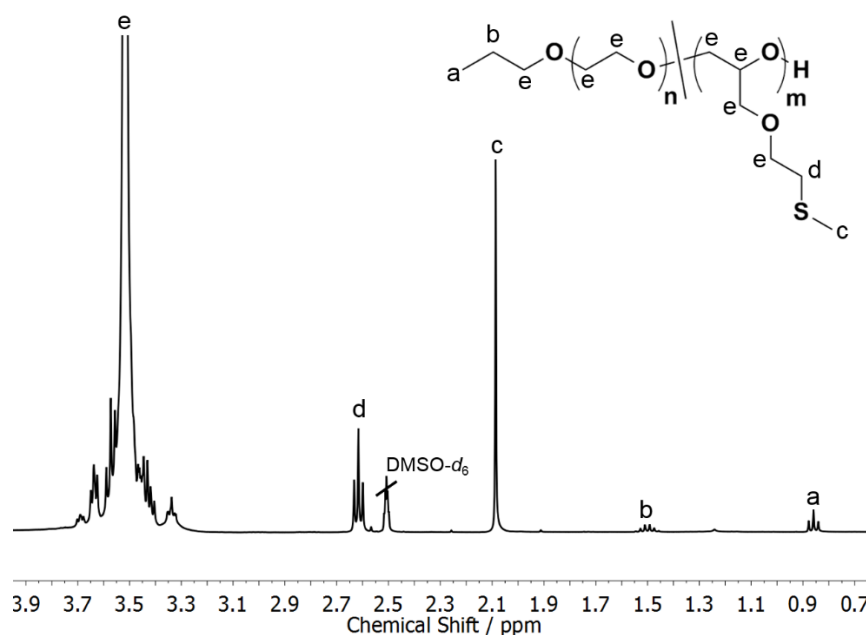T_c: Cloud point temperature determined via turbidity for c = 5 mg· mL^{ge}

Figure 2. ^{1}H NMR spectrum (400 MHz, DMSO-d_6) of PEG-*ran*-PTMEGE with 5.1 mol% MTEGE.

To gain further information about the resulting microstructure of PEG-*ran*-PMTEGE, we monitored the copolymerization of EO and MTEGE in a vacuum sealed NMR tube. Both monomers are consumed constantly throughout the polymerization, with full conversion after 10 h (Figure 3 (bottom) in DMSO-d_6 at 40 °C). Measurements revealed random copolymerization of MTEGE and EO with reactivity ratios of $r_{EO} = 0.92 \pm 0.02$ and $r_{MTEGE} = 1.06 \pm 0.02$ and a product of r_{EO} x $r_{MTEGE} = 0.98$. The values were determined from Figure 3 (top) by applying a nonterminal model of chain copolymerization recently introduced by Lynd and co-workers.[30] We propose that the slightly higher reactivity of MTEGE results from both an increased coordination to the cesium counter ion and an increased Lewis basicity of the epoxide ring compared to EO, as reported for other glycidyl ethers.[31] See the Supporting Information for characterization details (Figures S9 and S10).
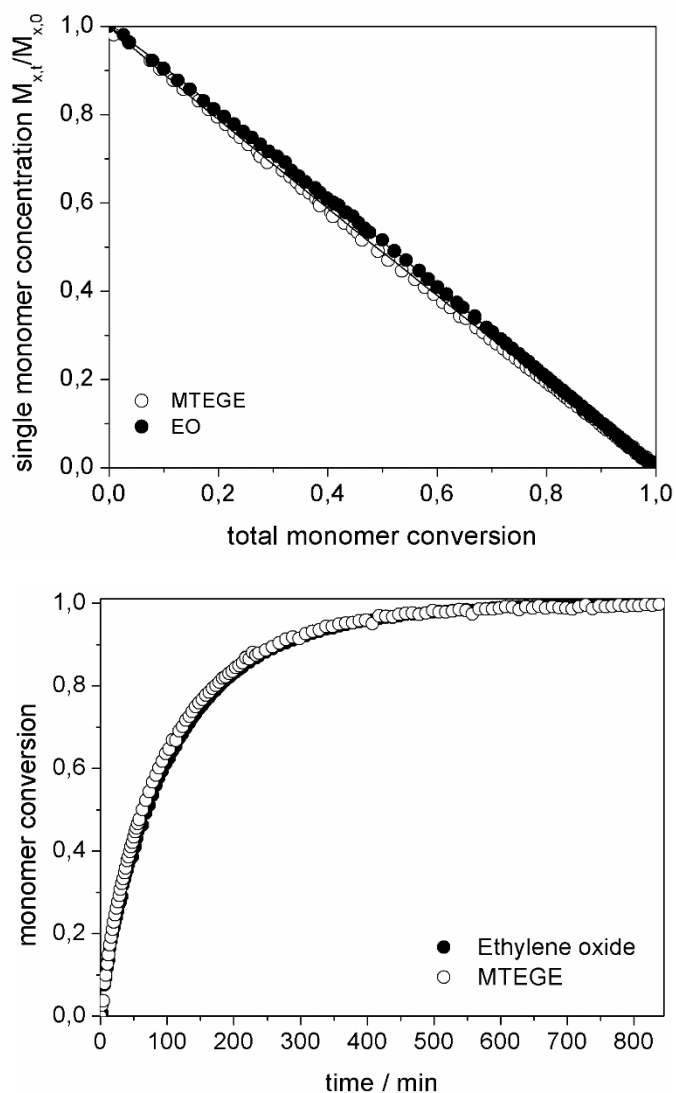
Figure 3. Top: Single monomer concentration versus total monomer conversion. Lines represent fits to the experimental data using the nonterminal model of chain copolymerization, proposed by Lynd and co-workers.[30] Bottom: Monomer conversion versus time. Statistical copolymerization was performed in DMSO-d_6 at 40 °C with the initial mole fractions n_{EO}=0.585 and n_{MTEGE}=0.415.

Inverse gated ^{13}C triad analysis further substantiates random microstructure of the copolymers. For simplicity, EO repeating units were abbreviated with *E* and MTEGE units with *S*, whereas *a* and *b* denote the methylene and methine carbon atom, respectively. Figure 4 illustrates a zoom-in of the characteristic region of the S_b signal of PMTEGE homopolymer, mPEG-*b*-PMTEGE block copolymer and various random copolymers. Focusing on the random copolymers, additional triads occur with increasing MTEGE

content (E-S_b-S, S-S_b-E and S-S_b-S) while the intensity of the E-S_b-E triad leads to the most prominent signal for all compositions. As expected, the E-S_b-E triad is absent for the block and homopolymer.
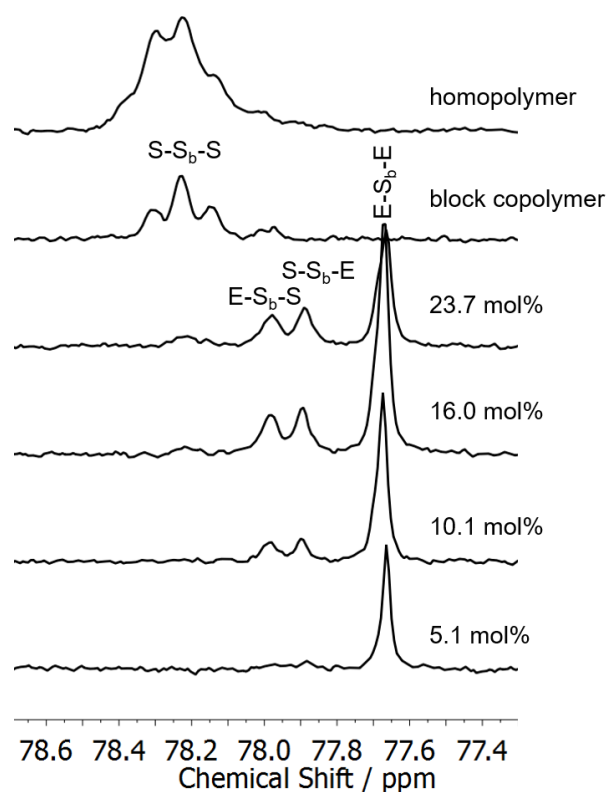

Figure 4. Zoom-in of the IG ^{13}C NMR spectra (DMSO-d_6, 100 MHz) of PMTEGE homopolymer, mPEG-*b*-PMTEGE block copolymer and various PEG-*ran*-PMTEGE copolymers, displaying the characteristic region of the S_b signal.

The region of EO centered triads is shown in Figure S11. Note that we refrained from assigning detailed triads in this region, due to a strong overlap of the EO- and S_a-centered triads with the signals of the MTEGE side chain (see also Figure S8). Nevertheless, the random copolymers possess more complex spectra than the block- and homopolymer, supporting the random microstructure.

The difference between random and block structures is also reflected by their thermal properties in bulk (Table 1). PEG itself is a highly crystalline polymer with a melting

temperature approaching 65 °C, when molecular weights exceed 2000 g·mol^{-1}.[32, 33] Randomly distributed MTEGE units along the PEG backbone strongly inhibit its crystallization, leading to a significant decrease of the melting temperature and enthalpy with increasing MTEGE content. For example, only 5.1 mol% MTEGE is required to cause a drop in the melting temperature by 30 °C. Completely amorphous structures are detected when 23 mol% MTEGE is present. In contrast, for mPEG$_{113}$-b-PMTEGE$_n$, only a marginal influence of the MTEGE amount on the melting temperature and enthalpy of the PEG block was detected (Table 1). In this case, the block structure still allows PEG chains to align and crystallize. As expected, the atactic PMTEGE homopolymer is fully amorphous with a T_g of -62 °C. For the random copolymers, glass transition temperatures are in the range of -61 °C to -64 °C, similar to other multi-functional PEGs bearing nonpolar side groups.[34] Interestingly, we only detected one T_g for all block copolymers. This suggests rather poor phase separation due to the structural similarity of both blocks and the relatively short PMTEGE block.

B. Properties in aqueous solution. For future biomedical applications, it is important to understand the behavior of thioether-functional PEG copolymers in aqueous solution and to determine potential self-assembly and aggregation. Random PEG-ran-PMTEGE copolymers with MTEGE ratios of 5-24 mol% are water soluble at room temperature, but turbid solutions are observed when samples are heated to a specific temperature. This so called "thermoresponsiveness" is a common feature of multi-functional PEGs, that bear hydrophobic units distributed along the polymer backbone, rendering them attractive for drug delivery applications.[28, 35] PEG itself is fully water-soluble up to ~ 100 °C, due to the specific bond distance of its oxygen atoms, which allows for beneficial hydrogen bonding with water.[36] The incorporation of hydrophobic moieties leads to a decrease of both the number of water molecules bound to PEG and their configurational entropy; the latter

results in a large entropy gain associated with their release, and therefore in an entropy-driven coil collapse upon heating. Polymers that exhibit phase transitions slightly above body temperature are interesting for medical applications such as therapeutic hypothermia.

With the incorporation of hydrophobic MTEGE units, one can tailor the aqueous solubility of PEG-*ran*-PMTEGE between 88 °C and 28 °C (5.1-23.7 mol%), as determined by turbidity measurements (Table 1, Figure 5). From Figure 5, one can conclude that MTEGE ratios between 16 and 20 mol% would be beneficial to cover the range near human body temperature. Repeated heating/cooling cycles show sharp phase transitions, complete reversibility and little to no hysteresis (Figure S12). In contrast, the described mPEG-*b*-PMTEGE block copolymers with molar fractions of MTEGE below 14 mol% show no cloud point temperatures in the range of 0-100 °C at concentrations of 5 mg·mL^{-1}. Only mPEG$_{113}$-*b*-PMTEGE$_{26}$, the block copolymer with the highest amount of MTEGE, reveals a cloud point of 95 °C. In analogy to PEG-*co*-polysulfides and PEG-*b*-poly(butylene oxide) diblocks, block copolymers of mPEG$_{113}$-*b*-PMTEGE$_n$ with n ≥ 9 show micellar gelation in water at high concentrations (20 wt%) at 25 °C.[16, 37] In contrast, no gelation is observed for random copolymers, and the solutions turn opaque when heated.

These results suggest that mPEG-*b*-PMTEGE block copolymers exhibit completely different aggregation behaviors in water in comparison to their random counterparts.
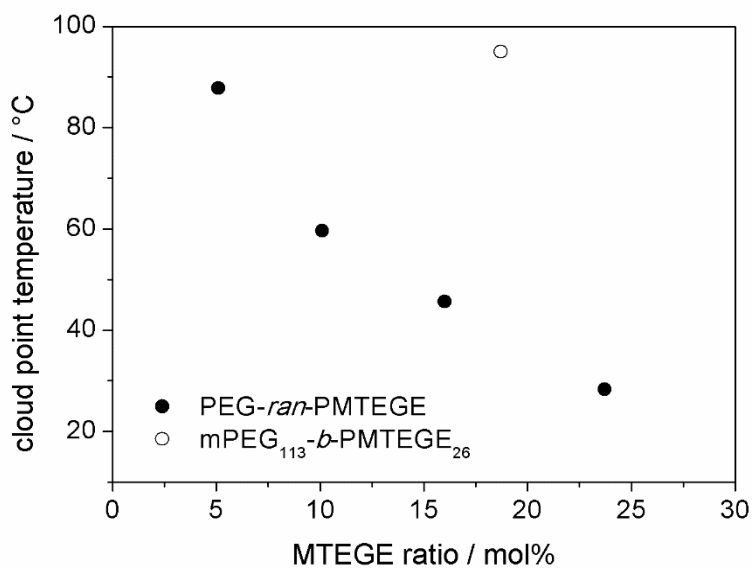
Figure 5. Cloud point temperatures plotted versus MTEGE content of PEG-*ran*-PMTEGE copolymers (solid spheres) and mPEG$_{113}$-*b*-PMTEGE$_{26}$ (hollow spheres). Error margins have been calculated from the standard deviation of the averaged values and are less than 1 °C.

To further elucidate their unique solubility behavior in water, we conducted dynamic light scattering (DLS) measurements. For the PEG-*ran*-PMTEGE copolymers, polydisperse samples at room temperature were observed, with the occurrence of unimers and larger aggregates. This can be attributed to a temperature-dependent association of PEG-*ran*-PMTEGE copolymers, already at temperatures below their respective cloud point (data not shown). Similar results were reported for other thermoresponsive polymers.[38–43]

In contrast to the random copolymers, block copolymers showed no strong thermoresponsiveness, suggesting well-defined self-assembly in water. We first conducted DLS in methanol, to ensure monomodal samples and to evaluate their respective hydrodynamic radius. For all samples, pure unimers were detected, showing an increase in the hydrodynamic radius with increasing MTEGE block length (Table S1). Intriguingly, when the block length of the hydrophobic block exceeds 6 units, aggregation of the block copolymers is forced by switching to an aqueous solution. For mPEG-*b*-PMTEGE$_n$ with

the longest hydrophobic block (n = 26 MTEGE units), a micelle size of roughly 30 nm can be observed with a low polydispersity (the largest particles being nearly monodisperse ($\mu_2 < 0.05$)). From Figures S13-16, one can observe that all experimental diffusion coefficients show no scattering angle dependency and low polydispersities as typical for micellar like assemblies. Fluorescence spectroscopy (with pyrene as a probe) was conducted to determine the CMC of all block copolymers, which still show self-assembly at a concentration of 1 g·L^{-1}, and are listed in Table S1. The CMCs range from 100 mg·L^{-1} to 1.5 mg·L^{-1} for mPEG$_{113}$-*b*-PMTEGE$_n$ with n = 9 and 26, respectively. These are in the range of values reported for PEG-*b*-poly(butylene oxide) diblock copolymers with similar hydrophobic block length[44, 45] and other PEG-based diblocks.[46, 47]

To gain further insight into the topology and aggregation number of the samples, we performed static light scattering (SLS) (Figure S17-18). Measurements in methanol and water prove that all samples show no angular dependency of the scattering intensity, indicating a radius of gyration (R_g) below 10 nm (Table S1). Hence, for the block copolymers with 19 and 26 MTEGE units, the rho-ratios ρ ($\rho \equiv$ "R_g/R_h" $= \langle R_g^2 \rangle_z^{1/2}/\langle 1/R_h \rangle_z^{-1}$) are below 1, which is in accordance with the micellar hypothesis ($\rho_{hard\ spheres} = 0.775$)[48]. From these results, we calculated the aggregation number Z (Kc/R in methanol versus Kc/R in water, see Supporting Information for details) (Table S1). One can observe a strong increase in Z with increasing MTEGE block length, also reflected by the increase of the hydrodynamic radius. Correspondingly, mPEG-*b*-PMTEGE block copolymers follow the scaling laws developed by Förster et al. for block copolymer micelles, which substantiates the micellar hypothesis.[49] This is clearly reflected by Figure 6, which summarizes the experimental results in agreement with the scaling behavior introduced by Förster et al.
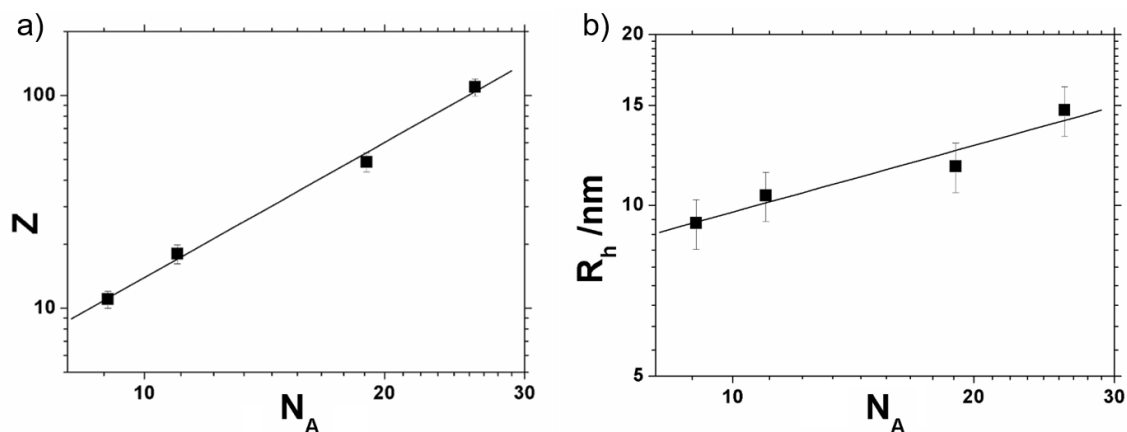
Figure 6. Scaling behavior of the aggregation number Z (a) and the hydrodynamic radius R_h (b) for mPEG$_{113}$-*b*-PMTEGE block copolymers with the block length N_A, as deduced from the polymer/low molar mass micellar aggregation theory by Förster et al.; exponents from theory 2 resp. 0.4, exp. found 2.1 resp. 0.39.

The aggregation number Z depends on the block length N_A of the hydrophobic block with an exponent of 2 (exp. 2.1), whereas the hydrodynamic radius (R_h) scales with the exponent of 0.4 on N_A (exp. 0.39), both determined from double logarithmic representation of the experimental results described in detail in the Supporting Information.

CryoTEM measurements further show the formation of micelles and support the light scattering results (Figure S19). However, a detailed analysis was not possible owing to the poor contrast of PEG, leading to rather diffuse images. SANS or SAXS measurements would be necessary to gain further information of the copolymers' morphology and inner structure.

C. Oxidation-sensitivity. Thioether can be selectively oxidized to sulfoxide or sulfone moieties, which leads to a strong increase in their dipole moment.[2, 50] Consequently, we expect a significant change in the polarity of PEG-PMTEGE copolymers upon oxidation of their MTEGE units, which should be reflected in their solubility properties in aqueous solution. To gain insight into the redox-sensitivity of MTEGE, we first monitored the

78

oxidation of mPEG-*b*-PMTEGE with H_2O_2 in a NMR tube. Experiments were performed in D_2O (296 K) with 1 wt% H_2O_2 solution and in deuterated buffer solution (NaD_2PO_4/Na_2DPO4; pD = 7.46[51]; 310 K), to predict the behavior at body temperature. Figure 7 shows a zoom-in of the important section of ^1H NMR spectra for oxidation in buffered solution. The oxidized polymer species is observed after a few minutes by the formation of sulfoxide groups: First, the singlet of the methyl group (-SC*H₃*) at 2.25 ppm shows a splitting, indicating the occurrence of adjacent oxidized moieties, followed by complete disappearance. Meanwhile, a new singlet appears at 2.78 ppm, representing the methyl group next to the sulfoxide group (-SOC*H₃*). Further, the methylene group (-C*H₂*SCH₃) at 2.74 ppm shifts downfield to 3.07 ppm-3.27 ppm and a new resonance at 3.95 ppm appears, corresponding to the neighboring methylene group (-C*H₂*CH₂SOCH₃). The signal integrals of the decreasing methyl group (-SC*H₃*) and the increasing methylene group (-C*H₂*SOCH₃) versus time, are illustrated in Figure 7 (right). Oxidation at 310 K (buffer solution) shows full conversion after 2.5 hours. In contrast, room temperature (296 K) slows down the reaction to 6 hours (Figure S22). Figure S23 depicts the respective SEC traces, which show a slight shift to lower molecular weights after oxidation. We attribute this observation to the change in polarity, leading to a different hydrodynamic volume. Furthermore, ^1H NMR spectroscopy confirmed preservation of the polymer backbone (M_n and MTEGE ratio remain constant after oxidation and dialysis). Notably, only sulfoxide moieties were detected (via NMR) under both 296 K and 310 K oxidation conditions, demonstrating that no further oxidation to sulfone groups occurs (Figure S24-25). These observations are in line with results reported by Tirelli and co-workers for poly(propylene sulfide) (PPS)[11, 15] and others,[52] who reported the selective oxidation of thioethers moieties to sulfoxides by treatment with diluted H_2O_2.

Hypochlorite (OCl⁻) is another biological oxidant generated during inflammatory processes[50] and was investigated as an additional oxidation agent. In contrast to hydrogen peroxide, treatment of mPEG-*b*-PMTEGE with 1 wt% sodium hypochlorite (NaOCl) solution leads to the formation of sulfone groups (Figure S26-S27). Note that the occurrence of additional signals in the ^{1}H NMR spectrum and a broadening in the SEC trace might indicate side reactions, such as polyether cleavage (Figure S28). Analogous results were reported by Tirelli and co-workers for oxidation of poly(propylene sulfide).[11]
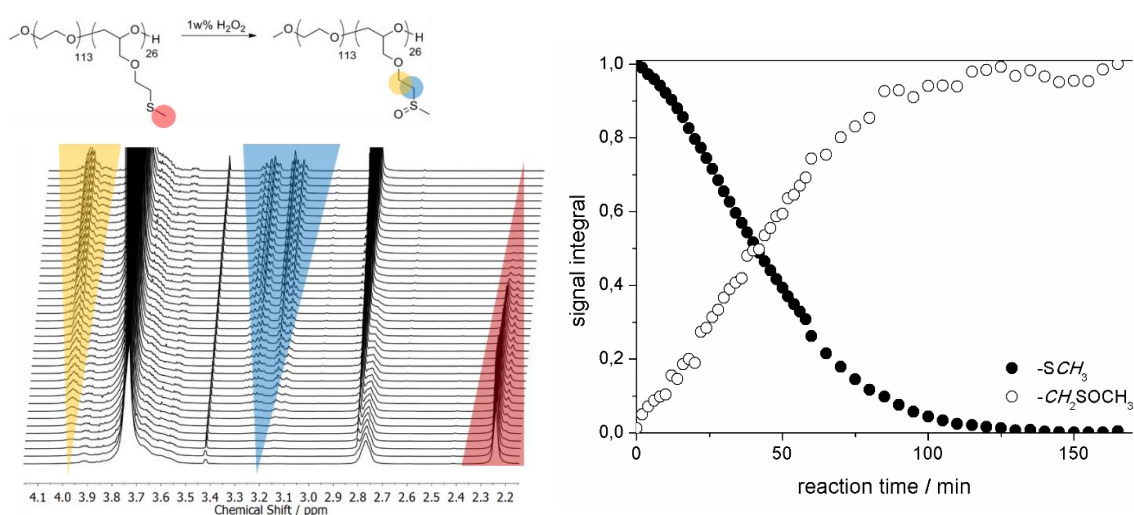

Figure 7. Selection of time-resolved ^{1}H NMR spectra (buffered D_2O, 400 MHz) of the oxidation of mPEG$_{113}$-*b*-PMTEGE$_{26}$ with 1 wt% H_2O_2 (left). Signal integral of the methyl signal (-SCH_3) and methylene signal (-CH_2SOCH$_3$) plotted versus reaction time for the oxidation of mPEG$_{113}$-*b*-PMTEGE$_{26}$ with H_2O_2 in buffered D_2O at 310 K (right).

The changes in polarity from a nonpolar thioether to polar sulfoxide or sulfone units strongly influences the glass transition temperature. While mPEG$_{113}$-*b*-PMTEGE$_{26}$ shows a T_g of -61 °C, the emerging dipole-dipole interactions cause a T_g of -33 °C for the sulfoxide derivative (mPEG$_{113}$-*b*-PMSOEGE$_{26}$) and a further increase to -15 °C for the sulfone derivative (mPEG$_{113}$-*b*-PMSO$_2$EGE$_{26}$). Sarapas and Tew reported similar results for linear poly(ether-thioethers) and their oxidized counterparts.[52]

After understanding the oxidation process on a molecular level, the question arises of how oxidation of the thioether units influences the solubility behavior of PEG-PMTEGE copolymers in water. First, we followed the oxidation process of the random PEG-*ran*-PMTEGE copolymers via turbidity measurements. An aqueous PEG-*ran*-PMTEGE solution (5 mg·mL^{-1}) with a cloud point of 28 °C was tempered to 37 °C and H$_2$O$_2$ solution was added under stirring. Directly after H$_2$O$_2$ addition, the transmitted laser light intensity increases, indicating the dissolution of aggregates due to increasing hydrophilicity of the oxidized species (Figure S29). After 8 minutes, an optically clear solution is observed with complete disappearance of aggregates. Similar results were reported by Chen and co-workers for linear poly(β-thioether ester).[17] Additionally, turbidity measurements of oxidized copolymers (PEG-*ran*-PMSOEGE) show fully water-soluble polymers and no cloud points were detected.

In particular, we were interested in the behavior of mPEG-*b*-PMTEGE block copolymers in aqueous solution with H$_2$O$_2$ treatment to investigate their potential as oxidation-responsive nanocarriers.[1, 12] To this end, we monitored the oxidation process of mPEG$_{113}$-*b*-PMTEGE$_{26}$ via DLS measurements in real-time. After the sample heating to 37 °C, H$_2$O$_2$ was added to the sample, followed by fast mixing (c$_{total}$ = 1 wt% H$_2$O$_2$). The temperature was kept at 37 °C during the measurement. Figure 8 shows the scattering intensity time traces versus time on a logarithmic scale.
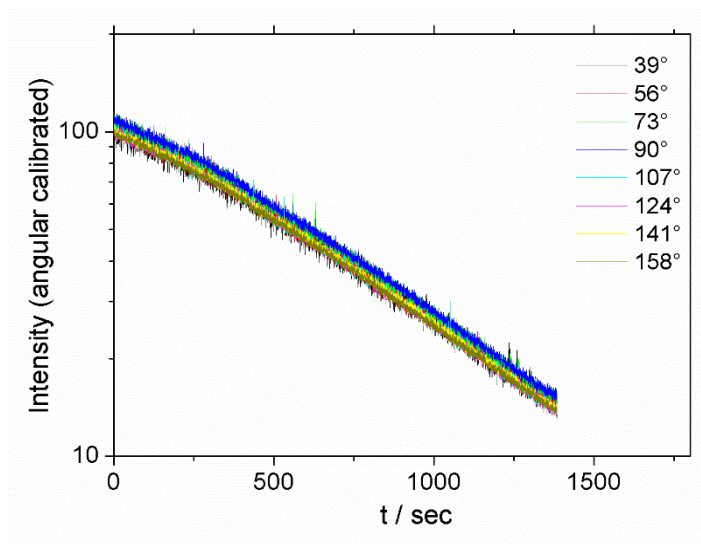
Figure 8. Angular dependent scattering intensity time traces (from multi-angular goniometer setup) for *in-situ* oxidation of mPEG$_{113}$-*b*-PMTEGE$_{26}$ (buffer solution, 37 °C, 1 wt% H$_2$O$_2$), shown on a logarithmic scale. The obvious change of the slope after 5 min is due to thermal equilibration.

After a thermal equilibration period of about 5 min, a linear decrease of the scattering intensity time traces can be observed. We attribute this linear decay to the oxidation of the nonpolar sulfides to polar sulfoxide groups, which leads to micelles with lower aggregation numbers (decrease in scattering intensity) and the formation of unimers (Scheme 3). Similar observations are reported for the disassembly of other H$_2$O$_2$ responsive or pH sensitive micelles. [17, 42, 53] Unfortunately, it was not possible to detect "spike" free intensity traces for oxidation times exceeding 20 min. This may be caused by several effects, e.g., formed oxygen bubbles may perturb the measurement, but also impurities of the H$_2$O$_2$ solution (not filtered) or the liberation of encapsulated impurities could lead to sudden increases in the scattering intensity. Huang et al. reported similar observations for DLS kinetic studies of acid sensitive polymeric micelles after complete hydrolysis. The authors observe bimodal distributions consisting of unimers and loose associates.[42] In analogy, Zhang et al. monitored the oxidation-responsiveness of phenylboronic acid-based polymers in DLS and described the formation of polymeric associates with a loose structure.[53]

82
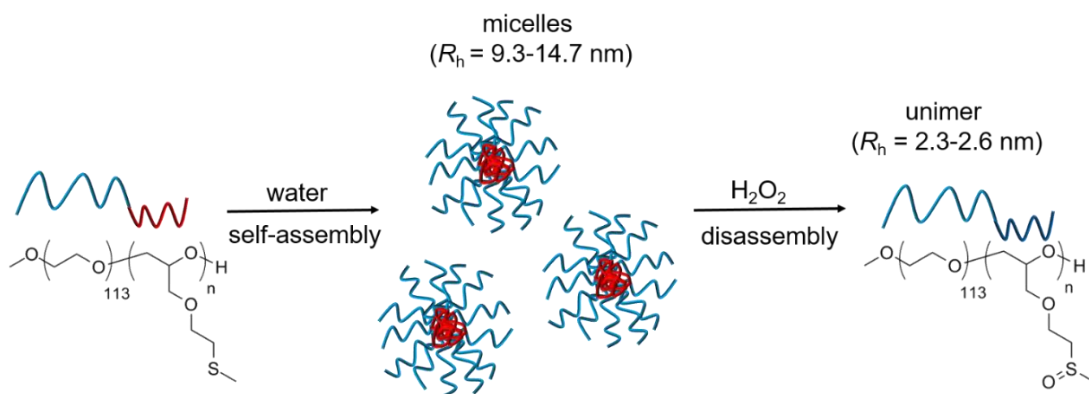
Scheme 3. Schematic of the micelle formation of mPEG$_{113}$-*b*-PMTEGE$_n$ block copolymers in water, followed by disruption upon treatment with H$_2$O$_2$. The hydrodynamic radii were determined by DLS measurements (Table S1 and Table S2).

To confirm our hypothesis of micelle dissociation and unimer formation, we performed DLS measurements of oxidized mPEG-*b*-PMSOEGE with 11 and 26 MSOEGE units. For both polymers, we detected pure unimers in water with hydrodynamic radii similar to their precursor polymers in methanol (Table S2). With the oxidation of MTEGE, the hydrophilic/hydrophobic balance of mPEG$_{113}$-*b*-PMTEGE$_n$ changes and leads to disassembly of the micelles into single polymer chains, as schematically shown in Scheme 3. Similar results were reported for the disassembly of PEG-polypropylene sulfide-PEG vesicles,[7] the dissolution of PEG-*b*-oligo(ethylene sulfide) fibrils[54] and the oxidation of OEGylated poly-L-cysteine.[14]

Having demonstrated successful disassembly of micelles as a consequence of the treatment with hydrogen peroxide, we investigated their potential as responsive nanocarriers. Nile Red, a hydrophobic fluorescence dye, was encapsulated in the micelles and their response to hydrogen peroxide (1 wt%) was studied.

Figure 9. Intensity of fluorescence emission of Nile Red, monitored as a function of time after addition of H_2O_2 solution to a block copolymer solution ($c_{polymer} = 0.5$ g·L^{-1}, $c_{H_2O_2} =$ 1 wt%, T = 25°C).

Figure 9 shows the intensity of the fluorescence emission of Nile Red recorded over time after addition of H_2O_2 to a block copolymer solution ($c_{polymer} = 0.5$ g·L^{-1}). Control measurements without H_2O_2 demonstrate stability of the micelles over the investigated timeframe, and no significant loss of Nile Red is observed (Figure S30). With the addition of hydrogen peroxide, the fluorescence intensity of Nile Red decreases, indicating release of the dye due to its insolubility in aqueous solution. Complete release was detected after 1 or 2 hours, for mPEG$_{113}$-*b*-PMTEGE$_n$ with n=11 and 26, respectively. For mPEG$_{113}$-*b*-PMTEGE$_{26}$ the intensity decrease follows a sigmoidal shape, which we attribute to an autoaccelerating character of the response in analogy to recent results by Tirelli and co-workers.[16] Significantly, the presented micelles respond faster to hydrogen peroxide than similar PEG (co)polysulfides (~8-24 h)[13, 16] structures and PEG-poly(β-thioethers) (~7 h).[19] Although the biologically relevant concentration of H_2O_2 for inflamed tissue is in the range of ~100 μM[55, 56], this is a first demonstration of the response of polyether based polysulfide analogs. Detailed concentration dependence will be investigated in the future. Overall, we

believe that mPEG-*b*-PMTEGE block copolymer architectures show potential as future redox-responsive drug vehicles and could be suitable for inflammation targeting.

D. Cell viability studies. PEG possesses excellent biocompatibility, very low immunogenicity, antigenicity and toxicity.[57] Low cytotoxicity is a crucial criterion for potential biomedical applications, and modification of PEG with thioether units may have an impact on these properties. Therefore, we conducted MTT assays to determine the effects of PEG-PMTEGE structures on the cellular metabolic activity of two different cell lines, HEK-293T cells (human embryonic kidney cells) and WEHI-164 cells (skin fibroblasts cells from mice), respectively. In a comparative study, mPEG itself and two samples of block and random PEG-PMTEGE copolymers with the highest amount of MTEGE were applied to seeded cells in concentrations of $1\text{-}1000\,\mu\text{g}\cdot\text{mL}^{-1}$. MTT assays were performed after an incubation time of 24 h. Results are displayed in Figure 10. Focusing on the random copolymers and HEK-293T cells, PEG_{137}-*ran*-PMTEGE_{26} with 16 mol% MTEGE affected the metabolic activity by less than 20% up to rather high concentrations of $100\,\mu\text{g}\cdot\text{mL}^{-1}$. With an increase of MTEGE to 23.7 mol%, which corresponds to 51 wt% MTEGE, cellular metabolic activity is slightly reduced. For a concentration of $1000\,\mu\text{g}\cdot\text{mL}^{-1}$, both samples drop below 80 % of metabolic activity of the control. Notably, both random copolymers showed no significant effect on the cellular metabolism of WEHI-164 cells, even at high concentrations of $1000\,\mu\text{g}\cdot\text{mL}^{-1}$.
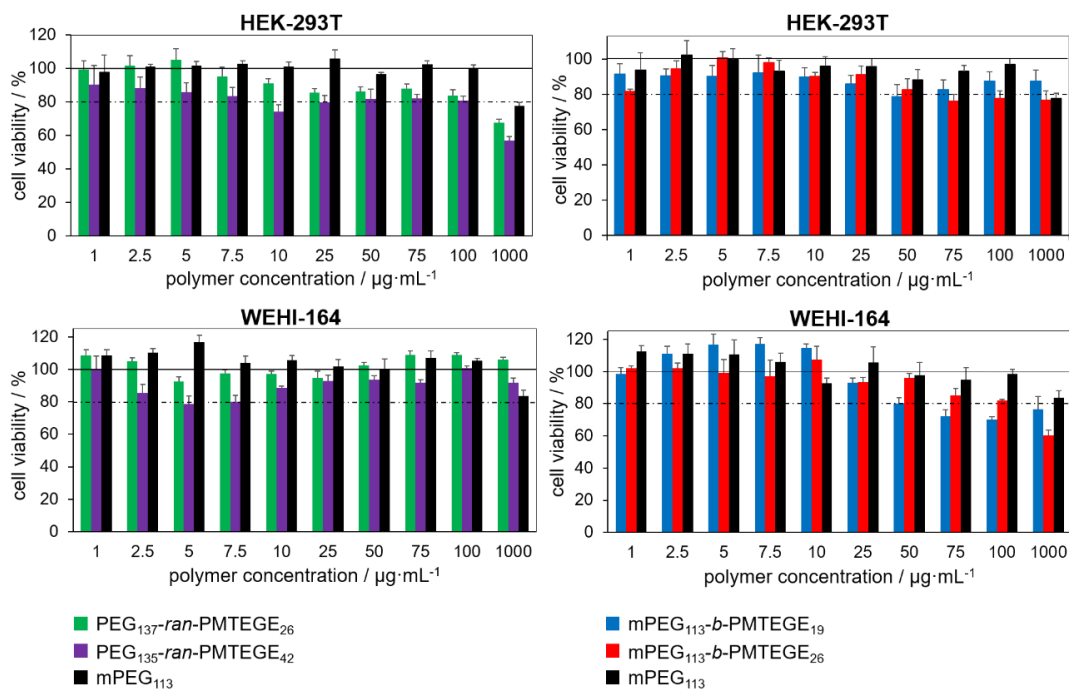
Figure 10. MTT assay of HEK-293T and WEHI-164 cells incubated with PEG-PMTEG random and block copolymers. For each type of polymer, copolymers with the highest amount MTEGE were tested. Results of mPEG$_{113}$ are shown for a better comparison. The metabolic activity of cells treated with 10 % PBS buffer corresponding to the highest volume of copolymer solution added to samples was set to 100 %. Graphs are representative of 2 independent experiments performed in triplicates. Data denote the mean±SEM of triplicates.

For the respective block copolymers, mPEG$_{113}$-*b*-PMTEGE$_{19}$ (14.1 mol%) showed biocompatibility up to 1000 μg·mL^{-1} for HEK-293T cells (Figure 10). The incorporation of 26 MTEGE units (18.7 mol%) at concentrations above 75 μg·mL^{-1} reduced cellular metabolic activity below the threshold of 80% of the control group. In comparison to HEK-293T, WEHI-164 cells were more sensitive towards the block copolymers.

With respect to envisaged inflammation targeting applications, it is particularly important, to which extent the oxidized products of mPEG-*b*-PMTEGE exert cytotoxic effects. To study this, we investigated the block copolymer with the highest amount of MTEGE. mPEG$_{113}$-*b*-PMTEGE$_{26}$ and its oxidized derivatives showed similar effects on HEK-293T cells as mPEG$_{113}$ itself (Figure 11). Regarding WEHI-164 cells, an inhibition of cellular

metabolic activity at high concentrations (1000 μg·mL^{-1}) was observed for mPEG$_{113}$-b-PMTEGE$_{26}$ and its sulfone derivative. In contrast, WEHI-164 cells incubated with mPEG$_{113}$-b-PMSOEGE$_{26}$ (sulfoxide units) exceeded 80% of metabolic activity of the control group, even at high concentrations (1000 μg·mL^{-1}), similar to neat mPEG$_{113}$. To sum up, mPEG$_{113}$-b-PMTEGE$_{26}$ and its oxidized derivatives had only marginal effects on the cellular metabolism of HEK-293T and WEHI-164 cells in the range up to 1000 μg·mL^{-1}, which is key for biomedical applications.

Figure 11. MTT assay of HEK-293T and WEHI-164 cells incubated with mPEG$_{113}$, mPEG$_{113}$-b-PMTEGE$_{26}$ and its oxidized derivatives, mPEG$_{113}$-b-PMSOEGE$_{26}$ (sulfoxide) and mPEG$_{113}$-b-PMSO$_2$EGE$_{26}$ (sulfone). The metabolic activity of cells treated with 10 % PBS buffer corresponding to the highest volume of block copolymer tested was set to 100 %. Graphs are representative of 2 independent experiments performed in triplicate. Data denote the mean±SEM of triplicates.

E. Post-Polymerization modification.

To highlight in a comprehensive manner the potential of MTEGE and thioether-functional PEGs, we further demonstrate their use as precursors for highly-functional sulfonium structures via click-type alkylation and alkoxylation. Positively charged sulfonium-PEGs are potential candidates for DNA/RNA complexation and represent an interesting polymer class themselves.

Alkylation. In contrast to common ethers, the sulfur in thioethers is nucleophilic and can react with alkyl halides to form sulfonium salts. Recently, Kramer and Deming applied this

concept to obtain various highly-functional and stable sulfonium derivatives based on poly(L-methionine).[4, 20, 58] Here, we "quaternized" the MTEGE units of mPEG-*b*-PMTEGE with bromoacetic acid or bromoacetamide to demonstrate their potential as precursors for highly functional sulfur-based polyelectrolytes (Figure 12, left). After modification, FT-IR spectra show new bands, that can be assigned to the carboxyl-group (1620 cm^{-1}) or the amide-group (1682 cm^{-1} (amide I) and 1624 cm^{-1} (amide II)), respectively (Figure 12, right).
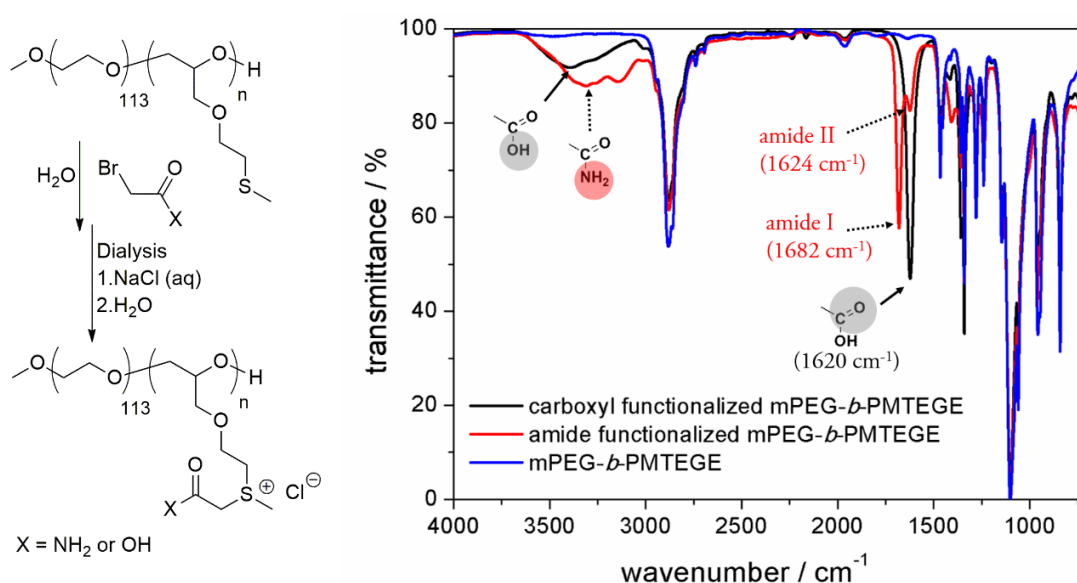
Figure 12. Left: Alkylation scheme. Right: FT-IR spectra of mPEG-*b*-PMTEGE (blue), carboxyl functionalized mPEG-*b*-PMTEGE (black) and amide functionalized block copolymer (red).

Successful modification can also be followed by ^{1}H and ^{13}C NMR spectroscopy. Figure S31 shows the ^{1}H NMR spectrum of amide-functional mPEG-*b*-PMTEGE. The methyl group at the sulfonium moiety shifted downfield to 3 ppm and a new resonance at 4 ppm appeared (-OC*H*$_2$CH$_2$S+). All other signals overlap with the backbone signal. Further, Figure S32 gives the respective ^{13}C NMR spectra: Both carbon atoms next to the sulfur atom shift downfield and two additional signals occur at 64.9 ppm (-O*C*H$_2$CH$_2$S+) and

166.3 ppm (-CONH$_2$). In analogy, the spectrum for carboxyl-functionalized polymer is shown in Figure S33. The introduction of highly polar functional groups further influence the thermal properties of the block copolymers. In DSC measurements, we observe a strong increase in T_g after alkylation (Table S3). We attribute the high T_g's to the introduced charges and the emerging hydrogen bonds between the carboxyl and amide groups, respectively. Interestingly, the T_g of carboxyl-functionalized polymers is higher than the respective amide-functionalized polymers, which is unexpected,[59] but might be caused by additional ionic interactions of the acid groups with the charged sulfonium moieties. Furthermore, TGA measurements show that sulfonium-PEG derivatives decompose around temperatures of ~130 °C (Figure S34). At high temperatures, primarily dealkylation occurs, as deduced from ^{1}H NMR spectra after heating of the samples (not shown). Yet, alkylated mPEG-b-PMTEGEs are stable under ambient conditions. The significance of sulfonium polyelectrolytes was demonstrated by Long and co-workers and Matyjaszewski and co-workers, who explored the use of methylated sulfonium poly(methyl)methacrylates for DNA and siRNA delivery.[21, 22] We believe that PEG-based sulfonium derivatives could be suitable alternatives to the above mentioned polymers, and their complexation and transport efficiencies need to be tested.

Alkoxylation. Recently, Gharakhanian and Deming demonstrated successful functionalization of thioethers with various epoxides as an alternative strategy to their alkylation (section *Alkylation*).[3] In an analogous manner, we can manipulate the reactivity of MTEGE by pH: At high pH, the nucleophilicity of the sulfide is not sufficient to ring-open an epoxide, and controlled AROP of the monomer can proceed, while at low pH the epoxide is activated and the sulfur(II) species is able to attack the epoxide ring. We studied this concept by addition of epichlorohydrin (ECH) (Figure S35), allyl glycidyl ether (AGE)

(Figure S36) and glycidyl propargyl ether (GPE) to mPEG-*b*-PMTEGE block copolymers.

Figure 13 illustrates the ^{1}H NMR spectrum of GPE-functionalized mPEG-*b*-PMTEGE.

Figure 13. ^{1}H NMR spectra (D$_2$O, 400 MHz) of mPEG$_{113}$-*b*-PMTEGE$_{19}$ and GPE-functionalized mPEG$_{113}$-*b*-PMTEGE$_{19}$ (left). TGA trace of GPE-functionalized mPEG$_{113}$-*b*-PMTEGE$_{19}$ (right).

The methyl-group at the charged sulfur atom shifts from 2.19 ppm to 3.04 ppm and additional signals at 4.03 ppm (-OC*H*$_2$CH$_2$S+), 4.29 ppm (HC≡CC*H*$_2$-) and 4.37 ppm (-CH$_2$C*H*OCH$_2$) appear. Note that the alkyne proton signal overlaps with the broad polyether backbone signal, which is not uncommon.[60] However, one can detect the characteristic signals of the alkyne group in the FT-IR spectrum (Figure S37). The respective HSQC spectrum of GPE-functionalized PEG-PMTEGE shows signal splitting of signals in close proximity to the sulfur atom (Figure S38). This phenomenon is explained by the use of racemic epoxides. After alkoxylation, a chiral sulfonium center is formed, and detected resonances might depend on the stereo information of the attached epoxide (*R*- vs *S*-). Alkoxylation with optically pure epoxides was not performed.

Similar to the alkylated derivatives, TGA measurements showed dealkylation at 120-130 °C, which is exemplarily shown for GPE functionalized mPEG-*b*-PMTEGE (Figure 13, right). Dealkylation or elimination during work-up of the reaction have not been observed. In summary, alkoxylated PEG-PMTEGE copolymers are stable at ambient

90

temperatures similar to the reported alkoxylated poly(L-methionine)[3] and enlarge the toolbox for highly functional sulfonium polyelectrolytes with polar polyether backbone.

2.1.5 Conclusion

We present a convenient synthesis of a novel epoxide monomer, 2-(methylthio)ethyl glycidyl ether (MTEGE), which can be copolymerized via AROP to yield well-defined thioether-functional PEGs. In a comprehensive study, synthesis and properties of random and block copolymers with PEG have been studied. The statistical copolymerization of MTEGE with EO was monitored via real-time ^{1}H NMR kinetics in DMSO, revealing an ideally random microstructure ($r_{EO} = 0.92 \pm 0.02$, $r_{MTEGE} = 1.06 \pm 0.02$). The random copolymers with 5-24 mol% MTEGE are water-soluble, with tunable cloud points in the range of 28-88 °C. In contrast, DLS studies show that $mPEG_{113}$-b-$PMTEGE_n$ block copolymers with $n \geq 9$ form defined micelles in water. Notably, disassembly of the micelles occurs when oxidized with 1 wt% H_2O_2, and pure unimers were detected. Hydrogen peroxide oxidizes the nonpolar thioethers-moieties to more polar sulfoxide groups, leading to a change in the hydrophilic/hydrophobic balance. Fluorescence studies with Nile Red show successful encapsulation and controlled release upon addition of dilute H_2O_2 after 1-2 hours, supporting the redox-responsive characteristics of the micellar nanocarriers. The oxidation-responsiveness represents the most intriguing feature of the mPEG-b-PMTEGE block copolymers and demonstrates their potential for future inflammation targeting. MTT assays employing HEK-293T and WEHI-164 cell lines demonstrated excellent biocompatibility of the thioether-PEGs and their oxidized derivatives.

Further, we demonstrated the use of thioether-PEGs as a precursor for sulfur-based polyelectrolytes. Alkylation and alkoxylation in aqueous solution render multi-functional sulfonium-derivatives bearing carboxyl-, amide-, chloro, allyl- or propargyl groups. These

tertiary sulfonium-PEGs are stable in aqueous solution under ambient temperatures. In conclusion, the presented thioether PEGs and their derivatives possess potential for a variety of applications, ranging from redox-sensitive nanotransporters and inflammation targeting,[12, 50, 56, 61, 62] to polyion complexes[21, 22] and surface modification.[63–65]

2.1.6 Acknowledgments

2.1.7 References

[1] Vo, C. D.; Kilcher, G.; Tirelli, N. *Macromol. Rapid Commun.* **2009**, *30*, 299–315.

[2] Oae, S. *Organic Chemistry of Sulfur*, Boston, MA, Springer US. **1977**.

[3] Gharakhanian, E. G.; Deming, T. J. *Biomacromolecules* **2015**, *16*, 1802–1806.

[4] Kramer, J. R.; Deming, T. J. *Biomacromolecules* **2012**, *13*, 1719–1723.

[5] Batz, H. G.; Hofmann, V.; Ringsdorf, H. *Die Makromolekulare Chemie* **1973**, *169*, 323–325.

[6] Hofmann, V.; Ringsdorf, H.; Muacevic, G. *Die Makromolekulare Chemie* **1975**, *176*, 1929–1943.

[7] Napoli, A.; Valentini, M.; Tirelli, N.; Müller, M.; Hubbell, J. A. *Nat Mater.* **2004**, *3*, 183–189.

[8] Napoli, A.; Boerakker, M. J.; Tirelli, N.; Nolte, R. J. M.;. Sommerdijk, N. A. J. M; Hubbell, J. A. *Langmuir* **2004**, *20*, 3487–3491.

[9] Napoli, A.; Bermudez, H.; Hubbell, J. A. *Langmuir* **2005**, *21*, 9149–9153.

[10] Wang, L.; Kilcher, G.; Tirelli, N. *Macromol. Biosci.* **2007**, *7*, 987–998.

[11] Carampin, P.; Lallana, E.; Laliturai, J.; Carroccio, S. C.; Puglisi, C.; Tirelli, N. *Macromol. Chem. Phys.* **2012**, *213*, 2052–2061.

[12] Lallana, E.; Tirelli, N. *Macromol. Chem. Phys.* **2013**, *214*, 143–158.

[13] Hu, P.; Tirelli, N. *Bioconjugate Chem.* **2012**, *23*, 438–449.

[14] Fu, X.; Ma, Y.; Shen, Y.; Fu, W.; Li, Z. *Biomacromolecules* **2014**, *15*, 1055–1061.

[15] Jeanmaire, D.; Laliturai, J.; Almalik, A.; Carampin, P.; d'Arcy, R.; Lallana, E.; Evans, R.; Winpenny, R. E. P.; Tirelli, N. *Polym. Chem.* **2014**, *5*, 1393–1404.

[16] d'Arcy, R.; Siani, A.; Lallana, E.; Tirelli, N. *Macromolecules* **2015**, *48*, 8108–8120.

[17] Xiao, C.; Ding, J.; Ma, L.; Yang, C.; Zhuang, X.; Chen, X. *Polym. Chem.* **2015**, *6*, 738–747.

[18] Allen, B. L.; Johnson, J. D.; Walker, J. P. *ACS Nano.* **2011**, *5*, 5263–5272.

[19] Wu, W.-X.; Yang, X.-L.; Liu, B.-Y.; Deng, Q.-F.; Xun, M.-M.; Wang, N.; Yu, X.-Q. *RSC Adv.* **2016**, *6*, 11870–11879.

[20] Kramer, J. R.; Deming, T. J. *J. Am. Chem. Soc.* **2014**, *136*, 5547–5550.

[21] Hemp, S. T.; Allen, M. H.; Smith, A. E.; Long, T. E. *ACS Macro Lett.* **2013**, *2*, 731–735.

[22] Mackenzie, M. C.; Shrivats, A. R.; Konkolewicz, D.; Averick, S. E.; McDermott, M. C.; Hollinger, J. O.; Matyjaszewski, K. *Biomacromolecules* **2015**, *16*, 236–245.

[23]   Herzberger, J.; Niederer, K.; Pohlit, H.; Seiwert, J.; Worm, M.; Wurm, F. R.; Frey, H. *Chem. Rev.* **2016**, *116*, 2170–2243.

[24]   Lee, J. C.; Litt, M. H.; Rogers, C. E *Macromolecules* **1997**, *30*, 3766–3774.

[25]   Lee, A.; Lundberg, P.; Klinger, D.; Lee, B. F.; Hawker, C. J.; Lynd, N. A. *Polym. Chem.* **2013**, 5735–5742.

[26]   Hans, M.; Keul, H.; Moeller, M. *Polymer* **2009**, *50*, 1103–1108.

[27]   Mangold, C.; Dingels, C.; Obermeier, B.; Frey, H.; Wurm, F. *Macromolecules* **2011**, *44*, 6326–6334.

[28]   Herzberger, J.; Kurzbach, D.; Werre, M.; Fischer, K.; Hinderberger, D.; Frey, H. *Macromolecules* **2014**, *47*, 7679–7690.

[29]   Niederer, K.; Schüll, C.; Leibig, D.; Johann, T.; Frey, H. *Macromolecules* **2016**, *49*, 1655–1665.

[30]   Beckingham, B. S.; Sanoja, G. E.; Lynd, N. A. *Macromolecules* **2015**, *48*, 6922–6930.

[31]   Lee, B. F.; Wolffs, M.; Delaney, K. T.; Sprafke, J. K.; Leibfarth, F. A.; Hawker, C. J.; Lynd, N. A. *Macromolecules* **2012**, *45*, 3722–3731.

[32]   Fuller, C. S., *Chem. Rev.* **1940**, *26*, 143–167.

[33]   Brandrup, J.; Immergut, E. H.; Grulke, E. A., *Polymer handbook, 4th edition*, 4th edition, New York, Chichester, Wiley. **2004**.

[34]   Müller, S. S.; Moers, C.; Frey, H. *Macromolecules* **2014**, *47*, 5492–5500.

[35]   Mangold, C.; Obermeier, B.; Wurm, F.; Frey, H. *Macromol. Rapid Commun.* **2011**, *32*, 1930–1934.

[36]   Shikata, T.; Okuzono, M.; Sugimoto, N. *Macromolecules* **2013**, 1956–1961.

[37]   Derici, L.; Ledger, S.; Mai, S.-M.; Booth, C.; W. Hamley, I.; Skov Pedersen, J. *Phys. Chem. Chem. Phys.* **1999**, *1*, 2773–2785.

[38]   Topp, M. D. C.; Dijkstra, P. J.; Talsma, H.; Feijen, H. *Macromolecules* **1997**, *30*, 8518–8520.

[39]   Kjøniksen, A.-L-; Nyström, B.; Tenhu, H. *Colloids Surf., A.* **2003**, *228*, 75–83.

[40]   Motokawa, R.; Morishita, K.; Koizumi, S.; Nakahira, T.; Annaka, M. *Macromolecules* **2005**, *38*, 5748–5760.

[41]   Yan, J.; Ji, W.; Chen, E.; Li, Z.; Liang, D *Macromolecules* **2008**, *41*, 4908–4913.

[42]   Huang, X.; Du, F.; Cheng, J.; Dong, Y.; Liang, D.; Ji, S.; Lin, S.-S.; Li, Z. *Macromolecules* **2009**, *42*, 783–790.

[43]   Kurzbach, D.; Wilms, V. S.; Frey, H.; Hinderberger, D. *ACS Macro Lett.* **2013**, 128–131.

[44]   Kelarakis, A.; i Havredaki, V.; Yu, G.-E.; Derici, L.; Booth, C. *Macromolecules* **1998**, *31*, 944–946.

[45]   Bedells, A. D.; Arafeh, R. M.; Yang, Z.; Attwood, D.; Heatley, F.; Padget, J. C.; Price, C.; Booth, C. *J. Chem. Soc., Faraday Trans.* **1993**, *89*, 1235–1242.

[46]   Wilhelm, M.; Zhao, C. L.; Wang, Y.; Xu, R.; Winnik, M. A.;Mura, J. L.; Riess, G.; Croucher, M. D. *Macromolecules* **1991**, *24*, 1033–1040.

[47]   Yasugi, K.; Nagasaki, Y.; Kato, M.; Kataoka, K. *J. Control. Release* **1999**, *62*, 89–100.

[48]   Stauch, O.; Schubert, R.; Savin, G.; Burchard, W. *Biomacromolecules* **2002**, *3*, 565–578.

[49]   Förster, S.; Zisenis, M.; Wenz, E.; Antonietti, M. *J. Chem. Phys.* **1996**, *104*, 9956–9970.

[50]   d'Arcy, R.; Tirelli, N. *Polym. Adv. Technol.* **2014**, *25*, 478–498.

[51]   Covington, A. K.; Paabo, M.; Robinson, R. A.; Bates, R.G. *Anal. Chem.* **1968**, *40*, 700–706.

[52]   Sarapas, J. M.; Tew, G. N. *Macromolecules* **2016**, *49*, 1154–1162.

[53]   Zhang, M.; Song, C.-C.; Ji, R.; Qiao, Z.-Y.; Yang, C.; Qiu, F.-Y.; Liang, D.-H.; Du, F.-S.; Li, Z.-C. *Polym. Chem.* **2016**, *7*, 1494–1504.

[54]   Brubaker, C. E.; Velluto, D.; Demurtas, D.; Phelps, E. A.; Hubbell, J. A. *ACS Nano* **2015**, *9*, 6872–6881.

[55]   Lux, C. G.; Joshi-Barr, S.; Nguyen, T.; Mahmoud, E.; Schopf, E.; Fomina, N.; Almutairi, A. *J. Am. Chem. Soc.* **2012**, *134*, 15758–15764.

[56]   Xu, Q.; He, C.; Xiao, C.; Chen, X. *Macromol. Biosci.* **2016**, *16*, 635–646.

[57]   Fruijtier-Pölloth, C. *Toxicol.* **2005**, *214*, 1–38.

[58]   Kramer, J. R.; Deming, T. J. *Chem. Commun.* **2013**, *49*, 5144–5146.

[59]   Herzberger, J.; Frey, H. *Macromolecules* **2015**, *48*, 8144–8153.

[60]   Thomas, A.; Niederer, K.; Wurm, F.; Frey, H. *Polym. Chem.* **2014**, *5*, 899–909.

[61]   Song, C.-C.; Du, F.-S.; Li, Z.-C., *J. Mater. Chem. B.* **2014**, *2*, 3413–3426.

[62]   Tapeinos, C.; Pandit, A. *Adv. Mater.* **2016**, DOI: 10.1002/adma.201505376.

[63]   Stouffer, J. M.; McCarthy, T. J. *Macromolecules* **1988**, *21*, 1204–1208.

[64]   Lenk, T. J.; Hallmark, V. M.; Rabolt, J. F.; Haeussling, L.; Ringsdorf, H. *Macromolecules* **1993**, *26*, 1230–1237.

[65]   Fujii, S.; McCarthy, T. J. *Langmuir* **2016**, *32*, 765–771.

2.1.8 Supporting Information

Terminology. Oxidized MTEGE is abbreviated as MSOEGE (corresponding to sulfoxide units) and as MSO₂EGE for the oxidation to sulfone groups.

Materials. EO, 2-(methylthio)ethanol and pyrene (for fluorescence, GC $\geq$ 99.0 %) were purchased from Sigma Aldrich. Poly(ethylene glycol) monomethyl ether (mPEG5000, M_n = 5000 g·mol^{-1}) was purchased from Fluka. Nile Red was received from Apollo Scientific. All other reagents were purchased from Acros Organics. Deuterated solvents were received from Deutero GmbH. All reagents were used as received if not otherwise stated. THF was stored over sodium, containing benzophenone and freshly distilled before each reaction. MTEGE was dried over CaH₂ and freshly distilled before polymerization. Dialysis bags (regenerated cellulose membranes, 1000 MWCO) were purchased from Orange Scientific.

Instrumentation. ^{1}H NMR spectra (400 MHz) and ^{13}C NMR spectra (100 MHz) were recorded using a Bruker Avance II HD 400 spectrometer equipped with a 5 mm BBFO-SmartProbe (Z-gradient probe) and an ATM as well as a SampleXPress 60 auto sampler. All spectra are referenced internally to residual proton signals of the deuterated solvent. ^{1}H NMR kinetic studies for copolymerization were conducted on a Bruker Avance III HD spectrometer equipped with a 5 mm BBFO SmartProbe and an ATM as well as a SampleXPress 60 auto sampler. Dried monomer was dissolved in DMSO-d_6 and transferred to a Norell S-500-VT-7 NMR tube (equipped with a Teflon stop-cock) under argon flow. The solution was cooled to -80 °C, followed by addition of the initiator solution (in DMSO-d_6) and pure DMSO-d_6, before EO was cryo-transferred into the tube. The polymerization was followed at 40 °C. For the first hour, proton NMRs were recorded every 2 min (16 scans). For the next 3 hours, measurements were conducted every 5 min (16 scans), followed by recording every 10 min for 14 h (16 scans).

SEC measurements were performed in DMF (containing 0.25 g L^{-1} lithium bromide as an additive) or in THF. For SEC measurements in DMF, an Agilent 1100 Series was used as an integrated instrument, including a PSS HEMA column (300/100/40 · 10^{-10} porosity) as well as a UV (275 nm) and a RI detector. Alternatively, SEC measurements in THF (flow rate 1 mL·min^{-1}) were performed with a MZ-Gel SD plus column (10^5/10^3/100 g mol^{-1}) at 20 °C, using a UV (254 nm) and RI detector. All calibrations were carried out using poly(ethylene glycol) standards purchased from Polymer Standards Service. DSC measurements were conducted under nitrogen atmosphere using a PerkinElmer DSC 8500 with PerkinElmer CLN2 in the temperature range of – 90 °C to 100 °C, at heating rates of 20 and 10 K · min^{-1} for the first and the second heating run, respectively. Thermogravimetric analysis (TGA) was carried out under nitrogen using a PerkinElmer TGA 6 thermogravimetric analyzer in the temperature range of 30−600 °C, with heating rates of 15 °C min^{-1}. Cloud point measurements were performed on a Jasco V-630 photospectrometer with a Jasco ETC-717 Peltier element through a 1 cm sample quartz cell. Copolymers were dissolved in Milli-Q water with a concentration of 5 mg·mL^{-1}. The optical transmittance of a light beam at 500 nm was observed and the transmitted laser light intensity was plotted versus the temperature of the sample cell. The cloud point temperatures were defined as inflection point of the turbidity profiles. Heating/cooling rates were 1 K·min^{-1} and values were recorded in 0.1 K steps. For CMC measurements, aqueous polymer stock solutions of 1 g·L^{-1} were prepared and further diluted to obtain solutions of 0.1 g·L^{-1}, 00.1 g·L^{-1} and 0.001 g·L^{-1}, respectively. For each measurement, first, a solution of pyrene in acetone was added to a vial, followed by evaporation of the acetone. Secondly, a calculated amount of stock solution and distilled water (Milli-Q) was added to obtain a final concentration of pyrene of 6·10^{-7} M in each sample. The samples were allowed to mix overnight, to completely solubilize the pyrene by the micelles. Overall, solutions in the concentration range of 1-1·10^{-4} g·L^{-1} block copolymer were prepared in nested interval

steps. CMC measurements were performed on a Jasco FP-6500 fluorescence spectrometer through a 1x1 cm quartz cell, recording the emission spectra of pyrene. The following parameters were chosen: excitation wavelength λ_{ex}=339 nm, slit$_{em}$ = 1 nm (for mPEG$_{113}$-b-PMTEGE$_{19}$: 3nm), slit$_{ex}$ = 1 nm (for mPEG$_{113}$-b-PMTEGE$_{19}$: 3nm), wavelength range = 320-460 nm, scan speed = 50 nm·min^{-1}, data interval = 0.2 nm, gain = high, response = 0.5-1 sec. The intensity ratio of I_1 = 373 nm and I_3 = 383.5 nm and the relative intensity were used to estimate the CMC. The CMC of mPEG$_{113}$-b-PMTEGE$_{26}$ was measured on a Varian Cary Eclipse spectrometer with the following parameters: λ_{ex}=339 nm, slit$_{em}$= 1.5 nm and slit$_{ex}$ = 5 nm, gain = high, wavelength range = 320-460 nm, scan speed = 60 nm·min^{-1}, data interval = 0.5 nm, response = 0.5 sec.

Nile Red release studies were performed in analogy to literature.[1, 2]A stock solution of Nile Red in acetone was prepared with a concentration of c = 6·10^{-4} M. 10µL of this stock solution was added to a vial, followed by evaporation of the acetone. Afterwards, 4 mL of aqueous polymer solution (c = 1g·L^{-1} in MilliQ water) was added and mixed overnight, to solubilize the Nile Red by the micelles. For each release study, 1.5 mL of this aqueous polymer solution (c=1g·L^{-1}) was mixed with 1.5 mL 2 wt% H$_2$O$_2$ solution, to obtain a final polymer concentration of 0.5 g·L^{-1} and 1wt % H$_2$O$_2$. Subsequently the intensity of fluorescence emission of Nile Red at 611 nm was recorded over time at room temperature (no stirring). The following measurement parameters were chosen: λ_{ex} = 557 nm, gain = 490 V* or high, response = 1 sec, slit$_{em}$ = 5 nm, slit$_{ex}$ = 5 nm, data invervall = 2 sec. Fluorescence spectra without added hydrogen peroxide were measured as controls. * for mPEG$_{113}$-b-PMTEGE$_{26}$

Static (SLS) and dynamic light scattering (DLS) were performed at 293.15 °C utilizing an ALV 3000 correlator, an ALV-SP86 goniometer equipped with an ALV High QE APD Avalanche photodiode fiber optical detection system, and a He-Ne laser (Uniphase, 22

mW, $\lambda = 632.8$ nm). For the unimer solutions in methanol and water (mPEG$_{113}$-b-PMTEGE$_x$ with x $\leq$6) with hydrodynamic radii well below 10 nm and therefore without angular dependency of the apparent diffusion coefficient, DLS was performed at angles of 30° (setup 1). Self-assembling samples in aqueous solutions were analyzed by DLS using a multi-angular detection goniometer (ALV-CGS-8F SLS/DLS 5022F) equipped with a He/Ne Laser (Uniphase, 25mW, λ=632.8nm), eight simultaneously working ALV7004 correlators connected to eight ALV high QE APD avalanche photodiode fiber optical detectors; detectors are separated by 17°, two independent simultaneous sets of measurement separated by 9° resulting in 16 angular dependent values covering an angular range from 30 to 158° thus allowing extrapolation to scattering angle zero with respect to polydispersities effects on diffusion coefficient. All measurements were performed at 20±0.1°C with the help of external ultra-thermostats (Lauda RKS 6C). Diffusion coefficients were determined from intensity autocorrelation functions after Siegert transformation (g$_1$(t)=sqrt(abs((g$_2$(t)-A)/A))*sign(g$_2$(t)) with A the experimentally measured baseline) by a non-linear fitting (Simplex algorithm) of the field autocorrelation function by applying mono- or biexponential fit functions. Hydrodynamic radii were calculated by applying the Stokes-Einstein equation. Static light scattering was conducted from $\theta = 30°$ to $\theta = 150°$ in steps of 2.5 or 5 degrees using the ALV SP-86 goniometer (setup 1) allowing the determination of the apparent squared radius of gyration $<R_g^2>_z >$ 10 nm; aggregation numbers were evaluated by the intensity ratios of the self-assembled systems in water extrapolated to zero scattering angle and the unimers in methanol (no angular dependency), which is allowed due to isorefractive solvent conditions. For samples with mPEG$_{113}$-b-PMETEG$_x$ x$\geq$11, both, concentration dependencies and critical aggregation concentration (cac) influences are neglected due to low concentration limit conditions (unimer) and cac well below 0.1 g·L^{-1} for the aggregates, see CMC

measurements. For the sample $mPEG_{113}$-b-$PMTEGE_9$ with a CMC of 0.1 $g \cdot L^{-1}$, c was corrected by c(CMC).

Samples were prepared in methanol (5mM LiBr), in water (5mM NaCl) and PBS-buffer solution with a concentration of 1 $g \cdot L^{-1}$. If not noted elsewhere, methanol solutions were passed through VWR Anatop filters (0.02 µm) and aqueous solutions were passed through VWR Anatop filters (0.02 µm) (for samples with $R_h \leq 3$ nm) or Millipore Millex-VV filters (0.1 µm) (for samples with $R_h > 3$ nm) into dust free cuvettes. Filtration loss was well below 10 %, as proofed by gravimetrical control.

Monitoring direct oxidation of mPEG-b-PMTEGE block copolymers via DLS: The block copolymer was dissolved in phosphate buffer (PBS, pH = 7.4, c=1g·L^{-1}) and filtered through a Millex-VV filter (0.1 µm) into a dust free cuvette. The sample was tempered at 37 °C for 30 min, followed by addition of H_2O_2 solution (not filtered) to obtain a total concentration of 1wt% H_2O_2 in the solution. After short mixing, light scattering measurements were performed at 37 °C with the multi-angular set up. Measurements were immediately started; after an equilibration time of 5 min, a linear intensity time dependency could be observed for each angular monitoring channel.

CryoTEM measurements. Cryogenic TEM imaging was performed by means of a Zeiss Libra® 120 under liquid N_2 cryo conditions on holey carbon-coated copper grids after freezing the solution with a Leica EM GP in liquid ethane at -180°C. The microscope was used at 120 kV acceleration voltage and the images were taken with a Gatan UltraScan® ccd camera.

MTT assays. Cytotoxic effects of polymer treatment were evaluated by MTT assay (Promega, Heidelberg, Germany). Cells from a fibroblast cell line (WEHI-164, 5×10^3) and human embryonic kidney cell line (HEK-293T, 5×10^3) were seeded in wells (100 μL)

of 96-well cell culture-treated plates. On the next day, copolymer was applied at different concentrations (1-1000 μg·mL^{-1}) to triplicates. Samples treated with the cytotoxic agent DMSO (10%) served as negative controls. After 24 h, metabolic activity of the cells was assessed by sequential addition of MTT substrate and stop solution, followed by quantification of formazan products in an ELISA plate reader as recommended by the manufacturer. Values shown are averages from at least 3 wells with the corresponding SEM as error bar. All values are normalized to the control (10% PBS buffer, equivalent to the highest volume of polymer solution added to samples).

Statistical copolymerization of EO and MTEGE. Copolymerization was performed in analogy to other literature-known PEG-glycidyl ether copolymers.[3] Cesium hydroxide monohydrate (1 equiv.), benzene (10 mL) and 2-propoxyethanol (1.05 equiv) were added into a dry Schlenk flask under argon atmosphere. The mixture was stirred and heated to 60 °C for 30 min, to generate the alkoxide species. Afterwards, benzene was removed under reduced pressure overnight at 50 °C to ensure a water-free environment. The next day, dry THF (~25 mL) was cryo-transferred into the flask and dry DMSO (3 mL) was added via syringe. Subsequently, the mixture was cooled to -80 °C with an ethanol/liquid nitrogen bath and EO was cryo-transferred from a graduated ampule into the reaction mixture, followed by addition of MTEGE via syringe. The polymerization was performed at 60 °C for 2 days. After cooling the flask to room temperature, termination was conducted with an excess of methanol. The solvents were removed under reduced pressure and the copolymers dialyzed against water to remove traces of DMSO and salts (MWCO = 1000 g·mol^{-1}), followed by drying via lyophilization.

Block copolymerization in bulk. Block copolymer synthesis was performed starting from mPEG-5000 as macroinitiator, as described for similar block copolymers.[4] Under an argon atmosphere, mPEG-5000 (1 equiv.) was added to a dry Schlenk flask, followed by cesium

hydroxide hydrate (0.9 equiv.) and benzene 10 mL. The mixture was stirred for 30 min at 60 °C, followed by removal of benzene under reduced pressure at 90 °C overnight. The next day, dry MTEGE was syringed into the flask and the polymerization was performed in bulk at 70 °C under vacuum for 2 days. After the flask was cooled down to room temperature, an excess of methanol was added. The block copolymers were dissolved in methanol and precipitated into ice cold diethyl ether. After drying under high-vacuum, the block copolymers were obtained in quantitative yield ≥ 90 %. Salts were removed via dialysis in water (MWCO = 1000 g·mol^{-1}), afterwards the polymer was dried via lyophilization.

^{1}H NMR kinetics of oxidation process. Oxidation of mPEG$_{113}$-*b*-PMTEGE$_{26}$ was monitored via ^{1}H NMR spectroscopy. 20 mg of the block copolymer were dissolved in 0.68 mL D$_2$O or deuterated phosphate buffer (pD = 7.46, pH = 7.01)[5] respectively. After addition of 20 µL H$_2$O$_2$ solution (~35 %, aq) (to obtain 1% solution) and short mixing, the tube was placed in the NMR setup. The oxidation in D$_2$O was performed at 296 K, and in buffer solution at elevated temperature (310 K), to predict a more biological surrounding. For the first hour, NMR spectra (16 scans) were recorded every 2 min, followed by every 5 min for 3 hours, afterwards the intervals were extended to every 10 min for 6 h.

Oxidation with H$_2$O$_2$-solution. Oxidation was conducted in 1wt% aqueous H$_2$O$_2$-solution for 24 h, followed by purification via dialysis against water (1000 MWCO) and freeze-drying. Yield after oxidation was ≥ 95 %, with some small loss due to dialysis.

Oxidation to sulfone groups. Oxidation to sulfone groups was performed in 1wt% aqueous NaOCl-solution for 24 h. Afterwards, the sample was dialyzed against water (1000 MWCO), followed by freeze-drying. Yields ≥ 90 %.

Post-polymerization functionalization via alkylation. A literature-known procedure was applied.[6] Exemplarily, 100 mg of mPEG-*b*-PMTEGE$_{19}$ was dissolved in 5 mL Milli-Q

water and alkylating agent (bromo acetic acid or bromo acetamide, 3 eq per MTEGE unit) was added. The reaction was stirred for 24 h at room temperature. Afterwards, the functionalized polymer was purified via dialysis against 0.1 M NaCl (for anion exchange), followed by water and drying via lyophilization. Small losses due to dialysis were observed (yield $\geq$ 90%).

Post-polymerization functionalization with epoxides. The reaction was performed in analogy to literature described by Gharakhanian and Deming.[7] 100 mg copolymer was dissolved in acetic acid (glacial), followed by addition of the epoxide (3 eq per MTEGE unit). The reaction was pursued at room temperature for 24 h, followed by removal of the acetic acid via dialysis against 3mM HCl with an additional dialysis against water. Afterwards, polymers were tried via lyophilization. Small losses due to dialysis were observed (yield $\geq$ 90%)
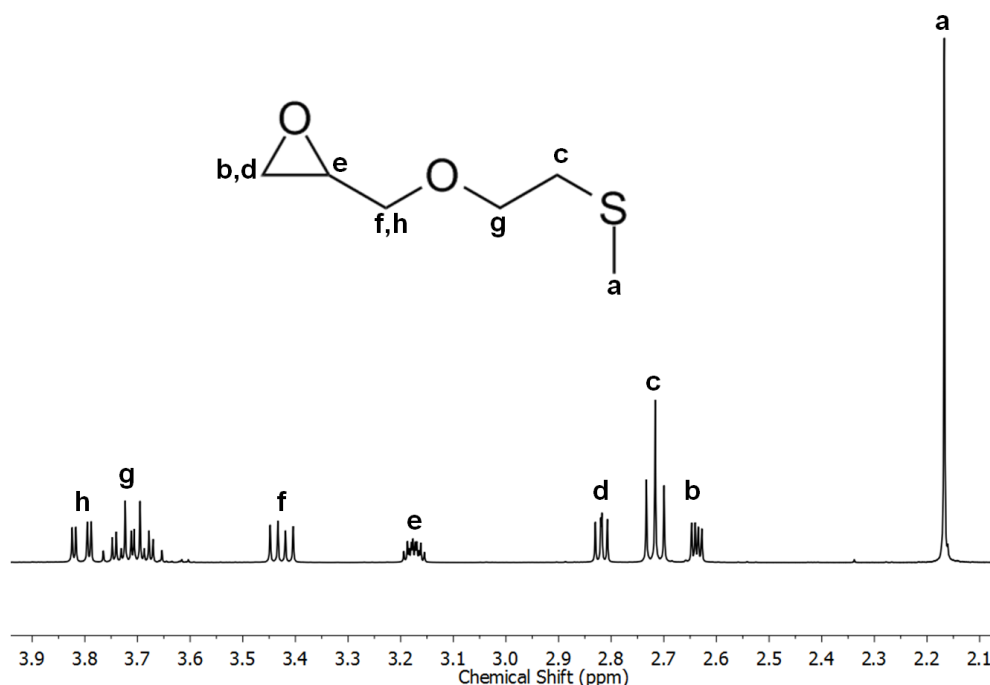
Figure S1. ^{1}H NMR spectrum (400 MHz, CDCl$_3$) of 2-(methylthio)ethyl glycidyl ether (MTEGE).
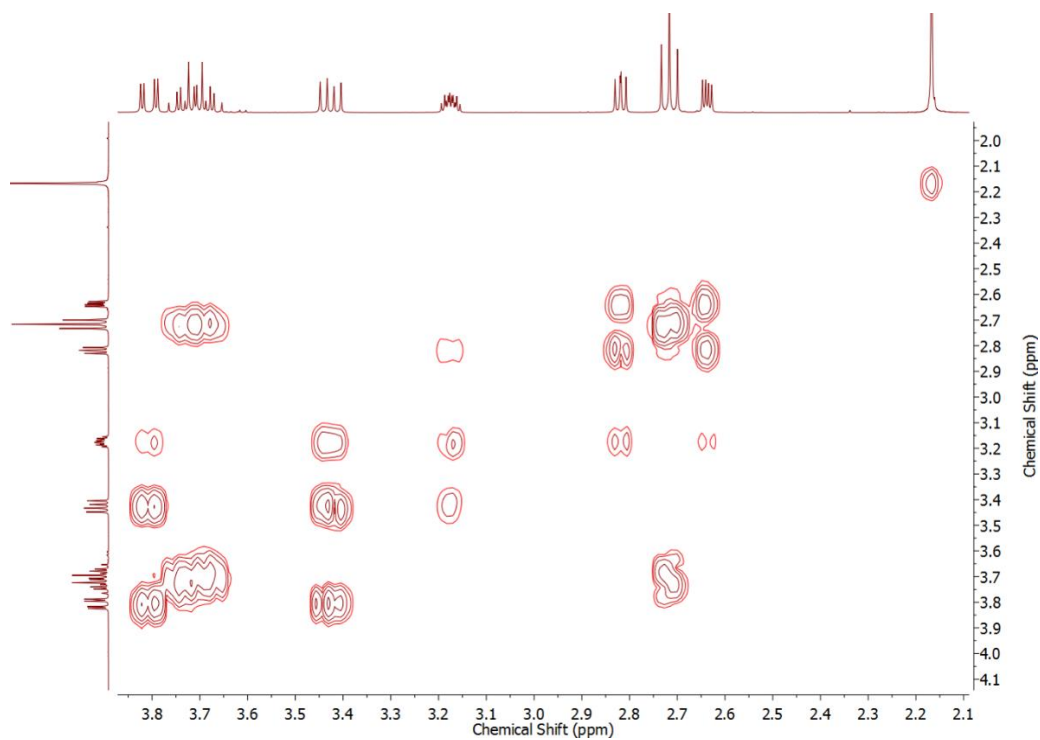
Figure S2. ^1H-^1H COSY NMR spectrum (CDCl$_3$) of MTEGE.
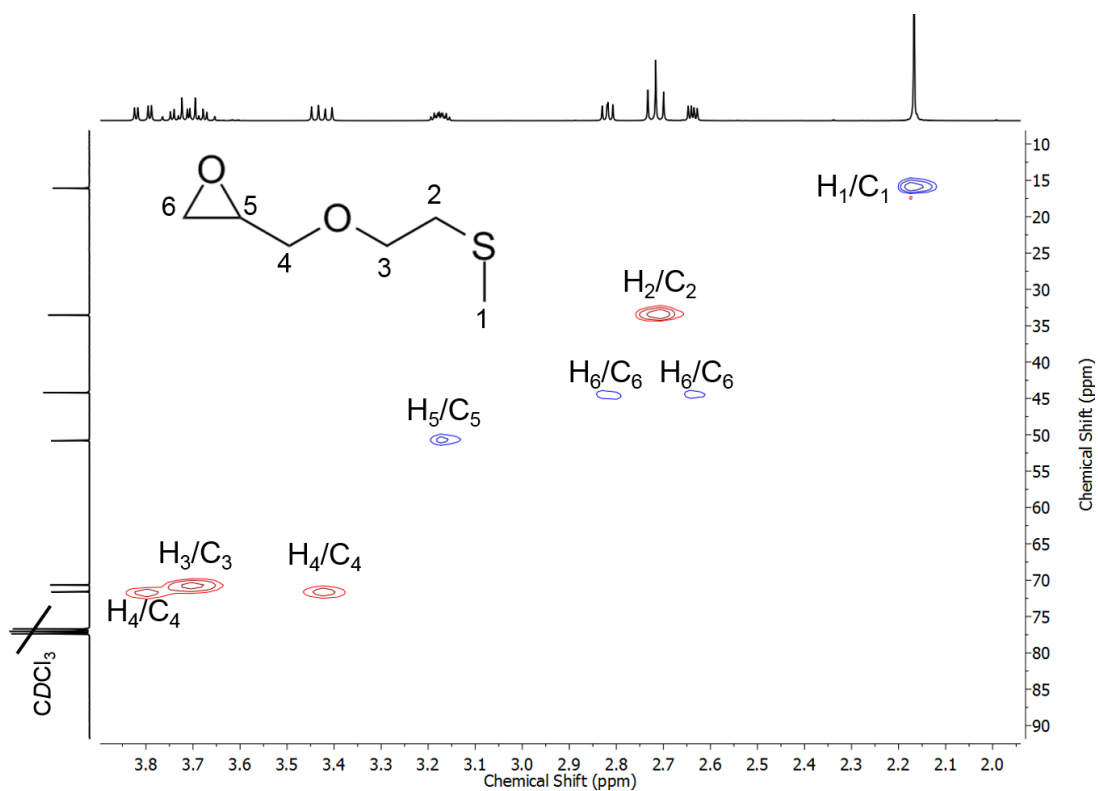
Figure S3. HSQC NMR spectrum (CDCl$_3$) of MTEGE. Phase information is given by coloration of cross peaks (red: methylene, blue: methine).
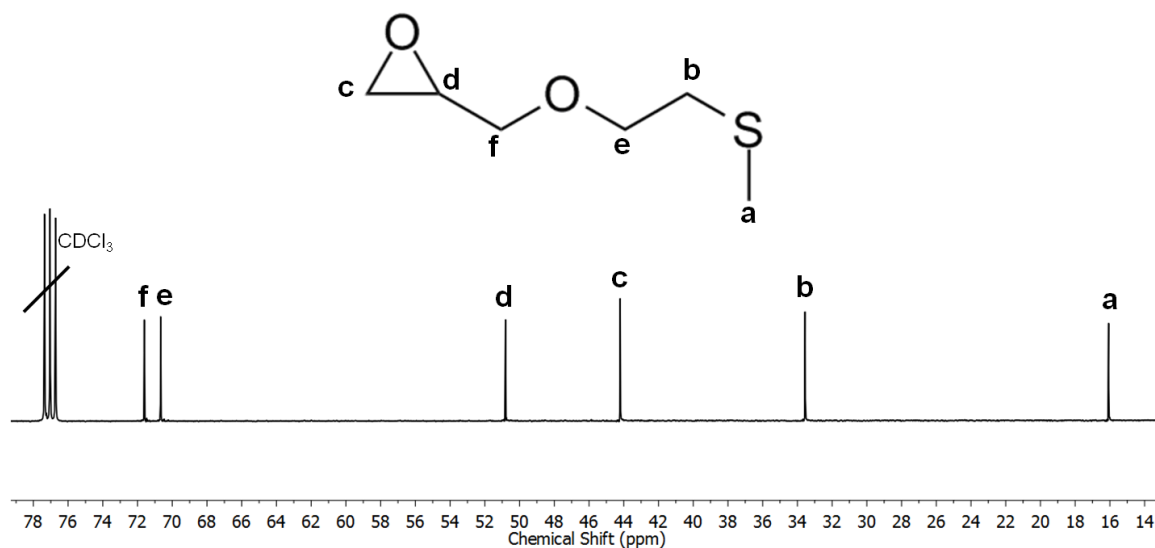
Figure S4. ^{13}C NMR spectrum (100 MHz, CDCl$_3$) of MTEGE.
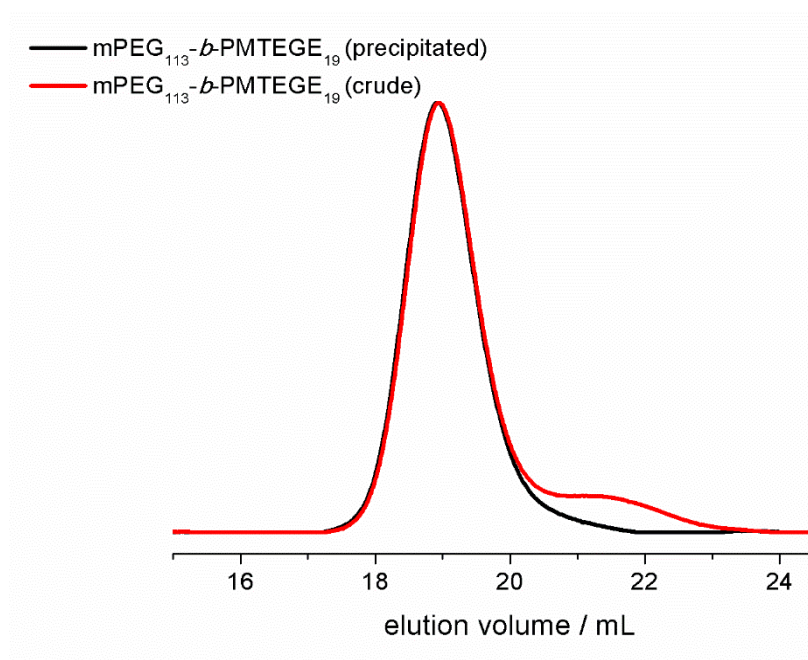
Figure S5. SEC elution traces (DMF, RI signal, PEG standard) of mPEG$_{113}$-*b*-PMTEGE$_{19}$ bevor (red line) and after precipitation (black line). We attribute the shoulder at higher elution time (lower molecular weight) to homopolymer formation, due to proton abstraction and double bond formation.[8]
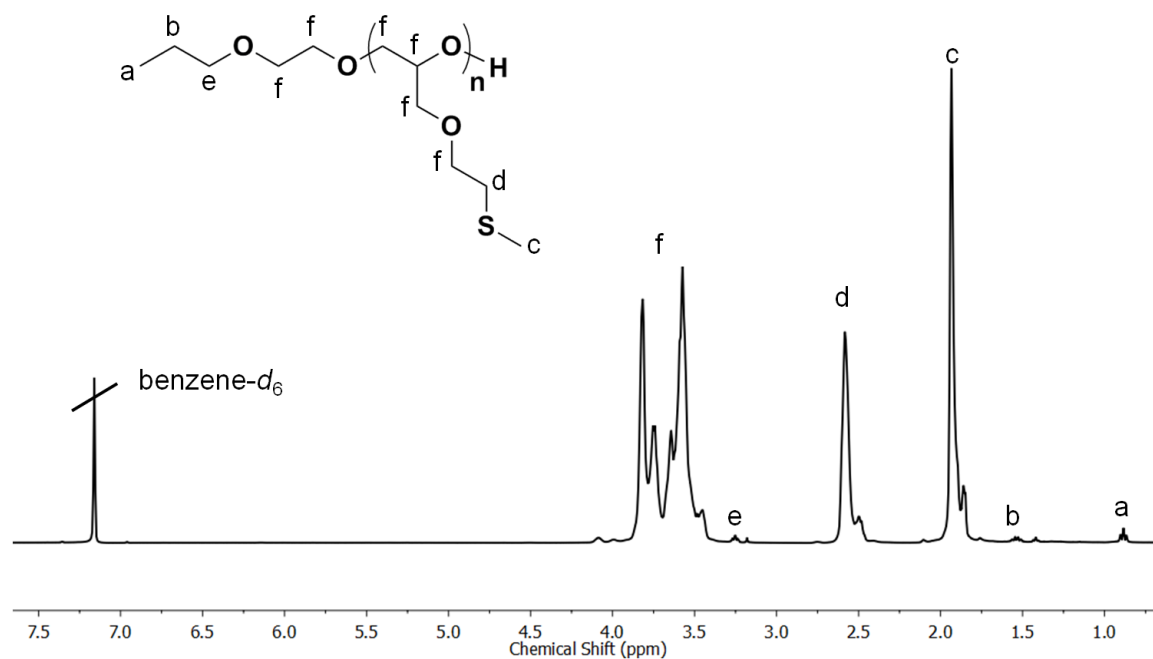
Figure S6. ^{1}H NMR spectrum (400 MHz, benzene-d_6) of PMTEGE homopolymer.
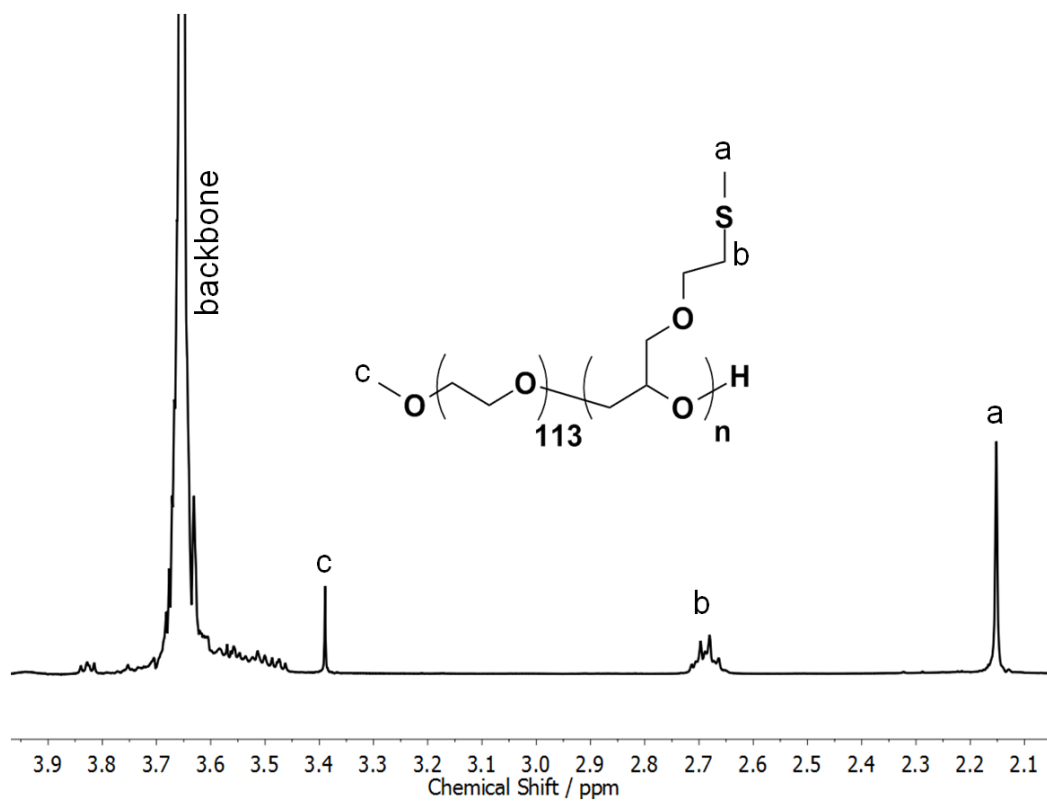
Figure S7. ^{1}H NMR spectrum (400 MHz, CDCl$_3$) of mPEG$_{113}$-b-PMTEGE block copolymer.

107
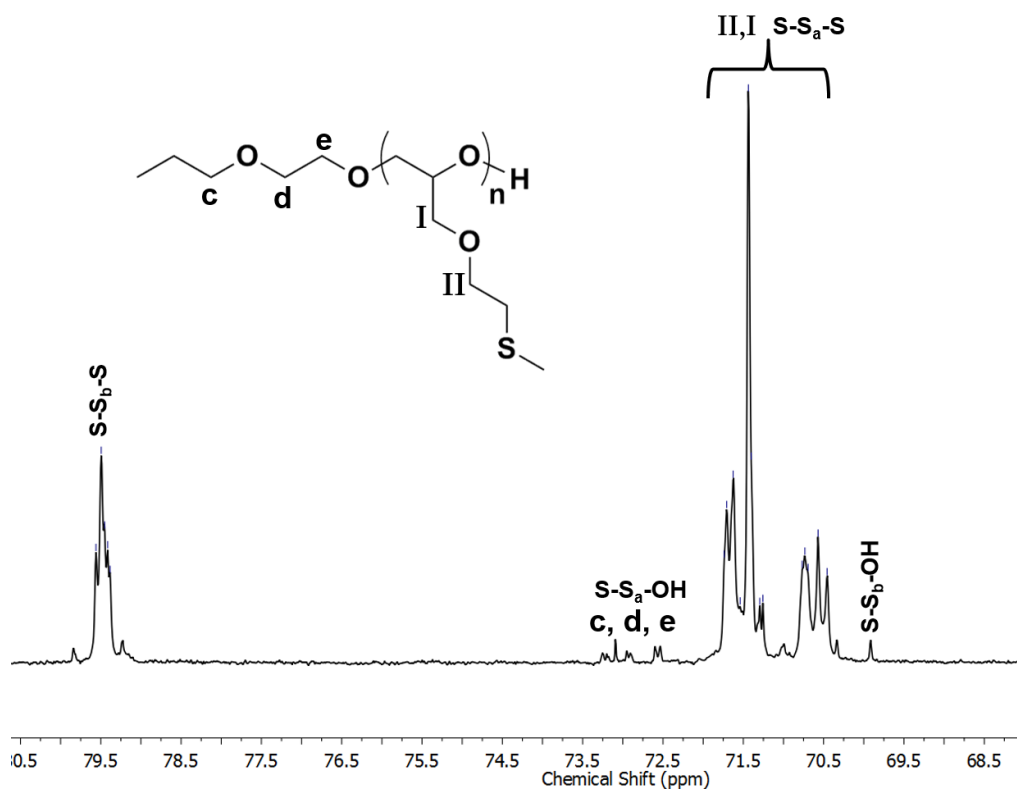
Figure S8. Important section of the ^{13}C NMR spectrum (100 MHz, benzene-d_6) of PMTEGE.

^{1}H NMR kinetic studies

^{1}H NMR spectra were recorded for 14 hours. Monomer consumption was followed by the respective protons at the epoxide ring (ethylene oxide, 4H, 2.62 ppm; MTEGE, 1H, 3.10 ppm) (Figure S9). Note, that the EO protons overlap with the methylene protons of MTEGE (-CH_2SCH$_3$), which have to be subtracted from the signal integral. With proceeding copolymerization, the highlighted proton signals of the epoxide rings decrease and the signal for the polymer backbone (3.4-3.6 ppm) increases. Integration of the highlighted signals allows to determine the exact monomer concentration for each spectrum and the copolymerization can be analyzed as illustrated in Figure 3.
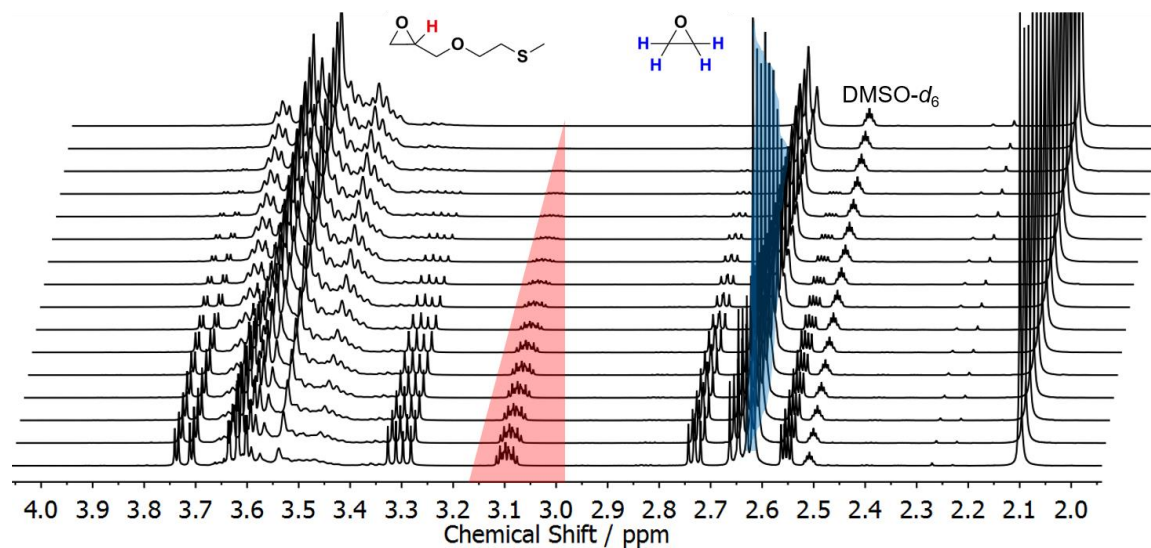
Figure S9. Selection of time-resolved ^{1}H NMR spectra (400 MHz, DMSO-d_6) for the statistical copolymerization of EO with MTEGE (mole fractions: $n_{EO} = 0.585$, $n_{MTEGE} = 0.415$) at 40 °C. The relevant signals are highlighted. Red: single proton of MTEGE (3.10 ppm); blue: protons of EO (2.62 ppm). Note, that the EO protons overlap with the methylene protons of MTEGE (-CH_2SCH$_3$). The shown spectra are a selection of 126 measured spectra, which were recorded in a period of 16 h.
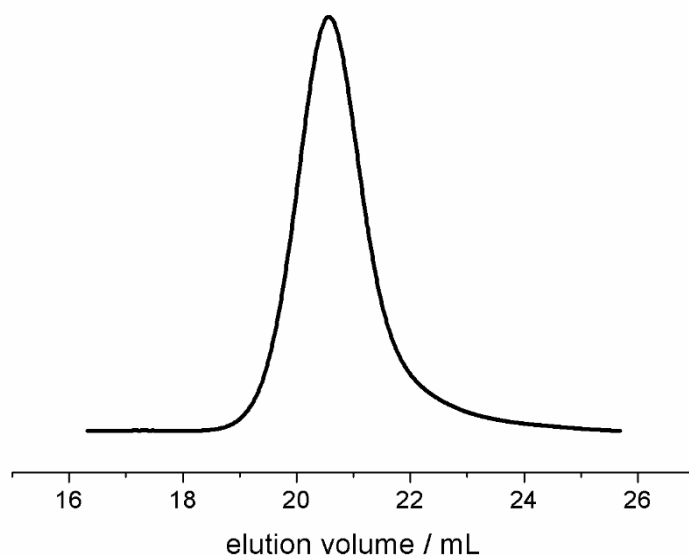
Figure S10. SEC elution trace (DMF, RI signal, PEG standard) of PEG-*ran*-PMTEGE copolymer; copolymerized in a NMR tube to study the reactivity of both monomers. EO/MTEGE (mole fractions: $n_{EO} = 0.585$, $n_{MTEGE} = 0.415$) in DMSO-d_6 at 40 °C. SEC data: $M_n = 2700$ g·mol^{-1}, PDI $= 1.12$.
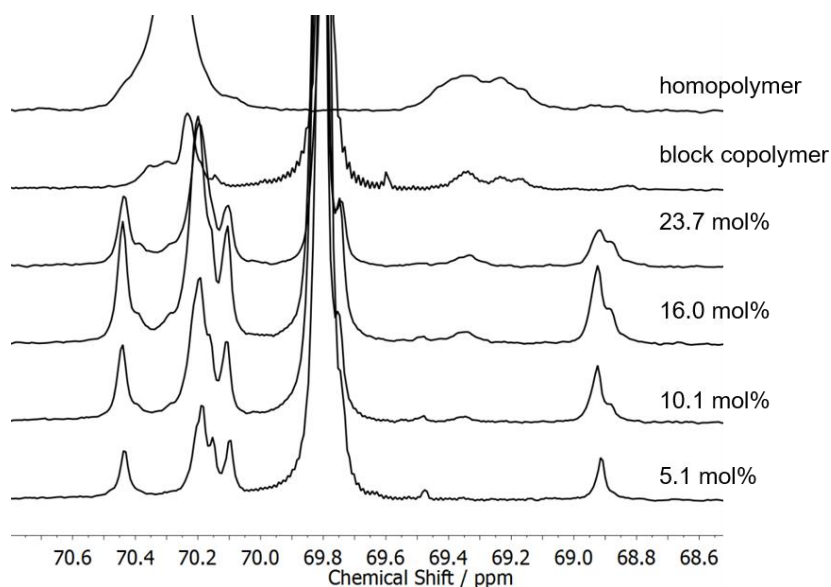
Figure S11. Enlargement of the IG ^{13}C NMR spectra (DMSO-d_6, 100 MHz) of PMTEGE homopolymer, mPEG-*b*-PMTEGE block copolymer and various random PEG-*ran*-PMTEGE copolymers, displaying the characteristic region of EO- and S$_a$-centered triads.
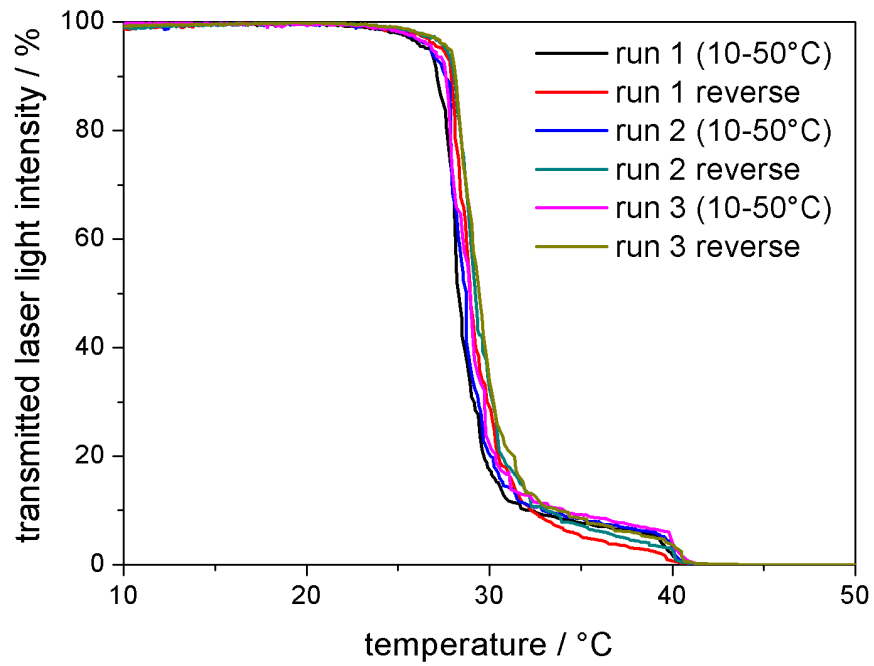
Figure S12. Transmitted laser light intensity versus temperature for PEG-*ran*-PMTEGE with 23.7 mol% MTEGE content (3 heating/cooling cycles).

Light scattering measurements

Table S1. Results of the light scattering experiments (DLS and SLS) and fluorescence spectroscopy of mPEG-*b*-PMTEGE block copolymers and mPEG homopolymer.

mPEG$_{113}$-*b*-PMTEGE$_x$	MTEGE/ mol %	MTEGE/ w %	$R_{h(CH3OH)}$/ nm	$R_{h(H2O)}$/ nm	$\mu_{2(H2O)}$	Z	$(Kc/R)_{q=0}$[*] in CH$_3$OH/ mol·g^{-1}	$(Kc/R)_{q=0}$[*] in H$_2$O/ mol·g^{-1}	CMC[#] (mg·L^{-1})
0	0	0	2.1	2.3					
4	3.4	11	2.1	2.6	-	0.66	6.98·10^{-5}	1.06·10^{-4}	
6	5.0	15	2.3	2.4	-	0.88	7.70·10^{-5}	8.71·10^{-5}	
9	7.4	21	2.3	9.3	0.12	9.6	6.07·10^{-5}	6.29·10^{-6}	100
11	8.9	25	2.5	10.4	0.09	18.0	5.95·10^{-5}	3.30·10^{-6}	30
19	14.4	36	2.5	11.7	<0.05	48.7	5.43·10^{-5}	1.12·10^{-6}	8
26	18.7	44	2.6	14.7	<0.05	109.6	4.44·10^{-5}	4.05·10^{-7}	1.5

[*])c = 1.0 g·L^{-1}; dn/dc = 0.1 mL·g^{-1}; R_g < 10 nm, [#]Calcuated from fluorescence spectroscopy
R_h: hydrodynamic radius, μ_2: normalized second cumulant, Z: aggregation number with Z = $(Kc/R)_{MeOH}$ / $(Kc/R)_{water}$ = M_{app}(water)/ M_{app}(MeOH) with the following assumption: specific refractive index increment dn/dc is identical for MeOH and water as a solvent; dn/dc(PEG) = 0.135 mL·g^{-1}, dn/dc(MTEGE) = 0.22 mL·g^{-1} (calculated).[9]

Dynamic light scattering
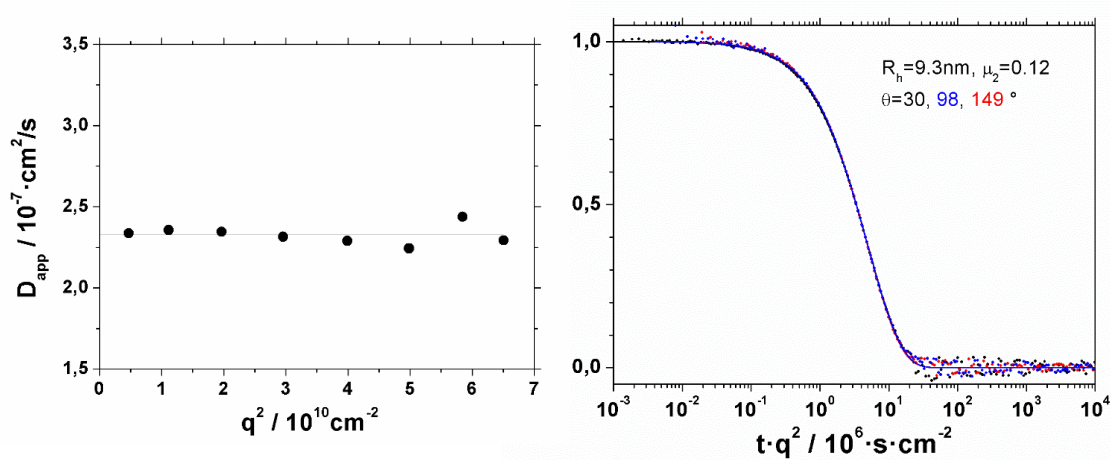
Figure S13. D_{app} versus q^2 for mPEG$_{113}$-*b*-PMTEGE$_9$ in H$_2$O (5mM NaCl) (left) and experimental autocorrelation function (right).
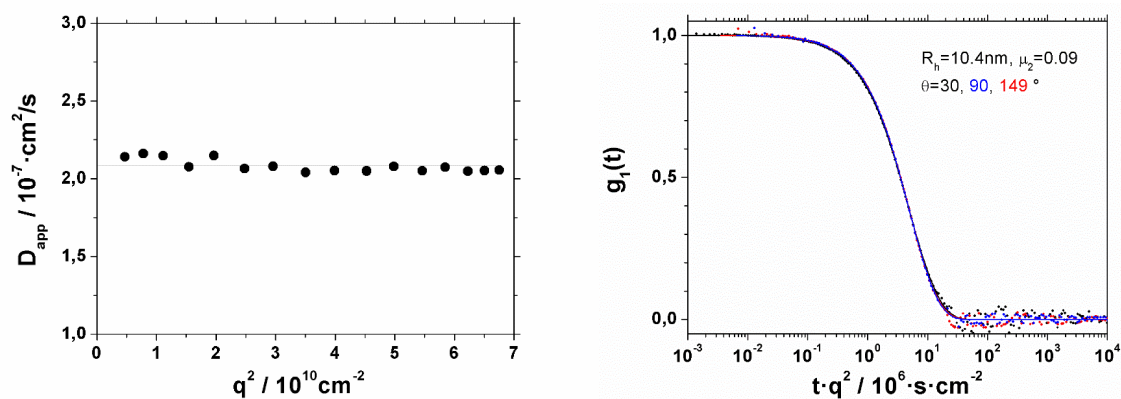
Figure S14. D_{app} versus q^2 for mPEG$_{113}$-*b*-PMTEGE$_{11}$ in H$_2$O (5mM NaCl) (left) and experimental autocorrelation function (right).
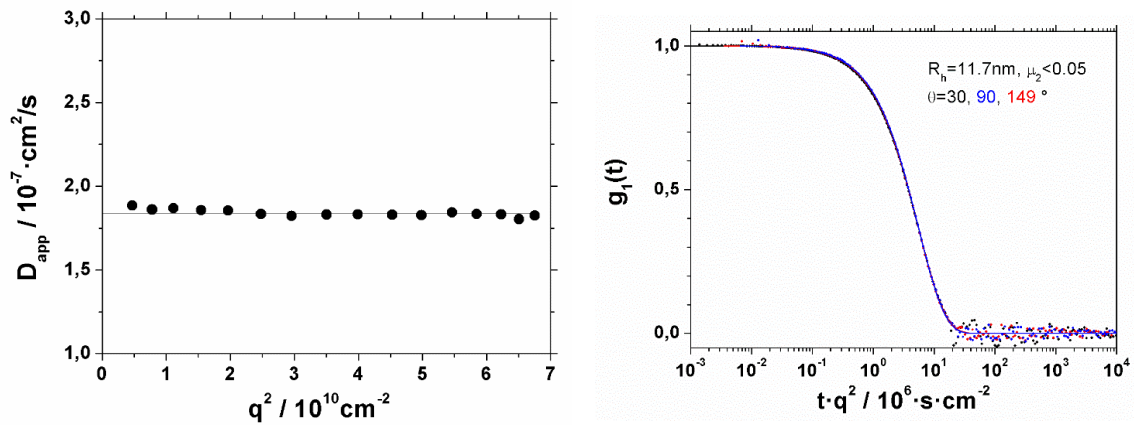
Figure S15. D_{app} versus q^2 for mPEG$_{113}$-*b*-PMTEGE$_{19}$ in H$_2$O (5mM NaCl) (left) and experimental autocorrelation function (right).
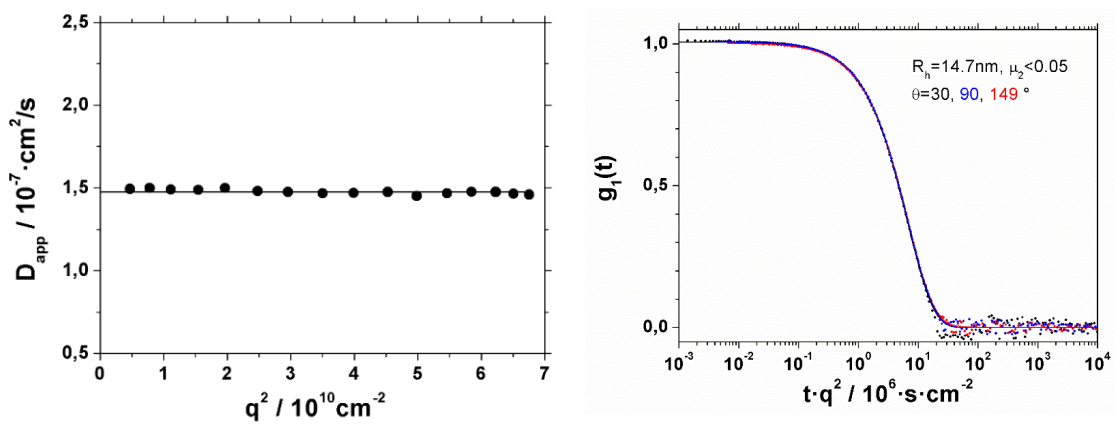
Figure S16. D_{app} versus q^2 for mPEG$_{113}$-*b*-PMTEGE$_{26}$ in H$_2$O (5mM NaCl) (left) and experimental autocorrelation function (right).

Static light scattering

Details/assumptions for data analysis:

1. Contrast factor (dn/dc) for each sample in methanol and water is roughly identical, which holds for PEG within 5% (refractive indices for water and methanol are 1.333 and 1.3288, respectively).

2. Concentration dependency of the scattering intensity is negligible (at a concentration of $c = 1 \text{g} \cdot \text{L}^{-1}$, unimers in methanol are measured at a high dilution limit, giving scattering intensities only twice as large as the pure solvent itself. In contrast, for micelles in aqueous solution, A_2 is expected to diminish, and therefore concentration dependence can also be neglected).

3. To ensure correct analysis, it is important, that concentration dependencies can be neglected; meaning that the concentration (c) has to be significantly higher than the respective critical aggregation concentration (cac, cmc). For mPEG-*b*-PMTEGE with 9 MTEGE units and a CMC of 0.1 $\text{g} \cdot \text{L}^{-1}$, the solution concentration c had to be corrected by the factor c(CMC). For all other block copolymers, the CMC is low enough (≤ 0.03 $\text{g} \cdot \text{L}^{-1}$) and can be neglected (see section *CMC measurements,* Figure S20 and S21 and Table S1).
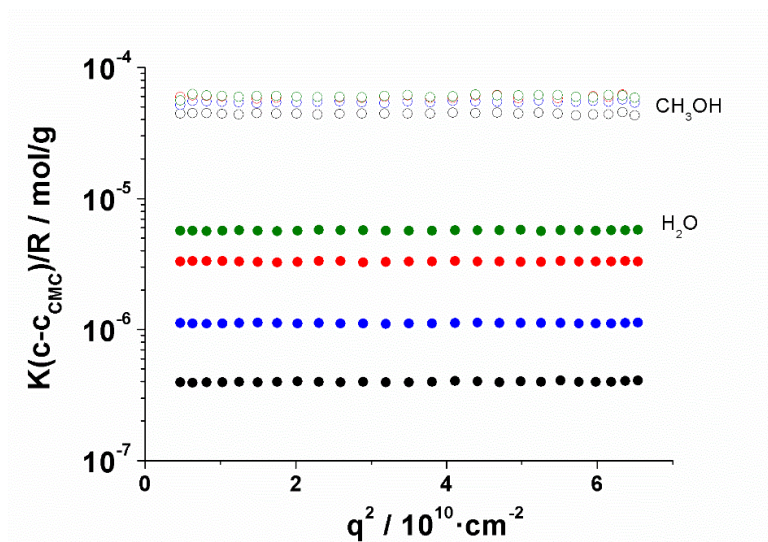
Figure S17. $K(c - c_{CMC})/R$ plotted versus q^2 for mPEG$_{113}$-b-PMTEGE$_n$ block copolymers (with n= 9 (green), 11 (red), 19 (blue), 26 (black) in methanol (hollow spheres) and water (solid spheres). For mPEG$_{113}$-b-PMTEGE$_9$, the solution concentration c was corrected by the CMC c_{CMC} = 0.1 g·L^{-1}. For the other block copolymers with n ≥ 11, the CMC is ≤ 0.03 g·L^{-1} and can be neglected. All (dn/dc) values are set to 0.1 mL·g^{-1}.
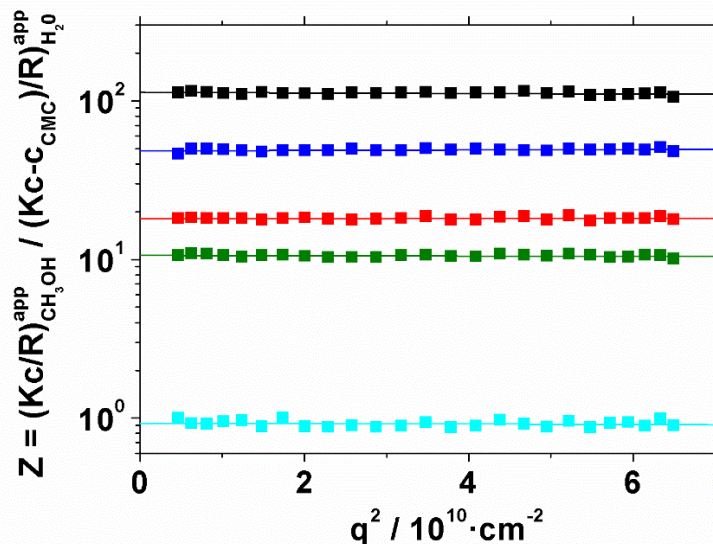
Figure S18. Aggregation number Z ($(Kc/R)^{app}_{CH_3OH}$ / $(Kc - c_{CMC}/R)^{app}_{H_2O}$) plotted versus q^2 for the block copolymers mPEG$_{113}$-b-MTEGE$_n$ (with n= 6 (light blue), 9 (green), 11 (red), 19 (dark blue), 26 (black)). For mPEG$_{113}$-b-PMTEGE$_9$, the solution concentration c was corrected by the CMC c_{CMC} = 0.1 g·L^{-1}. For the other block copolymers with n ≥ 11, the CMC is ≤ 0.03 g·L^{-1} and can be neglected.

Scaling laws developed by Förster et al.[10]

Förster et al. developed a simple theory of block copolymer micelle formation corresponding to the behavior of low molar mass surfactants ending up with two scaling law representations given by equation (1) and (2)

(1) $Z \propto N_B^{-0.8} \cdot N_A^2$

(2) $D \propto Z^{1/5} \cdot N_B^{3/5}$

with Z: aggregation number, N_A block length of core (MTEGE), N_B block length of corona polymer (PEG), D: aggregate dimension = hydrodynamic diameter

with (1) entering (2) equation (3) is obtainable including the corona contribution into constant

(3) $D/2 == R_h \propto N_A^{2/5}$

Including all contributions from the corona as a constant (same PEG for all samples) scaling behavior can be easily checked by plotting Z vs N_A (Figure 6a) and R_h vs N_A (Figure 6b) with double logarithmic scaling, yielding exponents of 2.1 and 0.39 vs. 2 and 0.4 from theory, clearly supporting the micellar assumption.

DLS results for oxidized mPEG-*b*-PMTEGE and DLS kinetic studies of the oxidation process are shown in the section below.
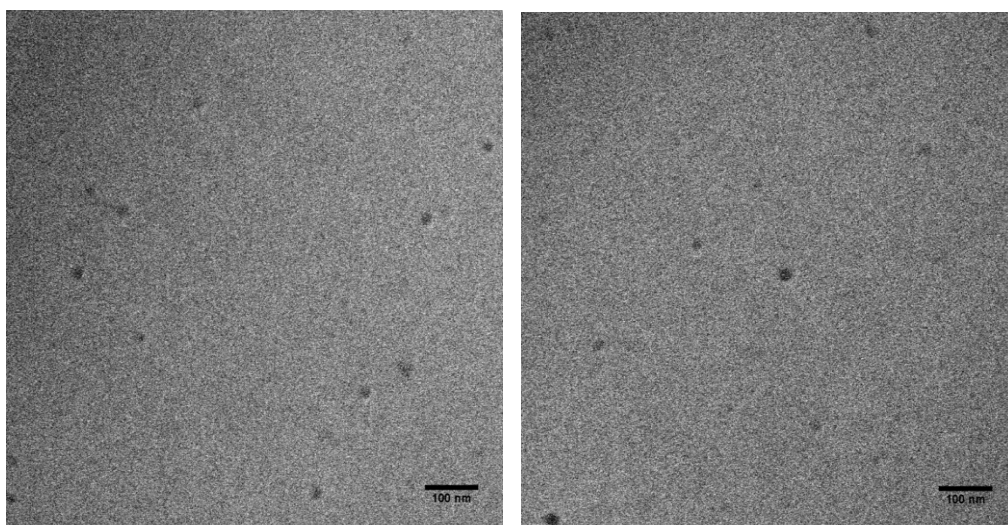
Figure S19. CryoTEM micrographs of mPEG$_{113}$-*b*-PMTEGE$_{19}$ in aqueous solution (1 g·L^{-1}, 5mM NaCl).

CMC measurements

Pyrene was used as a fluorescent probe to determine the CMC of the block copolymers which are still showing self-assembly in water at a concentration of 1 g·L^{-1} (determined by DLS, Table S1). CMCs were calculated by plotting the intensity ratio($I_{ratio} = I_1/I_3$) of the two characteristic vibrational bands of pyrene ($I_1 = 373$ nm, $I_3 = 383.5$ nm, emission spectrum) or the relative intensity versus the concentration of the block copolymer in water.[11] Two examples are depicted in Figures S20 and S21 and one can determine values of 0.1 g·L^{-1} for mPEG$_{113}$-*b*-PMTEGE$_9$ and 0.03 g·L^{-1} for mPEG$_{113}$-*b*-PMTEGE$_{11}$, respectively. The CMC values of all block copolymers are listed in Table S1.
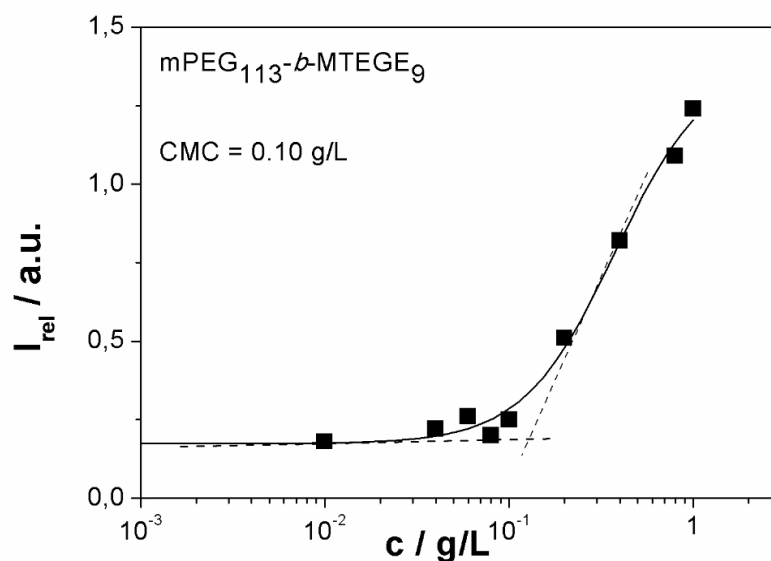
Figure S20. Relative intensity plotted versus concentration for the block copolymer mPEG$_{113}$-*b*-PMTEGE$_9$ with a pyrene concentration of $6 \cdot 10^{-7}$ mol$\cdot$L^{-1}. The CMC was determined to 0.10 g$\cdot$L^{-1}.
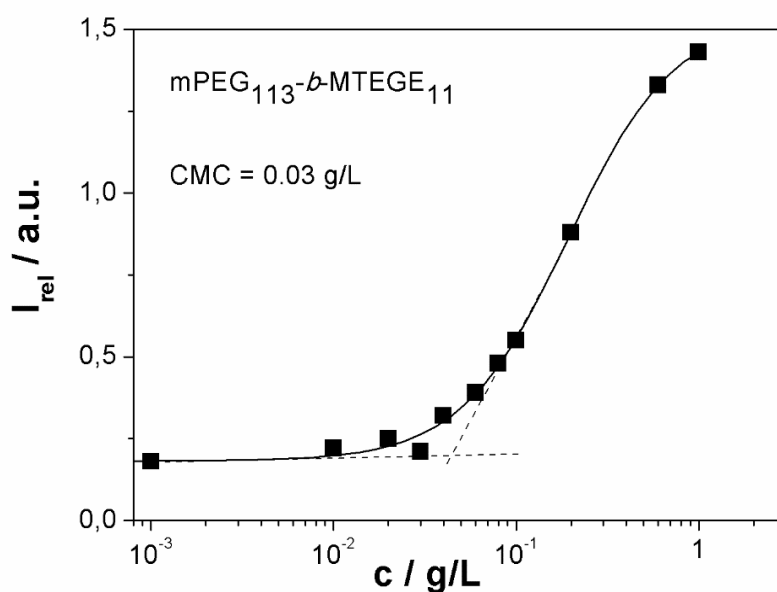
Figure S21. Relative intensity plotted versus concentration for the block copolymer mPEG$_{113}$-*b*-PMTEGE$_{11}$ with a pyrene concentration of $6 \cdot 10^{-7}$ mol$\cdot$L^{-1}. The CMC was determined to 0.03 g$\cdot$L^{-1}.

Oxidation-responsiveness
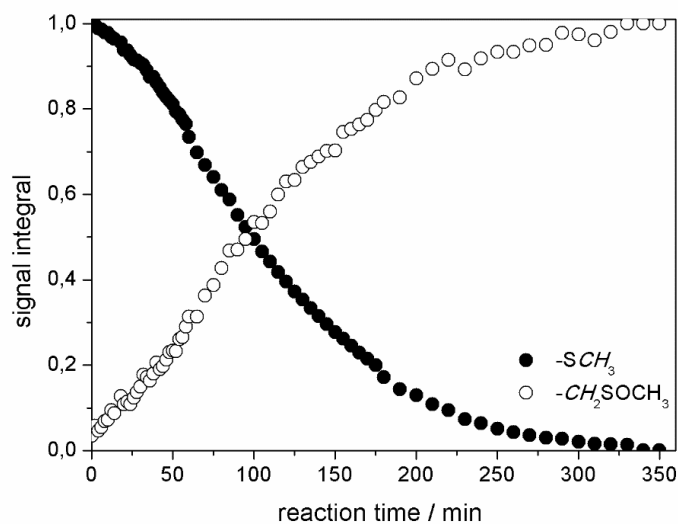
Figure S22. Signal integral of the methyl signal (-SC*H*$_3$) and methylene signal (-C*H*$_2$SOCH$_3$) plotted versus reaction time for the oxidation of mPEG$_{113}$-*b*-PMTEGE$_{26}$ with H$_2$O$_2$ (1wt%) in D$_2$O at 296 K.
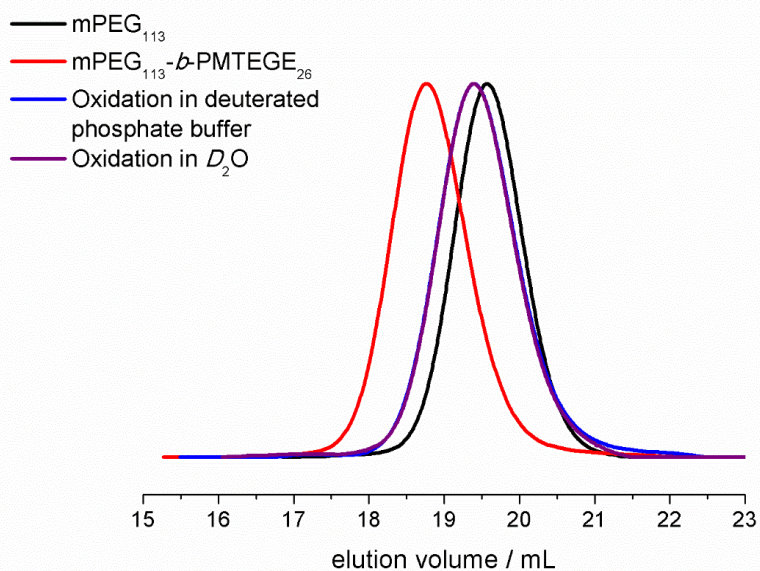
Figure S23. SEC elution traces (DMF, RI signal, PEG standard) of mPEG$_{113}$, mPEG$_{113}$-*b*-PMTEGE$_{26}$ block copolymer and oxidized species (mPEG$_{113}$-*b*-PMSOEGE$_{26}$). The oxidized block copolymers (oxidized in D$_2$O or deuterated buffer) show identical elution traces.

120
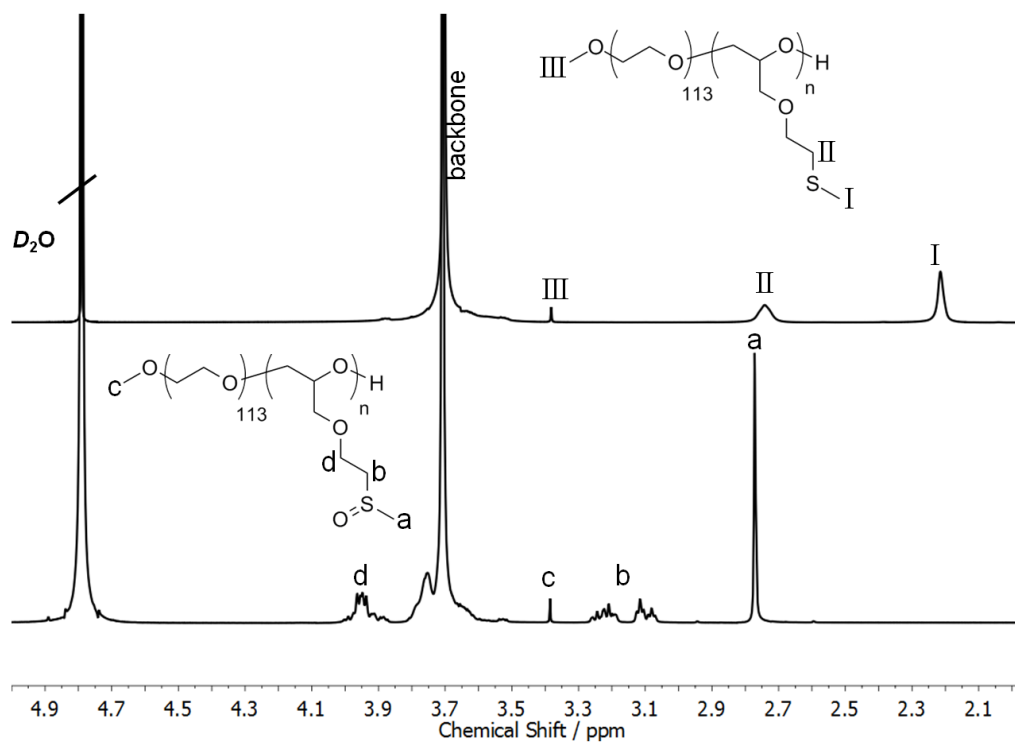
Figure S24. ^{1}H NMR spectra (400 MHz, D$_2$O) of mPEG$_{113}$-*b*-PMTEGE$_{26}$ block copolymer before (top) and after oxidation (bottom) to sulfoxide units.
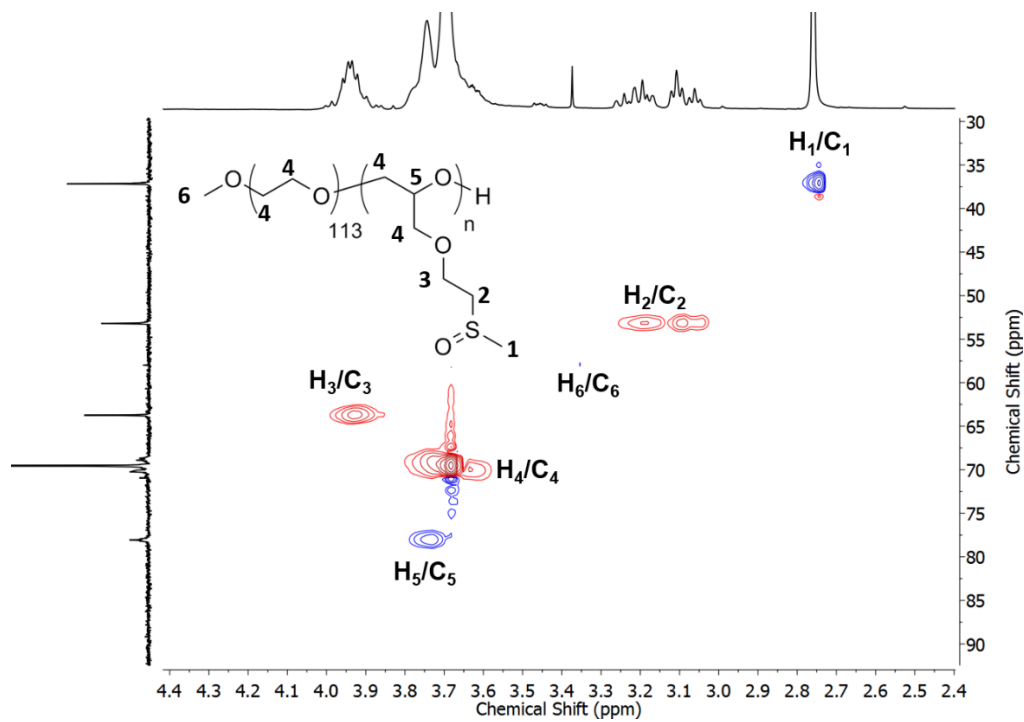
Figure S25. HSQC NMR spectrum (D$_2$O) of oxidized mPEG$_{113}$-*b*-PMTEGE$_{26}$. Sulfone species were not detected.
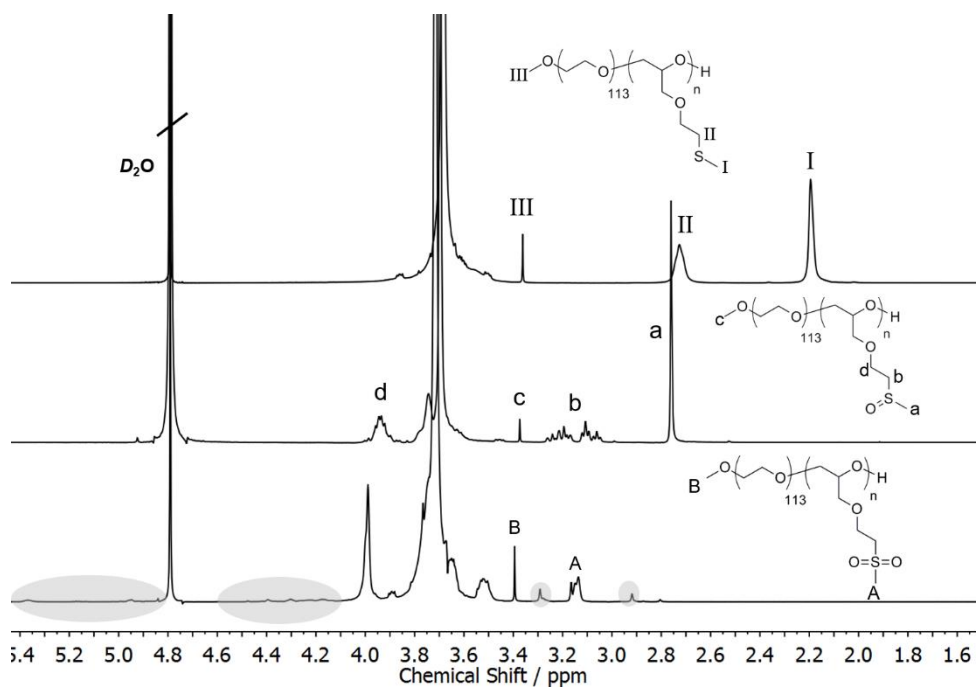
Figure S26. ^{1}H NMR spectra (400 MHz, D_2O) of mPEG-*b*-PMTEGE block copolymer before (top) and after oxidation with H_2O_2 (middle) and NaOCl-solution (bottom).
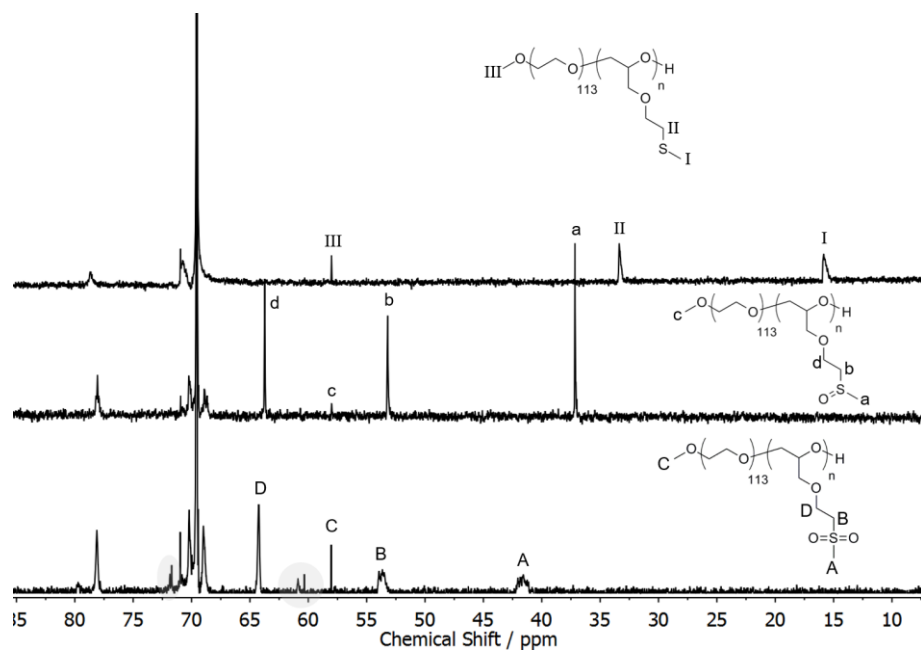
Figure S27. ^{13}C NMR spectra (100 MHz, D_2O) of mPEG-*b*-PMTEGE block copolymer before (top) and after oxidation with H_2O_2 (middle) and NaOCl-solution (bottom).
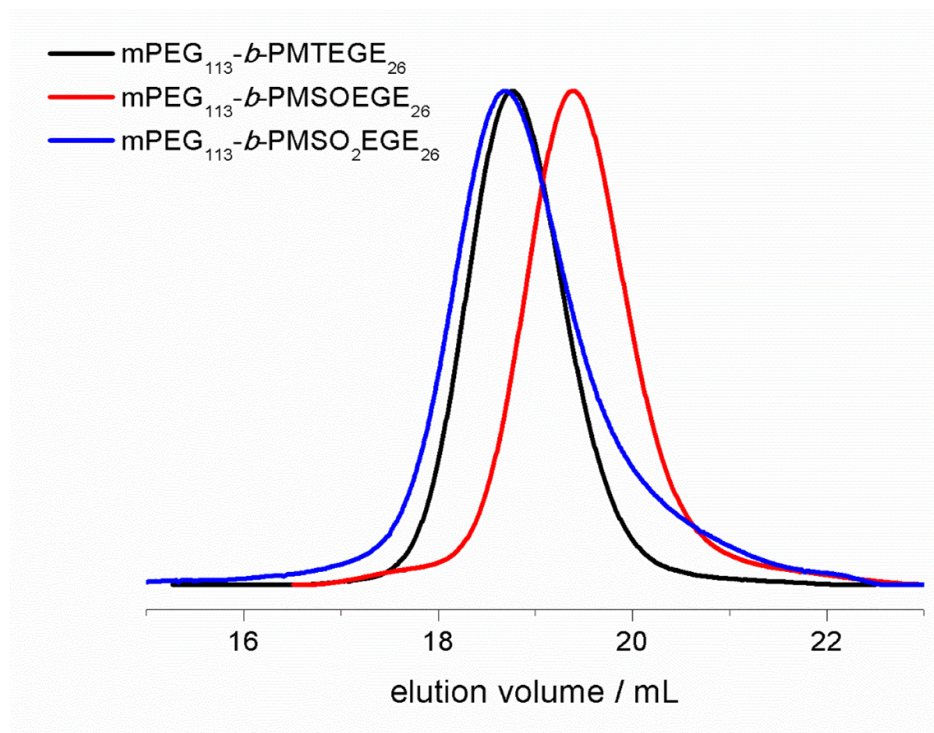
Figure S28. SEC elution traces (DMF, RI signal, PEG standard) of mPEG$_{113}$-*b*-PMTEGE$_{26}$ and the oxidized derivatives mPEG$_{113}$-*b*-PMSOEGE$_{26}$ (oxidized to sulfoxide) and mPEG$_{113}$-*b*-PMSO$_2$EGE$_{26}$ (oxidized to sulfone).
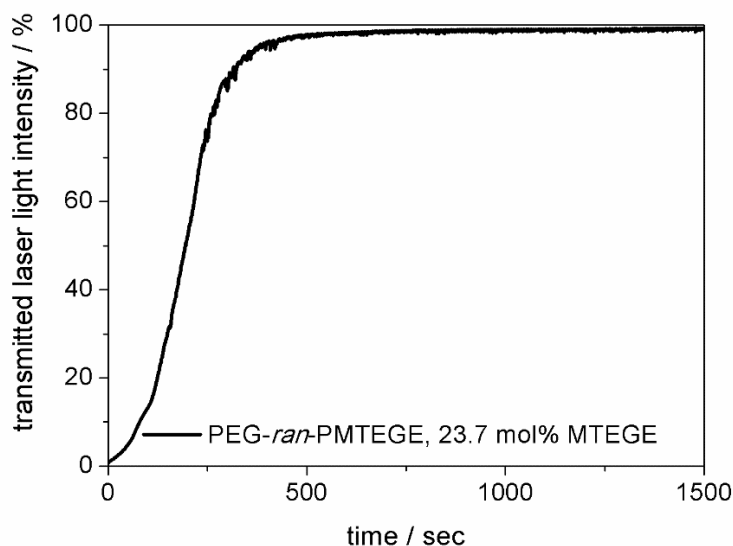
Figure S29. Monitoring the oxidation process of PEG-*ran*-PMTEGE in buffer solution at 37 °C via turbidity measurements. The graph shows the transmitted laser light intensity versus time after addition of H$_2$O$_2$ (1 wt%). A clear solution is detected after about 500 seconds.

Table S2. DLS data of mPEG-*b*-PMTEGE and their oxidized derivatives (mPEG-*b*-PMSOEGE) in water and methanol.

Sample	R_h (CH$_3$OH)/nm	R_h (H$_2$O)/nm
mPEG$_{113}$-*b*-PMTEGE$_{11}$	2.5	10.4
mPEG$_{113}$-*b*-PMSOEGE$_{11}$	2.6	2.6
mPEG$_{113}$-*b*-PMTEGE$_{26}$	2.6	14.7
mPEG$_{113}$-*b*-PMSOEGE$_{26}$	2.4	2.6

R_h: hydrodynamic radius
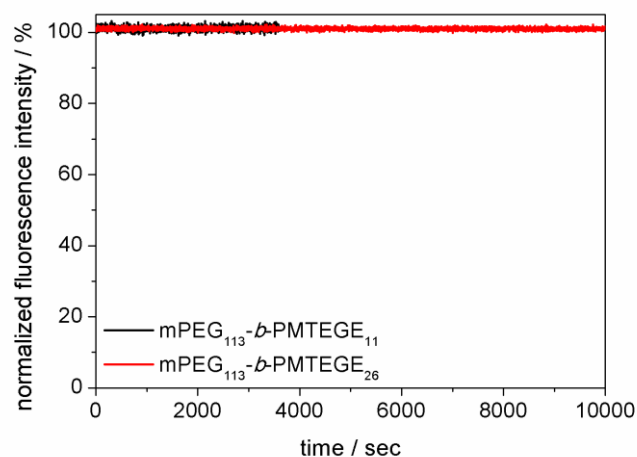
Figure S30. Intensity of fluorescence emission of Nile Red, monitored as a function of time for aqueous block copolymer solutions mPEG$_{113}$-*b*-PMTEGE$_n$ with n=11 and 26, respectively (c = 0.5 g·L^{-1}). Measurements show stability of micelles, when no H$_2$O$_2$ is added. (For oxidative release, see Figure 9, main manuscript).

Post-polymerization modification

1. Alkylation
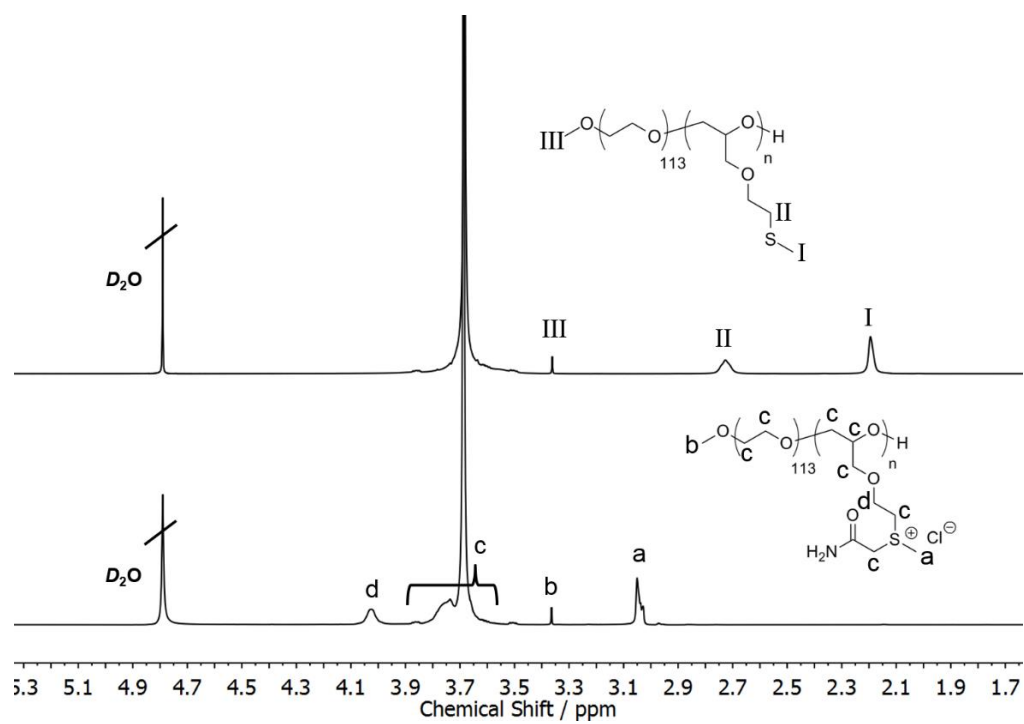
Figure S31. ^{1}H NMR spectra (400 MHz, D$_2$O) of mPEG-*b*-PMTEGE and amide functionalized block copolymer, respectively.
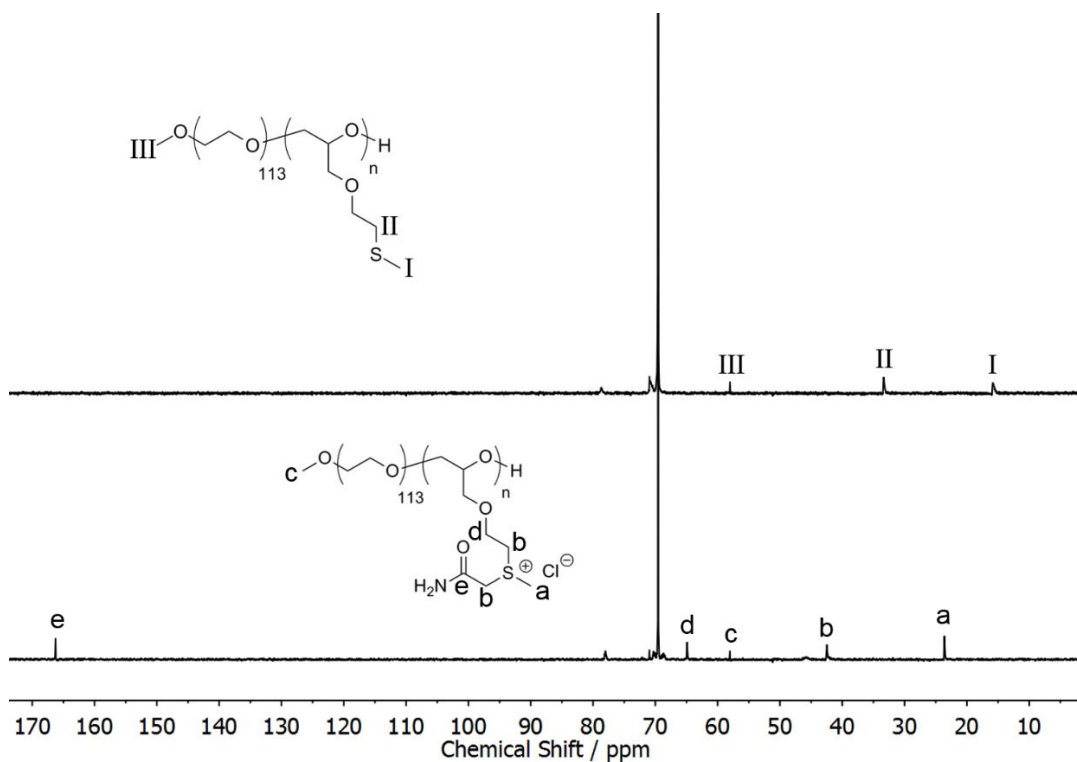
Figure S32. ^{13}C NMR spectra (100 MHz, D$_2$O) of mPEG-*b*-PMTEGE and amide functionalized block copolymer, respectively.
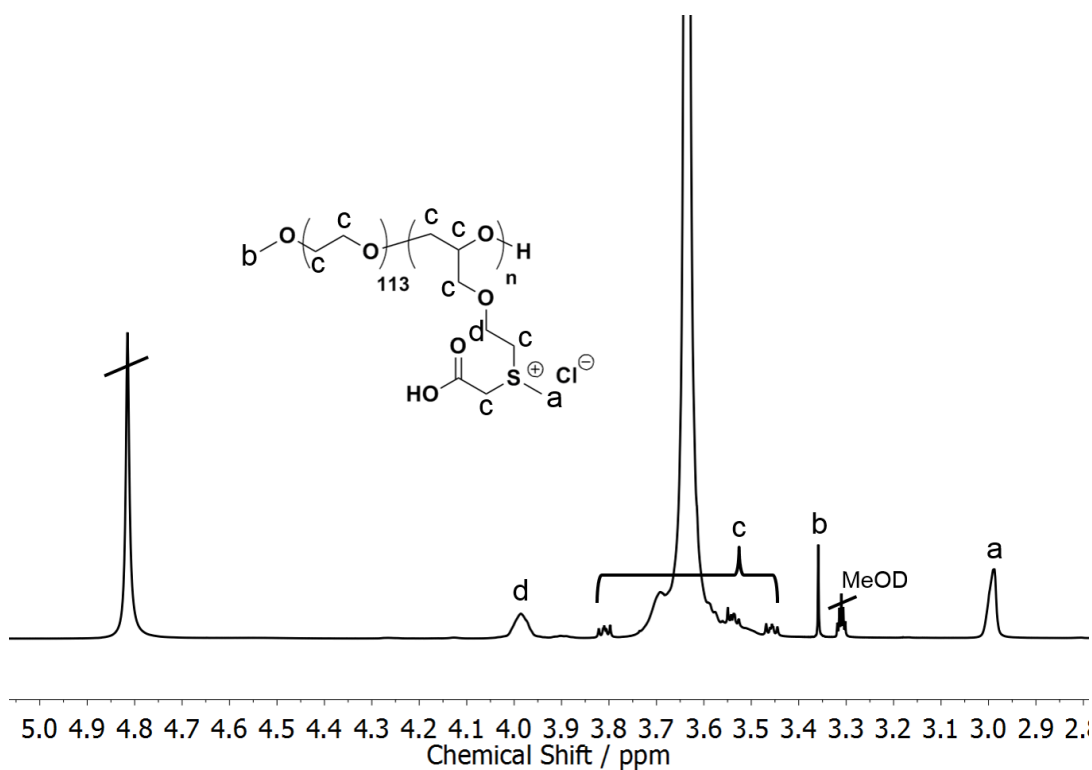
Figure S33. ^{1}H NMR spectra (400 MHz, MeOD) of mPEG-*b*-PMTEGE and carboxyl functionalized block copolymer, respectively.

Table S3. DSC data of alkylated block copolymers.

Sample	functionalization	T_g (°C)	T_m (°C)	ΔH (J·g^{-1})
mPEG$_{113}$-*b*-PMTEGE$_6$	---	-58	55	142
mPEG$_{113}$-*b*-PMTEGE$_6$	bromoacetic acid	-34	56	124
mPEG$_{113}$-*b*-PMTEGE$_6$	bromoacetamide	-42	54	111
mPEG$_{113}$-*b*-PMTEGE$_{19}$	---	-59	53	93
mPEG$_{113}$-*b*-PMTEGE$_{19}$	bromoacetic acid	-16	54	91
mPEG$_{113}$-*b*-PMTEGE$_{19}$	bromoacetamide	-22	50	76

T_g: glass transition temperature; T_m: melting temperature; ΔH: melting enthalpy.
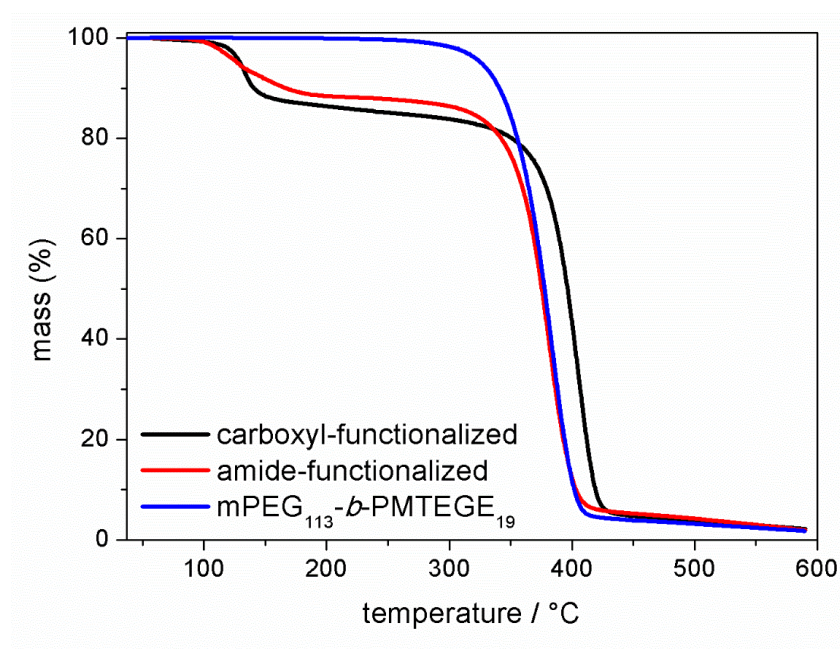
Figure S34. TGA traces of mPEG-*b*-PMTEGE$_{19}$ (blue) and respective alkylated derivatives.

2. Alkoxylation
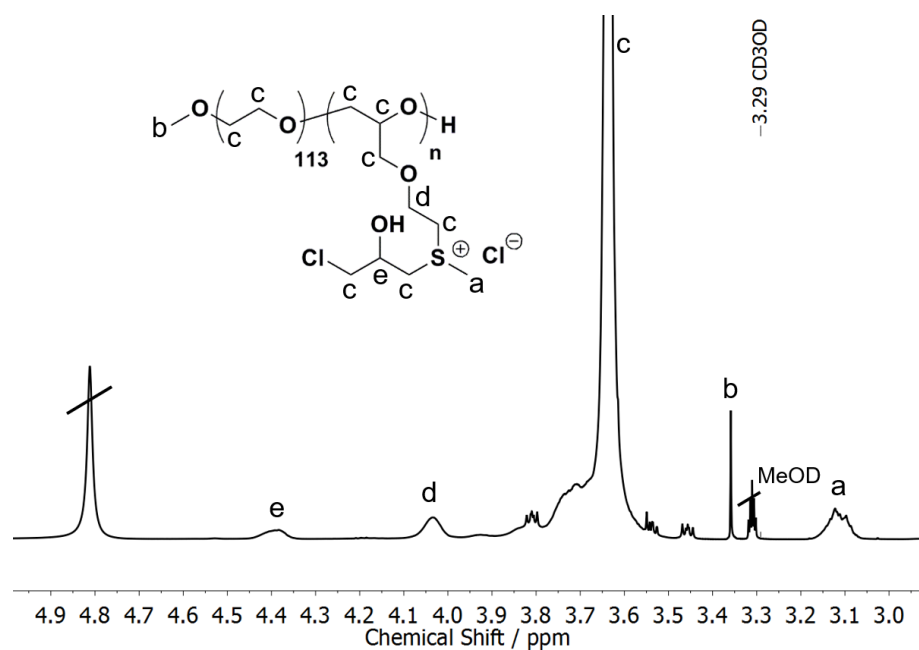
Figure S35. ^{1}H NMR (400 MHz, MeOD) of mPEG-*b*-PMTEGE functionalized with epichlorohydrin (ECH).
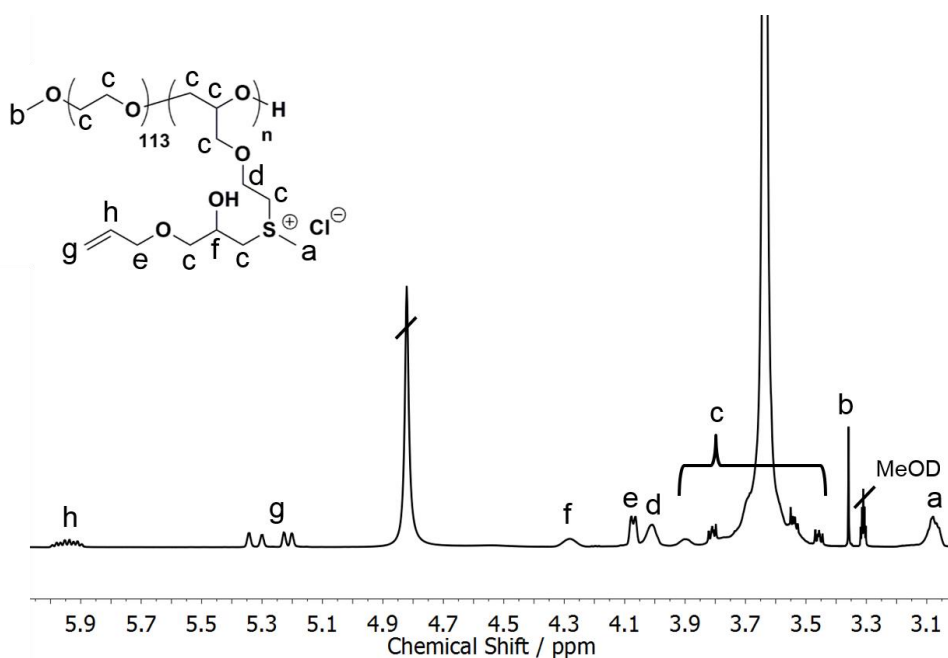
Figure S36. ^{1}H NMR (400 MHz, MeOD) of mPEG-*b*-PMTEGE functionalized with allyl glycidyl ether (AGE).
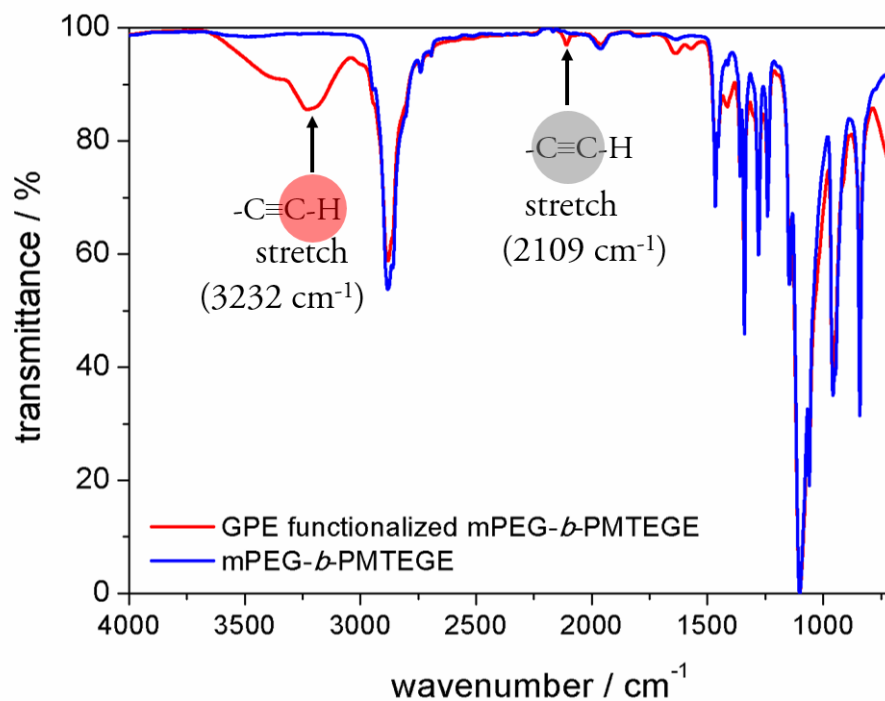
Figure S37. FT-IR spectra of mPEG-*b*-PMTEGE (blue) and GPE functionalized mPEG-*b*-PMTEGE (red).
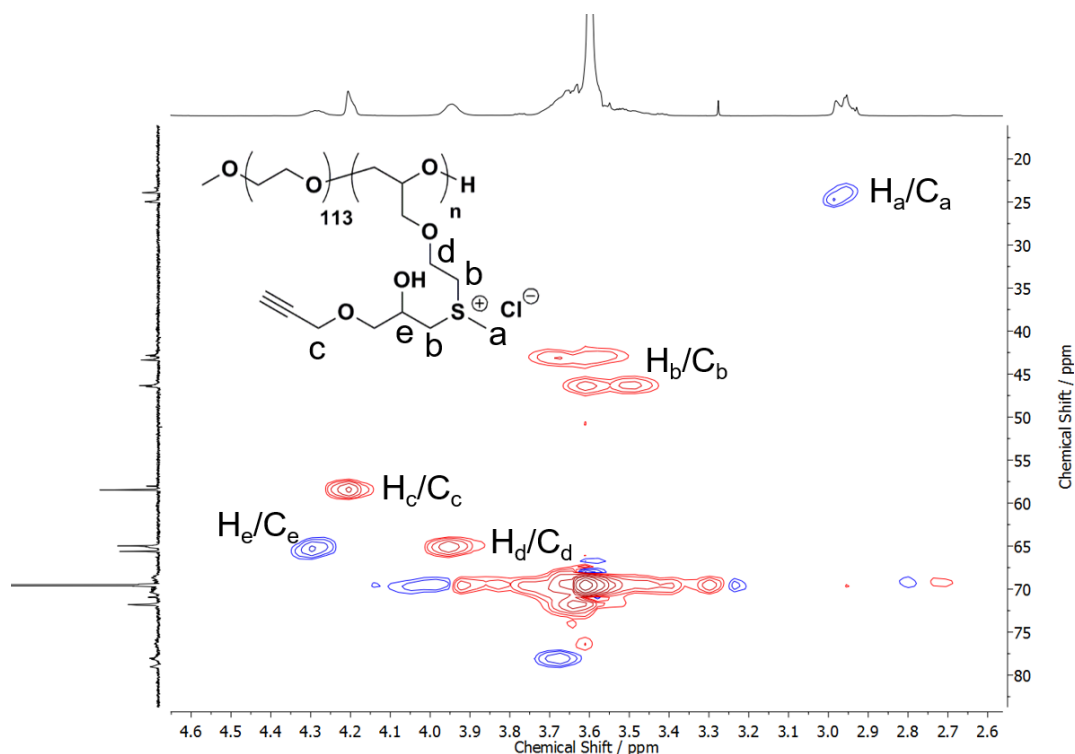
Figure S38. HSQC NMR (D$_2$O) of mPEG-*b*-PMTEGE functionalized with glycidyl propargyl ether (GPE). Phase information is given by coloration of cross peaks (red: methylene, blue: methine).

References

[1] d'Arcy, R.; Siani, A.; Lallana, E.; Tirelli, N. *Macromolecules.* **2015**, *48*, 8108–8120.

[2] Wu, W.-X.; Yang, X.-L.; Liu, B.-Y.; Deng, Q.-F.;Xun, M.-M.;Wang, N.;Yu, X.-Q. *RSC Adv.* **2016**, *6*, 11870–11879.

[3] Obermeier, B.; Frey, H. *Bioconjugate Chem.* **2011**, *22*, 436–444.

[4] Herzberger, J.; Kurzbach, D.; Werre, M.; Fischer, K.; Hinderberger, D.; Frey, H. *Macromolecules.* **2014**, *47*, 7679–7690.

[5] Covington, A. K.; Paabo, M.; Robinson, R. A.; Bates, R.G. *Anal. Chem.* **1968**, *40*, 700–706.

[6] Kramer, J. R.; Deming, T. J. *Biomacromolecules.* **2012**, *13*, 1719–1723.

[7] Gharakhanian, E. G. Deming, T. J. *Biomacromolecules.* **2015**, *16*, 1802–1806.

[8] Hans, M.; Keul, H.; Moeller, M. *Polymer.* **2009**, *50*, 1103–1108.

[9] Krevelen, D. W. van, *Properties of polymers: Their correlation with chemical structure, their numerical estimation and prediction from additive group contributions*, 2nd edition, Amsterdam, Elsevier. **1976**, p.222.

[10] Förster, S.; Zisenis, M.; Wenz, E.; Antonietti, M. *J. Chem. Phys.* **1996**, *104*, 9956–9970.

[11] Wilhelm, M.; Zhao, C. L.; Wang, Y.; Xu, R.; Winnik, M. A.;Mura, J. L.; Riess, G.; Croucher, M. D. *Macromolecules.* **1991**, *24*, 1033–1040.

3 Amino-functional

Poly(ethylene glycol) Copolymers

3.1 Glycidyl Amine Comonomers and Polyethers with Pendant Amino Groups

The following section is a contribution by the author of this thesis that was published as a part of *Chemical Reviews*, **2016**, *116*, 2170−2243 (Special Issue: Frontiers in Macromolecular and Supramolecular Science), titled: "Polymerization of Ethylene Oxide, Propylene Oxide, and Other Alkylene Oxides: Synthesis, Novel Polymer Architectures, and Bioconjugation".

Only very recently, multi amino-functional polyethers are increasingly studied, since they are promising candidates for a variety of applications ranging from surface modification to biomedicine.[1] While primary amino groups permit conjugation of biomolecules or low molecular weight compounds,[2–5] the value of tertiary amino groups should not be underestimated. Ordinary tertiary amine moieties permit triggering the polyethers' properties via the pH-value.[6–8] Further, their substituents can be modified, leading to tailor-made polyethers.[8–10] In addition, if a positively charged polyelectrolyte is desired, the tertiary amino groups can be simply quaternized. These cationic PEG-based polyethers may be promising polymer vectors for gene delivery.[11]

Different strategies can be pursued to introduce multiple amino functionalities at the polyether backbone. In general, different synthetic methods have to be applied for primary or tertiary amino groups. In this section, we focus on synthetic approaches based on post-polymerization reactions and direct copolymerization of EO/PO with glycidyl amine derivatives. A detailed overview of multiple amino-functional polyethers, including poly(meth)acrylate derivatives and their potential applications, was given by Wilms et al.[1]

3.1.1 Introduction of Primary Amino Groups

Obviously, the direct polymerization of epoxide monomers bearing primary amino groups is not feasible, since the nucleophilic nitrogen atom attacks the epoxide ring. Hence, post-polymerization strategies or the introduction of suitable protecting groups for amine-functional epoxide monomers are necessary. Koyama et al. were the first to obtain PEG with multiple primary amino moieties via copolymerization of ethylene oxide (EO) with allyl glycidyl ether (AGE) followed by thiol-ene coupling of 2-aminoethanethiol to the allylic groups of AGE (Scheme 1).[4] The authors further demonstrated the suitability of these amino-functional PEGs for DNA complexation.[12]
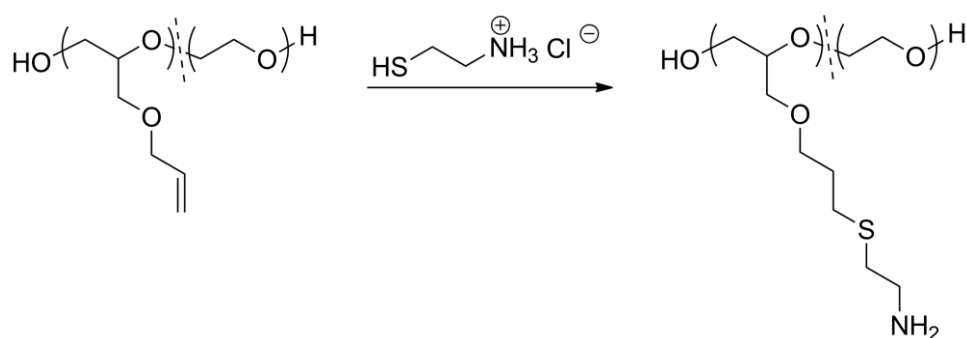
Scheme 1. Modification of PEG-*co*-PAGE copolymers with 2-aminoethanethiol.[4]

Another post-polymerization approach was reported by Li and Chau who synthesized a library of multifunctional PEGs by modifying the hydroxyl groups of *lin*PG-*co*-PEO.[13] The glycerol units were reacted with phthalimide potassium, followed by conversion into primary amines. However, this route shows a limited overall conversion for amino functions of only 34 %. Alternatively, Möller and coworkers applied the "activated monomer mechanism" to homo- and copolymerize epichlorohydrin (ECH) with ethoxyethyl glycidyl ether (EEGE), followed by the conversion of the chloride atoms of

ECH to azide groups. Eventually, the glycidyl azide segments were reduced, using triphenylphosphine to obtain primary amines at the polyether backbone (Scheme 2).[2]
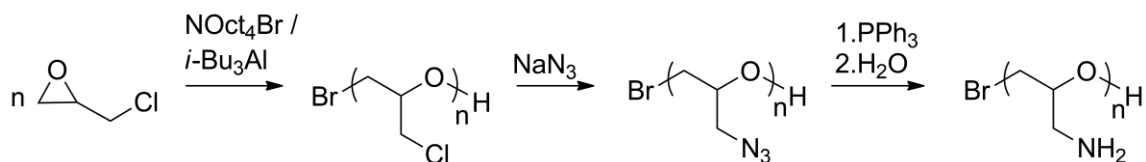
Scheme 2. Synthesis scheme for poly(glycidyl amine) (PGA) starting from epichlorohydrin (ECH).[2]

In general, postpolymerization modifications are often time-consuming and can suffer from a limited overall conversion. To overcome this problem, glycidyl amine derivatives bearing suitable protecting groups can be used as monomeric building blocks for the direct copolymerization with EO or PO. Our group introduced a protected glycidyl amine, dibenzyl amino glycidol (DBAG) (Scheme 3, left), accessible by a simple two-step transformation of epichlorohydrin with dibenzyl amine.[14] Copolymerization of 2-15 mol% of DBAG with EO yielded copolymers with a tapered microstructure containing EO rich segments near the initiator and DBAG rich segments near the chain terminus. Liberation of the primary amino groups was performed by catalytic hydrogenation, albeit requiring prolonged reaction times (1-8 days, Pearlman's catalyst). Only limited copolymer yields of 30-50 % were achieved due to interaction of the primary amino groups with the carbon-supported catalyst. In particular, this strong adhesion precluded the recovery of block copolymers. This strategy was improved by introduction of *N,N*-diallyl glycidyl amine (DAGA) (Scheme 3, middle).[15] This approach enabled the polymerization of well-defined gradient copolymers as well as block copolymers with DAGA ratios of 2.5-24 mol%. Furthermore, the time for cleavage of the protecting group was reduced from 1-8 days to several hours and yields were increased from 30-50 % to 85 % copolymer. In a following publication, the suitability of this comonomer as anchor for dye functionalization or for

134

drug conjugation was demonstrated.[16] In 2015, Satoh and Kakuchi et al. re-investigated the homopolymerization of DBAG to obtain poly(glycidyl amine) after release of the benzyl groups.[9] While the degree of polymerization of PDBAG was limited in the common AROP,[14] well-defined homopolymers with molecular weights ranging from 6200 $g \cdot mol^{-1}$ to 50,400 $g \cdot mol^{-1}$ and PDIs of 1.09-1.22 were obtained with the strong phosphazene base t-BuP$_4$ as a deprotonation agent. The authors attribute the high molecular weights to the mild reaction conditions (room temperature), which suppress weight limiting transfer reactions.[17] Cleavage of the benzyl protecting groups was performed under hydrogen atmosphere in a tetrahydrofuran/methanol mixture with palladium on carbon (Pd/C) as catalyst. This hydrogenation method allowed reducing the reaction time from 8 to 4 days. In contrast to the previous method described by Frey and coworkers,[14] no yield limiting interaction of the released amino groups with the catalyst surface was observed. Successful release of the amino groups was also reflected by the thermal properties of the homopolymers, whereas PDBAG reveals a T_g of 4.6 °C, the primary amino groups of PGA cause an extremely high T_g of 68.2 °C.

Further, polyethers with combined amino- and hydroxyl functionalities were obtained by copolymerization of DBAG with benzylglycidylether (BnGE) in a sequential and statistical manner and subsequent deprotection to PGA-linPG copolymers. This strategy is superior to previous results by Möller et al,[2] since only two reaction steps were required. Monomer reactivity ratios were determined to $r_{DBAG} = 0.8$ and $r_{BGE} = 3.24$, indicating a strong compositional drift, with DBAG rich segments near the terminus. From these results and other reported reactivity ratios of glycidyl amine derivatives, an overall lower reactivity of glycidyl amines compared to glycidyl ethers can be concluded.[6,8,14,15,18] Additionally, the authors described the homopolymerization of the optically pure (S)-DBAG, yielding amino-functional polyethers with an exclusive isotactic sterosequence.[9]

N,N-Dibenzyl amino glycidol
(DBAG)

N,N-Dially glycidyl amine
(DAGA)

Epicyanohydrin
(EPICH)
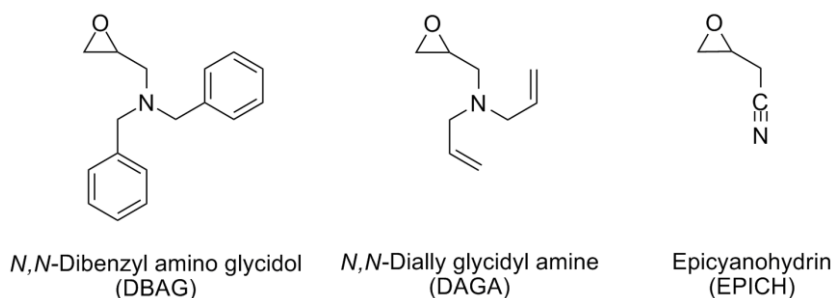
Scheme 3. Suitable monomers to obtain PEG with primary amino functionalities. *N,N*-Dibenzyl amino glycidol (DBAG),[14] *N,N*-Diallyl glycidyl amine (DAGA)[15] and epicyanohydrin (EPICH).[19]

Epicyanohydrin (EPICH) (Scheme 3, right) is a suitable alternative to the introduced protected glycidyl amine derivatives. This monomer allows the synthesis of amino-functional PEG by simple hydrogenation of the nitrile-group. In contrast to the glycidyl amine derivatives, EPICH cannot be polymerized by conventional AROP.[20, 21] Recently, our group demonstrated the successful incorporation of 4-16 mol% EPICH into PEG by the "activated monomer" method. However, the nitrile group is a strong electron withdrawing functional group and supports the transfer to monomer reaction described in the Introduction (Chapter 1.3.1) of this thesis, resulting in unsaturated chain ends.[19]

3.1.2 Secondary Amino Groups

Inspired by DBAG, Satoh and Kakuchi et al. very recently introduced a glycidyl amine derivative bearing only one cleavable substituent: *N*-benzyl-*N*-methylglycidylamine (BMGA) (Scheme 4).[9] Secondary amino-groups are obtained, after polymerization and subsequent cleavage of the benzyl-protecting group. The authors described homo-, block- as well as statistical (co)polymers of BMGA and DBAG, utilizing the phosphazene base *t*-BuP₄ as deprotonation agent and BuOH as initiator. Investigations on the monomer

incorporation revealed similar reactivity ratios for DBAG ($r_{DBAG} = 0.91$) and BMGA ($r_{BMGA} = 0.98$), resulting in a random monomer distribution.
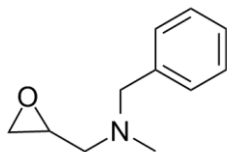
N-benzyl-*N*-methylglycidylamine
(BMGA)

Scheme 4. Suitable glycidyl amine derivative for secondary amino groups along the polyether backbone. *N*-benzyl-*N*-methylglycidylamine (BMGA).[9]

3.1.3 Tertiary Amino Groups

In contrast to primary amino groups, tertiary amino moieties do not interfere in the polymerization of epoxides as long as the nitrogen atom is shielded by its substituents. Considering alkyl glycidyl amine derivatives, the most simple one, *N,N*-dimethyl glycidyl amine, cannot be polymerized in a controlled manner, since the methyl groups do not sufficiently shield the nucleophilic nitrogen atom, which results in polycondensation reactions caused by the nucleophilic attack of the nitrogen at the epoxide ring.[22] In an interesting work Dhal and co-workers presented an indirect route to poly(*N,N*-dimethyl glycidyl amine) by nucleophilic substitution of poly(epichlorohydrin) (PECH) with dimethylamine.[23] The authors proposed that these polymers may show high potential as bile acid sequestrant after quaternization of the amino moieties with hydrophobic alkyl halides.

Expanding the alkyl chain of glycidyl amines from methyl to ethyl already permits successful controlled polymerization due to effective shielding of the nitrogen atom by the ethyl substituents. In this context, Ponomarenko et al. long ago already described the

copolymerization of PO and *N,N*-diethyl glycidyl amine (DEGA) (see Scheme 5) and calculated the copolymerization parameters using the Fineman-Ross equation, resulting in $r_{PO}=1.90$ and $r_{DEGA}=0.30$.[18] However, no further characterization of the resulting polymers was reported.

Reuss et al. introcuced the copolymerization of DEGA with EO. Well-definded tapered and block copolymer structures were obtained with DEGA ratios up to 29 mol%.[6] The block copolymers were shown to be suitable as dual reducing and capping agent for gold nanoparticle formation. Furthermore, these structures act as a precursor for cationic polyelectrolytes, simply obtained by quaternization of the amino moieties with methyl iodide. Most interesting, PEG-*co*-PDEGA copolymers showed temperature and pH-responsive behavior in aqueous solution, similar to the structurally related poly(*N,N*-dialkylaminoethyl methacrylates).[24] To elucidate the temperature-induced inverse phase transition, the authors measured the occurrence of nanoaggregates by continuous wave electron paramagnetic resonance (CW-EPR) spectroscopy and compared it to the macroscopic cloud points. Interestingly, stable nano-aggregates were formed long before macroscopic changes were detectable.[7,25] Following this strategy, Frey and coworkers expanded the library of alkyl glycidyl amines and synthesized derivatives with longer alkyl chains, *N,N*-di(*n*-butyl) glycidyl amine (DButGA), *N,N*-di(*n*-hexyl) glycidyl amine (DHexGA), *N,N*-di(*n*-octyl) glycidyl amine (DOctGA) (Scheme 5).[8] The authors investigated the influence of the alkyl chain length on the relative reactivity in the copolymerization with EO and the copolymers' thermal behavior in aqueous solution. Interestingly, *real-time* ^{1}H NMR kinetic studies showed no dependence of the relative reactivity on the alkyl chain length. All copolymers showed lower relative reactivity than EO, resulting in r-parameters of $r_{EO}=1.84$, $r_{ButGA}=0.49$; $r_{EO}=1.78$, $r_{OctGA}=0.42$.[8] These results document the formation of gradient structures with increasing glycidyl amine segments towards the chain end.

138

A highly hydrophobic glycidyl amine derivative, glycidyl-didodecylamine (GDDA), was introduced by Rangelov and Tsvetanov (Scheme 5).[26] However, to date, successful polymerizationof GDDA has not been achieved.
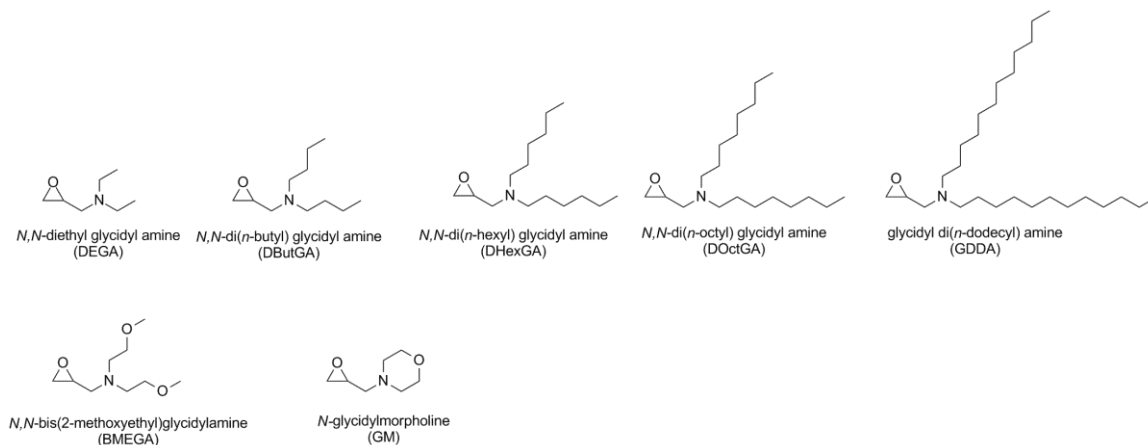
Scheme 5. Glycidyl amine derivatives based on tertiary amines. *N,N*-Diethyl glycidyl amine (DEGA),[6] *N,N*-di(*n*-butyl) glycidyl amine (DButGA),[8] *N,N*-di(*n*-hexyl) glycidyl amine (DHexGA),[8] *N,N*-di(*n*-octyl) glycidyl amine (DOctGA),[8] glycidyl di(*n*-dodecyl) amine (GDDA),[26] *N,N*-bis(2-methoxyethyl)glycidylamine (BMEGA)[9] and *N*-glycidylmorpholine (GM).[9]

As mentioned before, 2015, Satoh and co-workers presented more hydrophilic tertiary glycidyl amine derivates, *N,N*-bis(2-methoxyethyl)glycidylamine (BMEGA) and *N*-glycidylmorpholine (GM) (Scheme 5, bottom).[9] Unlike their hydrophobic counterparts, BMEGA and GM can be successfully homopolymerized. The authors report water-soluble polymers with degrees of polymerizations up to 200 and narrow PDI (< 1.18).

3.1.4 Other Polyether Derivatives Bearing Nitrogen Moieties

In 2009, Long and co-workers presented two imidazole-substituted epoxides, 1-tritylimidazole-2-epoxide and 1-tritylimidazole-4-epoxide (Scheme 6).[27] The trityl-protecting group allowed for polymerization by conventional AROP with *tert*-butoxide as

an initiator and facile removal by treatment with trifluoroacetic acid, yielding water-soluble homopolymers with degrees of polymerization up to 90. The polymers showed a buffering range within the pH ranges of 3 and 6.5 and are candidates for electroactive devices or biological complexation for nucleic acid binding. The strategy also offers access to polyether-based polymeric ionic liquids (PIL) with polar polyether backbone.

1-tritylimidazole-2-epoxide   1-tritylimidazole-4-epoxide   Tr =
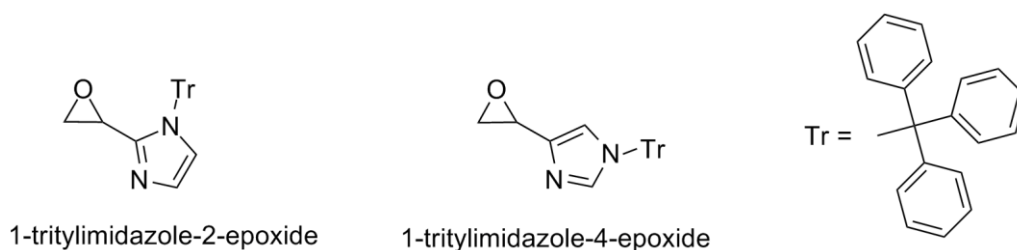
Scheme 6. Imidazole-substituted epoxides. 1-tritylimidazole-2-epoxide and 1-tritylimi-dazole-4-epoxide.[27]

Recently, Baker and co-workers reported poly(ionic liquids) (PILs) based on imidazolium ionic liquids grafted onto PEG.[28] The authors modified poly(epichorohydrin) with 1-butylimidazole, followed by an anion exchange with lithium bis(trifluoromethanesulfonyl)imide (LiTFSI) to obtain a polyether based PIL (Scheme 7). The described homopolymers showed a conductivity of around 10^{-3} S·cm^{-1} at 90 °C, which dropped to around 10^{-5} to 10^{-6} S·cm^{-1} at 30 °C, which is not sufficient for practical use.[29] This approach was improved by cationic copolymerization of 2-((2-(2-(2-methoxyethoxy)ethoxy)ethoxy)methyl)oxirane with epichlorohydrin, followed by modification of the ECH units. Copolymers with a 1:1 ratio of the mentioned monomers showed an improved conductivity of 10^{-4} S·cm^{-1} compared to the described homopolymers.[30]

140
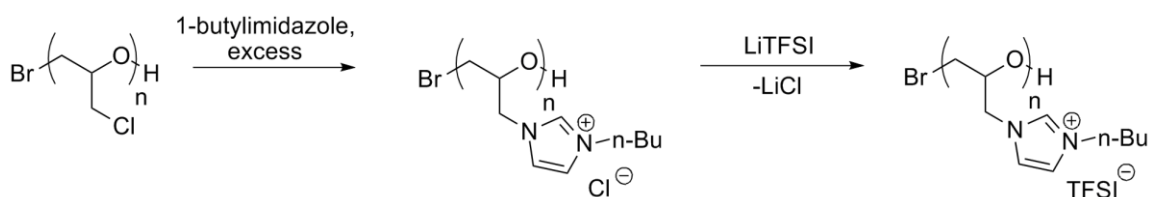
Scheme 7. Postpolymerization modification of PECH to obtain a polyether based PIL.[28]

Hawker and co-workers demonstrated the use of another imidazole derivative, histamine, for pH-responsive hydrogels. PAGE-*b*-PEO-*b*-PAGE triblock copolymers were modified with thiol-functional histamine units by thiol-ene-click chemistry.[31] A clear gel to sol transition was reported upon lowering the pH from 7 to 6.6, rendering this material suitable for drug delivery applications with pH as an active trigger.

Starting from PEG-*b*-PAGE copolymers, in 2005 Ulbrich and coworkers showed the introduction of multiple hydrazide functionalities at PEG. The allyl group of the AGE units were reacted with methyl sulfanyl acetate *via* click chemistry, followed by transformation of the methyl ester to the hydrazide with hydrazine hydrate (Scheme 8).[32] The hydrazide functionality reacts specifically with aldehydes, forming reversible hydrazone linkages under ambient conditions. This concept is particularly interesting for drug delivery based on aldehyde-containing drugs, such as doxorubicin or for glyco-targeting.[33, 34] Further, Sokolovskaya et al. applied the high reactivity of the hydrazide group to form acid-labile PEG-based hydrogels, suitable for controlled release applications.[35]
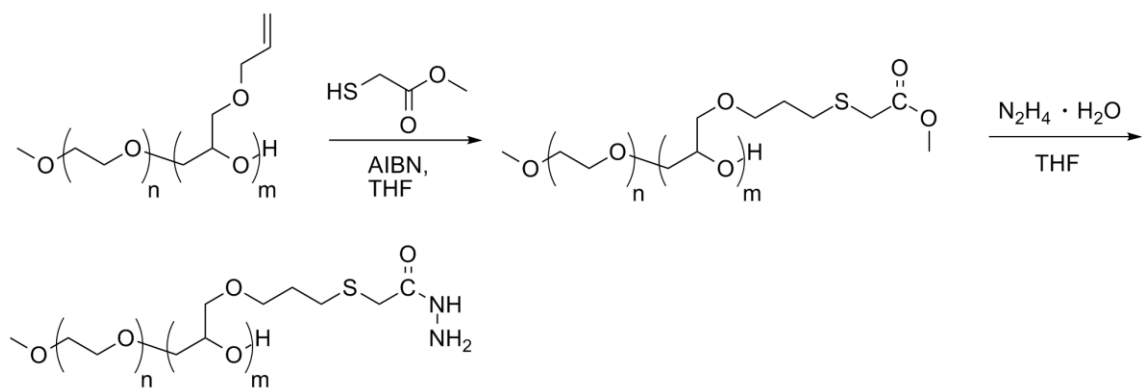
Scheme 8. Introduction of hydrazide functions into the polyether backbone.[32]

3.1.5 References

[1] Wilms, V. S.; Frey, H., Amino-functional Polyethers: Smart Materials for Applications in Solution and on Surfaces, *Polym. Int.* **2013**, *62*, 849–859.

[2] Meyer, J.; Keul, H.; Möller, M., Poly(glycidyl amine) and Copolymers with Glycidol and Glycidyl Amine Repeating Units: Synthesis and Characterization, *Macromolecules.* **2011**, *44*, 4082–4091.

[3] M.S. Thompson; T.P. Vadala; M.L. Vadala; Y. Lin; J.S. Riffle, Synthesis and Applications of Heterobifunctional Poly(ethylene oxide) Oligomers, *Polymer.* **2008**, *49*, 345–373.

[4] Koyama, Y.; Umehara, M.; Mizuno, A.; Itaba, M.; Yasukouchi, T.; Natsume, K.; Suginaka, A.; Watanabe, K., Synthesis of Novel Poly(ethylene glycol) Derivatives Having Pendant Amino Groups and Aggregating Behavior of Its Mixture with Fatty Acid in Water, *Bioconjugate Chem.* **1996**, *7*, 298–301.

[5] Obermeier, B.; Frey, H., Poly(ethylene glycol-*co*-allyl glycidyl ether)s: A PEG-Based Modular Synthetic Platform for Multiple Bioconjugation, *Bioconjugate Chem.* **2011**, *22*, 436–444.

[6] Reuss, V. S.; Werre, M.; Frey, H., Thermoresponsive Copolymers of Ethylene Oxide and *N,N*-Diethyl Glycidyl Amine: Polyether Polyelectrolytes and PEGylated Gold Nanoparticle Formation, *Macromol. Rapid Commun.* **2012**, *33*, 1556–1561.

[7] Kurzbach, D.; Wilms, V. S.; Frey, H.; Hinderberger, D., Impact of Amino-Functionalization on the Response of Poly(ethylene glycol) (PEG) to External Stimuli, *ACS Macro Lett.* **2013**, *2*, 128–131.

[8] Herzberger, J.; Kurzbach, D.; Werre, M.; Fischer, K.; Hinderberger, D.; Frey, H., Stimuli-Responsive Tertiary Amine Functional PEGs Based on *N,N*-Dialkylglycidylamines, *Macromolecules.* **2014**, *47*, 7679–7690.

[9] Isono, T.; Asai, S.; Satoh, Y.; Takaoka, T.; Tajima, K.; Kakuchi, T.; Satoh, T., Controlled/Living Ring-Opening Polymerization of Glycidylamine Derivatives Using *t*-Bu-P$_4$/Alcohol Initiating System Leading to Polyethers with Pendant Primary, Secondary, and Tertiary Amino Groups, *Macromolecules.* **2015**, *48*, 3217–3229.

[10] Lee, A.; Lundberg, P.; Klinger, D.; Lee, B. F.; Hawker, C. J.; Lynd, N. A., Physiologically relevant, pH-Responsive PEG-based Block and Statistical Copolymers with *N,N*-Diisopropylamine units, *Polym. Chem.* **2013**, 5735–5742.

[11]   Xu, F.; Yang, W., Polymer Vectors via Controlled/living Radical Polymerization for Gene Delivery, *Prog. Polym. Sci.* **2011**, *36*, 1099–1131.

[12]   Yoshikawa, K.; Yoshikawa, Y.; Koyama, Y.; Kanbe, T., Highly Effective Compaction of Long Duplex DNA Induced by Polyethylene Glycol with Pendant Amino Groups, *J. Am. Chem. Soc.* **1997**, *119*, 6473–6477.

[13]   Li, Z.; Chau, Y., Synthesis of Linear Polyether Polyol Derivatives as New Materials for Bioconjugation, *Bioconjugate Chem.* **2009**, *20*, 780–789.

[14]   Obermeier, B.; Wurm, F.; Frey, H., Amino Functional Poly(ethylene glycol) Copolymers via Protected Amino Glycidol, *Macromolecules.* **2010**, *43*, 2244–2251.

[15]   Reuss, V. S.; Obermeier, B.; Dingels, C.; Frey, H., *N,N*-Diallylglycidylamine: A Key Monomer for Amino-Functional Poly(ethylene glycol) Architectures, *Macromolecules.* **2012**, *45*, 4581–4589.

[16]   Wilms, V. S.; Bauer, H.; Tonhauser, C.; Schilmann, A.-M.; Müller, M.-C.; Tremel, W.; Frey, H., Catechol-Initiated Polyethers: Multifunctional Hydrophilic Ligands for PEGylation and Functionalization of Metal Oxide Nanoparticles, *Biomacromolecules.* **2013**, *14*, 193–199.

[17]   Hans, M.; Keul, H.; Moeller, M., Chain Transfer Reactions Limit the Molecular Weight of Polyglycidol Prepared via Alkali Metal based Initiating Systems, *Polymer.* **2009**, *50*, 1103–1108.

[18]   Ponomarenko, V. A.; Khomutov, A. M.; Il'chenko, S. I.; Ignatenko, A. V., The Effect of Substituents of the Anionic Polymerization of α-Oxides, *Polym. Sci.(USSR)* **1971**, *13*, 1735–1740.

[19]   Herzberger, J.; Frey, H., Epicyanohydrin: Polymerization by Monomer Activation Gives Access to Nitrile-, Amino-, and Carboxyl-Functional Poly(ethylene glycol), *Macromolecules.* **2015**, *48*, 8144–8153.

[20]   Wei, P. E.; Butler, P. E., Synthesis and Polymerization Studies of Several Chloro and Cyano Epoxides, *J. Polym. Sci. A Polym. Chem.* **1968**, *6*, 2461–2475.

[21]   Cantor, S. E.; Brindell, G. D.; Brett, T. J., Synthesis and Polymerization Studies of Cyano Epoxides, *J. Macromol. Sci. Part A.* **1973**, *7*, 1483–1508.

[22]   Burness, D. M.; Bayer, H. O., Synthesis and Reactions of Quaternary Salts of Glyeidyl Amines, *J. Org. Chem.* **1963**, *28*, 2283–2288.

[23]   Huval, C. C.; Bailey, M.J.; Holmes-Farley, S. R.; Mandeville, W. H.; Miller-Gilmore, K.; Sacchiero, R. J.; Dhal, Pradeep K., Amine Functionalized Polyethers as

144

Bile Acid Sequestrants: Synthesis and Biological Evaluation, *J. Macromol. Sci. Part A.* **2001**, *38*, 1559–1574.

[24]   Thavanesan, T.; Herbert, C.; Plamper, F. A., Insight in the Phase Separation Peculiarities of Poly(dialkylaminoethyl methacrylate)s, *Langmuir.* **2014**, *30*, 5609–5619.

[25]   Kurzbach, D.; Schömer, M.; Wilms, V. S.; Frey, H.; Hinderberger, D., How Structure-Related Collapse Mechanisms Determine Nanoscale Inhomogeneities in Thermoresponsive Polymers, *Macromolecules.* **2012**, *45*, 7535–7548.

[26]   Rangelov, S.; Tsvetanov, C., Towards the Synthesis of Amino-substituted Epoxides: Synthesis and Characterization of Glycidyldidodecylamine, *Des. Monomers Polym.* **2001**, *4*, 39–43.

[27]   Ramirez, S. M.; Layman, J. M.; Bissel, P.; Long, T. E., Ring-Opening Polymerization of Imidazole Epoxides for the Synthesis of Imidazole-Substituted Poly(ethylene oxides), *Macromolecules.* **2009**, *42*, 8010–8012.

[28]   Hu, H.; Yuan, W.; Lu, L.; Zhao, H.; Jia, Z.; Baker, G. L., Low Glass Transition Temperature Polymer Electrolyte Prepared from Ionic Liquid Grafted Polyethylene Oxide, *J. Polym. Sci. A: Polym. Chem.* **2014**, *52*, 2104–2110.

[29]   Mecerreyes, D., Polymeric Ionic Liquids: Broadening the Properties and Applications of Polyelectrolytes, *Prog. Polym. Sci.* **2011**, *36*, 1629–1648.

[30]   Hu, H.; Yuan, W.; Jia, Z.; Baker, G. L., Ionic Liquid-based Random Copolymers: A New Type of Polymer Electrolyte with Low Glass Transition Temperature, *RSC Adv.* **2015**, *5*, 3135–3140.

[31]   Lundberg, P.; Lynd, N. A.; Zhang, Y.; Zeng, X.; Krogstad, D. V.; Paffen, T.; Malkoch, M.; Nystrom, A. M.; Hawker, C. J., pH-Triggered Self-assembly of Biocompatible Histamine-functionalized Triblock Copolymers, *Soft Matter.* **2013**, *9*, 82–89.

[32]   Martin Hrubý; Čestmír Koňák; Karel Ulbrich, Polymeric Micellar pH-Sensitive Drug Delivery System for Doxorubicin, *J. Control. Release.* **2005**, *103*, 137–148.

[33]   Sokolovskaya, E.; Yoon, J.; Misra, A. C.; Bräse, S.; Lahann, J., Controlled Microstructuring of Janus Particles Based on a Multifunctional Poly(ethylene glycol), *Macromol. Rapid Commun.* **2013**, *34*, 1554–1559.

[34]   Zhou, L.; Cheng, R.; Tao, H.; Ma, S.; Guo, W.; Meng, F.; Liu, H.; Liu, Z.; Zhong, Z., Endosomal pH-Activatable Poly(ethylene oxide)-*graft*-Doxorubicin Prodrugs:

Synthesis, Drug Release, and Biodistribution in Tumor-Bearing Mice, *Biomacromolecules.* **2011**, *12*, 1460–1467.

[35]   Sokolovskaya, E.; Barner, L.; Bräse, S.; Lahann, J., Synthesis and On-Demand Gelation of Multifunctional Poly(ethylene glycol)-Based Polymers, *Macromol. Rapid Commun.* **2014**, *35*, 780-786.

3.2 Stimuli-Responsive Tertiary Amine-Functional PEGs Based on *N,N*-Dialkyl Glycidyl Amines

Jana Herzberger,[a,c] Dennis Kurzbach,[b] Mathias Werre,[a,c] Karl Fischer,[d]

Dariush Hinderberger,[e] Holger Frey[a,]*

[a] Institute of Organic Chemistry, Johannes Gutenberg-University Mainz, Duesbergweg 10-14, 55128 Mainz, Germany

[b] Department of Structural and Computational Biology, Max F. Perutz Laboratories Vienna Biocenter Campus 5, 1030 Vienna, Austria

[c] Graduate School Materials Science in Mainz , Staudingerweg 9, 55128 Mainz, Germany

[d] Institute of Physical Chemistry, Johannes Gutenberg-University Mainz, Jakob-Welder-Weg 11 , 55099 Mainz, Germany

[e] Institute of Chemistry, Martin-Luther-Universität Halle-Wittenberg, Von-Danckelmann-Platz 4, 06120 Halle (Saale), Germany

E-Mail: hfrey@uni-mainz.de
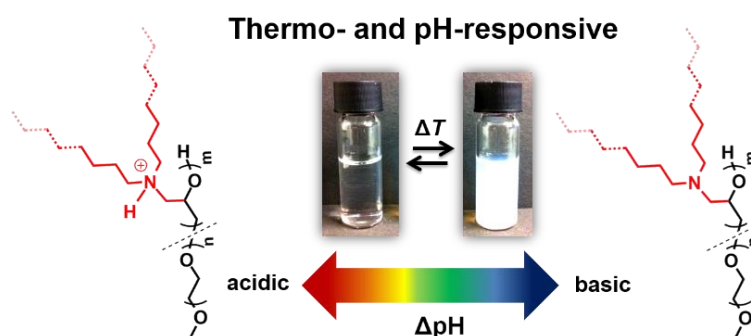
3.2.1 Abstract

Amine-functional poly(ethylene glycol) (PEG) copolymers have been prepared that exhibit thermo- and pH- responsive behavior in aqueous solution. Three novel tertiary di(n-alkyl) glycidyl amine monomers have been introduced for anionic ring opening copolymerization (AROcP) with ethylene oxide (EO): N,N-di(n-butyl) glycidyl amine (DButGA), N,N-di(n-hexyl) glycidyl amine (DHexGA) and N,N-di(n-octyl) glycidyl amine (DOctGA). Via controlled AROcP we synthesized well-defined ($M_w/M_n = 1.05$-1.14), water-soluble block- and gradient-type PEG copolymers, containing up to 25 mol% of the respective dialkyl glycidyl amine comonomer. Molecular weights ranged from 4900 to 12000 g·mol^{-1}. Detailed in-situ ^{1}H NMR kinetics and ^{13}C triad analyses elucidate the microstructures of the copolymers and the relative reactivity of the novel comonomers. Notably, the n-alkyl chain length had no significant influence on the relative reactivity of the glycidyl amine comonomers. Calculated reactivity ratios ranged from $r_{EO} = 1.84$, $r_{DButGA} = 0.49$ to $r_{EO} = 1.78$, $r_{DOctGA} = 0.42$, manifesting the formation of gradient copolymers. Thermo- and pH-responsive properties of these copolymers are precisely tunable by the comonomer ratio, and cloud points in aqueous solution can be adjusted between 21 °C and 93 °C. Electron paramagnetic resonance (EPR) spectroscopic studies with TEMPO as a spin-probe were conducted to elucidate host-guest interactions of the copolymers. Unexpectedly, the n-alkyl chain length of the different glycidyl amine comonomers only influences the inverse phase transition of the gradient copolymers, but not of the block copolymers on the nanoscale. Self-assembly of the block- and gradient-type copolymers in aqueous alkaline solution by both static and dynamic light scattering has also been investigated after confirming the existence of pure unimers in methanol.

3.2.2 Introduction

Poly(ethylene glycol) (PEG) is an extremely versatile material that distinguishes itself from other common simple polyethers, like poly(oxymethylene) (POM) or poly(propylene oxide) (PPO) by its remarkably high solubility in water,[1] high chain flexibility and biocompatibility.[2, 3] This unique combination of properties renders PEG a valuable compound in a vast variety of fields, e.g., for pharmaceutical and biomedical applications,[4, 5] nonionic surfactants[6] or soluble polymeric supports in phase transfer catalysis.[7]

The properties of PEG can be systematically expanded and manipulated by the incorporation of other epoxide-based comonomers into the polyether backbone. This is achieved by anionic ring opening copolymerization (AROcP) of ethylene oxide (EO) with various other comonomers.[8, 9] For example, thermo-responsive PEGs with adjustable cloud points can be generated by incorporating more hydrophobic comonomers, such as ethoxy vinyl glycidyl ether (EVGE)[10, 11] or allyl glycidyl ether (AGE)[12] into the PEG backbone. Recently, our group reported well-defined, amine-functional PEGs, which combine thermo- and pH-responsive behavior.[3, 13–16] The copolymerization of EO with *N,N*-diethyl glycidyl amine (DEGA) leads to temperature- and pH-responsive copolymers in the range between 42 °C and 97 °C with the main focus on prospective use in modern drug delivery strategies.[16, 14] Tsvetanov et al. introduced an even more hydrophobic glycidyl amine derivative, i.e., glycidyl di(dodecyl)amine (GDDA) to introduce high solubilizing power towards extremely hydrophobic drugs. However, to date successful polymerization of GDDA has not been achieved.[17] Besides the use for drug delivery strategies, Lynd and co-workers recently reported pH-responsive hydrogels prepared from symmetric triblock copolymers, based on *N,N*-diisopropyl ethanolamine glycidyl ether (DEGE) and PEG. These PDEGE-*b*-PEG-*b*-PDEGE hydrogels showed pH-sensitivity in a physiologically

relevant pH window and could be used for controlled drug release or as cell carriers.[18] Overall, amine-functional PEGs may represent promising candidates for biomedical applications, utilizing pH as their active trigger together with PEG's established biocompatibility.[5]
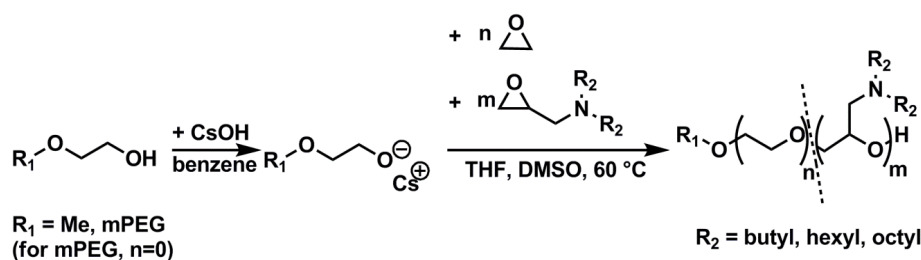
Scheme 1. Polymerization strategy for the concurrent copolymerization of EO and the respective DXGA monomer. For the block copolymerization, monomethoxy-PEG5000 (mPEG$_{113}$) was used as a macro-initiator. 2-Methoxyethanol was used as an initiator for the concurrent copolymerization.

In this work, we present the synthesis of novel water-soluble polyethers comprising different hydrophobically substituted, tertiary amine moieties, which can be used as a new and simple handle in tuning temperature- and pH-response of such polymers. To this end, we introduce three comonomer building blocks for concurrent AROcP with EO: *N,N*-di(*n*-butyl) glycidyl amine (DButGA), *N,N*-di(*n*-hexyl) glycidyl amine (DHexGA) and *N,N*-di(*n*-octyl) glycidyl amine (DOctGA) (Scheme 1). In the following, the glycidyl amine derivatives will be referred to as DXGA with X = But, Hex or Oct, respectively. We focus on a systematic study of the effect of the different *n*-alkyl chain lengths at the tertiary amine moiety and the consequent variation in the hydrophilic-hydrophobic balance on thermo- and pH-responsiveness of the aqueous polymer solutions. We demonstrate that inverse phase transition temperatures can be precisely triggered by the system pH due to the protic nature of the amines and thus can be adjusted by the respective *n*-alkyl chain of the amine.

150

Moreover, we utilize light scattering experiments to provide insight on the self-assembly of the copolymers in aqueous alkaline solution, which is expected to depend not only on the block length ratio but also on the copolymers' microstructure and their hydrophobicity, e.g. the chain length of the alkyl-substituent.

3.2.3 Experimental Section

All methods employed and the sources of all reagents used are given in the Supporting Information document.

Monomer synthesis (DXGA). The procedure described by Hovland et al.[19] for DButGA and DOctGA was modified. Epichlorohydrin (1.2 eq), water (0.15 eq, deionized) and the respective secondary amine (1.0 eq) were added to a round-bottom flask and stirred overnight at room temperature. After extraction of the mixture with 20 % aq K_2CO_3 solution, 36 % aqueous NaOH was added to the organic phase, followed by stirring at room temperature overnight. The organic phase, separated from the solids by centrifugation, was then dried over $MgSO_4$ and washed with diethyl ether. Filtration and fractional distillation under reduced pressure ($p = 6 \cdot 10^{-2}$ mbar) gave the respective product (yields 80-90 %) as a colorless liquid.

N,N-Di(*n*-butyl) glycidyl amine (DButGA)

Purification by distillation: $p = 6 \cdot 10^{-2}$ mbar, $T_b = 54\ °C$

^{1}H NMR (300 MHz, Chloroform-*d*): δ[ppm]: 3.09-3.03 (m, 1H, C*H*$_{ring}$), 2.78-2.70 (m, 2H, C*H'-H''*$_{,ring}$), 2.60-2.42 (m, 6H, N-C*H*$_2$), 1.49-1.25 (m, 8H, -C*H*$_2$-C*H*$_2$-), 0.94-0.89 (t, 7.2 Hz, 6H, -C*H*$_3$). ^{13}C NMR (75 MHz, Chloroform-*d*): δ[ppm]: 56.78, 54.34, 50.97, 45.38, 29.12, 20.62, 14.05.

N,N-Di(*n*-hexyl) glycidylamine (DHexGA)

Purification by distillation: $p = 6 \cdot 10^{-2}$ mbar, $T_b = 82\ °C$

^{1}H NMR (300 MHz, Chloroform-*d*): δ[ppm]: 3.09-3.04 (m, 1H, C*H*$_{ring}$), 2.79-2.71 (m, 2H, C*H'-H''*$_{,ring}$), 2.60-2.42 (m, 6H, N-C*H$_2$*), 1.50-1.38 (m, 4H,-N-CH$_2$-C*H$_2$*), 1.37-1.29 (m, 12H, -(CH$_2$)$_3$-), 0.91-0.87 (t, 7.0 Hz, 6H, -C*H$_3$*). ^{13}C NMR (75 MHz, Chloroform-*d*): δ[ppm]: 56.81, 54.70, 51.00, 45.38, 31.81, 27.18, 26.96, 22.65, 14.05.

N,N-Di(*n*-octyl) glycidylamine (DOctGA)

Purification by distillation: $p = 6 \cdot 10^{-2}$ mbar, $T_b = 100$ °C

^{1}H NMR (300 MHz, Chloroform-*d*): δ[ppm]: 3.09-3.04 (m, 1H, C*H*$_{ring}$), 2.80-2.74 (m, 2H, C*H'-H''*$_{,ring}$), 2.61-2.43 (m, 6H, N-C*H$_2$*), 1.55-1.40 (m, 4H,-N-CH$_2$-C*H$_2$*), 1.33-1.22 (m, 20H, -(CH$_2$)$_5$-), 0.91-0.86 (t, 6.9 Hz, 6H, -C*H$_3$*). ^{13}C NMR (75 MHz, Chloroform-*d*): δ[ppm]: 56.81, 54.68, 51.00, 45.40, 31.84, 29.55, 29.31, 27.51, 27.00, 22.65, 14.08.

Block copolymer synthesis in bulk. The typical procedure is based on previous work[14] and is exemplified for mPEG$_{113}$-*b*-PDButGA$_5$. 2 g of mPEG5000 (1 eq), 60 mg cesium hydroxide monohydrate (0.9 eq) and 10 mL benzene were added into a dry 100 mL Schlenk flask under argon atmosphere. The mixture was stirred for 30 min at 60 °C. Evaporation of the solvent under reduced pressure at 90 °C overnight afforded the partially (90 %) deprotonated initiator. After the required amount of the dry DXGA (0.37 g DButGA) was added via syringe, the reaction was stirred overnight at 70 °C. The reaction mixture was allowed to cool down to room temperature prior to termination with methanol (0.3 mL). The polymer was precipitated from methanol in cold diethyl ether. Filtration and drying in vacuum afforded the block copolymer in quantitative yields.

Concurrent copolymerization of EO and DXGA. Copolymerization was performed as previously described by Reuss et al.[14] Cesium hydroxide monohydrate (1 eq), benzene (10 mL) and 2-methoxy ethanol (1.05 eq) were added into a dry Schlenk flask under argon atmosphere. Stirring the mixture for 30 min at 60 °C followed by removing the solvent under reduced pressure overnight at 60 °C afforded the initiator. Dry THF (~ 25 mL) and DMSO (5 mL) were added to the reaction mixture. The mixture was cooled to -80 °C, and

the desired amount of EO was cryo-transferred from a graduated ampule into the reaction mixture. The respective, dry DXGA was syringed into the flask and the polymerization was performed for 24 h (DButGA) to 48 h (DHexGA, DOctGA) at 60 °C. After cooling to room temperature, methanol (0.3 mL) was added. The reaction mixture was precipitated into cold diethyl ether. Filtration and drying in vacuum afforded a gradient-like copolymer in almost quantitative yields (>95 %). Copolymers containing amounts of more than 10 % of DXGA were dissolved in methanol and purified by dialysis (MWCO = 1000 g·mol^{-1}).

3.2.4 Results and Discussion

A. Monomer synthesis and copolymerization with EO

Monomer (DXGA) synthesis. The di(*n*-alkyl) glycidyl amine derivatives (DXGA) can be synthesized in a modified two-step procedure. The synthesis was originally developed by Hovland et al. for DButGA and DOctGA and is described in the Experimental Section.[19] Mixing epichlorohydrin with the respective secondary amine leads to ring opening in the presence of water. Addition of sodium hydroxide solution affords the desired product by recyclization of the epoxide ring. We refrained from excessive heating during all reaction steps (to 30-70 °C)[19] to avoid condensation reactions.[17] The achieved yields of the DXGAs were in the range of 80 % to 90 %. Small losses are due to polymeric by-products, which are generated during distillation of the glycidyl amines due to nucleophilic attack of the amine at the epoxide ring. This side reaction has previously been observed for DEGA as well.[14] However, this undesired polymerization only occurs at elevated temperatures. At lower temperatures, it is prevented by the sterically demanding, long alkyl chains. As reported long ago, *N,N*-dimethyl glycidyl amine is not stable at room temperature due to the limited steric bulk and small shielding effect of the methyl groups.[20] Stable *N,N*-di(n-

alkyl) glycidyl amines are accessible only with ethyl or longer alkyl chains. On the other hand, purification by distillation obviously becomes more challenging with increasing chain length.

Concurrent copolymerization of EO and DXGA. AROcP copolymerization of DXGA was carried out with 3.8-25 mol% comonomer content, while the theoretical degree of polymerization (DP_n) was kept constant at $n = 113$ (see Table 1). Since we targeted copolymers exhibiting solubility in aqueous solution, higher contents of the DXGA comonomers were not explored in this work. The desired DXGA content is adjustable by the monomer feed ratio and was determined by ^{1}H NMR spectroscopy. Gel permeation chromatography (GPC) indicates well-defined copolymers with low polydispersity indices ($M_w/M_n = 1.05\text{-}1.14$) and monomodal molecular weight distributions (Figure S4a, Supporting Information). With increasing content of the hydrophobic DXGA, the relative hydrodynamic volume decreased, and the molecular weights determined by GPC (DMF, calibrated with PEG standards) differed increasingly from the absolute molecular weight obtained from NMR data (see Table 1). This is a well-known phenomenon for amine functional PEGs also observed in previous works in our group.[3, 14, 15] Eventually, absolute number average molecular weights (M_n) can be determined via ^{1}H NMR spectroscopy with an error of ±10 % due to signal overlap between the proton signals of the methoxy-group (initiator) and the backbone protons of PEG.[3]

Table 1. Characterization data for the series of PEG-*co*-PDXGA copolymers.

Composition[1]	DXGA content[1]	$M_n{}^1$/g·mol^{-1}	$M_n{}^2$/g·mol^{-1}	$M_w/M_n{}^2$
PEG$_{92}$-*co*-PDButGA$_4$	4.2 %	4790	5360	1.07
PEG$_{95}$-*co*-PDButGA$_6$	6.0 %	5160	5180	1.09
PEG$_{136}$-*co*-PDButGA$_{11}$	7.5 %	8020	4570	1.12
PEG$_{91}$-*co*-PDButGA$_{15}$	14.2 %	6780	3470	1.13
PEG$_{88}$-*co*-PDButGA$_{21}$	19.3 %	7760	3880	1.14
PEG$_{117}$-*co*-PDButGA$_{39}$	25.0 %	12360	3560	1.14
PEG$_{100}$-*co*-PDHexGA$_4$	3.8 %	5400	5440	1.07
PEG$_{95}$-*co*-PDHexGA$_6$	6.0 %	5630	5380	1.07
PEG$_{107}$-*co*-PDHexGA$_9$	7.8 %	6900	4490	1.11
PEG$_{106}$-*co*-PDHexGA$_{10}$	8.6 %	7100	4320	1.13
PEG$_{181}$-*co*-PDHexGA$_{33}$	15.4 %	15900	3020	1.13
PEG$_{194}$-*co*-PDHexGA$_{51}$	20.8 %	20800	2620	1.12
PEG$_{99}$-*co*-PDOctGA$_4$	3.9 %	5500	4630	1.05
PEG$_{114}$-*co*-PDOctGA$_7$	5.8 %	7170	4820	1.06
PEG$_{138}$-*co*-PDOctGA$_{14}$	9.2 %	10230	3800	1.10

[1] Obtained from ^{1}H NMR spectra; [2] Determined by GPC measurements in DMF (RI signal)

Block copolymerization of mPEG and DXGA. We also prepared copolymers with DXGA comonomer fractions ranging from 4.2 to 15.0 %, showing low dispersity indices (1.05-1.09) and monomodal weight distributions (see Table 2 and Figure S4b). GPC traces illustrate distinct shifts to higher molecular weights in comparison to the molecular weight of the macro-initiator mPEG5000. The achieved degrees of polymerization were slightly lower than anticipated, which we explain by chain transfer reactions to the monomer (Table 2 and Scheme S1, Supporting Information). This is a well-known limitation in alkali metal mediated AROcPs of epoxides.[21, 9] Concerning this reaction, a detailed ^{1}H,^{1}H-COSY (correlation spectroscopy) NMR spectrum is shown in the Supporting Information (Figure S5). In general, the transfer reaction can be efficiently suppressed by lowering the reaction

temperature. For this block copolymerization, a temperature of 70 °C has been observed to be suitable to minimize these transfer reactions.

Table 2. Characterization data for the series of PEG-*b*-PDXGA block copolymers.

Composition[1]	DXGA content[1]	DXGA content (th)	M_n^1/ g·mol^{-1}	M_n^2/ g·mol^{-1}	M_w/M_n^2
mPEG$_{113}$-*b*-PDButGA$_5$	4.2 %	4.2 %	5930	5570	1.05
mPEG$_{113}$-*b*-PDButGA$_8$	6.6 %	8.1 %	8480	6030	1.06
mPEG$_{113}$-*b*-PDButGA$_{17}$	13.1 %	15.0 %	8150	5770	1.07
mPEG$_{113}$-*b*-PDButGA$_{20}$	15.0 %	18.1 %	8700	5730	1.09
mPEG$_{113}$-*b*-PDHexGA$_5$	4.2 %	4.2 %	6200	5800	1.06
mPEG$_{113}$-*b*-PDHexGA$_8$	6.6 %	8.1 %	6930	6000	1.06
mPEG$_{113}$-*b*-PDHexGA$_{15}$	11.7 %	15.0 %	8620	5150	1.09
mPEG$_{113}$-*b*-PDOctGA$_5$	4.2 %	4.2 %	6490	5560	1.06
mPEG$_{113}$-*b*-PDOctGA$_7$	5.8 %	8.1 %	7080	5610	1.07

[1] Obtained from ^{1}H NMR spectra; [2] Determined by GPC measurements in DMF (RI signal)

^{13}C NMR triad analysis. ^{13}C NMR spectroscopy based triad analysis provides first insights into the microstructure of the copolymers generated by concurrent AROcP. The analyzed triads (i.e., sequences of three subsequent monomer units) were labeled as recently described for tapered EO/DEGA copolymers,[14] and as established for EO/PO copolymers.[22–24] Peak assignment was achieved by comparison with amine-functional PEGs[14, 3, 15] recently synthesized in our group, other block copolymer structures and various calculated spectra. Figure 1 shows the relevant region of the ^{13}C NMR spectrum of PEG-*co*-PDButGA with 6.0 % DButGA. The signals at 77.6 ppm, 71.7 ppm and 68.7 ppm found in the spectra of the random copolymers are absent in the ^{13}C NMR spectrum of the block copolymer (see Figure 2) and can be assigned as the *E-D$_b$-E*, *E-D$_a$-E* and *D-E$_a$-D* triads, respectively (*E* refers to the EO repeating unit and *D* refers to the DXGA repeating unit, *a* indicating the first methylene group and *b* the second of the central monomer unit). With

increasing DXGA content, the signal at 77.6 ppm broadens, indicating additional triads like *D-D_b-E*, while the signal of *E-D_b-E* remains the strongest resonance (see Figure 2). Note that no quantitative determination of the triad abundance was possible, however simple block structures could not be observed for the random copolymers. Similar results were also obtained for PEG-*co*-PDXGA copolymers with DHexGA and DOctGA. ^{1}H NMR kinetic studies were performed to elucidate the exact microstructure of the copolymers and the comonomers´ reactivity ratios.
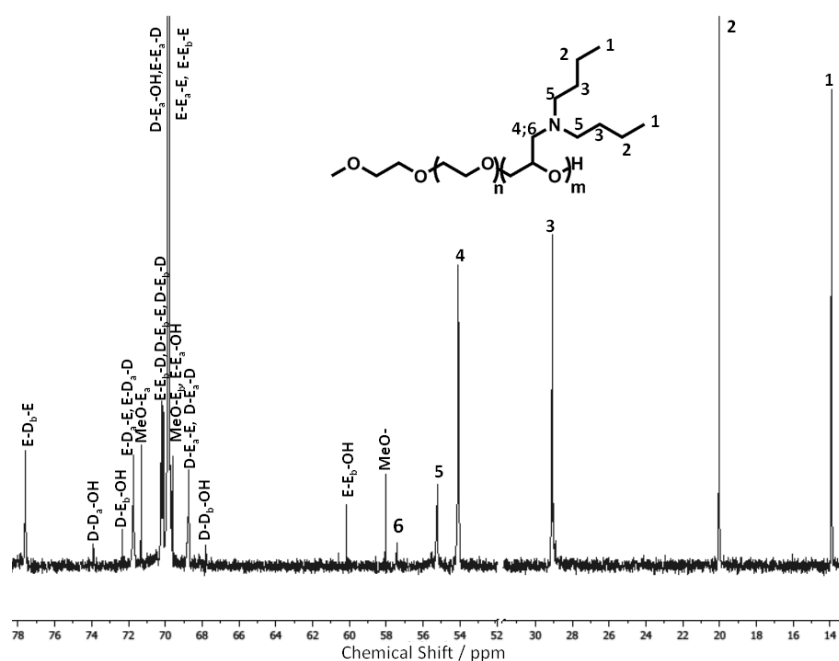
Figure 1. Relevant section of the ^{13}C NMR spectrum (75 MHz, DMSO-*d₆*) of PEG-*co*-PDButGA copolymer with a fraction of 6.0 % DButGA.
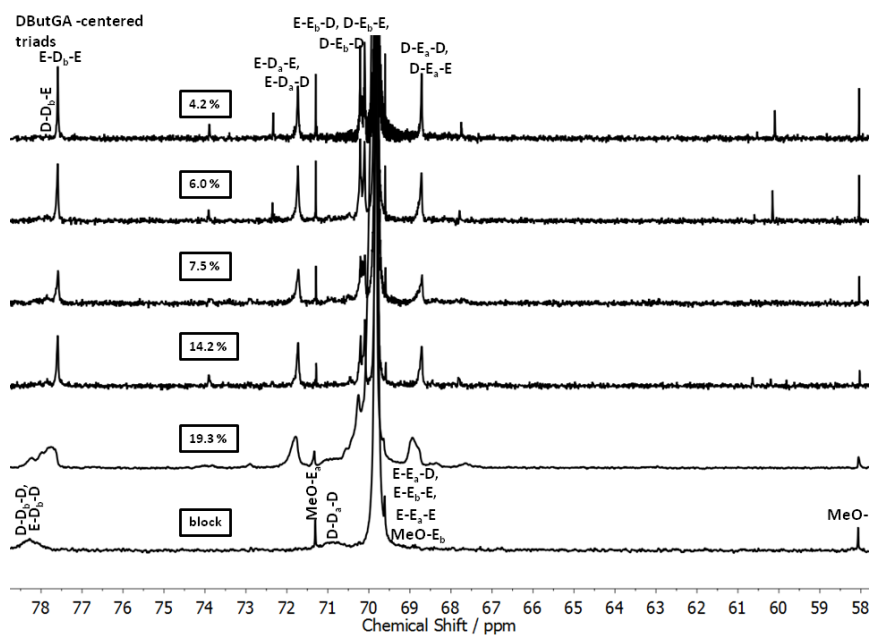
Figure 2. Relevant sections of the ^{13}C NMR spectra (75 MHz, DMSO-d_6) of mPEG$_{113}$-b-PDButGA$_{20}$ and PEG-co-PDButGA copolymers with 4.2 %, 6.0 %, 7.5 %, 14.2 % and 19.3 % DButGA fraction. The copolymer with 25.0 mol% DButGA showed poor solubility in DMSO-d_6 and could therefore not be employed for ^{13}C NMR measurements in this solvent.

^{1}H NMR _in situ_ kinetic studies. To compare the properties of the different PEG-co-PDXGA copolymers, it is important that the functional group distribution at the backbone is known. ^{1}H NMR spectroscopy was used to investigate the relative monomer reactivity by monitoring the different copolymerization reactions.[3, 12, 25] The reactions were carried out under reduced pressure in a solvent mixture of THF-d_8 and DMSO-d_6 (5:1) at 80 °C using 2-methoxy ethoxide as initiator. A higher reaction temperature compared to the reactions in flask (60 °C) is reasonable, since the lack of stirring can be expected to slow down the reaction time dramatically. Yet, this difference in reaction temperature does not affect the relative monomer reactivities.[3, 26, 24] The NMR tubes were prepared as described earlier,[3, 15, 14] measurements were conducted every 30 s and with increasing reaction time every 15 min. The monomer consumption was followed via integration of the decreasing signal areas of the monomer resonances at 2.55 ppm (methylene protons of EO (4 H),

highlighted in purple) and at 2.93 ppm (protons of the respective DXGA (1 H), highlighted in red). The area under the signals of the alkyl protons (butyl, hexyl or octyl) remained constant throughout the reaction. Therefore, these signals were used as an internal reference. Simultaneously, the growing polyether backbone was monitored by integrating the signal at 3.6 ppm (highlighted in green). Figure 3 shows the relevant section of the time-resolved ^{1}H NMR spectra for the copolymerization of EO and a DHexGA fraction of 10 %.
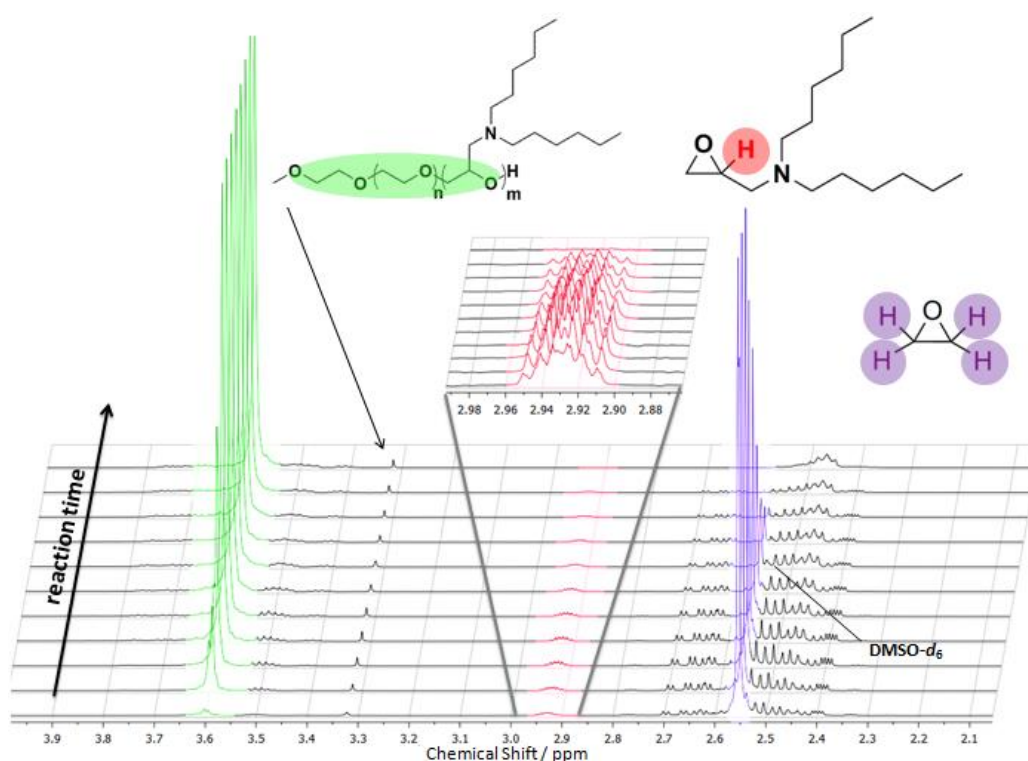
Figure 3. Time-resolved ^{1}H NMR spectra (400 MHz) for the copolymerization of EO and DHexGA (10 %) at 80 °C. The relevant signals are highlighted. Green: polymer backbone, red: single proton of DHexGA, purple: protons of EO. The shown spectra were recorded after 30 sec, 1 min, 2 min, 15 min, 30 min, 1 h, 2 h, 4 h, 6 h, 7 h and 8 h, respectively.

The polymerization rates are influenced by the steric bulk of the different DXGA comonomer (see Figure S6 in the Supporting Information). At a reaction temperature of 80 °C copolymerization of DButGA requires 30 min to achieve full monomer consumption. For DHexGA complete conversion was observed only after 8 h, and 23 h

were required to achieve full monomer consumption for the copolymerization of DOctGA and EO.

Figure 4 illustrates monomer consumption with increasing total conversion. Faster incorporation of EO into the growing polymer chain with progressing conversion can be observed, resulting in a distinct compositional drift, with EO enriched segments near the initiator and DXGA enriched segments near the terminus of the chains. Similar gradient copolymer structures are observed for all three DXGA monomers (Figure 4). Note that in analogy to these findings gradient structures were reported for other glycidyl amine derivatives polymerized in DMSO-d_6, such as *N,N*-dibenzyl amino glycidol (DBAG)[3], *N,N*-diallyl glycidyl amine (DAGA)[15] and DEGA.[14] For a better understanding of the AROcP, based on the NMR-data the monomer reactivity ratios (r-parameters) for the DXGA comonomers and EO were calculated using the Fineman-Ross formalism (Figure S7, Supporting Information).[27] Values for DButGA and DOctGA of $r_{EO} = 1.84$, $r_{DButGA} = 0.49$ and $r_{EO} = 1.78$, $r_{DOctGA} = 0.42$ reflect the higher reactivity of EO compared to the DXGA monomer and the similarity of the different reactivity ratios for all DXGA monomers. From these results, we can conclude that a similar gradient microstructure for all different DXGA copolymers is obtained. This is of importance, since this demonstrates – maybe in contrast to the chemist's intuition - that the alkyl chain length of the tertiary amine does not strongly influence the reactivity and microstructure by steric shielding, as opposed to the copolymerization of ethylene oxide with various alkyl oxiranes[28, 23–25] and as reported for several other epoxide monomers.[28, 29] Already in the 1970s, the copolymerization of PO and DEGA was investigated in terms of their relative reactivities based on the steric demand and the polarity of the respective substituents.[29] Unexpectedly, for the copolymerization of PO with DEGA reactivity ratios of $r_{PO} = 1.9$ and $r_{DEGA} = 0.3$ using the Fineman-Ross method were calculated. From these results, the polarity of the

160

nitrogen atom did not appear to increase the reactivity of DEGA, in analogy to our results. In contrast, for glycidyl ethers, a multi-dentate coordination of the additional oxygen atom with the counter-ion was proposed, which enhances the Lewis basicity of the monomer, resulting in a similar [26, 12] or even higher relative reactivity compared to EO[11, 18] and PO.[29] Consequently, we suppose that a similar multi-dentate coordination of the glycidyl amine comonomers with the counter-ion (here Cs^+) does not occur, based on the general shielding of the nitrogen in the tertiary amine derivatives. This assumption is also supported by results reported by Lynd et al. discussing a cation-coordination mechanism. They investigated the copolymerization of EO with several glycidyl ethers with the following observations: *N,N*-diisopropyl ethanolamine glycidyl ether (DEGE) (two oxygen atoms, one nitrogen atom) and allyl glycidyl ether (AGE) (two oxygen atoms) show quite similar reactivity ratios: $r_{DEGE} = 1.28\pm0.14$, $r_{EO} = 0.82\pm0.1$ and $r_{AGE} = 1.31 \pm0.26$, $r_{EO} = 0.54 \pm0.03$, whereas ethoxy vinyl glycidyl ether (EVGE) (three oxygen atoms) shows a higher reactivity ratio $r_{EVGE} = 3.50\pm0.90$ and $r_{EO} = 0.32\pm0.1$.[5, 11] From these results one can deduce that the additional nitrogen atom in DEGE does not increase reactivity.

In summary, the nitrogen atom of glycidyl amine derivatives does not appear to decrease the transition-state energy by coordination with the cation and therefore does not enhance the reactivity of the comonomer. Nevertheless, the AROcP is strongly influenced by the choice of the counter-ion as well as the polarity of the reaction solvent; consequently any comparison of different copolymer systems has to be handled with care.[30]
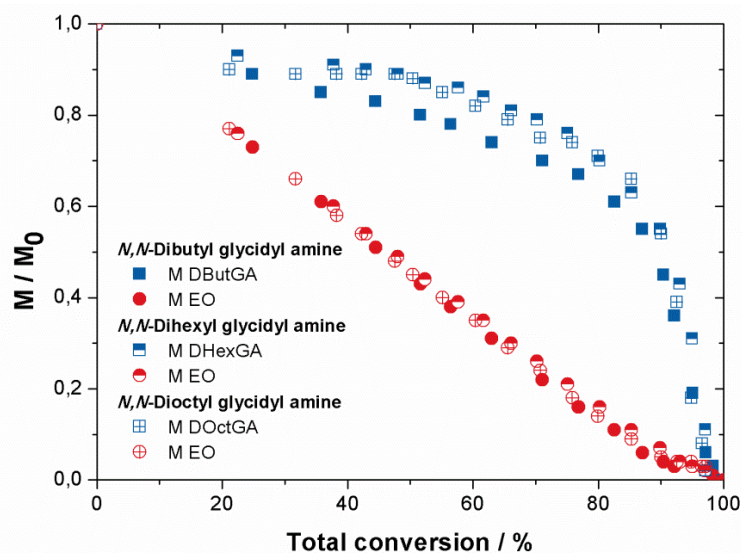
Figure 4. Fraction of initial monomer concentration of EO and the DXGA comonomer (10-15 %) versus total conversion for copolymerization at 80 °C, measured in a THF-d_8 and DMSO-d_6 (5:1 ratio) mixture.

B. Properties of the copolymers in bulk and solution

The thermal properties of the copolymers in bulk were studied by differential scanning calorimetry (DSC), aiming at differences between block- and gradient copolymers. PEG homopolymer with molecular weights exceeding 2000 g·mol^{-1} is a highly crystalline material with a melting temperature approaching 65 °C.[31] Copolymerization strongly affects the degree of crystallization. Thermal characteristics are also determined by the respective microstructure, as reported previously for other PEG-copolymers.[22, 3, 15, 32] For gradient copolymers obtained from concurrent copolymerization of DXGA and EO, a decreasing melting temperature and melting enthalpy with increasing DXGA content is observed (Table 3). We attribute this to destabilization of the crystal structure[22] by the bulky tertiary amines. Intriguingly, an incorporation of as little as 4 % of any DXGA in a gradient copolymer already decreases the melting temperature by ~ 20 °C. In comparison, for the block copolymers no significant influence of the DXGA content on the melting temperature

of the PEG block could be observed (Table 4), which indicates nanosegregation of both blocks. On the other hand, these results again confirm the conclusion that the gradient copolymers show no block-like structure and consequently no nanosegregated domains.

Table 3. Characterization data of PEG-*co*-PDXGA gradient copolymers from DSC.

Composition	DXGA content	T_g/°C	T_m/°C	ΔH/J·g^{-1}
PEG$_{92}$-*co*-PDButGA$_4$	4.2 %	-66	45	83
PEG$_{95}$-*co*-PDButGA$_6$	6.0 %	-68	42	74
PEG$_{136}$-*co*-PDButGA$_{11}$	7.5 %	-68	37	72
PEG$_{91}$-*co*-PDButGA$_{15}$	14.2 %	-72	15	32
PEG$_{88}$-*co*-PDButGA$_{21}$	19.3 %	-72	21	31
PEG$_{117}$-*co*-PDButGA$_{39}$	25.0 %	-73	15	26
PEG$_{100}$-*co*-PDHexGA$_4$	3.8 %	-71	46	80
PEG$_{95}$-*co*-PDHexGA$_6$	6.0 %	-74	42	71
PEG$_{107}$-*co*-PDHexGA$_9$	7.8 %	-74	38	72
PEG$_{106}$-*co*-PDHexGA$_{10}$	8.6 %	-77	35	64
PEG$_{181}$-*co*-PDHexGA$_{33}$	15.4 %	-76	30	38
PEG$_{194}$-co-PDHexGA$_{51}$	20.8 %	-78	12	25
PEG$_{99}$-*co*-PDOctGA$_4$	3.9 %	-70	49	92
PEG$_{113}$-*co*-PDOctGA$_7$	5.8 %	-75	45	81
PEG$_{138}$-*co*-PDOctGA$_{14}$	9.2 %	-74	43	57

T_g: glass transition temperature
T_m: melting temperature
ΔH: melting enthalpy

Table 4. Characterization data of mPEG$_{113}$-*b*-PDXGA block copolymers obtained by DSC.

Composition	DXGA content	T_g/°C	T_m/°C	ΔH/J·g^{-1}
mPEG$_{113}$	0 %	-53	64	186
mPEG$_{113}$-*b*-PDButGA$_5$	4.2 %	-60	57	139
mPEG$_{113}$-*b*-PDButGA$_8$	6.6 %	-69	54	125
mPEG$_{113}$-*b*-PDButGA$_{17}$	13.1 %	-72	54	92
mPEG$_{113}$-*b*-PDButGA$_{20}$	15.0 %	-73	55	88
mPEG$_{113}$-*b*-PDHexGA$_5$	4.2 %	---	56	131
mPEG$_{113}$-*b*-PDHexGA$_8$	6.6 %	-79	54	114
mPEG$_{113}$-*b*-PDHexGA$_{15}$	11.7 %	-78	56	89
mPEG$_{113}$-*b*-PDOctGA$_5$	4.2 %	-71	57	143
mPEG$_{113}$-*b*-PDOctGA$_7$	5.8 %	-76	55	113

T_g: glass transition temperature
T_m: melting temperature
ΔH: melting enthalpy

Stimuli-responsive behavior in aqueous solution. Recently we established an approach that combines macroscopic turbidity measurements with intrinsically local electron paramagnetic resonance (EPR) techniques to thoroughly describe the phase transition of LCST-exhibiting polymers.[33–35, 16] This approach exploits the fact that turbidimetry provides information on large-scale aggregation of polymers (leading to aggregates that are large enough to scatter incident light, i.e., > 0.5 µm), while spin-probing continuous wave (CW) EPR spectroscopy complementarily investigates the local (on length scales of a few nm) collapse behavior of a polymer of interest.[33–35, 16] For PEG-*co*-PDEGA copolymers, this approach has already revealed quite complex phase transition modes.[16] While the gradient copolymer shows cooperative coil-to-globule transitions on the nanoscale at temperatures below the macroscopically observable (by turbidimetry) cloud point, a block architecture facilitates a slowly percolating collapse, i.e., dehydration of the polymers that eventually leads to aggregation at the cloud point (see Figure 9). Interestingly, in both cases of block and gradient polymers, the onset of the nanophase separation observed by CW

EPR and the cloud point turned out to merge with increasing solution pH and consequently decreasing degree of protonation of the DEGA base.

Turbidimetric Characterization. PEG itself is known for its cloud point temperature of about 100 °C , which is dependent on its molecular weight in aqueous solutions.[36] The cloud point can be systematically lowered and tuned by copolymerization with hydrophobic comonomers.[32] Recently, our group introduced various amine-functional PEGs with cloud points ranging from 22 °C up to 97 °C.[13, 14] The cloud points were shown to depend on the incorporated comonomer content, the microstructure of the copolymer, the pH and the nature of the amine moieties. Here, we complementarily investigate how the length of alkyl side chains attached to tertiary amine moieties affects the cloud point of gradient and block copolymers. We systematically increase the alkyl chain length from *n*-butyl, to *n*-hexyl and *n*-octyl, but keep the degree of polymerization of the copolymers constant. Note that varying the length of the alkyl chain on the tertiary amine has a strong influence on the pK_a of a polymer with given comonomer ratio. It decreases with increasing steric demand of the alkyl chains from 9.6 (PEG-*co*-PDButGA) to 7.6 (PEG-*co*-PDHexGA) to 5.6 (PEG-*co*-PDOctGA) as determined by titration (Figure S9 and Figure S10, Supporting Information). For PEG-*co*-PDEGA a pK_a of 9.9 was reported.[16] The varying pK_a values might well result in different hydration energies of the polymers that in return determine the LCSTs/cloud points.[16]

Figure 5 displays the cloud points as a function of comonomer content for the different gradient copolymer series with no adjustment of the pH. Cloud points were measured at a concentration of 20 mg·mL^{-1} of an aqueous polymer solution. Measurements were repeated several times per copolymer, and the displayed cloud points are averaged values. Errors are calculated from the standard deviation of the averaged values and are less than 1 °C. Furthermore, heating and cooling cycles were monitored to study the occurrence of a hysteresis. For all copolymers, a thermal hysteresis between the heating and the cooling

profile can be observed. (Table S1 and Figure S8, Supporting Information). With an increasing ratio of hydrophobic to hydrophilic comonomers a significant shift of the cloud points occurs (Figure 5). At low comonomer ratios, the cloud point temperatures of PEG-*co*-PDXGA appear to be mainly influenced by the hydrophilic PEG segment, showing little influence by the alkyl chain lengths. Interestingly, with increasing comonomer ratio, a significant influence of the alkyl chain length can be observed, clearly resulting in lower cloud point temperatures.

Generally, PEG-*co*-PDButGA copolymers show lower cloud point temperatures than their PEG-*co*-PDEGA copolymer counterparts reported in literature.[14] Incorporating 14.2 % DButGA into PEG lowers the cloud point from 100 °C to 24 °C. Thus, cloud points at human body temperature are easily accessible with a low comonomer content, which is an attractive feature for future drug delivery applications. In contrast, a fraction of 15 % DEGA lowers the cloud point temperature to only 68 °C. Even an incorporation of 29 % DEGA leads to a transition temperature of only 55 °C.[14,16] A cloud point in the range of the human body temperature is only accessible at high pH (pH = 14, T_c = 42 °C) for DEGA-copolymers and therefore not applicable *in vivo*. In general, the longer *n*-alkyl chain in DButGA (in comparison to DEGA) leads to increasing hydrophobicity of the DButGA-based copolymers and, hence, decreasing cloud points. This feature is essential for the use in future biomedical applications, since one can rely on the unique, biocompatible PEG structure with tailor-made cloud points, albeit with only subtle structural alteration. A comparison of the gradient copolymers of DHexGA and DOctGA shows that with higher amount of incorporated DXGA the difference in the cloud point temperatures is even more significant. For instance, PEG-*co*-PDOctGA with a fraction of only 9.2 % DOctGA already shows a turbid solution at 0°C. In comparison, PEG-*co*-PDHexGA leads to a turbid solution at 0 °C with a comonomer ratio of 15.4 %.

166
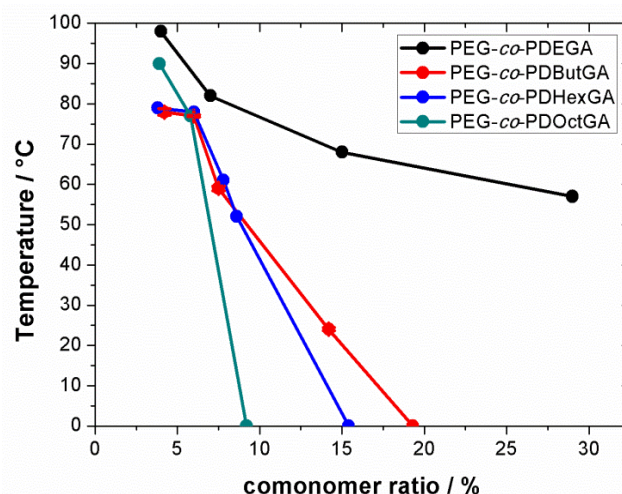
Figure 5. Cloud point temperatures as a function of the comonomer content. Black: PEG-*co*-PDEGA (data taken from Reuss et al.[14]) Red: PEG-*co*-PDButGA. Blue: PEG-*co*-PDHexGA. Green: PEG-*co*-PDOctGA. Note that the connecting lines are only to guide your eye. PEG-*co*-PDButGA with a comonomer ratio of 19.3 %, PEG-*co*-PDHexGA with 15.4 mol% DHexGA and PEG-*co*-PDOctGA with a comonomer fraction of 9.2 % show already turbid solutions at 0 °C.

To study the impact of pH, turbidity measurements were performed at different pH values as well. Cloud points were measured at pH 9, 11 and 14 for each gradient copolymer. The results are shown in Table 5, including the degree of protonation of the amines at a given pH (see Table 6). Figure 6 shows the correlation between pH and cloud point for the PEG-*co*-PDButGA copolymers (data for PEG-*co*-PDHexGA and PEG-*co*-PDOctGA see Figure S11 and Figure S12, Supporting Information). With increasing pH, the tertiary amine moieties become deprotonated and increasingly insoluble in aqueous solution, therefore the cloud point temperature decreases.

Table 5. Cloud point data at a given pH for PEG-*co*-PDXGA gradient copolymers.

No.	Composition	DXGA content	T_C/°C (pH=9)	T_C/°C (pH=11)	T_C/°C (pH=14)
1	PEG$_{92}$-*co*-PDButGA$_4$	4.2 %	100	78	71
2	PEG$_{95}$-*co*-PDButGA$_6$	6.0 %	100	76	69
3	PEG$_{123}$-*co*-PDButGA$_{11}$	7.5 %	86	59	53
4	PEG$_{91}$-*co*-PDButGA$_{15}$	14.2 %	37	24	21
5	PEG$_{100}$-*co*-PDHexGA$_4$	3.8 %	81	79	74
6	PEG$_{95}$-*co*-PDHexGA$_6$	6.0 %	80	78	76
7	PEG$_{107}$-*co*-PDHexGA$_9$	7.8 %	63	61	59
8	PEG$_{106}$-*co*-PDHexGA$_{10}$	8.6 %	52	51	45
9	PEG$_{99}$-*co*-PDOctGA$_4$	3.9 %	90	89	87
10	PEG$_{114}$-*co*-PDOctGA$_7$	5.8 %	77	75	69

T_C: cloud point temperature

Table 6. Degree of protonation of the respective amine moieties at a given pH.

Copolymer	pK_a	Degree of protonation at pH=9	Degree of protonation at pH=11	Degree of protonation at pH=14
PEG-*co*-PDButGA	9.6	76 %	3 %	0.03 %
PEG-*co*-PDHexGA	7.6	4 %	0.04 %	0.004 %
PEG-*co*-PDOctGA	5.6	0.04 %	0.004 %	0.0004 %
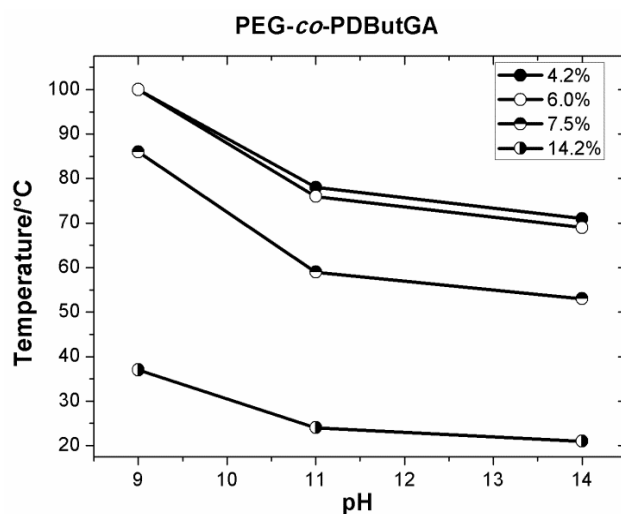
Figure 6. Cloud point temperature plotted versus pH for the series of PEG-*co*-PDButGA copolymers with varying DButGA fraction.

A comparison with the block copolymers is instructive: all PEG-*b*-PDXGA with 4.2 % DXGA fraction show no cloud point below 100 °C as well as PEG-*b*-PDButGA with 6.6 % DButGA fraction. Interestingly, all other PEG-*b*-PDXGA block copolymers with a DXGA fraction above 4 % yield turbid solutions already at 0 °C. Therefore, no diagram is shown for the block copolymers. This different behavior of aqueous copolymer solutions (gradient copolymers vs. block copolymers) once again supports the conclusion that no simple block structures are obtained by concurrent copolymerization of EO with DXGA.

CW EPR measurements. Figure 7 shows temperature profiles derived from turbidity measurements and from CW EPR spectroscopy on the amphiphilic spin-probe TEMPO (2,2,6,6-tetramethylpiperidin-1-)oxyl) in solutions of PEG-*co*-PDButGA and PEG-*co*-PDHexGA, respectively. Note that the EPR-derived profiles are based on the quantity χ_A. Here, χ_A is defined as the fraction of TEMPO probes diffusing freely in the aqueous polymer solutions. Correspondingly, $1-\chi_A$ denotes the fraction of TEMPO probes incorporated into collapsed, i.e., dehydrated and compacted PEG-*co*-PDButGA or PEG-

co-PDHexGA. The experimental details that lead to the χ_A functions have been described in detail.[33–35, 16] Spin probing CW EPR is sensitive for length scales below ~ 5 nm,[33] and thus one can state that a decreasing χ_A coincides with an advancing collapse of the polymers on nanoscopic length scales below approximately 5 nm.

From Figure 7, one can deduce that for PEG-*co*-PDButGA and PEG-*co*-PDHexGA the temperature difference between the onset of the nanoscale (EPR; $\chi_A < 1$) transition and the observable cloud point of the solutions increases with increasing content of the hydrophobic comonomers DButGA and DHexGA. Similar trends can be observed as for PEG-*co*-PDEGA.[14] This is a consequence of stronger hydrophobic interactions between the polymers at higher DXGA content that shift the cloud point to lower temperatures. In contrast, the onset of the nanoscale transition is not as markedly influenced by the hydrophobic content of the polymers. Their architecture on length scales below approximately 5 nm can be viewed as similar segments of a few DXGA monomers at any comonomer ratio, which dominate the nanoscale behavior (see references[33–35, 16] for details on this phenomenon). At high DXGA content, the two transitions almost merge (see Figure 7a), 14.2 % line). Most importantly, for PEG-*co*-PDButGA with a PDButGA content between 10 and 15 %, the two transitions fall into the medically relevant temperature range around body temperature (see Figure 7).

One can furthermore observe that on average more TEMPO spin probes interact with PEG-*co*-PDEGA[16] than with PEG-*co*-PDButGA and PEG-*co*-PDHexGA. This trend of diminishing interaction between TEMPO and the polymers with increasing side chain hydrophobicity is continued even for PEG-*co*-PDOctGA (see the Supporting Information for the corresponding data). This can be explained as follows: Earlier EPR and fluorescence studies on similar systems as the ones studied herein (aqueous solutions of amphiphilic copolymers with strongly hydrophobic side chains at one type of monomer, i.e.,

170

polysoaps[37, 38]) suggest that PEG-*co*-PDXGA copolymers form intramolecular micelles with the hydrophobic alkyl chains clustered in a micellar core (see Figure 9). This morphology will be increasingly fostered and more frequently adopted at lower temperatures with growing side chain length, as the hydrophobic micellar core becomes increasingly water-depleted (this is also reflected in our earlier study on PEG-*co*-PDEGA).[16]
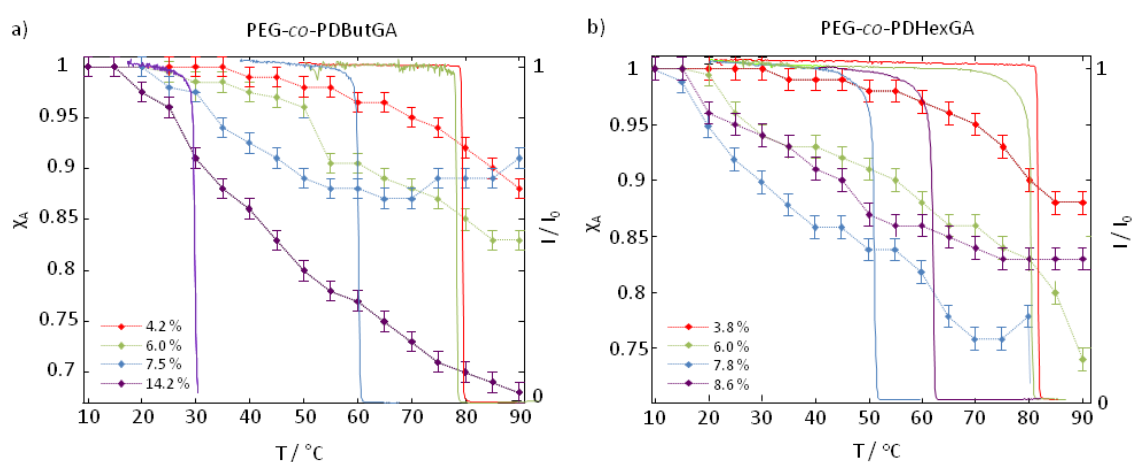
Figure 7. a) Fraction of TEMPO not incorporated into collapsed PEG-*co*-PDButGA domains, χ_A, as a function of temperature for different comonomer ratios (symbols connected by dashed lines). The corresponding turbidity measurements of the solutions (normalized transmitted light intensity, I/I_0) are shown as solid lines; b) fraction of TEMPO not incorporated into collapsed PEG-*co*-PDHexGA and corresponding turbidity profiles for different comonomer ratios. All measurements were performed using 1 wt.% polymer concentration.

Hence, as we observed on other PEG-based systems previously,[35] the strongly dehydrated apolar regions formed by PEG-*co*-PDXGA are less likely to interact with TEMPO with increasing side chain hydrophobicity and dense packing of the alkyl chains. This rationale also explains why in PEG-*co*-PDHexGA, the copolymer with the highest DHexGA fraction (8.6 %, see Figure 7b)) actually hosts a lower amount of spin probe at any given temperature than the copolymer with 7.8 % DHexGA. These results suggest that this is near

an optimum percentage for copolymer structures of DHexGA when thermally addressable (by small molecule probes) nanoscopic structures are intended.

Figure 8 shows data for the block analogues of PEG-*co*-PDButGA versus PEG-*co*-PDHexGA (mPEG-*b*-PDButGA versus mPEG-*b*-PDHexGA). For the block copolymers (Figure 8), similar general trends can be observed. For mPEG-*b*-PDButGA with increasing fraction of hydrophobic comonomer, the percentage of aggregate-incorporated TEMPO molecules at a given temperature increases (Figure 8a).
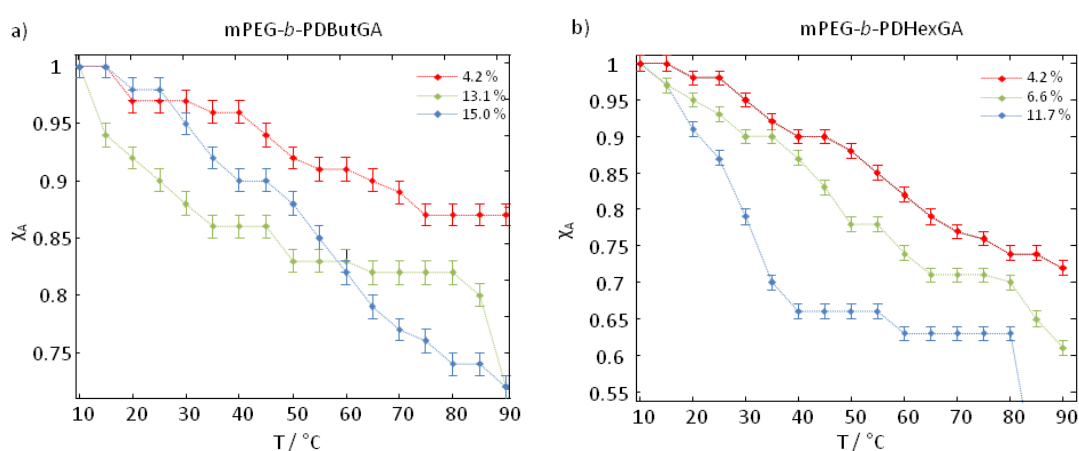
Figure 8. a) Fraction of TEMPO not incorporated into collapsed mPEG-*b*-PDButGA domains, χ_A, as a function of temperature for different comonomer ratios; b) fraction of TEMPO not incorporated into collapsed mPEG-*b*-PDHexGA domains, χ_A, as function of temperature for different comonomer ratios.

As in the case of gradient copolymers, the hexyl side chain bearing mPEG-*b*-PDHexGA at higher fractions of DHexGA (already above 6 %) actually hosts a lower amount of spin probe molecules at any given temperature than the copolymer with only 4 % DHexGA. This corroborates the above assumption that DHexGA at high monomer fractions forms nanoscopic structures that - due to high density - cannot take up TEMPO spin probes. Since the hydrophobic side groups are now concentrated in a block, it is not surprising that the optimum monomer fraction for small molecule uptake is significantly reduced from ~8 %

in the gradient-like copolymer to ~4 % in the block copolymer. This observation emphasizes the importance of the copolymers´ microstructure for their thermal behavior. We do not observe a significant decrease of χ_A with increasing side-chain length (when comparing mPEG-*b*-PDButGA and mPEG-*b*-PDHexGA see Figure 8b). This again might be a consequence of different (micellar) aggregate morphology[16] of block copolymers as compared to gradient-like copolymers (see Figure 9). Interestingly, we do not observe substantial differences in shapes of the χ_A profiles when the polymer architecture is altered from gradient to block structures for butyl and hexyl-side chain based copolymers. However, these differences in shape can be observed with ethyl-side chain based PEG-*co*-PDEGA and mPEG-*b*-PDEGA. Thus, increased side-chain hydrophobicity of the DXGA comonomers and the consequently fostered intramolecular micellization of the analogues gradient copolymers might prevent the cooperative nanoscale transition that was observed in gradient PEG-*co*-PDEGA, leading to similar profiles for both block- and gradient architectures. The assumption of intramolecular micellization below the cloud point is also in accordance with the fact that we did not observe significant pH-dependences of the χ_A profiles of mPEG-*b*-PDButGA and mPEG-*b*-PDHexGA (see the Supporting Information), while a strong pH-dependence was reported for mPEG-*b*-PDEGA.[16] Yet, for the more hydrophobic side chains (hexyl), clustering in a micellar core might lead to a decreasing influence of the degree of amine base protonation, lowering its influence on the phase transition mode significantly. However, due to the rather low fractions of TEMPO taken up by polymers with longer, more hydrophobic side chains, it is difficult to make conclusive statements (see the Supporting Information for the corresponding data) concerning the pH dependence on their transition.
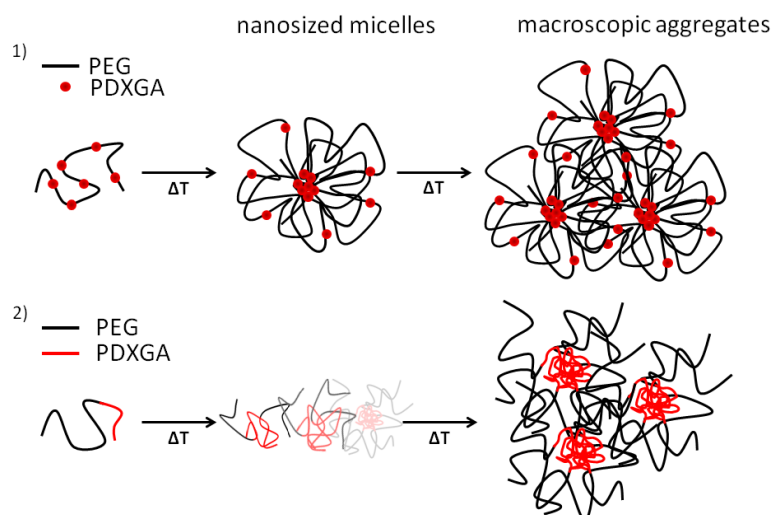
Figure 9. Proposed temperature transition mechanisms (according to Kurzbach et. al)[16] and micelle morphologies for 1) gradient copolymers and 2) block copolymers.

Note that some of the χ_A profiles in Figure 7 and Figure 8 show a steep decrease or an increase in χ_A at higher temperatures for some polymers. This has been observed earlier for PNiPAam hydrogels[39] and is a consequence of disproportionation of the TEMPO probes due to local acidic conditions, which catalyze redox reactions between two TEMPO probes.

Light scattering experiments. For a better understanding of the copolymers´ self-assembly in aqueous solution we also carried out light scattering experiments. First, DLS measurements were conducted in methanol to evaluate the hydrodynamic radius (R_h) of single copolymer chains and to ensure monomodal samples, without the presence of aggregates or traces of contamination. The hydrodynamic radii of the single copolymer chains ranged between 2 – 3 nm as expected for their range of molar masses (see Table S2 and S3 in the Supporting Information). The self-assembly studies were performed in an aqueous $Na_2CO_3/NaHCO_3$ buffer solution (pH = 10.8) to guarantee a consistent pH and degree of deprotonation of the tertiary amine moieties. DLS studies were combined with

SLS to further determine the topology and aggregation number of the assembled objects. From these experiments, well-defined structures were generally verified for the block copolymers with DXGA ratios below 5 mol% at a concentration of 1g·L⁻¹ (Figure S13-S15 and Table S2, Supporting Information). For mPEG$_{113}$-b-PDButGA$_5$, the dimensions of diffusing objects suggest a micelle-like structure ($\rho \approx 0.775$). More interestingly, for mPEG$_{113}$-b-PDHexGA$_5$ and mPEG$_{113}$-b-PDOctGA$_5$, we propose a vesicle-like structure based on the ρ ratio ($\rho \approx 1$) and the number of aggregation, which yields values of densities in an appropriate range (0.1-0.2 g·cm⁻³).[40] We note that with high DXGA content (> 5 mol%), larger aggregates (> 150 nm) are detected for all block copolymers at the given concentration of 1 g·L⁻¹. At the moment it is unclear, whether these sizes correspond to primary particles or are the result of secondary aggregation processes.

 In comparison, for gradient copolymers formed by random/concurrent copolymerization, well-defined solution structures are detected up to a DXGA fraction of 14.2 mol% (Table S3 and Figure S16-S20, Supporting Information). Note that for some gradient copolymers, a minor contribution of larger particles (≈ 100 nm) can be detected (not shown). This phenomenon has been already observed for PEG-co-PDEGA.[16] We assume that the minor contribution of larger particles is a consequence of impurities leading to further aggregation. This is supported by DLS of the samples in methanol (Table S3, Supporting Information).

Without discussing details, the block copolymers show the expected behavior concerning their self-assembly[41]; increasing volume fraction of the hydrophobic blocks forces the transition from single micelles with low aggregation numbers ($N_{agg.} = 30$) to vesicles with aggregation numbers of roughly $N_{agg.} = 600$. In comparison, equivalent gradient copolymers exhibit lower aggregation numbers and dimensions at comparable compositions. Furthermore the gradient copolymers allow considerably higher contents of hydrophobic constituents to form singular self assembled aggregates without secondary

aggregation compared to the block copolymers (Table S2 and S3, Supporting Information). These results support the proposed scheme (Figure 9), which was established by Kurzbach et. al for PEG-*co*-PDEGA copolymers based on computational studies and light scattering and refers to the structural similarity of PEG-*co*-PDXGA to polysoaps. However, to gain further inside into the morphology and inner structure SANS or SAXS measurements would be necessary.

3.2.5 Conclusion

Several new amine-functional PEG copolymers with pendant di(*n*-alkyl) amine moieties at the polyether backbone have been presented. Inspired by well-known, stimuli-responsive polybases, such as poly(*N,N*-dimethylaminoethylmethacrylate) (PDMAEMA) and poly(*N,N*-diethylaminoethylmethacrylate) (PDEAEMA)[42] based on vinyl monomer structures, we have introduced three *N,N*-di(*n*-alkyl) glycidyl amine comonomers (DButGA, DHexGA, DOctGA) and demonstrated successful copolymerization with ethylene oxide. PEG-copolymers with 3.8-25.0 mol% *n*-alkyl amine moieties were obtained. ^{1}H NMR kinetic studies, ^{13}C NMR triad analysis and differential scanning calorimetry confirmed a gradient microstructure for all PEG-*co*-PDXGA copolymers, albeit with no influence of the *n*-alkyl chain length on the monomers´ reactivity in the copolymerization with EO. Calculated r-parameters ranged between $r_{EO} = 1.84$, $r_{DButGA} = 0.49$ and $r_{EO} = 1.78$, $r_{DOctGA} = 0.42$. Light scattering experiments were conducted to study the self-assembly of the copolymers, where all block copolymers showed the formation of large aggregates when the content of DXGA (c = 1 g·L^{-1}) exceeded 5 mol%. Thermo- and pH-responsive behavior in aqueous solution represents the most intriguing feature of the novel polyether copolymers. This feature can be tailored and tuned by the comonomer ratio and has been analyzed in detail by both turbidity measurements and EPR

176

spectroscopy, studying the macroscopic and microscopic behavior, respectively. PEG-*co*-PDButGA with a comonomer ratio between 10 and 15% showed an inverse phase transition at the medically relevant temperature range around human body temperature. The thermal collapse and the related polymer-rich nanoscopic regions depend on the pH (amine-moieties), side chain length and copolymer architecture (block vs. gradient-like) in a complex manner. This renders these novel copolymers remarkably tunable, on both macroscopic and nanoscopic length scales. It is a promising feature that the novel glycidyl amine comonomers employed can be used to generate PEG copolymers with cloud points at physiological temperatures based on the incorporation of only a small fraction in a PEG structure. Altogether, we conclude that amine-functional PEG-based copolymers are a versatile class of pH-responsive polyethers that is promising not only for applications in drug targeting and delivery, but also for complex polyelectrolyte architectures in general. [5, 43]

3.2.6 Acknowledgements

3.2.7 References

[1]   a) R. Kjellander, E. Florin, *J. Chem. Soc., Faraday Trans. 1,* **1981**, *77*, 2053;
        b) T. Shikata, M. Okuzono, N. Sugimoto, *Macromolecules,* **2013**, *46*, 1965-1961.

[2]   a) A. Abuchowski, J. R. McCoy, N. C. Palczuk, T. van Es, F. F. Davis, *J. Biol.
        Chem.,* **1977**, *252*, 3582–3586; b) F. M. Veronese, G. Pasut, *Drug Discovery Today,*
        2005, *10*, 1451–1458.

[3]   B. Obermeier, F. Wurm, H. Frey, *Macromolecules,* **2010**, *43*, 2244–2251.

[4]   G. Pasut, F. M. Veronese, *J. Contr. Rel.,* **2012**, *161*, 461–472.

[5]   P. Lundberg, N. A. Lynd, Y. Zhang, X. Zeng, D. V. Krogstad, T. Paffen, M.
        Malkoch, A. M. Nystrom, C. J. Hawker, *Soft Matter,* **2013**, *9*, 82–89.

[6]   P. Alexandridis, T. Alan Hatton, *Colloids and Surfaces A: Physicochemical and
        Engineering Aspects,* **1995**, *96*, 1–46.

[7]   a) Y. Kimura, S. L. Regen, *J. Org. Chem.,* **1982**, *47*, 2493–2494; b) G. E. Totten,
        N. A. Clinton, *J. Macromol. Sci., Part C: Polym.Rev.,* **1988**, *28*, 293–337; c) D. E.
        Bergbreiter, J. Tian, C. Hongfa, *Chem. Rev.,* **2009**, *109*, 530–582.

[8]   a) C. Mangold, F. Wurm, H. Frey, *Polym. Chem.,* **2012**, *3*, 1714; b) B. Obermeier,
        F. Wurm, C. Mangold, H. Frey, *Angew. Chem. Int. Ed.,* **2011**, *50*, 7988–7997.

[9]   A.-L. Brocas, C. Mantzaridis, D. Tunc, S. Carlotti, *Progr. Polym.Sci.,* **2012**.

[10]   C. Mangold, C. Dingels, B. Obermeier, H. Frey, F. Wurm, *Macromolecules,* **2011**,
        44, 6326–6334.

[11]   B. F. Lee, M. Wolffs, K. T. Delaney, J. K. Sprafke, F. A. Leibfarth, C. J. Hawker,
        N. A. Lynd, *Macromolecules,* **2012**, *45*, 3722–3731.

[12]   B. Obermeier, H. Frey, *Bioconj. Chem.,* **2011**, *22*, 436–444.

[13]   C. Mangold, B. Obermeier, F. Wurm, H. Frey, *Macromol. Rapid Commun.,* **2011**,
        32, 1930–1934.

[14]   V. S. Reuss, M. Werre, H. Frey, *Macromol. Rapid Commun.,* **2012**, *33*, 1556–1561.

[15]   V. S. Reuss, B. Obermeier, C. Dingels, H. Frey, *Macromolecules,* **2012**, *45*, 4581–
        4589.

[16]   D. Kurzbach, V. S. Wilms, H. Frey, D. Hinderberger, *ACS Macro Lett.,* **2013**, 128–
        131.

[17]   S. Rangelov, C. Tsvetanov, *Des. Mon. Polym.,* **2001**, *4*, 39–43.

[18]   A. Lee, P. Lundberg, D. Klinger, B. F. Lee, C. J. Hawker, N. A. Lynd, *Polym.
        Chem.,* **2013**, *4*, 5735–5742.

[19]   R. Hovland, C. Gløgård, A. J. Aasen, J. Klaveness, *J. Chem. Soc., Perkin Trans. 2,* **2001**, 929–933.

[20]   D. M.Burness, O.H. Bayer, *J. Org. Chem.,* **1963**, *28*, 2283–2288.

[21]   M. Hans, H. Keul, M. Moeller, *Polymer,* **2009**, *50*, 1103–1108.

[22]   T. Hamaide, A. Goux, M.-F. Llauro, R. Spitz, A. Guyot, *Angew. Makromol. Chemie,* **1996**, *237*, 55–77.

[23]   V. Rejsek, D. Sauvanier, C. Billouard, P. Desbois, A. Deffieux, S. Carlotti, *Macromolecules,* **2007**, *40*, 6510–6514.

[24]   F. Heatley, G.-e. Yu, C. Booth, T. G. Blease, *Eur. Polym. J.,* **1991**, *27*, 573–579.

[25]   W. Zhang, J. Allgaier, R. Zorn, S. Willbold, *Macromolecules,* **2013**, *46*, 3931–3938.

[26]   C. Mangold, F. Wurm, B. Obermeier, H. Frey, *Macromolecules,* **2010**, *43*, 8511–8518.

[27]   a) M. Fineman, S. D. Ross, *J. Polym. Sci.,* **1950**, *5*, 259–262; b) A. Natalello, M. Werre, A. Alkan, H. Frey, *Macromolecules,* **2013**, *46*, 8467–8471.

[28]   A. Stolarzewicz, D. Neugebauer, *Macrom. Chem. Phys.,* **1999**, *200*, 2467–2470.

[29]   V. A. Ponomarenko, A. M. Khomutov, S. I. Il'chenko, A. V. Ignatenko, *Polymer Science U.S.S.R.,* **1971**, *13*, 1735–1740.

[30]   S. Boileau, A. Deffieux, D.Lassalle, F.Menezes, B.Vidal, *Tetrahedron Lett.,* **1978**, *19*, 1767–1770.

[31]   Fuller, C. S., *Chem. Rev.,* **1940**, *26*, 143–167.

[32]   C. Tonhauser, A. Alkan, M. Schömer, C. Dingels, S. Ritz, V. Mailänder, H. Frey, F. R. Wurm, *Macromolecules,* **2013**, *46*, 647–655.

[33]   D. Kurzbach, M. J. N. Junk, D. Hinderberger, *Macromol. Rapid Commun.,* **2013**, *34*, 119–134.

[34]   D. Kurzbach, M. N. Reh, D. Hinderberger, *Chem. Phys. Chem.,* **2011**, *12*, 3566–3572.

[35]   D. Kurzbach, M. Schömer, V. S. Wilms, H. Frey, D. Hinderberger, *Macromolecules,* **2012**, *45*, 7535–7548.

[36]   S. Saeki, N. Kuwahara, M. Nakata, M. Kaneko, *Polymer,* **1976**, *17*, 685–689.

[37]   A. Laschewsky, *Adv. Polym. Sci.*, **1995**, *124*, 1-86.

[38]   M. Hemmelmann, D. Kurzbach, K. Koynov, D. Hinderberger, R. Zentel, *Biomacromolecules,* **2012**, *13*, 4065-4075.

[39]   M. J. N. Junk, U. Jonas, D. Hinderberger, *Small,* **2008**, *4*, 1485–1493.

[40]   M. Antonietti, S. Förster, *Adv. Mat.,* **2003**, *15*, 1323–1333.

[41]   a) M. S. Nikolic, C. Olsson, A. Salcher, A. Kornowski, A. Rank, R. Schubert, A. Frömsdorf, H. Weller, S. Förster, *Angew. Chem. Int. Ed.,* **2009**, *48*, 2752–2754; b) D. Duque, *J. Chem. Phys.,* **2003**, *119*, 5701–5704; c) S. Förster, M. Zisenis, E. Wenz, M. Antonietti, *J. Chem. Phys.,* **1996**, *104*, 9956–9970.

[42]   a) E. S. Gil, S. M. Hudson, *Progr. Polym. Sci.,* **2004**, *29*, 1173–1222; b) W. Jaeger, J. Bohrisch, A. Laschewsky, *Progr. Polym. Sci.,* **2010**, *35*, 511–577; c) T. Thavanesan, C. Herbert, F. A. Plamper, *Langmuir,* **2014**, *30*, 5609–5619.

[43]   a) N. Murthy, J. Campbell, N. Fausto, A. S. Hoffman, P. S. Stayton, *Bioconj. Chem.,* **2003**, *14*, 412–419; b) V. S. Wilms, H. Frey, *Polym. Int.,* **2013**, *62*, 849–859; c) J. Meyer, H. Keul, M. Möller, *Macromolecules,* **2011**, *44*, 4082–4091.

3.2.8 Supporting Information

Instrumentation. ^{1}H NMR spectra (300 MHz) and ^{13}C NMR spectra (75 MHz) were recorded using a Bruker Avance III HD 300 spectrometer equipped with a 5 mm BBFO Z-gradient probe with an automated tuning and matching device (ATM) as well as a B-ACS 60 auto sampler. Kinetic studies using ^{1}H NMR spectroscopy were investigated on a Bruker Avance III HD 400 apparatus operated at 400 MHz with a 5 mm BBFO-SmartProbe (Z-gradient) and an ATM as well as a SampleXPress 60 auto sampler. For kinetic studies, a ^{1}H NMR spectrum with 8 scans was recorded every 30 seconds at elevated temperatures of 80 °C. The reaction conditions for the kinetic studies were equivalent to the conditions in flask to obtain comparable data. All spectra were referenced internally to residual proton signals of the deuterated solvent (CDCl$_3$, DMSO-d_6 or THF-d_8). GPC measurements were performed in DMF (containing 0.25 g·L^{-1} lithium bromide as an additive). An Agilent 1100 Series was used as an integrated instrument, including a PSS HEMA column ($10^6/10^5/10^4$ A) a UV (275 nm) and a RI detector. Calibration was carried out using poly(ethylene glycol) standards purchased from Polymer Standards Service.

DSC measurements were performed under nitrogen atmosphere using a PerkinElmer DSC 8500 with PerkinElmer CLN2 in the temperature range from – 100 °C to 100 °C at heating rates of 20 and 10 K·min^{-1} for the first and the second heating run, respectively.

Cloud points were determined in Milli-Q water at a concentration of 20 mg·mL^{-1} and observed by optical transmittance of a light beam (λ = 670 nm). Transmitted laser light intensity was plotted versus the temperature of the sample cell. The cloud point temperatures were determined as inflection point of the turbidity profiles. The measurements were performed on a Jasco V-630 photospectrometer with a Jasco ETC-717 Peltier element or a Tepper turbidimeter TP1 through a 1 cm sample quartz cell. The

heating/cooling rate was 1 K min^{-1}, and values were recorded in 1 K steps. The different pH values were adjusted by adding conc. HCl (aq.) or 50w% NaOH solution via Eppendorf pipettes. Titrations of the polyethers were performed using 0.1 mol·L^{-1} HCl (aq.) or 0.1 mol·L^{-1} NaOH (aq.) were repeated three times for each copolymer. pH measurements were performed by using a pH electrode from HANNA instruments.

Static (SLS) and dynamic light scattering (DLS) were performed at 293.15 K utilizing an ALV 3000 correlator, an ALV-SP86 goniometer equipped with an ALV High QE APD Avalanche photodiode fiber optical detection system, and a He-Ne laser (Uniphase, 22 mW, $\lambda = 632.8$ nm). For the unimer solutions in methanol with hydrodynamic radii well below 10 nnm and therefore without angular dependency of the apparent diffusion coefficient DLS was performed at angles of 20° or 30° (setup 1). Self-assembling samples in aqueous solutions were analyzed by DLS using a multiangular detection goniometer (ALV-CGS-8F SLS/DLS 5022F) equipped with a He/Ne Laser (Uniphase, 25 mW, $\lambda=632.8$ nm), eight simultaneously working ALV7004 correlators connected to eight ALV high QE APD avalanche photodiode fiber optical detectors; detectors are separated by 17°, two independent simultaneous sets of measurement separated by 9° resulting in 16 angular dependent values covering an angular range from 30 to 158° thus allowing extrapolation to scattering angle zero with respect to polydispersities effects on diffusion coefficient. All measurements were performed at 20±0.1 °C with the help of external ultra-thermostats (Lauda RKS 6C). Diffusion coefficients were determined from intensity autocorrelation functions after Siegert transformation (g_1(t)=sqrt(abs((g_2(t)-A)/A))*sign(g_2(t)) with A the experimentally measured baseline) by a non-linear fitting (Simplex algorithm) of the field autocorrelation function by applying mono- or biexponential fit functions, and the polydispersity was evaluated by cumulant analysis in terms of the normalized second cumulant μ_2 (Figure S21). Hydrodynamic radii were calculated by applying the Stokes-Einstein equation. Static light scattering was conducted from $\theta = 30°$ to $\theta = 150°$ in steps of

182

2.5 or 5 degrees using the ALV SP-86 goniometer (setup 1) allowing the determination of the apparent squared radius of gyration $<R_g^2>_z$; aggregation numbers were evaluated by the intensity ratios of the self-assembled systems in water extrapolated to zero scattering angle and the unimers in methanol (no angular dependency), which is allowed due to isorefractive conditions; both, concentration dependencies and citrical aggregation concentration (cac) influences are neglected due to low concentration limit conditions (unimer) and cac well below 0.1 $g \cdot L^{-1}$ for the aggregates, which has been tested for the most hydrophilic sample (not shown) by DLS.

Samples were prepared in methanol (25mM LiBr), in 0.1 M HCL solution and in $Na_2CO_3/NaHCO_3$ buffer solution (pH = 10.8) with a concentration of 1 $g \cdot L^{-1}$. If not noted elsewhere, methanol solutions were passed through Millex-LG filters (0.2 μm) and aqueous solutions were passed through Acrodisc GHP filters (0.2 μm or 0.45 μm pore size) into dust free cuvettes.

Continuous wave (CW) EPR spectra at X-band (~9.4 GHz) were measured on a Magnettech (Berlin, Germany) MiniScope MS200 benchtop CW EPR spectrometer with a variable-temperature cooling/heating unit. The sample volume was always large enough to fill the complete resonator volume in the probehead (>300 μL). Each sample was left at the particular temperature for exactly 5 minutes to equilibrate. Changes in mole fractions of species A or B after longer periods of time were not detected. Typical experimental parameters were: modulation amplitude of 0.06 mT and sweep width of 10 mT. Details on data analysis and EPR sample preparation are summarized in the section of EPR CW measurements.

Reagents. Poly(ethylene glycol) monomethyl ether (mPEG5000, M_n = 5000 $g \cdot mol^{-1}$) was purchased from Fluka. *N,N*-Di(*n*-butyl) amine, epichlorohydrin (99 %), sodium hydroxide and ethylene oxide (99.5 %) were purchased from Aldrich. Chloroform-*d,* DMSO-*d₆,* THF-

d8, NaOD and DCl were purchased from Deutero GmbH. *N,N*-di(*n*-hexyl) amine was purchased from Abcr. All other solvents and reagents were ordered from Acros Organics.
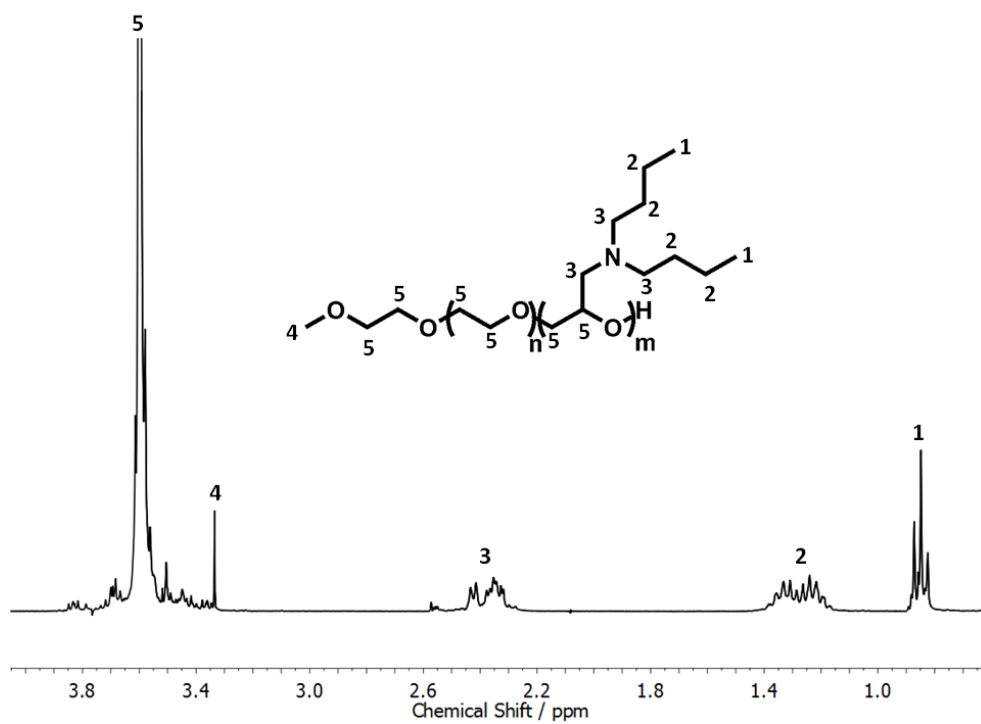
Figure S1. ^{1}H NMR spectrum (300 MHz, C*D*Cl$_3$) of PEG-*co*-PDButGA.
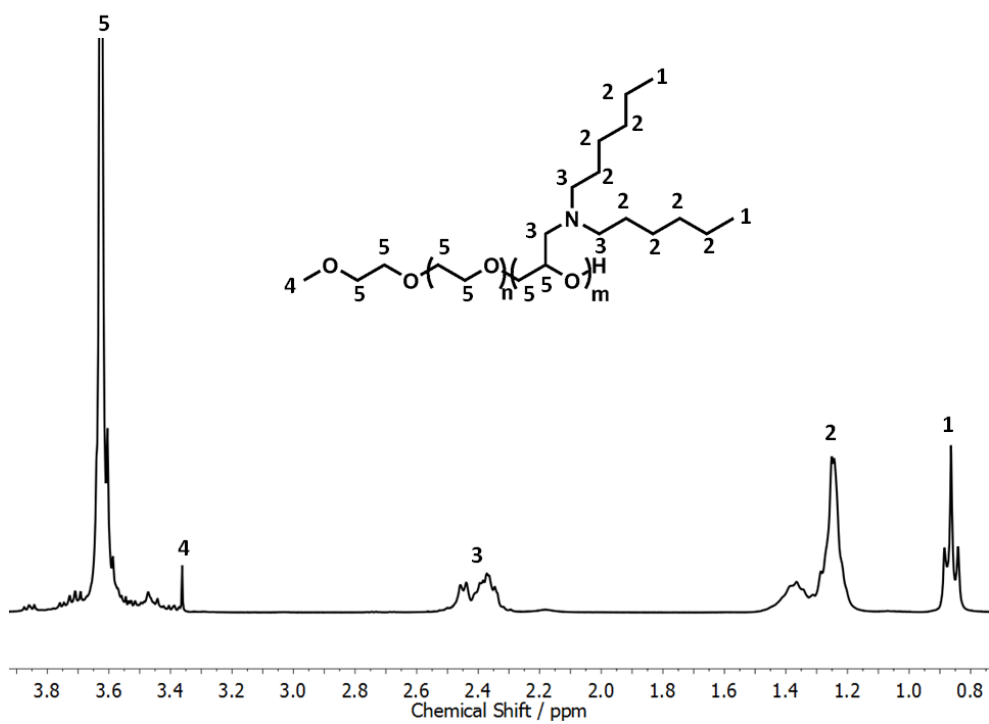
Figure S2. ^{1}H NMR spectrum (300 MHz, CDCl$_3$) of PEG-*co*-PDHexGA.
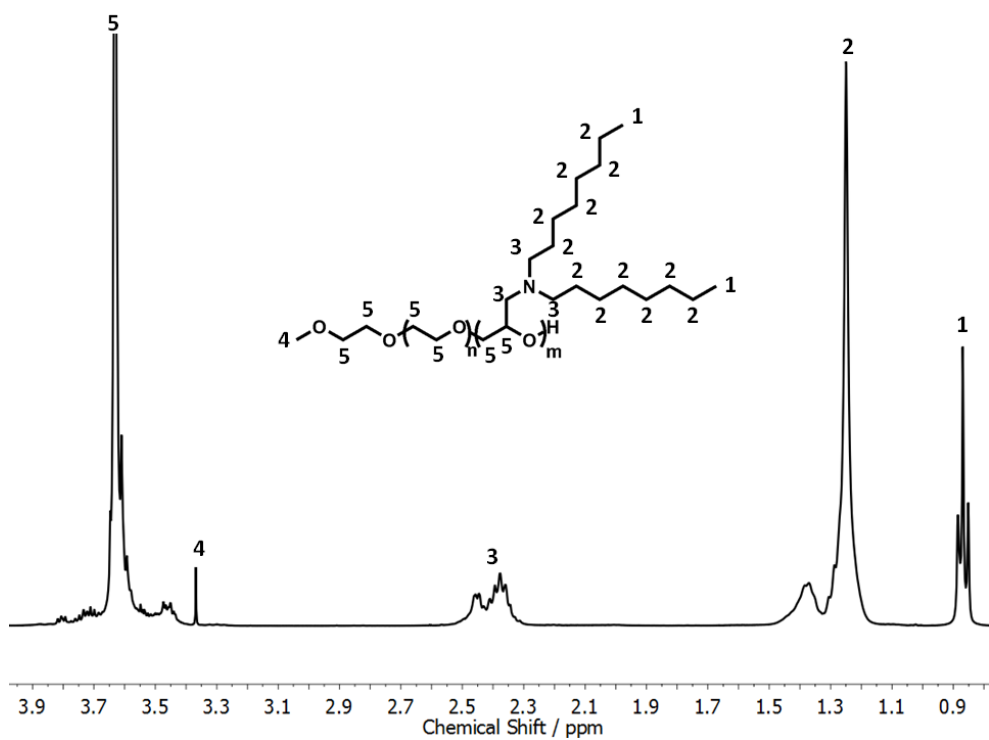
Figure S3. ^{1}H NMR spectrum (300 MHz, CDCl$_3$) of PEG-*co*-PDOctGA.
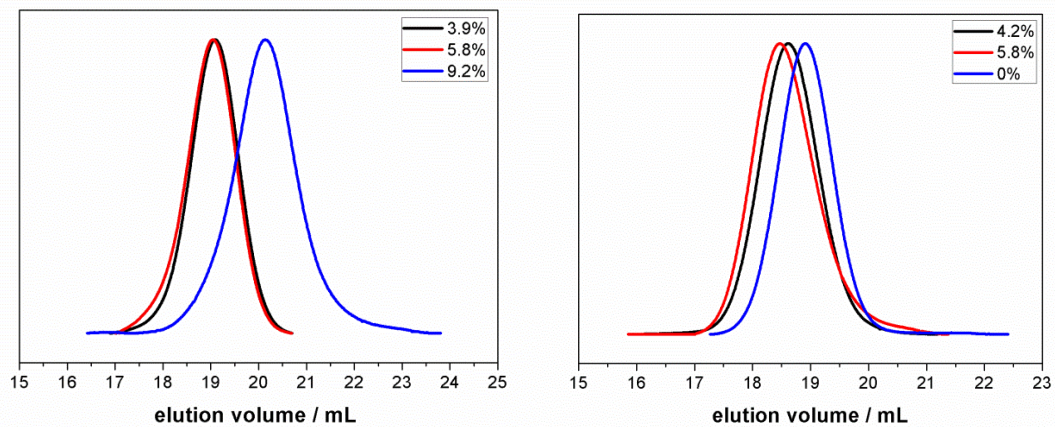
Figure S4. GPC elution traces (DMF, RI detection, PEG standards) of (left) PEG-*co*-PDOctGA and (right) mPEG-*b*-PDOctGA.
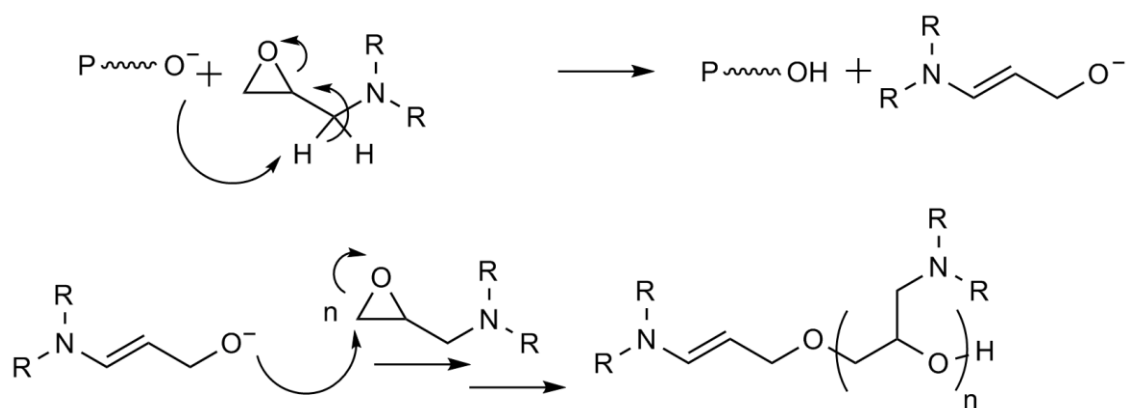
Scheme S1. Chain transfer to monomer.
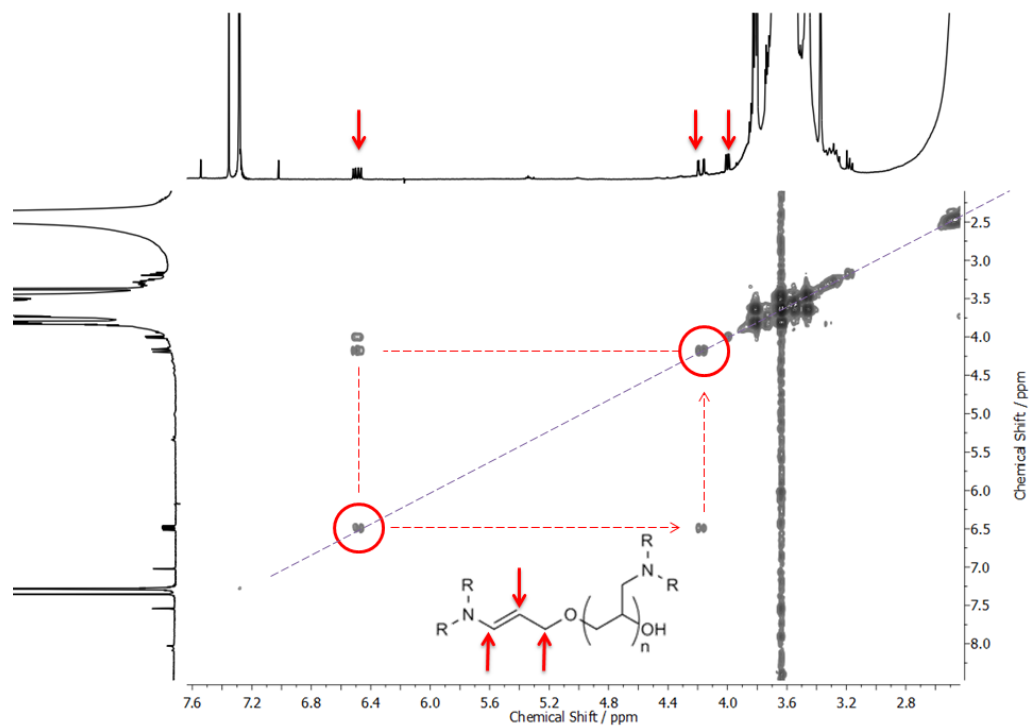
Figure S5. ^{1}H,^{1}H COSY NMR of the reaction solution of PEG-*b*-PDOctGA before precipitation in diethyl ether.

^{1}H NMR kinetic studies
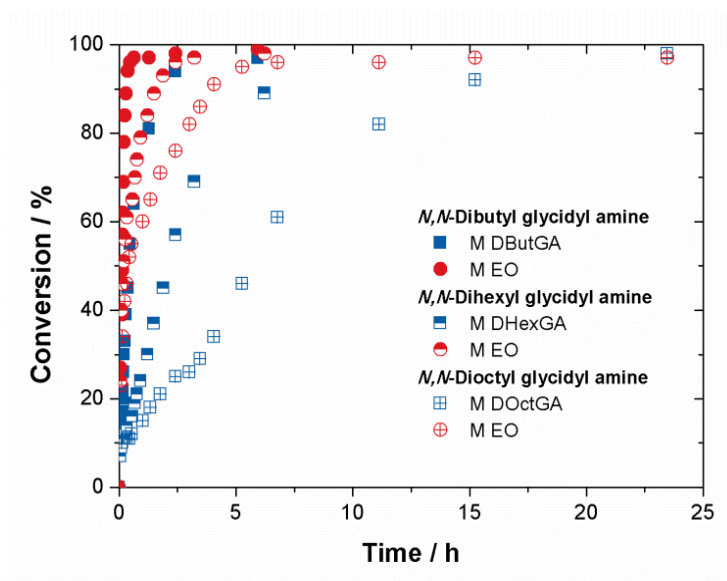
Figure S6. Monomer conversion versus time plots for copolymerization of EO and the different DXGA monomers (ca. 10-15 %) at 80 °C.

Copolymerization:

$$P_1^- + M_1 \xrightarrow{k_{11}} P_1 M_1^-$$

$$P_1^- + M_2 \xrightarrow{k_{12}} P_1 M_2^-$$

$$P_2^- + M_1 \xrightarrow{k_{21}} P_2 M_1^-$$

$$P_2^- + M_2 \xrightarrow{k_{22}} P_2 M_2^-$$
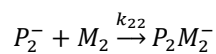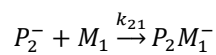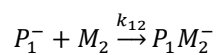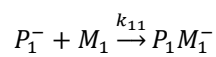
P_1^-; P_2^-: active chain end

M_1; M_2: monomer

k: reactivity constant

Fineman-Ross equation: $x \cdot \frac{1-X}{X} = -\frac{x^2}{X}r_1 + r_2$ with $r_1 = \frac{k_{11}}{k_{12}}$ and $r_2 = \frac{k_{22}}{k_{21}}$

x: mole fraction of the stock

X: mole fraction of the polymer at certain mole fractions of the stock

r_1: reactivity ratio for monomer M_1

r_2: reactivity ratio for monomer M_2
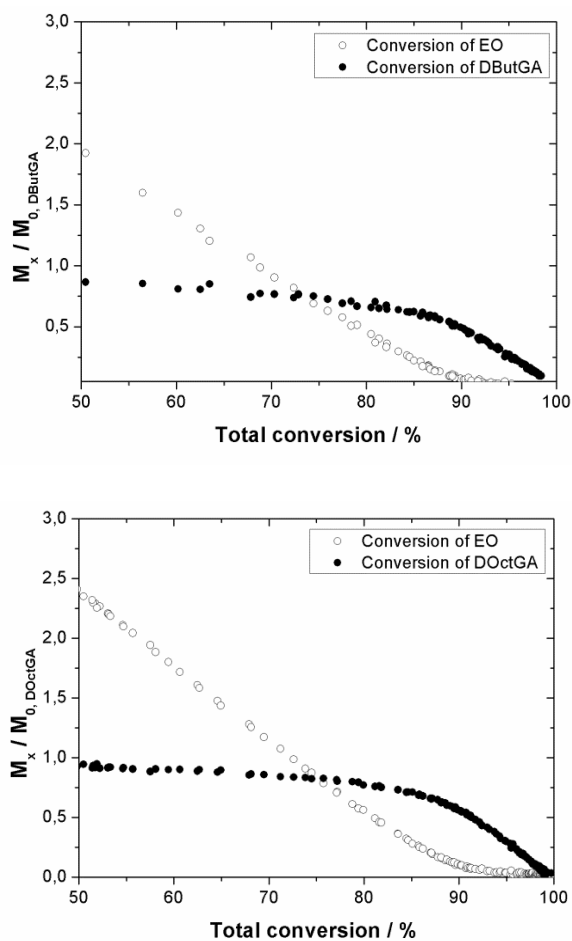
Figure S7. Monomer concentration plotted versus total conversion for EO and (top) DButGA and (bottom) DOctGA, respectively.

Cloud point measurements
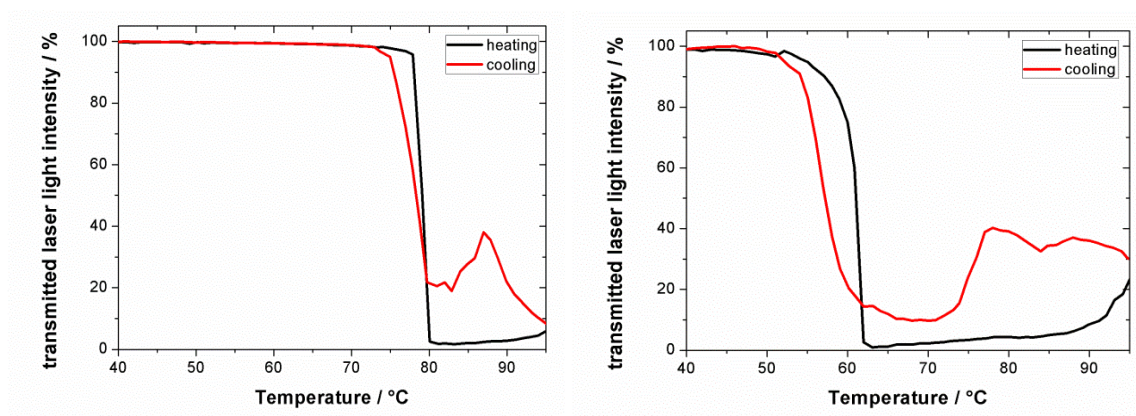
Figure S8. Heating and cooling cycles of PEG-*co*-PDHexGA with 3.8 % (left side) and 7.8 % (right side) DHexGA content. The diagrams show the transmitted laser light intensity plotted versus the temperature.

Copolymers	T_c /°C heating	T_c /°C cooling
PEG$_{92}$-*co*-PDButGA$_4$	78	76
PEG$_{95}$-*co*-PDButGA$_6$	77	77
PEG$_{136}$-*co*-PDButGA$_{11}$	59	60
PEG$_{91}$-*co*-PDButGA$_{15}$	24	22
PEG$_{100}$-*co*-PDHexGA$_4$	79	78
PEG$_{95}$-*co*-PDHexGA$_6$	78	79
PEG$_{107}$-*co*-PDHexGA$_9$	61	57
PEG$_{106}$-*co*-PDHexGA$_{10}$	52	---
PEG$_{99}$-*co*-PDOctGA$_4$	90	87
PEG$_{114}$-*co*-PDOctGA$_7$	77	78

Table S1. Cloud points of heating and cooling cycles. The aqueous solution of PEG$_{106}$-*co*-PDHexGA$_{10}$ stayed turbid for several hours after cooling back to room temperature. Therefore, no $T_{c, cooling}$ is provided.
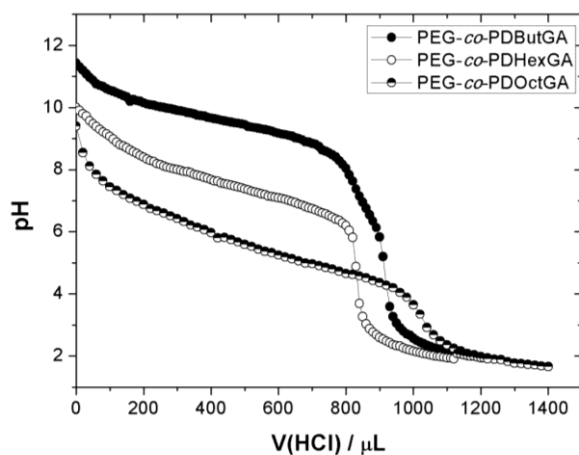
Figure S9. pH titration profiles of PEG-*co*-PDButGA, PEG-*co*-PDHexGA and PEG-*co*-PDOctGA at 5wt % with 0.1M HCl solution. Titrations were repeated three times for each copolymer. Here, a representative titration curve for each copolymer class is shown. The pK_a's can be estimated to be 9.6, 7.6 and 5.6 respectively.
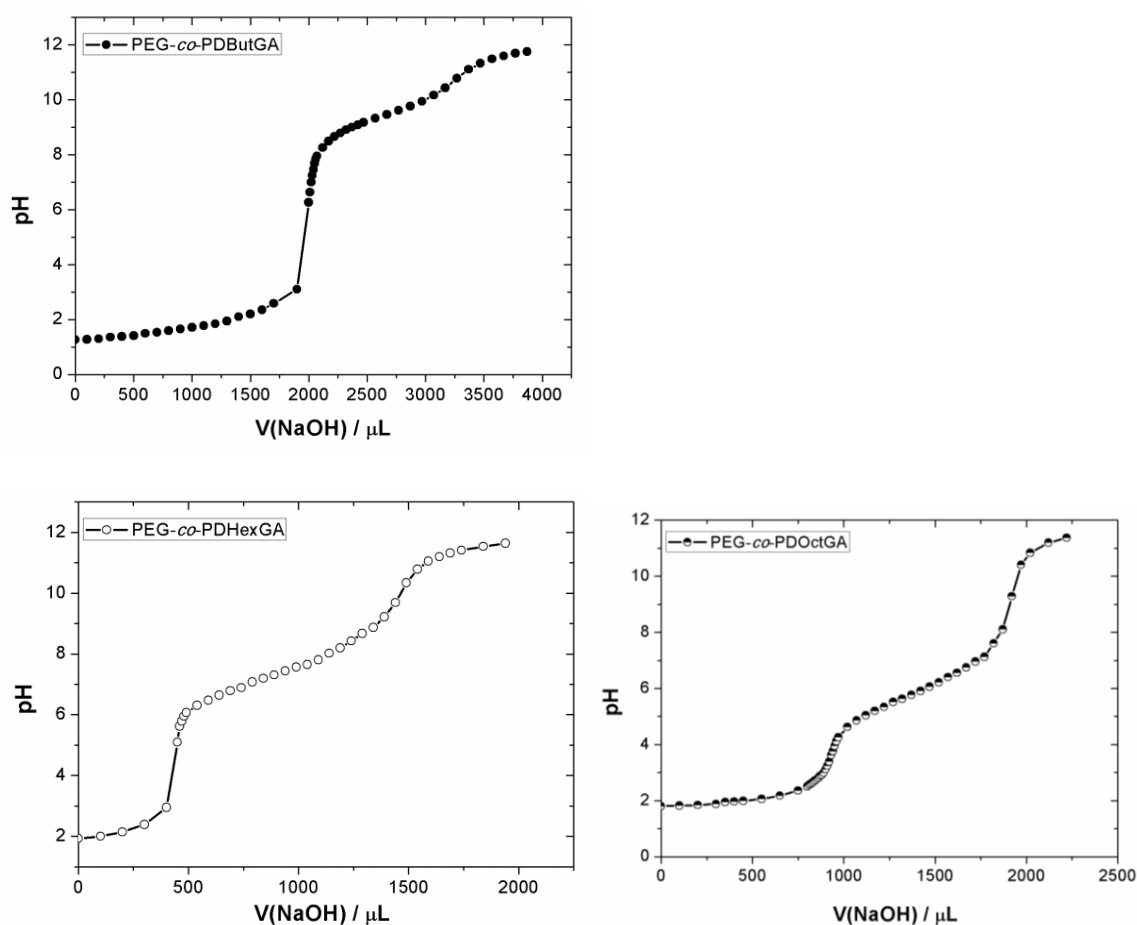
Figure S10. pH titration profiles of PEG-*co*-PDButGA (upper left), PEG-*co*-PDHexGA (upper right) and PEG-*co*-PDOctGA (bottom) at 5wt % with 0.1M NaOH solution, after acidification. Titrations were repeated three times for each copolymer. One representative

titration curve for each copolymer class is shown. In general, the copolymers show a buffering capacity to where pH ≈ pK_a.
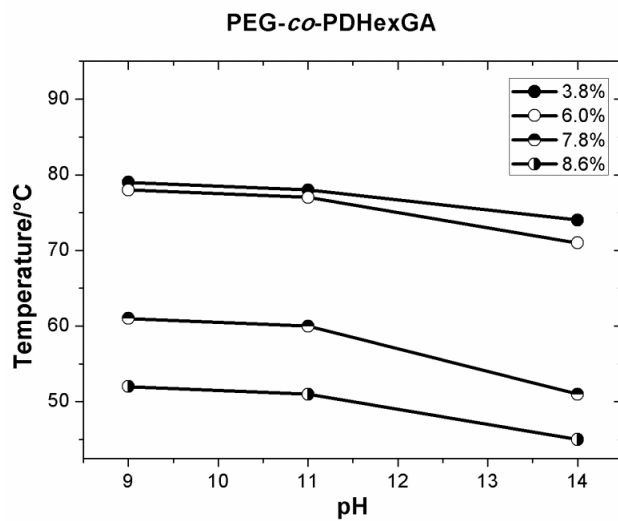
Figure S11. Cloud point temperature plotted versus pH for the series of PEG-*co*-PDHexGA copolymers with varying DHexGA fraction.
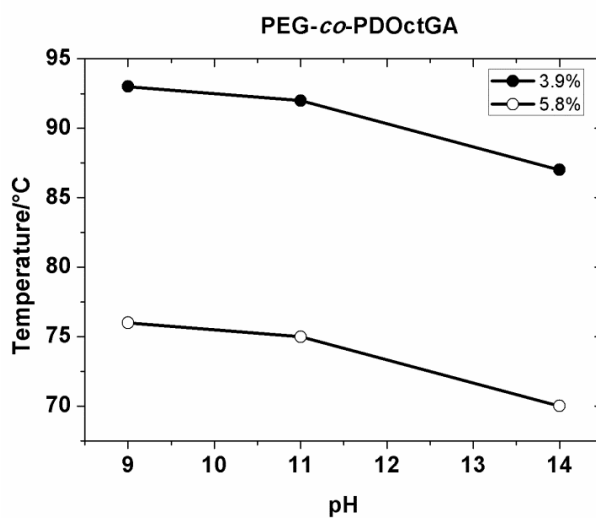
Figure S12. Cloud point temperature plotted versus pH for the series of PEG-*co*-PDOctGA copolymers with varying DOctGA fraction.

Light scattering measurements

Table S2. Results of the light scattering experiments for the mPEG-*b*-PDXGA block copolymers.

Polymer	DXGA content / %	Solvent	R_h / nm	μ_2	R_g / nm	$N_{agg.}$
mPEG$_{113}$	0	Methanol	2.2	---	---	---
mPEG$_{113}$-*b*-PDButGA$_5$	4.2	Methanol	2.7	**---**	**---**	**---**
		Buffer solution	10.3	0.08	<10	34
mPEG$_{113}$-*b*-PDHexGA$_5$	4.2	Methanol	2.3	---	---	---
		Buffer solution	26	0.16	33.5	360
mPEG$_{113}$-*b*-PDOctGA$_5$	4.2	Methanol	2.3	---	---	---
		Buffer solution	48	0.2	48.1	590

R_h = hydrodynamic radius R_g = radius of gyration μ_2 = normalized second cumulant

$N_{agg.}$ = number of aggregation

Table S3. Results of the light scattering experiments for the PEG-*co*-PDXGA gradient copolymers.

Polymer	DXGA content / %	Solvent	R_h / nm	μ_2	R_g / nm	$N_{agg.}$
PEG$_{95}$-*co*-PDButGA$_6$	6.0	Methanol	2.2	---	---	---
		Buffer solution	6	0.15	$\leq$10	7
PEG$_{91}$-*co*-PDButGA$_{15}$	14.2	Methanol	3.5/115[a]	---	---	---
		Buffer solution	7/100[a]	---	25[b]	---
PEG$_{95}$-*co*-PDHexGA$_6$	6.0	Methanol	2.1	---	---	---
		Buffer solution	11.2	0.2	17.3	56
PEG$_{107}$-*co*-PDHexGA$_9$	7.8	Methanol	2.3			
		Buffer solution	8.1	0.1	13	36
PEG$_{106}$-*co*-PDHexGA$_{10}$	8.6	Methanol	2/45[a]			
		Buffer solution	10/110[a]	0.1	34[b]	60
PEG$_{99}$-*co*-PDOctGA$_4$	3.9	Methanol	2.1	---	---	---
		Buffer solution	7.7	---	<10	---
PEG$_{114}$-*co*-PDOctGA$_7$	5.8	Methanol	2.3			
		Buffer solution	24	0.17	34.9	190

R_h = hydrodynamic radius R_g = radius of gyration μ_2 = normalized second cumulant

$N_{agg.}$ = number of aggregation

[a] Bimodal distribution with a minor contribution of large particles.

[b] Apparent radius of gyration, which is related to a bimodal distribution detected by DLS.
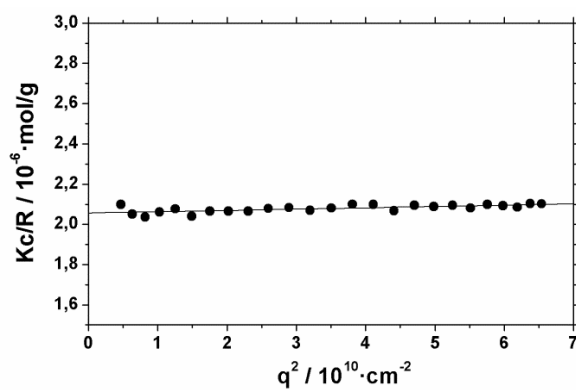
Figure S13. Static light scattering (Na$_2$CO$_3$/NaHCO$_3$-buffer, c = 1 g·L^{-1}) of mPEG$_{113}$-*b*-PDButGA$_5$ (no angular dependency of DLS (not shown)).
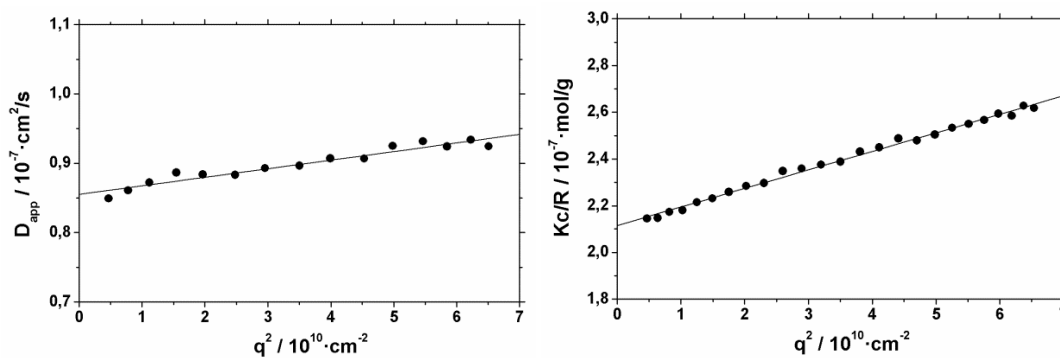
Figure S14. Dynamic and static light scattering (Na$_2$CO$_3$/NaHCO$_3$-buffer, c = 1 g·L^{-1}) of mPEG$_{113}$-*b*-PDHexGA$_5$.
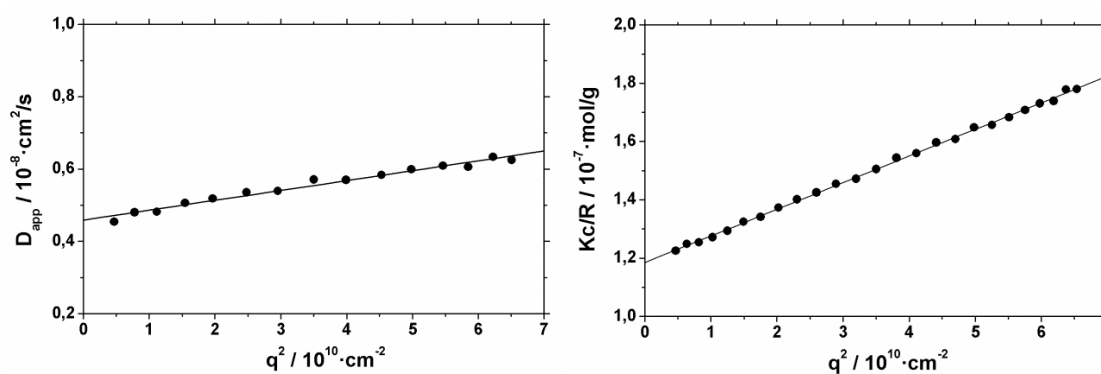
Figure S15. Dynamic and static light scattering (Na$_2$CO$_3$/NaHCO$_3$-buffer, c = 1 g·L^{-1}) of mPEG$_{113}$-*b*-PDOctGA$_5$.
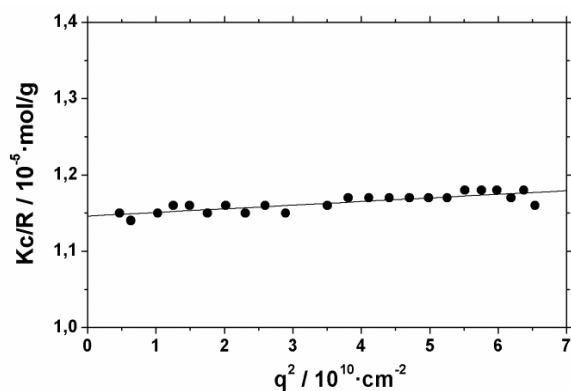
Figure S16. Static light scattering (Na$_2$CO$_3$/NaHCO$_3$-buffer, c = 1 g·L^{-1}) of PEG$_{95}$-*co*-PDButGA$_6$ (no angular dependency of DLS (not shown)).
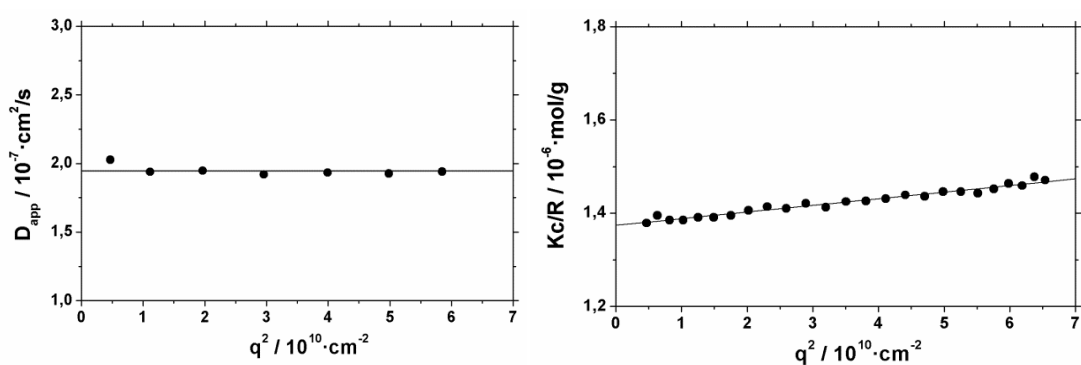
Figure S17. Dynamic and static light scattering (Na$_2$CO$_3$/NaHCO$_3$-buffer, c = 1 g·L^{-1}) of PEG$_{95}$-*co*-PDHexGA$_6$.
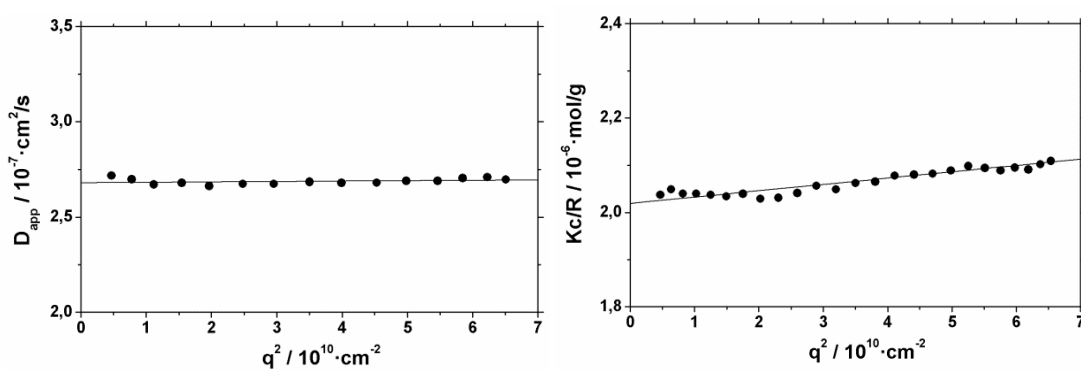
Figure S18. Dynamic and static light scattering (Na$_2$CO$_3$/NaHCO$_3$-buffer, c = 1 g·L^{-1}) of PEG$_{107}$-*co*-PDHexGA$_9$.
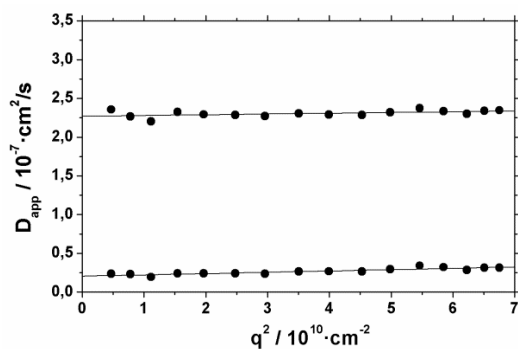
Figure S19. Dynamic light scattering (Na_2CO_3/$NaHCO_3$-buffer, c = 1 g·L^{-1}) of PEG_{106}-*co*-$PDHexGA_{10}$ with a bimodal distribution corresponding to micelles of Rh≅10 nm and larger aggregates with Rh≅100 nm; static light scattering not shown due to physical meaningless.
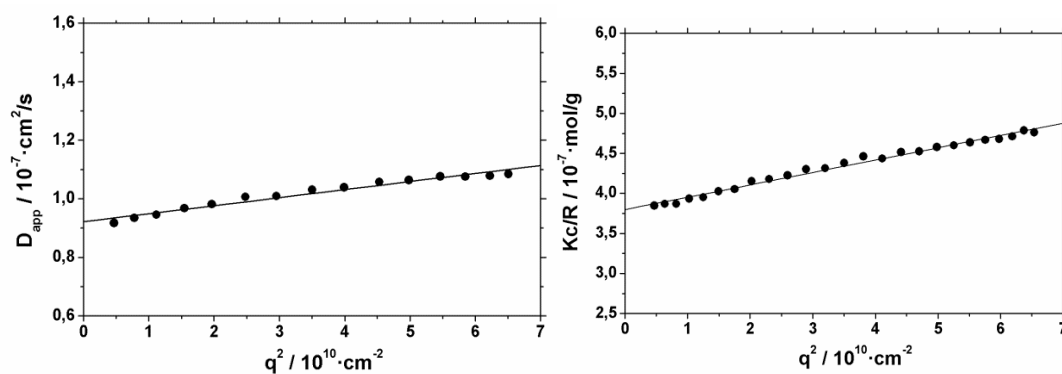
Figure S20. Dynamic and static light scattering (Na_2CO_3/$NaHCO_3$-buffer, c = 1 g·L^{-1}) of PEG_{114}-*co*-$PDOctGA_7$.
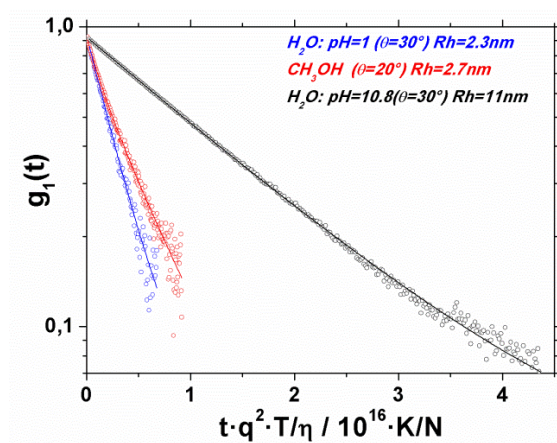
Figure S21. Comparison of the experimental autocorrelation functions (universal reduced plot with respect to different experimental conditions) of $mPEG_{113}$-*b*-$PButGA_5$ in methanol, aqueous acidic and aqueous alkaline solution plotted (c = 1 g·L^{-1}); data in methanol and acidic water are normalized to the experimental intercept of the AKF from alkaline water).

197

CW EPR measurements

Sample Preparation.

In all cases, 0.2 mM aqueous TEMPO *solutions* were freshly prepared and the required amount of polymer was dissolved subsequently in the TEMPO solution to yield 1 wt% polymer concentration. Afterwards, the solution was transferred to 3 mm outer diameter quartz tubes. All substances not newly reported herein are commercially available and were used without further purification.

EPR Spectroscopy.

CW EPR spectra at X-band (~9.4 GHz) were measured on a Magnettech (Berlin, Germany) MiniScope MS200 benchtop CW EPR spectrometer with a variable-temperature cooling/heating unit. The sample volume was always large enough to fill the complete resonator volume in the probehead (>300 μL). Each sample was left at the particular temperature for exactly 5 minutes to equilibrate. Changes in mole fractions of species A or B after longer periods of time were not detected. Typical experimental parameters were: modulation amplitude of 0.06 mT and sweep width of 10 mT.

Data Analysis.

All spectral simulations were performed with home-written programs in MATLAB (The MathWorks, Inc.) employing the EasySpin toolbox for EPR spectroscopy.[1] Simulations of CW EPR spectra in fluid solution were performed by using a model, which is based on the fast-motion theory and a program developed by Freed and Fraenkel as implemented in EasySpin.[2] These simulations can account for the effect of intermediate or slow rotational diffusion of the radical on the EPR spectra. All reported values for hyperfine-coupling parameters and spectral fractions were obtained from simulating the experimental CW EPR spectra. The hyperfine-coupling constants are given in MHz throughout this article. 1 MHz corresponds to 0.0357 mT at a magnetic field of 336 mT. The evolution of the spin-probe concentration over time was determined by double integration of the spectra. Typical simulation values were, depending on pH, temperature and polymer architecture: $g_{iso,A}$ = 2.0056 – 2.0059; $A_{iso,A}$ = 47.6 – 48.7 MHz; $\tau_{c,A}$ = 0.01 – 0.02 ns; $g_{iso,B}$ = 2.0061 – 2.0062; $A_{iso,B}$ = 44.5 – 46.75 MHz; $\tau_{c,B}$ = 0.16 – 0.25 ns.

The errors of the χ_A values stem from uncertainties in the spectral simulations. The simulations include a scaling of the two spectral components, A and B. The overall normalized spectrum is simulated as $S = \chi_A \cdot A + (1-\chi_A) \cdot B$. χ_A is fitted to optimize the computational reproduction of the experimental spectra. The error bars in the χ_A functions represent the uncertainty of the fitting process. The errors include the maximum variance of the χ_A values.

pH Dependence.
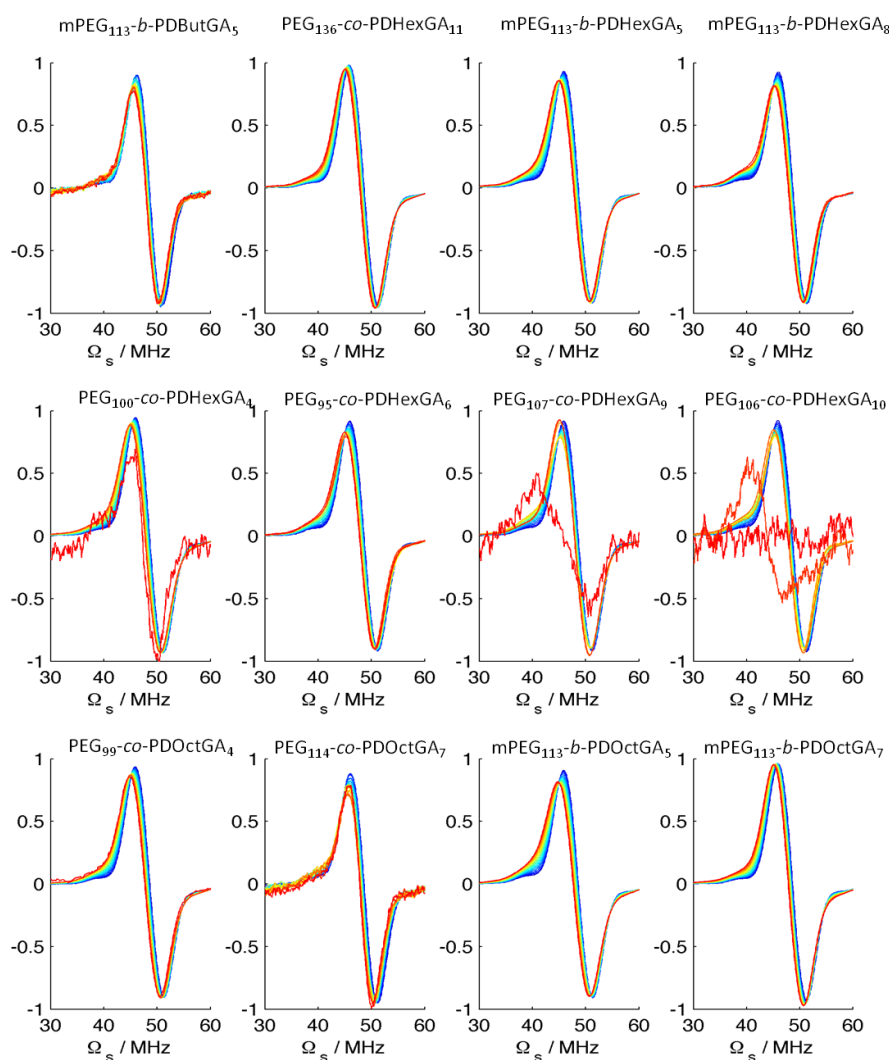
Figure EPRS1. High field transitions of the different polymers under investigation at pH 9. c(TEMPO) = 0.2 mM; c(polymer) = 1 wt%. The colors display the different temperatures of the measurements going from 10 °C (blue) to 90 °C (red) in steps of 5 °C.
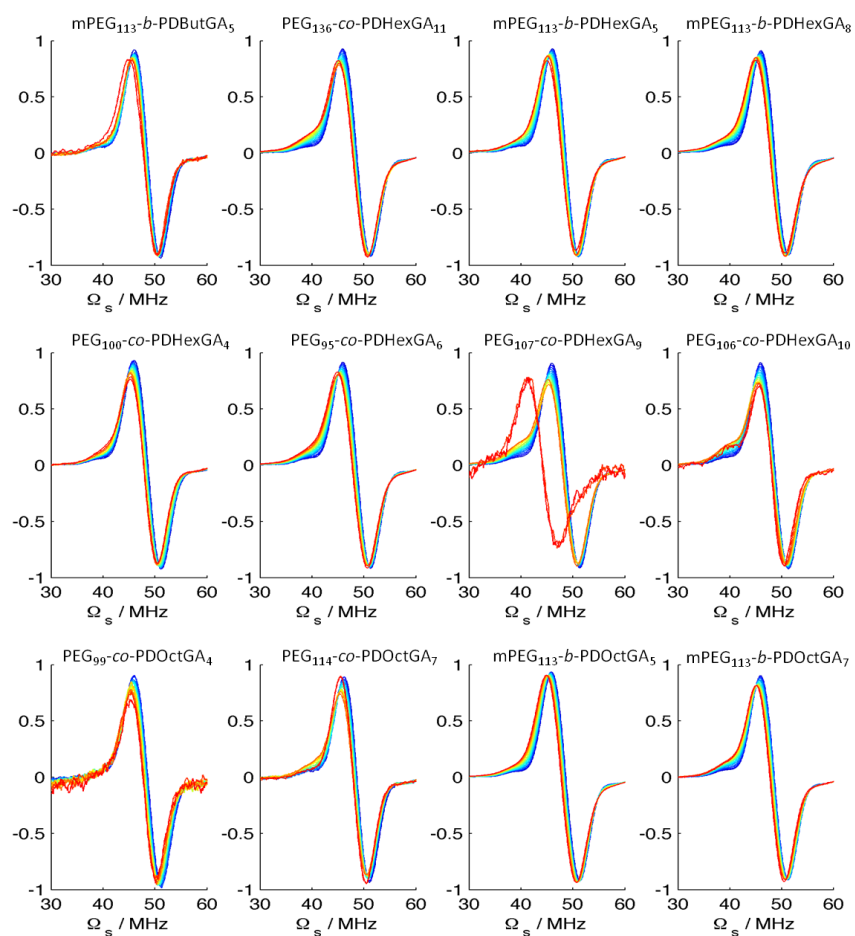
Figure EPRS2. High field transitions of the different polymers under investigation at pH 11. c(TEMPO) = 0.2 mM; c(polymer) = 1 wt%. The colors display the different temperatures of the measurements going from 10 °C (blue) to 90 °C (red) in steps of 5 °C.
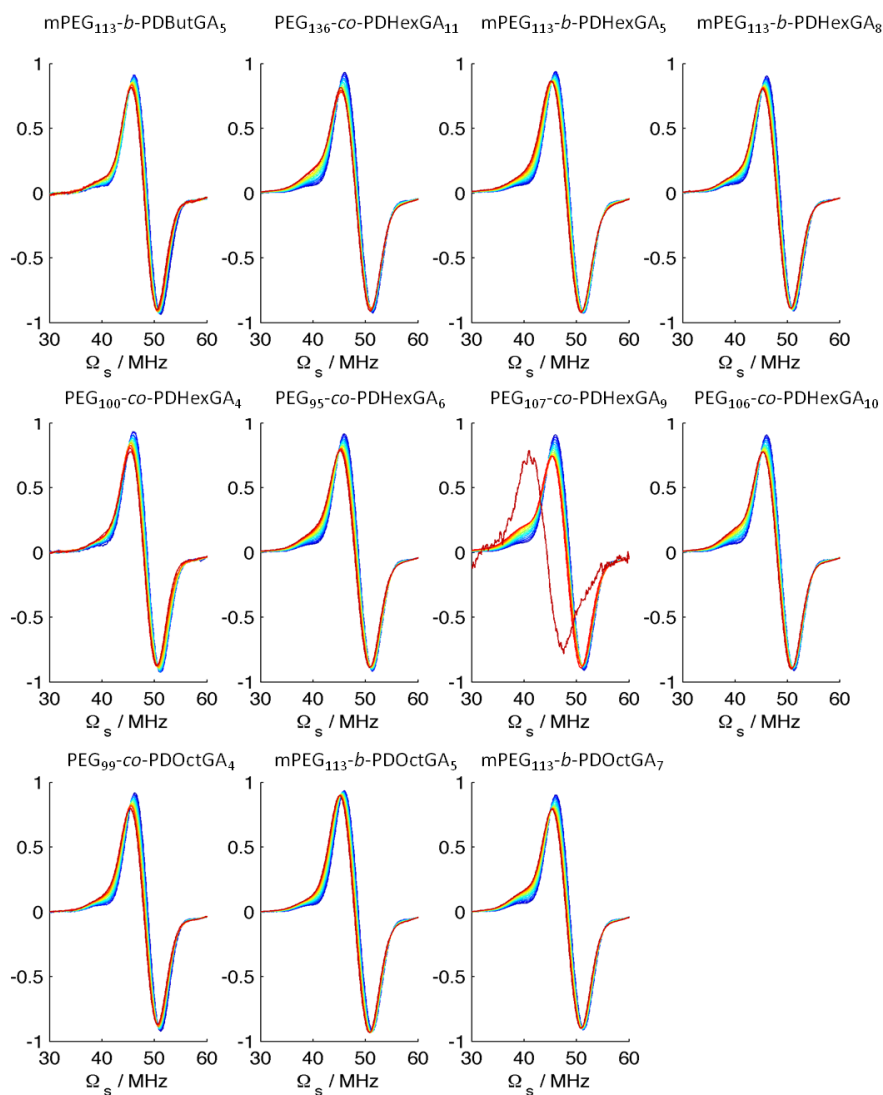
Figure EPRS3. High field transitions of the different polymers under investigation at pH 14. c(TEMPO) = 0.2 mM; c(polymer) = 1 wt%. The colors display the different temperatures of the measurements, going from 10 °C (blue) to 90 °C (red) in steps of 5 °C.

References

[1]   S. Stoll, A. Schweiger. *J. Magn. Reson.* **2006**, *178*, 42–55.

[2] J. H. Freed, G. K. Fraenkel. *J. Chem. Phys.* **1963**, *39*, 326–348.

3.3 Structure-Property Study of Novel Copolyethers Based on PEG with Pendant Quaternary Ammoniums Obtained by Post-Polymerization Modification of Poly(glycidyl amine) Precursors

Jana Herzberger,[a,b] Holger Frey[a,b]* and Daniel Taton[c]*

[a]Institute of Organic Chemistry, Johannes Gutenberg-University Mainz, Duesbergweg 10-14, 55128 Mainz, Germany

[b]Graduate School Materials Science in Mainz, Staudinger Weg 9, 55128 Mainz, Germany

[c]Laboratoire de Chimie des Polymères Organiques, Université de Bordeaux, IPB-ENSCBP, Pessac Cedex, France

*E-Mail: hfrey@uni-mainz.de and taton@enscbp.fr

unpublished results
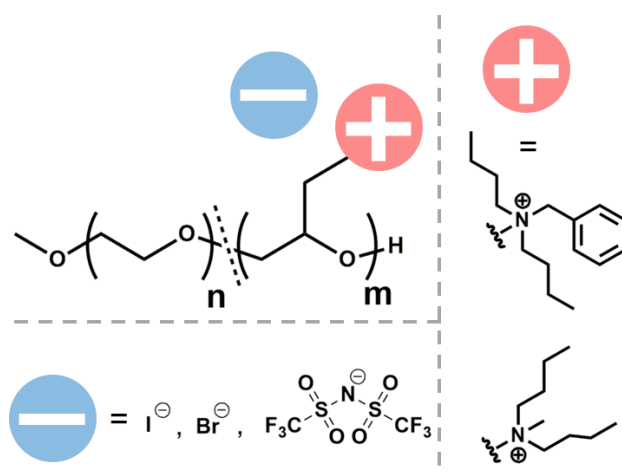
3.3.1 Abstract

Quaternary ammonium-functional polymers constituted of a copolyether backbone, featuring bis(trifluoromethylsulfonyl)imide (TFSI) counterions were synthesized in a two-step procedure, from neutral copolymers based on PEG and poly(glycidyl amine)s involving post-polymerization modification followed by an anion exchange reaction. Such cationically charged copolyehers with mobile TFSI anions, represent a novel class of poly(ionic liquid)s (PILs). Neutral precursor polymers, namely, diblock, triblock and gradient PEG-*co*-poly(*N,N*-di(*n*-butyl) glycidyl amine)s (PEG-*co*-PDButGA and PEG-*b*-PDButGA) copolymers with molecular weights in the range of 4,300-11,300 g·mol^{-1} and DButGA ratios up to 53 mol% were prepared by anionic ring opening polymerization (AROP) and exhibited low polydispersity (PDI < 1.16). Quaternization of tertiary amino groups of PEG-*co*-PDButGA and PEG-*b*-PDButGA structures was carried out in presence of benzyl bromide or methyl iodide. Thermal behavior and stability of the different copolymers were assessed by differential scanning calorimetry (DSC) and thermogravimetric analysis (TGA). After quaternization with either reagent, polyether-type polyelectrolytes showed an increased glass transition temperatures (T_gs) in the range of 6-83 °C (compared to -71 °C to -73 °C for the parent neutral copolymers) and a thermal degradation around $T_{d,5wt\%}$ ~ 150-200 °C. After anion exchange with LiTFSI, the T_g of the resulting copolyethers significantly decreased (-33 °C to 18 °C) as expected, while showing an increased thermal stability ($T_{d,5wt\%}$~250-330 °C). Overall, polymers bearing methyl units showed superior thermal stability compared to their benzyl counterparts, and possessed lower T_g's. Yet, PILs with benzyl moieties are expected to exhibit a higher mechanical stability. These results prove promising and open possibilities to apply ammonium-functionalized copolyethers, for instance, as single-ion solid polymer electrolytes, and in this respect, ion conductivity measurements are ongoing.

3.3.2 Introduction

Poly(ethylene glycol) (PEG) is one of the most studied polymer for solid polymer electrolytes (SPEs). This is due to the fact that PEG exhibits a high thermal stability while possessing an extremely flexible backbone, which leads to high ion mobility. Further, its ability to dissolve and complex ionic species render it highly valuable as a SPE.[1–4] Mixtures of PEO and lithium salts show an ionic conductivity as high as 10^{-3} S·cm^{-1} at 90 °C, which is still several magnitudes lower than the respective ion conductivity of liquid molecular electrolytes.[5] However, safety concerns, such as solvent leakage or flammability shift the interest from liquid electrolytes to SPEs. Consequently, researchers have been developing strategies to increase the ion conductivity of polymeric materials, to provide non-volatile and safe alternatives. As potential candidates, poly(ionic liquid)s (PILs) have attracted considerable attention in the last decade.[6–8] PILs can be deemed as polymeric versions of molecular ionic liquids (ILs). In PILs, however, cations or anions of each monomer unit are covalently tethered to the polymer backbone, only the counterions being mobile, in contrast to ILs. In PILs, cations (e.g. imidazolium, pyridinium, pyrrolidinium, phosphonium, triazolium) and anions (e.g. Cl$^-$, Br$^-$, BF$_4^-$, CH$_3$SO$_3^-$, (CF$_3$SO$_2$)$_2$N$^-$ = Tf$_2$N$^-$) can be judiciously combined using tools of polymer chemistry. Various PIL structures have thus been investigated as SPEs for energy application devices. They are mainly based on a rigid hydrocarbon backbone, though, this is not favorable for ionic transport.[9, 10] A general strategy to increase the ion mobility of PILs is to introduce flexible ethylene glycol or short oligo(ethylene glycol) units to the IL moiety.[11–14] Alternatively, Drockenmuller and co-workers demonstrated high ion conductivity for a 1,2,3-triazolium-based ionene-type main chain polymer, consisting of flexible triethylene glycol repeating units.[15] Surprisingly, only a handful of studies have described PILs based on a true PEG-type (polyether) backbone with side-chain charged functionalities, which is likely to cause synthetic complications.

Recently, Hu et al. have synthesized imidazolium-based structures by post-polymerization functionalization of polyepichlorohydrin (PECH). The authors report ion conductivities reaching 10^{-5} S·cm^{-1} at 30 °C.[16] The conductivity was further increased to 10^{-4} S·cm^{-1} when additional oligo(ethylene glycol) units were incorporated *via* copolymerization of epichlorohydrin and a glycidyl ether derivative.[17] Consequently, neutral and flexible glycidyl ether units allow for increasing ion mobility by likely acting as spacers for the charges. Further, Ikeda et al. have investigated PIL structures based on glycidyl triazole units, giving anhydrous ion conductivities in the range of 1.1-$1.5 \cdot 10^{-5}$ S cm^{-1} at 30 °C.[18, 19] In a follow-up work, the same authors demonstrated that glycidyl triazole polymers bearing quaternary ammonium moieties exhibit lower ion conductivities than their imidazolium counterparts ($9.8 \cdot 10^{-6}$ S cm^{-1} at 30 °C).[20]

In this work we introduce a novel class of PILs consisting of a flexible polyether backbone. Based on our expertise in the design of functional PEG derivatives by anionic ring opening polymerization (AROP), we prepared unprecedented ammonium-functional copolyethers *via* quaternization of PEG-*co*-poly(*N,N*-di(*n*-butyl) glycidyl amine) (PEG-*co*-PDButGA and PEG-*b*-PDButGA) copolymers. We rely on a simple two-step post-polymerization modification involving quaternization and anion exchange reaction. Di-, triblock and gradient copolymers were designed with cationic moieties constituting up to 53 mol% of the repeating units. Neutral precursor polymers were synthesized by AROP, possessing low PDIs (< 1.16). Quaternization was conducted in the presence of benzyl bromide or methyl iodide, forming the corresponding quaternized copolyethers quantitatively. After anion exchange with LiTFSI, the resulting TFSI-containing copolymers were characterized by various techniques. Given their molecular features and thermal properties, these copolymers might be candidates as SPEs, their ion conductivity being planned to be investigated in the near future.

3.3.3 Experimental Section

Nomenclature. *N,N*-di(*n*-butyl) glycidyl amine is abbreviated as DButGA. After quaternization, the cationic segment is abbreviated as QDButGA, while QBnDButGA indicates quaternization with benzyl bromide and QCH$_3$DButGA quaternization with methyl iodide, respectively.

Materials. Methyl iodide and benzyl bromide were purchased from Sigma Aldrich. Lithium bis(trifluoromethanesulfonyl)imide (LiTFSI) was received from TCI. Deuterated solvents were purchased from Euriso-Top GmbH.

Instrumentation. ^{1}H and ^{13}C NMR spectra were recorded on a Bruker Avance 400 spectrometer equipped with a 5 mm Bruker multinuclear direct cryoprobe. Thermo-gravimetric analyses (TGA) were conducted on a TA instruments Q50 from 30°C to 600°C with a heating rate of 15 °C·min^{-1} under nitrogen flow. The weight loss was recorded as a function of temperature. Differential scanning calorimetry analyses (DSC) were performed on a DSC t/T modulation LN$_2$ heating from -90 °C to 130 °C with a heating/cooling rate of 10 °C·min^{-1}. Molar masses of all samples were determined by size exclusion chromatography (SEC) in THF, containing 10 mmol·L^{-1} LiTFSI, as the eluent, using light scattering (LS) and refractive index (RI) signals. For LS analysis, dn/dc value were set to 0.185 mL·g^{-1}.

Gradient and block PEG-PDButGA copolymers. The synthesis of PEG-PDButGA gradient and block copolymers is described elsewhere.[21]

Quaternization with benzyl bromide or methyl iodide. 500 mg PEG-PDButGA gradient or block copolymer were dissolved in a mixture of methanol and tetrahydrofuran (3:1). Subsequently, 3 equiv (per amino group) benzyl bromide or methyl iodide were added and the quaternization was performed at 60 °C for 12 h. Subsequent to cooling to room

temperature, the polymer was precipitated twice in diethyl ether (room temperature). Drying under high vacuum gave the quaternized product in yields of 80 %.

Anion exchange with LiTFSI. A modified literature procedure was applied.[22] 200 mg of quaternized polymer was dissolved in methanol (2 mL), 2.5 equiv LiTFSI (per amino group) dissolved in methanol (2 mL) were added, and the mixture was stirred for 12 h at room temperature. Purification was conducted via dialysis. The methanol solution was added to a dialysis bag (MWCO =1000, regenerated cellulose) and dialyzed against DI water (24 h, 6 solvent changes), to remove salts. All polymers precipitated during the dialysis procedure, indicating successful ion exchange. After drying in high vacuum, the product was obtained in quantitative yields.

3.3.4 Results and Discussion

Tertiary amino-functional PEGs were prepared *via* AROP of ethylene oxide (EO) and *N,N*-di(*n*-butyl) glycidyl amine (DButGA) or by homopolymerization of DButGA applying a PEG macroinitiator, according to a literature procedure.[21] In particular, gradient, di- and triblock copolymers were synthesized and polymers with low PDIs (< 1.16) and molecular weights in the range of 4,300-11,300 g·mol^{-1} were obtained (Table 1).

Table 1. Characterization data of neutral dialkyl-amine functional precursor copolymers, synthesized *via* AROP.

Precursor polymers^a	$M_n{}^a$ /g·mol^{-1}	$M_n{}^b$ /g·mol^{-1}	$M_w{}^b$/g·mol^{-1}	$M_w/M_n{}^b$	$T_g{}^c$/°C	$T_m{}^c$/°C
mPEG$_{45}$-*b*-PDButGA$_{25}$	6600	4150	4800	1.16	-72	40
PEG$_{45}$-(*b*-PDButGA$_{25}$)$_2$	11300	5020	5260	1.05	-72	22
PEG$_{35}$-co-PDButGA$_{15}$	4300	2570	2620	1.02	-71	4
PEG$_{25}$-co-PDButGA$_{25}$	5700	3210	3370	1.05	-73	---

^{a}Calculated by ^{1}H NMR spectroscopy.
^{b}Determined by SEC (THF/10 mM LiTFSI, MALLS detector with dn/dc of polystyrene).
^{c}Obtained by DSC measurements.

Quaternization was conducted using benzyl bromide or methyl iodide, followed by anion exchange with bis(trifluoromethane)sulfonimide lithium (LiTFSI), yielding copolyether-based PILs (Scheme 1). Characterization data are summarized in Tables 2 and 3. Quaternization was performed in a mixture of methanol/THF. The addition of THF was necessary to fully solubilize the parent neutral copolymers. After quaternization, the resulting samples featuring chloride or iodide counter anions proved to be water-soluble. In contrast, the TFSI-containing PEG-PQDButGA derivatives obtained after anion exchange did not dissolve in water, but were found to be soluble in THF.
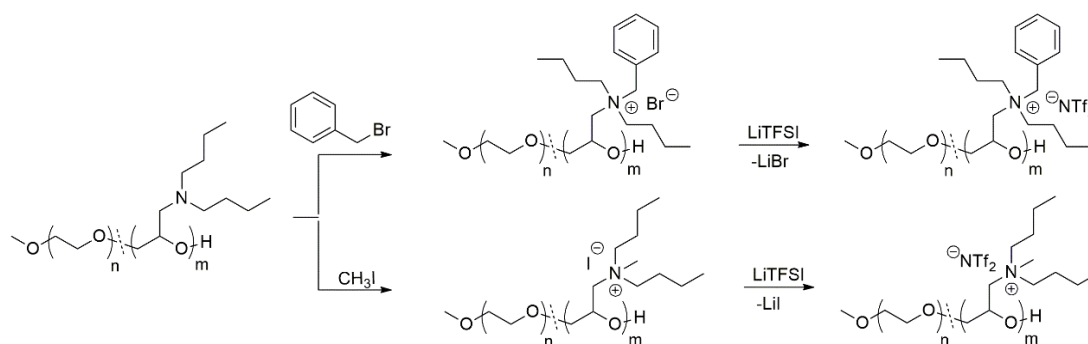
Scheme 1. Quaternization of PEG-*co*-PDButGA copolymers with benzyl bromide and methyl iodide, respectively, followed by anion exchange with bis(trifluoromethane)sulfonimide lithium (LiTFSI).

The quaternization step was monitored by ^{1}H NMR spectroscopy (Figure 1). After reaction, the resonances of the methylene groups (-NCH_2-) in direct neighborhood to the nitrogen atom of DButGA segments shifted downfield to 3.24 ppm. Further, the adjacent methylene groups CH_2-CH_2-CH$_3$, showed a distinct splitting at 1.34 ppm and 1.79 ppm, respectively. After quaternization with benzyl bromide, characteristic signals of the benzyl group appeared at 7.5-8.0 ppm. In analogy, after quaternization with methyl iodide the methyl group is detected at 3.36 ppm.
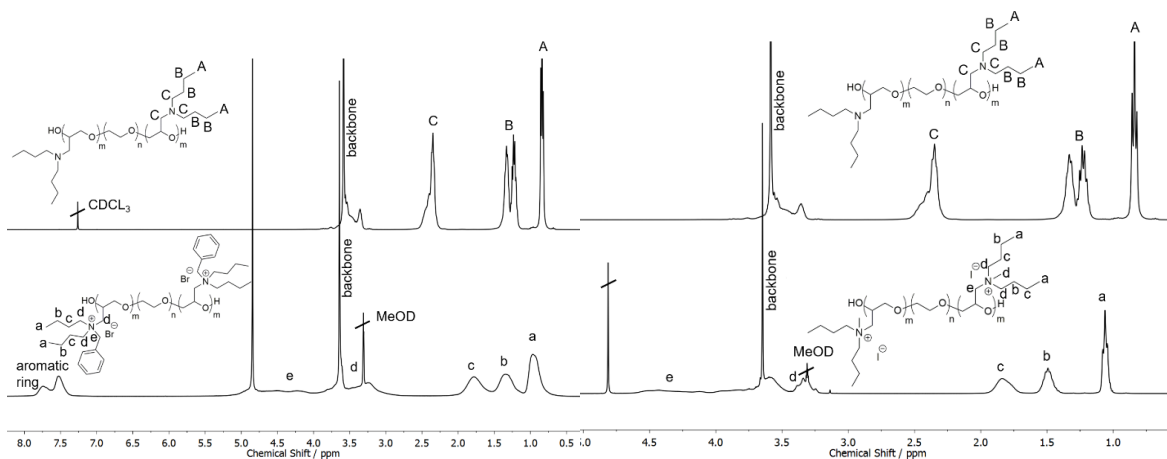
Figure 1. ^{1}H NMR spectra (400 MHz) of (PDButGA$_{25}$)$_2$-*b*-PEG before (top, CDCl$_3$) and after quaternization (bottom, MeOD). Quaternized with benzyl bromide (left) and methyl iodide (right), respectively.

^{13}C NMR spectroscopy confirmed the successful modification. Indeed, the resonances of the benzyl group appeared at 129-134 ppm (Figure S1), while a new resonance at 50.9 ppm was detected, which was assigned to the methyl group in PEG-*co*-PQCH$_3$DButGA (Figure S1). Characterization of neutral amino-functionalized PEG derivatives by regular SEC in THF with DButGA ratios above 25 mol% was not possible, likely due to strong interaction with the column materials of the SEC set up. Consequently, we analyzed the parent polymers and ammonium-functionalized copolyethers using a SEC set-up under conditions established by Matyjaszewski et al.[23] The results are listed in Tables 1-3. Exemplarily, Figure 2 shows SEC traces of PEG-*co*-PDButGA copolymers and the TFSI-containing charged counterparts. After quaternization, the SEC signal shifted to shorter elution times, that was, to a higher molecular weight. Also, PEG-*co*-PQDButGA quaternized with benzyl moieties eluted faster than homologues with methyl moieties, indicating higher molecular weights. Note that the listed molecular weight values in Tables 1-3 are not absolute values,

and were obtained using the refractive index increment (dn/dc) of polystyrene. SEC traces of the other polymers are shown in the Supporting Information (Figure S2).
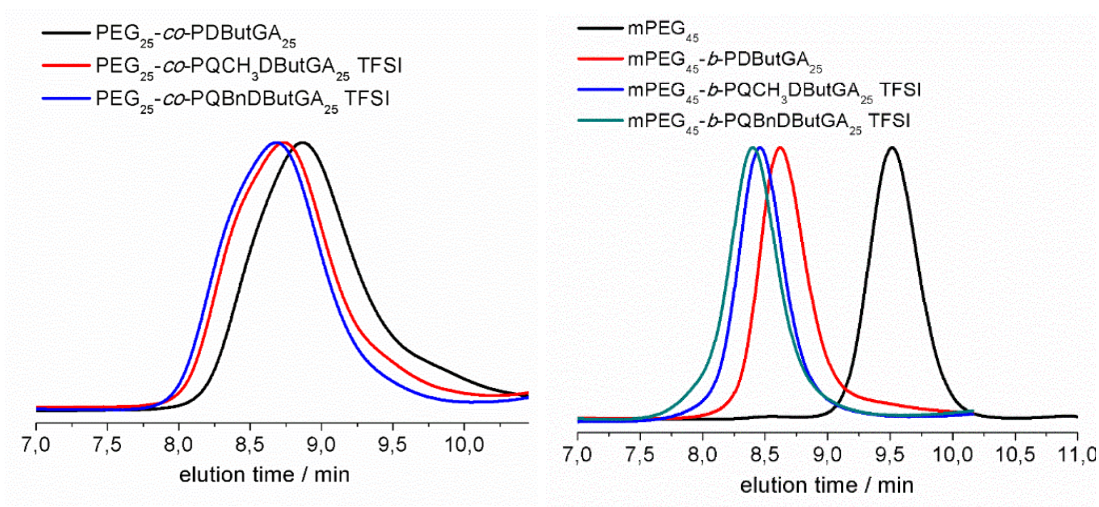
Figure 2. SEC traces (THF/10 mM LiTFSI, RI signal) of PEG$_{25}$-*co*-PDButGA$_{25}$ and quaternized derivatives (left) and mPEG$_{45}$, mPEG$_{45}$-*b*-PDButGA$_{25}$ and quaternized derivatives (right).

Table 2. Characterization data of charged PEG-*co*-PQCH₃DButGA samples.

Charged samples	$T_g{}^a$/°C (Iodide)	$T_m{}^a$/°C (Iodide)	$T_g{}^a$/°C (TFSI)	$T_m{}^a$/°C (TFSI)	$M_n{}^b$/g·mol⁻¹	$M_n{}^c$/g·mol⁻¹ (TFSI)	PDI
mPEG$_{45}$-*b*-PQCH$_3$DButGA$_{25}$	T_{g1}=-58, T_{g2}= 53	6	18	---	7000	3530	1.19
PEG$_{45}$-(*b*-PQCH$_3$DButGA$_{25}$)$_2$	83	---	1	---	12000	5070	1.05
PEG$_{35}$-*co*-PQCH$_3$DButGA$_{15}$	6	---	-33	---	4540	2510	1.06
PEG$_{25}$-*co*-PQCH$_3$DButGA$_{25}$	53	---	-15	---	6100	2530	1.06

^{a}Determined *via* DSC measurements.
^{b}Calculated from ^{1}H NMR spectrum.
^{c}Obtained *via* SEC (THF/1 mM LiTFSI, LS signal, dn/dc 0.185 mL·g⁻¹)

Table 3. Characterization data of charged PEG-*co*-PQBnDButGA samples.

Charged samples	T_g^a/°C (Br)	T_m^a/°C (Br)	T_g^a/°C (TFSI)	T_m^a/°C (TFSI)	M_n^b/g·mol^{-1}	M_n^c/g·mol^{-1} (TFSI)	PDI
mPEG$_{45}$-*b*-PQBnDButGA$_{25}$	T_{g1}=-55, T_{g2}= 15	---	45	---	8900	5580	1.05
PEG$_{45}$-(*b*-PQBnDButGA$_{25}$)$_2$	25	---	22	---	15800	8560	1.03
PEG$_{35}$-*co*-PQBnDButGA$_{15}$	32	---	-6	---	5680	2950	1.06
PEG$_{25}$-*co*-PQBnDButGA$_{25}$	79	---	9	---	8000	3760	1.03

[a]Determined *via* DSC measurements.
[b]Calculated from ^{1}H NMR spectrum.
[c]Obtained *via* SEC (THF/1 mM LiTFSI, LS signal, dn/dc 0.185 mL·g^{-1})

FT-IR spectroscopy confirmed the successful anion exchange (Figure 3). The IR spectrum of LiTFSI showed characteristic bands in the region of 1000-1400 cm^{-1}, which can be assigned to the asymmetric and symmetric stretching vibration of the SO$_2$ structure, respectively.[24, 25] After anion exchange, these characteristic bands appeared in the spectrum of PEG$_{25}$-*co*-PQCH$_3$DButGA$_{25}$ TFSI, indicating the presence of TFSI anions. Note that the characteristic bands of the copolyether are weak compared to the vibrations of the TFSI counterion.
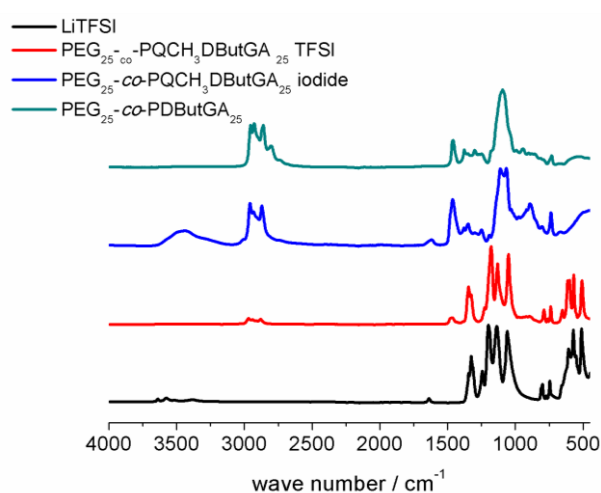
Figure 3. FT-IR spectra (absorbance) of LiTFSI, PEG$_{25}$-*co*-PDButGA$_{25}$ (cyan) and after quaternization PEG$_{25}$-*co*-PQCH3DButGA25 with iodide (blue) or TFSI (red) as counterion.

Bulk thermal properties. The thermal stability of all copolyether-based PILs was investigated by TGA. Figure 4 shows the thermograms of PEG$_{25}$-*co*-PDButGA$_{25}$, quaternized PEG-*co*-PQDButGA with CH$_3$I and BnBr, respectively, and after anion exchange with LiTFSI. Neutral PEG-*co*-PDButGA showed thermal degradation at around 370 °C (thermal decomposition at 5% weight loss), which is marginally lower than neat mPEG2000 ($T_d = 380°C$). After quaternization with benzyl bromide, however, the thermal stability dropped to ~150 °C.
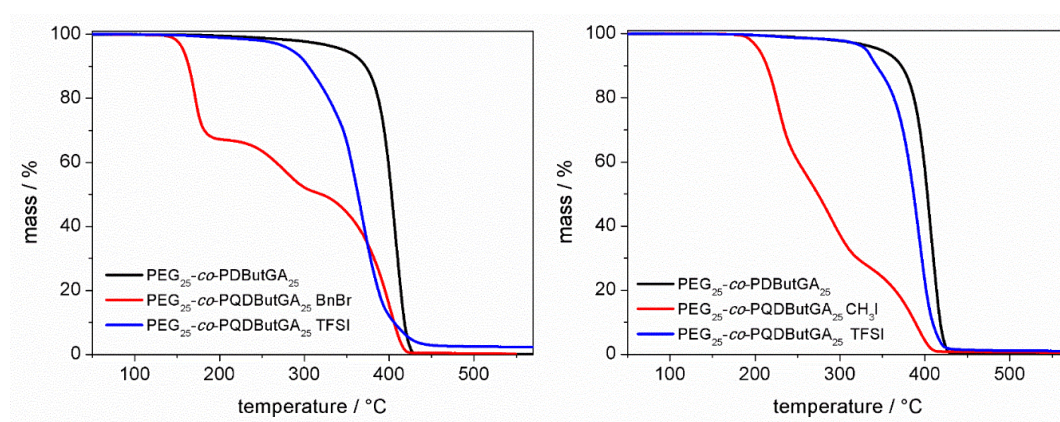
Figure 4. TGA traces of PEG$_{25}$-*co*-PDButGA$_{25}$ and quaternized derivatives. Left: Initial polymer (black), after quaternization with benzyl bromide (red) and after anion exchange (blue). Right: Initial polymer (black), after quaternization with methyl iodide (red) and after anion exchange (blue).

This can be explained by the degradation of the quaternized copolyether by debenzylation at this temperature.[26] The PEG$_{25}$-*co*-PQBnDButGA$_{25}$ was heated to 200 °C and the resulting sample was analyzed by ^{1}H NMR spectroscopy. After heating, additional signals of released benzyl bromide were detected, indicating that the reverse Menschutkin reaction did occur upon heating (Figure S3).
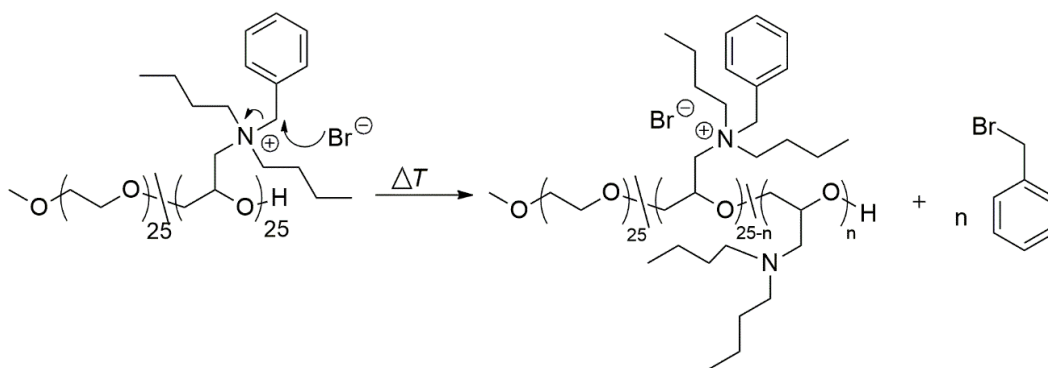
Scheme 2. Proposed release of benzyl bromide and formation of neutral PEG-*co*-PDButGA after heating of PEG-*co*-PQBnDButGA.

The degradation mechanism likely occurs by the attack of the bromide counterion onto the α-carbon, regenerating benzyl bromide and uncharged PEG$_{25}$-*co*-PDButGA$_{25}$, as illustrated in Scheme 2 (see Figure S3, middle). However, Hofmann elimination and other degradation pathways cannot be ruled out.[26] After heating the polymer to 320°C, almost full debenzylation occurred and the amount of amino groups decreased as well (Figure S3, bottom). Notably, after anion exchange with LiTFSI, the thermal stability of the charged polymer increased to 270 °C. In contrast, PEG$_{25}$-*co*-PQCH$_3$DButGA$_{25}$, quaternized with methyl iodide, showed a higher initial thermal stability, the first degradation being detected around 200°C. After anion exchange with LiTFSI, the thermal stability of PEG$_{25}$-*co*-PQCH$_3$DButGA$_{25}$ increased to 330°C. TGA traces of all other polymers showed a similar behavior and are shown in the Supporting Information (Figure S4-S6).

Bulk thermal properties of all samples were further investigated by differential scanning calorimetry (DSC). The flexible amino-functional PEG-based copolyethers showed a glass transition temperature in the range of -71 to -73°C (Table 1), in analogy to literature values.[21] For the di- and triblock copolymer, no second T_g of the PEG segment was detected and the melting temperature of PEG was slightly lowered (T_m= 40 and 20, respectively), likely due to a solvating effect of the PDButGA block on PEG. As expected, the gradient

copolymers showed a stronger influence of the amino-functionality on the melting temperature of PEG. PEG-*co*-PDButGA with 30 mol% DButGA revealed a melting temperature of 4 °C, while 50 mol% DButGA led to a completely amorphous structure. After quaternization, a strong increase in T_g was noted (Tables 2 and 3). For example, PEG$_{25}$-*co*-PQBnDButGA$_{25}$ exhibited a T_g of 79 °C. Quaternization with methyl iodide led to a T_g of 53°C. Unfortunately, the T_g valued of the di- and triblock copolymers were difficult to detect. The general trend was that a strong increase in T_g with quaternization was observed, due to the introduced charges. After anion exchange, from iodide/bromide to the bulky and strongly delocalized TFSI$^-$ counterion, a decrease in T_g was noted. As an example the T_g of PEG$_{25}$-*co*-PQDButGA$_{25}$ droped from 79 °C (PEG$_{25}$-*co*-PQBnDButGA$_{25}$ Br) to 9 °C (PEG$_{25}$-*co*-PQBnDButGA$_{25}$ TFSI) and from 53 °C(PEG$_{25}$-*co*-PQCH$_3$DButGA$_{25}$ I) to -15 °C (PEG$_{25}$-*co*-PQCH$_3$DButGA$_{25}$ TFSI).

3.3.5 Conclusion

We have introduced quaternized ammonium-functional PEG-based copolyethers deemed as a novel family of poly(ionic liquid)s. Tertiary amino-PEGs (PEG-*co*-PDButGA, PEG-*b*-PDButGA), with a gradient, di- and triblock copolymer structure were investigated as precursor polymers that were subjected to a quaternization reaction with benzyl bromide or methyl iodide. Regarding the different quaternization agents (BnBr or CH$_3$I), a higher thermal stability of ammonium-functional PEGs with methyl substituents was observed, reaching $T_{d,5wt\%} \sim 330$ °C for PEG-PQCH$_3$DButGA bearing TFSI counterions. Further, a lower T_g of the methyl-functionalized structures is detected. However, PILs based on benzyl moieties might provide a better mechanical stability. Overall, these structures show promising thermal stability together with rather low T_gs, which holds great promise for a use of these materials as solid polymer electrolytes with high ion mobility.

3.3.6 Acknowledgements

3.3.7 References

[1] S. Lascaud; M. Perrier; A. Vallee; S. Besner; J. Prud'homme; M. Armand, Phase Diagrams and Conductivity Behavior of Poly(ethylene oxide)-Molten Salt Rubbery Electrolytes, *Macromolecules.* **1994**, *27*, 7469–7477.

[2] W. Gorecki; M. Jeannin; E. Belorizky; C. Roux; M. Armand, Physical Properties of Solid Polymer Electrolyte PEO(LiTFSI) Complexes, *J. Phys. Condens. Matter.* **1995**, *7*, 6823-6832.

[3] O. Borodin; G. D. Smith, Mechanism of Ion Transport in Amorphous Poly(ethylene oxide)/LiTFSI from Molecular Dynamics Simulations, *Macromolecules.* **2006**, *39*, 1620–1629.

[4] G. Zardalidis; E. Ioannou; S. Pispas; G. Floudas, Relating Structure, Viscoelasticity, and Local Mobility to Conductivity in PEO/LiTf Electrolytes, *Macromolecules.* **2013**, *46*, 2705–2714.

[5] D. M. Pesko; M. A. Webb; Y. Jung; Q. Zheng; T. F. Miller; G. W. Coates; N. P. Balsara, Universal Relationship between Conductivity and Solvation-Site Connectivity in Ether-Based Polymer Electrolytes, *Macromolecules.* **2016**, *49*, 5244–5255.

[6] D. Mecerreyes, Polymeric ionic liquids: Broadening the Properties and Applications of Polyelectrolytes, *Prog. Polym. Sci.* **2011**, *36*, 1629–1648.

[7] J. Yuan; D. Mecerreyes; M. Antonietti, Poly(ionic liquid)s: An update, *Prog. Polym. Sci.* **2013**, *38*, 1009–1036.

[8] I. Osada; H. de Vries; B. Scrosati; S. Passerini, Ionic-Liquid-Based Polymer Electrolytes for Battery Applications, *Angew. Chem. Int. Ed.* **2016**, *55*, 500–513.

[9] A.-L. Pont; R. Marcilla; I. De Meatza; H. Grande; D. Mecerreyes, Pyrrolidinium-based Polymeric Ionic Liquids as Mechanically and Electrochemically Stable Polymer Electrolytes, *J. Power Sources.* **2009**, *188*, 558–563.

[10] G.B. Appetecchi; G.-T. Kim; M. Montanino; M. Carewska; R. Marcilla; D. Mecerreyes; I. De Meatza, Ternary Polymer Electrolytes Containing Pyrrolidinium-Based Polymeric Ionic Liquids for Lithium Batteries, *J. Power Sources.* **2010**, *195*, 3668–3675.

[11] M. Lee; U. H. Choi; R. H. Colby; H. W. Gibson, Ion Conduction in Imidazolium Acrylate Ionic Liquids and their Polymers, *Chem. Mater.* **2010**, *22*, 5814–5822.

[12] M. Döbbelin; I. Azcune; M. Bedu; A. Ruiz de Luzuriaga; A. Genua; V. Jovanovski; G. Cabañero; I. Odriozola, Synthesis of Pyrrolidinium-Based Poly(ionic liquid)

Electrolytes with Poly(ethylene glycol) Side Chains, *Chem. Mater.* **2012**, *24*, 1583–1590.

[13]   R. Sood; B. Zhang; A. Serghei; J. Bernard; E. Drockenmuller, Triethylene Glycol-based Poly(1,2,3-triazolium acrylate)s with Enhanced Ionic Conductivity, *Polym. Chem.* **2015**, *6*, 3521–3528.

[14]   F. Fan; Y.Wang; T. Hong; M. F. Heres; T.Saito; A.P. Sokolov, Ion Conduction in Polymerized Ionic Liquids with Different Pendant Groups, *Macromolecules.* **2015**, *48*, 4461–4470.

[15]   B. P. Mudraboyina; M. M. Obadia; I. Allaoua; R. Sood; A. Serghei; E. Drockenmuller, 1,2,3-Triazolium-Based Poly(ionic liquid)s with Enhanced Ion Conducting Properties Obtained through a Click Chemistry Polyaddition Strategy, *Chem. Mater.* **2014**, *26*, 1720–1726.

[16]   H. Hu; W. Yuan; L. Lu; H. Zhao; Z. Jia; G. L. Baker, Low Glass Transition Temperature Polymer Electrolyte Prepared from Ionic Liquid Grafted Polyethylene Oxide, *J. Polym. Sci. Part A: Polym. Chem.* **2014**, *52*, 2104–2110.

[17]   H. Hu; W. Yuan; Z. Jia; G. L. Baker, Ionic Liquid-Based Random Copolymers: a New Type of Polymer Electrolyte with Low Glass Transition Temperature, *RSC Adv.* **2015**, *5*, 3135–3140.

[18]   T. Ikeda; I. Nagao; S. Moriyama; J.-D. Kim, Synthesis and Characterization of Glycidyl-Polymer-based Poly(ionic liquid)s: Highly Designable Polyelectrolytes with a Poly(ethylene glycol) Main Chain, *RSC Adv.* **2015**, *5*, 87940–87947.

[19]   T. Ikeda; S. Moriyama; J.-D. Kim, Imidazolium-based Poly(ionic liquid)s with Poly(ethylene oxide) Main Chains: Effects of Spacer and Tail Structures on Ionic Conductivity, *J. Polym. Sci. Part A: Polym. Chem.* **2016**, *54*, 2896–2906.

[20]   Ikeda, T.; Moriyama, S.; Kim, J., Quaternary Ammonium Cation Functionalized Poly(Ionic Liquid)s with Poly(Ethylene Oxide) Main Chains, *Macromol. Chem. Phys.* **2016**, doi: 10.1002/macp.201600282.

[21]   J. Herzberger; D. Kurzbach; M. Werre; K. Fischer; D. Hinderberger; H. Frey, Stimuli-Responsive Tertiary Amine Functional PEGs Based on *N,N*-Dialkylglycidylamines, *Macromolecules.* **2014**, *47*, 7679–7690.

[22]   J. Pinaud; J. Vignolle; Y. Gnanou; D. Taton, Poly(*N*-heterocyclic-carbene)s and their CO2 Adducts as Recyclable Polymer-Supported Organocatalysts for Benzoin Condensation and Transesterification Reactions, *Macromolecules.* **2011**, *44*, 1900–1908.

[23]   H. He; M. Zhong; B. Adzima; D. Luebke; H. Nulwala; K. Matyjaszewski, A Simple and Universal Gel Permeation Chromatography Technique for Precise Molecular Weight Characterization of Well-Defined Poly(ionic liquid)s, *J. Am. Chem. Soc.* **2013**, *135*, 4227–4230.

[24]   I. Rey; P. Johansson; J. Lindgren; J. C. Lassègues; J. Grondin; and L. Servant, Spectroscopic and Theoretical Study of $(CF_3SO_2)_2N^-$ ($TFSI^-$) and $(CF_3SO_2)_2NH$ (HTFSI), *J. Phys. Chem. A.* **1998**, *102*, 3249–3258.

[25]   J.-C. Lassègues; J. Grondin; C. Aupetit; P. Johansson, Spectroscopic Identification of the Lithium Ion Transporting Species in LiTFSI-Doped Ionic Liquids, *J. Phys. Chem. A.* **2009**, *113*, 305–314.

[26]   S. R. Williams; T. E. Long, Recent Advances in the Synthesis and Structure–Property Relationships of Ammonium Ionenes, *Prog. Polym. Sci.* **2009**, *34*, 762–782.
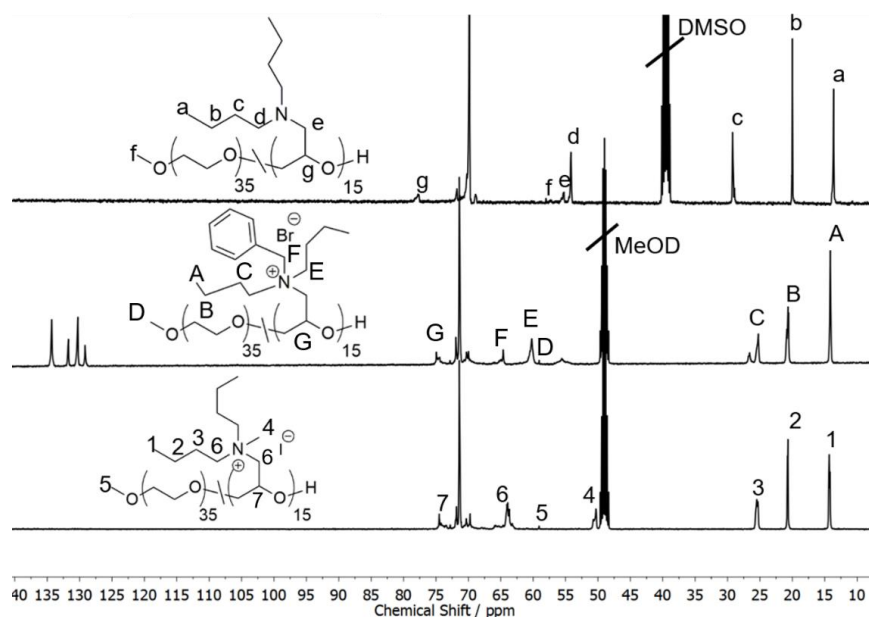
Figure S1. ^{13}C NMR (100 MHz) spectra of PEG$_{35}$-co-PDButGA$_{15}$ (top, DMSO-d_6) and PEG$_{35}$-co-PQDButGA$_{15}$ quaternized with benzyl bromide (middle, MeOD) and PEG$_{35}$-co-PQDButGA$_{15}$ quaternized with methyl iodide (bottom, MeOD).
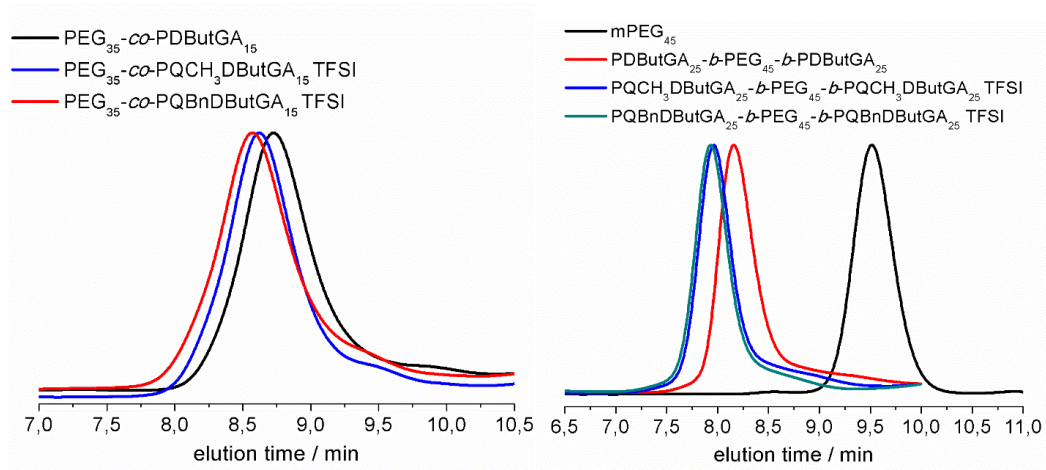
Figure S2. SEC traces (THF/10 mM LiTFSI, RI signal) of PEG$_{35}$-co-PDButGA$_{15}$ and quaternized derivatives (left) and mPEG$_{45}$, PEG$_{45}$-b-(PDButGA$_{25}$)$_2$ and quaternized derivatives (right).
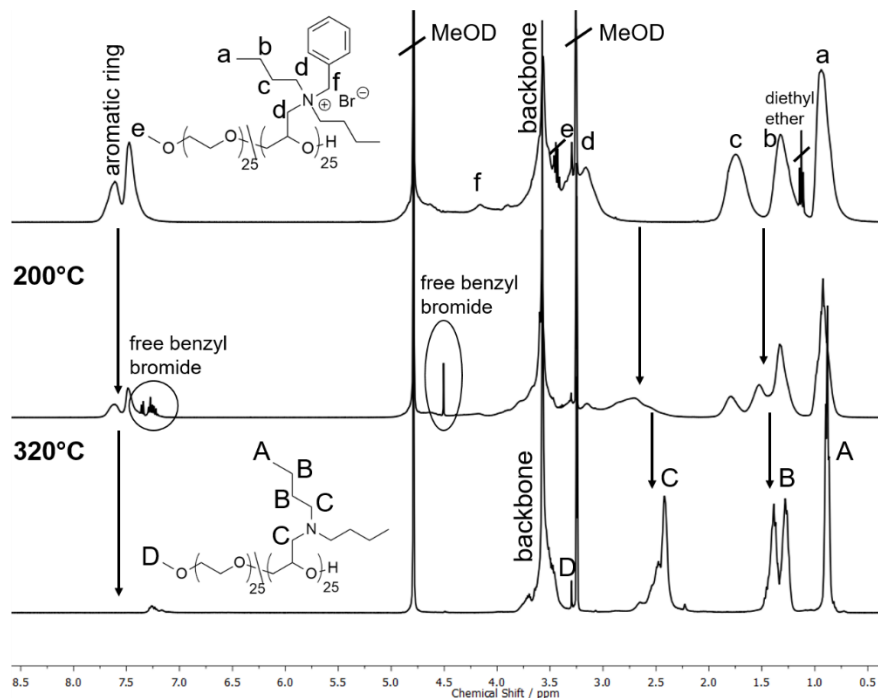
Figure S3. ^{1}H NMR spectra (400 MHz, MeOD) of PEG$_{25}$-*co*-PQBnDButGA$_{25}$ (top), after heating to 200 °C (middle) and after heating to 320 °C (bottom).
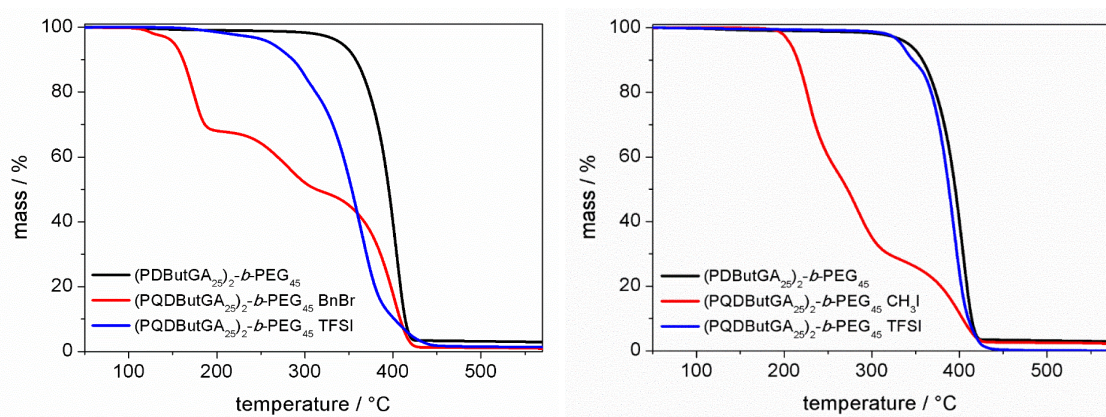
Figure S4. TGA traces of (PDButGA$_{25}$)$_2$-*b*-PEG$_{45}$ and quaternized derivatives. Left: Initial polymer (black), after quaternization with benzyl bromide (red) and after anion exchange (blue). Right: Initial polymer (black), after quaternization with methyl iodide (red) and after anion exchange (blue).
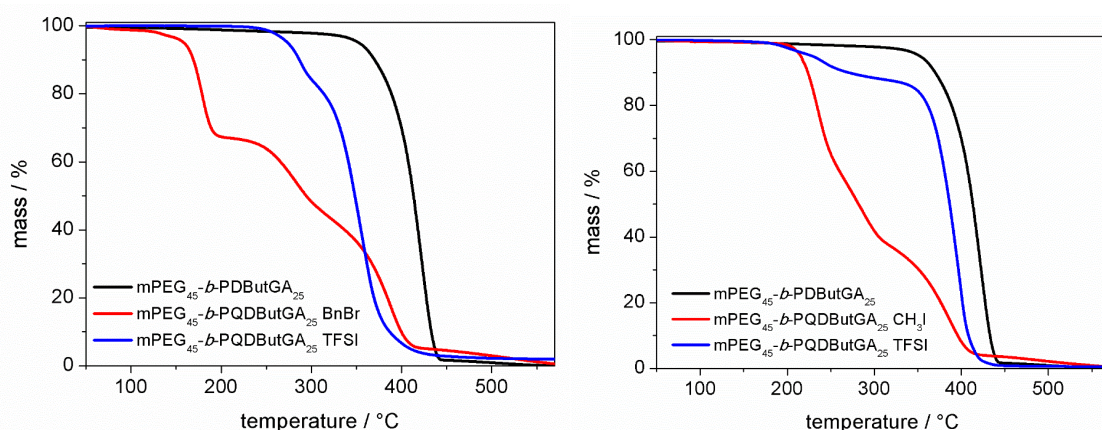
Figure S5. TGA traces of mPEG$_{45}$-*b*- PDButGA$_{25}$ and quaternized derivatives. Right: Initial polymer (black), after quaternization with benzyl bromide (red) and after anion exchange (blue). Right: Initial polymer (black), after quaternization with methyl iodide (red) and after anion exchange (blue).
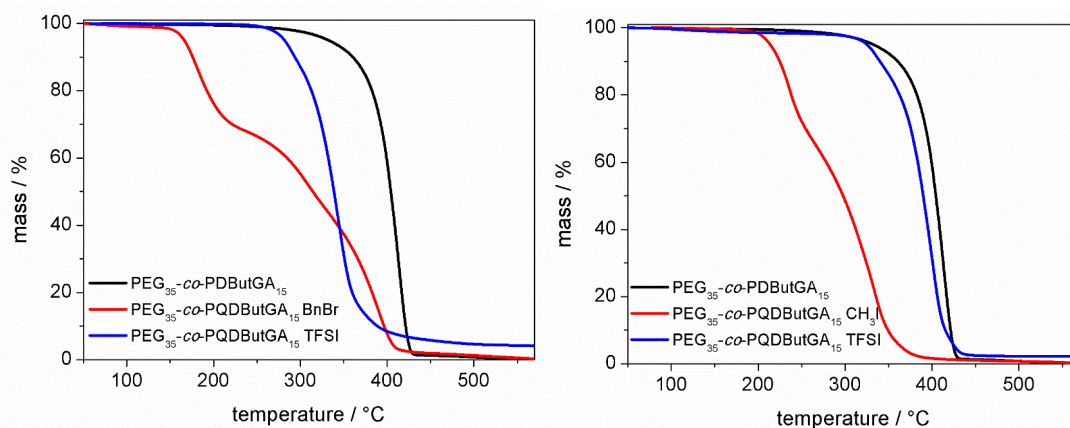
Figure S6. TGA traces of PEG$_{35}$-*co*- PDButGA$_{15}$ and quaternized derivatives. Left: Initial polymer (black), after quaternization with benzyl bromide (red) and after anion exchange (blue). Right: Initial polymer (black), after quaternization with methyl iodide (red) and after anion exchange (blue).

3.4 Epicyanohydrin: Polymerization by Monomer Activation Gives Access to Nitrile-, Amino- and Carboxyl-Functional Poly(ethylene glycol)

Jana Herzberger,[a,b] Holger Frey [a,]*

[a] Department of Organic Chemistry, Johannes Gutenberg-University Mainz, Duesbergweg 10-14, 55128 Mainz, Germany

[b] Graduate School Materials Science in Mainz , Staudingerweg 9, 55128 Mainz, Germany

*E-Mail: hfrey@uni-mainz.de
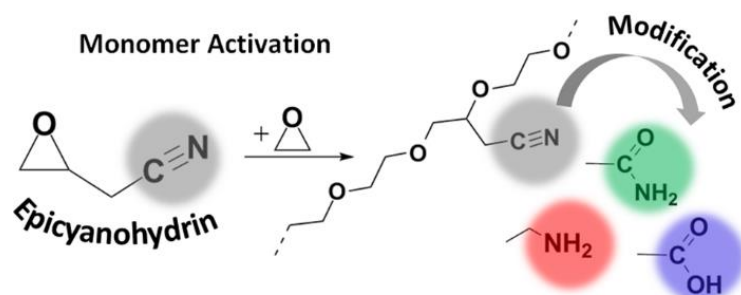
3.4.1 Abstract

Both homo- and copolymerization of the hitherto non-polymerizable epoxide monomer epicyanohydrin (EPICH) with ethylene oxide (EO) have been studied, employing the monomer activation technique. Tetraoctylammonium bromide or tetrabutylammonium iodide were used as initiators, combined with i-Bu$_3$Al to activate the EPICH monomer. The EPICH content was varied from 4-16 mol%, yielding well-defined PEG-co-PEPICH copolymers with molecular weights M_n (SEC) ranging from 3,700 to 8,800 g·mol^{-1}. The nitrile groups of the resulting polyethers were further reduced or hydrolyzed to introduce amino-, amide- or carboxyl groups at the polyether backbone, respectively, circumventing protecting group chemistry. Successful transformation of the functional groups was proven by SEC measurements, ^{1}H NMR, ^{13}C NMR and FT-IR spectroscopy. These carboxyl-functional PEG copolymers are anionic polyelectrolytes consisting only of purely aliphatic polyether structures with carboxyl groups. The hydrolyzed PEPICH homopolymers represent the first polyether based analogues of poly(acrylamide) and poly(acrylic acid). In pronounced contrast to poly(acrylic acid), carboxyl-functional PEPICH shows excellent aqueous solubility even at low pH.

3.4.2 Introduction

Poly(ethylene glycol) (PEG) is a widely used material that is implemented in an immense variety of biomedical and pharmaceutical applications[1, 2] as well as in large-scale industrial processes, for instance as a segment of non-ionic surfactants or in polyols for polyurethane foam production.[3] Conventional PEG is a simple polyether with ethylene glycol repeating units and one hydroxyl group at each chain end, which is highly soluble both in water and in many organic solvents. Yet, the low functionality of poly(ethylene glycol) (PEG) can be a limiting parameter for its use in specialty applications such as drug delivery,[2, 4, 5] bioconjugation[6,7] or polymer-supported catalysis.[8] The need for PEG with higher functionality has motivated intense research efforts to synthesize novel components, either via appropriate initiator and terminating agents[9] or via epoxide building blocks.[10] The latter can be copolymerized with ethylene oxide (EO) and yield multi-functional PEG (*mf*-PEG) with high loading capacity.[11–13] Here, we present a simple strategy to introduce nitrile-, amino- , amide- or carboxyl groups at the PEG backbone by copolymerization of EO with an unusual epoxide monomer, epicyanohydrin (EPICH), followed by post-polymerization reactions.

Ammonium- or carboxyl groups at the polyether backbone are desirable to generate polyether-based polyelectrolytes, which have hardly been investigated to date. In this context, copolymerization of allyl glycidyl ether (AGE) with ethylene oxide (EO) has been exploited to generate a platform for post-polymerization modification via thiol-ene coupling.[14–18] Following this approach, amino- or carboxyl groups can be coupled to the PEG backbone, which are attractive for further bioconjugation purposes. Alternatively, protected amino-functional epoxides can be directly polymerized to release multi-amino functional polyethers,[19–21] or a detour via copolymerization of epichlorohydrin can be applied.[22]

In this work, we introduce the polymerization of the challenging epoxide monomer epicyanohydrin (EPICH). This monomer enables direct access to nitrile-, amino-, amide- or carboxyl functional PEG without the use of odorous thiol compounds or extensive protecting group chemistry. The first report on EPICH dates back to 1870[23, 24] and first attempts to polymerize EPICH were described by Wei and Butler in the 1970ies.[25] The authors report EPICH to be a non-polymerizable monomer due to a proposed "dimer" formation. In 1973, Cantor *et al.* confirmed that EPICH was non-polymerizable, using a catalyst system developed by Vandenberg *et al.*[26] The strong electron-withdrawing character of the nitrile group next to the methylene group increases the positive character of the carbon atom and weakens the C-H-bond. This favors the formation of double bonds over the ring-opening reaction. In the current work, we applied the activated-monomer technique[27–29] to achieve polymerization of this epoxide, aiming at both PEPICH homopolymers and copolymers of EO and EPICH (Scheme 1).
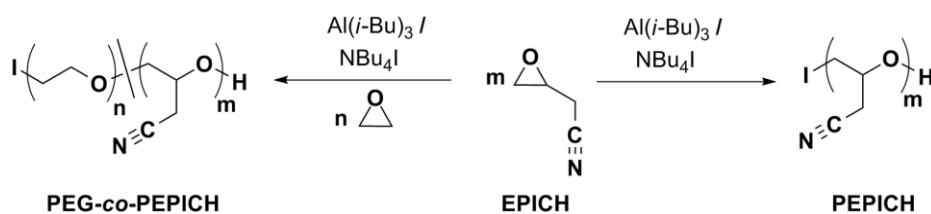
Scheme 1. Synthetic strategy for the copolymerization of EPICH and EO (left) and the synthesis of PEPICH homopolymer (right) via the activated monomer technique.

3.4.3 Experimental Part

Terminology. In this work, amino-, amide- and carboxyl-functional polyethers are named according to the underlying theoretical monomers and abbreviated as follows: "2-oxiraneethanamine" (OEA) in poly(2-oxiraneethanamine), "2-oxiraneacetamide" (OAm) in poly(2-oxiraneacetamide) and "2-oxiraneacetic acid" (OAa) in poly(2-oxiraneacetic acid). The homopolymer poly(epicyanohydrin) is named according to the monomer "epicyanohydrin", which is generally abbreviated as EPICH.[23, 26]

Reagents. Allyl cyanide was purchased from TCI, meta-chloroperoxybenzoic acid (mCPBA) (77% in water), ethylene oxide, mPEG5000, PEG1500, dichloromethane and hydrogen peroxide-urea adduct were purchased from SigmaAldrich. All other solvents and reagents were ordered from Acros Organics. The Raney cobalt catalyst (Grace 2724, in slurry) was purchased from Grace Catalysts Technologies. Deuterated solvents were received from Deutero GmbH. Dialysis membrane tubings were purchased from Sigma Aldrich or Orange Scientific, respectively. For dialysis in chloroform, a membrane of regenerated cellulose (benzoylated) was used. For dialysis in protic solvents, regular regenerated cellulose membranes were applied.

Instrumentation. ^{1}H NMR spectra (400 MHz) and ^{13}C NMR spectra (100 MHz) were recorded using a Bruker Avance III HD 400 spectrometer equipped with a 5 mm BBFO-SmartProbe (Z-gradient probe) and an ATM as well as a SampleXPress 60 auto sampler. All spectra are referenced internally to residual proton signals of the deuterated solvent (CDCl$_3$, DMSO-d_6 or D$_2$O). SEC measurements were performed in DMF (containing 0.25 g·L^{-1} lithium bromide as an additive) or THF, respectively. For SEC measurements in DMF, an Agilent 1100 Series was used as an integrated instrument, including a PSS HEMA column (300/100/40), a UV (275 nm) and a RI detector. Alternatively, SEC measurements in THF (flow rate 1 mL·min^{-1}) were performed with a MZ-Gel SD plus column

($10^5/10^3/100$ g·mol^{-1}) at 20°C, using a UV (254 nm) and RI detector. All calibrations were carried out using poly(ethylene glycol) standards purchased from Polymer Standards Service. DSC measurements were performed under nitrogen atmosphere using a PerkinElmer DSC 8500 with PerkinElmer CLN2 in the temperature range from -100 °C to 100 °C at heating rates of 20 and 10 K·min^{-1} for the first and the second heating run, respectively.

FT-IR measurements were recorded on a Thermo Scientific Nicolet iS10. Matrix-assisted laser desorption/ionization-time-of-flight (MALDI-ToF) measurements were performed on a Shimadzu Axima CFR MALDI-ToF mass spectrometer equipped with a nitrogen laser delivering 3 ns laser pulses at 337 nm. 2′,4′,6′-Trihydroxyacetophenone monohydrate (THAP) was used as a matrix.

Monomer synthesis (Epicyanohydrin). Epicyanohydrin (EPICH) was synthesized as described in literature, applying minor changes.[30, 31] 12 mL of allyl cyanide were dissolved in 300 mL of dichloromethane and stirred for 14 days at room temperature. Within the first three days, 20 g of mCPBA were added each day to the stirred solution. At full conversion, the precipitated meta-chlorobenzoic acid was filtered off, and the excess of mCPBA was removed by slow addition of a saturated aqueous solution of NaHSO$_3$ to the cooled solution. Subsequently, the organic phase was separated and washed with a saturated aqueous solution of NaHCO$_3$ followed by drying over MgSO$_4$. The product was purified by distillation under reduced pressure. $p = 1$ mbar, *b.p.* = 59 °C, 70 % yield. The monomer was stored in the dark at -18 °C and dried over CaH$_2$ directly before use.

^{1}H NMR (400 MHz, CDCl$_3$, δ): 3.24-3.20 (m, 1H, C*H*), 2.90-2.88 (t, 1H, C*H*$_{2a,ring}$, $J = 4.4$ Hz), 2.76-2.74 (m, 3H, C*H*$_{2b,ring}$, -C*H*$_2$CN);

^{13}C NMR (100 MHz, CDCl$_3$, δ): 115.60 (*C*N), 46.78 (*C*H$_{2,ring}$), 46.22 (*C*H$_{ring}$), 21.21 (*C*H$_2$CN).

Homopolymerization (PEPICH). Epicyanohydrin (EPICH) was polymerized similar to a literature protocol described for ethoxyethyl glycidyl ether applying the monomer activation technique.[32] As a typical procedure, tetraoctylammonium bromide or tetrabutylammonium iodide (1 eq) was freeze-dried with benzene overnight, and the flask was backfilled with argon. Chlorobenzene was added under argon atmosphere via syringe ($c = 1$ mol$\cdot$L^{-1}). The solution was cooled to 0 °C before the dry monomer was syringed in, followed by *i*-Bu$_3$Al (5 eq) solution in toluene. The solution was slowly warmed up to 25 °C and terminated after 24 h by addition of ethanol. The crude polymer was subsequently dissolved in THF and precipitated into methanol (room temperature). This purification step was repeated twice to ensure complete removal of the ammonium salts, which was confirmed by NMR.

Copolymerization of EO with EPICH (PEG-co-PEPICH). Here, an exemplary synthesis protocol is described for the synthesis of the PEG$_{190}$-*co*-PEPICH$_{10}$ copolymer with 5 mol% EPICH content. 77.5 mg of tetrabutyl ammonium iodide (1 eq) was dissolved in 5 mL benzene and freeze-dried under vacuum to remove residual water. The flask was backfilled with argon and 15 ml of chlorobenzene were added via syringe. For the transfer of EO into the flask, vacuum was applied and 2 mL (190 eq) of ethylene oxide were distilled into a graduate ampoule in the cold and subsequently into the reaction flask, using an ethanol/liquid nitrogen cooling bath (-80 °C). The flask was sealed, backfilled with argon and 0.16 mL (10 eq) of freshly distilled EPICH was introduced by syringe via septum. The reaction was initiated at -15 °C by addition of *i*-Bu$_3$Al solution in toluene (2 eq, 0.42 mL) and slowly allowed to warm up to room temperature. After 24 h, termination was performed by addition of an excess of ethanol (1 mL), and the polymer was precipitated into ice cold diethyl ether. Dialysis in chloroform (MWCO = 2000 g$\cdot$mol^{-1}) was performed to remove residual tetrabutylammonium salts. Drying under high vacuum at 40 °C afforded the copolymer in yields of ca. 80-90 %.

Derivatization of the hydroxyl groups with phenyl isocyanate. The dried polymer (100 mg) was dissolved in anhydrous THF (3 mL) and heated to 50 °C under argon atmosphere. Subsequently, an excess of phenyl isocyanate (0.5 mL) was added. The solution was stirred for 12 h and cooled to room temperature. Excess of phenyl isocyanate was removed by addition of methanol. The solution was precipitated into ice cold diethyl ether and the modified polymer was additionally purified by dialysis against methanol (MWCO = 1000 g·mol^{-1}). The yields were in the range of 85-90 %.

Synthesis of poly(ethylene glycol)-co-poly(2-oxiraneethanamine) (PEG-co-POEA). A modified literature procedure, analogous to the procedure reported for the poly(propylene imine) dendrimer synthesis was applied.[33] 100 mg of the copolymer were dissolved in 20 mL DI water and placed in a pressure vessel. After addition of a Raney cobalt catalyst (Grace 2724, in slurry), the hydrogenation was carried out under stirring at 40 °C and 100 atm H_2 for 7 days. The catalyst was removed by filtration, and the solution was acidified with 2 mL of 1 M HCl and nitrogen was bubbled through the solution for 1 day. Then the solution was purified by dialysis for 1 day against DI water (MWCO = 1000 g·mol^{-1}) to remove hydrochloric acid traces. A small loss of product due to dialysis was observed. Yield ≥ 80 %.

Derivatization reaction of the amino groups with acetic anhydride. The derivatization was carried out in THF according to a literature procedure, reported by our group.[19] PEG-*co*-POEA with OEA ratios above 13 mol% were dissolved in DMF instead of THF, caused by poor solubility in THF.[22] The product was purified by dialysis against methanol (MWCO = 1000 g·mol^{-1}). Yield ≥ 85 %.

Synthesis of poly(ethylene glycol)-co-poly(2-oxiraneacetamide) (PEG-co-POAm) and poly(2-oxiraneacetamide) (POAm). A published procedure for the mild conversion of nitrile groups to amide groups was applied.[34] 400 mg of PEG-*co*-PEPICH with 6 mol%

EPICH units were dissolved in 10 mL water/acetone (1:1). 150 mg of hydrogen peroxide-urea adduct (4 eq), and 20 mg of anhydrous potassium carbonate were added to the reaction flask and the mixture was stirred for 1-2 days at room temperature. After complete conversion, the solvents were removed under vacuum and the polymer was isolated by extraction with dichloromethane. The conversion was quantitative. POAm homopolymers were not soluble in dichloromethane and were purified via dialysis against DI water (MWCO = 1000 g·mol⁻¹). A small loss of product due to dialysis was observed. Yield ≥ 85 %.

Synthesis of poly(ethylene glycol)-co-poly(2-oxiraneacetic acid) (PEG-co-POAa) and poly(2-oxiraneacetic acid) (POAa). The amide containing (co)polymer (200 mg) was dissolved in 6 M HCl (10 mL) and stirred for 7 days at room temperature to ensure a complete hydrolysis.[35] After complete conversion of the amide groups into carboxyl groups, the solvent was removed by vacuum and the polymer was dialyzed against DI water (MWCO = 1000 g·mol⁻¹). A small loss of product due to dialysis was observed. Yield ≥ 90 %.

Cleavage of the copolymer and homopolymer backbone. 100 mg of the (co)polymer was dissolved in anhydrous THF (3 mL), and an excess of sodium ethoxide (150 mg) was added to the reaction mixture. Subsequently, the solution was heated to 70 °C for 12 hours. After the mixture was cooled down to room temperature, the excess of sodium ethoxide was quenched by addition of DI water and the solution was neutralized by addition of aqueous HCl solution. The solvent was removed by rotary evaporation and the residual polymer characterized without further purification; characterization data are discussed in the main text. Yields were not determined.

3.4.4 Results and Discussion

A. Monomer Synthesis and (Co)polymerization of EPICH and EO.

Monomer (EPICH) Synthesis. The synthesis of EPICH was accomplished by facile oxidation of commercially available allyl nitrile with mCPBA. Minor modifications of a literature procedure yielded 70 % of the monomer after purification by distillation. We did not observe formation of the 4-hydroxybut-2-enenitrile contaminant, which was mentioned by some authors.[30, 31] ^{1}H and ^{13}C NMR spectra confirmed the purity of the product (Figure S1 and Figure S2). We recommend to avoid extensive heating of the monomer and storage at -18 °C to prevent isomerization to 4-hydroxybut-2-enenitrile.

Homopolymerization of EPICH. According to literature, EPICH is non-polymerizable, due to the strong electron withdrawing character of the cyano group and the resulting acidic characteristics of the methylene protons.[25, 26] However, we assumed that the "activated monomer" technique, introduced by Deffieux and Carlotti *et al.* in 2004, might permit successful polymerization of EPICH, since in this case no strongly basic alkoxide initiators are employed and low reaction temperatures are chosen.[27, 28] The reaction mechanism is illustrated in Scheme 2. Triisobutylaluminum (catalyst) forms a nucleophilic "ate" complex with tetrabutylammonium iodide (initiator) (step 1). In addition, excess triisobutyl-aluminum reduces the electron density of the epoxide ring via coordination (step 2). Subsequently, initiation proceeds through nucleophilic attack of the "ate" complex at the activated epoxide ring (step 3). Chain growth continues until all monomer is consumed (step 4). Addition of excess ethanol terminates the reaction (step 5). The polymerization was carried out in chlorobenzene, as discussed below.
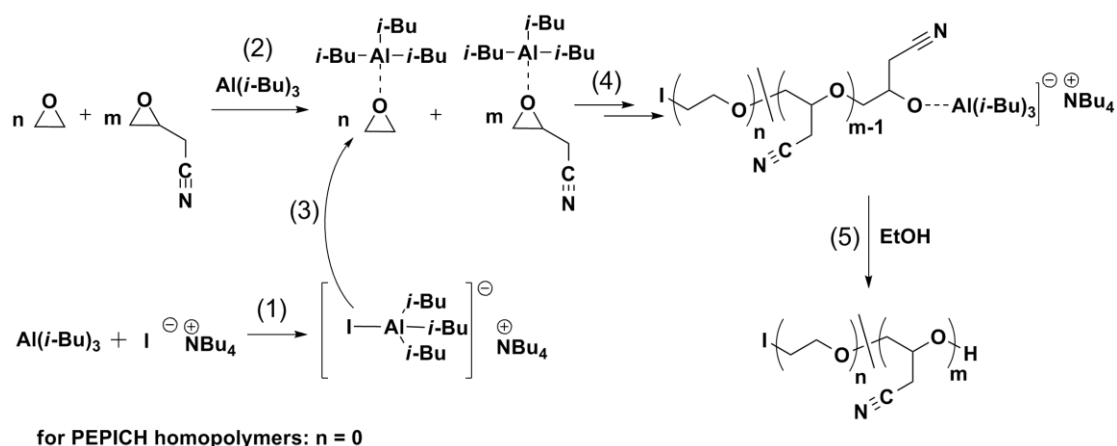
Scheme 2. (Co)polymerization mechanism of EPICH and EO; (1) formation of the "ate"-complex; (2) activation of the epoxide ring through complexation with triisobutylaluminum; (3) initiation through nucleophilic attack; (4) chain growth; (5) termination with excess ethanol.

PEPICH homopolymers with molecular weights M_n up to 2,500 g·mol^{-1} (DP = 30) were obtained, while PDIs ranged from 1.08 to 1.14. Molecular weights have been determined via SEC measurements and by ^{1}H NMR spectroscopy after derivatization of the terminal hydroxyl group with phenyl isocyanate (Table 1 and Figure 1). Detailed NMR characterization showed that the molecular weights of the homopolymers are limited due to precipitation of the product during polymerization and the occurrence of transfer to the EPICH monomer, resulting in unsaturated chain ends (Scheme 3), despite the absence of strong bases in the polymerization.
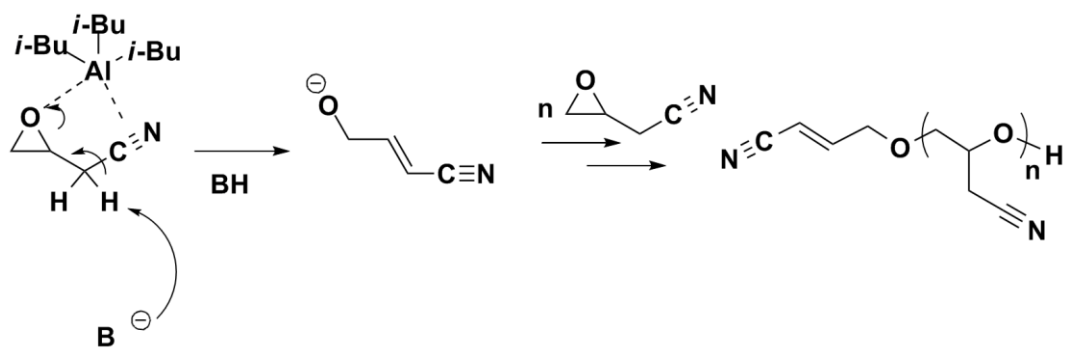
Scheme 3. Side reaction induced by base (B), resulting in PEPICH homopolymer with an unsaturated chain end.

The side reaction shown in Scheme 3 is a common molecular weight limiting pathway for epoxide derivatives and usually occurs under harsh reaction conditions (strong bases, high reaction temperatures).[36] In our case, the use of dichloromethane as an alternative solvent with higher polarity than chlorobenzene appeared to facilitate this side reaction, and only short oligomers ($M_n \leq 1000$ g·mol^{-1}) of PEPICH with very broad PDIs ($M_w/M_n > 3$) were obtained. An alternative solvent to chlorobenzene that on the one hand prevents precipitation of the PEPICH homopolymer, on the other hand does not facilitate the undesired proton abstraction was not found.

In general, the activated monomer technique is a well-known approach to suppress the described side reaction and thereby to achieve high molecular weight polyethers.[27, 28, 32, 37–39] Even epoxide derivatives bearing electron withdrawing groups, such as chlorinated or fluorinated oxirane monomers can be successfully polymerized with this powerful technique.[22, 40–44] Yet, the extremely strong electron withdrawing character of the nitrile group in EPICH and the emerging mesomeric stabilization enable even weak bases to abstract a proton from the methylene group adjacent to the nitrile group. Consequently, an unsaturated alkoxide is formed, which acts further as an initiator, strongly lowering molecular weights in comparison to the targeted values (Scheme 3). This proton abstraction was confirmed by the occurrence of double bonds in ^{1}H and ^{13}C NMR spectra (Figure S3 and Figure S4). Furthermore, MALDI-ToF measurements confirmed two main distributions for PEPICH, both polymer initiated via iodide and via unsaturated alkoxide species (Figure S5, Supporting Information). Note, that the variety of possible initiating species and counterions impede a complete assignment of the subdistributions in MALDI spectra. To minimize the described proton abstraction, low catalyst/initiator ratios have to be chosen and low temperatures and weak bases should be used as initiators. Based on this rationale, we favored tetrabutylammonium iodide as an initiator over the more common tetraoctylammonium bromide. The tetrabutylammonium ion is less sterically hindered than

its tetraoctylammonium analogue. Therefore we assume that it attaches stronger to the polymer chain end and may aid to impede proton abstraction. Additionally, iodide is a weaker base than bromide albeit a stronger nucleophile and may thus lower proton abstraction. Nevertheless, NMR studies showed that the obtained PEPICH samples are only initiated to about 40-50 % by the chosen initiator and the other 50-60 % of the chains are initiated by the described unsaturated species.

Concurrent Copolymerization of EPICH and EO. The copolymerization of EO and EPICH was performed in analogy to the described homopolymerization of EPICH (Scheme 2).[27, 28] Copolymers with molar fractions of 4-16 mol% EPICH were synthesized, aiming at water-soluble materials with a minority fraction of the EPICH comonomer. The EPICH ratios were calculated by comparing the proton signals of the CH_2CN methylene group (2.60-2.85 ppm) with the polyether backbone signals (3.40-3.80 ppm), as shown in Figure 1.
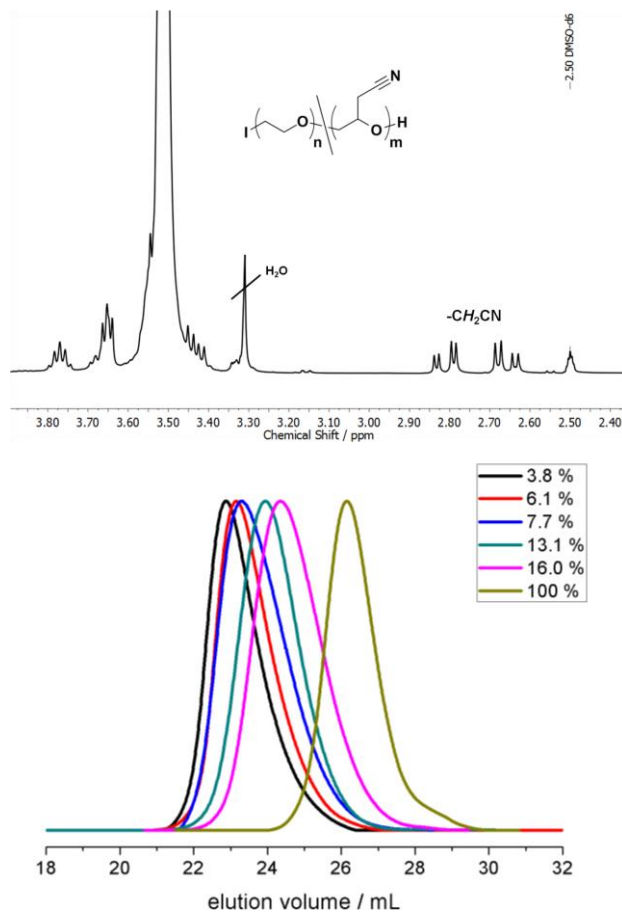
Figure 1. ^{1}H NMR spectrum (400 MHz, DMSO-*d₆*) of PEG-*co*-PEPICH with 6.1 mol% EPICH (top); SEC elution traces (THF, RI detection, PEG standards) of PEG-*co*-PEPICH copolymers with varied EPICH content and PEPICH homopolymer (bottom).

Molecular weights of the EO/EPICH copolymers were determined by SEC (THF, PEG standards) and ranged from 3,700 to 8,800 g·mol⁻¹ with moderate PDIs (1.24-1.35) (Figure 1 and Table 1). Due to the nature of the applied initiator, ^{1}H NMR spectroscopy can not be used to calculate absolute molecular weights of the copolymers. Hence, we derivatized the terminal hydroxyl groups of the PEG-*co*-PEPICH copolymers with phenyl isocyanate to obtain an integrable end group for ^{1}H NMR spectroscopy (Figure S6). Determined molecular weights confirmed the data obtained by SEC and are also listed in Table 1. Still, these values only represent absolute molecular weights, if full conversion is realized and no hydroxyl initiated species occurred during the polymerization process. Further, the iodide initiator is a good leaving group and additional hydroxyl end groups could have been

formed during the workup process of the polymers. Consequently, we assume that the listed molecular weights most likely underestimate the actual molecular weights.

In general, we adjusted the catalyst to initiator ratio for each copolymer composition. Full monomer conversion was proven by monitoring residual EO and EPICH signals *via* ^{1}H NMR spectroscopy. A higher catalyst amount for high EPICH ratios was necessary to ensure full conversion (Table 1). As observed for the homopolymerization, the described side reaction leading to unsaturated end groups lowered the estimated molecular weight of the copolymers (Scheme 3). For PEG-*co*-PEPICH copolymers with low EPICH content, less than 10 % of the polymer chains were initiated by the unsaturated species. For EPICH ratios exceeding 7 mol%, we observed that about 80 % of the polymer chains were initiated by tetrabutylammonium iodide and up to 20 % due to side reaction (see Table 1).

Table 1. Copolymerization of EO with EPICH using [*i*-Bu$_3$Al]/[NBu$_4$I] (chlorobenzene, -15°C, c_{EO} = 3 mol·L^{-1}).

No.	[*i*-Bu$_3$Al]/ [NBu$_4$I]	EPICH content (mol%)[a]	Copolymer composition[c]	M_n[b] (g·mol^{-1})	M_n[c] (g·mol^{-1})	M_w/M_n[b]	AEG[d] (%)
1	2	3.8	PEG$_{152}$-*co*-PEPICH$_6$	8800	7200	1.24	5
2	2	6.1	PEG$_{138}$-*co*-PEPICH$_9$	7300	6800	1.31	7
3	3	7.7	PEG$_{144}$-*co*-PEPICH$_{12}$	6100	7300	1.35	20
4	5	13.1	PEG$_{79}$-*co*-PEPICH$_{12}$	5000	4500	1.30	22
5	5	16.0	PEG$_{58}$-*co*-PEPICH$_{11}$	3700	3500	1.27	18
6	5	100	PEPICH$_{26}$	1800	2200	1.10	60

[a]Obtained from ^{1}H NMR spectra.
[b]Determined by SEC measurements in THF (RI signal, PEG standards).
[c]Calculated by ^{1}H NMR spectra after derivatization of the hydroxyl end group with phenyl isocyanate.
[d]AEG = Percentage of chains with an allylic end group (AEG). Calculated in analogy to Moeller and coworkers by ^{1}H NMR spectra after derivatization of the hydroxyl end group with phenyl isocyanate.[36]

¹³C NMR Triad Analysis. ¹³C NMR triad analysis was performed to gain a qualitative insight into the microstructure of the synthesized PEG-*co*-PEPICH copolymers. For this purpose, we recorded *inverse gated* (IG) ¹³C NMR spectra of PEG, PEPICH and PEG-*co*-PEPICH with various EPICH content. We assigned the triads relying on 2D NMR spectra and literature spectra of random EO based copolymers.[19, 45–47] In Figure 2, EPICH centered triads are labeled with N and EO centered triads with E, whereas *a* and *b* denote the first and second carbon atom. The IG ¹³C NMR spectrum of PEPICH shows four main resonances, corresponding to the branch nitrile (118.30 ppm), the backbone methine (74.20 ppm), backbone methylene (69.36-70.09 ppm) and the branch methylene carbons (19.93 ppm) (Figure S4). The observed signals show further splitting into higher stereosequences, similar to atactic polyepichlorohydrin synthesized by the activated monomer technique.[40]

Figure 2 shows the important section of the IG ¹³C NMR spectrum and the respective triad assignment of PEG-*co*-PEPICH with 13.1 mol% EPICH. For a better interpretation, we listed the different IG ¹³C NMR spectra of PEG, PEG-*co*-PEPICH and PEPICH (Figure 3). The increasing signal intensity of the E-N-E triad with increasing EPICH content and the remaining low intensity for N-E-N or N-N-N triads indicate a rather random or gradient microstructure, respectively, and a blocky structure of the copolymers can be excluded.
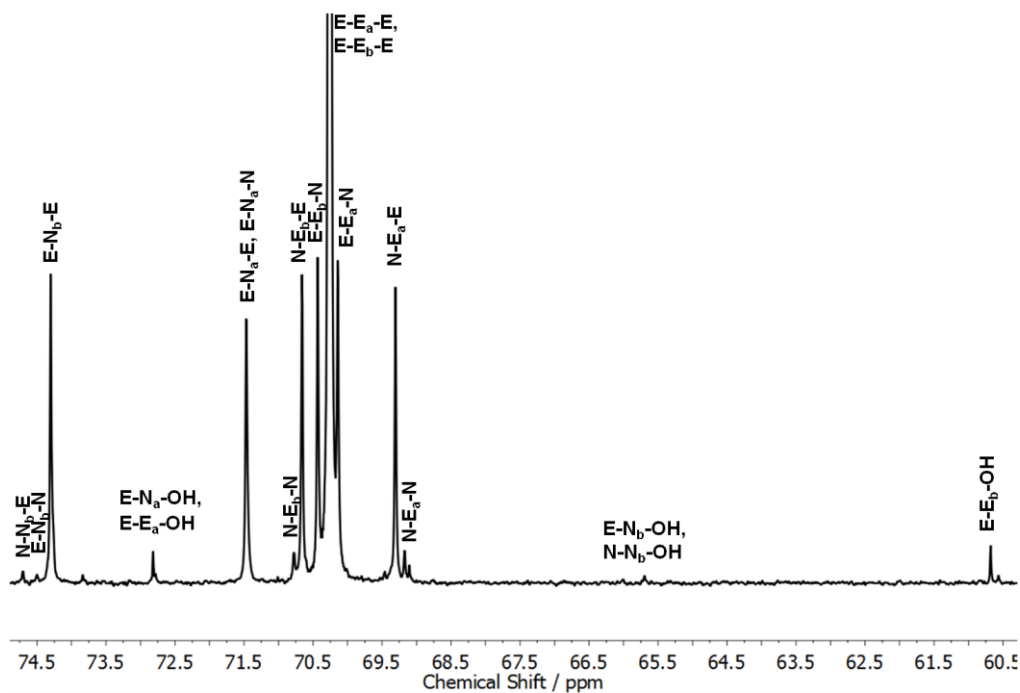
Figure 2. Relevant section of the IG ^{13}C NMR spectrum (100 MHz, DMSO-d_6) of PEG-*co*-PEPICH with 13.1 mol% EPICH.
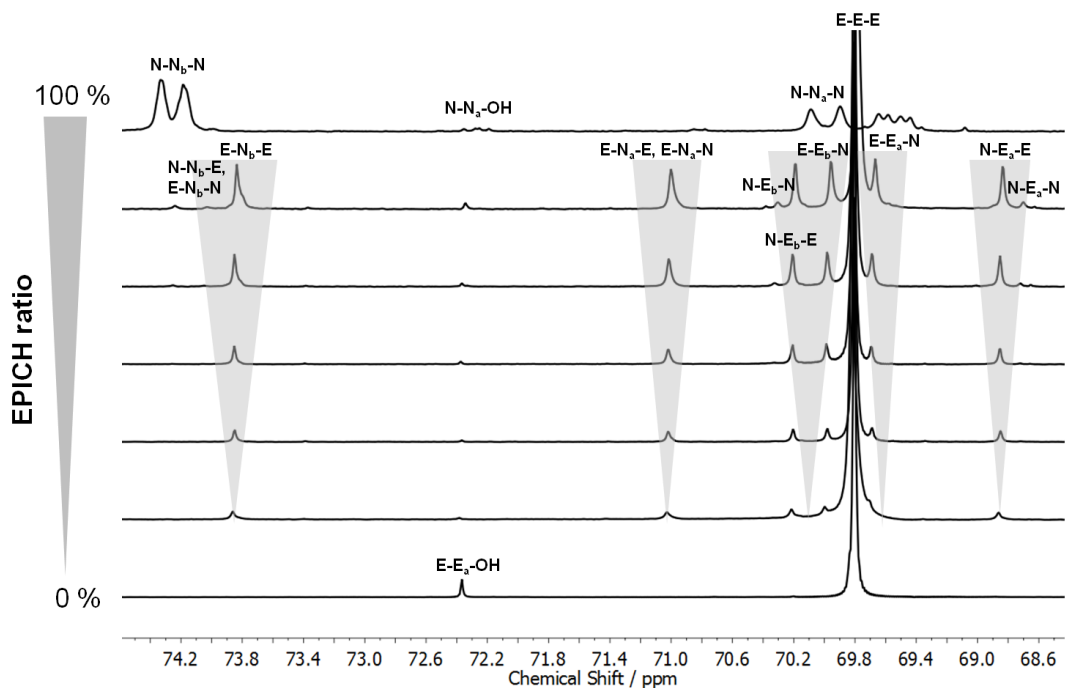
Figure 3. Relevant section of IG ^{13}C NMR spectra (100 MHz, DMSO-d_6) of PEG, PEG-*co*-PEPICH copolymer with various mol% EPICH (3.8%, 6.1%, 7.7%, 13.1%, 16.0%) and PEPICH homopolymer.

238

For further investigation of the microstructure, the polymer backbone was deliberately cleaved by retro-Michael addition (Scheme S1, Supporting Information) with sodium ethoxide in THF, and the fragments were analyzed by SEC measurements (Figure S7, Supporting Information). PEG-*co*-PEPICH with 7 mol% EPICH and a molecular weight of $M_n = 4,800$ g·mol^{-1} showed, after treatment with sodium ethoxide in THF, a molecular weight of about 700 g·mol^{-1}, indicating a nearly random distribution of the nitrile groups along the polymer backbone (Figure S7, Supporting Information). Note, that cleavage can occur at any EPICH segment within the polymer, both at isolated N-N-N triads as well as random E-N-E units, respectively. The PEPICH homopolymer was also treated with sodium ethoxide to demonstrate almost complete cleavage of the polymer backbone (Figure S8, Supporting Information). As control experiment, commercial mPEG5000 without EPICH units shows no alteration after treatment with sodium ethoxide (Figure S9, Supporting Information). In summary, these results can be taken as an indication for a random microstructure rather than a pronounced monomer gradient.

Thermal Properties of PEPICH and PEG-co-PEPICH (co)polymers. We conducted DSC measurements to investigate the effect of nitrile groups on melting behavior and the glass transition temperature (T_g) of PEG-*co*-PEPICH (co)polymers (Table 2).

The atactic PEPICH homopolymer is an amorphous material with a glass transition temperature of T_g = -14 °C. The T_g of PEPICH is in good agreement with other polyethers bearing polar side groups, e.g. poly(epichlorohydrin) (T_g = -25 °C to -20 °C)[22, 48, 49] or the nitrile functional poly(3-(2-cyano ethoxy)methyl-3'-methyloxetane) with T_g = -18 °C.[50]

For the copolymers, we observed a strong influence of the EPICH content on the melting temperature and melting enthalpy. Figure 4 shows the melting temperatures of PEG-*co*-PEPICH copolymers plotted as a function of the content of incorporated EPICH. Fitting of the experimental data and interpolation to a comonomer content of 0 %, i.e., PEG

homopolymer, results in a melting temperature of about 61 °C, which is in good agreement with the known melting temperature for mPEG5000 (T_m = 64 °C). If a block-type structure had been obtained, one would expect a melting temperature for the PEG segments close to the melting temperature of mPEG itself. Thus, our results are in line with a random or gradient distribution of EPICH within the polyether backbone and are consistent with the data obtained via ^{13}C triad analysis and cleavage experiments. The thermal properties of the post-modified (co)polymers are listed in the respective section.

Table 2. Characterization data of PEG-*co*-PEPICH copolymers and PEPICH homopolymer obtained by DSC measurements.

No.	EPICH content / %	T_g/°C	T_c/°C	T_m/°C	ΔH/J·g^{-1}
mPEG5000	0	-53	---	64	186
1	3.8	- 48	---	44	84
2	6.1	-49	---	36	58
3	7.7	- 48	---	28	60
4	13.1	-52	-11	5	20
5	16.0	-46	---	---	---
6	100	-14	---	---	---

T_g: glass transition temperature
T_m: melting temperature
ΔH: melting enthalpy
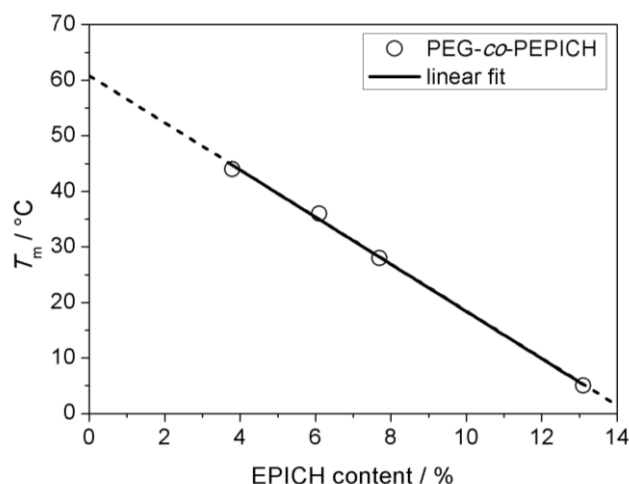
Figure 4. Melting temperature (T_m) of PEG-*co*-PEPICH copolymers versus EPICH content and linear fit (black line).

B. Post-Polymerization Modification.

The nitrile groups of PEG-*co*-PEPICH and PEPICH (co)polymers can be directly converted into amino or carboxyl groups via amide groups, respectively. The simple transformation of the incorporated nitrile units to various multi-functional PEGs reflects the promising potential of the EPICH monomer and gives access to merely polyether-based polyelectrolyte structures.

Amino groups. Amino-functional PEG was obtained by hydrogenation of PEG-*co*-PEPICH using a Raney cobalt catalyst (Scheme 4). The reaction was carried out in water at 40 °C for 7 days. The hydrogenation of nitriles into primary amines is a complex reaction, which can be accompanied by side reactions. The formation of secondary and tertiary amines is often observed in literature, caused by the interaction of primary amines with residual nitriles.[33, 51] Therefore, the reaction conditions have to be carefully chosen. The applied procedure in the current work is well-known for the synthesis of poly(propylene imine) dendrimers and suitable for hydrogenation of nitrile groups.[33] We observed the formation of ammonium carbamate species during the hydrogenation process. This is tentatively

attributed to reaction of the formed primary amines with dissolved CO_2 in the DI water (Scheme S2). The reversible formation of ammonium carbamates is a literature-known phenomenon and represents the principle of CO_2-stimuli responsive amino-functional materials.[52, 53] Here, these ammonium carbamate structures act as protecting group for the amino groups and prevent further reaction with the residual nitrile groups. Consequently no secondary or tertiary amines can be formed. After removal of the Raney cobalt catalyst, the ammonium carbamate functional PEG was dissolved in 1 M hydrochloric acid and the amino groups were released by bubbling nitrogen through the aqueous polymer solution. Successful release of the amino moieties was proven by ^1H and ^{13}C NMR spectroscopy (Figure S10-S12). After acidic treatment, the characteristic signal of the carbamate species in the ^{13}C NMR spectrum at 170.8 ppm vanished and the resonances for the methylene groups next to the amino-group at 28.2 ppm and 37.2 ppm appeared (Supporting Information, Figure S10). Further NMR spectroscopy revealed the cleavage of the iodide initiator, resulting in proton signals at 1.09 ppm and 3.5 ppm and ^{13}C signals at 14 ppm and 66 pm, caused by the formed methyl-group (Scheme 4).
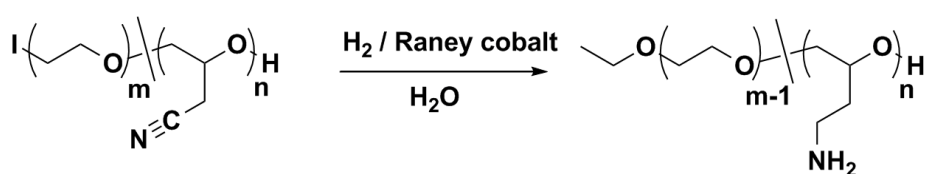
Scheme 4. Reaction scheme to obtain amino-functional PEG (PEG-*co*-POEA) through hydrogenation with cleavage of the iodide initiator.

Successful conversion was also confirmed by FT-IR spectroscopy (Figure S13). After hydrogenation, the absorption band of the nitrile group (2247 cm^{-1}) disappeared and characteristic bands of primary amines in the region of 3400 cm^{-1} to 3100 cm^{-1} appeared, corresponding to the symmetrical and asymmetrical stretching of the N-H bond. A new absorption band at 1609 cm^{-1} corresponds to the N-H bend. The measured peaks are in good

agreement with reported literature values of poly(glycidyl amine).[22] Additionally, the amino-functions were derivatized with acetic anhydride as a model reaction (Scheme 5). SEC measurements of the derivatized species confirm a monomodal distribution with a slight shift to lower molecular weights, attributed to a change in hydrodynamic volume and slight interactions of the secondary amide groups with the column material (Figure 5).
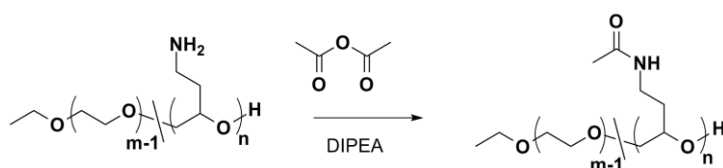
Scheme 5. Derivatization of PEG-*co*-POEA with acetic anhydride.[19]
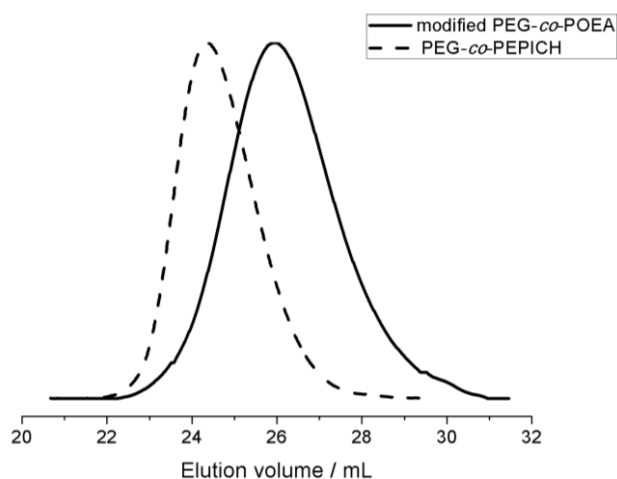
Figure 5. SEC elution traces (THF, RI detection, PEG standards) of PEG-*co*-PEPICH (dashed line) and PEG-*co*-Poly(2-oxiraneethanacetamid) (solid line) with 16 mol% EPICH.

Thermal Properties of PEG-co-POEA. The thermal properties of PEG-*co*-POEA copolymers are listed in the Supporting Information (Table S1). Copolymers with 3.8-6.1 mol% OEA show no change in melting temperature to their nitrile analogues. For PEG-*co*-POEA with 7.7 mol% OEA, an increased melting temperature ($T_m = 34$ °C) compared to the respective PEG-*co*-PEPICH ($T_m = 28$ °C) was detected. A similar trend is described

in literature for poly(ethylene glycol)-*co*-poly(glycidyl amine) (PEG-*co*-PGA).[19] Obermeier *et al.* observed an increased melting temperature for PEG-*co*-PGA copolymers compared to the respective precursor polymers, e.g., poly(ethylene glycol)-*co*-poly(dibenzyl amino glycidol) (PEG-*co*-PDBAG). This was explained with the occurrence of hydrogen bonds between the amino groups. In our case, the 2-oxiranethanamine unit possesses an additional methylene group, compared to the glycidyl amine unit. Therefore, we propose that the increase in chain flexibility compensates for the occurrence of hydrogen bonds for samples with low molar fractions of OEA. The occurrence of hydrogen bonding within the polymer structure also influences the glass transition temperatures.[21] In particular PEG-*co*-POEA with 13.1 and 16.0 mol% OEA show a jump in T_g of ∼ 25°C.

Amide and Carboxyl Moieties. The direct conversion of nitrile units into carboxylic acid units, as described by Zhang *et al.* for nitrile-functional initiators, is not possible for PEG-*co*-PEPICH.[54] Harsh alkaline conditions induce *β*-elimination reactions at the glycidyl nitrile unit, followed by subsequent cleavage of the polymer backbone. Furthermore, strongly acidic conditions at elevated temperatures induce cleavage of the polyether backbone. Consequently, we chose a different approach and synthesized amide groups first, followed by conversion into carboxyl groups (Scheme 6).
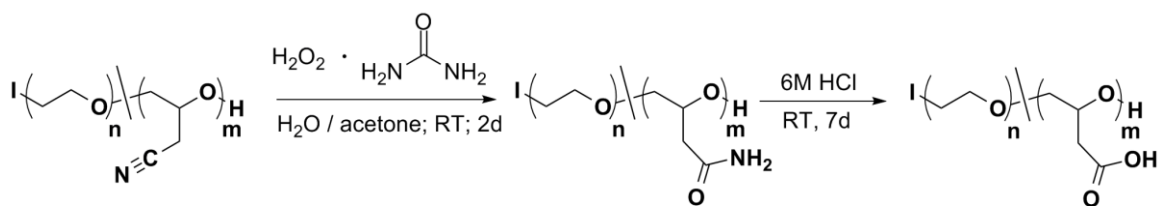
for PEPICH homopolymer: n = 0

Scheme 6. Post-polymerization modification scheme to obtain carboxyl and amide functional (co)polymers: Mild oxidization of the nitrile group with hydrogen peroxide urea complex to obtain amide functional PEG-*co*-POAm or POAm (co)polymers is followed by hydrolysis of the amide group in aqueous hydrochloric acid solution.

Use of the hydrogen peroxide – urea adduct permits mild and simple conversion of nitriles into amides.[34] Subsequently, the amide groups of the (co)polymers were successfully converted into carboxyl groups by hydrolysis in hydrochloric acid solution at room temperature. ^{1}H and ^{13}C NMR measurement confirmed successful and quantitative reactions (Figure 6 and Figure S14). Figure 6 shows the ^{1}H NMR of PEG-*co*-PEPICH, PEG-*co*-POAm and PEG-*co*-POAa. The methylene group adjacent to the functional group shows a clear shift from 2.85 ppm (CH_2CN) to 2.53 ppm (CH_2CONH$_2$) and finally to 2.6 ppm (CH_2COOH). These results were confirmed by ^{13}C NMR spectroscopy (Figure S14). After treatment with the hydrogen peroxide-urea complex, the *C*N-resonance at 118.9 ppm vanished and a new resonance for the *C*ONH$_2$ at 176.0 ppm occurred. Additionally, the carbon atom of the methylene group showed a clear shift from 19.7 ppm (*C*H$_2$CN) to 37.5 ppm (*C*H$_2$CONH$_2$). After complete hydrolysis to the carboxylic acid, the resonance of the carbonyl-group shifted from 176.0 ppm (*C*ONH$_2$) to 175.2 ppm (*C*OOH) and the methylene group from 37.5 ppm (*C*H$_2$CONH$_2$) to 36.5 ppm (*C*H$_2$COOH). Similar results were observed for the respective PEPICH homopolymers (Figures S15-S18, Supp. Inf.).
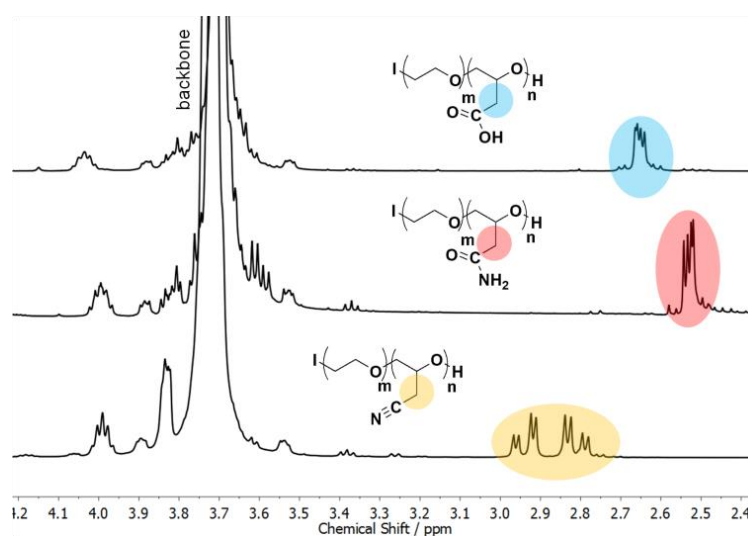
Figure 6. Relevant region of the ^{1}H NMR spectra (400 MHz, D$_2$O) of PEG-*co*-PEPICH (yellow), PEG-*co*-POAm (red) and PEG-*co*-POAa (blue).

Together with SEC measurements, the results confirm that the integrity of the PEG-*co*-POAm copolymers was maintained. Figure 7 shows the SEC traces of PEG-*co*-PEPICH with 16.1 mol% EPICH and the respective PEG-*co*-POAm. Note, that the slight shift is probably due to interactions of the primary amide groups with the column material and the overall change in hydrodynamic volume after post-polymerization modification. Interestingly, the POAm homopolymer showed no solubility in common organic solvents and only turbid solutions in water were obtained, which we attribute to strong hydrogen bonding interaction between the polymer chains. Thus, no SEC measurements of the POAm homopolymer could be conducted. Further, no SEC traces of carboxyl acid functional (co)polymers were recorded, due to interactions of the acid groups with the column material.

Interestingly, in contrast to the amide functional POAm homopolymers, the acid functional POAa homopolymers show excellent water solubility in the whole pH range of water (even in 1M HCl, pH < pK_s). This behavior differs from the known solubility behavior of poly(acrylic acid), which only possesses good water solubility in the salt state. We assume that the low molecular weight of POAm homopolymers in combination with the hydrophilic and extremely flexible polyether backbone lead to good water solubility, even at low pH.

Additionally, FT-IR spectroscopy was carried out to confirm successful hydrolysis. Figure 7 shows the conversion of PEG-*co*-PEPICH to PEG-*co*-POAm and PEG-*co*-POAa. After treatment of PEG-*co*-PEPICH with the urea·H_2O_2 adduct, the adsorption at 2247 cm^{-1} (-CN group) disappeared and a new peak at 1670 cm^{-1} and three new absorption bands at 3210 cm^{-1}, 3345 cm^{-1} and 3428 cm^{-1} appeared, due to the carbonyl group of the amide and the N-H stretching. The characteristic absorption band for the polyether backbone (1094 cm^{-1}) showed no alteration. After hydrolysis, the carbonyl frequency shifted to

246

1729 cm^{-1}, confirming successful conversion of amide groups to carboxyl groups. IR spectra for the respective homopolymers are depicted in the Supporting Information (Figure S19) and show similar results.
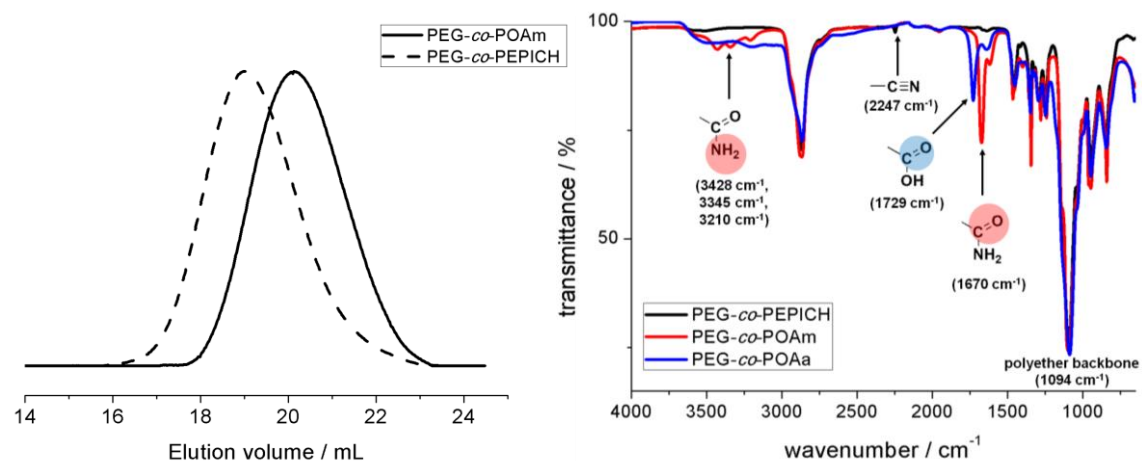
Figure 7. Left: SEC elution traces (DMF, RI detection, PEG standards) of PEG-*co*-POAm (solid trace) and PEG-*co*-PEPICH (dashed trace) with 16 mol% functional group. Right: FT-IR spectra of PEG-*co*-PEPICH (black line), PEG-*co*-POAm (red line) and PEG-*co*-POAa (blue line).

Additional MALDI-ToF MS measurements demonstrate successful modification of the PEPICH homopolymer to POAm and POAa, respectively, as shown in Figures S20-S21. However, the variety of initiating species and counterions impedes complete peak assignment of the modified homopolymers. Nevertheless, the main distribution confirms a successful conversion and reflects the respective repeating units.

Thermal Properties of PEG-co-POAm, PEG-co-POAa, POAm and POAa. We studied the thermal behavior of the respective *mf*-PEGs in order to evaluate the influence of the amide and carboxyl functional group on the polymer structure (Table S2). A pronounced change of the thermal properties can only be observed with high molar fractions (>13 mol%) of incorporated functional comonomer. In particular, for PEG-*co*-PEPICH with 16 mol% EPICH, the T_g increases from -46 °C (nitrile) to -30 °C (amide). This trend is even stronger for the respective homopolymer. While PEPICH shows a glass transition temperature

of -14 °C, POAm, the poly(acrylamide) analogue reveals a T_g of 55 °C. This extremely high T_g is explained by strong hydrogen bonding between the respective amide groups. After hydrolysis to POAa, the T_g drops from 55°C to 29 °C, reflecting weaker molecular interactions, in analogy to poly(acrylamide) ($T_g = 165$ °C) and poly(acrylic acid) ($T_g = 105$ °C) (Scheme 7).[55]
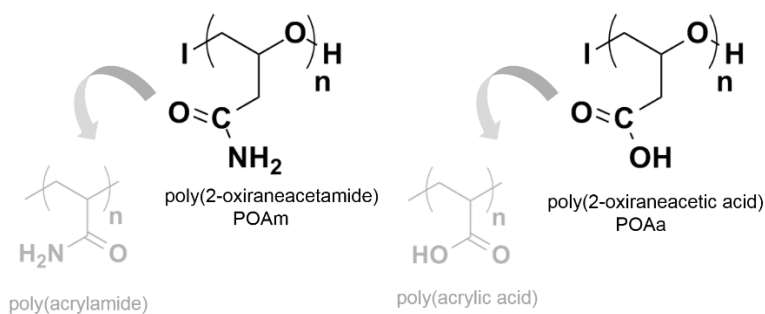
Scheme 7. Modified PEPICH homopolymers, poly(2-oxiraneacetamide) (POAm) and poly(2-oxiraneacetic acid) (POAa) and carbon-backbone based analogues: poly(acrylamide) and poly(acrylic acid), respectively.

3.4.5 Conclusion

Both the poly(epicyanohydrin) (PEPICH) homopolymer and a variety copolymers of epicyanohydrin and ethylene oxide have been prepared by applying the "activated monomer" approach. For the random copolymers, the EPICH ratio was varied between 4-16 mol% and molecular weights ranging from 3,700 to 8,8000 g·mol^{-1} with rather narrow molecular weight distributions ($M_w/M_n = 1.24 - 1.35$) were obtained, albeit molecular weight limiting transfer reactions could not be completely suppressed. Note that in this work deliberately low molar fractions of EPICH (4-16 mol%) were chosen to maintain PEG's outstanding properties while extending its functionality. From detailed ^{13}C NMR triad analysis, cleavage experiments and thermal properties, a random or slightly gradient-like distribution of EPICH in PEG-*co*-PEPICH was derived.

248

To the best of our knowledge, PEG-*co*-PEPICH copolymers represent the first functional PEG derivatives containing nitrile groups at the polymer chain. To date, only nitrile based initiators have been applied to synthesize heterobifunctional PEG. [54, 56, 57] In facile post-polymerization reactions multiple amino, amide or carboxyl groups at the polyether chain were accessible. The respective homopolymers represent polyether based analogues of poly(acrylamide) and poly(acrylic acid), albeit with higher hydrophilicity than their carbon backbone analogues.

PEPICH and PEG-*co*-PEPICH (co)polymers could also be promising candidates as polymer matrix for lithium batteries, as reported for similar oxetane based structures.[50, 58, 59] The novel multi-functional polyethers offer intriguing potential regarding polyion complexes, layer-by-layer assembly and may also be suitable multifunctional linkers for pharmaceutically active compounds.[60–65]

3.4.6 Acknowledgements

3.4.7 References

[1] S. N. S. Alconcel, A. S. Baas, H. D. Maynard, *Polym. Chem.* **2011**, *2*, 1442–1448.

[2] G. Pasut, F. M. Veronese, *J. Control. Release.* **2012**, *161*, 461–472.

[3] H.-W. Engels, H.-G. Pirkl, R. Albers, R. W. Albach, J. Krause, A. Hoffmann, H. Casselmann, J. Dormish, *Angew. Chem. Int. Ed.* **2013**, *52*, 9422–9441.

[4] K. Knop, R. Hoogenboom, D. Fischer, U. S. Schubert, *Angew. Chem.* **2010**, *122*, 6430–6452.

[5] F. M. Veronese, G. Pasut, *Drug Discovery Today.* **2005**, *10*, 1451–1458.

[6] F. M. Veronese, *Biomaterials.* **2001**, *22*, 405–417.

[7] E. M. Pelegri-O'Day, E.-W. Lin, H. D. Maynard, *J. Am. Chem. Soc.* **2014**, *136*, 14323–14332.

[8] D. E. Bergbreiter, J. Tian, C. Hongfa, *Chem. Rev.* **2009**, *109*, 530–582.

[9] M.S. Thompson, T.P. Vadala, M.L. Vadala, Y. Lin, J.S. Riffle, *Polymer.* **2008**, *49*, 345–373.

[10] B. Obermeier, F. Wurm, C. Mangold, H. Frey, *Angew. Chem. Int. Ed.* **2011**, *50*, 7988–7997.

[11] Z. Li, Y. Chau, *Bioconjugate Chem.* **2009**, *20*, 780–789.

[12] C. Mangold, F. Wurm, H. Frey, *Polym. Chem.* **2012**, *3*, 1714–1721.

[13] J. Herzberger, D. Kurzbach, M. Werre, K. Fischer, D. Hinderberger, H. Frey, *Macromolecules.* **2014**, *47*, 7679–7690.

[14] Y. Koyama, M. Umehara, A. Mizuno, M. Itaba, T. Yasukouchi, K. Natsume, A. Suginaka, K. Watanabe, *Bioconjugate Chem.* **1996**, *7*, 298–301.

[15] B. Obermeier, H. Frey, *Bioconjugate Chem.* **2011**, *22*, 436–444.

[16] B. F. Lee, M. J. Kade, J. A. Chute, N. Gupta, L. M. Campos, G. H. Fredrickson, E. J. Kramer, N. A. Lynd, C. J. Hawker, *J. Polym. Sci. A Polym. Chem.* **2011**, *49*, 4498–4504.

[17] P. Lundberg, N. A. Lynd, Y. Zhang, X. Zeng, D. V. Krogstad, T. Paffen, M. Malkoch, A. M. Nystrom, C. J. Hawker, *Soft Matter.* **2013**, *9*, 82–89.

[18] K. M. Mattson, A. A. Latimer, A. J. McGrath, N. A. Lynd, P. Lundberg, Z. M. Hudson, C. J. Hawker, *J. Polym. Sci. A Polym. Chem.* **2015**, DOI:10.1002/pola.27749.

[19] B. Obermeier, F. Wurm, H. Frey, *Macromolecules.* **2010**, *43*, 2244–2251.

[20] V. S. Reuss, B. Obermeier, C. Dingels, H. Frey, *Macromolecules.* **2012**, *45*, 4581–4589.

[21]   T. Isono, S. Asai, Y. Satoh, T. Takaoka, K. Tajima, T. Kakuchi, T. Satoh, *Macromolecules.* **2015**, *48*, 3217–3229.

[22]   J. Meyer, H. Keul, M. Möller, *Macromolecules.* **2011**, *44*, 4082–4091.

[23]   F. O. Pazschke, *Journal für Praktische Chemie.* **1870**, 82–101.

[24]   W. Hartenstein, *Journal für Praktische Chemie.* **1873**, *7*, 295–318.

[25]   P. E. Wei, P. E. Butler, *J. Polym. Sci. A Polym. Chem.* **1968**, *6*, 2461–2475.

[26]   S. E. Cantor, G. D. Brindell, T. J. Brett, *J. Macromol. Sci. A.* **1973**, *7*, 1483–1508.

[27]   C. Billouard, S. Carlotti, P. Desbois, A. Deffieux, *Macromolecules.* **2004**, *37*, 4038–4043.

[28]   A. Labbé, S. Carlotti, C. Billouard, P. Desbois, A. Deffieux, *Macromolecules.* **2007**, *40*, 7842–7847.

[29]   A.-L. Brocas, C. Mantzaridis, D. Tunc, S. Carlotti, *Prog. Polym. Sci.* **2013**, 845–873.

[30]   F. F. Fleming, Q. Wang, O. W. Steward, *J. Org. Chem.* **2001**, *66*, 2171–2174.

[31]   F. Rua, M. Buffard, L. Sedo-Cabezon, G. Hernandez-Mir, A. de la Torre, S. Saldana-Ruiz, C. Chabbert, J. M. Bayona, A. Messeguer, J. Llorens, *Toxicol. Sci.* **2013**, *135*, 182–192.

[32]   M. Gervais, A.-L. Brocas, G. Cendejas, A. Deffieux, S. Carlotti, *Macromolecules.* **2010**, *43*, 1778–1784.

[33]   E. M. M. de Brabander-van den Berg, E. W. Meijer, *Angew. Chem. Int. Ed. Engl.* **1993**, *32*, 1308–1311.

[34]   R. Balicki, Ł. Kaczmarek, *Synthetic Commun.* **1993**, *23*, 3149–3155.

[35]   I. B. Rietveld, W. G. Bouwman, M. W. P. L. Baars, R. K. Heenan, *Macromolecules.* **2001**, *34*, 8380–8383.

[36]   M. Hans, H. Keul, M. Moeller, *Polymer.* **2009**, *50*, 1103–1108.

[37]   M. Gervais, A.-L. Brocas, A. Deffieux, E. Ibarboure, S. Carlotti, *Pure Appl. Chem.* **2012**, *84*, 2103–2111.

[38]   S. S. Müller, C. Moers, H. Frey, *Macromolecules.* **2014**, *47*, 5492–5500.

[39]   K. Roos, S. Carlotti, *Eur. Polym. J.* **2015**, *70*, 240–246.

[40]   S. Carlotti, A. Labbé, V. Rejsek, S. Doutaz, M. Gervais, A. Deffieux, *Macromolecules.* **2008**, *41*, 7058–7062.

[41]   K. Sakakibara, K. Nakano, K. Nozaki, *Chem. Commun.* **2006**, 3334–3336.

[42]   K. Sakakibara, K. Nakano, K. Nozaki, *Macromolecules.* **2007**, *40*, 6136–6142.

[43]   A.-L. Brocas, M. Gervais, S. Carlotti, S. Pispas, *Polym. Chem.* **2012**, *3*, 2148.

[44]   P. Lundberg, B. F. Lee, S. A. van den Berg, E. D. Pressly, A. Lee, C. J. Hawker, N. A. Lynd, *ACS Macro Lett.* **2012**, *1*, 1240–1243.

[45]   F. Heatley, G. Yu, C. Booth, T. G. Blease, *Eur. Polym. J.* **1991**, *27*, 573–579.

[46]   T. Hamaide, A. Goux, M.-F. Llauro, R. Spitz, A. Guyot, *Angew. Makromol. Chemie.* **1996**, *237*, 55–77.

[47]   V. Rejsek, D. Sauvanier, C. Billouard, P. Desbois, A. Deffieux, S. Carlotti, *Macromolecules.* **2007**, *40*, 6510–6514.

[48]   M.I. Chipara, D. Barb, P.V. Notingher, L. Georgescu, T. Sarbu, *Polymer.* **1996**, *37*, 707–712.

[49]   A. C. Fernandes, J. W. Barlow, D. R. Paul, *J. Appl. Polym. Sci.* **1984**, *29*, 1971–1983.

[50]   L. Ye, Z.-g. Feng, Y.-f. Su, F. Wu, S. Chen, G.-q. Wang, *Polym. Int.* **2005**, *54*, 1440–1448.

[51]   C. Wörner, R. Mülhaupt, *Angew. Chem. Int. Ed. Engl.* **1993**, *32*, 1306–1308.

[52]   E. Carretti, L. Dei, P. Baglioni, R. G. Weiss, *J. Am. Chem. Soc.* **2003**, *125*, 5121–5129.

[53]   S. Lin, P. Theato, *Macromol. Rapid Commun.* **2013**, *34*, 1118–1133.

[54]   S. Zhang, J. Du, R. Sun, X. Li, D. Yang, S. Zhang, C. Xiong, Y. Peng, *React. Funct. Polym.* **2003**, *56*, 17–25.

[55] SigmaAldrich, *https://www.sigmaaldrich.com/content/dam/sigma-aldrich/docs/Aldrich/General_Information/thermal_transitions_of_homopolymers.pdf.*

[56]   H. Schlaad, H. Kukula, J. Rudloff, I. Below, *Macromolecules.* **2001**, *34*, 4302–4304.

[57]   Y. Nagasaki, M. Iijima, M. Kato, K. Kataoka, *Bioconjugate Chem.* **1995**, *6*, 702–704.

[58]   Y. Shintani, H. Tsutsumi, *J. Power Sources.* **2010**, *195*, 2863–2869.

[59]   H. Tsutsumi, A. Suzuki, *Solid State Ionics.* **2014**, *262*, 761–764.

[60]   J. N. Hunt, K. E. Feldman, N. A. Lynd, J. Deek, L. M. Campos, J. M. Spruell, B. M. Hernandez, E. J. Kramer, C. J. Hawker, *Adv. Mater.* **2011**, *23*, 2327–2331.

[61]   M. Lemmers, J. Sprakel, I. K. Voets, J. van der Gucht, C. M. A. C. Stuart, *Angew. Chem. Int. Ed.* **2010**, *49*, 708–711.

[62]   S. Lv, W. Song, Z. Tang, M. Li, H. Yu, H. Hong, X. Chen, *Mol. Pharm.* **2014**, *11*, 1562–1574.

[63]   F. Xiang, S. M. Ward, T. M. Givens, J. C. Grunlan, *Soft Matter.* **2015**, *11*, 1001–1007.

[64]   S. de Santis, R. D. Ladogana, M. Diociaiuti, G. Masci, *Macromolecules.* **2010**, *43*, 1992–2001.

[65]   A. Wibowo, K. Osada, H. Matsuda, Y. Anraku, H. Hirose, A. Kishimura, K. Kataoka, *Macromolecules.* **2014**, *47*, 3086–3092.
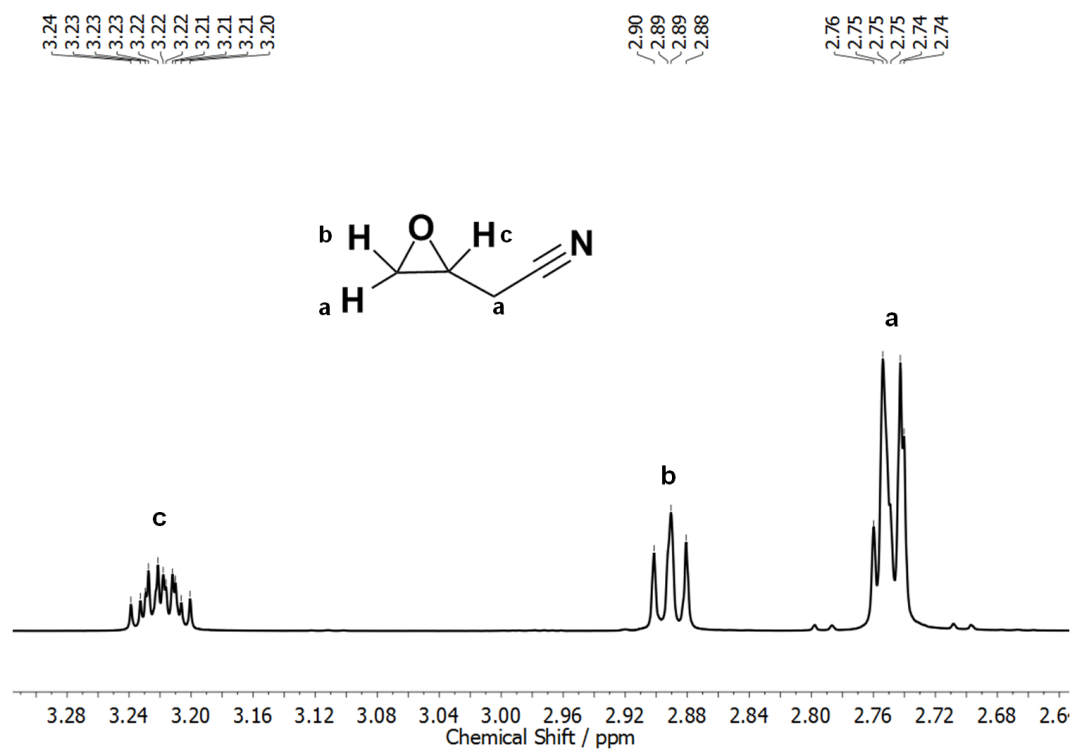
Figure S1. ^{1}H NMR spectrum (400 MHz, CDCl$_3$) of epicyanohydrin (EPICH).
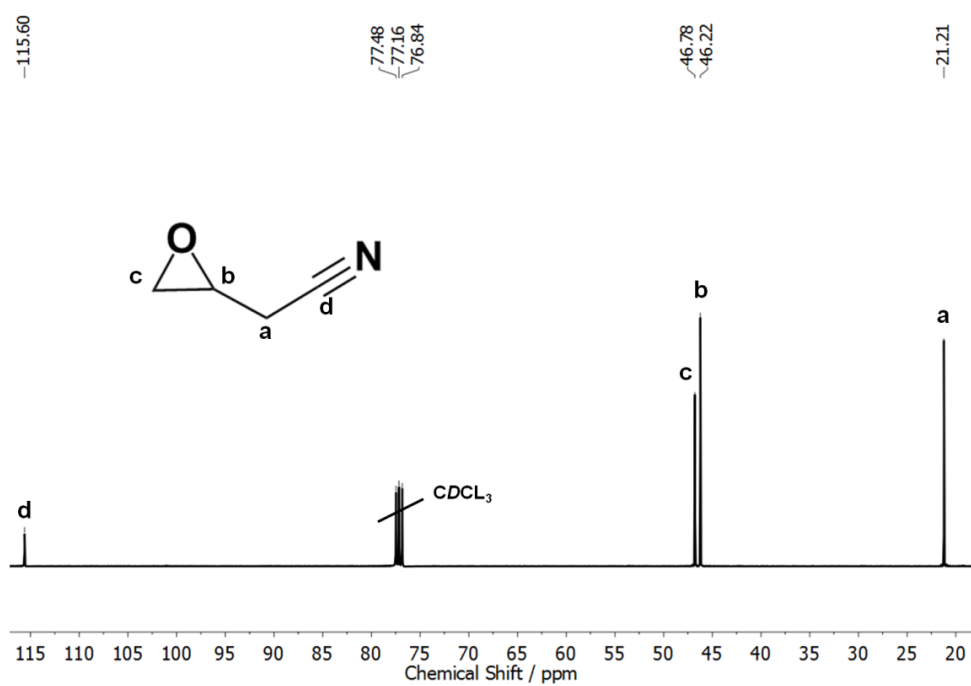
Figure S2. ^{13}C NMR spectrum (100 MHz, CDCl$_3$) of EPICH.
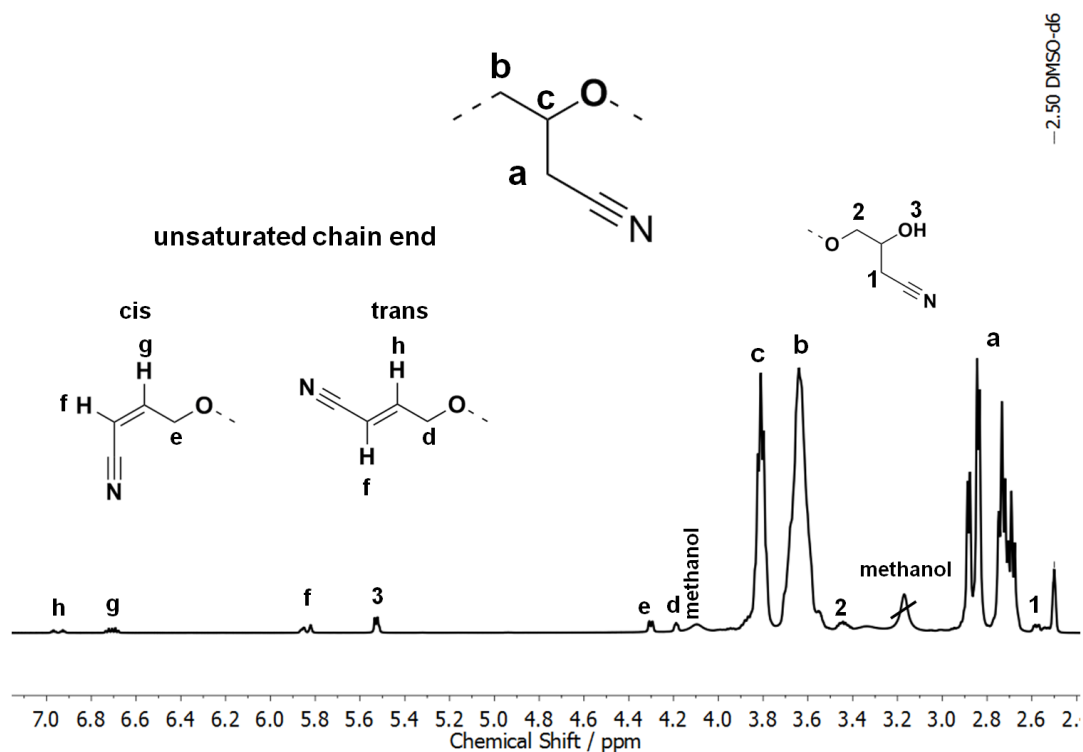
Figure S3. ^{1}H NMR spectrum (400 MHz, DMSO-d_6) of PEPICH homopolymer.
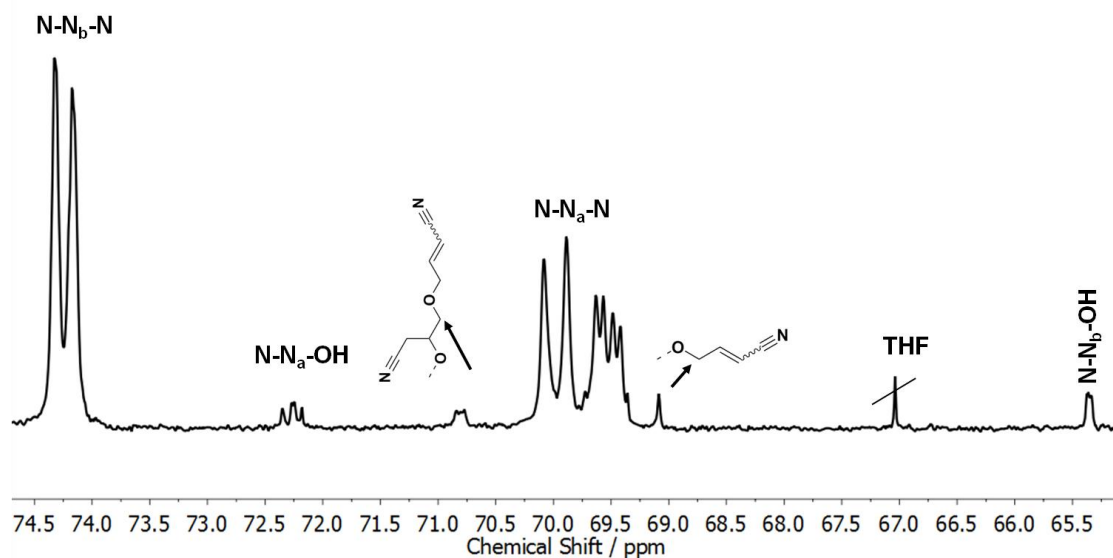
Figure S4. Important section of the IG ^{13}C NMR spectrum (100 MHz, DMSO-d_6) of PEPICH homopolymer; "N" is an abbreviation for the EPICH unit.
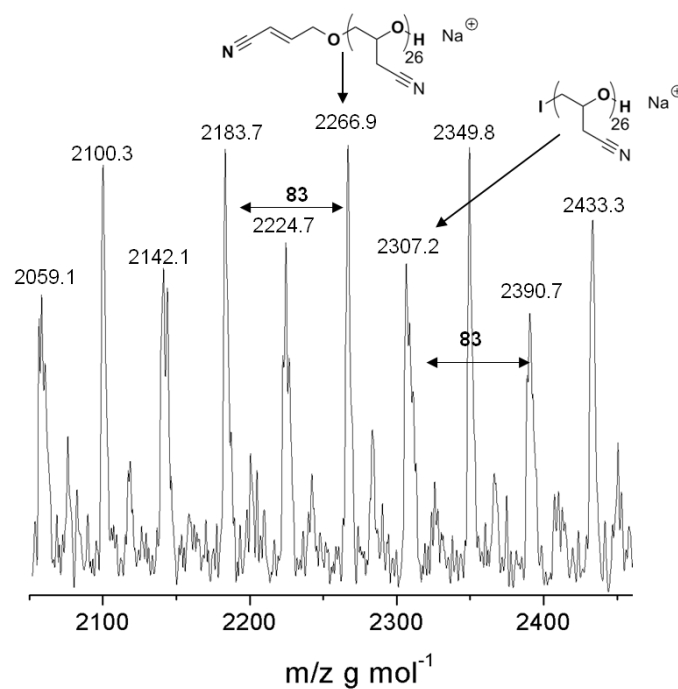
Figure S5. Expanded MALDI-ToF mass spectrum of PEPICH$_{26}$ with peak assignment (linear mode, matrix: THAP). One repeating unit of EPICH (83 g·mol^{-1}) is marked by black arrows. Main distributions correspond to the sodium adduct of PEPICH$_{26}$, initiated via iodide and unsaturated species, respectively.
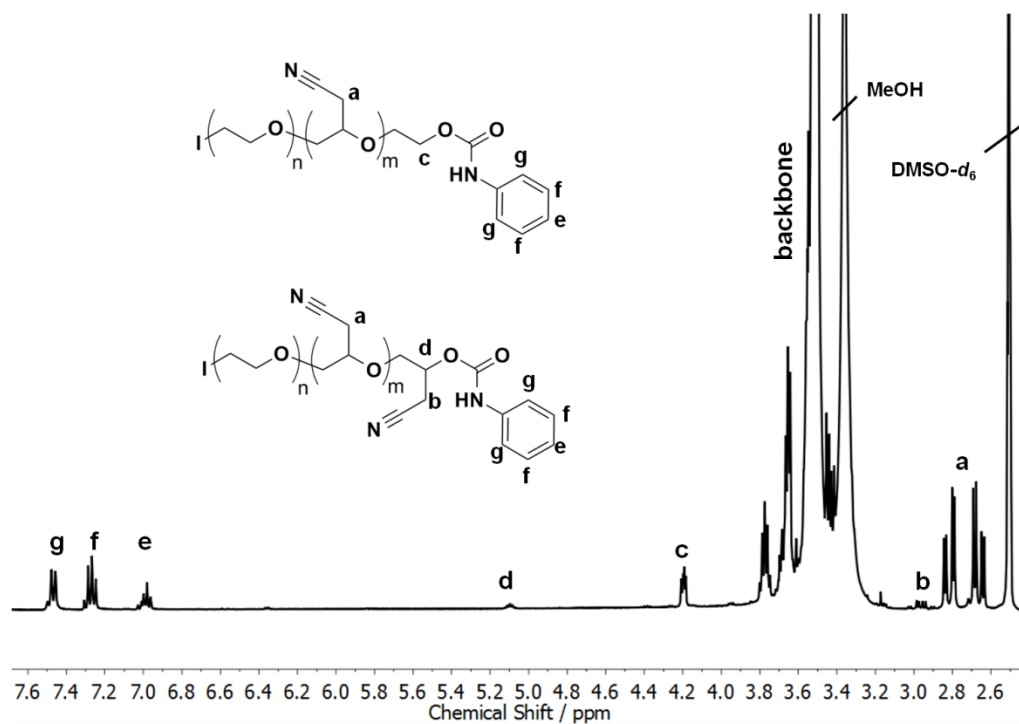
Figure S6. ^{1}H NMR (400 MHz, DMSO-d_6) of PEG-*co*-PEPICH copolymer, functionalized with phenyl isocyanate.
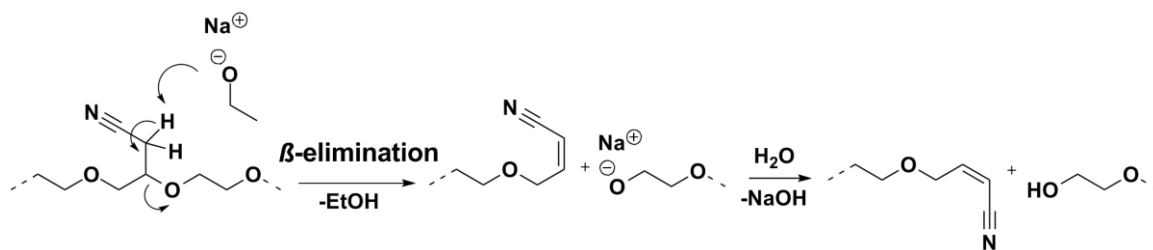
Scheme S1. *β*-elimination (Retro-Michael addition), exemplarily shown for an E-N-E triad and resulting cleavage of the PEG-*co*-PEPICH backbone.
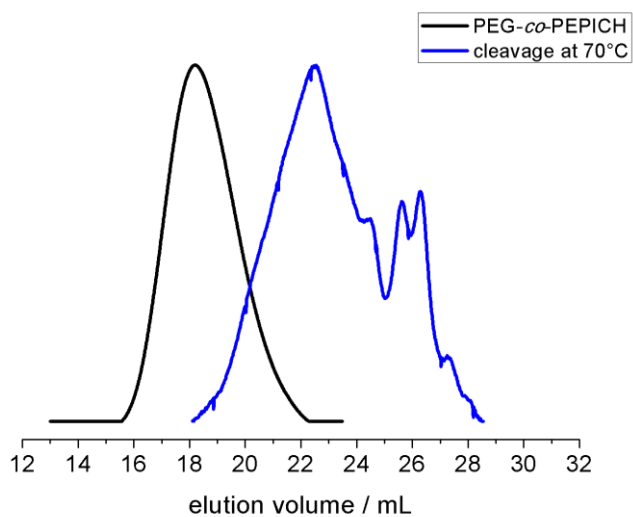
Figure S7. SEC elution traces (DMF, RI detection, PEG standards) of PEG-*co*-PEPICH copolymer (7 mol% EPICH) before cleavage (black line) and after cleavage at 70 °C (blue line).
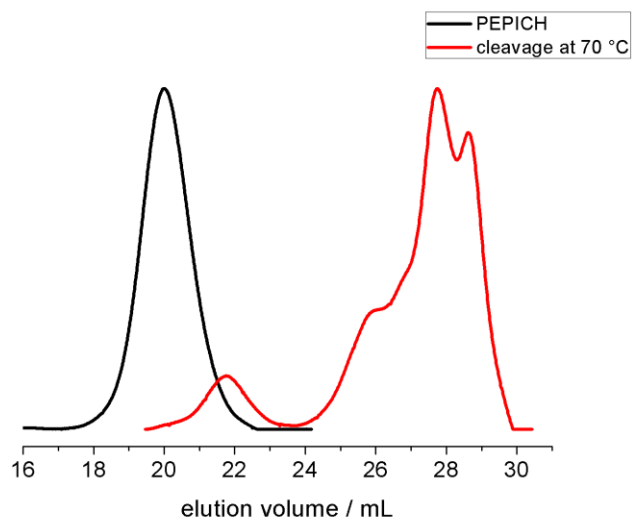
Figure S8. SEC elution traces (DMF, RI detection, PEG standards) of PEPICH homopolymer before cleavage (black line) and after cleavage at 70 °C (red line).
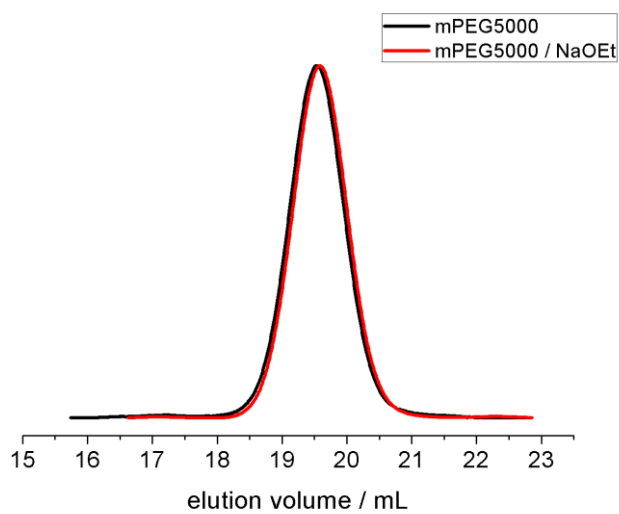
Figure S9. SEC elution traces (DMF, RI detection, PEG standards) of mPEG5000 before cleavage (black line) and after treatment with sodium ethoxide solution at 70 °C (red line).
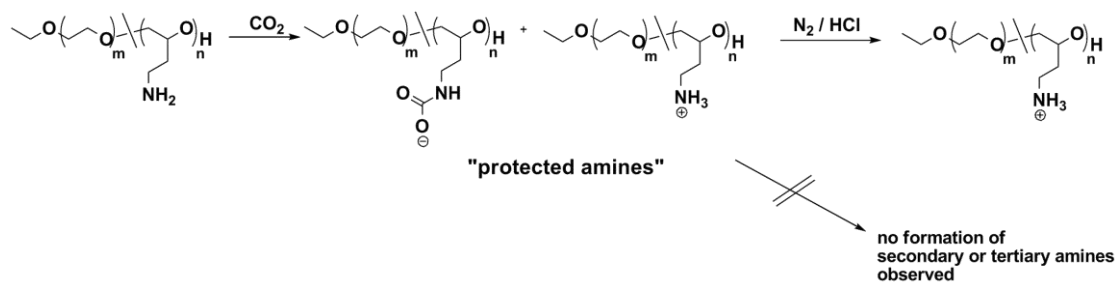
Scheme S2. Reaction of amino moieties with carbon dioxide to ammonium carbamates, followed by release of the amino groups *via* N_2/HCl.
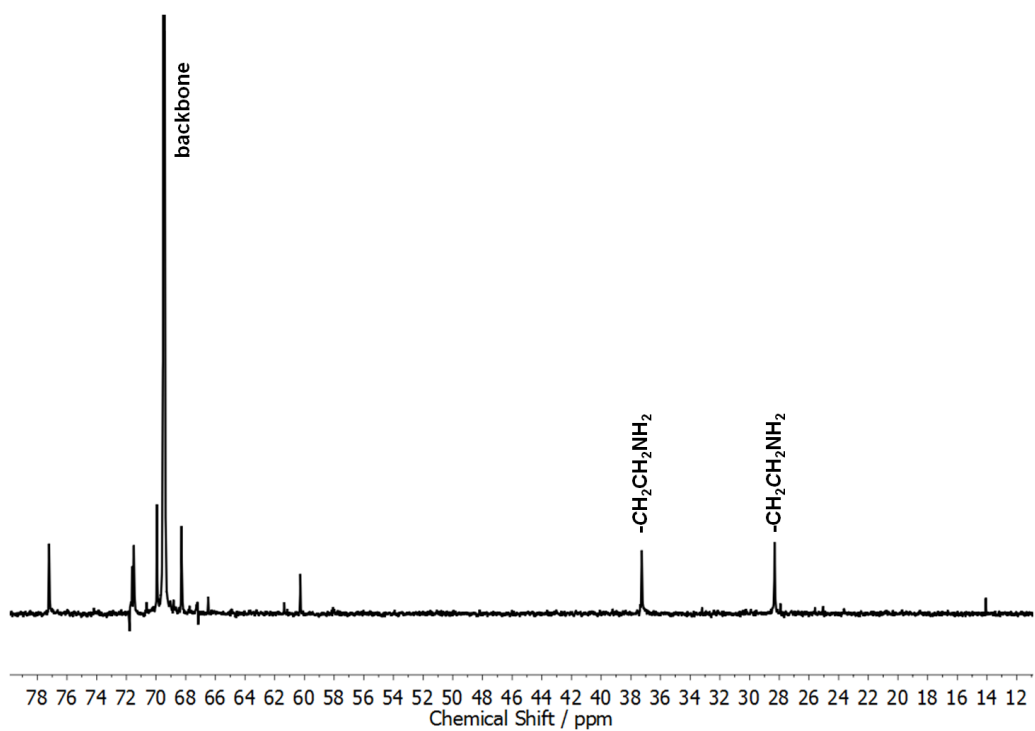
Figure S10. ^{13}C NMR (100 MHz, D_2O) of PEG-*co*-POEA with 6.1 % OEA.
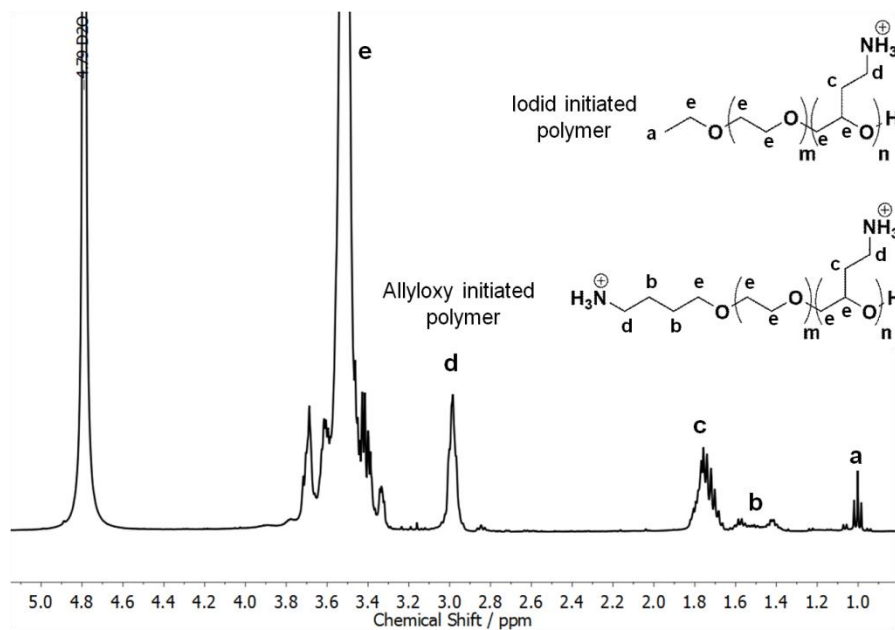
Figure S11. ^{1}H NMR spectrum (400 MHz, D$_2$O) of PEG-*co*-POEA with 6.1 % OEA.
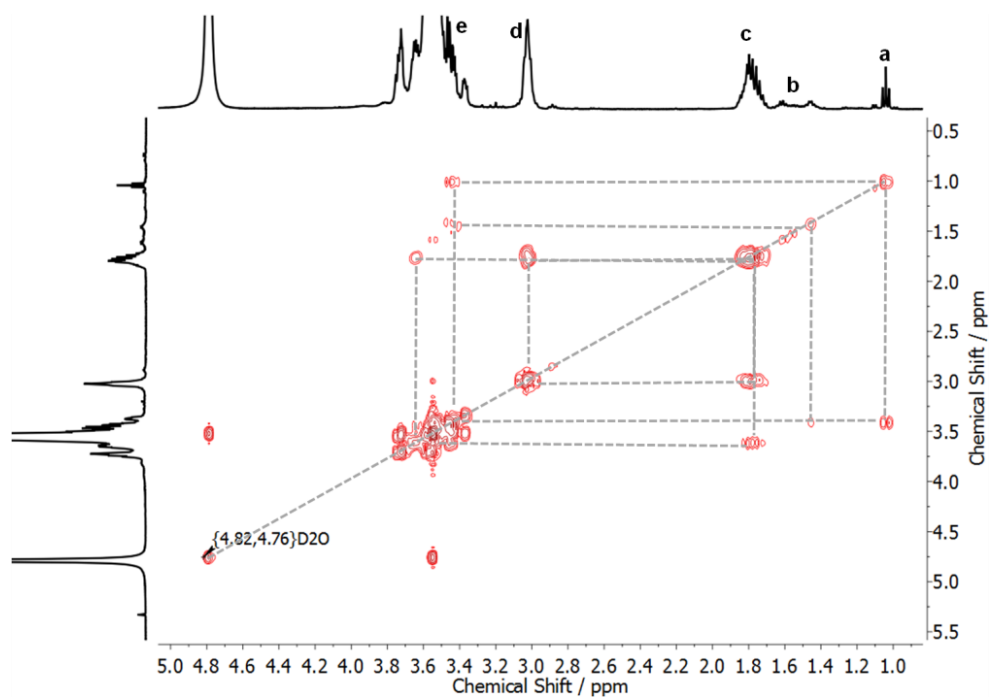
Figure S12. ^{1}H, ^{1}H COSY NMR (400 MHz, D$_2$O) of PEG-*co*-POEA with 6.1 % OEA.
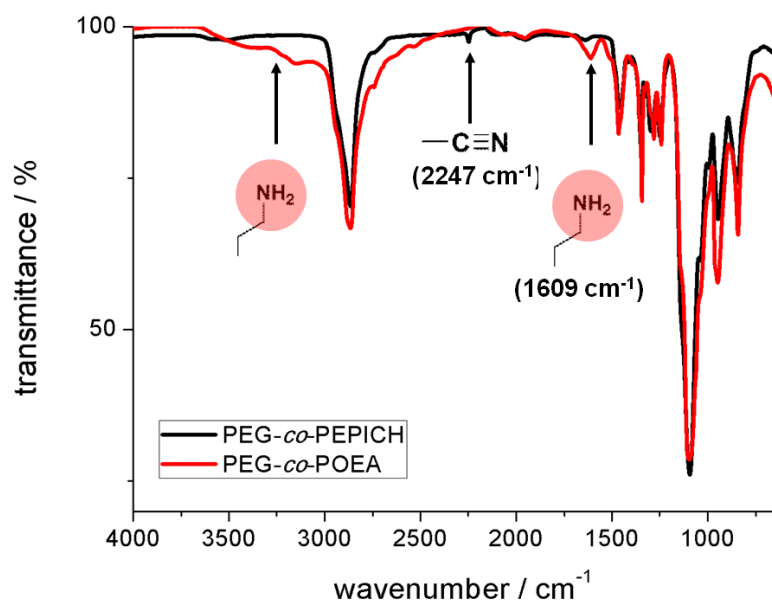
Figure S13. FT-IR spectra of PEG-*co*-PEPICH (black line) and amino-functional PEG-*co*-POEA (red line).

Table S1. Thermal properties of PEG-*co*-PEPICH and PEG-*co*-POEA obtained from differential scanning calorimetry (DSC) measurements.

Copolymer	[a]FG content / %	T_g/°C	T_m/°C	T_{rc} / °C	ΔH/J·g^{-1}
PEG-*co*-PEPICH	3.8	-48	44	---	87
PEG-*co*-POEA	3.8	-43	44	---	78
PEG-*co*-PEPICH	6.1	-49	36	---	58
PEG-*co*-POEA	6.1	-40	36	---	61
PEG-*co*-PEPICH	7.7	-48	28	---	63
PEG-*co*-POEA	7.7	-44	34	-13	47
PEG-*co*-PEPICH	13.1	-52	5	-11	20
PEG-*co*-POEA	13.1	-27	---	---	---
PEG-*co*-PEPICH	16.0	-46	---	---	---
PEG-*co*-POEA	16.0	-22	---	---	---

[a]FG = functional group

T_g: glass transition temperature
T_m: melting temperature
ΔH: melting enthalpy
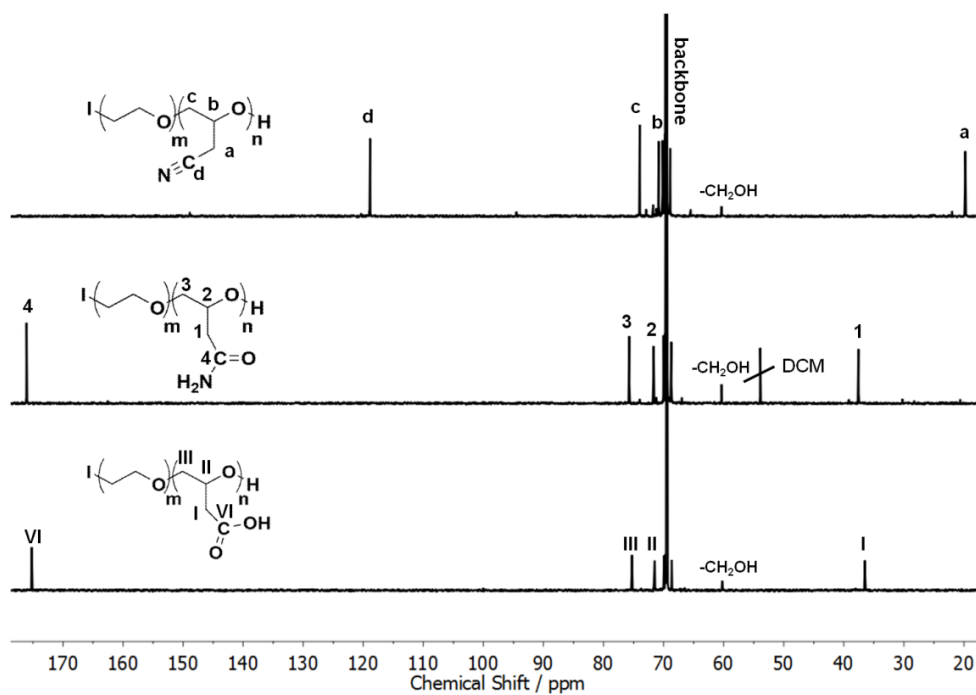
Figure S14. ^{13}C NMR spectra (100 MHz, D$_2$O) of PEG-*co*-PEPICH (top), PEG-*co*-POAm and PEG-*co*-POAa (bottom), respectively.
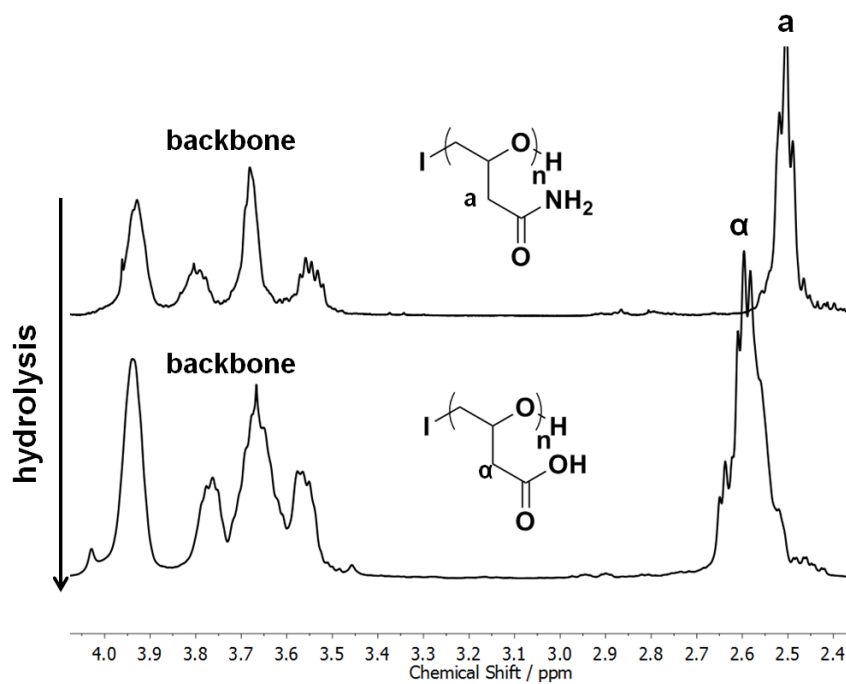
Figure S15. Important sections of ^{1}H NMR spectra (400 MHz, D$_2$O) of poly(2-oxiraneacetamide) (POAm) (top) and poly(2-oxiraneacetic acid) (POAa) (bottom).
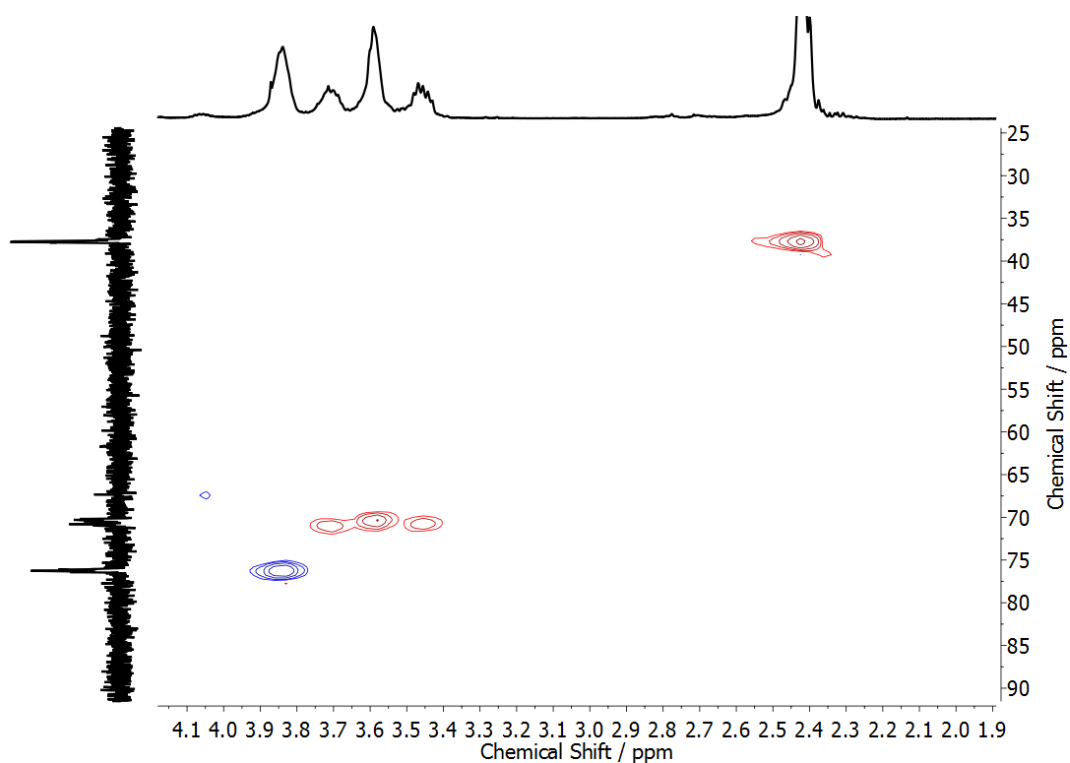
Figure S16. ^{1}H- ^{13}C-HSQC NMR spectrum (D$_2$O) of poly(2-oxiraneacetamide). Phase information is given by coloration of cross peaks (red: methylene, blue: methine).
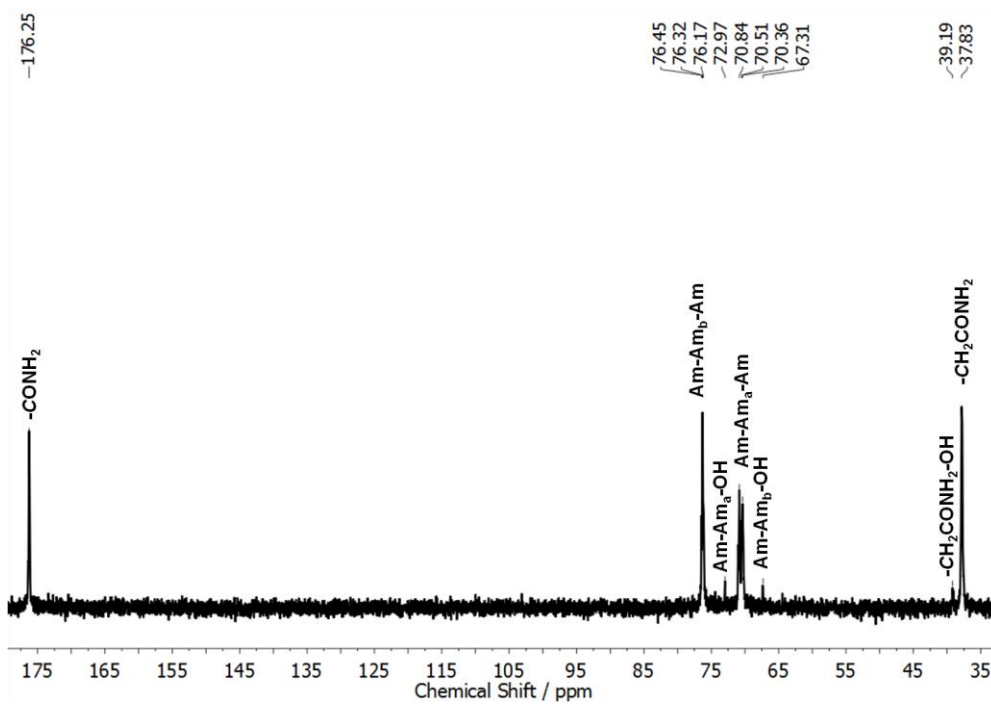
Figure S17. ^{13}C NMR spectrum (100 MHz, D_2O) of poly(2-oxiraneacetamide) homopolymer. 2-oxiraneacetamide unit is abbreviated as "Am".
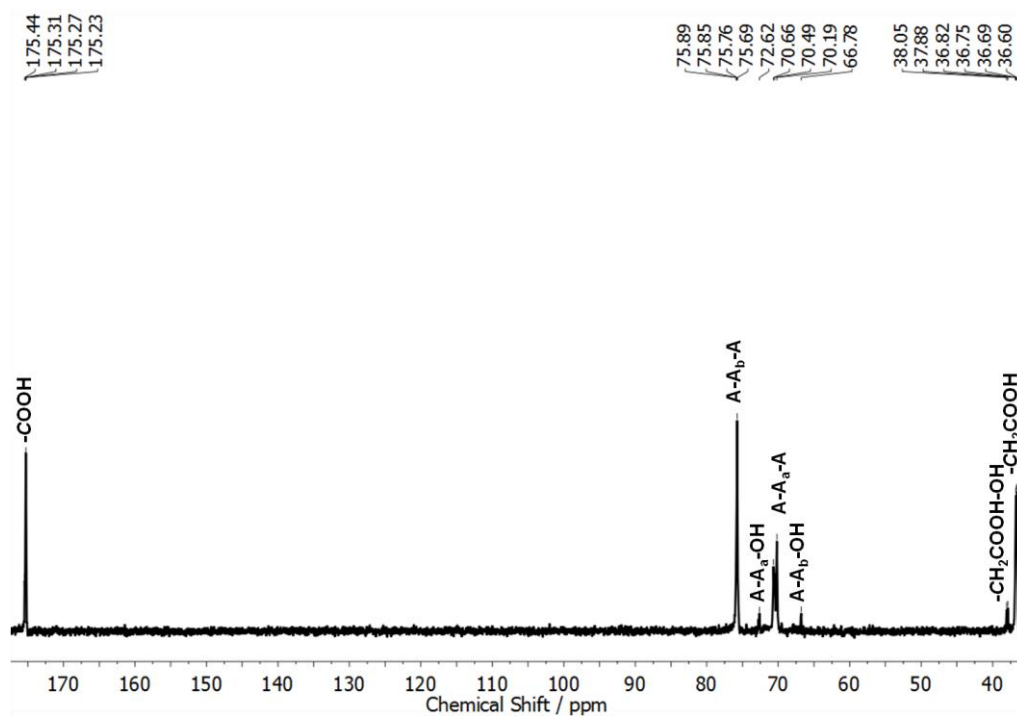
Figure S18. ^{13}C NMR spectrum (100 MHz, D_2O) of poly(2-oxiraneacetic acid) homopolymer. 2-oxiraneacetic acid unit is abbreviated as "A".
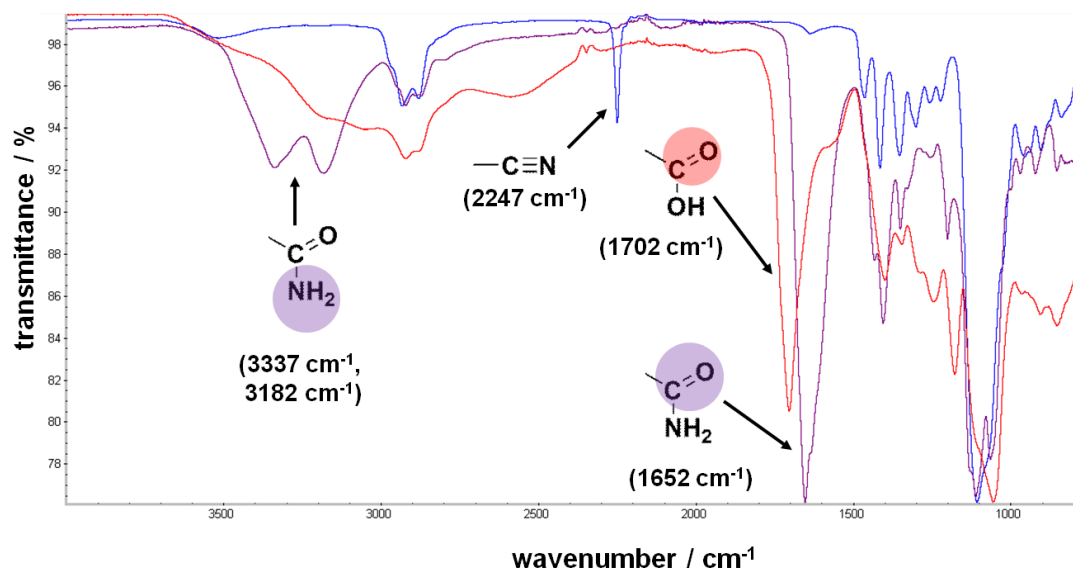
Figure S19. FT-IR spectra of PEPICH (blue line), POAm (violet line) and POAa (red line).

264
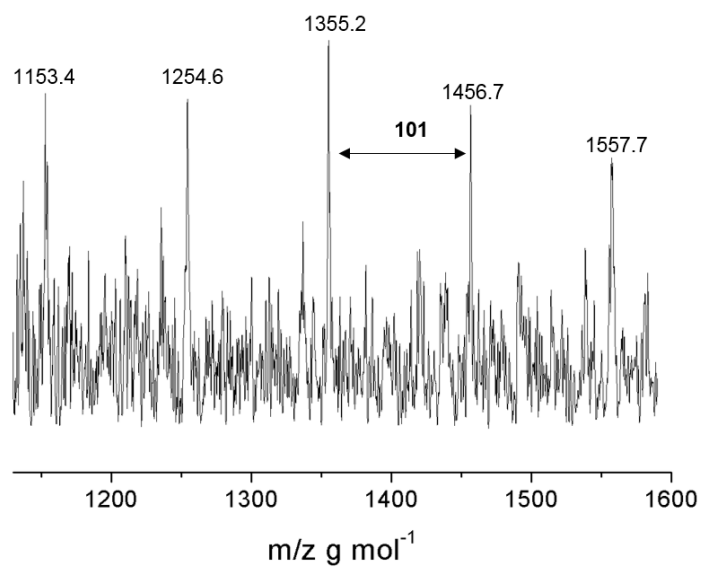
Figure S20. Expanded MALDI-ToF mass spectrum of amide functional POAm homopolymer (linear mode, matrix: THAP). The repeating unit difference for OAm (101 g·mol^{-1}) is marked by a black arrow.
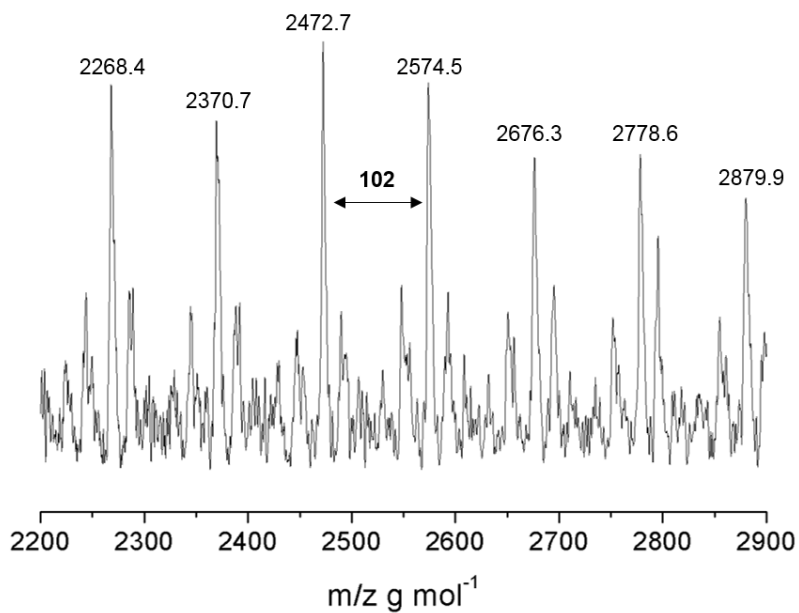
Figure S21. Expanded MALDI-ToF mass spectrum of carboxyl functional POAa homopolymer (linear mode, matrix: THAP). The repeating unit mass difference for OAa (102 g·mol^{-1}) is marked by a black arrow.

Table S2. Thermal properties of PEG-*co*-PEPICH, PEG-*co*-POAm and PEG-*co*-POAa copolymers obtained from differential scanning calorimetry (DSC) measurements.

Copolymer	[a]FG content / %	T_g/°C	T_m/°C	T_{rc} / °C	ΔH/J·g^{-1}
PEG-*co*-PEPICH	3.8	-48	44	---	87
PEG-*co*-POAm	3.8	-48	38	-27	57
PEG-*co*-POAa	3.8	-37	42	---	71
PEG-*co*-PEPICH	6.1	-49	36	---	58
PEG-*co*-POAm	6.1	-48	32	-24	53
PEG-*co*-POAa	6.1	-55	29	-37	63
PEG-*co*-PEPICH	7.7	- 48	28	---	63
PEG-*co*-POAm	7.7	-48	29	-23	53
PEG-*co*-POAa	7.7	-52	28	-32	60
PEG-*co*-PEPICH	13.1	-52	5	-11	20
PEG-*co*-POAm	13.1	-40	---	---	---
PEG-*co*-POAa	13.1	-45	---	---	---
PEG-*co*-PEPICH	16.0	-46	---	---	---
PEG-*co*-POAm	16.0	-30	---	---	---
PEG-*co*-POAa	16.0	-36	---	---	---
PEPICH	100	-14	---	---	---
POAm	100	55	---	---	---
POAa	100	29	---	---	---

[a]FG = functional group

T_g: glass transition temperature
T_m: melting temperature
ΔH: melting enthalpy

Table S3. Thermal properties of PEG-*co*-PEPICH, PEG-*co*-POAm and PEG-*co*-POAa copolymers obtained from differential scanning calorimetry (DSC) measurements.

Copolymer	^{a}FG content / %	T_g/°C	T_m/°C	T_{rc} / °C	ΔH/J·g^{-1}
PEG-*co*-PEPICH	3.8	-48	44	---	87
PEG-*co*-POAm	3.8	-48	38	-27	57
PEG-*co*-POAa	3.8	-37	42	---	71
PEG-*co*-PEPICH	6.1	-49	36	---	58
PEG-*co*-POAm	6.1	-48	32	-24	53
PEG-*co*-POAa	6.1	-55	29	-37	63
PEG-*co*-PEPICH	7.7	- 48	28	---	63
PEG-*co*-POAm	7.7	-48	29	-23	53
PEG-*co*-POAa	7.7	-52	28	-32	60
PEG-*co*-PEPICH	13.1	-52	5	-11	20
PEG-*co*-POAm	13.1	-40	---	---	---
PEG-*co*-POAa	13.1	-45	---	---	---
PEG-*co*-PEPICH	16.0	-46	---	---	---
PEG-*co*-POAm	16.0	-30	---	---	---
PEG-*co*-POAa	16.0	-36	---	---	---
PEPICH	100	-14	---	---	---
POAm	100	55	---	---	---
POAa	100	29	---	---	---

^{a}FG = functional group

T_g: glass transition temperature
T_m: melting temperature
ΔH: melting enthalp

4 Alkyne-functional

Poly(ethylene glycol) Copolymers

4.1 "Clickable PEG" via Anionic Copolymerization of Ethylene Oxide and Glycidyl Propargyl Ether

Jana Herzberger,[a,b] Daniel Leibig,[a,b] Jens Langhanki,[a] Christian Moers [a,b] Till Opatz,[a]

Holger Frey [a,b]*

[a] Institute of Organic Chemistry, Johannes Gutenberg University Mainz, Duesbergweg 10-14, D-55128 Mainz, Germany

[b] Graduate School Materials Science in Mainz, Staudingerweg 9, D-55128 Mainz, Germany

*E-Mail: hfrey@uni-mainz.de

to be submitted
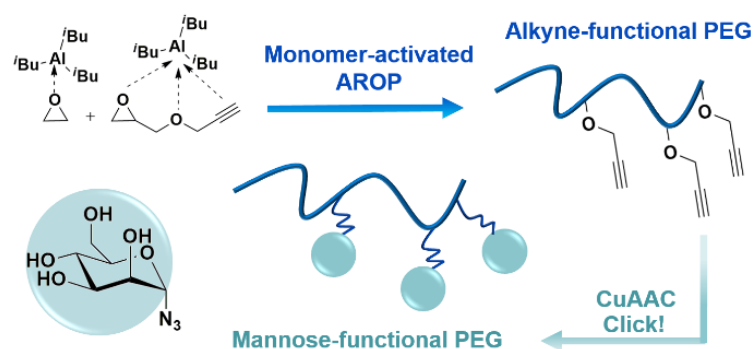
4.1.1 Abstract

A straight forward synthesis of poly(ethylene glycol) (PEG) with multiple alkyne units distributed along the polymer chain is presented. Direct access to clickable PEG is achieved by the monomer-activated anionic ring-opening copolymerization (AROP) of ethylene oxide (EO) with glycidyl propargyl ether (GPgE). Notably for successful polymerization no protection of the alkyne unit is required owing to the mild reaction conditions. Defined PEG-*co*-PGPgE and PGPgE (co)polymers with PDIs of 1.18-1.60 and molecular weights of $M_n = 3,000 - 9,500$ g·mol^{-1} were prepared. *In-situ* ^{1}H NMR kinetic studies revealed remarkably disparate reactivity ratios of $r_{EO} = 14.8$ and $r_{GPgE} = 0.076$, representing a pronounced compositional drift with EO rich segments close to the initiator and GPgE units near the chain terminus, i.e. copolymers with a steep monomer gradient. Copper(I)-catalyzed azide-alkyne cycloaddition (CuAAC) with mannopyranosyl azide leads to PEG-based glycopolymers and highlights the potential of alkyne-functional PEGs as a universal scaffold for a range of biomedical applications.

4.1.2 Introduction

Poly(ethylene glycol) (PEG) is a highly valuable polymer for biomedical and pharmaceutical applications due to its non-toxicity, non-immunogenicity, resistance to protein absorption and extremely high water-solubility.[1] Commercially available products include PEG derivatives as food additives in ice cream, as surfactants in cosmetics or as a shielding component in drug delivery systems.[2] The latter implements the covalent attachment of active molecules to PEG and in this context, many synthetic routes are described to design specific α,ω-bifunctional PEGs to achieve quantitative coupling reactions.[3] However, an increased number of functionalities is an appealing approach to increase the loading capacity of PEG. For example, the attachment of a targeting functionality as well as therapeutic and diagnostic agents to one multifunctional polymer would then be possible. Besides, increasing the amount of pendant groups along the PEG backbone allows for tailoring of physical and chemical properties for specific purposes, e.g. incorporating simple methyl groups via glycidyl methyl ether or propylene oxide copolymerization suppresses PEGs crystallinity and its water-solubility can be adjusted.[4,5] The preparation of multi-functional PEGs is often tedious, requiring specific synthetic strategies starting from substituted epoxide monomers that are compatible with the applied polymerization reaction.[6] Consequently, monomers bearing clickable moieties are eligible alternatives, giving access to versatile functionalization opportunities via post-polymerization modification. For example, a library of active molecules or dyes is commercially established for copper(I)-catalyzed azide-alkyne cycloaddition (CuAAC) and many synthetic strategies have been reported for the preparation of alkyne functional polymers as universal scaffolds.[7]

In the context of the synthesis of PEG, anionic polymerization of alkyne functional epoxides, such as glycidyl propargyl ether (GPgE), is challenging due to the acidity of the acetylenic proton, interfering with the living mechanism. Thus, PEGs bearing multiple alkyne units have only been described via post-polymerization methods starting from linear polyglycerol.[8,9] However, this method is rather time-consuming, requiring first the polymerization of protected glycidol, followed by deprotection to generate hydroxyl groups and further conversion with propargyl bromide. Importantly, Schüll et al. demonstrated that direct anionic ring-opening polymerization (AROP) of GPgE is possible when copolymerized with glycidol applying the so-called „slow monomer addition".[10] Low monomer concentrations and a decrease of the local basicity are the key features to prepare alkyne-functional hyperbranched structures. Regarding linear multi-functional PEGs, a decreased basicity of the growing chain end can be realized by employing the monomer-activated AROP.[11] Initiation with an ammonium halide/Lewis acid complex and activation of the epoxide ring allow for polymerizations at low temperatures (0-25 °C) in hydrocarbon solvents. Because of the low basicity of the living species, this method is well-established for substituted epoxides bearing sensitive or strongly electron withdrawing moieties, such as epichlorohydrin,[12] fluorine-containing epoxides,[13] epicyanohydrin[14] and glycidyl methacrylate.[15]

Herein, we introduce an approach to prepare alkyne-functional PEGs that are suitable for copper(I)-catalyzed azide-alkyne cycloaddition (CuAAC). The monomer-activated technique enables the direct anionic copolymerization of glycidyl propargyl ether (GPgE) with ethylene oxide (EO) (Scheme 1). Both monomers are commercially available and no protection of the alkyne moiety of GPgE is necessary. Further, the attachment of mannopyranosyl azide highlights their potential as scaffolds for bioactive molecules and diverse applications.
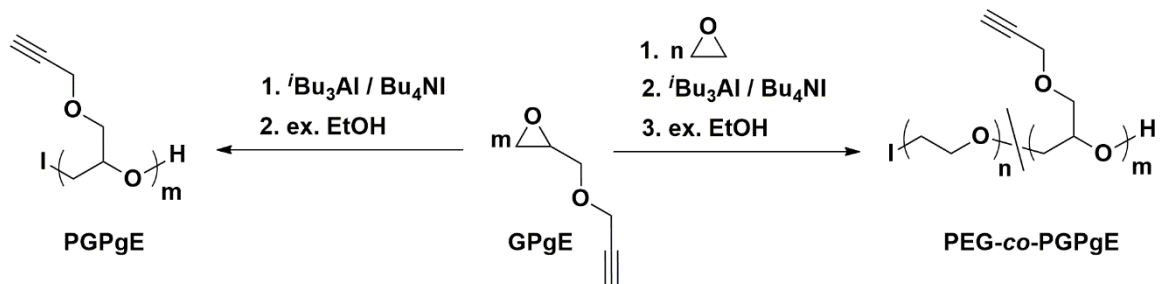
Scheme 1. Alkyne-functional PEG (PEG-*co*-PGPgE) and PGPgE homopolymer, directly accessible via monomer-activated anionic (co)polymerization of GPgE and EO.

4.1.3 Results and Discussion

PEG-*co*-PGPgE copolymers and PGPgE homopolymers with PDIs of 1.18-1.6 and molecular weights in the range of $M_n = 3,000 - 9,500$ g·mol^{-1} were prepared via monomer-activated AROP (Figure 1, Table 1). For a successful polymerization, purification of commercially available GPgE via simple cryogenic distillation was sufficient (Figure S1-2). Overall, we varied the GPgE content from 2.0 to 15.6 mol% and generated PGPgE homopolymers. Comonomer ratios were calculated from ^{1}H NMR spectra by comparing the proton resonance of the methylene group (-CH_2C≡CH, $\delta = 4.20$ ppm) to the broad polymer backbone signals ($\delta = 3.40$-3.82 ppm).
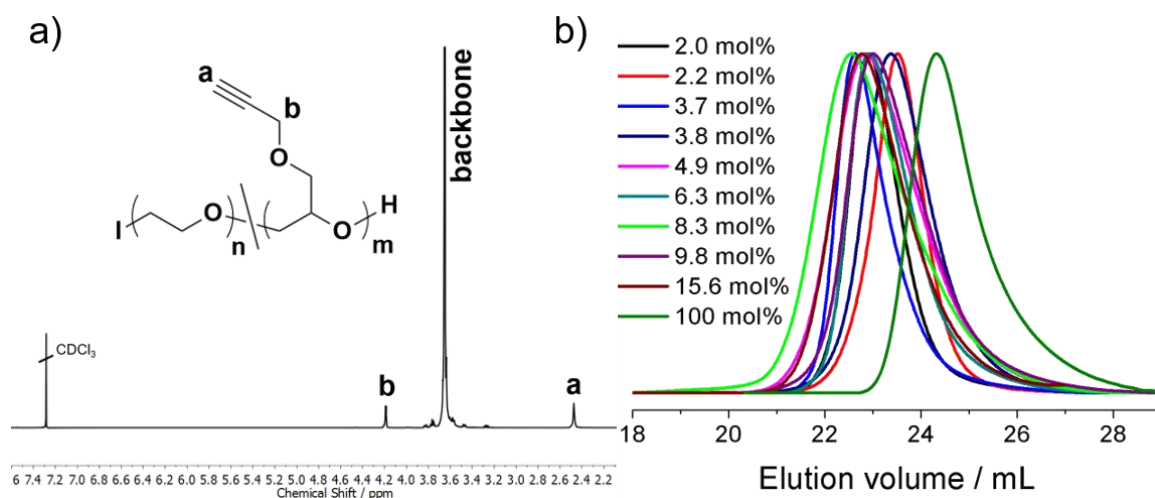
Figure 1. (a) ^{1}H NMR spectrum (400 MHz, CDCl$_3$) of PEG-*co*-PGPgE and (b) SEC elution traces (THF, RI signal, PEG standard) of various PEG-*co*-PGPgE copolymers and PGPgE homopolymer.

274

The comonomer ratios in the polyethers formed are in good agreement with theoretical ones and vary marginally due to the difficulty in measuring liquid EO. It should be noted that in some deuterated solvents such as D_2O and DMSO-d_6, the resonance of the acetylenic proton appears in the same range as the broad polymer backbone signal and is not clearly distinguishable. The maximum content of GPgE in PEG-*co*-PGPgE copolymers is limited due to the reactivity differences of both monomers. The presence of an additional oxygen atom in GPgE requires an increased amount of catalyst (^{i}Bu$_3$Al), however this induces a very high reactivity of EO, which leads to a broadening of the molecular weight distribution. Consequently, defined copolymers are accessible with GPgE ratios up to 15 mol%. This phenomenon is repeatedly observed for other comonomer systems and a limiting factor if the reactivity of both comonomers differs strongly.[16] Catalyst to initiator ratios of 3 are sufficient to generate GPgE homopolymers with DP = 30, while higher molecular weights require an increased amount of catalyst (4-5 equiv). Figure S3 shows a ^{1}H NMR spectrum of the homopolymer. PGPgE$_{30}$ is well soluble in THF, DMF, chloroform, benzene and DMSO, but insoluble in water and methanol. In contrast, all copolymers are soluble in aqueous solution at room temperature. A thermo-induced coil-to-globule transition and precipitation of the copolymer occurs at 75 °C for PEG-*co*-PGPgE with the highest amount of GPgE (15.6 mol%) at a concentration of 5 mg·mL^{-1}.

Table 1. Characterization data of PEG-*co*-PGPgE copolymers and PGPgE homopolymers generated with [^{i}Bu$_3$Al]/[TBAI] in chlorobenzene.

No.	[^{i}Bu$_3$Al]/ [TBAI]	GPgEth /mol%	GPgE^a /mol%	$M_n{}^b$	$M_w/M_n{}^b$	T_g/°C	T_m/°C	ΔH_m/J·g^{-1}
1	1.4	2.0	2.0	7140	1.19	-52	52	126
2	1.5	2.5	2.2	7540	1.20	-50	51	118
3	1.8	4.0	3.7	7770	1.23	-51	50	106
4	2	4.0	3.8	6900	1.34	-50	48	112
5	3	5.0	4.9	8100	1.59	-48	49	93
6	2.2	5.0	6.0	6200	1.25	-50	42	78
7	3	9.0	8.3	9530	1.56	-47	43	79
8	2.5	10.0	9.8	7290	1.51	-44	43	74
9	3	15.0	15.6	9130	1.37	-51	37	55
10	3	100	100	3030	1.18	-39	---	---

^{a}Obtained from ^{1}H NMR spectra
^{b}Determined via SEC (THF, RI signal, PEG standard)
T_g: Glass transition temperature
T_m: Melting temperature
ΔH_m: Melting enthalpy

Recent *in situ* ^{1}H NMR kinetic studies of the copolymerization of EO with ethoxy ethyl glycidyl ether (EEGE) under monomer-activated AROP conditions showed a lowering of the reactivity of EEGE, leading to strongly tapered structures.[17] These results encouraged us to investigate the reactivity ratios of the current EO/GPgE system in the same manner. Details on the sample preparation and data analysis are given in the Supporting Information (Figures S4-S7). After ~160 min (at $T = 10$ °C), EO was fully reacted, while only 40 % of GPgE was incorporated into the polymer chain (Figure S5b). Total monomer conversion was reached after 280 min at $T = 15$ °C. From the collected NMR data, reactivity ratios

were calculated, applying the nonterminal model of chain copolymerization, introduced by Lynd and co-workers.[18] Reactivity ratios of $r_{EO} = 14.8$ and $r_{GPgE} = 0.076$ ($r_{EO}{\cdot}r_{GPgE} = 1.12$) reveal a tapered structure, with EO rich segments close to the initiator and GPgE rich segments near the terminus (Figures S5a and S6). To visualize the reactivity ratios and to demonstrate the tapered nature of PEG-*co*-PGPgE copolymers, we illustrate the monomer compositional drift schematically in two hypothetical copolymers with (a) 50 mol% GPgE (Scheme 2 a) and 10 mol% GPgE (Scheme 2 b). The latter reflects the tapered structure of the synthesized copolymers with comonomer ratios in the range of 2-15.6 mol% GPgE (Table 1).

Scheme 2. Illustration of the monomer distribution of a PEG-*co*-PGPgE copolymer

P(EO-*co*-GPgE) with $r_{EO} = 14.8$ and $r_{GPgE} = 0.076$

a) 50 mol% GPgE
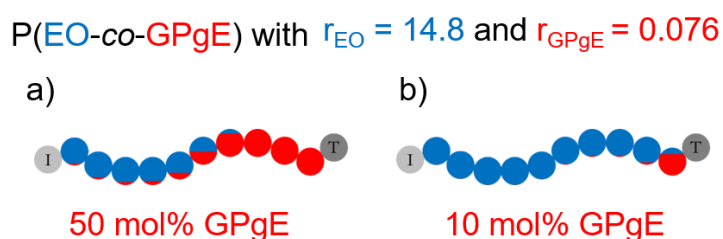
b) 10 mol% GPgE

consisting of a) 50 mol% GPgE and b) 10 mol% GPgE. GPgE is depicted in red and EO in blue. "I" denotes the initiator and "T" implies the terminus of the polymer chain.

These results are in analogy to our previous studies on the copolymerization of EO with EEGE. When copolymerized under monomer-activated conditions with EO, GPgE and EEGE behave similar ($r_{EO} = 8.0$ and $r_{EEGE} = 0.125$).[17] We assume that the attachment of the larger glycidyl ethers (GPgE and EEGE) to the growing 'ate' complex is sterically hindered compared to the small EO molecule. Consequently, the relative reactivity of EO is much higher. In analogy, Müller et al. reported gradient-like structures for poly(ethylene glycol-*co*-glycidyl methyl ether) (PEG-*co*-PGME) copolymers, based on bulk thermal properties and ^{13}C triad analysis.[5]

The monomer compositional profile is also confirmed by ^{13}C NMR spectroscopy (see Supporting Information for details and Figures S8-S9). The G-G$_b$-G triad appears already at low GPgE ratios (~4 mol%), and a splitting of the resonances of the alkyne-carbons (-CH$_2$$C$≡CH at 80.5 ppm and -CH$_2$C≡$C$H at 75.2 ppm, respectively) is observed (Figure S9). This splitting reflects an interaction of the alkyne group with adjacent monomer units and differs, if EO or GPgE units are located in direct neighborhood. Similar results were reported for the methyl group of GME in PEG-*co*-PGME.[5] The formation of an almost homopolymer PEG block in PEG-*co*-PGPgE copolymers is also reflected in their bulk thermal properties (Table 1). While PEG (> 2000 g·mol^{-1}) is a crystalline material (T$_{m, PEG2000}$ = 56 °C)[19], random incorporation of substituted epoxides should lower its melting temperature dramatically. Only little influence of the small amount of incorporated GPgE units on the melting temperature is detected, confirming the presence of block-like structures (see Table 1). In particular, PEG-*co*-PGPgE obtained via statistical copolymerization with 15.6 mol% GPgE and a molecular weight of ~9000 g·mol^{-1} showed a melting temperature of 37 °C. A missing second T_g is not contradictive, given that GPgE segments are rather short.

The potential of alkyne-functional PEGs for post-functionalization via click-reaction was demonstrated by attaching mannopyranosyl azide via CuAAC, leading to PEG-based glycopolymers (Scheme 3). Glycopolymers are macromolecules bearing pendant saccharide moieties and play an important role in studying multivalent interactions, such as protein-saccharide binding. Since the 1980ies, researchers have been interested in synthesizing glycopolymers and studying their affinity to lectins, e.g. Concanavalin A (Con A).[20] To date, glycopolymers based on a PEG backbone are not well explored, due to the difficulty of synthesizing multi-functional PEGs.[8,21] In the current

work, we decorated the PEG-*co*-PGPgE copolymers and PGPgE hompolymer with mannopyranosyl azide (α-D-mannopyranosyl azide) as shown in Scheme 3.
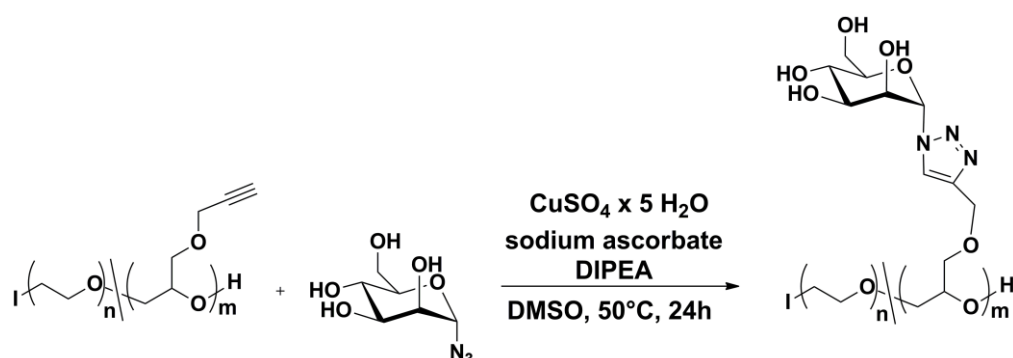
Scheme 3. CuAAC of PEG-*co*-PGPgE with mannopyranosyl azide leading to sugar-functionalized PEG.

The applied mannopyranosyl azide was synthesized as described in literature.[22] After successful CuAAC, a shift to smaller elution volumes ($\cong$ higher molecular weights) is observed in SEC for mannose-functionalized PEG-*co*-PGPgE (Figure 2b). Additionally, the resonance of the propargylic methylene group (4.25 ppm) in the ^{1}H NMR spectrum disappeared, while the characteristic signals of the formed triazole ring (8.25 ppm) and the adjacent H-1 proton of the mannose (6.13 ppm) and the methylene group (4.72 ppm) emerge (Figure 2a). The proton resonances of the attached sugar residues overlap with the broad polymer backbone signals, but are clearly visible in the ^{13}C NMR spectra (see Figure S10).
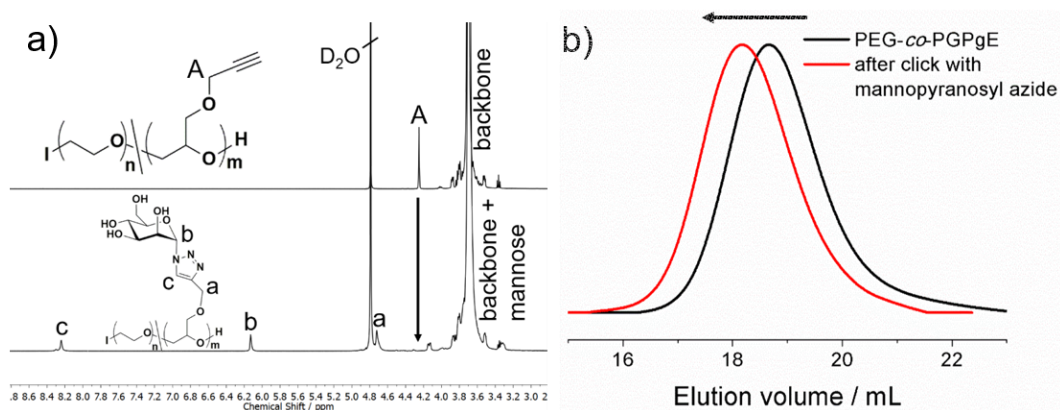
Figure 2. (a) ^{1}H NMR spectrum (D$_2$O, 400 MHz) of PEG-*co*-PGPgE before and after click with mannopyranosyl azide. (b) SEC traces (DMF, RI signal, PEG standard) of PEG-*co*-PGPgE (3.7 mol% GPgE) before and after click with mannopyranosyl azide.

Additionally, we functionalized PGPgE homopolymer with mannopyranosyl azide to obtain a glycopolymer solely based on a polyether backbone. The SEC traces are shown in Figure S11 and show a clear shift from PGPgE homopolymer to sugar functionalized PGPgE. After attachment of mannopyranosyl azide, the homopolymer became fully water-soluble. ^{1}H and HSQC NMR are depicted in Figures S12 and S13 and confirm full conversion of the alkyne moiety. Cu traces were successfully removed via an ion exchange resin (Chelex® 100). Regarding the thermal properties in bulk, functionalization with sugar-moieties leads to a strong increase in T_g. In particular, the T_g of PEG-*co*-PGPgE with 3.7 mol% shifts from -51 °C to -27 °C after modification (Table S1). Most significantly, a substantial jump from -39 °C to +35 °C is observed for the sugar-functionalized PGPgE homopolymer.

4.1.4 Conclusion

In summary, we have developed a simple synthetic strategy to prepare the first example of alkyne-functional PEGs by direct copolymerization of EO and GPgE. Monomer-activation via Lewis acid and initiation with an ammonium halide/Lewis acid complex permits polymerization under mild conditions. Demanding protection/deprotection of GPgE is not required. SEC analysis shows monomodal molecular weight distributions with moderate to narrow PDIs (< 1.6). PEG-*co*-PGPgE copolymers reveal a strongly tapered monomer profile reflected by the reactivity ratios of $r_{EO} = 14.8$ and $r_{GPgE} = 0.076$. The most intriguing feature of alkyne-functional PEGs is their universal platform character for CuAAC click reactions in general. We quantitatively decorated PEG-*co*-PGPgE copolymers and PGPgE homopolymer with multiple mannosyl units and generated PEG based glycopolymers, which might be suitable for cell targeting due to their multivalent character.[23] However, we believe that alkyne-functional PEG has many applications beyond the biomedical field. In

particular, it is a versatile polyether platform for any functional material, benefiting from the highly flexible and polar PEG backbone. Future work will aim at optimization catalyst/initiator ratios and detailed biomedical studies of a variety of bio-conjugates.

4.1.5 Acknowledgements

4.1.6 References

[1] J. Herzberger, K. Niederer, H. Pohlit, J. Seiwert, M. Worm, F. R. Wurm and H. Frey, *Chem. Rev.*, 2016, **116**, 2170–2243.

[2] a) K. Knop, R. Hoogenboom, D. Fischer and U. S. Schubert, *Ang. Chem. Int. Ed.*, 2010, **49**, 6288–6308; b) S. N. S. Alconcel, A. S. Baas and H. D. Maynard, *Polym. Chem.*, 2011, **2**, 1442–1448; c) G. Pasut and F. M. Veronese, *J. Control. Release*, 2012, **161**, 461–472;

[3] M. S. Thompson, T. P. Vadala, M. L. Vadala, Y. Lin and J. S. Riffle, *Polymer*, 2008, **49**, 345–373.

[4] T. Hamaide, A. Goux, M.-F. Llauro, R. Spitz and A. Guyot, *Angew. Makromol. Chemie*, 1996, **237**, 55–77.

[5] S. S. Müller, C. Moers and H. Frey, *Macromolecules*, 2014, **47**, 5492–5500.

[6] B. Obermeier, F. Wurm, C. Mangold and H. Frey, *Angew. Chem. Int. Ed.*, 2011, **50**, 7988–7997.

[7] a) B. Parrish, R. B. Breitenkamp and T. Emrick, *J. Am. Chem. Soc.*, 2005, **127**, 7404–7410; b) V. Ladmiral, G. Mantovani, G. J. Clarkson, S. Cauet, J. L. Irwin and D. M. Haddleton, *J. Am. Chem. Soc.*, 2006, **128**, 4823–4830; c) D. Quémener, M. Le Hellaye, C. Bissett, T. P. Davis, C. Barner-Kowollik and M. H. Stenzel, *J. Polym. Sci. A Polym. Chem.*, 2008, **46**, 155–173; d) R. K. Iha, K. L. Wooley, A. M. Nyström, D. J. Burke, M. J. Kade and C. J. Hawker, *Chem. Rev.*, 2009, **109**, 5620–5686; e) C. Secker, J. W. R. and H. Schlaad, *Eur. Polym. J.*, 2015, **62**, 394–399;

[8] M. Erberich, H. Keul and M. Möller, *Macromolecules*, 2007, **40**, 3070–3079.

[9] Z. Li and Y. Chau, *Bioconjugate Chem.*, 2009, **20**, 780–789.

[10] C. Schüll, T. Gieshoff and H. Frey, *Polym. Chem.*, 2013, **4**, 4730–4736.

[11] a) A. Labbé, S. Carlotti, C. Billouard, P. Desbois and A. Deffieux, *Macromolecules*, 2007, **40**, 7842–7847; b) A.-L. Brocas, C. Mantzaridis, D. Tunc and S. Carlotti, *Prog. Polym. Sci.*, 2013, 845–873;

[12] S. Carlotti, A. Labbé, V. Rejsek, S. Doutaz, M. Gervais and A. Deffieux, *Macromolecules*, 2008, **41**, 7058–7062.

[13] a) K. Sakakibara, K. Nakano and K. Nozaki, *Chem. Commun.*, 2006, 3334–3336; b) K. Sakakibara, K. Nakano and K. Nozaki, *Macromolecules*, 2007, **40**, 6136–6142;

[14] J. Herzberger and H. Frey, *Macromolecules*, 2015, **48**, 8144–8153.

[15] A. Labbé, A.-L. Brocas, E. Ibarboure, T. Ishizone, A. Hirao, A. Deffieux and S. Carlotti, *Macromolecules*, 2011, **44**, 6356–6364.

[16] M. Gervais, A.-L. Brocas, G. Cendejas, A. Deffieux and S. Carlotti, *Macromolecules*, 2010, **43**, 1778–1784.

[17] J. Herzberger, D. Leibig, J. C. Liermann and H. Frey, *ACS Macro Lett.*, 2016, **5**, 1206-1211.

[18] B. S. Beckingham, G. E. Sanoja and N. A. Lynd, *Macromolecules*, 2015, **48**, 6922–6930.

[19] Y. K. Godovsky, G. L. Slonimsky and N. M. Garbar, *J. polym. sci., Polym. symp.*, 1972, **38**, 1–21.

[20] Y. Miura, Y. Hoshino and H. Seto, *Chem. Rev.*, 2016, **116**, 1673–1692.

[21] M. J. Barthel, U. Mansfeld, S. Hoeppener, J. A. Czaplewska, F. H. Schacher and U. S. Schubert, *Soft Matter*, 2013, **9**, 3509–3520.

[22] a) V. Percec, P. Leowanawat, H.-J. Sun, O. Kulikov, C. D. Nusbaum, T. M. Tran, A. Bertin, D. A. Wilson, M. Peterca, S. Zhang, N. P. Kamat, K. Vargo, D. Moock, E. D. Johnston, D. A. Hammer, D. J. Pochan, Y. Chen, Y. M. Chabre, T. C. Shiao, M. Bergeron-Brlek, S. André, R. Roy, H.-J. Gabius and P. A. Heiney, *J. Am. Chem. Soc.*, 2013, **135**, 9055–9077; b) B. Kang, P. Okwieka, S. Schöttler, S. Winzen, J. Langhanki, K. Mohr, T. Opatz, V. Mailänder, K. Landfester and F. R. Wurm, *Ang. Chem. Int. Ed.*, 2015, **54**, 7436–7440;

[23] C. Fasting, C. A. Schalley, M. Weber, O. Seitz, S. Hecht, B. Koksch, J. Dernedde, C. Graf, E.-W. Knapp and R. Haag, *Ang. Chem. Int. Ed.*, 2012, **51**, 10472–10498.

4.1.7 Supporting Information

Materials. Ethylene oxide (EO), glycidyl propargyl ether (GPgE), chlorobenzene and Chelex® 100 sodium form (50-100 mesh, dry) were purchased from Sigma-Aldrich. GPgE was freshly distilled from CaH_2 prior to use (see Figure S1-S2 for detailed analysis). Deuterated chlorobenzene was received from Deutero GmbH and dried over CaH_2 and freshly distilled prior to use. Tetra(*n*-butyl) ammonium iodide (TBAI) and all other were reagents were reagent grade and purchased from Acros Organics. Anhydrous chlorobenzene was stirred over CaH_2 and freshly distilled before use. If not otherwise stated, the chemicals were used as received.

General procedures. All reactions involving air or moisture sensitive reagents or intermediates were performed under an inert atmosphere of argon in glassware that was oven dried. Reaction temperatures referred to the temperature of the particular cooling/heating bath. Chromatography was performed using flash chromatography of the indicated solvent system on 35-70 µm silica gel (*Acros Organics*) unless otherwise noted. Reactions were monitored by thin-layer chromatography (TLC) carried out on 0.25 mm E. Merck silica gel plates (60F$_{254}$) using an 1M ethanolic solution of sulfuric acid with 0.2% 3-methoxyphenol and heat as developing agents.

Instrumentation. ^{1}H NMR spectra (400 MHz) and ^{13}C NMR spectra (100 MHz) were recorded using a Bruker *Bruker Avance-II 400* MHz spectrometer equipped with a 5 mm BBFO-SmartProbe (Z-gradient probe) and an ATM as well as a SampleXPress 60 auto sampler. Chemical shifts were referenced to the deuterated solvent (e.g., for $CDCl_3$, $\delta = 7.26$ ppm and 77.16 ppm for ^{1}H and ^{13}C NMR, respectively) and reported in parts per million (ppm, δ) relative to tetramethylsilane (TMS, $\delta = 0.00$ ppm).[1] (1) Coupling constants (*J*) were reported in Hz and the splitting abbreviations used were: s, singlet; d, doublet; t,

triplet; m, multiplet; br, broad SEC measurements were performed in DMF (containing 0.25 g L^{-1} lithium bromide as an additive) or in THF. For SEC measurements in DMF, an Agilent 1100 Series was used as an integrated instrument, including a PSS HEMA column (300/100/40 · 10^{-10} porosity) as well as a UV (275 nm) and a RI detector. Alternatively, SEC measurements in THF (flow rate 1 mL·min^{-1}) were performed with a MZ-Gel SD plus column (10^5/10^3/100 g mol^{-1}) at 20 °C, using a UV (254 nm) and RI detector. All calibrations were carried out using poly(ethylene glycol) standards purchased from Polymer Standards Service. ^{1}H NMR kinetic studies to monitor copolymerization were conducted on a Bruker Avance III HD spectrometer equipped with a 5 mm BBFO SmartProbe and an ATM as well as a SampleXPress 60 auto sampler. DSC measurements were performed under nitrogen atmosphere using a PerkinElmer DSC 8500 with PerkinElmer CLN2 in the temperature range from – 100 °C to 100 °C (sugar functionalized materials were only heated to 60 °C) at heating rates of 20 and 10 K·min^{-1} for the first and the second heating run, respectively. Specific reactions were monitored by LC-MS on a 1200 HPLC-unit from *Agilent Technologies* with binary pump and integrated diode array detector coupled to a LC/MSD-Trap-mass-spectrometer from *Bruker*. Ionization was achieved by an electron-spray-ionization source (ESI) or an atmospheric-pressure-chemical-ionization source (APCI). High-resolution masses were recorded on a *Waters QTof-Ultima 3*-Instrument with *Lockspray*-Interface and a suitable external calibrant. Infrared spectra were recorded as FT-IR spectra using a diamond ATR unit and are reported in terms of frequency of absorption (ν, cm^{-1}).

***In situ* ^{1}H NMR kinetic studies of copolymerization.** Measurements were conducted according to a literature procedure.[2] A NMR tube suitable for high pressure and high vacuum Norell S-500-VT-7 NMR tube (equipped with a Teflon stop-cock) was applied. The tube was evacuated and filled with (1) 0.1 mL initiator solution (24 mg TBAI in 0.5 mL

chlorobenzene-d_5) followed by (2) 0.3 mL neat chlorobenzene, (3) 60 µL TIBAL solution in toluene (1.1 M, 5 euqiv), (4) 0.2 mL neat chlorobenzene and (5) 21 µL GPgE monomer under argon flow and repeated cooling with an acetone/dry ice bath. Afterwards, the tube was evacuated under cooling and EO was cryo-transferred into the tube (~20 µL). Before the measurement, the tube was shaking vigorously and subsequently placed in the NMR spectrometer (T=0 °C). After the temperature in the spectrometer was constant (~10 min, $\Delta T = 0.1$ K), the first spectrum was recorded. Sample spinning was turned off. Spectra were recorded with 16 scans with 2 min-intervals. After 1h at 0 °C, the temperature was raised to 5 °C, all other parameters were kept constant. After another hour, the temperature was set to 10 °C and then to 15 °C. The measurement was stopped after full conversion (~5 h).

Synthesis of poly(ethylene glycol-*co*-glycidyl propargyl ether) (PEG-*co*-PGgPE) copolymers. Here, an exemplary synthesis protocol is described for the synthesis of PEG$_{195}$-*co*-PGPgE$_5$ with 2.5 mol% GPgE content. TBAI (1 equiv, 83.5 mg) were dissolved in 5 mL benzene and freeze dried under vacuum to remove residual water. The flask was backfilled with argon and 15 ml of chlorobenzene were added via syringe. For the transfer of EO into the flask, vacuum was applied and EO (190 equiv, 2 mL) was cryo-transferred into a graduate ampoule and subsequently into the reaction flask, using an ethanol/liquid nitrogen cooling bath (-80 °C). The flask was sealed, backfilled with argon and 0.12 mL (5 equiv) of freshly distilled GPgE was added via septum by syringe. The reaction was initiated at -15 °C (ice/NaCl bath) by addition of 0.3 mL *i*-Bu$_3$Al solution in toluene (1.5 equiv, 1.1 M in toluene) and slowly allowed to warm up to room temperature. After 24 h, termination was performed by addition of an excess of ethanol (1 mL) and the polymer was precipitated into ice cold diethyl ether. Dialysis in methanol and then DI water (MWCO = 2000 g·mol^{-1}) was performed to remove residual tetra(*n*-butyl) ammonium salts. Small loss was observed due to dialysis. Afterwards, copolymers were dried via

lyophilization for DSC measurements. Note, direct purification of the polymers is recommended to extend their shelf life. Small amounts of basic impurities lead to crosslinking. Purified polymers were stored in the dark at -18 °C and are stable for several weeks.

Homopolymerization (PGPgE). GPgE was polymerized similar to a literature procedure described for epicyanohydrin by applying monomer-activated AROP.[3] As a typical procedure, TBAI (1equiv) was added to a Schlenk flask, freeze-dried with benzene overnight and backfilled with argon. Chlorobenzene was added under argon atmosphere via syringe ($c = 1$ mol·L^{-1}). The solution was cooled to 0 °C before the dry monomer was syringed in, followed by ^{i}Bu$_3$Al solution in toluene (3-4 equiv). Polymerization was conducted under argon atmosphere and the solution was allowed to slowly reach room temperature and was terminated after 24 h by addition of ethanol. The crude polymer was dissolved in THF and precipitated into methanol (room temperature). This purification step was repeated twice to remove tetra(*n*-butyl)ammonium salts and the homopolymer was obtained in quantitative yield. Alternatively, tetra(*n*-butyl)ammonium salts can be removed via consecutive washing of the reaction mixture with saturated NaHCO$_3$ solution, NaCl solution (10%), and water in analogy to reports by Osterwinter et al.[4]

Mannopyranosyl azide.
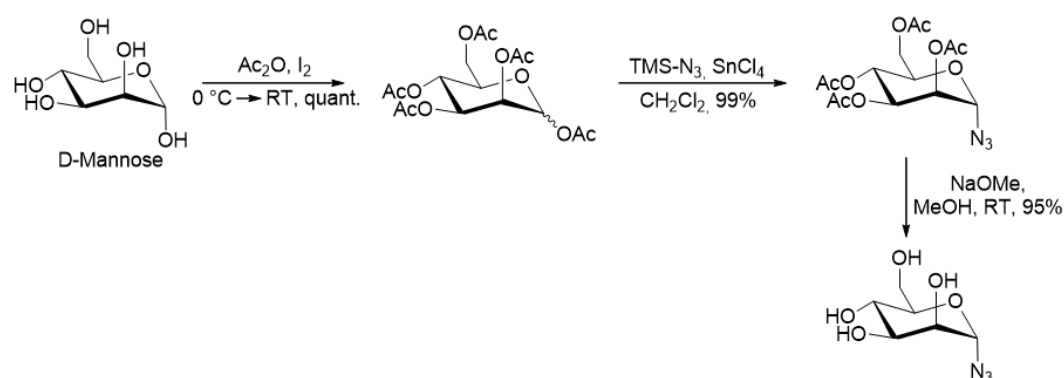
Scheme S1. Synthesis scheme of mannopyranosyl azide, starting from D-mannose.

1,2,3,4,6-Penta-*O*-acetyl-D-mannopyranose. Iodine (560 mg, 2.2 mmol, 0.04 equiv.) and acetic anhydride (50 ml) were mixed under Ar-atmosphere. D-Mannose (10 g, 55.5 mmol, 1 equiv.) was added portion by portion at 0 °C. After stirring for 30 min at 0 °C and additionally for 18 hours at room temperature TLC (cyclohexane/toluene/ethylacetate 3:3:1) showed complete consumption of the starting material. The reaction mixture was diluted with CH_2Cl_2 (50 ml) and was washed twice with cold saturated aqueous Na_2SO_3 solution (2x 80 ml), then with a saturated aqueous solution of $NaHCO_3$ (4x 50 ml). The separated organic layer was dried over anhydrous Na_2SO_4. The solvent was removed *in vacuo* to afford the desired peracetylated D-mannose (21.5 g, 55.1 mmol, 99%, mixture of both anomers α/β 12:88) as a yellowish high viscous oil.

R_f 0.30 (silica gel, cyclohexane/toluene/ethyl acetate, 3:3:1);

Signals assignable to α-anomer: ^{1}H NMR, COSY (600 MHz, CDCl$_3$) δ (ppm) = 6.09 (d, ^3J = 1.9 Hz, 1H, H-1), 5.34–5.36 (m, 2H, H-3, H-4), 5.25–5.27 (m, 1H, H-2), 4.28 (dd, ^2J = 12.4 Hz, ^3J = 4.9 Hz, 1H, H-6a), 4.10 (dd, ^2J = 12.4 Hz, ^3J = 2.5 Hz, 1H, H-6b), 4.03-4.07 (m, 1H, H-5), 2.18, 2.17, 2.10, 2.05, 2.01 (5x s, 15H, COC*H$_3$*); ^{13}C NMR, HSQC, HMBC (151 MHz, CDCl$_3$) δ (ppm) = 170.8, 170.2, 169.9, 169.7, 168.2 (5x *C*OCH$_3$), 90.7 (C-1), 70.7 (C-5), 68.8 (C-3), 68.4 (C-2), 65.6 (C-4), 62.2 (C-6), 21.0, 20.9, 20.9, 20.8, 20.8 (5x COCH$_3$).

The spectral data are in accordance with literature.[5]

2,3,4,6-Tetra-*O*-acetyl-α-D-mannopyranosyl azide. 1,2,3,4,6-Penta-*O*-acetyl-D-mannopyranose (13.6 g, 34.9 mmol, 1 equiv.) was dissolved in anhydrous CH_2Cl_2 (140 ml) under argon atmosphere. Trimethylsilyl azide (16.1 g, 18.5 ml, 139 mmol, 4 equiv.) and tin(IV) chloride (2.37 g, 1.06 ml, 9.1 mmol, 0.26 equiv.) was added. After stirring for four hours at room temperature, TLC (cyclohexane/toluene/ethylacetate 3:3:1) showed

complete consumption of the starting material. The reaction mixture was washed successively with saturated aqueous $NaHCO_3$ solution (100ml), water (100 ml) and brine (100 ml). The organic layer was dried over anhydrous Na_2SO_4. The solvent was removed *in vacuo* and the residue was purified by flash column chromatography (cyclohexane/ ehtylacetate, 3:1) to afford the title compound (12.9 g, 34.4 mmol, 99%) as a clear, colorless oil.

R_f 0.49 (silica gel, cyclohexane/toluene/ethyl acetate, 3:3:1);

^{1}H NMR, COSY (400 MHz, CDCl₃) δ (ppm) = 5.38 (d, ^3J = 1.9 Hz, 1H, H-1), 5.14 (dd, ^3J = 3.0 Hz, ^3J = 1.9 Hz, 1H, H-2), 5.30–5.21 (m, 2H, H-3, H-4), 4.32-4.27 (m, 1H, H-6a), 4.17–4.11 (m, 2H, H-5, H-6b), 2.16, 2.10, 2.04, 1.98 (4x s, 12H, COC*H₃*); ^{13}C NMR, HSQC, HMBC (100.6 MHz, CDCl₃) δ (ppm) = 170.7, 170.0, 169.9, 169.7 (4x *C*OCH₃), 87.6 (C-1), 70.7 (C-5), 69.3 (C-2), 68.3 (C-3), 65.7 (C-4), 62.2 (C-6), 21.0, 20.8, 20.8, 20.7 (4x COC*H₃*).

The spectral data are in accordance with literature.[5]

α-D-Mannopyranosyl azide. 2,3,4,6-Tetra-*O*-acetyl-α-D-mannopyranosyl azide (10 g, 26.8 mmol) was dissolved in methanol (100 ml) and sodium methoxide was added until pH 9–10 (approx. 60 mg). The reaction mixture was stirred at room temperature for 16 hours. Subsequently the solution was neutralized by Amberlite 120 H⁺ resin until pH 7. The mixture was filtered over Celite which was washed thoroughly with methanol. The solvent was removed *in vacuo* to afford the desired α-D-Mannopyranosyl azide (5.23 g, 25.5 mmol, 95%) as a colorless syrup.

^{1}H NMR, COSY (400 MHz, CDCl₃) δ (ppm) = 5.43 (d, ^3J = 1.9 Hz, 1H, H-1), 3.91–3.87 (m, 1H, H-6a), 3.85 (dd, ^3J = 3.3 Hz, ^3J = 1.9 Hz, 1H, H-2), 3.79–3.69 (m, 3H, H-3, H-5,

H-6b), 3.65-3.59 (m, 1H, H-4); ^{13}C NMR, HSQC, HMBC (100.6 MHz, CDCl$_3$)

δ (ppm) = 89.7 (C-1), 74.6 (C-5), 69.8, 69.7 (C-2, C-3), 66.3 (C-4), 60.7 (C-6).

The spectral data are in accordance with literature.[5]

Copper(I)-catalyzed azide-alkyne cycloaddition (CuAAC). A literature known procedure was applied.[6] For example, 100 mg PEG-*co*-PGPgE (1 equiv) was placed in a Schlenk flask and dissolved in 15 mL DMSO (anhydrous) and mannopyranosyl azide (1.5 equiv per propargyl unit) and diisopropylethylamine (DIPEA) (0.3 equiv per propargyl unit) were added. The mixture was degassed by three freeze-pump-thaw cycles and subsequently copper sulfate pentahydrate (0.3 equiv per propargyl unit) and sodium ascorbic acid (0.6 equiv per propargyl unit) were added under argon flow. The solution was heated to 50 °C and stirred for 24 h under argon atmosphere. Afterwards, the flask was opened and DMSO was removed under vacuum. The polymer was dissolved in water and Chelex®100 was added and stirred for 12 h, changed and stirred for another 12 h to remove copper traces. Afterwards, the polymer was dissolved in DI water and dialyzed for 1 day (MWCO = 2000 g·mol^{-1}) to remove excess of mannose azide and residual DMSO. Products were obtained after lyophilizing as pale yellow solids (yield = 90%). Functionalized PGPgE homopolymer was treated for 1 week with ion exchange resin (Chelex®100) for sufficient removal of copper traces.
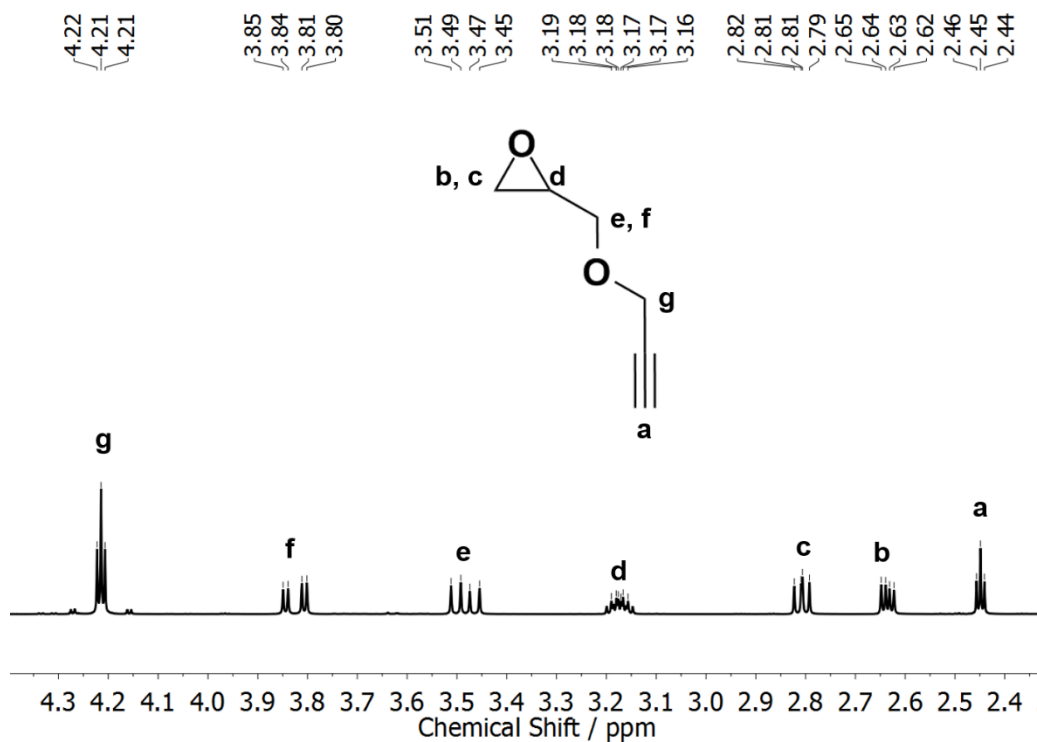
Figure S1. ^{1}H NMR spectrum (400 MHz, CDCl$_3$) of commercially available GPgE after purification via distillation.
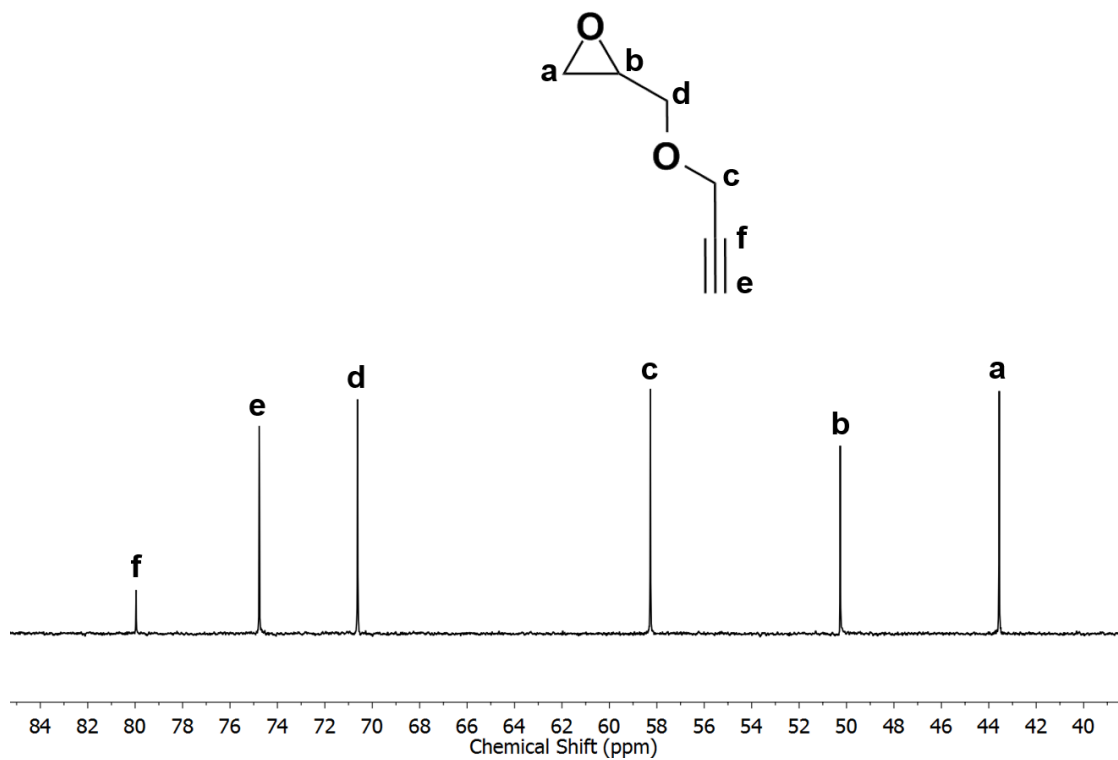
Figure S2. ^{13}C NMR spectrum (100 MHz, benzene-d_6) of commercially available GPgE after distillation.
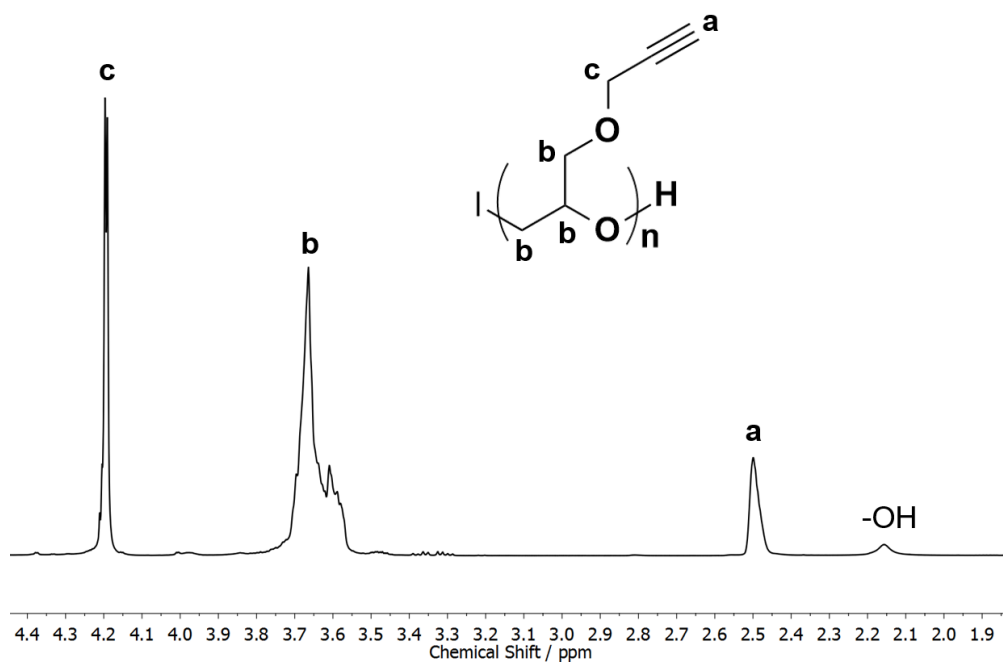
Figure S3. ^{1}H NMR spectrum (400 MHz, CDCl$_3$) of PGPgE homopolymer.
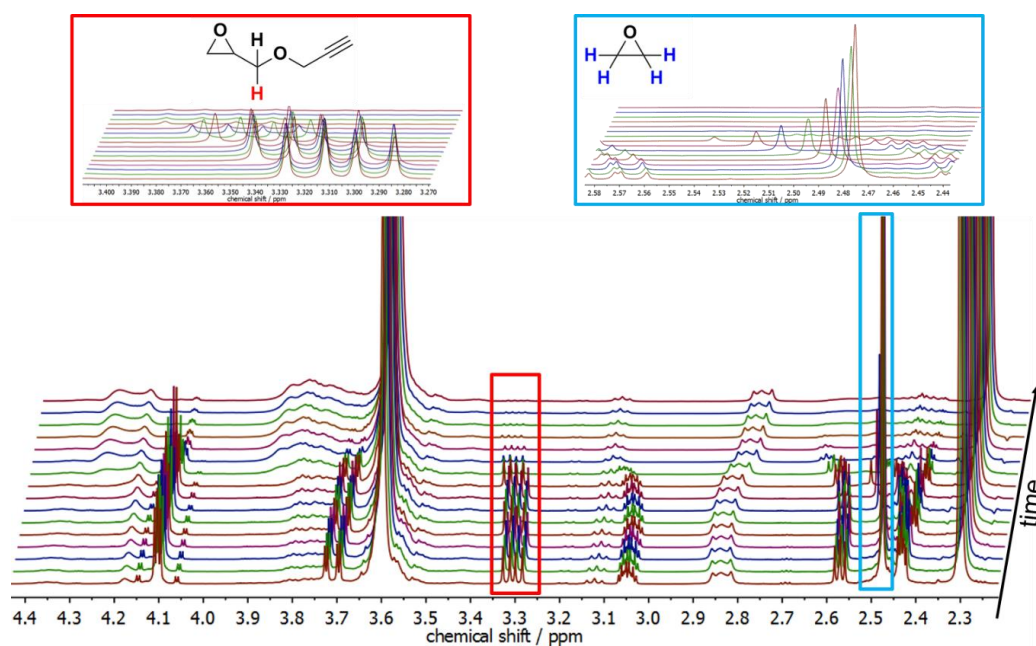
Figure S4. Subset of ^{1}H NMR spectra (400 MHz, chlrobenze-d_5) of the copolymerization of EO with GPgE, applying the activated monomer technique. Insets expand region of interest, showing the proton signals used to calculate the respective monomer conversion
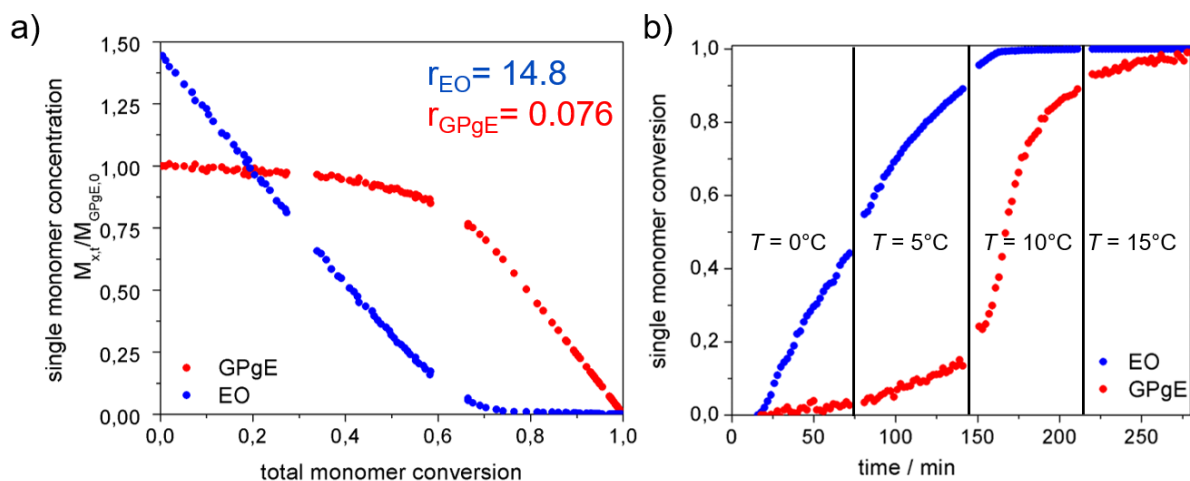
Figure S5. a) Single monomer concentrations normalized by the initial concentration of GPgE plotted versus total monomer conversion and b) single monomer conversions plotted versus time. n(EO) = 59 mol% and n(GPgE) = 41 mol% with a catalyst/initiator ratio of 5, initiated at 0 °C.
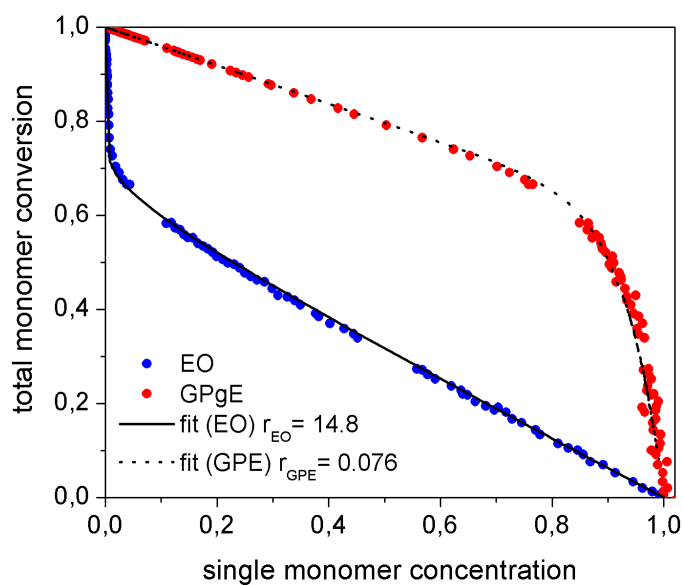
Figure S6. Total monomer conversion plotted as a function of the individual monomer concentration for EO (blue) and GPgE (red). Reactivity ratios are calculated from the respective fits (EO: solid line; GPgE: dashed line) in analogy to literature.[7]
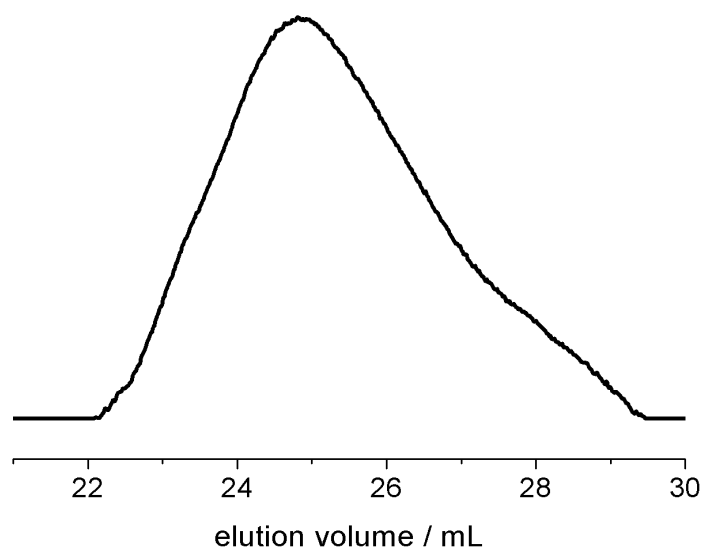
Figure S7. SEC elution trace (THF, RI signal, PEG standard) of PEG-*co*-PGPgE copolymer generated in a NMR tube to study the respective reactivity ratios of EO and GPgE under monomer-activated AROP conditions. Mole fractions: n(EO) = 59 mol% and n(GPgE) = 41 mol% with a catalyst/initiator ratio of 5 equiv, initiated at 0 °C. SEC data: M_n = 3000 g·mol^{-1}, PDI = 1.77.

^{13}C triad analysis. Figure S8 shows the IG ^{13}C NMR spectrum of PEG-*co*-PGPgE copolymer. A collection of IG ^{13}C NMR spectra of PGPgE homopolymer and PEG-*co*-PGPgE copolymers with 2.0-15.6 mol% GPE content in benzene-d_6 is shown in S9. Triad assignment was performed in analogy to literature-known functional PEGs[8] and with the help of 2D spectra and simulated ^{13}C NMR spectra (ChemDraw Ultra 10.0). GPgE units are labeled with *G*, while *a* denotes the methylene carbon and *b* the methine carbon of GPgE. *E* refers to EO units.
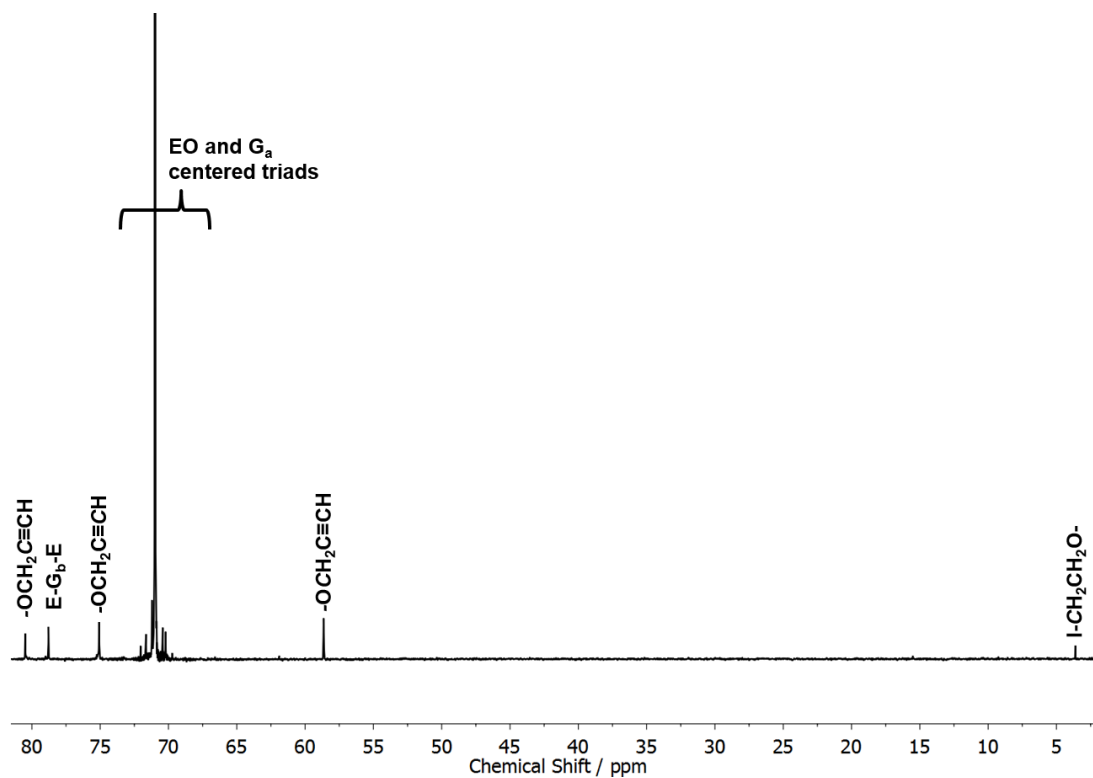
Figure S8. ^{13}C NMR spectrum (100 MHz, benzene-d_6) of PEG-*co*-PGPgE. EO units are abbreviated with E and GPgE units with G, whereas *a* denotes the methylene and *b* the methine carbon.
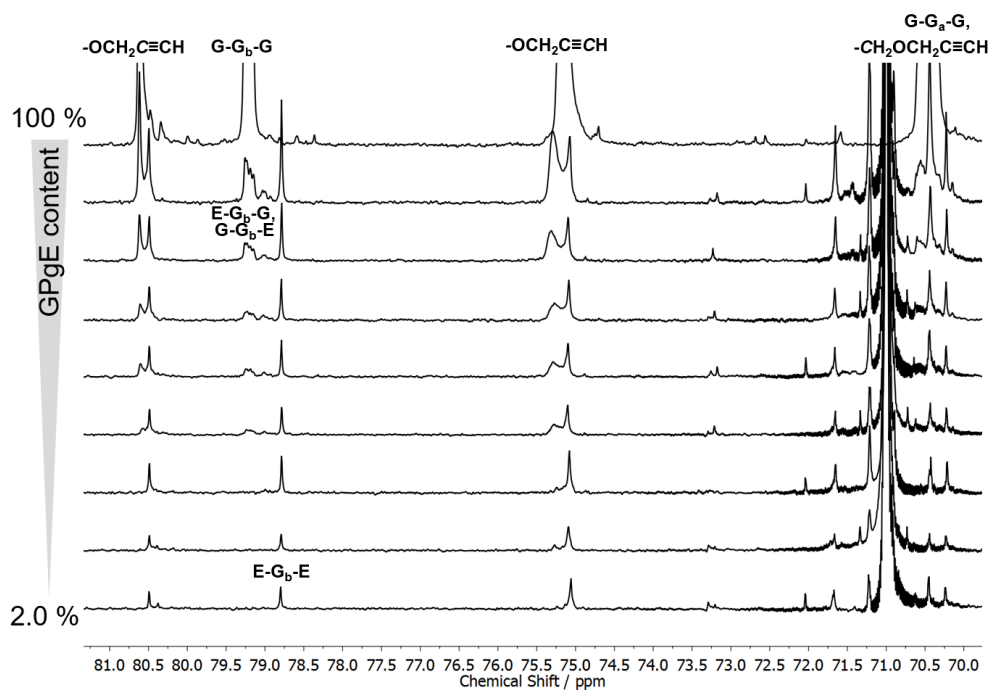
Figure S9. Important region of IG ^{13}C NMR spectra (100 MHz, benzene-d_6) of PGPgE homopolymer and various PEG-*co*-PGPgE copolymers (2.0 - 15.6 mol%).
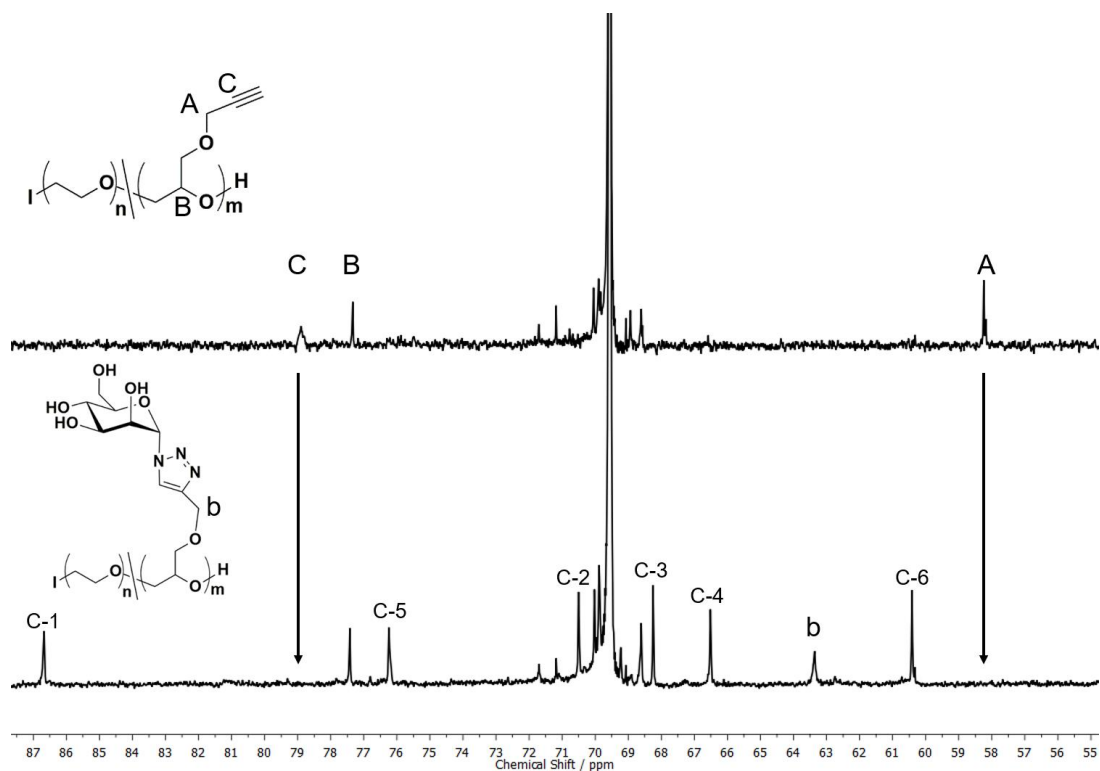
Figure S10. Relevant section of ^{13}C NMR spectra (100 MHz, D$_2$O) of PEG-*co*-PGPgE before (top) and after click with mannopyranosyl azide (bottom).
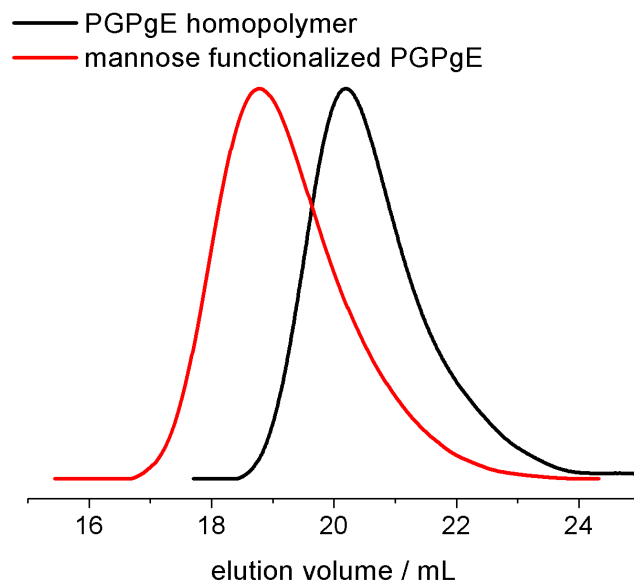
Figure S11. SEC traces (DMF, RI signal, PEG standard) of PGPgE$_{30}$ homopolymer (black line) and mannose-functionalized PGPgE$_{30}$ (red line).
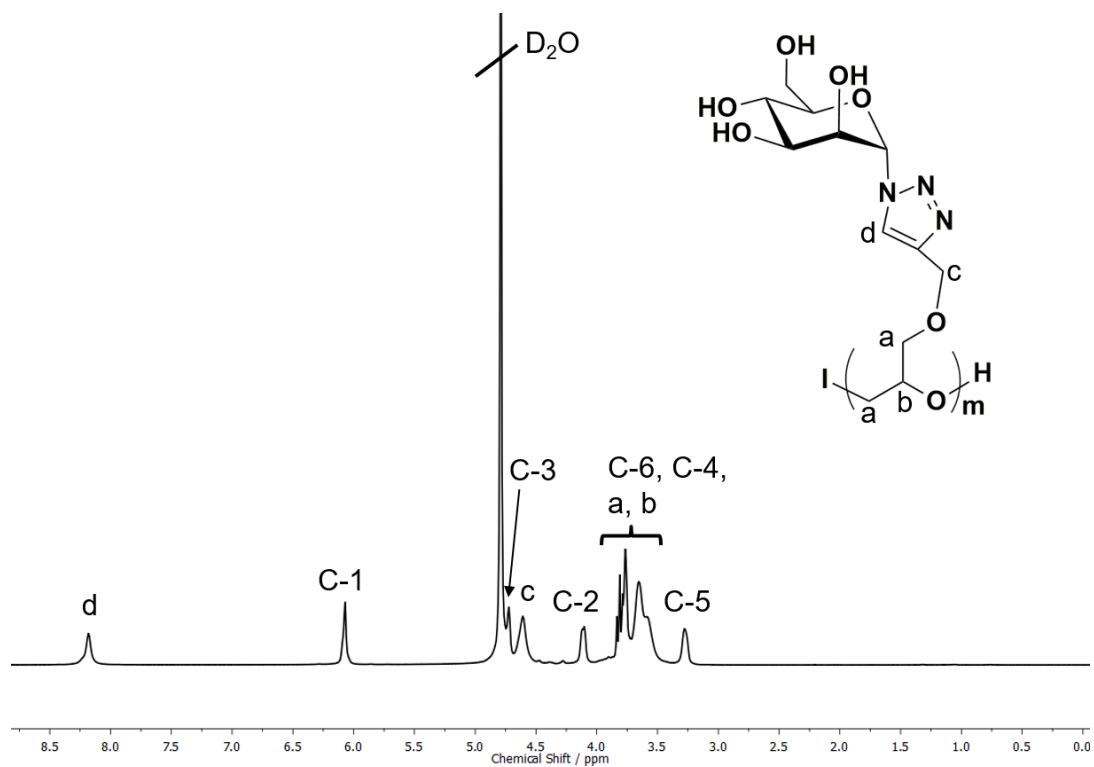
Figure S12. ^{1}H NMR (400 MHz, D_2O) of mannose-functionalized PGPgE$_{30}$ homopolymer.
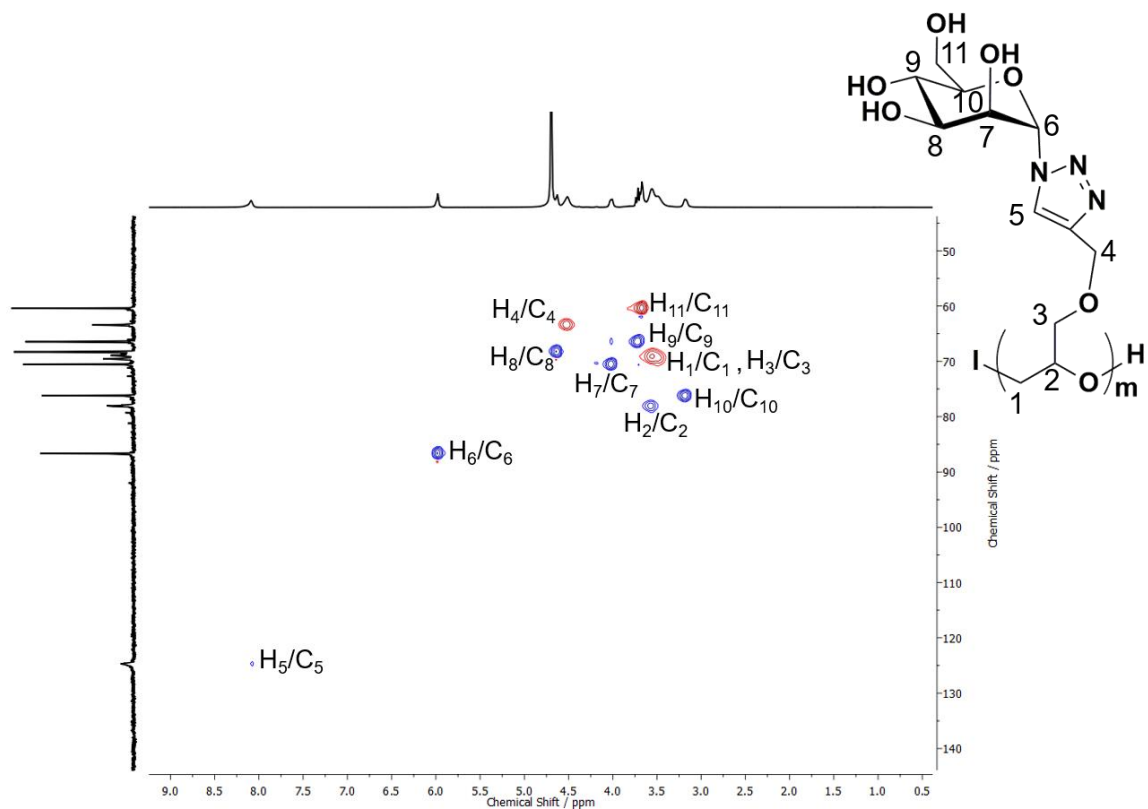
Figure S13. HSQC NMR (400 MHz/100 MHz, D_2O) of mannose-functionalized PGPgE$_{30}$ homopolymer.

Table S1. DSC data of PEG-*co*-PGPgE copolymer and PGPgE homopolymer before and after CuAAC with mannopyranosyl azide.

GPgE / mol%	Functionalization	T_g / °C	T_m / °C	ΔH/J·g^{-1}
2.0	---	-52	52	126
2.0	mannopyranosyl azide	-34	51	109
3.7	---	-51	50	106
3.7	mannopyranosyl azide	-27	48	76
100	---	-39	---	---
100	mannopyranosyl azide	35		

References

[1] G. R. Fulmer, A. J. M. Miller, N. H. Sherden, H. E. Gottlieb, A. Nudelman, B. M. Stoltz, J.E. Bercaw and K. I. Goldberg, *Organometallics*, 2010, **29**, 2176–2179.

[2] J. Herzberger, D. Leibig, J. C. Liermann and H. Frey, *ACS Macro Lett.*, 2016, **5**, 1206-1211.

[3] J. Herzberger and H. Frey, *Macromolecules*, 2015, **48**, 8144–8153.

[4] C. Osterwinter, C. Schubert, C. Tonhauser, D. Wilms, H. Frey and C. Friedrich, *Macromolecules*, 2015, **48**, 119–130.

[5] V. Percec, P. Leowanawat, H.-J. Sun, O. Kulikov, C. D. Nusbaum, T. M. Tran, A. Bertin, D. A. Wilson, M. Peterca, S. Zhang, N. P. Kamat, K. Vargo, D. Moock, E. D. Johnston, D. A. Hammer, D. J. Pochan, Y. Chen, Y. M. Chabre, T. C. Shiao, M. Bergeron-Brlek, S. André, R. Roy, H.-J. Gabius and P. A. Heiney, *J. Am. Chem. Soc.*, 2013, **135**, 9055–9077.

[6] C. Schüll, T. Gieshoff and H. Frey, *Polym. Chem.*, 2013, **4**, 4730–4736.

[7] B. S. Beckingham, G. E. Sanoja and N. A. Lynd, *Macromolecules*, 2015, **48**, 6922–6930.

[8] a) F. Heatley, G. Yu, C. Booth and T. G. Blease, *Eur. Polym. J.*, 1991, **27**, 573–579; b) T. Hamaide, A. Goux, M.-F. Llauro, R. Spitz and A. Guyot, *Angew. Makromol. Chemie*, 1996, **237**, 55–77; c) J. Herzberger, K. Fischer, D. Leibig, M. Bros, R. Thiermann and H. Frey, *J. Am. Chem. Soc.*, 2016, **138**, 9212–9223;

5 Monomer Distribution in Polyether Copolymers

5.1 Conventional Oxyanionic versus Monomer-Activated Anionic Copolymerization of Ethylene Oxide with Glycidyl Ethers: Striking Differences in Reactivity Ratios

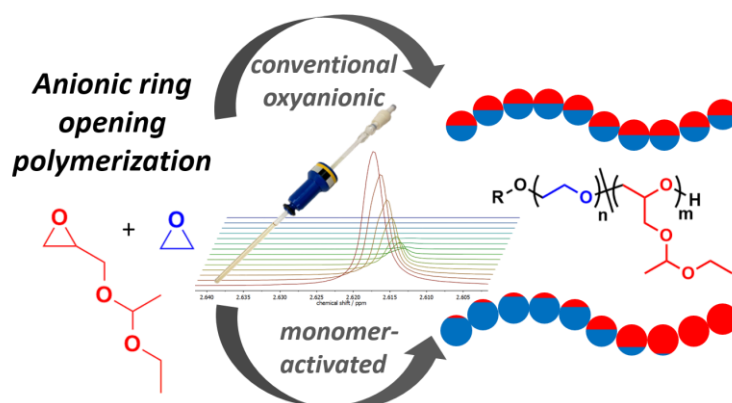*Jana Herzberger,[1,2,‡] Daniel Leibig,[1,2,‡] Johannes C. Liermann,[1] and Holger Frey[1,2]**

[1] Institute of Organic Chemistry, Johannes Gutenberg University Mainz, Duesbergweg 10-14, D-55128 Mainz, Germany

[2] Graduate School Materials Science in Mainz, Staudingerweg 9, D-55128 Mainz, Germany

*E-mail: hfrey@uni-mainz.de

[‡] These authors have contributed equally to this work.

5.1.1 Abstract

Detailed understanding of the monomer distribution in copolymers is essential to tailor their properties. For the first time, we have been able to utilize *in situ* ^{1}H NMR spectroscopy to monitor the monomer-activated anionic ring opening copolymerization (AROP) of ethylene oxide (EO) with a glycidyl ether comonomer, namely ethoxy ethyl glycidyl ether (EEGE). We determine reactivity ratios and draw a direct comparison to conventional oxyanionic ROP. Surprisingly, the respective monomer reactivities differ strongly between the different types of AROP. Under conventional oxyanionic conditions similar monomer reactivities of EO and EEGE are observed, leading to random structures ($r_{EO} = 1.05 \pm 0.02$, $r_{EEGE} = 0.94 \pm 0.02$). Addition of a cation complexing agent (18-crown-6) showed no influence on the relative reactivity of EO and EEGE ($r_{EO} = r_{EEGE} = 1.00 \pm 0.02$). In striking contrast, monomer-activated AROP produces very different monomer reactivities, affording strongly tapered copolymer structures ($r_{EO} = 8.00 \pm 0.16$, $r_{EEGE} = 0.125 \pm 0.003$). These results highlight the importance of understanding reactivity ratios of comonomer pairs under certain polymerization conditions, at the same time demonstrating the ability to generate both random and strongly tapered P(EO-*co*-EEGE) polyethers by simple one-pot statistical anionic copolymerization. These observations may be generally valid for the copolymerization of EO and glycidyl ethers.

5.1.2 Introduction

Glycidyl ethers are one of the most common epoxide monomer classes for copolymerization with ethylene oxide (EO) to prepare multifunctional poly(ethyelene glycol)s (PEGs).[1–9] Such structures are promising for a variety of biomedical and pharmaceutical purposes,[3, 10–12] due to their biocompatibility and water-solubility and have also gained attention as potential polymer electrolytes for lithium ion batteries.[13, 14] In general, their properties strongly depend on the monomer composition profile in the copolymer chain. For example, solubility behavior in aqueous solution differs for random or block-type structures. While random copolymers often form large thermoresponsive aggregates in the micrometer range, block copolymers can self-assemble into defined micelles.[9] In this context, understanding the distribution of functional groups along the PEG chain is highly relevant. Unfortunately, determining the reactivity ratios of these systems is challenging due to the toxicity and volatility of EO. Post-polymerization analysis techniques such as ^{13}C triad analysis often provide first insight into the monomer distribution, but determining precise reactivity ratios is commonly tedious.[15] Alternatively, *in situ* monitoring of the copolymerization is instrumental, which can be conducted via IR[16–19], Raman,[20, 21] UV[22, 23] and NMR spectroscopy. Our group previously reported *in situ* ^{1}H NMR kinetic studies of anionic ring opening polymerization (AROP) of epoxides in vacuum sealed NMR tubes, with the main advantage of the technique being noninvasive.[24] Since then, this technique has been employed to monitor the monomer conversion of a variety of copolymerizations,[25–28] including the highly sensitive carbanionic living copolymerization.[29, 30]

Statistical copolymerization can lead to random, gradient, tapered or block copolymers, predefined by the reactivity of the respective comonomers and growing chain ends under

the given polymerization conditions.[31] For copolymerization of EO with glycidyl ethers, the use of conventional anionic ring opening copolymerization (AROP) initiated with alkoxides leads to random structures with reactivity ratios close to r = 1.[32] Interestingly, bulky substituents generally show only little or no influence on the reactivity ratios of glycidyl ethers.[7, 33, 34]

As an alternative route, the monomer-activated AROP introduced by Carlotti and Deffieux has gained much attention for the preparation of high molecular weight polyethers from glycidyl ether monomers.[35] In contrast to conventional oxyanionic ROP, transfer to monomer is suppressed due to mild polymerization conditions. In particular, the epoxide ring is activated via coordination to a Lewis acid (trialkylaluminum compound), the initiating species is a weak nucleophile (e.g. tetraoctylammonium bromide/ trialkylaluminum complex), and polymerization proceeds at low temperatures in hydrocarbon solvents (Scheme 1, left). Yet, while EO/glycidyl ether systems are well-studied under conventional AROP conditions, little is known about their relative reactivity using monomer-activated AROP.[36] Currently, researchers use both methods interchangeably without considering different results concerning the monomer distribution in the copolymers. Consequently, the question arises whether different polymerization conditions (conventional oxyanionic vs. monomer activation) influence the relative reactivity of EO and glycidyl ethers, thus leading to polyethers with different monomer compositional profiles.

Motivated by this fundamental question, we have utilized *in situ* ^{1}H NMR spectroscopy to compare the kinetics of the statistical copolymerization of EO with ethoxy ethyl glycidyl ether (EEGE) under (i) monomer-activated AROP (Scheme 1, left) and (ii) conventional oxyanionic ROP (Scheme 1, right) conditions. Both measurements were conducted in vacuum-sealed NMR tubes, applying noninvasive ^{1}H NMR spectroscopy. In particular,

EEGE was chosen as a model glycidyl ether, since it is a well-established monomer for AROP.[37] For the activated monomer technique, we employed a specific temperature program (0-25 °C) to monitor the reaction, as it is commonly conducted (initiation at low temperature and slowly reaching room temperature with proceeding polymerization). Note that toluene was chosen as a common solvent for the monomer-activated AROP, while DMSO was applied for the oxyanionic ROP to ensure good solvation of the active chain end.
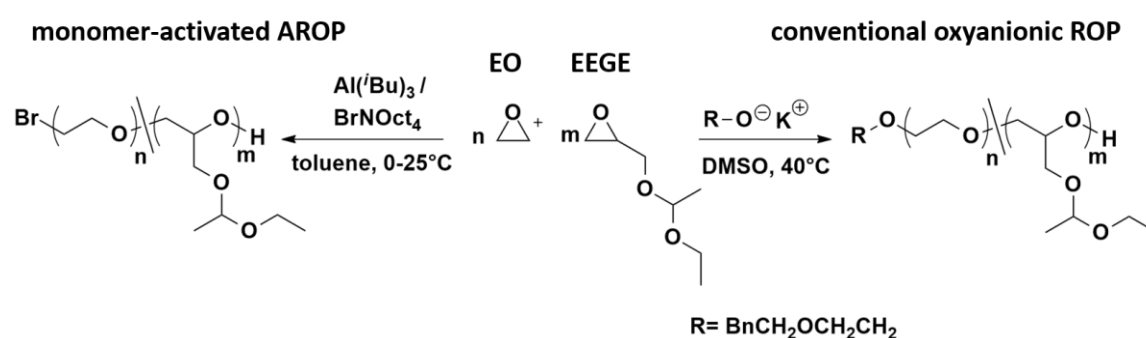
Scheme 1. Anionic ring opening copolymerization (AROP) of EO and EEGE under monomer-activated (left) and conventional oxyanionic ROP conditions (right).

The AROP of EEGE starting from an alkali metal alkoxide initiator was first reported by Taton et al.[38] and since then, has attracted increased attention.[37, 39-41] Statistical copolymerization of EEGE with EO gives access to hydroxyl-functional PEGs after release of the protecting group of EEGE.[1, 2, 4] Such copolymers are not only valuable due to their increased hydrophilicity, but the additional hydroxyl groups render them suitable precursors for post-polymerization modification.[3, 10, 42] Consequently, knowing the monomer composition profile of P(EO-*co*-EEGE) copolymers is crucial for their future applications as "multifunctional PEG".

5.1.3 Results and Discussion

Conventional oxyanionic ring opening polymerization. In 2008, Huang and co-workers studied the copolymerization of EEGE with EO under conventional AROP conditions (potassium salt of triethylene glycol in THF/DMSO) and reported reactivity ratios of $r_{EO} = 1.20$ and $r_{EEGE} = 0.76$, determined by the YBR method.[2] Note that the reactivity ratios r, are defined as $r_{EO} = k_{EO,EO}/k_{EO,EEGE}$ and $r_{EEGE} = k_{EEGE,EEGE}/k_{EEGE,EO}$ with k being the respective rate constant.[31] As expected, an almost random copolymer structure was obtained. For a comprehensive study we have reinvestigated the statistical copolymerization of EO/EEGE under conventional oxyanionic conditions by *in situ* ^{1}H NMR kinetics. With this approach misinterpretation due to different analytical methods or calculation models can be excluded, and the results can be directly compared to the monomer-activated approach. Real-time ^{1}H NMR studies of the statistical copolymerization of EO and EEGE under conventional AROP conditions were performed in analogy to other EO/glycidyl ether systems.[9] Copolymerization was initiated with potassium 2-(benzyloxy)ethoxide and conducted in DMSO-d_6 at 40 °C. Monomer conversion was monitored over time by integrating the respective ring proton signals (EO, $\delta = 2.62$ ppm, s, 4H; EEGE, $\delta = 2.73$ ppm, ddd, 1H). With proceeding polymerization, monomer signals decrease, while broad backbone signals emerge at 3.40-3.66 ppm (see Figure S1).
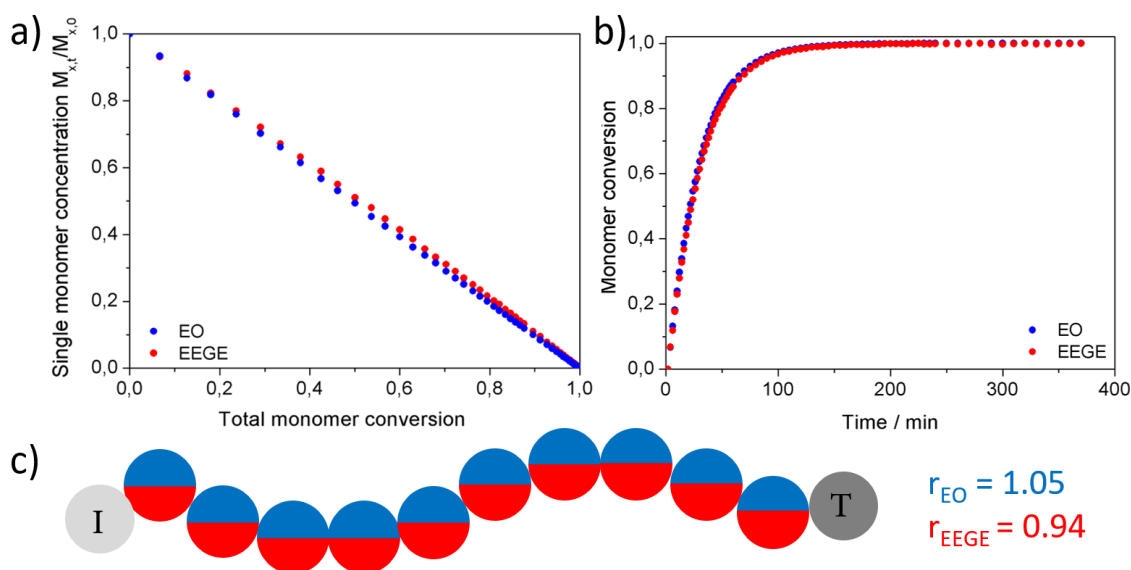
Figure 1. a) Single monomer concentration plotted versus total monomer conversion for the oxyanionic copolymerization. b) Monomer conversion versus time. c) Illustration of the monomer distribution of a P(EO-*co*-EEGE) copolymer consisting of 50 mol% EO and EEGE. Here, "I" denotes the initiator and "T" implies the terminus of the chains formed.

From *in situ* NMR data, Figure 1a and b were generated (see Supporting Information for details regarding data analysis). Slightly faster incorporation of EO into the polymer chain is detected (Figure 1a) and full conversion is reached for both monomers at 40 °C after 6 h (Figure 1b). Note, first-order time conversion plots confirm the absence of termination events and are depicted in Figure S2. To quantify this data, we calculated reactivity ratios according to the nonterminal model of chain copolymerization, recently introduced by Lynd and co-workers (Figure S3).[26] From our *in situ* data we obtain reactivity ratios of $r_{EO} = 1.05 \pm 0.02$ and $r_{EEGE} = 0.94 \pm 0.02$, which are in accordance with reported literature values ($r_{EO} = 1.20 \pm 0.01$ and $r_{EEGE} = 0.76 \pm 0.02$),[2] reflecting a random copolymerization. The reactivity ratios are visualized in Figure 1c, showing a hypothetical P(EO-*co*-EEGE) copolymer model with a 1:1 comonomer ratio. It should be mentioned that slight deviations from the reported reactivity ratios are likely due to different solvents (THF vs. DMSO) or metal counterions (potassium vs. cesium) and can vary marginally with the employed

calculation method or sample preparation (Kelen Tüdos,[43] Fineman-Ross,[44] Skeist[45] and others), but are within the same range.[15, 46]

In general, steric and electronic properties have to be considered when evaluating the reactivity of monomers in copolymerizations. Regarding steric properties, similar reactivity of EEGE and EO seems counterintuitive, since one would expect the ring opening of EEGE to be sterically hindered, in analogy to propylene oxide.[15] However, it is well-known that coordination of the counterion (potassium in this case) to the epoxide ring activates C-O bond cleavage[47–50], which should be facilitated for EEGE due to its additional oxygen atoms. In this context, DFT calculations of analogous glycidyl ethers revealed lower transition state energies for the attachment of the glycidyl ether to the growing chain end due to (i) better complexation of the potassium counterion and (ii) increased Lewis basicity of the epoxide ring compared to EO.[6] Consequently, we believe that both reasons account for the high reactivity of EEGE under conventional AROP conditions. In this context, we were further interested in understanding the influence of a cation complexing agent (here 18-crown-6) on the respective comonomer reactivities. It is known that in the copolymerization of EO and PO the addition of 18-crown-6 shows no impact on the respective reactivity ratios.[51] However, complexation of the potassium cation by 18-crown-6 may influence the reactivity of EEGE. Therefore, analogous *in situ* NMR measurements with addition of 18-crown-6 (2 equiv per equiv potassium) were conducted. No significant impact on the relative reactivity ratios was observed. This data is shown in the Supporting Information (Figure S5-S9). Reactivity ratios of $r_{EO} = r_{EEGE} = 1.00 \pm 0.02$ indicate ideally random copolymerization behavior. We assume that the large amount of EEGE monomer competes with the crown-ether regarding the coordination to the potassium counterion, and additional crown-ether therefore does not influence the relative reactivity of both monomers.

Monomer-activated AROP. Carlotti, Deffieux and co-workers introduced an alternative polymerization technique to conventional oxyanionic ROP, which is the so-called monomer-activated AROP.[52] In contrast to conventional AROP conditions, weak nucleophiles (e.g. tetraoctylammonium bromide/triisobutylaluminum (TIBAL) complex) are employed as the initiator. Together with an activation of the epoxide by a Lewis acid (TIBAL), this allows for copolymerization at low temperatures in hydrocarbon solvents.[53] A mechanistic overview is shown in Scheme 2. As a consequence of the mild polymerization conditions, transfer to monomer is suppressed and the monomer-activated approach has become a well-established alternative to generate particularly high molecular weight polyether homo- and copolymers.[36, 52]
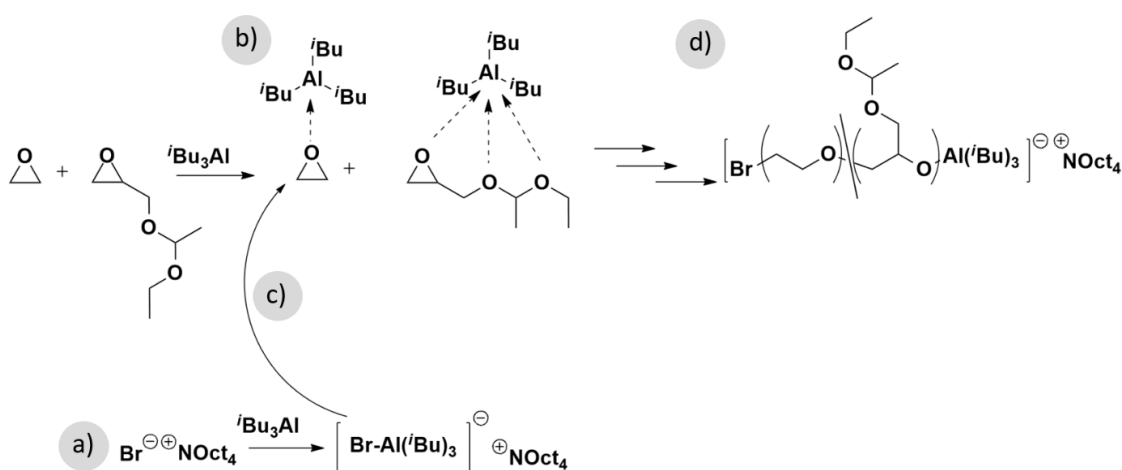
Scheme 2. Mechanism of the monomer-activated AROP of EO and EEGE: a) formation of initiating 'ate' complex; b) activation of monomers via complexation to TIBAL; c) initiation of copolymerization. d) propagation via growing 'ate' center.[36]

Carlotti, Deffieux and co-workers briefly mentioned reactivity ratios for PO systems, e.g. for the PO/EEGE comonomer pair of $r_{PO} = 3.58$ and $r_{EEGE} = 0.18$.[36] Interestingly, our group assessed a higher reactivity of EEGE under conventional oxyanionic conditions (DMSO, 40 °C, potassium alkoxide initiator).[54] Unfortunately, reactivity ratios of this system were not calculated. However, these results suggest inverted reactivities for the same comonomer pair, when copolymerized under conventional or monomer-activated AROP. To study the

copolymerization of EO/EEGE under monomer-activated conditions, we implemented a temperature program to monitor copolymerization *in situ* in a NMR tube. First, we assessed a suitable polymerization temperature, at which initiation takes place. Reported initiation temperatures range from -30 to 0 °C and the reaction is allowed to slowly reach room temperature while the polymerization proceeds.[36, 53] Interestingly, at reaction temperatures below 0 °C no significant monomer conversion was detected via NMR. While we assume, that a lack of stirring slows down the reaction, it is important that no significant polymerization takes place at temperatures below 0 °C (catalyst/initiator ratio = 5). Consequently, copolymerization measurements were started at 0 °C and ramped up in steps of 5 °C per hour (See Supporting Information for temperature profile and details on sample preparation). In a separate experiment, we monitored EEGE in toluene-d_8 at different temperatures (-10 °C to 20 °C) with and without added TIBAL to assess temperature-induced differences of the thermodynamic stability of the EEGE-TIBAL complex. As expected, the oxirane protons show a clear shift to low field, when EEGE is complexed. However, this shift remains constant with temperature and indicates steady behavior (Table S1).

Figure S10 displays a selection of the collected ^{1}H NMR data during copolymerization. As expected, the proton resonances shift with each temperature step. From the respective proton integrals, the monomer conversion was calculated, as plotted in Figure 2a and b. Full conversion was reached after 3.5 hours at 10 °C and the measurement was stopped. A high catalyst/initiator ratio was chosen (5 equiv), to ensure fast copolymerization and full conversion without the need for stirring. First-order time-conversion plots (Figure S11) confirm the absence of termination reactions. From Figure S12, we calculated the respective, strongly disparate reactivity ratios $r_{EO} = 8.00 \pm 0.16$ and $r_{EEGE} = 0.125 \pm 0.003$. These ratios reflect a strongly tapered polymer structure with EO rich segments at the

initiator and EEGE rich segments close to the terminus. The reactivity ratios are schematically illustrated in Figure 2c, which depicts the monomer gradient in a P(EO-*co*-EEGE) copolymer with 50 mol% EO and EEGE.
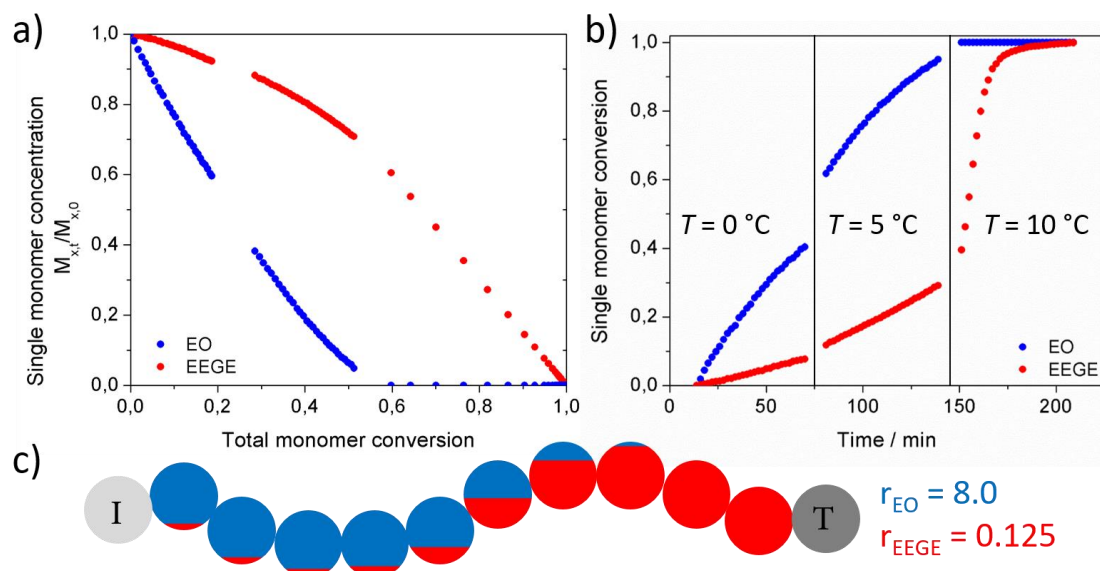

Figure 2. a) Single monomer concentration plotted versus total monomer conversion applying the monomer-activated AROP b) Respective monomer conversion plotted versus time. Note that no data is collected during temperature change. c) Illustration of the monomer distribution of a P(EO-*co*-EEGE) copolymer consisting of 50 mol% EO and EEGE "I" denotes initiator and "T" implies the terminus.

Intriguingly, the obtained reactivity ratios differ strongly from those obtained via conventional oxyanionic ROP, the incorporation of EO being strongly preferred over EEGE. First, it should be mentioned that toluene serves as solvent in the monomer-activated AROP (versus DMSO), which will have an impact on the reactivity ratios, as known for other ionic polymerizations.[55] Further electronic effects have to be considered. EEGE possesses three oxygen atoms, which can interact with the Lewis acid. In contrast, EO only exhibits one oxygen atom, and activation of the oxirane ring might be increased compared to EEGE. Yet, while we suggest that electronic properties are the reason for the high reactivity of glycidyl ethers under conventional oxyanionic ROP conditions, steric

hindrance gains importance for the low reactivity of EEGE in the monomer-activated AROP.

In the monomer-activated AROP, the growing center consists of an "ate"-complex composed of an alkoxide chain end that interacts with a Lewis acid and the bulky organic tetra(n-octyl)ammonium counterion (Scheme 2). In addition, the monomer is activated via coordination to the Lewis acid (TIBAL) and therefore its attachment to the bulky active chain end is sterically impeded. Previous works showed a pronounced retardation of the reaction of PO in an EO/PO system when copolymerized under monomer-activated conditions.[53] In analogy, a gradient structure was reported for the copolymerization of EO with glycidyl methyl ether (GME) under monomer-activated conditions.[56] Although no reactivity ratios were determined, ^{13}C triad analysis and thermal properties in bulk suggested a gradient like structure. In general, the incorporation of glycidyl ether units into the PEG backbone impedes ordering of PEG chains and the degree of crystallization is lowered or fully suppressed. In particular, the authors report a melting temperature around 17 °C for a P(EO-co-GME) copolymer with 55 mol% GME and a molecular weight of 15,000 g·mol^{-1}, indicating the existence of pronounced PEG segments. For comparison, commercially available methoxyPEG with a molecular weight of 550 g·mol^{-1} possesses a melting temperature of 12.5 °C, which increases to 37.5 °C for mPEG-1100[56] and reaches 66 °C for high molecular weight PEGs.[57]

To study the consequences of the tapered structure for the bulk thermal properties we synthesized P(EO-co-EEGE) copolymers with two different comonomer compositions via monomer-activated AROP (Table S2, Figure S14). Both copolymers (48 mol% and 33 mol% EEGE and M_n in the range of 15,100-19,800 g·mol^{-1}) show melting endotherms for PEG segments at temperatures of 13 °C and 22 °C, respectively. For the conventional anionic copolymerization Mangold et al. showed that more than 23 mol% EEGE units lead

to fully amorphous materials.[4] For completeness, block copolymers of polyethylene oxide-*b*-linear polyglycerol (PEO-*b*-*lin*PG) show melting temperatures of 43 °C (PEO$_{45}$-*b*-*lin*PG$_{34}$) and 54 °C (PEO$_{113}$-*lin*PG$_{13}$).[58] Overall, a strong influence of EEGE on the thermal properties of P(EO-*co*-EEGE) is reported for copolymers prepared via conventional oxyanionic ROP, while the monomer-activated AROP still leads to semi-crystalline material despite high EEGE content (~50 mol%). These findings reflect that copolymerization via monomer-activation produces tapered structures and long PEG segments are formed that can crystallize.

5.1.4 Conclusion

In conclusion, real-time ^{1}H NMR kinetic studies of the statistical anionic ring opening copolymerization (AROP) of EEGE with EO reveals that P(EO-*co*-EEGE) copolymers with strikingly different monomer distributions are obtained, depending on the copolymerization conditions. In particular, the conventional oxyanionic approach leads to random copolymers ($r_{EO} = 1.05 \pm 0.02$, $r_{EEGE} = 0.94 \pm 0.02$), while activation by a Lewis acid and the use of a bulky counterion drastically lower the reactivity of EEGE, leading to strongly tapered structures ($r_{EO} = 8.00 \pm 0.16$ and $r_{EEGE} = 0.125 \pm 0.003$). Consequently, choice of the initiator system enables tailoring of the monomer distribution in glycidyl ether-based polyethers, while still maintaining the living character of AROP. In particular, P(EO-*co*-EEGE) copolymers with block-like structures and high molecular weights are accessible, which are inaccessible via oxyanionic ROP due to molecular weight limiting monomer transfer reactions. We believe that these observations are not only limited to EEGE, but are rather general for glycidyl ethers, offering enormous potential for polyether-based gradient copolymer structures.

5.1.5 Acknowledgements

5.1.6 References

[1] Dimitrov, P.; Hasan, E.; Rangelov, S.; Trzebicka, B.; Dworak, A.; Tsvetanov, C. B. High Molecular Weight Functionalized Poly(ethylene oxide). *Polymer.* **2002**, *43*, 7171–7178.

[2] Pang, X.; Jing, R.; Huang, J. Synthesis of Amphiphilic Macrocyclic Graft Copolymer Consisting of a Poly(ethylene oxide) Ring and Multi-poly(ε-caprolactone) Lateral Chains. *Polymer.* **2008**, *49*, 893–900.

[3] Li, Z.; Chau, Y. Synthesis of Linear Polyether Polyol Derivatives as New Materials for Bioconjugation. *Bioconjugate Chem.* **2009**, *20*, 780–789.

[4] Mangold, C.; Wurm, F.; Obermeier, B.; Frey, H. Hetero-Multifunctional Poly(ethylene glycol) Copolymers with Multiple Hydroxyl Groups and a Single Terminal Functionality. *Macromol. Rapid Commun.* **2010**, *31*, 258–264.

[5] Obermeier, B.; Frey, H. Poly(ethylene glycol-*co*-allyl glycidyl ether)s: A PEG-Based Modular Synthetic Platform for Multiple Bioconjugation. *Bioconjugate Chem.* **2011**, *22*, 436–444.

[6] Lee, B. F.; Wolffs, M.; Delaney, K. T.; Sprafke, J. K.; Leibfarth, F. A.; Hawker, C. J.; Lynd, N. A. Reactivity Ratios and Mechanistic Insight for Anionic Ring-Opening Copolymerization of Epoxides. *Macromolecules.* **2012**, *45*, 3722–3731.

[7] Lee, A.; Lundberg, P.; Klinger, D.; Lee, B. F.; Hawker, C. J.; Lynd, N. A. Physiologically relevant, pH-Responsive PEG-based Block and Statistical Copolymers with *N,N*-diisopropylamine Units, *Polym. Chem.* **2013**, 5735–5742.

[8] Mattson, K. M.; Latimer, A. A.; McGrath, A. J.; Lynd, N. A.; Lundberg, P.; Hudson, Z. M.; Hawker, C. J. A facile Synthesis of Catechol-functionalized Poly(ethylene oxide) Block and Random Copolymers. *J. Polym. Sci. A Polym. Chem.* **2015**, *53*, 2685-2692.

[9] Herzberger, J.; Fischer, K.; Leibig, D.; Bros, M.; Thiermann, R.; Frey, H. Oxidation-Responsive and "Clickable" Poly(ethylene glycol) via Copolymerization of 2-(Methylthio)ethyl Glycidyl Ether, *J. Am. Chem. Soc.* **2016**, *138*, 9212–9223.

[10] Zhou, P.; Li, Z.; Chau, Y. Synthesis, Characterization, and In Vivo Evaluation of Poly(ethylene oxide-*co*-glycidol)-Platinate Conjugate. *Eur. J. Pharm. Sci.* **2010**, *41*, 464–472.

[11] Sakae, M.; Ito, T.; Yoshihara, C.; Iida-Tanaka, N.; Yanagie, H.; Eriguchi, M.; Koyama, Y. Highly Efficient In Vivo Gene Transfection by Plasmid/PEI Complexes

coated by Anionic 5PEG6 Derivatives Bearing Carboxyl Groups and 5RGD6 Peptide. *Biomed. Pharmacother.* **2008**, *62*, 448–453.

[12]   Obermeier, B.; Wurm, F.; Mangold, C.; Frey, H. Multifunctional Poly(ethylene glycol)s. *Angew. Chem. Int. Ed.* **2011**, *50*, 7988–7997.

[13]   Matoba, Y.; Matsui, S.; Tabuchi, M.; Sakai, T. Electrochemical Properties of Composite Polymer Electrolyte Applied to Rechargeable Lithium Polymer Battery. *J. Power Sources.* **2004**, *137*, 284–287.

[14]   Barteau, K. P.; Wolffs, M.; Lynd, N. A.; Fredrickson, G. H.; Kramer, E. J.; Hawker, C. J. Allyl Glycidyl Ether-Based Polymer Electrolytes for Room Temperature Lithium Batteries. *Macromolecules.* **2013**, *46*, 8988–8994.

[15]   Heatley, F.; Yu, G.; Booth, C.; Blease, T. G. Determination of Reactivity Ratios for the Anionic Copolymerization of Ethylene Oxide and Propylene Oxide in Bulk, *Eur. Polym. J.* **1991**, *27*, 573–579.

[16]   Long, T. E.; Liu, H. Y.; Schell, B. A.; Teegarden, D. M.; Uerz, D. S. Determination of Solution Polymerization Kinetics by Near-Infrared Spectroscopy. Living Anionic Polymerization Processes. *Macromolecules.* **1993**, *26*, 6237–6242.

[17] Pasquale, A. J.; Long, T. E. Real-Time Monitoring of the Stable Free Radical Polymerization of Styrene via in-Situ Mid-Infrared Spectroscopy. *Macromolecules.* **1999**, *32*, 7954–7957.

[18]   Fontoura, J. M. R.; Santos, A. F.; Silva, F. M.; Lenzi, M. K.; Lima, E. L.; Pinto, J. C. Monitoring and Control of Styrene Solution Polymerization using NIR Spectroscopy. *J. Appl. Polym. Sci.* **2003**, *90*, 1273–1289.

[19]   Shaikh, S.; Puskas, J. E.; Kaszas, G. A New High-throughput Approach to Measure Copolymerization Reactivity Ratios Using Real-time FTIR Monitoring. *J. Polym. Sci. Part A: Polym. Chem.* **2004**, *42*, 4084–4100.

[20]   Wang, C.; Vickers, T. J.; Schlenoff, J. B.; Mann, C. K. *In Situ* Monitoring of Emulsion Polymerization Using Fiber-Optic Raman Spectroscopy. *Appl spectrosc.* **1992**, *46*, 1729–1731.

[21]   van den Brink, M.; Pepers, M.; van Herk, A. M.; German,A. L. On-Line Monitoring and Composition Control of the Emulsion Copolymerization of VeoVA 9 and Butyl Acrylate by Raman Spectroscopy. *Polym. React. Eng.* **2001**, *9*, 101–133.

[22]   Alb, A. M.; Enohnyaket, P.; Drenski, M. F.; Head, A.; Reed, A. W.; Reed, W. F. Online Monitoring of Copolymerization Involving Comonomers of Similar Spectral Characteristics. *Macromolecules.* **2006**, *39*, 5705–5713.

[23]   Quinebèche, S.; Navarro, C.; Gnanou, Y.; Fontanille, M. In Situ mid-IR and UV–Visible Spectroscopies Applied to the Determination of Kinetic Parameters in the Anionic Copolymerization of Styrene and Isoprene. *Polymer.* **2009**, *50*, 1351–1357.

[24]   Obermeier, B.; Wurm, F.; Frey, H. Amino Functional Poly(ethylene glycol) Copolymers via Protected Amino Glycidol. *Macromolecules.* **2010**, *43*, 2244–2251.

[25]   Zhang, W.; Allgaier, J.; Zorn, R.; Willbold, S. Determination of the Compositional Profile for Tapered Copolymers of Ethylene Oxide and 1,2-Butylene Oxide by In-situ-NMR. *Macromolecules.* **2013**, *46*, 3931–3938.

[26]   Beckingham, B. S.; Sanoja, G. E.; Lynd, N. A. Simple and Accurate Determination of Reactivity Ratios Using a Nonterminal Model of Chain Copolymerization. *Macromolecules.* **2015**, *48*, 6922–6930.

[27]   Rieger, E.; Alkan, A.; Manhart, A.; Wagner, M.; Wurm, F. R. Sequence-Controlled Polymers via Simultaneous Living Anionic Copolymerization of Competing Monomers. *Macromol. Rapid Commun.* **2016**, *37*, 833–839.

[28]   Wu, Z.-c.; Liu, Y.; Wei, W.; Chen, F.-s.; Qiu, G.-x.; Xiong, H.-M., Reaction Kinetics in anionic copolymerization, *Chin J Polym Sci.* **2016**, *34*, 431–438.

[29]   Natalello, A.; Werre, M.; Alkan, A.; Frey, H. Monomer Sequence Distribution Monitoring in Living Carbanionic Copolymerization by Real-Time ^{1}H NMR Spectroscopy. *Macromolecules.* **2013**, *46*, 8467–8471.

[30]   Leibig, D.; Müller, A. H. E.; Frey, H. Anionic Polymerization of Vinylcatechol Derivatives: Reversal of the Monomer Gradient Directed by the Position of the Catechol Moiety in the Copolymerization with Styrene. *Macromolecules.* **2016**, *49*, 4792–4801.

[31]   Mayo, F. R.; Lewis, F. M. Copolymerization. I. A Basis for Comparing the Behavior of Monomers in Copolymerization; The Copolymerization of Styrene and Methyl Methacrylate *J. Am. Chem. Soc.* **1944**, *66*, 1594–1601.

[32]   Herzberger, J.; Niederer, K.; Pohlit, H.; Seiwert, J.; Worm, M.; Wurm, F. R.; Frey, H. Polymerization of Ethylene Oxide, Propylene Oxide, and Other Alkylene Oxides: Synthesis, Novel Polymer Architectures, and Bioconjugation. *Chem. Rev.* **2016**, *116*, 2170–2243.

[33]   Mangold, C.; Wurm, F.; Obermeier, B.; Frey, H. "Functional Poly(ethylene glycol)": PEG-Based Random Copolymers with 1,2-Diol Side Chains and Terminal Amino Functionality. *Macromolecules.* **2010**, *43*, 8511–8518.

[34] Niederer, K.; Schüll, C.; Leibig, D.; Johann, T.; Frey, H. Catechol Acetonide Glycidyl Ether (CAGE): A Functional Epoxide Monomer for Linear and Hyperbranched Multi-Catechol Functional Polyether Architectures. *Macromolecules.* **2016**, *49*, 1655–1665.

[35] Brocas, A.-L.; Mantzaridis, C.; Tunc, D.; Carlotti, S. Polyether synthesis: From Activated or Metal-Free Anionic Ring-Opening Polymerization of Epoxides to Functionalization. *Prog. Polym. Sci.* **2013**, 845–873.

[36] Gervais, M.; Brocas, A.-L.; Cendejas, G.; Deffieux, A.; Carlotti, S. Synthesis of Linear High Molar Mass Glycidol-Based Polymers by Monomer-Activated Anionic Polymerization. *Macromolecules.* **2010**, *43*, 1778–1784.

[37] Thomas, A.; Müller, S. S.; Frey, H. Beyond Poly(ethylene glycol): Linear Polyglycerol as a Multifunctional Polyether for Biomedical and Pharmaceutical Applications. *Biomacromolecules.* **2014**, *15*, 1935–1954.

[38] Taton, D.; Le Borgne, A.; Sepulchre, M.; Spassky, N. Synthesis of Chiral and Racemic functional Polymers from Glycidol and Thioglycidol. *Macromol. Chem. Phys.* **1994**, *195*, 139–148.

[39] Dworak, A.; Panchev, I.; Trzebicka, B.; Walach, W. Hydrophilic and Amphiphilic Copolymers of 2,3-Epoxypropanol-1. *Macromol. Symp.* **2000**, *153*, 233–242.

[40] Halacheva, S.; Rangelov, S.; Tsvetanov, C. Poly(glycidol)-Based Analogues to Pluronic Block Copolymers. Synthesis and Aqueous Solution Properties. *Macromolecules.* **2006**, *39*, 6845–6852.

[41] Hans, M.; Keul, H.; Möller, M. Chain Transfer Reactions Limit the Molecular Weight of Polyglycidol Prepared via Alkali Metal Based Initiating Systems. *Polymer.* **2009**, *50*, 1103–1108.

[42] Erberich, M.; Keul, H.; Möller, M. Polyglycidols with Two Orthogonal Protective Groups: Preparation, Selective Deprotection, and Functionalization. *Macromolecules.* **2007**, *40*, 3070–3079.

[43] Kelen, T; Tüdos, F. Analysis of the Linear Methods for Determining Copolymerization Reactivity Ratios. I. A New Improved Linear Graphic Method. *J. Macromol. Sci: Part A.* **1975**, *9*, 1–27.

[44] Fineman, M.; Ross, S. D., Linear Method for Determining Monomer Reactivity Ratios in Copolymerization, *J. Polym. Sci.* **1950**, *5*, 259–262.

[45] Irving, S. Copolymerization: the Composition Distribution Curve. *J. Am. Chem. Soc.* **1946**, *68*, 1781–1784.

[46]   Reinicke, S.; Schmelz, J.; Lapp, A.; Karg, M.; Hellweg, T.; Schmalz, H. Smart Hydrogels Based on Double Responsive Triblock Terpolymers. *Soft Matter.* **2009**, *5*, 2648–2657.

[47]   Ponomarenko, V. A.; Khomutov, A. M.; Il'chenko, S. I.; Ignatenko, A. V. The Effect of Substituents of the Anionic Polymerization of α-Oxides. *Polym. Sci. (USSR)* **1971**, *13*, 1735–1740.

[48]   Chang, C. J.; Kiesel, R. F.; Hogen-Esch, T. E. Specific Cation Participation in Alkali-Carbanion Initiated Epoxide Cleavage Reactions. *J. Am. Chem. Soc.* **1973**, *95*, 8446–8448.

[49]   Boileau, S.; Deffieux, A.; Lassalle, D.; Menezes, F.; Vidal, B. Reactivities of Anionic Species for the Ring Opening of Ethylene Oxide. *Tetrahedron Lett.* **1978**, *19*, 1767–1770.

[50]   Harder, S.; van Lenthe, J. H.; van Eikema, H.; Nicolaas J. R.; Schleyer, P. v. R., Nucleophilic Ring Opening of Epoxides by Organolithium Compounds: Ab Initio Mechanisms. *J. Am. Chem. Soc.* **1994**, *116*, 2508–2514.

[51]   Deng, Y.; Ding, J.; Yu, G.; Mobbs, R. H.; Heatley, F.; Price, C.; Booth, C. Preparation and Properties of *Stat*-copoly(oxyethylene-oxypropylene)-*block*-poly (oxyethylene): Use of Crown Ether in the Anionic Copolymerization of Propylene Oxide and Ethylene Oxide. *Polymer.* **1992**, *33*, 1959–1962.

[52]   Labbé, A.; Carlotti, S.; Billouard, C.; Desbois, P.; Deffieux, A. Controlled High-Speed Anionic Polymerization of Propylene Oxide Initiated by Onium Salts in the Presence of Triisobutylaluminum. *Macromolecules.* **2007**, *40*, 7842–7847.

[53]   Rejsek, V.; Sauvanier, D.; Billouard, C.; Desbois, P.; Deffieux, A.; Carlotti, S. Controlled Anionic Homo- and Copolymerization of Ethylene Oxide and Propylene Oxide by Monomer Activation. *Macromolecules.* **2007**, *40*, 6510–6514.

[54]   Schömer, M.; Frey, H. Water-Soluble "Poly(propylene oxide)" by Random Copolymerization of Propylene Oxide with a Protected Glycidol Monomer. *Macromolecules.* **2012**, *45*, 3039–3046.

[55] Yang, M.-H.; Chou, C.; Lin, C.-H., Effect of Solvent and Promoter on the Reactivity Ratios in the Copolymerization of Hexamethylcyclotrisiloxane and Hexaphenylcyclotrisiloxane. *J. Polym. Res*. **1995**, *2*, 197-201.

[56]   Müller, S. S.; Moers, C.; Frey, H. A Challenging Comonomer Pair: Copolymerization of Ethylene Oxide and Glycidyl Methyl Ether to Thermoresponsive Polyethers. *Macromolecules.* **2014**, *47*, 5492–5500.

320

[57]   Mandelkern, L. The Crystallization of Flexible Polymer Molecules, *Chem. Rev.* **1956**, *56*, 903–958.

[58]   Wurm, F.; Nieberle, J.; Frey, H. Double-Hydrophilic Linear-Hyperbranched Block Copolymers Based on Poly(ethylene oxide) and Poly(glycerol). *Macromolecules.* **2008**, *41*, 1184–1188.

5.1.7 Supporting Information

Materials. EO and 18-crown-6 were purchased from Sigma Aldrich. Potassium *tert*-butoxide, 2-(benzyloxy)ethanol and triisobutylaluminum (1.1 M in toluene) were received from Acros Organics. Deuterated solvents (toluene-d_8 and DMSO-d_6) were purchased from Deutero GmbH. Tetra(*n*-octyl)ammonium bromide (TOAB) was received from TCI. Benzene (anhydrous) was purchased from Alfa Aesar. All chemicals were used as received if not otherwise stated. Toluene-d_8 was freshly distilled from CaH_2 before use. EEGE was synthesized as described in literature.[1] For each polymerization, EEGE was dried over CaH_2 and freshly distilled.

Instrumentation. In situ ^{1}H NMR kinetic studies were conducted on a Bruker Avance III HD 400 MHz spectrometer equipped with a 5 mm BBFO SmartProbe. Regular ^{1}H NMR spectra (400 MHz) and ^{13}C NMR spectra (100 MHz) were recorded using a Bruker Avance II HD 400 spectrometer equipped with a 5 mm BBFO SmartProbe (Z-gradient probe) and an ATM as well as a SampleXPress 60 auto sampler. All spectra are referenced internally to residual proton signals of the deuterated solvent. SEC measurements were performed in DMF (containing 0.25 g L^{-1} lithium bromide as additive). An Agilent 1100 Series was used as an integrated instrument, including a PSS HEMA column ($300/100/40 \cdot 10^{-10}$ porosity) as well as a UV (275 nm) and a RI detector. All calibrations were carried out using poly(ethylene glycol) standards purchased from Polymer Standards Service. Differential scanning calorimetry (DSC) measurements were conducted under nitrogen atmosphere using a PerkinElmer DSC 8500 with PerkinElmer CLN2 in the temperature range of – 90 °C to 100 °C, at heating rates of 20 and 10 K·min^{-1} for the first and the second heating run, respectively.

Data analysis: All spectra are referenced internally to residual proton signals of the deuterated solvent. Phase and baseline correction were performed manually for each spectrum. Afterwards, the area under each proton signal was determined and normalized to the starting concentration of the monomer.

Note: Ethylene oxide is a highly toxic gas and precautions must be taken before handling. Addition of ethylene oxide to the NMR tube was conducted via graduate ampoule. However, it is rather difficult to measure such small amounts needed for the copolymerization. Consequently, comonomer ratios and calculated molecular weights can vary with each measurement.

Monomer-activated copolymerization of EO with EEGE. The polymerization was conducted according to literature.[2] For example, TOAB (1 equiv, 60 mg) was added to an anionic flask, dissolved in benzene and freeze-dried overnight. The next day, dry toluene (10 mL) and freshly distilled EEGE (100 equiv, 1.6 mL) were added under argon atmosphere, cooled with liquid nitrogen and vacuum was applied. Subsequently, EO (100 equiv, 0.5 mL) was cryo-transferred into the flask. The flask was cooled with an ice/sodium chloride bath and the required amount of TIBAL (3-5 equiv) was added via gastight syringe. The polymerization was conducted under vacuum for 24 h and terminated with an excess of ethanol. The solvent was removed in vacuum and the mixture was dissolved in methanol and dialyzed for 24 h. Yields were in the range of 80-90 %. P(EO$_{200}$-*co*-EEGE$_{200}$) initiated with 5 equiv TIBAL and terminated after 24 h showed a total conversion of 80 %.

Sample preparation for ^{1}H NMR kinetic studies:

Anionic ring opening copolymerization of EO with EEGE with an alkali metal alkoxide as initiator. 49 mg of potassium *tert*-butoxide (1 equiv) were placed in a Schlenk tube and

5 mL benzene were added, followed by 65 µL 2-(benzyloxy)ethanol (1.05 equiv). The mixture was stirred for 30 min at 60 °C before benzene was removed under vacuum overnight at 40 °C. The next day, the initiator salt was dissolved in 2 mL DMSO-d_6 (solution A). A Norell S-500-VT-7 NMR tube was evacuated and 0.1 mL of solution A were added under argon atmosphere, followed by 0.3 mL DMSO-d_6. The mixture was cooled down with an acetone/dry ice bath and 70 µL EEGE (22 equiv), followed by 0.3 mL DMSO-d_6 were syringed in under argon atmosphere. The mixture was cooled down with liquid nitrogen and evacuated under high vacuum. Subsequently, EO (~40 µL, 40 equiv) was cryotransfered to the NMR tube under static vacuum and the tube was sealed with a Teflon stop-cock. The tube was warmed up to room temperature, shook vigorously to homogenize the solution and placed in a NMR spectrometer with the probe gas flow adjusted to 40 °C. After the temperature in the probehead was stable (~10 min, $\Delta T = 0.1$ K), the first spectrum was recorded. Sample spinning was turned off. Spectra were recorded with 16 scans at 2-minute intervals during the first hour, then at 5-minute intervals for 2 hours, and afterwards with 10-minute intervals.

The P(EO-*co*-EEGE) copolymer isolated from the NMR had an average number molecular weight of $M_n = 4300$ g·mol^{-1} and a PDI of 1.15 (Figure S4).

Anionic ring opening copolymerization of EO with EEGE with an alkali metal alkoxide as initiator and crown ether as complexing agent. A similar procedure was conducted as described above. The initiator solution was prepared as follows: 10.1 mg potassium *tert*-butoxide (0.5 equiv) were placed into a Schlenk tube, followed by 2.5 mL benzene, 25.7 µL 2-(benzyloxy)ethanol (1 equiv) and 47.8 mg 18-crown-6 (1 equiv). The mixture was dried overnight, to obtain the initiator salt. The next day, 1 mL DMSO-d_6 were added. From this solution, 0.2 mL were placed into the NMR tube. Further, 70 µL EEGE (13 equiv) were used and about 20 µL EO (13 equiv). Measurements were conducted at 35 °C.

The P(EO-*co*-EEGE) copolymer isolated from the NMR had an average number molecular weight of $M_n = 2300$ g·mol^{-1} and a PDI of 1.08 (Figure S9).

Monomer-activated anionic ring opening copolymerization of EO with EEGE. 35.45 mg tetra(n-octyl)ammonium bromide (TOAB) was added to a Schlenk flask and freeze-dried with 5 mL benzene overnight. The next day, 0.5 mL dry toluene-d_8 were added to prepare the initiator solution. A Norell S-500-VT-7 NMR tube was evacuated and 0.1 mL of the initiator solution (TOAB, 1 equiv) was added under argon atmosphere, followed by 0.3 mL neat toluene-d_8. The mixture was cooled down with an acetone/dry ice bath and 60 μL TIBAL solution (1.1 M in toluene, 5 equiv) was added via syringe, followed by 0.2 mL toluene-d_8 and 45 μL EEGE (24 equiv) under argon atmosphere. The mixture was cooled down with liquid nitrogen and evacuated under high vacuum. Subsequently, EO (~10 μL, 12 equiv) was cryo-transferred to the NMR tube under static vacuum and the tube was sealed with a Teflon stop-cock and kept at -40 °C. Before the measurement, the tube was shaken vigorously to homogenize the solution and placed in a NMR spectrometer with the probe gas flow adjusted to 0 °C. After the temperature in the probehead was stable (~10 min, $\Delta T = 0.1$ K), the first spectrum was recorded. Sample spinning was turned off. Spectra were recorded with 16 scans at 2 min-intervals. After 1h at 0 °C, the temperature was raised to 5 °C, all other parameters were kept constant. After another hour, the temperature was set to 10 °C. The measurement was stopped after full conversion (3.5 h).

The copolymer isolated from the NMR had an average number molecular weight of $M_n = 4900$ g·mol^{-1} and a PDI of 2.2 (Figure S13).
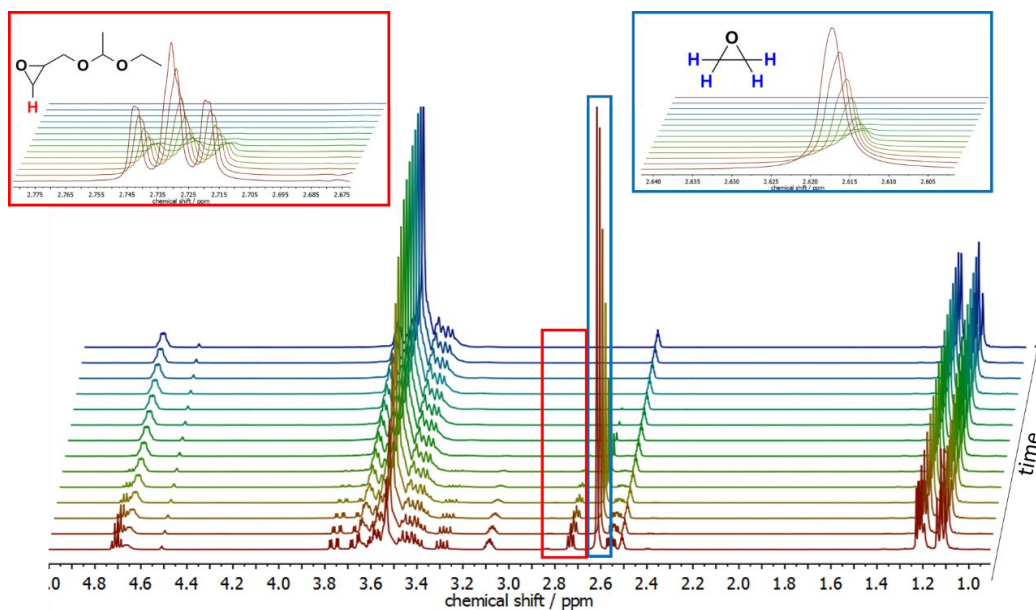
Figure S1. Bottom: Selection of ¹H NMR spectra (400 MHz, DMSO-d_6, 40 °C) recorded during the *in situ* ¹H NMR kinetic studies of the copolymerization of EO (65 mol%) and EEGE (35 mol%) at 40 °C in DMSO-d_6. Top: Enlargement of the respective proton signals used to calculate the monomer conversion (EEGE highlighted in red and EO highlighted in blue).
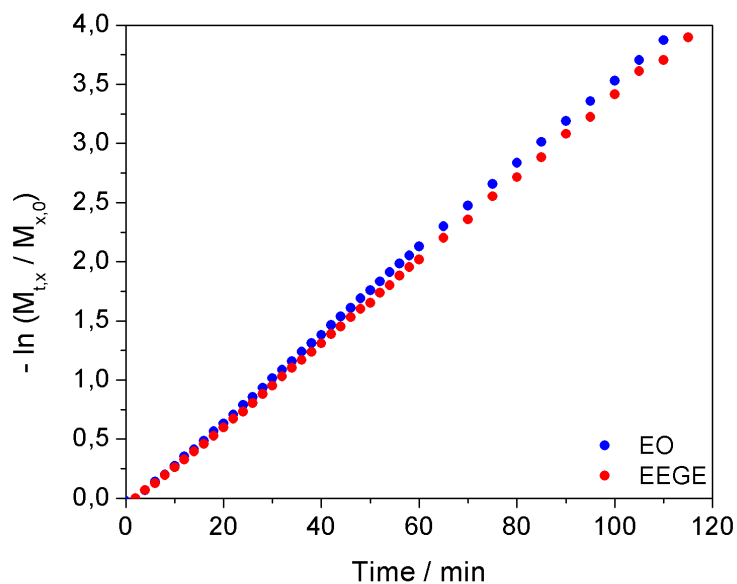

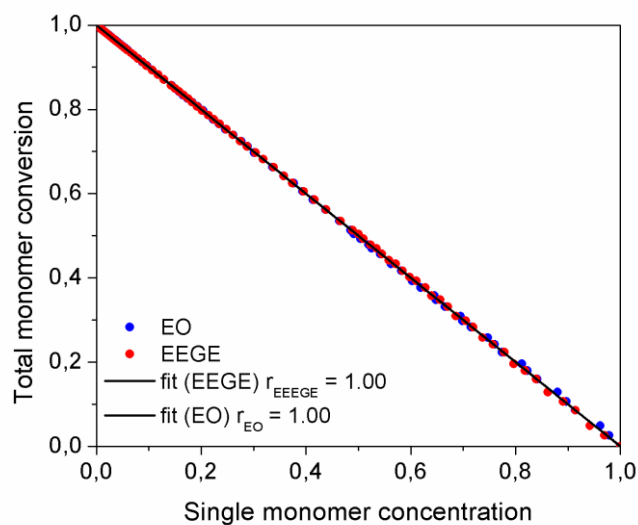**Figure S2.** First-order time-conversion plot for the copolymerization of EO (blue) and EEGE (red) in DMSO-d_6 at 40 °C.
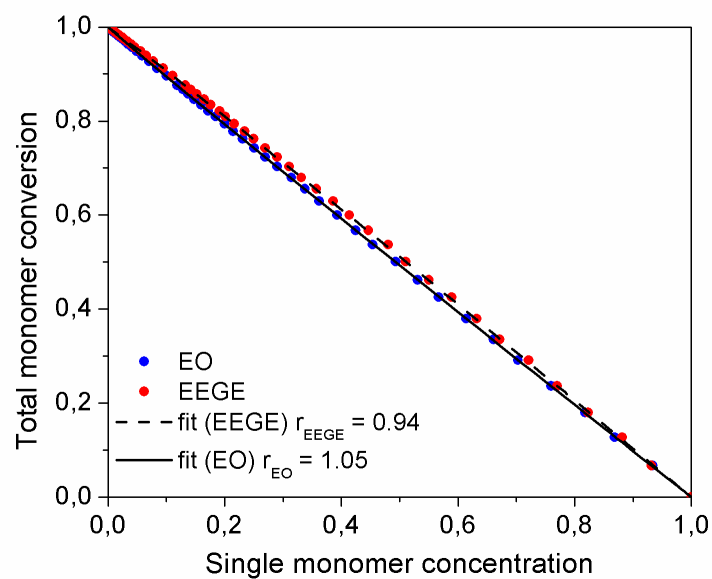
Figure S3. Total monomer conversion plotted as a function of the individual monomer concentration for EO (blue) and EEGE (red) for conventional AROP (potassium 2-(benzyloxy)ethanolate in DMSO-d_6). Reactivity ratios are calculated from the respective fits (EEGE: dashed line, EO: solid line) in analogy to literature.[3]
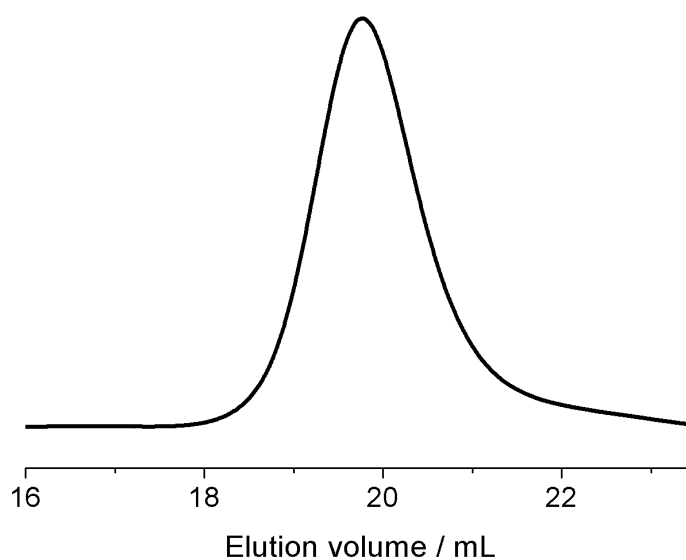
Figure S4. SEC trace (DMF, RI signal, PEG standard) of P(EO-*co*-EEGE) initiated with potassium 2-(benzyloxy)ethanolate in DMSO-d_6.
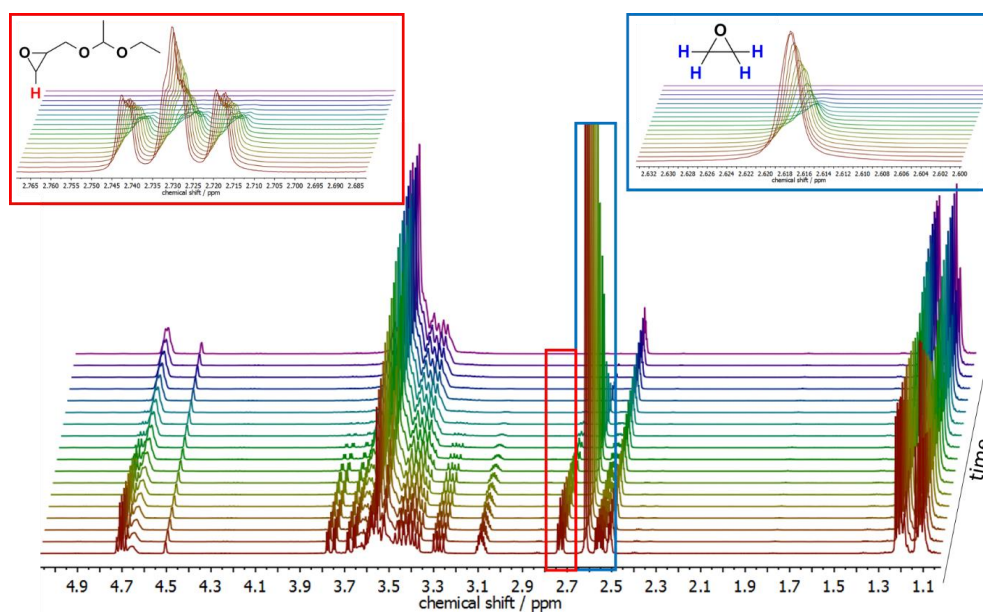
Figure S5. Bottom: Selection of ^{1}H NMR spectra (400 MHz, DMSO-d_6, 35 °C) recorded during the *in situ* NMR kinetic studies of the copolymerization of EO and EEGE at 35 °C in DMSO-d_6 with 18-crown-6 as complexing agent (2 equiv per equiv potassium). Top: Enlargement of the respective proton signals, used to calculate the monomer conversion (EEGE highlighted in red and EO highlighted in blue).
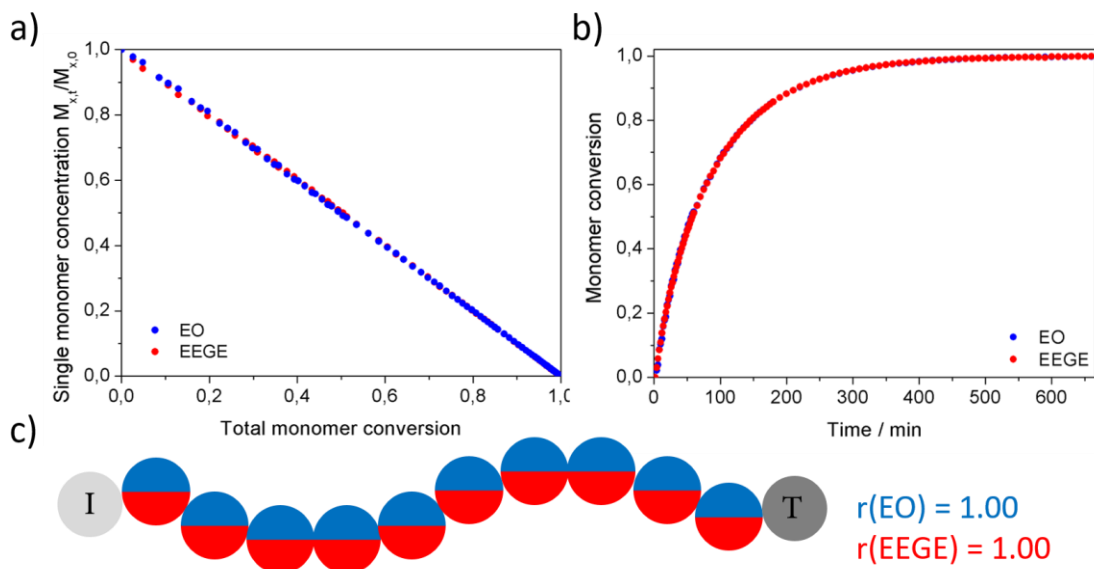
Figure S6. a) Single monomer concentration plotted versus overall monomer conversion for the copolymerization of EO (blue) and EEGE (red) in DMSO-d_6 at 35°C with 18-crown-6 as complexing agent. Mole fractions of n(EO) = 49 mol% and n(EEGE) = 51 mol%. b) Respective monomer conversion plotted versus time. Full conversion was reached after 10 h. c) Illustration of the monomer distribution of a P(EO-*co*-EEGE) copolymer consisting of 50 mol% EO and 50 mol% EEGE with $r_{EO} = 1.00 \pm 0.02$ and $r_{EEGE} = 1.00 \pm 0.02$. "I" denotes initiator and "T" implies the terminus.

Figure S7. Total monomer conversion plotted as a function of the individual monomer concentration for EO (blue) and EEGE (red) (DMSO-d_6 at 35°C, potassium 2-(benzyloxy)ethanolate, 18-crown-6). Reactivity ratios are calculated from the respective fits in analogy to literature.[3]
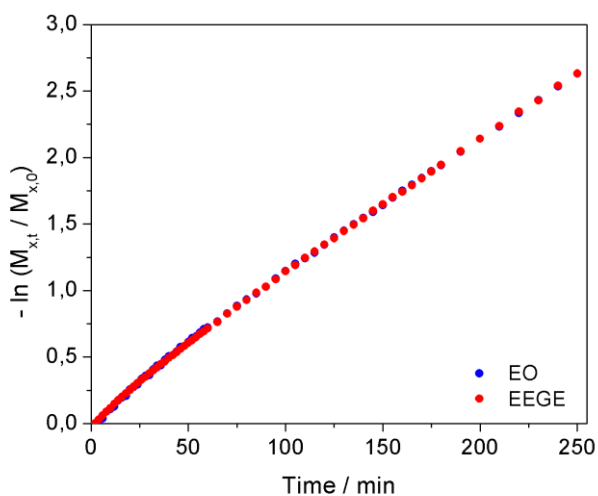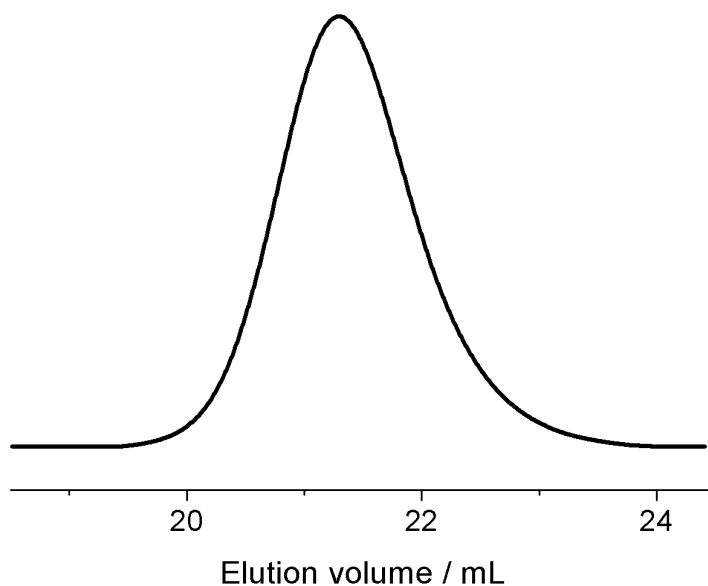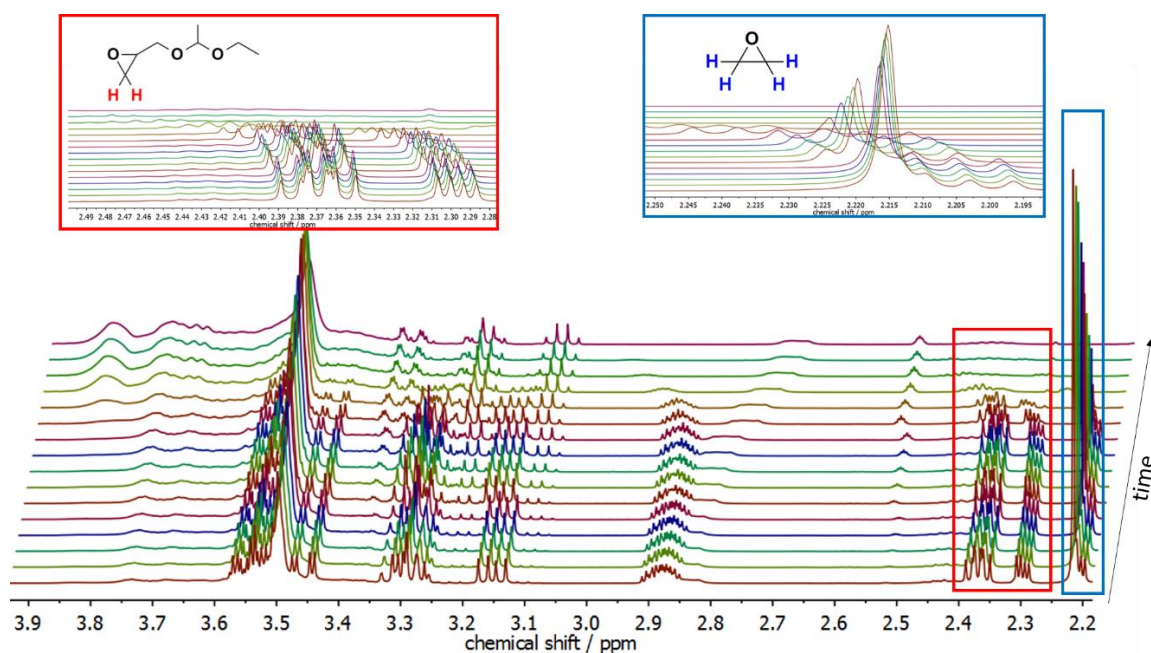

Figure S8. First-order time-conversion plot for the copolymerization of EO (blue) and EEGE (red) in DMSO-d_6 at 35 °C with 18-crown-6 as complexing agent and potassium 2-(benzyloxy)ethanolate as initiator.

Figure S9. SEC trace (DMF, RI signal, PEG standard) of P(EO-*co*-EEGE) initiated with potassium 2-(benzyloxy)ethanolate in the presence of 18-crown-6 in DMSO-*d*₆.

Figure S10. Bottom: Selection of ¹H NMR spectra (400 MHz, toluene-*d*₈, 0 °C, 5 °C, 10 °C) recorded during the *in situ* NMR kinetic studies of the copolymerization of EO (33 mol%) and EEGE (67 mol%) employing the monomer-activated AROP with a catalyst/initiator ratio of 5 equiv. Top: Enlargement of the respective proton signals, used to calculate the monomer conversion (EEGE highlighted in red and EO highlighted in blue). Note, the shift of the proton signals results from the respective temperature changes (0 °C, 5 °C, 10 °C).
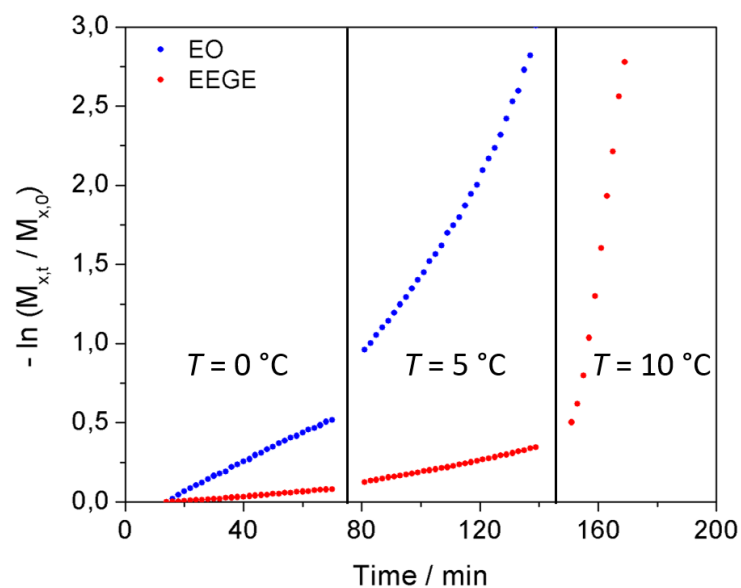
Figure S11. First-order time-conversion plot for the copolymerization of EO (blue) and EEGE (red) in toluene-d_8 employing the monomer-activated AROP. Note that no data was collected during temperature step and that rate constants depend on temperature interval (0 °C, 5 °C and 10 °C).
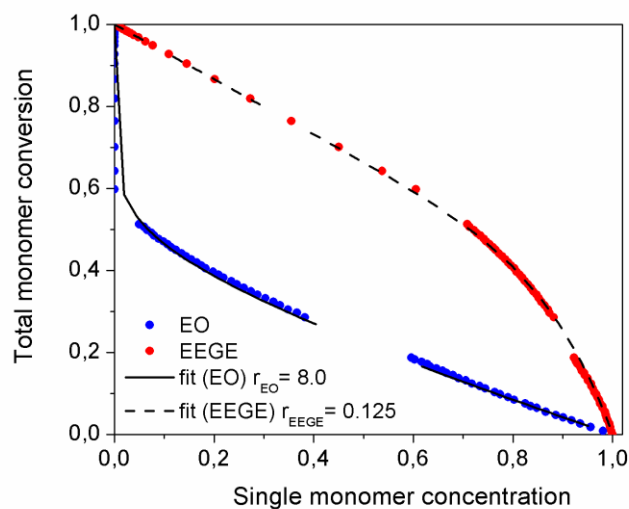

Figure S12. Total monomer conversion plotted as a function of the individual monomer concentration for EO (blue) and EEGE (red) for the activated-monomer AROP. Reactivity ratios are calculated from the respective fits (EO: solid line; EEGE: dashed line) in analogy to literature.[3]
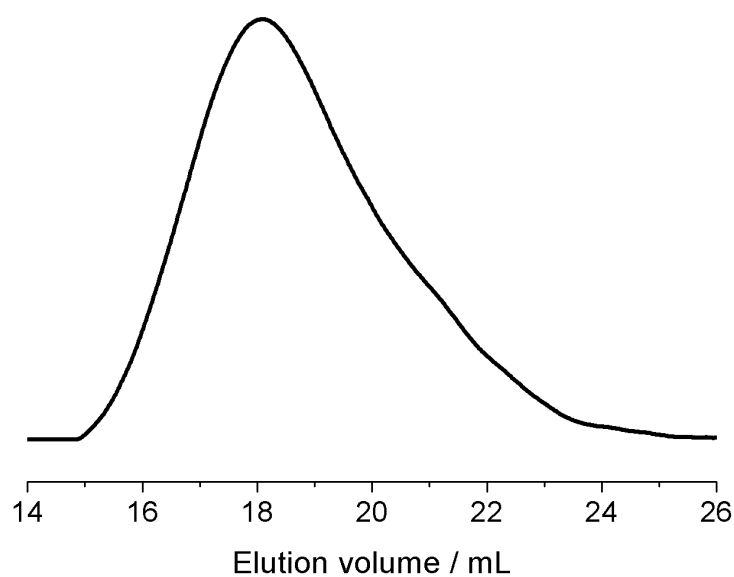
Figure S13. SEC trace (DMF, RI signal, PEG standard) of P(EO-*co*-EEGE) initiated with TOAB/TIBAL in toluene-d_8.

Table S1. Oxirane ring proton shifts of EEGE in toluene-d_8 at different temperatures (-10 °C to 20 °C) with added TIBAL and without TIBAL. [EEGE]/[TIBAL] = 9

T/°C	Oxirane proton signal CH			Oxirane proton signal C$H_{2,a}$			Oxirane proton signal C$H_{2,b}$		
	δ/ppm TIBAL added	δ/ppm no TIBAL	$\Delta\delta$/ppm	δ/ppm TIBAL added	δ/ppm no TIBAL	$\Delta\delta$/ppm	δ/ppm TIBAL added	δ/ppm no TIBAL	$\Delta\delta$/ppm
-10	2.89	2.87	0.02	2.36	2.34	0.02	2.25	2.22	0.03
-5	2.89	2.87	0.02	2.37	2.34	0.03	2.25	2.23	0.02
0	2.89	2.87	0.02	2.37	2.35	0.02	2.26	2.23	0.03
5	2.89	2.87	0.02	2.37	2.35	0.02	2.26	2.23	0.03
10	2.89	2.87	0.02	2.37	2.35	0.02	2.27	2.24	0.03
15	2.89	2.87	0.02	2.38	2.35	0.03	2.27	2.24	0.03
20	2.89	2.87	0.02	2.39	2.36	0.03	2.28	2.24	0.04

Table S2. DSC data of P(EO-*co*-EEGE) copolymers, prepared via monomer-activated AROP. Initiation at -5 °C.

EEGE/mol%[a]	[^{i}Bu$_3$Al]/ TOAB	M_n[b]/ mol·g^{-1}	PDI[b]	T_g/°C	T_m/°C	ΔH/J·g^{-1}
48	3	15,100	1.6*	-64	13	11
33	5	19,800	1.8**	-63	22	15

[a]comonomer ratio was determined by ^{1}H NMR spectroscopy
[b]determined via SEC (DMF, RI signal, PEG standard)
*after dialysis in methanol with 6-8 kDa MWCO (before: PDI = 1.7), 10 wt% loss after dialysis
**after dialysis in methanol with 25 kDa MWCO (before: PDI = 1.9), 15 wt% loss after dialysis
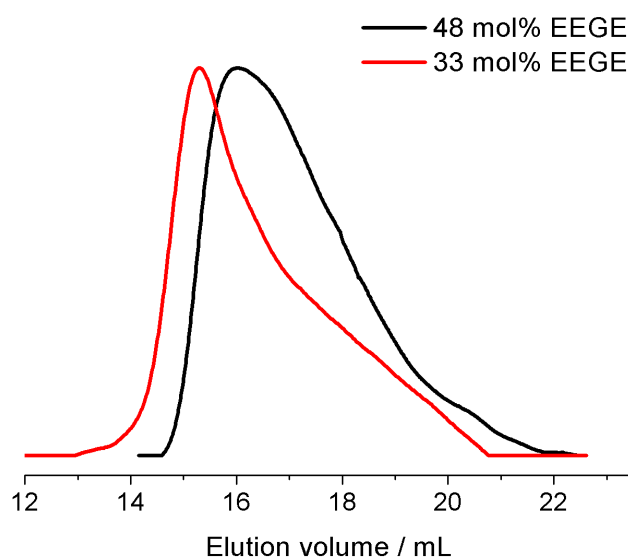

Figure S14. SEC traces (DMF, RI signal, PEG standard) of P(EO-co-EEGE) copolymers with 48 mol% (black line) and 33 mol% EEGE, prepared by monomer-activated AROP.

References

[1] Fitton, A. O.; Hill, J.; Jane, D. E.; Millar, R. Synthesis of Simple Oxetanes Carrying Reactive 2-Substituents. *Synthesis.* **1987**, *1987*, 1140–1142.

[2] Gervais, M.; Brocas, A.-L.; Cendejas, G.; Deffieux, A.; Carlotti, S. Synthesis of Linear High Molar Mass Glycidol-Based Polymers by Monomer-Activated Anionic Polymerization. *Macromolecules.* **2010**, *43*, 1778–1784.

[3] Beckingham, B.S.; Sanoja, G.E.; Lynd, N. A. Simple and Accurate Determination of Reactivity Ratios Using a Nonterminal Model of Chain Copolymerization. *Macromolecules.* **2015**, *48*, 6922–6930.
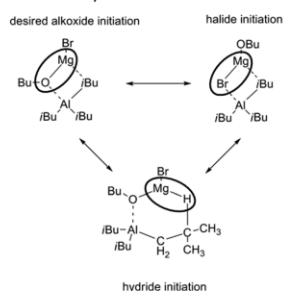
Appendix

Appendix A1

Reprinted with permission from Herzberger, J.; Niederer, K.; Pohlit, H.; Seiwert, J.; Worm, M.; Wurm, F. R.; Frey, H. *Chem. Rev.* **2016**, 116, 2170-2243. Copyright 2016 American Chemical Society.

Scheme 9. Proposed Initiation Species for Grignard/Alcohol/Triisobutylaluminum System[86]

difficult and time-consuming. Simple precipitation of the polymer often leads to unsatisfactory results. Column chromatography or long-term dialysis can be performed, albeit with reduction of the polymer yield.[97] More hydrophobic polyethers, such as PEEGE, can also be purified by consecutive washing with saturated $NaHCO_3$ solution, NaCl solution (10%), and water.[94]

Direct calculation of the absolute M_n via ^{1}H NMR spectroscopy using ^{1}H NMR signals of the initiator is generally not possible for the activated monomer approach, given the nature of the initiator species (bromide, chloride, and azide). In the literature, molecular weights are determined by SEC measurements (refractive index signal or UV signal). However, molecular weights analyzed by a general SEC setup are not absolute values. Alternatively, end-group functionalization or absolute methods, such as static light scattering, have to be performed. Even though the formation of unsaturated end-groups can be mainly suppressed, undesired initiation by hydride or *iso*-butyl groups was also reported (Scheme 6e).[80,84]

In summary, the "activated monomer mechanism" has become a well-established alternative to the conventional AROP within the past decade and is a crucial method, both to prepare high molecular weight polyethers and to polymerize a broad family of epoxides bearing functional groups to generate novel functional polyethers.

2.4. N-Heterocyclic Carbenes (NHCs) and N-Heterocyclic Olefins (NHOs) as Organocatalysts for Metal-Free Polyether Synthesis

N-Heterocyclic carbenes (NHCs) have seen a tremendous development since the turn of the millennium and are known as efficient ligands of transition metal complexes[107,108] or as organocatalysts for reactions, such as the benzoin condensation or the Stetter-reaction.[109−111] Recently, Taton et al. reviewed the

use of *N*-heterocyclic carbenes (NHCs) in organocatalysis, mainly focusing on general macromolecular chemistry.[112,113] In 2015, Naumann and Dove further highlighted a current trend regarding NHCs as organocatalysts for various polymerizations.[114,115] Here we summarize current reports devoted to NHCs as initiators and/or as organocatalysts for the metal-free ROP of epoxides.

In 1991, Arduengo et al. presented the first crystalline diaminocarbene and introduced the class of *N*-heterocyclic carbenes (NHC).[116] While the first step-growth polymerization via NHC catalysis followed in the late 1990s,[117,118] the use for EO polymerization was not established until 2009, when it was introduced in a seminal work by Taton and Gnanou et al.[119] The authors showed that the strong nucleophilicity of 1,3-bis-(diisopropyl)imidazol-2-ylidene enabled the direct attack at the methylene group of EO, generating an imidazolium alkoxide for further polymerization of EO. The proposed polymerization mechanism is based on the formation of a zwitterionic species (imidazolium alkoxide), as displayed in Scheme 10. Termination with suitable nucleophiles releases the NHC and affords well-defined α,ω-bifunctional PEG.

This technique enabled the controlled synthesis of heterotelechelic PEG up to 13 000 g·mol^{-1}, with narrow molecular weight distributions without the need to remove metallic initiators. Most important, no cyclic species were detected. In general, the NHC method allows for facile synthesis of azide-functional PEG, which is suitable for subsequent azide−alkyne click-chemistry. Furthermore, the authors demonstrated the versatility of the NHC method by combining the ring-opening polymerization of epoxides with cyclic esters. In particular, PEG-*b*-PCL block copolymers were synthesized by simple addition of ε-caprolactone (CL) to the NHC-initiated PEG-chain.

In addition, Taton et al. demonstrated the successful polymerization of EO by using NHC as a true organocatalyst. A typical procedure relies on a ratio of [NHC]/[NuE]/[EO] = 0.1:1:100, whereas NuE (Nu = nucleophilic and E = electrophilic part, e.g., $PhCH_2OH$, $HC≡CH_2OH$, N_3SiMe_3, and $PhCH_2OSiMe_3$) represents the chain regulator.[120] Well-defined, heterotelechelic PEGs up to 12 000 g·mol^{-1} were synthesized with narrow molecular weight distributions (PDI = 1.07−1.15). As an example, Figure 3 shows the MALDI TOF MS spectrum of α-propargyl,ω-hydroxyl heterodifunctional PEG, confirming the absence of any side products and the preservation of the alkyne functionality during polymerization.[120]

The authors considered two possible mechanisms, based on either monomer activation (path a) or chain-end activation (path b) by the NHC, as illustrated in Scheme 11.

Motivated by the successful metal-free synthesis of PEG, Taton et al. also implemented the NHC method for the polymerization of PO.[121] Yet, low monomer conversion (≤40%)

Scheme 10. Proposed Reaction Scheme of the Zwitterionic ROP of EO[119]

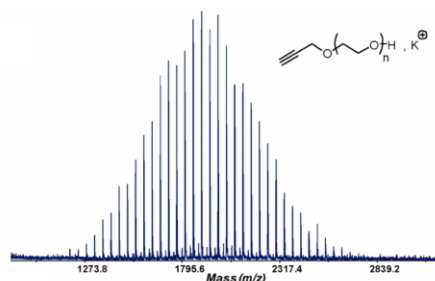Nu = N$_3$, OH, Benzyl alkoxide
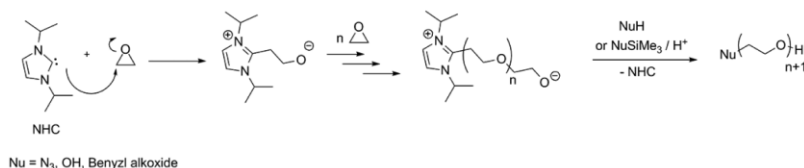
Figure 3. MALDI TOF MS of α-propargyl,ω-hydroxyl heterodifunctional PEO. Adapted with permission from Raynaud, J.; Absalon, C.; Gnanou, Y.; Taton, D. *Macromolecules* **2010**, *43*, 2814−2823.[120] Copyright 2010 American Chemical Society.

was observed and the absence of unsaturated impurities was only ensured for low molecular weight PPOs (4500 g·mol^{-1}).

Recently, Lindner et al. reported several NHC−CO$_2$ adducts as feasible precatalysts for the homopolymerization of PO and the block copolymerization with ε-caprolactone (CL) or block and random copolymerization with (S,S)-lactide (LA), respectively.[122] NHC−CO$_2$ adducts are thermally labile progenitors that allow the in situ generation of NHCs (Scheme 12), as recently reviewed by Naumann and Buchmeiser.[123] The homopolymerization of PO was performed by release of the

Scheme 12. Example of a CO$_2$-Protected NHC[122]
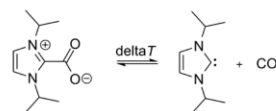
NHC at 120 °C and initiation with diethylene glycol. Oligomeric PPO with narrow MWD (1.08−1.23) was obtained. Moreover, the authors presented block copolymers of PO and CL, and block and random copolymers of PO and LA, respectively. In contrast to pure PPO, the copolymers showed rather poor monomer conversion and broad MWD (PDI = 1.38−1.77), assumingly a result of transesterification or backbiting reactions.

In summary, NHCs are suitable initiators and/or catalysts to synthesize α,ω-bifunctional PEGs. To date, the successful polymerization of EO and the synthesis of low molecular weight PPO as well as several block copolymers have been presented. It is obvious that this method could also show promising results for other epoxide-based monomers, for instance to generate multifunctional PEG. Further, the random copolymerization of epoxides with cyclic esters is feasible and warrants further study that may lead to unprecedented copolymer structures.[119,122] Nevertheless, NHCs are highly reactive and sensitive compounds and careful handling is necessary. Moisture should be avoided and storage at low temperatures is suggested. However, recently developed imidazolium-2-carboxylates and (benz)imidazolium hydrogen carbonates that can be viewed as masked *N*-

Scheme 11. Proposed mechanisms for the ring-opening polymerization of EO catalyzed by NHC. (a) via monomer activation; (b) via chain-end activation.[120]

Nu = benzyl alkoxide, propargyl alkoxide, N$_3$,
E= H or SiMe$_3$

337
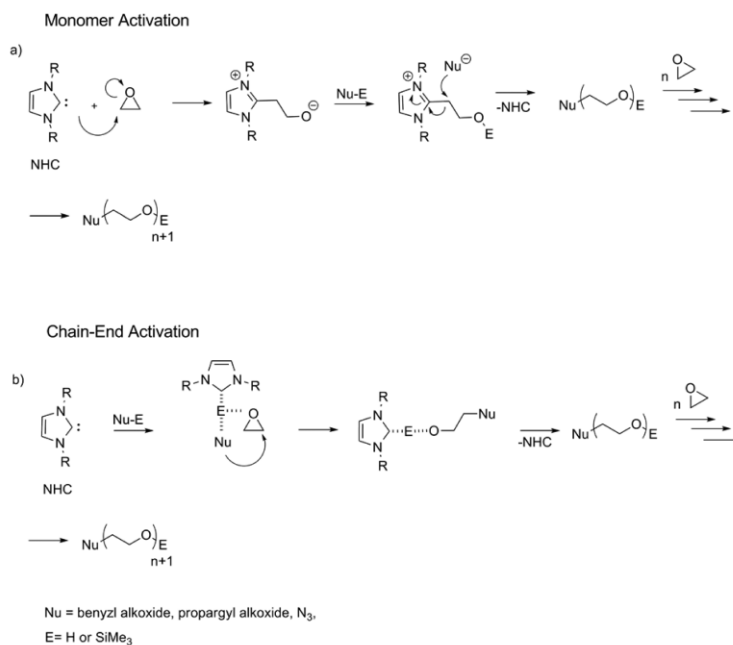
heterocyclic carbenes permit use for polymerization of various monomers (lactide, MMA) at room temperature and possess greatly improved storage stability.[124] Therefore, intriguing potential for the polymerization of epoxide monomers can be envisaged.

A further step to metal-free polymer synthesis was reported by Naumann and Dove et al., who applied *N*-heterocyclic olefins (NHOs) as organic catalyst for the controlled polymerization of PO.[125] NHOs are highly polarized alkenes with considerable electron density on their exocyclic carbon atom, as illustrated in Scheme 13.[126] To some extent, they combine NHC-like adaptability and carbanionic reactivity. NHOs are air sensitive and should be preferably stored at cold temperatures.[126−128]

Scheme 13. Mesomeric Structure of NHOs, Showing the Strong Charge Delocalization[125]
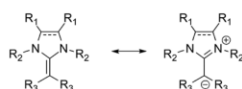
Naumann and Dove et al. prepared a library of NHOs and studied their structural influence on PO polymerization. Similarly as for the NHCs, the authors proposed two possible mechanisms for the polymerization of PO with NHO, which are in agreement with the "monomer activation" and "chain end activation" shown exemplarily in Scheme 11 for NHCs. For NHOs, the zwitterionic "monomer activation" leads to the occurrence of high molecular weight impurities but is mainly disfavored for NHOs. The authors demonstrate that the zwitterionic mechanism can be suppressed completely by increasing steric hindrance and basicity of the catalytically active site. Consequently, the most suitable NHO for ROP of epoxides is shown in Scheme 14, bearing two methyl moieties at the exocyclic carbon atom.

Scheme 14. Suitable NHO Catalyst to Obtain Well-Defined PPO[125]

Overall, PPO with molecular weights in the range of 2000−12 000 g·mol^{-1} and narrow PDIs below 1.06 were prepared. Despite the high turnover number (TON) of about 2200, the polymerization of PO with organic catalysts is rather slow, e.g., 88% conversion of PO with ratios of 1:10:1000 ([NHO]/[BnOH]/[PO]) was reached in 68 h. Nevertheless, NHOs represent a promising class of catalysts for novel polymer structures.

2.5. Phosphazene Bases: Metal-Free Initiators

Another metal-free polymerization technique relies on the use of phosphazene bases as deprotonation or complexation agents. While various reviews and books have covered the use of phosphazene bases for living anionic polymerizations,[25,73,129−132] herein an overview of their general use for epoxide polymerization and focus on recent achievements will be presented.

Phosphazene bases, also known as "Schwesinger Bases", belong to the family of neutral Brönsted "super" bases, which are highly basic but only weakly nucleophilic (selected phosphazene bases in Scheme 15).[133−135] Despite their exceptional structure,

Scheme 15. Chemical Structure and Respective pK$_a$ Value of Relevant Phosphazene Bases for Epoxide Polymerization^a
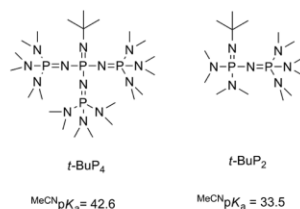

^{a}1-*tert*-Butyl-4,4,4-tris(dimethylamino)-2,2-bis[tris(dimethyl-amino)-phosphoranylidenamino]-2λ^5, 4λ^5- catenadi(phosphazene) (*t*-BuP$_4$) and 1-*tert*-butyl-2,2,4,4,4-pentakis(dimethylamino)-2λ^5,4λ^5-catenadi-(phosphazene) (*t*-BuP$_2$).

phosphazene bases are commercially available, chemically and thermally stable, and soluble in nonpolar and moderately polar organic solvents (e.g., hexane, toluene, and THF).[133] Nevertheless, the commercially available phosphazene bases may contain their respective isomers as impurities, which could have an influence on their reactivity.[136] In 1996, Möller and co-workers introduced the first polymerization of EO with *t*-BuP$_4$ as a deprotonation agent.[137] In the family of phosphazene bases, *t*-BuP$_4$ is one of the strongest phosphazene bases with a pK$_a$ of 42.6 (in acetonitrile)[134] and is typically used for the ROP of epoxides (Scheme 15). As an alternative to phosphazene bases, Rexin and Mülhaupt investigated several bulky phosphonium salts as deprotonation agents for PO polymerization.[138,139] At polymerization temperatures of 100 °C, the total degree of unsaturations was lowered, compared to known phosphazene bases, albeit lower polymerization rates were observed.[138] Recently, Hadjichristidis and Gnanou et al. reported the first successful use of the less conjugated and consequently milder *t*-BuP$_2$ (^{MeCN}pK$_a$ = 33.5)[134] for the polymerization of EO (Scheme 15).[140] This approach enabled an elegant one-pot synthesis of polyether-polyester block terpolymers (PEO-*b*-PCL-*b*-PLA) with no occurrence of chain transfer reactions (PDI = 1.10).[140] However, prolonged reaction times have been reported for the EO polymerization with *t*-BuP$_2$, and no successful polymerizations of other epoxides have been demonstrated to date. For example, only *t*-BuP$_4$ enabled successful polymerization of 1,2-butene oxide (BO), but neither *t*-BuP$_1$, *t*-BuP$_2$, nor TiBP, which is due to insufficient basicity.[141] Consequently, *t*-BuP$_4$ remains the standard phosphazene base for epoxide polymerization, e.g., EEGE,[142] AGE,[143] glycidyl methyl ether (GME),[144] ethyl glycidyl ether (EGE),[144] PO,[141] *tert*-butyl glycidyl ether (*t*BuGE),[141] and benzyl glycidyl ether (BnGE).[141]

The salient feature of phosphazene bases and especially *t*-BuP$_4$ for epoxide ROP is that they are metal-free and thus alternative deprotonation agents to common alkali hydroxides. After deprotonation, the bulky phosphazenium cation [*t*-BuP$_4$]H$^+$ represents a soft counterion with low tendency for ion-pair association. Consequently, high polymerization rates also in nonpolar solvents under mild reaction temperatures can be observed, as the chain end is highly reactive. Usually, the ratio of phosphazene base:initiator is close to 1, but also lower ratios (as low as 0.01 equiv) have been reported but are accompanied by

338

Scheme 16. Synthesis of Figure-Eight Shaped Amphiphilic Block Copolyethers Based on Decyl Glycidyl Ether and 2-(2-(2-Methoxyethoxy)ethoxy)ethyl Glycidyl Ether[155]

R₁ = -(CH₂)₉CH₃   R₂ = -(CH₂CH₂O)₃CH₃
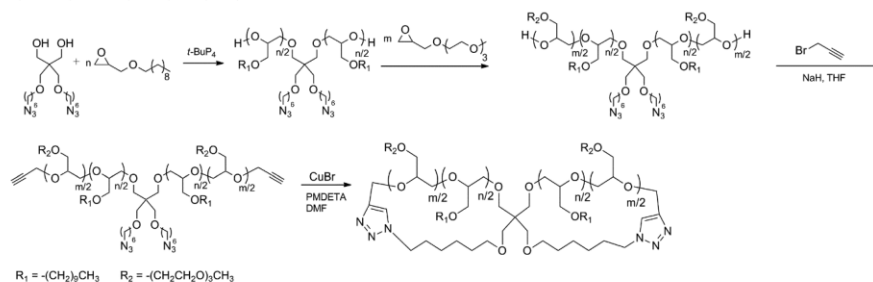
Scheme 17. One-Pot Synthesis of Poly(styrene)-*block*-poly(ethylene oxide)-*block*-poly(ethoxyethyl glycidyl ether) (PS-*b*-PEO-*b*-PEEGE) Triblock Terpolymers and Subsequent Deprotection to Poly(styrene)-*block*-poly(ethylene oxide)-*block*-*lin*poly(glycerol)[157]
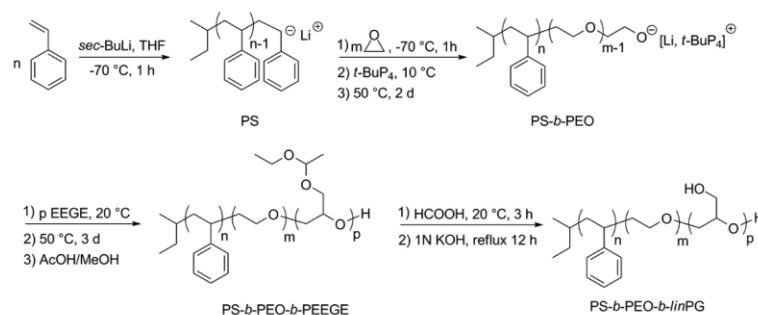
longer reaction times.[130,145−147] Suitable initiators range from common alcohols[148−151] to secondary amides[152,153] and carboxylic acids.[147] Kakuchi and Satoh et al. demonstrated the power of the phosphazene base approach by polymerizing less reactive monomers, such as styrene oxide,[150] BO,[141,153,154] decyl glycidyl ether and 2-(2-(2-methoxyethoxy)ethoxy)ethyl glycidyl ether[155] as well as several glycidyl amine derivatives (see also section 3.2).[151] Based on a selection of these monomers, the authors synthesized linear, cyclic, figure-eight-shaped, and tadpole-shaped amphiphilic block copolyethers starting from α,ω-bifunctional initiators, bearing an alcohol and an azide functionality (Scheme 16).[155]

Alternatively, phosphazene bases can be used as complexation agent and enable ROP of epoxides starting from anions bearing lithium as a counterion.[142,148,156] In general, lithium alkoxides are not applicable for epoxide polymerization due to the strong interaction of the lithium cation with the alkoxide. Addition of phosphazene bases breaks down the ion association of lithium cations with the alkoxides, and polymerization can proceed. Thus, switching from carbanionic polymerization to oxyanionic polymerization is possible, permitting the one-pot synthesis of a variety of promising block copolymers. For example, Müller and Schmalz et al. presented poly(styrene)-*block*-poly(ethylene oxide)-*block*-poly(ethoxyethyl glycidyl ether) (PS-*b*-PEO-*b*-PEEGE) triblock terpolymers in a one-pot procedure (Scheme 17) that were deprotected to afford PS-*b*-PEO-*b*-*lin*PG with a

linear polyglycerol block (*lin*PG).[157] Narrow PDIs of 1.02 confirm the living character of the polymerization.

Other examples are PS-*b*-PEO,[148] PB-*b*-PEO,[158−160] PI-*b*-PEO,[158,161] PB-*b*-PI-*b*-PEO,[162] PS-*b*-*lin*PG,[163] P2VP-*b*-PEO-*b*-P(GME-*co*-EGE),[144] and polystyrene-*block*-poly(*p*-hydroxystyrene-*graft*-ethylene oxide)[164] block copolymers. Further, the switch from oxyanionic to carbanionic polymerization was demonstrated for EO and dimethylaminoethyl methacrylate (DMAEMA), but only PEO-*b*-PDMAEMA block copolymers with moderate PDIs (1.40−1.70) were obtained.[165]

In 2012, Carlotti and co-workers combined *t*-BuP₄ with the "activated monomer technique" for the rapid polymerization of PO at room temperature (see section 2.3).[90] PPO with molecular weights up to 80 000 g·mol⁻¹ was obtained. However, the authors reported the occurrence of unsaturated chain ends indicating the occurrence of transfer reactions despite the high molecular weight; consequently the combination of both methods did not lead to a significant improvement of the common "activated monomer technique".

Phosphazene bases can also function as organocatalyst for the polymerization of cyclic esters e.g., lactide (LA)[166] and ε-caprolactone (CL).[140] In general, ideal catalysts are weaker phosphazene bases such as BEMP, *t*-BuP₁ or *t*-BuP₂ to suppress undesired transesterification reactions.[140,166,167] The use of the strong *t*-BuP₄ base affords polyesters with rather broad PDIs.[168] Yet, this approach permits the synthesis of random polyester-polyether copolymers, as it was demonstrated for the

339

Scheme 18. Copolymerization Scheme of Reaction of *ε*-CL with *t*BuGE[a]
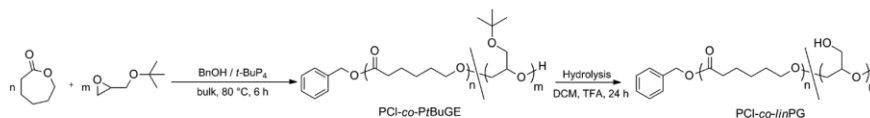
[a]Release of the hydroxyl groups renders PCL-*co-lin*PG copolymers.[169]

Scheme 19. Reaction Scheme of the "Catalyst Switch" Approach for the Block Copolymerization of EO/BO with *ε*-Caprolcatone/ *δ*-Valerolactone or Trimethylene Carbonate[145]
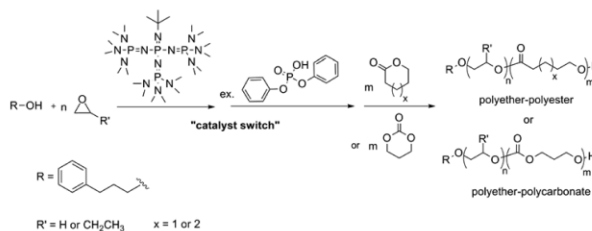
copolymerization of *ε*-caprolactone (CL) with *tert*-butyl glycidyl ether (*t*BuGE) (Scheme 18).[169] CL ratios were varied from 0 to 100 mol %, resulting in (co)polymers with molecular weights ranging from 1.38×10^{-4} to 4.92×10^{-4} g·mol^{-1} and moderate PDIs 1.28–1.43. After cleavage of the *tert*-butyl protecting group, the PCL-*co-lin*PG copolymers with PCL < 72 mol % showed faster enzymatic degradation than pure PCL. The authors attribute the accelerated biodegradation to the lower degree of crystallization and higher hydrophilicity of PCL-*co-lin*PG than PCL, induced by the incorporated glycerol units.

Recently, Hadjichristidis and Gnanou et al. utilized a "catalyst switch" for the sequential one-pot polymerization of polyether-polyester/polycarbonate block copolymers by applying a combination of phosphazene bases and diphenyl phosphate (DPP).[145] As mentioned before, the strong basicity of *t*-Bu$_4$P promotes chain transfer reactions during the ROP of cyclic esters or cyclic carbonates leading to relatively broad PDIs.[145,168,169] By the addition of DPP, the phosphazene base was neutralized and subsequently DPP acted as acidic catalyst for the polymerization of cyclic esters: a basic to acidic catalyst switch. Various epoxides (EO, BO) were polymerized by using an alcohol/*t*-Bu$_4$P system, followed by excess addition of DPP and the respective cyclic ester (CL, *δ*-valerolactone) and/or cyclic carbonate (trimethylene carbonate, TMC) (Scheme 19). Block copolymers and triblock terpolymers with molecular weights up to 19 000 g·mol^{-1} and narrow PDIs in the range of 1.04–1.17 were obtained (Figure 4).[145] The authors report a retardation effect of the phosphazenium diphenyl phosphate on the polymerization rates of the cyclic esters. Thus, the ratio of *t*-BuP$_4$ should be kept at a minimum (0.2 equiv).

In 2015, the same group expanded the scope of the "catalyst switch" strategy by synthesizing linear- and three- arm star-tetrablock quarterpolymers based on the same monomers.[146] To expand the toolbox of suitable monomers, Hadjichristidis and Zhao demonstrated the successful preparation of block copolymers based on BO or 2-ethylhexyl glycidyl ether (EHGE) with various substituted lactones, namely *δ*-hexalactone (HL), *δ*-nonalactone (NL), and *δ*-decalactone (DL).[170]
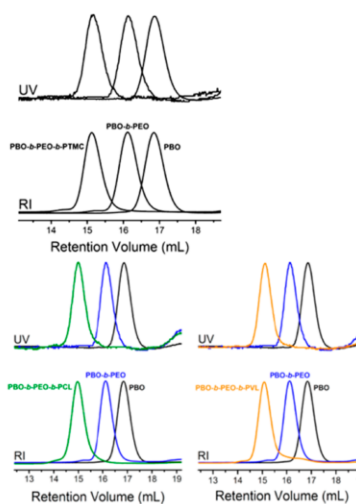

Figure 4. SEC traces of isolated products of PBO, PBO-*b*-PEO, PBO-*b*-PEO-*b*-PCL, PBO-*b*-PEO-*b*-PVL, and PBO-*b*-PEO-*b*-PTMC respectively, synthesized via "catalyst switch" strategy.[145] Adapted with permission from Zhao, J.; Pahovnik, D.; Gnanou, Y.; Hadjichristidis, N. *Macromolecules* **2014**, *47*, 3814–3822. Copyright 2014 American Chemical Society.

In summary, phosphazene bases permit the synthesis of unprecedented and "challenging" block copolymer pairs with polyether block, such as vinyl polymer-based block copolymers (PS, PI, PB, PVP) with-polyether and polyether-polyester/-carbonate, and also random polyester/polyether copolymers, in a one-pot reaction with no need for isolation or purification after individual synthetic steps. In spite of these advantages, it should be kept in mind that removal of phosphazene bases can be time-consuming and challenging and is not always considered in the

340

respective works. A suitable procedure for this purpose is the purification via filtration over alumina.[151,155] However, oftentimes polymers are purified merely by simple precipitation, and the phosphazene base may remain in the polymer. Especially with a focus on future biomedical applications, complete removal of the charged phosphazene bases is mandatory, since phosphazene base cations are critically discussed with respect to their toxicity. More specifically, preliminary in vitro studies on several human cell lines suggest that t-BuP$_4$ exhibits high cytotoxicity, the toxic species being most probably the corresponding phosphazenium ion.[171] Consequently, one might consider avoiding the use of phosphazene bases for biological or biomedical purposes completely. To date, phosphazene bases have attracted minor attention for industrial polyether synthesis, which might be due to their rather high cost in comparison to established alkoxides.

2.6. Heterogeneous Catalysis—Double Metal Cyanide Catalysts for Epoxide Polymerization

An increasingly important method, yet currently only employed for specialty polyols in industry, particularly for high molecular weight polyalkylene ether polyols is based on the so-called "double metal cyanide catalysts" (DMC).[172] This catalytic system was first developed by General Tire and Rubber in 1966[173] and has its primary use in the preparation of high-quality polyols for the polyurethane (PU) production.[174−178] A detailed overview was given by Ionescu in "Chemistry and Technology of Polyols for Polyurethanes".[179] Clearly, major progress has been made in this area in the last 15 years. Here, we will give a brief overview of the DMC method and will focus on novel polyether structures obtained with the DMC catalyst.

While this method is well-established for industrial purposes, it has attracted minor attention in the scientific community. High polymerization temperatures, elevated pressures, and a complex catalyst preparation procedure, followed by difficult characterization of the actual catalyst structure render this approach less attractive for scientific purposes. However, the DMC method is applicable to large scale processes. The formation of unsaturated impurities is suppressed, and high molecular weight polyalkylene ether polyols can be achieved. Especially in the industrial production of polyols based on PPO, where mainly potassium hydroxide (KOH) is applied as a deprotonating agent and metal salts have to be removed after polymerization, the DMC catalyst can be a suitable alternative, enabling a continuous process with no need for further purification steps. Nevertheless, the DMC method includes various challenges and limitations, which are discussed in the following.

DMC is a heterogeneous catalyst with the general structure of $M^1_u[M^2(CN)_6]_v \cdot xM^1X_w \cdot yL \cdot zH_2O$, where M^1 = Zn, M^2 = Co, Fe. L is an organic complexing agent, such as $tert$-butyl alcohol, diglyme, or other.[180,181] A proposed structure of the DMC catalyst is shown in Scheme 20.[182]

Detailed analysis of the DMC structure is difficult, which is due to its insoluble character and the strong dependence of the crystal structure on the preparation procedure.[180,183,184] Since 1966, intense research efforts were performed to increase the catalytic efficiency of the DMC catalyst with the focus on cost-efficient and eco-friendly[185] systems for industrial applications.[174,181,186−189] In particular, novel complexing agents/cocomplexing agents,[174,188,190,191] numerous additives,[181,186,187,189] and various metal centers[172,184,192−195] were investigated to increase the performance of the DMC. To date, catalyst concentrations of as little as 15−50 ppm are sufficient to

**Scheme 20. Proposed Structure of the Active Site of Zn−Co(III) DMC Catalyst**[a]
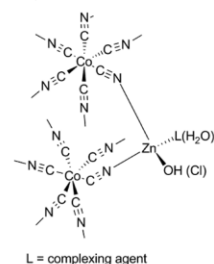
L = complexing agent

[a]Here, the Zn−OH structure acts as the initiating group. L represents a complexing agent, used during the preparation of the catalyst, e.g., $tert$-butanol.[182]

obtain suitable polyols within short reaction times, and the catalyst can remain in the polymers.[179,190] Consequently, no additional purification (filtration of salts) is necessary and the overall production steps are reduced.

Scheme 21 shows the mechanism proposed by Huang et al. and Kim et al. for the DMC-catalyzed PO polymerization.[174,181] The active sites of the DMC are believed to be cationic coordinative, however fully conclusive evidence of the proposed mechanism is still lacking, given by the heterogeneous character of the DMC. It is supposed that the polymerization center forms in two stages: (I) The inactive $(CN)_2ZnCl_2$ species interacts with the added initiator or a present ligand to form a dormant site at the catalyst surface. (II) Coordination of PO and subsequent replacement of a ligand (ROH) take place, followed by the attack of PO and the formation of the active center. Eventually, propagation occurs by nucleophilic attack of the growing PPO chain on activated PO molecules and proceeds until the monomer is consumed completely. The DMC method generates a strict head-to-tail regiosequence and a random configurational sequence of the resulting PPO.[196] The active polymer chain cannot be terminated by protic species; consequently no functional end groups can be introduced via a terminating agent.[196] However, after complete polymerization, the active polymer-DMC adduct is dormant, and the polymer chains can be reactivated by monomer addition at any time. Note that a fast intermolecular chain transfer (VI) between the active polymer chain and dormant hydroxyl-terminated polymer chains ensures narrow molecular weight distributions (e.g., $M_w/M_n < 1.1$ for $M_n < 6000$ g·mol^{-1}).[174] Further, the occurrence of unsaturated PPO chains (IV−V) is reduced to around 0.003 mequiv/g, compared to conventional KOH catalyzed PPO with 0.04−0.10 mequiv/g, which represents a significant advantage of the DMC-method for the preparation of specialty polyols.[174] In general, molecular weight distributions and amounts of unsaturated species are strongly influenced by the chosen DMC catalyst system and can vary significantly in literature.

Although unsaturated structures are suppressed, the DMC method possesses some characteristic challenges and limitations. The main characteristic of the DMC is the occurrence of an induction time, before actual chain growth can be observed. The substitution of the soft organic ligands by PO molecules leads to a general induction period of 20−30 min up to several hours. Consequently, in a common reaction procedure, the DMC has to be activated first, before the actual polymerization takes

341

Scheme 21. Proposed Mechanism of DMC-Catalyzed PO ROP,[181] Including Proposed Side Reactions and the Intermolecular Chain Transfer[174]
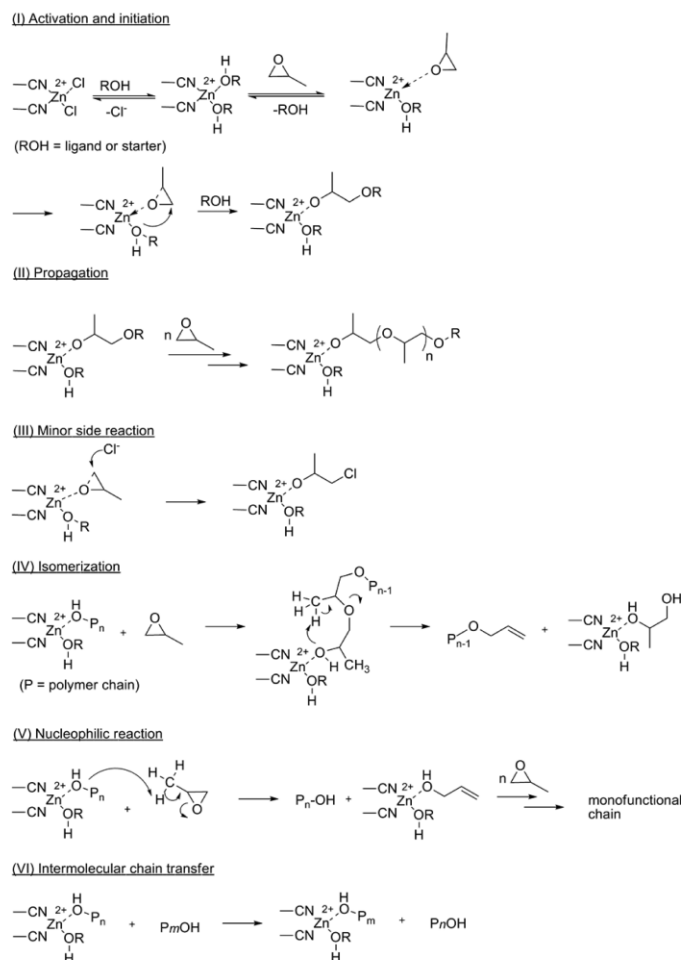
place.[196,197] However, after the induction period, the reaction rate exceeds that of the conventional AROP (Figure 5). Several approaches to avoid an induction period are described in patent literature but will not be discussed in detail here.[198,199]

A major drawback of the DMC catalysis for the polyol industry is the target to produce reactive (EO)-capped polyols with primary hydroxyl termini. These compounds represent an important class of polyols for flexible PU foams. However, if EO is added to a PPO-based polyol, the DMC catalyst leads to a heterogeneous mixture of unreacted PPO-polyol and highly ethoxylated PPO or PEO homopolymer.[200] Consequently, KOH catalysis still remains the method of choice to prepare EO-capped polyols. Additionally, the DMC catalyst shows limitations toward common initiator systems. In particular,

initiators having good coordination capability such as ethylene glycol, glycerol, low-carbon amines, low-carbon acids and urea act as inhibitors and preclude the coordination of PO at the catalyst.[174,181] Therefore, industrially relevant polyols based on sorbitol or sugars are not accessible via DMC catalysis. Suitable initiators are low molecular weight PPOs ($400-700$ g·mol^{-1}) or noncomplexing alcohols.[196] In addition alkaline species deactivate the catalyst surface and impede polymerization. In contrast, long-chain carboxylic acids do not interfere with the catalyst and can be present throughout the polymerization, allowing for novel polyol derivatives.[196]

Another challenging characteristic of the DMC is the occurrence of high molecular weight polymer impurities ($100\,000-400\,000$ Da) in very small quantities ($60-400$
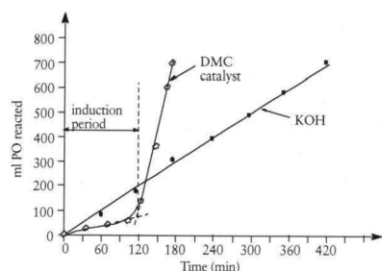
342

Figure 5. PO consumption versus time in PO polymerization with DMC catalysts and conventional KOH. (Reaction conditions: $T = 110$ °C; $p = 300$ MPa; catalyst concentration: $c(\text{KOH}) = 0.25\%$ and $c(\text{DMC}) = 200$ ppm (0.02%).)[179] Adapted with permission from M. Ionescu, Rapra Technology, 2005. Copyright 2005 Smithers RAPRA Technology.

ppm).[177,179] To date, intense research has been performed to understand and suppress the formation of high molecular weight tails. Several approaches are described in the patent literature, which, however, are beyond the scope of this article.[201−203]

Considering the tolerance of the DMC catalyst toward epoxide monomers, unexpected observations were reported. As opposed to conventional AROP, ethylene oxide exhibits lower reactivity toward the DMC catalysts than PO. Complexation and activation of PO is considered to be favored, based on the high electron density on the oxygen atom, given by the positive inductive effect of the methylene group. In comparison, EO is less basic than PO, leading to a lower complexation constant.[204] In general, literature mostly reports the homopolymerization of PO or focuses on the copolymerization with carbon dioxide.[205−213] Only little has been reported on other epoxide based copolymers. However, Huang et al. reported the random copolymerization of PO with EO using a DMC system.[214] Narrow molecular weight distributions (PDI = 1.2−1.3) were obtained with low molecular weight fractions of EO (<30%). At higher EO fractions (>78%), turbid solutions were observed, caused by the crystallization of long PEO homopolymer fractions. In 2012, Sun et al. reported the homopolymerization of epichlorohydrin (ECH) with tri-(2-hydroxyethyl) isocyanurate as an initiator, followed by the use of PECH as chain extender for PU elastomers.[215] Recently, the homopolymerization of racemic ECH, *S*-ECH, and *R*-ECH was reinvestigated by Zhang et al.[182] Regioregular PECH was obtained with a head-to-tail content exceeding 99%, molecular weights ranging from 900 to 2700 g/mol and PDIs of 1.42 to 1.72. Cyclic or oligomeric byproducts were completely suppressed. Given by the special nature of the DMC catalyst, extraordinary copolymers are accessible, which cannot be obtained by conventional AROP. For example, Langanke et al. reported PPO-*b*-pFA-*b*-PPO and PEO-*b*-pFA-*b*-PEO triblock copolymers initiated from paraformaldehyde (pFA) as a macroinitiator ($M_w/M_n = 1.11−1.48$).[216] Further, the tolerance of the DMC catalyst to ester groups has been exploited to create a new class of biobased polyols for the PU industry, starting from vegetable oils such as castor oil.[217−219]

Chen and co-workers reported the copolymerization of PO with maleic anhydride (MA) to obtain polyether-ester structures (Scheme 22).[220] Copolymers of molecular weights up to 3000 g·mol^{-1} and moderate PDIs of 1.35 to 1.54 were reported, with a catalyst efficiency of 10 kg polymer/g catalyst. The reactivity

Scheme 22. Reaction Scheme for the Copolymerization of PO with Maleic Anhydride[220]
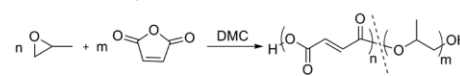
ratios of MA and PO were calculated by the extended Kelen-Tüdös equation with values of $r_1(\text{MA}) = 0$ and $r_2(\text{PO}) = 0.286$. Copolymers with the monomer ratio MA/PO ≥ 1 were almost alternating, whereas homopolymers of MA are not accessible by DMC.

In 2010, Kim and co-workers extended the library of alternating copolymers of PO and cyclic acid anhydrides.[221] The authors reported the copolymerization of PO with succinic anhydride (SA), maleic anhydride (MA), phthalic anhydride (PA), and glutaric anhydride (GA), respectively. Comonomer ratios were varied from 0 to 50 mol % with molecular weights up to 7000 g·mol^{-1} and narrow PDIs below 1.5. However, with increasing molar ratio of cyclic anhydride the polymer yields decreased to less than 30%. The reactivity ratios were calculated by the extended Kelen-Tüdös equation under the assumption that r_{AA} for any cyclic acid anhydride is zero. The reported reactivity ratios for PO are 0.34, 0.28, and 0.26 for PO/SA, PO/MA, and PO/PA copolymerization, respectively.

In addition to the intriguing copolymers of PO and cyclic anhydrides, the DMC technique enables the copolymerization of CO_2 with various epoxides such as propylene oxide, cyclohexene oxide, epichlorohydrin, and styrene oxide, which are discussed elsewhere.[205−213] In summary, DMC catalysis is a powerful method for novel high molecular weight polyether structures; however, this research field is by no means mature yet and offers promise for the future. It is also worth noting that to date many of the new materials obtained by this technique were characterized only to a very limited extent with respect to their properties.

2.7. Cationic Polymerization

The cationic ROP (CROP) of oxygen-containing heterocycles plays an important role for the preparation of the commercial products poly(oxymethylene) (POM, polyacetal), a highly crystalline engineering plastic prepared by ROP of trioxane as well as for the synthesis of poly(tetrahydrofuran) (polyTHF),[222] which is used for soft-elastic segments in thermoplastic elastomers, such as polyurethanes (Lycra) and polyesters (Hytrel). Generally, four-membered and higher cyclic ethers polymerize by cationic mechanism only (with a few rather unusual exceptions that have been mentioned in literature). The basic mechanistic principles of the CROP of heterocycles are well understood, based on work carried out by various groups from the 1960ies to the 1980ies, summarized in excellent reviews by Kubisa and Penczek et al.[223−225] The CROP is rarely used for the polymerization of EO or PO, since the formation of considerable amounts of cyclic polyether byproducts cannot be avoided, which is due to "backbiting" processes, i.e., intramolecular chain transfer.[30,226] For this reason and due to the low number of recent works on the CROP of epoxides this section of the current review is rather brief, and merely the basic principles will be outlined.

The active species in CROP are typically secondary or tertiary oxonium ions, and two fundamentally different mechanisms have to be considered that are illustrated in Figure 6: The activated chain-end mechanism (ACE) that is based on a tertiary oxonium ion located at the chain and as an active center. A nucleophilic attack of the oxygen atom in the cyclic monomer at a carbon

343

Sia	sialyl
siRNA	small interfering ribonucleic acid
tBuGE	*tert*-butylglycidylether
t-Bu-P4	1-*tert*-butyl-4,4,4-tris(dimethylamino)-2,2-bis[tris(dimethylamino)-phosphoranylidenamino]-2Λ5,4Λ5-catenadi(phosphazene)
Tc	cloud point
Tg	glass transition temperature
THF	tetrahydrofuran
Thr	threonine
TMC	trimethylene carbonate
TME	trimethylolethane
TMP	trimethylolpropane
TNF-α	tumor necrosis factor alpha
TON	turn over number
TRAIL	tumor necrosis factor-related apoptosis inducing ligand
T-T	tail to tail
Tyr	tyrosin
UV/vis	ultraviolet−visible spectroscopy
VEGF	heparin binding growth factor
VfcGE	vinyl ferrocenyl glycidyl ether

REFERENCES

(1) Polymer Science: A Comprehensive Reference. *Ring-Opening Polymerization and Special Polymerization Processes*; Penczek, S.; Grubbs, R. H., Eds.; Elsevier: Amsterdam, 2012; Vol. 4.

(2) Carlotti, S. and Peruch, F. *Cyclic Monomers: Epoxides, Lactide, Lactones, Lactams, Cyclic Silicon-Containing Monomers, Cyclic Carbonates, and Others. Anionic Polymerization: Principles, Practice, Strength, Consequences and Applications*; Hadjichristidis, N., Hirao, A., Eds.; Springer, 2015; pp 191−306.

(3) Dudev, T.; Lim, C. Ring Strain Energies from Ab Initio Calculations. *J. Am. Chem. Soc.* 1998, 120, 4450−4458.

(4) Wurtz, C. A. Mémoire Sur L'oxyde D'éthylène Et Les Alcools Polyéthyléniques. *Ann. Chim. Phys.* 1863, 69, 317−354.

(5) Staudinger, H.; Schweitzer, O. Über Hochpolymere Verbindungen, 20. Mitteil.: Über Die Poly-Äthylenoxyde. *Ber. Dtsch. Chem. Ges. B* 1929, 62, 2395−2405.

(6) Flory, P. J. Molecular Size Distribution in Ethylene Oxide Polymers. *J. Am. Chem. Soc.* 1940, 62, 1561−1565.

(7) Kosswig, K. *Ullmann's Encyclopedia of Industrial Chemistry*; Wiley-VCH Verlag GmbH & Co. KGaA: Berlin, 2000.

(8) Robson, R. J.; Dennis, E. A. The Size, Shape, and Hydration of Nonionic Surfactant Micelles. Triton X-100. *J. Phys. Chem.* 1977, 81, 1075−1078.

(9) Hargreaves, A. E.; Hargreaves, T. *Chemical Formulation: An Overview of Surfactant-Based Preparations Used in Everyday Life*; Royal Society of Chemistry: London, 2003; Vol. 32.

(10) Dingels, C.; Schömer, M.; Frey, H. Die vielen Gesichter des Poly(ethylenglykol)s. *Chem. Unserer Zeit* 2011, 45, 338−349.

(11) Fruijtier-Pölloth, C. Safety Assessment on Polyethylene Glycols (PEGs) and Their Derivatives as Used in Cosmetic Products. *Toxicology* 2005, 214, 1−38.

(12) Klein, R.; Wurm, F. R. Aliphatic Polyethers: Classical Polymers for the 21st Century. *Macromol. Rapid Commun.* 2015, 36, 1147−1165.

(13) Kjellander, R.; Florin, E. Water Structure and Changes in Thermal Stability of the System Poly(ethylene oxide)−Water. *J. Chem. Soc., Faraday Trans. 1* 1981, 77, 2053−2077.

(14) Veronese, F. M.; Pasut, G. PEGylation, Successful Approach to Drug Delivery. *Drug Discovery Today* 2005, 10, 1451−1458.

(15) Lasic, D. D.; Needham, D. The "Stealth" Liposome: A Prototypical Biomaterial. *Chem. Rev.* 1995, 95, 2601−2628.

(16) Knop, K.; Hoogenboom, R.; Fischer, D.; Schubert, U. S. Poly(ethylene glycol) in Drug Delivery: Pros and Cons as Well as Potential Alternatives. *Angew. Chem., Int. Ed.* 2010, 49, 6288−6308.

(17) Pelegri-O'Day, E. M.; Lin, E. W.; Maynard, H. D. Therapeutic Protein-Polymer Conjugates: Advancing Beyond PEGylation. *J. Am. Chem. Soc.* 2014, 136, 14323−14332.

(18) Dimitrov, I.; Tsvetanov, C. B. in *Polymer Science: A Comprehensive Reference*; Vol. 4, pp 551−569; Penczek, S.; Grubbs, R. H., Eds.; Matyjaszewski, K., Möller, M. Series Eds.; Elsevier: Amsterdam, 2012.

(19) Dingels, C.; Frey, H. In *Hierarchical Macromolecular Structures: 60 Years after the Staudinger Nobel Prize II*; 1st ed.; Percec, V., Ed.; Springer International Publishing: 2013; Vol. 262, 167−190.

(20) Dai, S.; Tam, K. C. Isothermal Titration Calorimetric Studies on the Temperature Dependence of Binding Interactions between Poly(propylene glycol)s and Sodium Dodecyl Sulfate. *Langmuir* 2004, 20, 2177−2183.

(21) Gagnon, S. D. In *Encyclopedia of Polymer Science and Technology*; John Wiley & Sons, Inc.: 2002.

(22) Chattopadhyay, D.; Raju, K. Structural Engineering of Polyurethane Coatings for High Performance Applications. *Prog. Polym. Sci.* 2007, 32, 352−418.

(23) Arnold, C. *CHEmanager* 2013, 19−20.

(24) Schillén, K.; Claesson, P. M.; Malmsten, M.; Linse, P.; Booth, C. Properties of Poly(ethylene oxide)−Poly(butylene oxide) Diblock Copolymers at the Interface between Hydrophobic Surfaces and Water. *J. Phys. Chem. B* 1997, 101, 4238−4252.

(25) Deffieux, A.; Carlotti, S.; Barrère, A. in *Polymer Science: A Comprehensive Reference*; Vol. 4, pp 117−140; Penczek, S.; Grubbs, R. H., Eds.; Matyjaszewski, K., Möller, M. Series Eds.; Elsevier: Amsterdam, 2012.

(26) Deffieux, A.; Boileau, S. Anionic Polymerization of Ethylene Oxide with Cryptates as Counterions: 1. *Polymer* 1977, 18, 1047−1050.

(27) Stolarzewicz, A.; Neugebauer, D.; Grobelny, Z. Influence of the Crown Ether Concentration and the Addition of Tert-Butyl Alcohol on Anionic Polymerization of (Butoxymethyl)Oxirane Initiated by Potassium Tert-Butoxide. *Macromol. Chem. Phys.* 1995, 196, 1295−1300.

(28) Stolarzewicz, A.; Neugebauer, D.; Grobelny, J. Potassium Hydride — the New Initiator for Anionic Polymerization of Oxiranes. *Macromol. Rapid Commun.* 1996, 17, 787−793.

(29) Tsvetanov, C.; Dimitrov, I.; Doytcheva, M.; Petrova, E.; Dotcheva, D.; Stamenova, R. In *Applications of Anionic Polymerization Research*; Quirk, R., Ed.; American Chemical Society: Washington DC, 1997, 236.

(30) Penczek, S.; Cypryk, M.; Duda, A.; Kubisa, P.; Slomkowski, S. Living Ring-Opening Polymerizations of Heterocyclic Monomers. *Prog. Polym. Sci.* 2007, 32, 247−282.

(31) Solovyanov, A. A.; Kazanski, K. S. Kinetics and Mechanism of Anionic Polymerization of Ethylene-Oxide in Ether Solutions. *Vysokomol. Soedin. A* 1972, 14, 1063−1070.

(32) Pearson, R. G. Hard and Soft Acids and Bases. *J. Am. Chem. Soc.* 1963, 85, 3533−3539.

(33) Hsieh, H.; Quirk, R. P. *Anionic Polymerization: Principles and Practical Applications*; CRC Press, 1996.

(34) Quirk, R. P.; You, F.; Wesdemiotis, C.; Arnould, M. A. Anionic Synthesis and Characterization of ω-Hydroxyl-Functionalized Poly (1, 3-cyclohexadiene). *Macromolecules* 2004, 37, 1234−1242.

(35) Tonhauser, C.; Frey, H. A Road Less Traveled to Functional Polymers: Epoxide Termination in Living Carbanionic Polymer Synthesis. *Macromol. Rapid Commun.* 2010, 31, 1938−1947.

(36) Quirk, R. P.; Guo, Y.; Wesdemiotis, C.; Arnould, M. A. Investigation of Ethylene Oxide Oligomerization During Functionalization of Poly(butadienyl)lithium Using MALDI-ToF MS and ¹H NMR Analyses. *Polymer* 2004, 45, 3423−3428.

(37) Encyclopedia of Polymer Science and Engineering, Vol. 2, *Anionic Polymerization to Cationic Polymerization*, Mark, H. F., Kroschwitz, J. I., Eds. 1985, 17, 377−377, DOI: 10.1002/pi.4980170412.

(38) Wojtech, V. B. Zur Darstellung Hochmolekularer Polyäthylenoxyde. *Makromol. Chem.* 1963, 66, 180−195.

344

(39) Mangold, C.; Wurm, F.; Frey, H. Functional PEG-Based Polymers with Reactive Groups Via Anionic ROP of Tailor-Made Epoxides. *Polym. Chem.* **2012**, *3*, 1714.

(40) Enjalbal, C.; Ribière, P.; Lamaty, F.; Yadav-Bhatnagar, N.; Martinez, J.; Aubagnac, J.-L. MALDI-ToF MS Analysis of Soluble PEG Based Multi-Step Synthetic Reaction Mixtures with Automated Detection of Reaction Failure. *J. Am. Soc. Mass Spectrom.* **2005**, *16*, 670−678.

(41) Kemptner, J.; Marchetti-Deschmann, M.; Siekmann, J.; Turecek, P. L.; Schwarz, H. P.; Allmaier, G. Gemma and MALDI-ToF MS of Reactive PEGs for Pharmaceutical Applications. *J. Pharm. Biomed. Anal.* **2010**, *52*, 432−437.

(42) Tsvetanov, C. B.; Petrova, E. B.; Panayotov, I. M. Polymerization of 1,2-Epoxides Initiated by Tetraalkyl Aluminates. I. Polymerization of Ethylene Oxide in the Presence of Sodium Tetrabutyl Aluminate. *J. Macromol. Sci., Chem.* **1985**, *22*, 1309−1324.

(43) Arkhipovich, G. N.; Dubrovskii, S. A.; Kazanskii, K. S.; Shupik, A. N. Complexing of Na⁺ Ion with Polyethylene Glycol. *Polym. Sci. U.S.S.R.* **1981**, *23*, 1827−1841.

(44) Ptitsyna, N. V.; Ovsyannikova, S. V.; Gel'fer, T. M.; Kazanskii, K. S. Synthesis of Polyethylene Glycols of Molecular Weight above 10,000 by Anionic Polymerization. *Polym. Sci. U.S.S.R.* **1980**, *22*, 2779−2786.

(45) Kazanskii, K. Donor-Acceptor and Solvation Interactions in Anionic Polymerization of Some Heterocycles. *Pure Appl. Chem.* **1981**, *53*, 1645−1661.

(46) Sigwalt, P.; Boileau, S. Reactivities of Ions and Ion-Pairs in Anionic Polymerizations of Epoxides and Episulfides. *J. Polym. Sci. C Polym. Symp.* **1978**, *62*, 51−64.

(47) Boileau, S. *Anionic Polymerization: Kinetics, Mechanisms and Synthesis*; American Chemical Society: Washington DC, 1981.

(48) Berlinova, I. V.; Panayotov, I. M.; Tsvetanov, C. B. Ionic Equilibriums in Living Polymer-Solutions of Ethylene-Oxide with Cesium. *Vysokomol. Soedin. S. B* **1978**, *20*, 839−342.

(49) Berlinova, I. V.; Panayotov, I. M.; Tsvetanov, C. B. Influence of the Polyether Chain on the Dissociation of "Living" Polymers Obtained in the Anionic Polymerization of Ethylene Oxide. *Eur. Polym. J.* **1977**, *13*, 757−760.

(50) Szwarc, M. *Carbanions, Living Polymers, and Electron Transfer Processes*; Interscience Publishers: New York, 1968.

(51) Szwarc, M. *Ionic Polymerization Fundamentals*; Hanser, 1996.

(52) Chang, C.; Kiesel, R.; Hogen-Esch, T. Specific Cation Participation in Alkali-Carbanion Initiated Epoxide Cleavage Reactions. *J. Am. Chem. Soc.* **1973**, *95*, 8446−8448.

(53) Vinogradova, L. V.; Zgonnik, V. N.; Il'ina, A. A.; Docheva, D.; Tsvetanov, C. Anionic Polymerization in Oxiranes. Polymerization of Methyl Methacrylate and 2-Vinylpyridine in Ethylene Oxide. *Macromolecules* **1992**, *25*, 6733−6738.

(54) Price, C.; Carmelit, D. Reactions of Epoxides in Dimethyl Sulfoxide Catalyzed by Potassium t-Butoxide. *J. Am. Chem. Soc.* **1966**, *88*, 4039.

(55) Gagnon, S. D. *Encyclopedia of Polymer Science and Engineering*; 2nd ed.; Wiley-Interscience: New York, 1985; Vol. 6.

(56) Wegener, G.; Brandt, M.; Duda, L.; Hofmann, J.; Klesczewski, B.; Koch, D.; Kumpf, R.-J.; Orzesek, H.; Pirkl, H.-G.; Six, C. Trends in Industrial Catalysis in the Polyurethane Industry. *Appl. Catal., A* **2001**, *221*, 303−335.

(57) Price, C. Polyethers. *Acc. Chem. Res.* **1974**, *7*, 294−301.

(58) Sloop, S. E.; Lerner, M. M.; Stephens, T. S.; Tipton, A. L.; Paull, D. G.; Stenger-Smith, J. D. Cross-Linking Poly(ethylene oxide) and Poly[oxymethylene-oligo (oxyethylene)] with Ultraviolet Radiation. *J. Appl. Polym. Sci.* **1994**, *53*, 1563−1572.

(59) Doytcheva, M.; Dotcheva, D.; Stamenova, R.; Orahovats, A.; Tsvetanov, C.; Leder, J. Ultraviolet-Induced Crosslinking of Solid Poly(ethylene oxide). *J. Appl. Polym. Sci.* **1997**, *64*, 2299−2307.

(60) Tsvetanov, C. B.; Stamenova, R.; Riess, G.; Ferrand, M.; Limal, D. U.S. Patent 20050043429 A1, 2003.

(61) Doytcheva, M.; Petrova, E.; Stamenova, R.; Tsvetanov, C.; Riess, G. UV-Induced Cross-Linking of Poly(ethylene oxide) in Aqueous Solution. *Macromol. Mater. Eng.* **2004**, *289*, 676−680.

(62) Hill, F. N.; Fitzpatrick, J. T.; Bailey, J. F. E.; Union Carbide Corp: U.S. Patent 2,969,402, 1961.

(63) Miller, R. A.; Price, C. C. Polyethers. Vii. Aluminum Catalysts for Polymerization of Ethylene Oxide. *J. Polym. Sci.* **1959**, *34*, 161−163.

(64) Vandenberg, E. Organometallic Catalysts for Polymerizing Monosubstituted Epoxides. *J. Polym. Sci.* **1960**, *47*, 486−489.

(65) Osgan, M.; Teyssie, P. Polymerization of Heterocyclic Monomers. *J. Polym. Sci., Part B: Polym. Lett.* **1967**, *5*, 789.

(66) Hsieh, H. Polymerization of Alkylene Oxides with Trialkylaluminum, Metal Acetylacetonates, and Water. *J. Appl. Polym. Sci.* **1971**, *15*, 2425−2438.

(67) Zhang, Y.; Shen, Z. *Acta. Polym. Sin.* **1998**, *6*, 469.

(68) Dimitrov, P.; Hasan, E.; Rangelov, S.; Trzebicka, B.; Dworak, A.; Tsvetanov, C. B. High Molecular Weight Functionalized Poly(ethylene oxide). *Polymer* **2002**, *43*, 7171−7178.

(69) Goeke, G. L.; Karol, F. J.; Union Carbide Corporation: U.S. Patent 4193892 A, 1980.

(70) Kazanskii, K.; Tarasov, A.; Paleyeva, I. Y.; Dubrovskii, S. High Molecular Suspension Polymerization of Ethylene Oxide under the Action of Diphenylcalcium. *Polym. Sci. U.S.S.R.* **1978**, *20*, 442−452.

(71) (a) Berlinova, I. V.; Panayotov, I. M.; Tsvetanov, K. B. Ionic Equilibriums in Living Polymer-Solutions of Ethylene-Oxide with Cesium Antion. *Vysokomol. Soedin. B* **1978**, *20*, 839−842. (b) Bulgarian Patent 25,142, 1978.

(72) Billouard, C.; Carlotti, S.; Desbois, P.; Deffieux, A. "Controlled" High-Speed Anionic Polymerization of Propylene Oxide Initiated by Alkali Metal Alkoxide/Trialkylaluminum Systems. *Macromolecules* **2004**, *37*, 4038−4043.

(73) Brocas, A.-L.; Mantzaridis, C.; Tunc, D.; Carlotti, S. Polyether Synthesis: From Activated or Metal-Free Anionic Ring-Opening Polymerization of Epoxides to Functionalization. *Prog. Polym. Sci.* **2013**, *38*, 845−873.

(74) Aida, T.; Inoue, S. Living Polymerization of Epoxides with Metalloporphyrin and Synthesis of Block Copolymers with Controlled Chain Lengths. *Macromolecules* **1981**, *14*, 1162−1166.

(75) Aida, T.; Mizuta, R.; Yoshida, Y.; Inoue, S. Polymerization of Epoxides Catalysed by Metalloporphine. *Makromol. Chem.* **1981**, *182*, 1073−1079.

(76) Sugimoto, H.; Kawamura, C.; Kuroki, M.; Aida, T.; Inoue, S. Lewis Acid-Assisted Anionic Ring-Opening Polymerization of Epoxide by the Aluminum Complexes of Porphyrin, Phthalocyanine, Tetraazaannulene, and Schiff Base as Initiators. *Macromolecules* **1994**, *27*, 2013−2018.

(77) Akatsuka, M.; Aida, T.; Inoue, S. High-Speed "Immortal" Polymerization of Epoxides with Aluminum Porphyrin. Acceleration of Propagation and Chain-Transfer Reactions by a Lewis Acid. *Macromolecules* **1994**, *27*, 2820−2825.

(78) Aida, T.; Inoue, S. Metalloporphyrins as Initiators for Living and Immortal Polymerizations. *Acc. Chem. Res.* **1996**, *29*, 39−48.

(79) Braune, W.; Okuda, J. An Efficient Method for Controlled Propylene Oxide Polymerization: The Significance of Bimetallic Activation in Aluminum Lewis Acids. *Angew. Chem., Int. Ed.* **2003**, *42*, 64−68.

(80) Labbé, A.; Carlotti, S.; Billouard, C.; Desbois, P.; Deffieux, A. Controlled High-Speed Anionic Polymerization of Propylene Oxide Initiated by Onium Salts in the Presence of Triisobutylaluminum. *Macromolecules* **2007**, *40*, 7842−7847.

(81) Deffieux, A.; Carlotti, S.; Desbois, P. New Perspectives in Living/Controlled Anionic Polymerization. *Macromol. Symp.* **2005**, *229*, 24−31.

(82) Carlotti, S.; Desbois, P.; Billouard, C.; Deffieux, A. Reactivity Control in Anionic Polymerization of Ethylenic and Heterocyclic Monomers through Formation of 'Ate' Complexes. *Polym. Int.* **2006**, *55*, 1126−1131.

(83) Gervais, M.; Labbé, A. l.; Carlotti, S.; Deffieux, A. Direct Synthesis of α-Azido,ω -Hydroxypolyethers by Monomer-Activated Anionic Polymerization. *Macromolecules* **2009**, *42*, 2395−2400.

(84) Sakakibara, K.; Nakano, K.; Nozaki, K. Regio-Controlled Ring-Opening Polymerization of Perfluoroalkyl-Substituted Epoxides. *Chem. Commun.* **2006**, 3334−3336.

(85) Sakakibara, K.; Nakano, K.; Nozaki, K. Regioregular Polymerization of Fluorine-Containing Epoxides. *Macromolecules* **2007**, *40*, 6136−6142.

(86) Roos, K.; Carlotti, S. Grignard-Based Anionic Ring-Opening Polymerization of Propylene Oxide Activated by Triisobutylaluminum. *Eur. Polym. J.* **2015**, *70*, 240−246.

(87) Herzberger, J.; Frey, H. Epicyanohydrin: Polymerization by Monomer Activation Gives Access to Nitrile-, Amino-, and Carboxyl-Functional Poly(ethylene glycol). *Macromolecules* **2015**, *48*, 8144−8153.

(88) Rejsek, V.; Sauvanier, D.; Billouard, C.; Desbois, P.; Deffieux, A.; Carlotti, S. Controlled Anionic Homo- and Copolymerization of Ethylene Oxide and Propylene Oxide by Monomer Activation. *Macromolecules* **2007**, *40*, 6510−6514.

(89) Gervais, M.; Brocas, A.-L.; Cendejas, G.; Deffieux, A.; Carlotti, S. Synthesis of Linear High Molar Mass Glycidol-Based Polymers by Monomer-Activated Anionic Polymerization. *Macromolecules* **2010**, *43*, 1778−1784.

(90) Brocas, A.-L.; Deffieux, A.; Le Malicot, N.; Carlotti, S. Combination of Phosphazene Base and Triisobutylaluminum for the Rapid Synthesis of Polyhydroxy Telechelic Poly(propylene oxide). *Polym. Chem.* **2012**, *3*, 1189−1195.

(91) Pierre, L. E. S.; Price, C. C. The Room Temperature Polymerization of Propylene Oxide. *J. Am. Chem. Soc.* **1956**, *78*, 3432−3436.

(92) Quirk, R. P.; Lizarraga, G. M. Anionic Synthesis of Well-Defined, Poly[(styrene)-block-(propylene oxide)] Block Copolymers. *Macromol. Chem. Phys.* **2000**, *201*, 1395−1404.

(93) Grobelny, Z.; Matlengiewicz, M.; Jurek, J.; Michalak, M.; Kwapulińska, D.; Swinarew, A.; Schab-Balcerzak, E. The Influence of Macrocyclic Ligands and Water on Propylene Oxide Polymerization Initiated with Anhydrous Potassium Hydroxide in Tetrahydrofuran. *Eur. Polym. J.* **2013**, *49*, 3277−3288.

(94) Osterwinter, C.; Schubert, C.; Tonhauser, C.; Wilms, D.; Frey, H.; Friedrich, C. Rheological Consequences of Hydrogen Bonding: Linear Viscoelastic Response of Linear Polyglycerol and Its Permethylated Analogues as a General Model for Hydroxyl-Functional Polymers. *Macromolecules* **2015**, *48*, 119−130.

(95) Brocas, A.-L.; Gervais, M.; Carlotti, S.; Pispas, S. Amphiphilic Diblock Copolymers Based on Ethylene Oxide and Epoxides Bearing Aliphatic Side Chains. *Polym. Chem.* **2012**, *3*, 2148.

(96) Gervais, M.; Brocas, A.-L.; Deffieux, A.; Ibarboure, E.; Carlotti, S. Rapid and Controlled Synthesis of Hydrophobic Polyethers by Monomer Activation. *Pure Appl. Chem.* **2012**, *84*, 2103−2111.

(97) Müller, S. S.; Moers, C.; Frey, H. A Challenging Comonomer Pair: Copolymerization of Ethylene Oxide and Glycidyl Methyl Ether to Thermoresponsive Polyethers. *Macromolecules* **2014**, *47*, 5492−5500.

(98) Labbé, A. l.; Brocas, A.-L.; Ibarboure, E.; Ishizone, T.; Hirao, A.; Deffieux, A.; Carlotti, S. Selective Ring-Opening Polymerization of Glycidyl Methacrylate: Toward the Synthesis of Cross-Linked (Co)-polyethers with Thermoresponsive Properties. *Macromolecules* **2011**, *44*, 6356−6364.

(99) Labbé, A.; Carlotti, S.; Deffieux, A.; Hirao, A. Controlled Polymerization of Glycidyl Methyl Ether Initiated by Onium Salt/Triisobutylaluminum and Investigation of the Polymer LCST. *Macromol. Symp.* **2007**, *249−250*, 392−397.

(100) Carlotti, S.; Labbé, A. l.; Rejsek, V.; Doutaz, S. p.; Gervais, M.; Deffieux, A. Living/Controlled Anionic Polymerization and Copolymerization of Epichlorohydrin with Tetraoctylammonium Bromide−Triisobutylaluminum Initiating Systems. *Macromolecules* **2008**, *41*, 7058−7062.

(101) Lundberg, P.; Lee, B. F.; van den Berg, S. A.; Pressly, E. D.; Lee, A.; Hawker, C. J.; Lynd, N. A. Poly[(ethylene oxide)-co-(methylene ethylene oxide)]: A Hydrolytically Degradable Poly(ethylene oxide) Platform. *ACS Macro Lett.* **2012**, *1*, 1240−1243.

(102) Meyer, J.; Keul, H.; Möller, M. Poly(glycidyl amine) and Copolymers with Glycidol and Glycidyl Amine Repeating Units: Synthesis and Characterization. *Macromolecules* **2011**, *44*, 4082−4091.

(103) Hu, H.; Yuan, W.; Lu, L.; Zhao, H.; Jia, Z.; Baker, G. L. Low Glass Transition Temperature Polymer Electrolyte Prepared from Ionic Liquid Grafted Polyethylene Oxide. *J. Polym. Sci., Part A: Polym. Chem.* **2014**, *52*, 2104−2110.

(104) Brocas, A.-L.; Cendejas, G.; Caillol, S.; Deffieux, A.; Carlotti, S. Controlled Synthesis of Polyepichlorohydrin with Pendant Cyclic Carbonate Functions for Isocyanate-Free Polyurethane Networks. *J. Polym. Sci., Part A: Polym. Chem.* **2011**, *49*, 2677−2684.

(105) Rejsek, V.; Desbois, P.; Deffieux, A.; Carlotti, S. Polymerization of Ethylene Oxide Initiated by Lithium Derivatives Via the Monomer-Activated Approach: Application to the Direct Synthesis of PS-*b*-PEO and PI-*b*-PEO Diblock Copolymers. *Polymer* **2010**, *51*, 5674−5679.

(106) Babu, H. V.; Muralidharan, K. Polyethers with Phosphate Pendant Groups by Monomer Activated Anionic Ring Opening Polymerization: Syntheses, Characterization and Their Lithium-Ion Conductivities. *Polymer* **2014**, *55*, 83−94.

(107) Hahn, F. E. Heterocyclic Carbenes. *Angew. Chem., Int. Ed.* **2006**, *45*, 1348−1352.

(108) Herrmann, W. A. N-Heterocyclic Carbenes: A New Concept in Organometallic Catalysis. *Angew. Chem., Int. Ed.* **2002**, *41*, 1290−1309.

(109) Enders, D.; Niemeier, O.; Henseler, A. Organocatalysis by N-Heterocyclic Carbenes. *Chem. Rev.* **2007**, *107*, 5606−5655.

(110) Marion, N.; Díez-González, S.; Nolan, S. P. N-Heterocyclic Carbenes as Organocatalysts. *Angew. Chem., Int. Ed.* **2007**, *46*, 2988−3000.

(111) Flanigan, D. M.; Romanov-Michailidis, F.; White, N. A.; Rovis, T. Organocatalytic Reactions Enabled by N-Heterocyclic Carbenes. *Chem. Rev.* **2015**, *115*, 9307−9387.

(112) Fèvre, M.; Pinaud, J.; Gnanou, Y.; Vignolle, J.; Taton, D. N-Heterocyclic Carbenes (NHCs) as Organocatalysts and Structural Components in Metal-Free Polymer Synthesis. *Chem. Soc. Rev.* **2013**, *42*, 2142−2172.

(113) Fèvre, M.; Vignolle, J.; Gnanou, Y.; Taton, D. in *Polymer Science: A Comprehensive Reference*; Penczek, S., Grubbs, R. H., Eds.; Elsevier: Amsterdam, 2012; Vol. *4*, pp 67−115.

(114) Naumann, S.; Dove, A. P. N-Heterocyclic Carbenes as Organocatalysts for Polymerizations: Trends and Frontiers. *Polym. Chem.* **2015**, *6*, 3185−3200.

(115) Naumann, S.; Dove, A. P. N-Heterocyclic Carbenes for Metal-Free Polymerization Catalysis: An Update. *Polym. Int.* **2015**, DOI: 10.1002/pi.5034.

(116) Arduengo, A. J.; Harlow, R. L.; Kline, M. A Stable Crystalline Carbene. *J. Am. Chem. Soc.* **1991**, *113*, 361−363.

(117) Jones, R. A.; Karatza, M.; Voro, T. N.; Civcir, P. U.; Franck, A.; Ozturk, O.; Seaman, J. P.; Whitmore, A. P.; Williamson, D. J. Extended Heterocyclic Systems 1. The Synthesis and Characterisation of Pyrrolylpyridines, Alternating Pyrrole: Pyridine Oligomers and Polymers, and Related Systems. *Tetrahedron* **1996**, *52*, 8707−8724.

(118) Jones, R. A.; Civcir, P. U. Extended Heterocyclic Systems 2. The Synthesis and Characterisation of (2-Furyl)pyridines, (2-Thienyl)-pyridines, and Furan-Pyridine and Thiophene-Pyridine Oligomers. *Tetrahedron* **1997**, *53*, 11529−11540.

(119) Raynaud, J.; Absalon, C.; Gnanou, Y.; Taton, D. N-Heterocyclic Carbene-Induced Zwitterionic Ring-Opening Polymerization of Ethylene Oxide and Direct Synthesis of α,ω-Difunctionalized Poly(ethylene oxide)s and Poly(ethylene oxide)-*b*-Poly(ε-caprolactone) Block Copolymers. *J. Am. Chem. Soc.* **2009**, *131*, 3201−3209.

(120) Raynaud, J.; Absalon, C.; Gnanou, Y.; Taton, D. N-Heterocyclic Carbene-Organocatalyzed Ring-Opening Polymerization of Ethylene Oxide in the Presence of Alcohols or Trimethylsilyl Nucleophiles as Chain Moderators for the Synthesis of α,ω-Heterodifunctionalized Poly(ethylene oxide)s. *Macromolecules* **2010**, *43*, 2814−2823.

(121) Raynaud, J.; Ottou, W. N.; Gnanou, Y.; Taton, D. Metal-Free and Solvent-Free Access to α,ω-Heterodifunctionalized Poly(propylene oxide)s by N-Heterocyclic Carbene-Induced Ring Opening Polymerization. *Chem. Commun.* **2010**, *46*, 3203−3205.

346

(122) Lindner, R.; Lejkowski, M. L.; Lavy, S.; Deglmann, P.; Wiss, K. T.; Zarbakhsh, S.; Meyer, L.; Limbach, M. Ring-Opening Polymerization and Copolymerization of Propylene Oxide Catalyzed by *N*-Heterocyclic Carbenes. *ChemCatChem* **2014**, *6*, 618−625.

(123) Naumann, S.; Buchmeiser, M. R. Liberation of *N*-Heterocyclic Carbenes (NHCs) from Thermally Labile Progenitors: Protected NHCs as Versatile Tools in Organo- and Polymerization Catalysis. *Catal. Sci. Technol.* **2014**, *4*, 2466.

(124) Fèvre, M.; Vignolle, J.; Taton, D. Azolium Hydrogen Carbonates and Azolium Carboxylates as Organic Pre-Catalysts for *N*-Heterocyclic Carbene-Catalysed Group Transfer and Ring-Opening Polymerisations. *Polym. Chem.* **2013**, *4*, 1995−2003.

(125) Naumann, S.; Thomas, A. W.; Dove, A. P. *N*-Heterocyclic Olefins as Organocatalysts for Polymerization: Preparation of Well-Defined Poly(propylene oxide). *Angew. Chem., Int. Ed.* **2015**, *54*, 9550−9554.

(126) Kuhn, N.; Bohnen, H.; Kreutzberg, J.; Blaser, D.; Boese, R. 1,3,4,5-Tetramethyl-2-Methyleneimidazoline-an Ylidic Olefin. *J. Chem. Soc., Chem. Commun.* **1993**, 1136−1137.

(127) Kronig, S.; Jones, P. G.; Tamm, M. Preparation of 2-Alkylidene-Substituted 1,3,4,5-Tetramethylimidazolines and Their Reactivity Towards Rh^I Complexes and B(C$_6$F$_5$)$_3$. *Eur. J. Inorg. Chem.* **2013**, *2013*, 2301−2314.

(128) Fürstner, A.; Alcarazo, M.; Goddard, R.; Lehmann, C. W. Coordination Chemistry of Ene-1,1-Diamines and a Prototype "Carbodicarbene". *Angew. Chem., Int. Ed.* **2008**, *47*, 3210−3214.

(129) Boileau, S.; Illy, N. Activation in Anionic Polymerization: Why Phosphazene Bases Are Very Exciting Promoters. *Prog. Polym. Sci.* **2011**, *36*, 1132−1151.

(130) Zhao, J.; Hadjichristidis, N. A.; Gnanou, Y. Phosphazene-Promoted Anionic Polymerization. *Polimery* **2014**, *59*, 49−59.

(131) Hirao, A.; Goseki, R.; Ishizone, T. Advances in Living Anionic Polymerization: From Functional Monomers, Polymerization Systems, to Macromolecular Architectures. *Macromolecules* **2014**, *47*, 1883−1905.

(132) Zhao, J.; Hadjichristidis, N. A.; Schlaad, H. In *Anionic Polymerization*; Hadjichristidis, N., Hirao, A., Eds.; Springer: Japan, 2015; pp 429−449.

(133) Schwesinger, R.; Schlemper, H. Peralkylated Polyaminophosphazenes— Extremely Strong, Neutral Nitrogen Bases. *Angew. Chem., Int. Ed. Engl.* **1987**, *26*, 1167−1169.

(134) Schwesinger, R.; Hasenfratz, C.; Schlemper, H.; Walz, L.; Peters, E.-M.; Peters, K.; von Schnering, H. G. How Strong and How Hindered Can Uncharged Phosphazene Bases Be? *Angew. Chem., Int. Ed. Engl.* **1993**, *32*, 1361−1363.

(135) Schwesinger, R.; Schlemper, H.; Hasenfratz, C.; Willaredt, J.; Dambacher, T.; Breuer, T.; Ottaway, C.; Fletschinger, M.; Boele, J.; Fritz, H.; et al. Extremely Strong, Uncharged Auxiliary Bases; Monomeric and Polymer-Supported Polyaminophosphazenes (P$_2$−P$_5$). *Liebigs Ann. Chem.* **1996**, *1996*, 1055−1081.

(136) Solladié-Cavallo, A.; Liptaj, T.; Schmitt, M.; Solgadi, A. Iso-Propyl Phenylacetate: Formation of a Single Enolate with *t*-BuP$_4$ as Base. *Tetrahedron Lett.* **2002**, *43*, 415−418.

(137) Eßwein, B.; Steidl, N. M.; Möller, M. Anionic Polymerization of Oxirane in the Presence of the Polyiminophosphazene Base *t*-BuP$_4$. *Macromol. Rapid Commun.* **1996**, *17*, 143−148.

(138) Rexin, O.; Mülhaupt, R. Anionic Ring-Opening Polymerization of Propylene Oxide in the Presence of Phosphonium Catalysts. *J. Polym. Sci., Part A: Polym. Chem.* **2002**, *40*, 864−873.

(139) Rexin, O.; Mülhaupt, R. Anionic Ring-Opening Polymerization of Propylene Oxide in the Presence of Phosphonium Catalysts at Various Temperatures. *Macromol. Chem. Phys.* **2003**, *204*, 1102−1109.

(140) Zhao, J.; Pahovnik, D.; Gnanou, Y.; Hadjichristidis, N. Sequential Polymerization of Ethylene Oxide, *ε*-Caprolactone and L-Lactide: A One-Pot Metal-Free Route to Tri- and Pentablock Terpolymers. *Polym. Chem.* **2014**, *5*, 3750−3753.

(141) Misaka, H.; Tamura, E.; Makiguchi, K.; Kamoshida, K.; Sakai, R.; Satoh, T.; Kakuchi, T. Synthesis of End-Functionalized Polyethers by Phosphazene Base-Catalyzed Ring-Opening Polymerization of 1,2-Butylene Oxide and Glycidyl Ether. *J. Polym. Sci., Part A: Polym. Chem.* **2012**, *50*, 1941−1952.

(142) Keul, H.; Möller, M. Synthesis and Degradation of Biomedical Materials Based on Linear and Star Shaped Polyglycidols. *J. Polym. Sci., Part A: Polym. Chem.* **2009**, *47*, 3209−3231.

(143) Kwon, W.; Rho, Y.; Kamoshida, K.; Kwon, K. H.; Jeong, Y. C.; Kim, J.; Misaka, H.; Shin, T. J.; Kim, J.; Kim, K.-W.; et al. Well-Defined Functional Linear Aliphatic Diblock Copolyethers: A Versatile Linear Aliphatic Polyether Platform for Selective Functionalizations and Various Nanostructures. *Adv. Funct. Mater.* **2012**, *22*, 5194−5208.

(144) Reinicke, S.; Schmelz, J.; Lapp, A.; Karg, M.; Hellweg, T.; Schmalz, H. Smart Hydrogels Based on Double Responsive Triblock Terpolymers. *Soft Matter* **2009**, *5*, 2648−2657.

(145) Zhao, J.; Pahovnik, D.; Gnanou, Y.; Hadjichristidis, N. Catalyst Switch" Strategy for the Sequential Metal-Free Polymerization of Epoxides and Cyclic Esters/Carbonate. *Macromolecules* **2014**, *47*, 3814−3822.

(146) Zhao, J.; Pahovnik, D.; Gnanou, Y.; Hadjichristidis, N. One-Pot Synthesis of Linear- and Three-Arm Star-Tetrablock Quarterpolymers Via Sequential Metal-Free Ring-Opening Polymerization Using a "Catalyst Switch" Strategy. *J. Polym. Sci., Part A: Polym. Chem.* **2015**, *53*, 304−312.

(147) Zhao, J.; Pahovnik, D.; Gnanou, Y.; Hadjichristidis, N. Phosphazene-Promoted Metal-Free Ring-Opening Polymerization of Ethylene Oxide Initiated by Carboxylic Acid. *Macromolecules* **2014**, *47*, 1693−1698.

(148) Esswein, B.; Möller, M. Polymerization of Ethylene Oxide with Alkyllithium Compounds and the Phosphazene Base "*t*-BuP$_4$. *Angew. Chem., Int. Ed. Engl.* **1996**, *35*, 623−625.

(149) Zhao, J.; Schlaad, H.; Weidner, S.; Antonietti, M. Synthesis of Terpene-Poly(ethylene oxide)S by *t*-BuP$_4$-Promoted Anionic Ring-Opening Polymerization. *Polym. Chem.* **2012**, *3*, 1763−1768.

(150) Misaka, H.; Sakai, R.; Satoh, T.; Kakuchi, T. Synthesis of High Molecular Weight and End-Functionalized Poly(Styrene Oxide) by Living Ring-Opening Polymerization of Styrene Oxide Using the Alcohol/Phosphazene Base Initiating System. *Macromolecules* **2011**, *44*, 9099−9107.

(151) Isono, T.; Asai, S.; Satoh, Y.; Takaoka, T.; Tajima, K.; Kakuchi, T.; Satoh, T. Controlled/Living Ring-Opening Polymerization of Glycidylamine Derivatives Using *t*-BuP$_4$/Alcohol Initiating System Leading to Polyethers with Pendant Primary, Secondary, and Tertiary Amino Groups. *Macromolecules* **2015**, *48*, 3217−3229.

(152) Zhao, J.; Alamri, H.; Hadjichristidis, N. A Facile Metal-Free "Grafting-from" Route from Acrylamide-Based Substrate toward Complex Macromolecular Combs. *Chem. Commun.* **2013**, *49*, 7079−7081.

(153) Dentzer, L.; Bray, C.; Noinville, S.; Illy, N.; Guégan, P. Phosphazene-Promoted Metal-Free Ring-Opening Polymerization of 1,2-Epoxybutane Initiated by Secondary Amides. *Macromolecules* **2015**, *48*, 7755−7764.

(154) Isono, T.; Kamoshida, K.; Satoh, Y.; Takaoka, T.; Sato, S.-i.; Satoh, T.; Kakuchi, T. Synthesis of Star- and Figure-Eight-Shaped Polyethers by *t*-BuP$_4$-Catalyzed Ring-Opening Polymerization of Butylene Oxide. *Macromolecules* **2013**, *46*, 3841−3849.

(155) Isono, T.; Satoh, Y.; Miyachi, K.; Chen, Y.; Sato, S.-i.; Tajima, K.; Satoh, T.; Kakuchi, T. Synthesis of Linear, Cyclic, Figure-Eight-Shaped, and Tadpole-Shaped Amphiphilic Block Copolyethers via *t*-BuP$_4$ Catalyzed Ring-Opening Polymerization of Hydrophilic and Hydrophobic Glycidyl Ethers. *Macromolecules* **2014**, *47*, 2853−2863.

(156) Schmalz, H.; Lanzendörfer, M. G.; Abetz, V.; Müller, A. H. E. Anionic Polymerization of Ethylene Oxide in the Presence of the Phosphazene Base *t*-BuP$_4$ − Kinetic Investigations Using In-Situ Ft-NIR Spectroscopy and MALDI-ToF MS. *Macromol. Chem. Phys.* **2003**, *204*, 1056−1071.

(157) Toy, A. A.; Reinicke, S.; Müller, A. H. E.; Schmalz, H. One-Pot Synthesis of Polyglycidol-Containing Block Copolymers with Alkyllithium Initiators Using the Phosphazene Base *t*-BuP$_4$. *Macromolecules* **2007**, *40*, 5241−5244.

(158) Förster, S.; Krämer, E. Synthesis of PB−PEO and PI−PEO Block Copolymers with Alkyllithium Initiators and the Phosphazene Base t-BuP₄. *Macromolecules* **1999**, *32*, 2783−2785.

(159) Pispas, S.; Hadjichristidis, N. Aggregation Behavior of Poly(butadiene-b-ethylene oxide) Block Copolymers in Dilute Aqueous Solutions: Effect of Concentration, Temperature, Ionic Strength, and Type of Surfactant. *Langmuir* **2003**, *19*, 48−54.

(160) Justynska, J.; Hordyjewicz, Z.; Schlaad, H. Toward a Toolbox of Functional Block Copolymers Via Free-Radical Addition of Mercaptans. *Polymer* **2005**, *46*, 12057−12064.

(161) Floudas, G.; Vazaiou, B.; Schipper, F.; Ulrich, R.; Wiesner, U.; Iatrou, H.; Hadjichristidis, N. Poly(ethylene oxide-b-isoprene) Diblock Copolymer Phase Diagram. *Macromolecules* **2001**, *34*, 2947−2957.

(162) Schmalz, H.; Knoll, A.; Müller, A. J.; Abetz, V. Synthesis and Characterization of ABC Triblock Copolymers with Two Different Crystalline End Blocks: Influence of Confinement on Crystallization Behavior and Morphology. *Macromolecules* **2002**, *35*, 10004−10013.

(163) Siebert, M.; Albrecht, K.; Spiertz, R.; Keul, H.; Moller, M. Reactive Amphiphilic Block Copolymers for the Preparation of Hybrid Organic/Inorganic Materials with Covalent Interactions. *Soft Matter* **2011**, *7*, 587−594.

(164) Zhao, J.; Mountrichas, G.; Zhang, G.; Pispas, S. Amphiphilic Polystyrene-b-Poly(p-hydroxystyrene-g-ethylene oxide) Block−Graft Copolymers via a Combination of Conventional and Metal-Free Anionic Polymerization. *Macromolecules* **2009**, *42*, 8661−8668.

(165) Schacher, F.; Müllner, M.; Schmalz, H.; Müller, A. H. E. New Block Copolymers with Poly(N,N-dimethylaminoethyl methacrylate) as a Double Stimuli-Responsive Block. *Macromol. Chem. Phys.* **2009**, *210*, 256−262.

(166) Zhang, L.; Nederberg, F.; Messman, J. M.; Pratt, R. C.; Hedrick, J. L.; Wade, C. G. Organocatalytic Stereoselective Ring-Opening Polymerization of Lactide with Dimeric Phosphazene Bases. *J. Am. Chem. Soc.* **2007**, *129*, 12610−12611.

(167) Zhang, L.; Nederberg, F.; Pratt, R. C.; Waymouth, R. M.; Hedrick, J. L.; Wade, C. G. Phosphazene Bases: A New Category of Organocatalysts for the Living Ring-Opening Polymerization of Cyclic Esters. *Macromolecules* **2007**, *40*, 4154−4158.

(168) Yang, H.; Xu, J.; Pispas, S.; Zhang, G. Hybrid Copolymerization of ε-Caprolactone and Methyl Methacrylate. *Macromolecules* **2012**, *45*, 3312−3317.

(169) Xu, J.; Yang, J.; Ye, X.; Ma, C.; Zhang, G.; Pispas, S. Synthesis and Properties of Amphiphilic and Biodegradable Poly(ε-Caprolactone-co-glycidol) Copolymers. *J. Polym. Sci., Part A: Polym. Chem.* **2015**, *53*, 846−853.

(170) Zhao, J.; Hadjichristidis, N. Polymerization of 5-Alkyl δ-Lactones Catalyzed by Diphenyl Phosphate and Their Sequential Organocatalytic Polymerization with Monosubstituted Epoxides. *Polym. Chem.* **2015**, *6*, 2659−2668.

(171) Penelle, J. *unpublished results* **2015**.

(172) Chen, S.; Xu, N.; Shi, J. Structure and Properties of Polyether Polyols Catalyzed by Fe/Zn Double Metal Cyanide Complex Catalyst. *Prog. Org. Coat.* **2004**, *49*, 125−129.

(173) Johnston, H. R.; Gen Tire & Rubber Co: U.S. Patent 3,278,459, 1966.

(174) Kim, I.; Ahn, J.-T.; Ha, C. S.; Yang, C. S.; Park, I. Polymerization of Propylene Oxide by Using Double Metal Cyanide Catalysts and the Application to Polyurethane Elastomer. *Polymer* **2003**, *44*, 3417−3428.

(175) Ehlers, S.; Bayer Aktiengesellschaft: U.S. Patent 6,486,361, 2002.

(176) Ostrowski, T.; BASF Aktiengesellschaft: U.S. Patent 7,968,754, 2005.

(177) Eleveld, M. B.; Shell Oil Company: U.S. Patent 6,977,236, 2005.

(178) Buckley, B. J.; Dow Global Technologies LLC: U.S. Patent 20140094534 A1, 2012.

(179) Ionescu, M. *Chemistry and Technology of Polyols for Polyurethanes*; Rapra Technology, 2005.

(180) Huang, Y. J.; Qi, G. R.; Chen, L. S. Effects of Morphology and Composition on Catalytic Performance of Double Metal Cyanide Complex Catalyst. *Appl. Catal., A* **2003**, *240*, 263−271.

(181) Huang, Y.-J.; Zhang, X.-H.; Hua, Z.-J.; Chen, S.-L.; Qi, G.-R. Ring-Opening Polymerization of Propylene Oxide Catalyzed by a Calcium-Chloride-Modified Zinc-Cobalt Double Metal-Cyanide Complex. *Macromol. Chem. Phys.* **2010**, *211*, 1229−1237.

(182) Wei, R.-J.; Zhang, Y.-Y.; Zhang, X.-H.; Du, B.-Y.; Fan, Z.-Q. Regio-Selective Synthesis of Polyepichlorohydrin Diol Using Zn-Co(III) Double Metal Cyanide Complex. *RSC Adv.* **2014**, *4*, 21765−21771.

(183) Zhang, X.-H.; Hua, Z.-J.; Chen, S.; Liu, F.; Sun, X.-K.; Qi, G.-R. Role of Zinc Chloride and Complexing Agents in Highly Active Double Metal Cyanide Catalysts for Ring-Opening Polymerization of Propylene Oxide. *Appl. Catal., A* **2007**, *325*, 91−98.

(184) Chen, S.; Zhang, P.; Chen, L. Fe/Zn Double Metal Cyanide (DMC) Catalyzed Ring-Opening Polymerization of Propylene Oxide: Part 3. Synthesis of DMC Catalysts. *Prog. Org. Coat.* **2004**, *50*, 269−272.

(185) Yoon, J. H.; Lee, I. K.; Choi, H. Y.; Choi, E. J.; Yoon, J. H.; Shim, S. E.; Kim, I. Double Metal Cyanide Catalysts Bearing Lactate Esters as eco-Friendly Complexing Agents for the Synthesis of Highly Pure Polyols. *Green Chem.* **2011**, *13*, 631−639.

(186) Kim, I.; Anas, K.; Lee, S.; Ha, C.-S.; Park, D.-W. Tuning of the Activity and Induction Period of Double Metal Cyanide Catalyzed Ring-Opening Polymerizations of Propylene Oxide by Using Ionic Liquids. *Catal. Today* **2008**, *131*, 541−547.

(187) Huang, Y. J.; Zhang, X. H.; Hua, Z. J.; Qi, G. R. Calcium Chloride Doped Zinc-Cobalt Metal-Cyanide Complex: Unexpected Highly Activity Towards Ring-Opening Polymerization of Propylene Oxide. *Chin. Chem. Lett.* **2010**, *21*, 897−901.

(188) Lee, S. H.; Lee, I. K.; Ha, J. Y.; Jo, J. K.; Park, I.; Ha, C.-S.; Suh, H.; Kim, I. Tuning of the Activity and Induction Period of the Polymerization of Propylene Oxide Catalyzed by Double Metal Cyanide Complexes Bearing β-Alkoxy Alcohols as Complexing Agents. *Ind. Eng. Chem. Res.* **2010**, *49*, 4107−4116.

(189) Lee, S.; Baek, S. T.; Anas, K.; Ha, C.-S.; Park, D.-W.; Lee, J. W.; Kim, I. Tuning of Activity, Induction Period and Polymer Properties of Double Metal Cyanide Catalyzed Ring-Opening Polymerizations of Propylene Oxide by Using Quaternary Ammonium Salts. *Polymer* **2007**, *48*, 4361−4367.

(190) Ooms, P.; Bayer Aktiengesellschaft: U.S. Patent 6,376,420, 2002.

(191) Ooms, P.; Bayer Aktiengesellschaft: U.S. Patent 6,953,765, 2005.

(192) Kim, I.; Ahn, J.-T.; Lee, S.-H.; Ha, C.-S.; Park, D.-W. Preparation of Multi-Metal Cyanide Catalysts and Ring-Opening Polymerization of Propylene Oxide. *Catal. Today* **2004**, *93−95*, 511−516.

(193) Lee, S. H.; Byun, S. H.; Baek, S. T.; Seo, H. S.; Park, D.-W.; Ha, C.-S.; Kim, I. Multi-Metal Cyanide Catalysts for Ring-Opening Polymerization of Propylene Oxide. *Catal. Today* **2008**, *132*, 170−177.

(194) Byun, S.; Seo, H.; Lee, S.; Ha, C.-S.; Kim, I. Zn(II)-Co(III)-Fe(III) Multi-Metal Cyanide Complexes as Highly Active Catalysts for Ring-Opening Polymerization of Propylene Oxide. *Macromol. Res.* **2007**, *15*, 393−395.

(195) Yu, S. J.; Liu, Y.; Byeon, S. J.; Park, D. W.; Kim, I. Ring-Opening Polymerization of Propylene Oxide by Double Metal Cyanide Catalysts Prepared by Reacting CoCl₂ with Various Metal Cyanide Salts. *Catal. Today* **2014**, *232*, 75−81.

(196) Huang, Y.-J.; Qi, G.-R.; Wang, Y.-H. Controlled Ring-Opening Polymerization of Propylene Oxide Catalyzed by Double Metal-Cyanide Complex. *J. Polym. Sci., Part A: Polym. Chem.* **2002**, *40*, 1142−1150.

(197) Wu, L.-C.; Yu, A.-F.; Zhang, M.; Liu, B.-H.; Chen, L.-B. DMC Catalyzed Epoxide Polymerization: Induction Period, Kinetics, and Mechanism. *J. Appl. Polym. Sci.* **2004**, *92*, 1302−1309.

(198) Televantos, Y.; Le-Khac, Bi. ARCO Chemical Technology; U.S. Patent 5,767,323, 1998.

(199) Hayes, J. E. Bayer Antwerp; U.S. Patent 6,835,801, 2004.

(200) Kaushiva, B. D. Bayer Materialscience Llc; U.S. Patent 7,005,552 B2, 2006.

(201) Pazos, J. F. Arco Chemical Technology; U.S. Patent 5,777,177, 1998.

(202) McDaniel, K. G.; Combs, G. G. Bayer Materialsscience, Llc; U.S. Patent 20140275632 A1, 2014.

348

(203) Laitar, D. S.; Babb, D. A.; Villa, C. M.; Keaton, R.; Masy, J.-P. U.S. Patent 2,013,028,9236, 2013.

(204) Clement, K. S. Dow Global Technologies, Inc.; U.S. Patent 6,642,423, 2002.

(205) Darensbourg, D. J.; Adams, M. J.; Yarbrough, J. C. Toward the Design of Double Metal Cyanides for the Copolymerization of CO_2 and Epoxides. *Inorg. Chem.* **2001**, *40*, 6543−6544.

(206) Chen, S.; Hua, Z.; Fang, Z.; Qi, G. Copolymerization of Carbon Dioxide and Propylene Oxide with Highly Effective Zinc Hexacyanocobaltate(III)-Based Coordination Catalyst. *Polymer* **2004**, *45*, 6519−6524.

(207) Robertson, N. J.; Qin, Z.; Dallinger, G. C.; Lobkovsky, E. B.; Lee, S.; Coates, G. W. Two-Dimensional Double Metal Cyanide Complexes: Highly Active Catalysts for the Homopolymerization of Propylene Oxide and Copolymerization of Propylene Oxide and Carbon Dioxide. *Dalton Transactions* **2006**, 5390−5395.

(208) Sun, X.-K.; Zhang, X.-H.; Chen, S.; Du, B.-Y.; Wang, Q.; Fan, Z.-Q.; Qi, G.-R. One-Pot Terpolymerization of CO_2, Cyclohexene Oxide and Maleic Anhydride Using a Highly Active Heterogeneous Double Metal Cyanide Complex Catalyst. *Polymer* **2010**, *51*, 5719−5725.

(209) Sun, X.-K.; Zhang, X.-H.; Wei, R.-J.; Du, B.-Y.; Wang, Q.; Fan, Z.-Q.; Qi, G.-R. Mechanistic Insight into Initiation and Chain Transfer Reaction of CO_2/Cyclohexene Oxide Copolymerization Catalyzed by Zinc-Cobalt Double Metal Cyanide Complex Catalysts. *J. Polym. Sci., Part A: Polym. Chem.* **2012**, *50*, 2924−2934.

(210) Wei, R.-J.; Zhang, X.-H.; Du, B.-Y.; Fan, Z.-Q.; Qi, G.-R. Selective Production of Poly(carbonate−*co*−ether) over Cyclic Carbonate for Epichlorohydrin and CO_2 Copolymerization Via Heterogeneous Catalysis of Zn−Co (III) Double Metal Cyanide Complex. *Polymer* **2013**, *54*, 6357−6362.

(211) Wei, R.-J.; Zhang, X.-H.; Du, B.-Y.; Sun, X.-K.; Fan, Z.-Q.; Qi, G.-R. Highly Regioselective and Alternating Copolymerization of Racemic Styrene Oxide and Carbon Dioxide Via Heterogeneous Double Metal Cyanide Complex Catalyst. *Macromolecules* **2013**, *46*, 3693−3697.

(212) Wei, R.-J.; Zhang, X.-H.; Zhang, Y.-Y.; Du, B.-Y.; Fan, Z.-Q.; Qi, G.-R. Functional Poly(carbonate-*co*-ether) Synthesis from Glycidyl Methacrylate/CO_2 Copolymerization Catalyzed by Zn-Co(III) Double Metal Cyanide Complex Catalyst. *RSC Adv.* **2014**, *4*, 3188−3194.

(213) Sebastian, J.; Srinivas, D. Effects of Method of Preparation on Catalytic Activity of Co−Zn Double-Metal Cyanide Catalysts for Copolymerization of CO_2 and Epoxide. *Appl. Catal., A* **2014**, *482*, 300−308.

(214) Yi-jun, H.; Guo-rong, Q.; Guan-xi, C. Random Copolymer of Propylene Oxide and Ethylene Oxide Prepared by Double Metal Cyanide Complex Catalyst. *Chin. J. Polym. Sci.* **2002**, *20*, 453−459.

(215) Gu, Y.; Dong, X.; Sun, D. X. Synthesis of Novel Polyether Polyol by Using Double Metal Cyanide. *J. Macromol. Sci., Part A: Pure Appl.Chem.* **2012**, *49*, 586−590.

(216) Langanke, J.; Hofmann, J.; Gürtler, C.; Wolf, A. Facile Synthesis of Formaldehyde-Based Polyether(-Carbonate) Polyols. *J. Polym. Sci., Part A: Polym. Chem.* **2015**, *53*, 2071−2074.

(217) Hager S. L.; Reese, M. M. N.; Neal, B. L. Bayer Material Science Llc.; U.S. Patent 20130210951 A1, 2013.

(218) Kunst, A.; Löffler, A.; Lutter, H.-D.; Han, W.; Müller, J. BASF SE; U.S. Patent 20110269863 A1, 2011.

(219) Desroches, M.; Escouvois, M.; Auvergne, R.; Caillol, S.; Boutevin, B. From Vegetable Oils to Polyurethanes: Synthetic Routes to Polyols and Main Industrial Products. *Polym. Rev.* **2012**, *52*, 38−79.

(220) Hua, Z.; Sun, D. X. Ring-Opening Copolymerization of Maleic Anhydride with Propylene Oxide by Double-Metal Cyanide. *J. Appl. Polym. Sci.* **2004**, *93*, 1788−1792.

(221) Suh, H. S.; Ha, J. Y.; Yoon, J. H.; Ha, C.-S.; Suh, H.; Kim, I. Polyester Polyol Synthesis by Alternating Copolymerization of Propylene Oxide with Cyclic Acid Anhydrides by Using Double Metal Cyanide Catalyst. *React. Funct. Polym.* **2010**, *70*, 288−293.

(222) Dreyfuss, P. *Poly (tetrahydrofuran)*; CRC Press: New York, 1982; Vol. 8.

(223) Penczek, S.; Kubisa, P.; Matyjaszewski, K. *Cationic Ring-Opening Polymerization*; Springer-Verlag: Berlin, 1985; Vol. I, II.

(224) Penczek, S. Cationic Ring-Opening Polymerization (CROP) Major Mechanistic Phenomena. *J. Polym. Sci., Part A: Polym. Chem.* **2000**, *38*, 1919−1933.

(225) Kubisa, P. In *Polymer Science: A Comprehensive Reference*; Penczek, S., Grubbs, R. H., Eds.; Elsevier: Amsterdam, 2012; Vol. 4, pp 141−163.

(226) Hoogenboom, R. *Handbook of Ring-Opening Polymerization*; Wiley Online Library: Weinheim, 2009; Vol. 6.

(227) Kobayashi, S.; Morikawa, K.; Saegusa, T. Superacids and Their Derivatives. X. Mechanistic Studies of Selective Cyclodimerization of Ethylene Oxide by Superacid Ester Catalysts. *Polym. J.* **1979**, *11*, 405−412.

(228) Kern, R. J. Twelve-membered Polyether Rings. Cyclic Tetramers of some Olefin Oxides. *J. Org. Chem.* **1968**, *33*, 388−390.

(229) Penczek, S.; Kubisa, P.; Szymański, R. Activated Monomer Propagation in Cationic Polymerizations. *Makromol. Chem., Macromol. Symp.* **1986**, *3*, 203−220.

(230) Kubisa, P.; Penczek, S. Cationic Activated Monomer Polymerization of Heterocyclic Monomers. *Prog. Polym. Sci.* **1999**, *24*, 1409−1437.

(231) Goethals, E. J. Cationic Polymerization and Related Processes: Proceedings of 6th International Symposium Held in Ghent, Belgium, 30. Aug. 02. Sept. 1983, Acad. Pr.: London, 1984.

(232) Brzezińska, K.; Szymański, R.; Kubisa, P.; Penczek, S. Activated Monomer Mechanism in Cationic Polymerization, 1. Ethylene Oxide, Formulation of Mechanism. *Makromol. Chem., Rapid Commun.* **1986**, *7*, 1−4.

(233) Kubisa, P.; Bednarek, M.; Biedroń, T.; Biela, T.; Penczek, S. Progress in Activated Monomer Polymerization. Kinetics of AM Polymerization. *Macromol. Symp.* **2000**, *153*, 217−226.

(234) Biedron, T.; Brzezinska, K.; Kubisa, P.; Penczek, S. Macromonomers by Activated Polymerization of Oxiranes. Synthesis and Polymerization. *Polym. Int.* **1995**, *36*, 73−80.

(235) Huang, W.; Zhou, Y.; Yan, D. Direct Synthesis of Amphiphilic Block Copolymers from Glycidyl Methacrylate and Poly(ethylene glycol) by Cationic Ring-Opening Polymerization and Supramolecular Self-Assembly thereof. *J. Polym. Sci., Part A: Polym. Chem.* **2005**, *43*, 2038−2047.

(236) Bednarek, M.; Kubisa, P.; Penczek, S. Coexistence of Activated Monomer and Active Chain End Mechanisms in Cationic Copolymerization of Tetrahydrofuran with Ethylene Oxide. *Macromolecules* **1999**, *32*, 5257−5263.

(237) Yahiaoui, A.; Hachemaoui, A.; Belbachir, M. Cationic Polymerization of Ethylene Oxide with Maghnite-H as a Clay Catalyst in the Presence of Ethylene Glycol. *J. Appl. Polym. Sci.* **2009**, *113*, 535−540.

(238) Kubisa, P. *Cationic Copolymerization of Heterocyclics, in Cationic Polymerizations*; Marcel Dekker: New York, 1996.

(239) Thompson, M. S.; Vadala, T. P.; Vadala, M. L.; Lin, Y.; Riffle, J. S. Synthesis and Applications of Heterobifunctional Poly(ethylene oxide) Oligomers. *Polymer* **2008**, *49*, 345−373.

(240) Tasdelen, M. A.; Kahveci, M. U.; Yagci, Y. Telechelic Polymers by Living and Controlled/Living Polymerization Methods. *Prog. Polym. Sci.* **2011**, *36*, 455−567.

(241) Obermeier, B.; Wurm, F.; Mangold, C.; Frey, H. Multifunctional Poly(ethylene glycol)s. *Angew. Chem., Int. Ed.* **2011**, *50*, 7988−7997.

(242) Barthel, M. J.; Schacher, F. H.; Schubert, U. S. Poly(ethylene oxide) (PEO)-Based ABC Triblock Terpolymers − Synthetic Complexity vs. Application Benefits. *Polym. Chem.* **2014**, *5*, 2647−2662.

(243) Yang, S.; Kim, Y.; Kim, H. C.; Siddique, A. B.; Youn, G.; Kim, H. J.; Park, H. J.; Lee, J. Y.; Kim, S.; Kim, J. Azide-Based Heterobifunctional Poly(ethylene oxide)S: NaN_3-Initiated "Living" Polymerization of Ethylene Oxide and Chain End Functionalizations. *Polym. Chem.* **2016**, DOI: 10.1039/C5PY01444A.

(244) Odian, G. *Principles of Polymerization*; John Wiley & Sons, Inc.: New York, 2004; pp 544−618.

(245) Cammas, S.; Nagasaki, Y.; Kataoka, K. Heterobifunctional Poly(ethylene oxide): Synthesis Of.Alpha.-Methoxy-.Omega.-Amino and.Alpha.-Hydroxy-.Omega.-Amino PEOs with the same Molecular Weights. *Bioconjugate Chem.* **1995**, *6*, 226−230.

349

Appendix A2

Thioether-bearing Hyperbranched Polyether Polyols with Methionine-like Side-Chains: A Versatile Platform for Orthogonal Functionalization
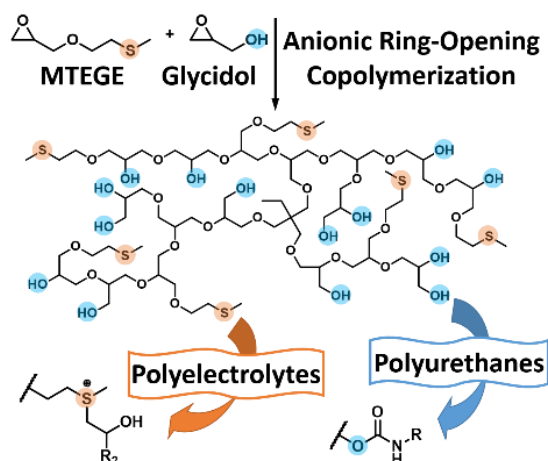
Jan Seiwert[a], Jana Herzberger,[a,b] Daniel Leibig,[a,b] Holger Frey[a,b]*

[a]Institute of Organic Chemistry, Johannes Gutenberg University, Duesbergweg10-14, 55128 Mainz, Germany

[b]Graduate School Materials Science in Mainz (MAINZ), Staudingerweg 9, 55128 Mainz, Germany

E-mail: hfrey@uni-mainz.de

Abstract

The synthesis of thioether-bearing hyperbranched polyether polyols based on an AB/AB$_2$ type copolymerization (cyclic latent monomers) is introduced. The polymers are prepared by anionic ring-opening multibranching copolymerization of glycidol and 2-(methylthio)ethyl glycidyl ether (MTEGE), which is conveniently accessible in a single etherification step. Slow monomer addition provides control over molecular weights. Moderate dispersities (Đ = 1.48 to 1.85) are obtained, given the hyperbranched structure. *In situ* ^{1}H NMR copolymerization kinetics revealed reactivity ratios of $r_G = 3.7$ and $r_{MTEGE} = 0.27$. Using slow monomer addition, copolymer composition can be systematically varied, allowing for the adjustment of the hydroxyl/thioether ratio, the degree of branching (DB = 0.36-0.48), thermal properties and cloud point temperatures in aqueous solution in the range of 29°C to 75 °C. Thioether oxidation to sulfoxides enables to tailor the copolymers' solubility profile. Use of these copolymers as a versatile, multifunctional platform for orthogonal modification is highlighted. The methyl sulfide groups can be selectively alkoxylated, using propylene oxide, allyl glycidyl ether or furfuryl glycidyl ether, resulting in functional hyperbranched polyelectrolytes. Reaction of the alcohol groups with benzyl isocyanate demonstrates successful orthogonal functionalization.

Introduction

Since 1999 both linear and hyperbranched polyglycerols (PG) have been established as a multifunctional alternative to poly(ethylene glycol) (PEG), the gold standard polyether for pharmaceutical application.[1] Both polyethers share excellent biocompatibility and good solubility in polar solvents.[2] In addition, the compact, three-dimensional structure of hyperbranched polyglycerol (*hb*PG) adds several dendrimer-like features. Hyperbranched polyglycerol possesses a high number of hydroxyl groups as well as a lower intrinsic viscosity than PEG and does not crystallize.[3] In contrast to many other hyperbranched polymers, polyglycerol can be prepared with control over molecular weight and narrow to moderate molecular weight distributions using multibranching anionic ring-opening polymerization and slow addition of the glycidol monomer.[3, 4] The slow monomer addition (SMA) procedure enables complete incorporation of the initiating core molecule and lowers the probability of chain transfer reactions.[5] Similarly controlled multibranching polymerization procedures often involve specifically designed monomers or core molecules, ruling out large-scale applications of the resulting materials, whereas *hb*PG can be prepared on a kilogram scale from commercial reagents.[6]

Polyglycerol-based materials bearing different functional groups in addition to the many hydroxyl groups are of special interest, e.g., for biomedical purposes and surface modification.[7] They can be accessed via various synthetic strategies. Initiating the polymerization from a heterofunctional polyol results in *hb*PG polymers containing exactly one functional moiety at the focal point of the branched structure, such as a single alkyne, amine, cholesterol or catechol group.[8] Furthermore, *hb*PG end groups can be partly modified after polymerization to obtain a large variety of functional materials.[9] This strategy commonly requires multi-step procedures and thorough purification. Copolymerization of glycidol with functional glycidyl ethers on the other hand provides an

elegant way of introducing certain functional groups into *hb*PG directly in a single step. Via this approach the introduction of allyl, alkyne, phenyl, ferrocene, maleimide, and catechol moieties as well as stimuli-responsive cleaving sites into the hyperbranched polyether structure was accomplished.[10–13]

In this work we present the synthesis of methyl-thioether-bearing hyperbranched polyglycerol by random anionic copolymerization of glycidol and 2-(methylthio)ethyl glycidyl ether (MTEGE) (Scheme 1).[14] The thioether side chain resembles the functional moiety of methionine, an essential α-amino acid. In contrast to linear copolymers of ethylene oxide and MTEGE, which were introduced previously, the presented hyperbranched copolymers prepared from glycidol and MTEGE comprise high numbers of both, thioether and alcohol groups. Either functional group can be selectively modified by orthogonal post-polymerization modification, leading to highly functionalized hyperbranched polyether structures. Sulfur opens manifold possibilities for modification by either oxidation or alkylation.[15, 16] Recently, also alkoxylation of thioethers using miscellaneous epoxides has been explored as a convenient click functionalization.[17] Additionally, polyether polyols are known to form urethane linkages by reaction with isocyanates. This renders thioether-bearing polyglycerol a multifunctional platform for a wide range of further modifications.

MTEGE Monomer Synthesis:
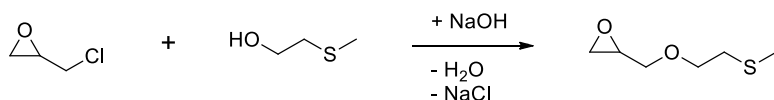
Copolymerization:
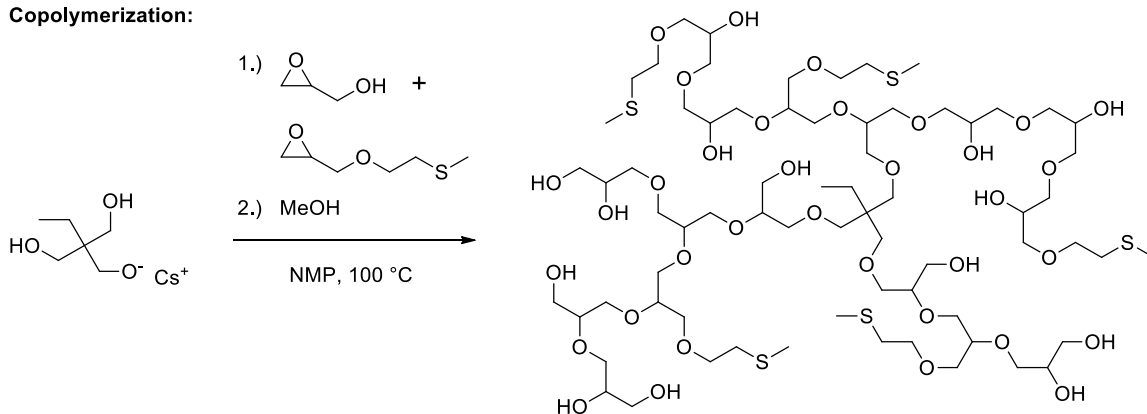
Scheme 1. Synthesis of hyperbranched copolymers from MTEGE and glycidol.

Experimental Section

Monomer Synthesis: 2-(Methylthio)ethyl Glycidyl Ether (MTEGE)

The synthesis protocol has been slightly improved with respect to the recently published procedure.[14] 10 mL (115 mmol, 1 eq.) 2-(Methylthio)ethanol was placed in a three-necked flask equipped with a mechanical stirrer and a dropping funnel. 4,6 g (115 mmol, 1 eq.) crushed NaOH pellets were added and the mixture was stirred at room temperature until most NaOH was dissolved. After cooling to 0 °C, 18 mL (230 mmol, 2 eq.) epichlorohydrin (ECH) was added dropwise and the mixture was stirred for two days. Subsequently, the formed salt was removed via centrifugation. Diethyl ether was added to the organic phase and the combined mixture was washed three times with brine solution. Afterwards, the solvent was removed under vacuum and the crude product was dried over MgSO$_4$. Purification was conducted via fractionated vacuum distillation ($p = 0.006$ mbar, $T_b = 60$°C) and MTEGE was isolated as a colorless liquid (yield: 60-70 %).

^{1}H NMR (400 MHz, CDCl$_3$, δ): 3.86 – 3.60 (m, 3H, CH-C$\underline{H}$H-O, O-C$\underline{H}_2$-CH$_2$); 3.43 (dd, J = 11.6, 5.9 Hz, 1H, , CH-CH$\underline{H}$-O); 3.18 (ddt , J = 5.9, 4.2, 2.8 Hz, 1H, H$_2$C(O)C$\underline{H}$); 2.82 (dd, J = 5.0, 4.2 Hz, 1H, $\underline{H}$HC(O)CH); 2.72 (t, J = 6.7 Hz, 2H, CH$_2$-S); 2.64 (dd, J = 5.0, 2.8 Hz, 1H, H$\underline{H}$C(O)CH); 2.17 (s, 3H, S-CH$_3$).

^{13}C NMR (100 MHz, CDCl$_3$, δ): 71.7 (CH-$\underline{C}$H$_2$-O), 70.8 (O-$\underline{C}$H$_2$-CH$_2$), 50.9 (H$_2$C(O)$\underline{C}$H), 44.3 (H$_2$$\underline{C}$(O)CH), 33.7 (CH$_2$-S), 16.2 (S-CH$_3$).

FDMS m/z: [M$^+$] calc. for C$_6$H$_{12}$O$_2$S, 148.06; found, 148.2.

Copolymerization of MTEGE and Glycidol

General procedure: In a Schlenk flask equipped with a magnetic stirrer, 67 mg (0.5 mmol, 1.0 eq.) trimethylolpropane (TMP) was dissolved in methanol, partly deprotonated with 28 mg (0.17 mmol, 0.3 eq.) cesium hydroxide monohydrate and dried in vacuum overnight at room temperature. Subsequently, the initiator was dissolved in 1 mL N-methyl-2-pyrrolidone (NMP) and heated to 100 °C under argon atmosphere. In a separate flask, the monomers MTEGE and glycidol were mixed under argon atmosphere and diluted with NMP in a volume ratio of 1:1. The solution was added dropwise to the initiator at a rate of 0.2 mL h^{-1} using a syringe pump. The polymerization was terminated with methanol 1 h after completion of the monomer addition. After removal of the solvent, the resulting pale brown oil was precipitated from MeOH into cold diethyl ether and then dried in vacuum at 50 °C for 24 h (yield 80 - 90%).

^{1}H NMR (400 MHz, DMSO-d_6, δ): 4.85 – 4.08 (br, OH); 4.05 – 3.05 (m, O-CH, O-CH$_2$); 2.61 (t, J = 6.7 Hz, CH$_2$-S); 2.07 (s, S-CH$_3$); 1.38 – 1.18 (m, 2H, C$\underline{H}_2$-CH$_3$ (TMP)); 0.87 – 0.72 (m, 3H, CH$_3$ (TMP)).

^{13}C NMR (DMSO-d_6, 100 MHz, δ): 80.30 – 79.45 (m, CH G$_{1,3\text{-Linear}}$); 78.68 – 77.63 (m, CH G$_{\text{Dendritic}}$, CH M$_{\text{Linear}}$); 72.92 (s, 2 CH$_2$ G$_{1,4\text{-Linear}}$); 72.26 (s, 2 CH$_2$ M$_{\text{Terminal}}$); 72.04 –

70.41 (m, 2 CH$_2$ G$_{Dendritic}$, CH G$_{Terminal}$, CH$_2$ G$_{Terminal}$); 70.39 − 69.93 (m, 2 CH$_2$ M$_{Linear}$); 69.61 − 68.37 (m, CH$_2$ G$_{1,3\text{-}Linear}$, CH-OH G$_{1,4\text{-}Linear}$, O-C̲H$_2$-CH$_2$-S M$_{Linear}$, O-C̲H$_2$-CH$_2$-S M$_{Terminal}$); 63.12 (s, CH$_2$-OH G$_{Terminal}$); 61.56 − 60.70 (m, CH$_2$-OH G$_{1,3\text{-}Linear}$); 32.69 (s, CH$_2$-S M$_{Linear}$, CH$_2$-S M$_{Terminal}$); 15.28 32.69 (s, S-CH$_3$ M$_{Linear}$, S-CH$_3$ M$_{Terminal}$).

Results and Discussion

Monomer synthesis

2-(Methylthio)ethyl glycidyl ether (MTEGE) was synthesized from the commercially available reagents epichlorohydrin and 2-(methylthio)ethanol in a single, straightforward etherification step (Scheme 1).[14] Successful synthesis was confirmed by ^{1}H and ^{13}C NMR spectroscopy (Figure S1) as well as mass spectrometry. Purification of the monomer by repeated fractionated distillation gave yields of 60 to 70% and allowed recollecting unreacted 2-(methylthio)ethanol. Column chromatography was found to be unsuitable for purification of MTEGE, due to side reactions with the column material (silica or aluminum oxide).

Copolymerization of MTEGE and Glycidol and Copolymer Characterization

The anionic ring-opening multibranching copolymerization of MTEGE with glycidol was carried out in analogy to the established procedure for the synthesis of polyglycerol-based copolymers (Scheme 1).[10–12] A mixture of both monomers was added slowly to a cesium alkoxide initiator in *N*-methyl-2-pyrrolidone, at 100 °C. The copolymer composition was systematically varied from 10% to 40% MTEGE content. [1]H and quantitative Inverse Gated ^{13}C NMR spectroscopy prove controlled incorporation of the MTEGE comonomer (Figure S2, Figure S3). The slightly lower MTEGE contents determined from the ^{1}H NMR spectra

356

can be attributed to an overlap of the polymer backbone signal between 3.05 and 4.05 ppm and the water signal at 3.33 ppm resulting from moisture in the NMR solvent. Average molecular weights can be calculated from the ^{1}H NMR spectra, as it is known for other polyglycerol copolymers prepared by slow monomer addition, using the methyl group of the initiator as a reference. Molecular weights in the range of 3890 to 6980 g mol^{-1} are found, matching the theoretical values well. Due to the low hydrodynamic volume of the compact, hyperbranched polymer structure in solution, size-exclusion chromatography based on linear PEG standards yields lower apparent molecular weights ranging from 1060 to 4080 g mol^{-1}.[18, 5] Taking the hyperbranched structure into account, moderate, mostly monomodal molecular weight distributions with dispersity in the range of Đ = 1.48 to 1.85 were obtained (Figure S4 - Figure S8). Table 1 summarizes the characterization data for the *hb*(PG-*co*-PMTEGE) copolymers.

Table 1. Characterization data of the *hb*(PG-*co*-PMTEGE) copolymers.

No.	Sample name[a]	MTEGE% theo	MTEGE%[b]	MTEGE%[c]	DB%[c]	M_n Theo (g·mol^{-1})	M_n[b] (g·mol^{-1})	M_n[d] (g·mol^{-1})	Đ[d]	T_g[e] (°C)	T_{cp}[f] (°C)
1	*hb*(PG$_{44}$-*co*-PMTEGE$_4$)	10	7	9	48	3370	3890	1060	1.85	-27	-
2	*hb*(PG$_{36}$-*co*-PMTEGE$_6$)	20	15	16	48	3690	3740	1750	1.51	-27	-
3	*hb*(PG$_{46}$-*co*-PMTEGE$_{13}$)	30	22	30	42	4950	5490	2170	1.48	-31	75
4	*hb*(PG$_{32}$-*co*-PMTEGE$_{18}$)	40	36	41	36	5320	5220	2160	1.58	-34	29
5	*hb*(PG$_{78}$-*co*-PMTEGE$_7$)	10	8	10	56	6310	6980	4080	1.49	-25	-

[a] Terminology: Samples are named according to the number of comonomer units *hb*(PG$_x$-*co*-PMTEGE$_y$), where x is the absolute number of G units and y the absolute number of MTEGE units, calculated from ^{1}H NMR spectra, [b] determined by ^{1}H NMR, [c] determined by Inverse Gated ^{13}C NMR, [d] SEC, [e] obtained by DSC, [f] cloud point temperatures, measured by turbidimetry.

The copolymerization kinetics of MTEGE and glycidol was investigated using *in situ* ^{1}H NMR spectroscopy. In order to ensure a safe reaction in the NMR tube, we altered the

polymerization protocol described above and performed the copolymerization in deuterated DMSO-d_6 at 60 °C without slow monomer addition. *In situ* NMR spectroscopy allows monitoring the single monomer conversion in real time. Figure 1 and Figure S11 demonstrate that MTEGE is consumed somewhat slower than glycidol in a batch copolymerization. Since the monomer feed ratio shifts continuously and is observed during the entire course of the polymerization, a single experiment provides sufficient data to calculate reactivity ratios according to the Fineman-Ross formalism: $r_G = 3.7 \pm 0.3$ and $r_{MTEGE} = 0.27 \pm 0.02$.[19] This implies that batch copolymerization of glycidol and MTEGE leads to a gradient compositional profile with a PG-rich center and a PMTEGE-rich periphery. It should be noted, however, that the reactivity gap is sufficiently small to obtain approximately random copolymers when using the slow monomer addition procedure. This was confirmed by taking NMR samples during a copolymerization under conventional slow monomer addition conditions (Figure S9). At an addition rate of 0.2 mL h^{-1}, both comonomers react sufficiently fast to avoid accumulation of the less reactive MTEGE in the reaction mixture. The composition of the growing copolymer remains largely constant during the copolymerization, equating the monomer feed ratio (Figure S10).

Figure 1. Single monomer conversion plot of glycidol and MTEGE in DMSO-d_6 at 60 °C versus time.

The degree of branching is a key parameter to describe the structure of a hyperbranched polymer. It can assume values between 0 (linear, no branching) and 1 (dendrimer-like, completely branched). For the *hb*(PG-*co*-PMTEGE) copolymers, inverse gated ^{13}C NMR spectroscopy reveals the characteristic signal pattern of a hyperbranched polyglycerol copolymer (Figure S3). The spectra enable to distinguish and quantify dendritic (D), linear (L) and terminal (T) repeating units. Due to the multiple chain ends of the branched structure, the spectra of the copolymers show considerably more terminal MTEGE units than the linear PMTEGE homopolymer (Figure S15). The degree of branching (DB) can be calculated according to Equation 1.[20]

$$DB = \frac{2D}{2D+L}$$
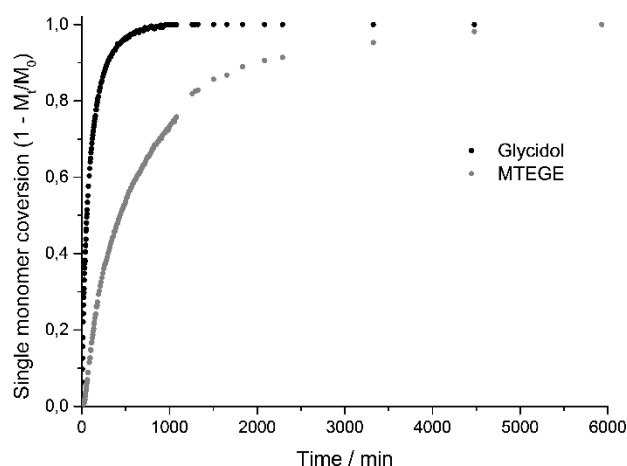
(1)

As expected, the DB decreases from 0.48 to 0.36 with increasing MTEGE content, because only glycidol can form dendritic repeating units, whereas MTEGE forms linear and terminal units exclusively.

The composition and DB affect the thermal properties of the copolymers. Differential scanning calorimetry (DSC) measurements reveal a decrease in the glass transition temperature from -27 °C to -44 °C with increasing MTEGE content. This finding can be ascribed to the reduced hydroxyl group density and therefore weaker hydrogen bonding as well as the flexible methyl-thioethyl alkyl chains.

Post-polymerization Modification

The two different types of functional groups of *hb*(PG-*co*-PMTEGE) offer the possibility for orthogonal modification. Unlike the oxygen of an ether group, the sulfur of a thioether moiety can be easily oxidized, forming a sulfoxide or a sulfone. Treating the copolymers

with acidified hydrogen peroxide solution for 30 min at room temperature selectively transforms the thioether moieties into the corresponding sulfoxides.[16] Complete disappearance of signals of the thioether-neighboring methylene and methyl groups in the ^{1}H NMR proves complete conversion (Figure S16). After oxidation, the methylene and methyl signals reappear at 2.78 - 3.10 ppm and 2.57 ppm. Converting thioethers into sulfoxides increases the local dipole moment of the group.[21] On the macroscopic scale, one can observe the impact of the increasing polarity by temperature-dependent turbidimetry of aqueous copolymer solutions before and after oxidation. Figure 2 and Figure S17 show that before oxidation, hb(PG$_{46}$-co-PMTEGE$_{13}$) and hb(PG$_{32}$-co-PMTEGE$_{16}$) exhibit thermoresponsive solubility with demixing above a cloud point of 29 °C and 75 °C, respectively. By oxidizing the thioether moieties, however, both copolymers become completely water-soluble at all temperatures.
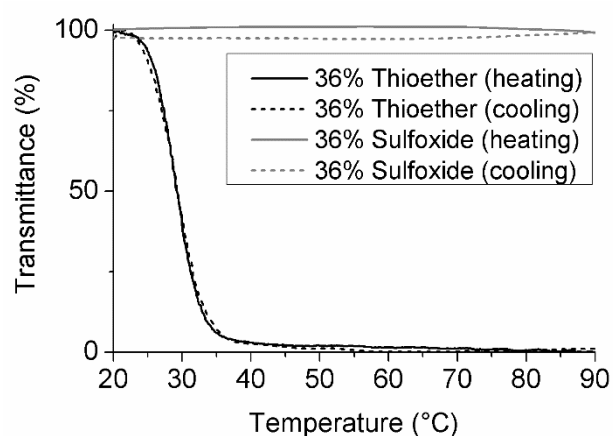
Figure 2. Intensity of transmitted laser light versus temperature for hb(PG$_{32}$-co-PMTEGE$_{18}$) in aqueous solution (c = 5 mg mL^{-1}) before and after oxidation of the thioether moieties.

Besides their oxidation-responsiveness, thioether groups can act as Lewis bases. They can react with electrophiles to form sulfonium cations; e.g. they open epoxide rings in a nucleophilic addition under acidic conditions.[17] Trialkylsulfonium compounds, such as the commercially available drug S-adenosyl methionine, are generally more stable and

accessible under milder conditions than the strongly alkylating trialkyl oxonium cations. This is a result of the higher Lewis basicity of thioethers in comparison to ethers. Capitalizing on this feature, *hb*(PG-*co*-PMTEGE) was dissolved in glacial acetic acid to alkoxylate the thioether moieties within 24 h at room temperature using the commercially available epoxides propylene oxide, allyl glycidyl ether (AGE) and furfuryl glycidyl ether (FGE) (Figure 3). Allyl and furfuryl functionalized polymers are known for their use in thiol-ene click and Diels-Alder click chemistry.[22] By dialyzing the modified polymers against diluted hydrochloric acid, the acetate anions were exchanged with chloride anions. The thioether groups were converted into sulfonium cations with 96-99% conversion, as can be deduced from the signal shift of the neighboring methyl group in the ^{1}H NMR spectra from 2.08 to 3.05 ppm. In addition, the characteristic signals of the attached methyl (1.22 ppm, Figure S18), allyl (5.17, 5.29 and 5.88 ppm, Figure S19) and furfuryl groups (4.46, 6.44, 7.64 ppm, Figure 3) appear after modification. Comparison of their intensity with the shifted thioether methyl signal confirms that under the acidic reaction conditions applied, the epoxides selectively react with the thioether moieties, but clearly not with hydroxyl groups. Strikingly, this is exactly the opposite reactivity in contrast to the alkoxide-mediated ring-opening during the polymerization that leaves the thioether groups unchanged.

361
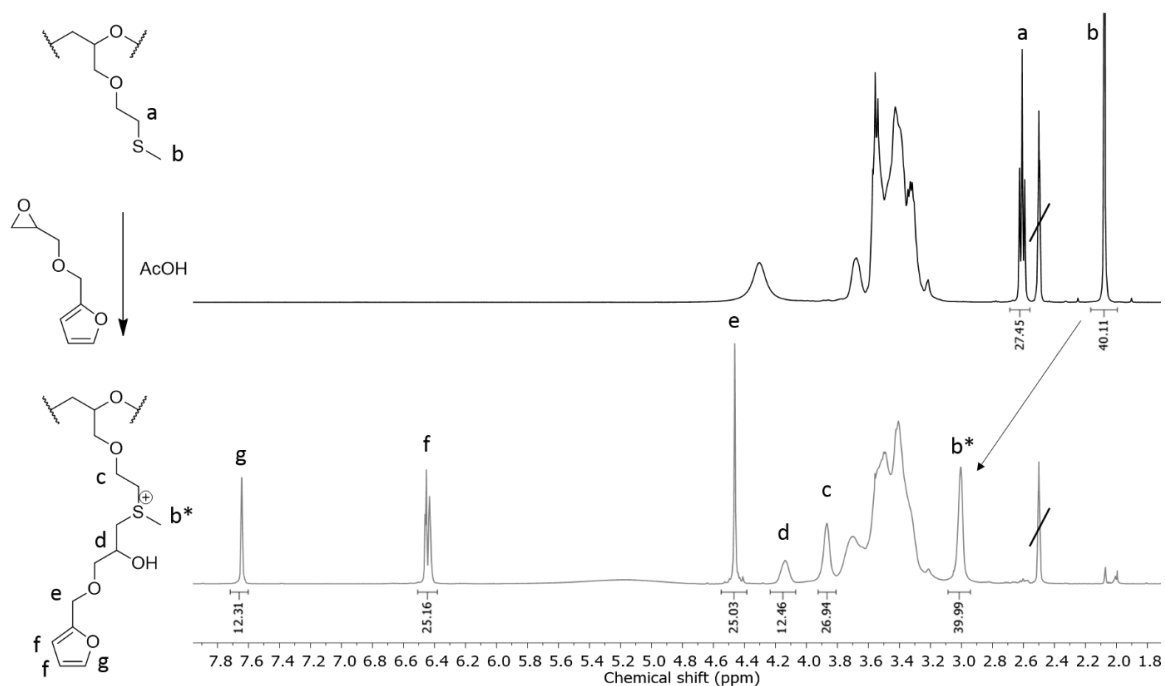
Figure 3. ^{1}H NMR spectra of *hb*(PG$_{46}$-*co*-PMTEGE$_{13}$) before (black, top) and after (grey, bottom) modification of the thioether groups with furfuryl glycidyl ether (400 MHz, DMSO-d_6).

As a proof of principle experiment to demonstrate that the hydroxyl groups can also be modified selectively, *hb*(PG$_{46}$-*co*-PMTEGE$_{13}$) was reacted with phenyl isocyanate as a model compound to obtain urethanes. Figure S20 shows the new aromatic and NH-signals of the phenyl urethane groups in the downfield area of the ^{1}H NMR spectrum between 6.74 and 8.15 ppm. Furthermore, the chemical shift of the thioether-related signals remains unchanged in the ^{1}H NMR and ^{13}C NMR (Figure S21) spectra, proving selective modification of the hydroxyl groups. The urethane-functionalized polymer exhibits an increased glass transition temperature of 26 °C, due to reduced chain flexibility and increased hydrogen bonding. The material exhibits a strong UV signal in the SEC due to the aromatic end groups, and the SEC trace is shifted towards higher molecular weights (Figure S22).

Conclusions

We have introduced hyperbranched, thioether-bearing polyether polyols as a versatile platform for modification, employing the easily accessible MTEGE as a new comonomer for anionic ring-opening multibranching polymerization of glycidol. A series of copolymers with systematically varied MTEGE incorporation between 7 and 36% was synthesized with good control over molecular weight, degree of branching and thermal properties. Real time NMR kinetic studies elucidated the reactivity ratios of the two comonomers, revealing a sufficiently small difference in reactivity that allows polymerization under slow monomer addition conditions.

Copolymerization of the hydrophilic glycidol with the hydrophobic MTEGE monomer permits tailoring the aqueous solubility, resulting in thermoresponsive behavior with cloud point temperatures in a wide temperature range between 29 and 75 °C. By oxidizing the thioether groups of the thermoresponsive copolymers with hydrogen peroxide, the solubility can be switched to fully water-soluble. This is an intriguing feature for potential application as e.g., an oxidation-responsive surface coating material. Functional sulfonium derivatives are conveniently accessible from the reaction of *hb*(PG-*co*-PMTEGE) with epoxides under acidic conditions. This was demonstrated using propylene oxide, allyl glycidyl ether and furfuryl glycidyl ether. Based on the large variety of available epoxides,[23] we envision *hb*(PG-*co*-PMTEGE) as a universal platform to create a library of heterofunctional hyperbranched polyelectrolytes and potentially as an unusual epoxy curing agent. Furthermore, the possibility to selectively modify the hydroxyl groups with isocyanates potentially renders these materials functional polyol building blocks for polyurethanes.

Acknowledgements

References

[1] a) D. Wilms, S. E. Stiriba, H. Frey, *Acc. Chem. Res.* **2010**, *43*, 129; b) M. Schömer, C. Schüll, H. Frey, *J. Polym. Sci. A Polym. Chem.* **2013**, *51*, 995; c) A. Thomas, S. S. Müller, H. Frey, *Biomacromolecules.* **2014**, *15*, 1935;

[2] R. K. Kainthan, J. Janzen, E. Levin, D. V. Devine, D. E. Brooks, *Biomacromolecules.* **2006**, *7*, 703.

[3] A. Sunder, R. Hanselmann, H. Frey, R. Mülhaupt, *Macromolecules.* **1999**, *32*, 4240.

[4] a) W. Radke, G. Litvinenko, A. H. E. Müller, *Macromolecules.* **1998**, *31*, 239; b) R. Hanselmann, D. Hölter, H. Frey, *Macromolecules.* **1998**, *31*, 3790; c) R. K. Kainthan, E. B. Muliawan, S. G. Hatzikiriakos, D. E. Brooks, *Macromolecules.* **2006**, *39*, 7708;

[5] J. Seiwert, D. Leibig, U. Kemmer-Jonas, M. Bauer, I. Perevyazko, J. Preis, H. Frey, *Macromolecules.* **2016**, *49*, 38.

[6] a) P. Bharathi, J. S. Moore, *Macromolecules.* **2000**, *33*, 3212; b) D. P. Bernal, L. Bedrossian, K. Collins, E. Fossum, *Macromolecules.* **2003**, *36*, 333; c) Y. Ohta, S. Fujii, A. Yokoyama, T. Furuyama, M. Uchiyama, T. Yokozawa, *Angew. Chem. Int. Ed.* **2009**, *48*, 5942; d) D. Konkolewicz, A. Gray-Weale, S. Perrier, *J. Am. Chem. Soc.* **2009**, *131*, 18075; e) J.-Y. Chen, M. Smet, J.-C. Zhang, W.-K. Shao, X. Li, K. Zhang, Y. Fu, Y.-H. Jiao, T. Sun, W. Dehaen, F.-C. Liu, E.-H. Han, *Polym. Chem.* **2014**, *5*, 2401; f) Y. Shi, R. W. Graff, X. Cao, X. Wang, H. Gao, *Angew. Chem. Int. Ed.* **2015**, *54*, 7631; g) A. B. Cook, R. Barbey, J. A. Burns, S. Perrier, *Macromolecules.* **2016**, *49*, 1296; h) X. Cao, Y. Shi, X. Wang, R. W. Graff, H. Gao, *Macromolecules.* **2016**, *49*, 760;

[7] a) M. Calderon, M. A. Quadir, S. K. Sharma, R. Haag, *Adv. Mater.* **2010**, *22*, 190; b) J. Khandare, M. Calderon, N. M. Dagia, R. Haag, *Chem. Soc. Rev.* **2012**, *41*, 2824; c) E. Moore, H. Thissen, N. H. Voelcker, *Prog. Surf. Sci.* **2013**, *88*, 213; d) H. Zhang, M.

W. Grinstaff, *Macromol. Rapid Commun.* **2014**, *35*, 1906; e) E. Mohammadifar, A. Nemati Kharat, M. Adeli, *J. Mater. Chem. B.* **2015**, *3*, 3896;

[8]   a) A. Zill, A. L. Rutz, R. E. Kohman, Am Alkilany, C. J. Murphy, H. Kong, S. C. Zimmerman, *Chem. Commun.* **2011**, *47*, 1279; b) A. M. Hofmann, F. Wurm, E. Huhn, T. Nawroth, P. Langguth, H. Frey, *Biomacromolecules.* **2010**, *11*, 568; c) C. Schüll, L. Nuhn, C. Mangold, E. Christ, R. Zentel, H. Frey, *Macromolecules.* **2012**, *45*, 5901; d) A. Thomas, H. Bauer, A.-M. Schilmann, K. Fischer, W. Tremel, H. Frey, *Macromolecules.* **2014**, *47*, 4557;

[9]   a) S. Roller, H. Zhou, R. Haag, *Mol. Divers.* **2005**, *9*, 305; b) Tziveleka L. A., C. Kontoyianni, Z. Sideratou, D. Tsiourvas, C. M. Paleos, *Macromol. Biosci.* **2006**, *6*, 161; c) I. Papp, J. Dernedde, S. Enders, R. Haag, *Chem. Commun.* **2008**, 5851; d) D. Gröger, M. Kerschnitzki, M. Weinhart, S. Reimann, T. Schneider, B. Kohl, W. Wagermaier, G. Schulze-Tanzil, P. Fratzl, R. Haag, *Adv. Healthcare Mater.* **2014**, *3*, 375; e) Q. Wei, S. Krysiak, K. Achazi, T. Becherer, P. L. Noeske, F. Paulus, H. Liebe, I. Grunwald, J. Dernedde, A. Hartwig, T. Hugel, R. Haag, *Colloids Surf. B Biointerfaces.* **2014**, *122*, 684; f) Y. Yu, H. Frey, *Langmuir.* **2015**, *31*, 13101; g) D. Pranantyo, L. Q. Xu, K. G. Neoh, E.-T. Kang, S. L.-M. Teo, *Ind. Eng. Chem. Res.* **2016**, *55*, 1890;

[10]   A. Sunder, H. Türk, R. Haag, H. Frey, *Macromolecules.* **2000**, *33*, 7682.

[11]   C. Schüll, T. Gieshoff, H. Frey, *Polym. Chem.* **2013**, *4*, 4730.

[12]   A. Alkan, R. Klein, S. I. Shylin, U. Kemmer-Jonas, H. Frey, F. R. Wurm, *Polym. Chem.* **2015**, *6*, 7112.

[13]   a) R. Klein, F. Übel, H. Frey, *Macromol. Rapid Commun.* **2015**, *36*, 1822; b) K. Niederer, C. Schüll, D. Leibig, T. Johann, H. Frey, *Macromolecules.* **2016**, *49*, 1655; c) C. Tonhauser, C. Schüll, C. Dingels, H. Frey, *ACS Macro Lett.* **2012**, *1*, 1094; d) R. A. Shenoi, J. K. Narayanannair, J. L. Hamilton, B. F. Lai, S. Horte, R. K. Kainthan, J. P. Varghese, K. G. Rajeev, M. Manoharan, J. N. Kizhakkedathu, *J. Am. Chem. Soc.* **2012**, *134*, 14945; e) R. A. Shenoi, I. Chafeeva, B. F. L. Lai, S. Horte, J. N. Kizhakkedathu, *J. Polym. Sci. A Polym. Chem.* **2015**, *53*, 2104; f) S. Son, E. Shin, B.-S. Kim, *Macromolecules.* **2015**, *48*, 600;

[14]   J. Herzberger, K. Fischer, D. Leibig, M. Bros, R. Thiermann, H. Frey, *J. Am. Chem. Soc.* **2016**, DOI: 10.1021/jacs.6b04548.

[15]   a) H. G. Batz, V. Hofmann, H. Ringsdorf, *Makromol. Chem.* **1973**, *169*, 323; b) V. Hofmann, H. Ringsdorf, G. Muacevic, *Makromol. Chem.* **1975**, *176*, 1929; c) A.

Napoli, M. Valentini, N. Tirelli, M. Muller, J. A. Hubbell, *Nat. Mater.* **2004**, *3*, 183; d) B. L. Allen, J. D. Johnson, J. P. Walker, *ACS Nano.* **2011**, *5*, 5263; e) P. Carampin, E. Lallana, J. Laliturai, S. C. Carroccio, C. Puglisi, N. Tirelli, *Macromol. Chem. Phys.* **2012**, *213*, 2052; f) J. R. Kramer, T. J. Deming, *Biomacromolecules.* **2012**, *13*, 1719; g) J. R. Kramer, T. J. Deming, *Chem. Commun.* **2013**, *49*, 5144; h) S. T. Hemp, M. H. Allen, A. E. Smith, T. E. Long, *ACS Macro Lett.* **2013**, *2*, 731; i) J. R. Kramer, T. J. Deming, *J. Am. Chem. Soc.* **2014**, *136*, 5547; j) M. C. Mackenzie, A. R. Shrivats, D. Konkolewicz, S. E. Averick, M. C. McDermott, J. O. Hollinger, K. Matyjaszewski, *Biomacromolecules.* **2015**, *16*, 236;

[16] A. R. Rodriguez, Kramer, JR, T. J. Deming, *Biomacromolecules.* **2013**, *14*, 3610.

[17] E. G. Gharakhanian, T. J. Deming, *Biomacromolecules.* **2015**, *16*, 1802.

[18] I. Perevyazko, J. Seiwert, M. Schömer, H. Frey, U. S. Schubert, G. M. Pavlov, *Macromolecules.* **2015**, *48*, 5887.

[19] M. Fineman, S. D. Ross, *J. Polym. Sci.* **1950**, *5*, 259.

[20] H. Frey, D. Hölter, *Acta Polym.* **1999**, *50*, 67.

[21] R. d'Arcy, N. Tirelli, *Polym. Adv. Technol.* **2014**, *25*, 478.

[22] a) C. E. Hoyle, A. B. Lowe, C. N. Bowman, *Chem. Soc. Rev.* **2010**, *39*, 1355; b) K. Kempe, A. Krieg, C. R. Becer, U. S. Schubert, *Chem. Soc. Rev.* **2012**, *41*, 176; c) A. Gandini, *Prog. Polym. Sci.* **2013**, *38*, 1;

[23] J. Herzberger, K. Niederer, H. Pohlit, J. Seiwert, M. Worm, F. R. Wurm, H. Frey, *Chem. Rev.* **2016**, *116*, 2170.

Supporting Information

Materials

Solvents and reagents were obtained from *Sigma Aldrich* and *Acros Organics*, respectively. DMSO-d_6 and CDCl$_3$ were received from *Deutero GmbH*. MTEGE, Glycidol (96%) and *N*-methyl-2-pyrrolidone (99.5%) were dried over calcium hydride (CaH$_2$) and distilled in vacuum directly prior to use. Phenyl isocyanate was freshly distilled prior to use. Epichlorohydrin (99%), 2-(methylthio)ethanol (99%) and all other reagents and solvents were used as received.

Instrumentation

NMR spectra were recorded on a *Bruker* Advance III HD 400 (5 mm BBFO-SmartProbe with z-gradient and ATM) at 400 MHz (^{1}H) and 100 MHz (^{13}C). The residual signals of the deuterated solvent were utilized as an internal reference.

Analytical SEC measurements in DMF (containing 0.25 g L^{-1} of lithium bromide) were performed on an *Agilent* 1100 series instrument, including a *PSS* HEMA column (10^6/10^4/10^2 Å porosity) and UV and RI detector. Poly(ethylene glycol) standards (*Polymer Standards Service GmbH*) were employed for calibration.

Purification by SEC was performed in CHCl$_3$, at 25 °C and a flow rate of 3.5 mL min^{-1} using a LC-91XX Next Series Recycling Preparative HPLC Anlage by *Japan Analytical Industry Co. Ltd.*. A Jaigel-2H column (upper exclusion limit $5 \cdot 10^3$ g mol^{-1}) and a UV and RI detector were used.

Differential scanning calorimetry (DSC) was measured using a *PerkinElmer* 8500 thermal analysis system and a *PerkinElmer* CLN2 thermal analysis controller in the temperature range from -90 to +20 °C at a heating rate of 10 K min^{-1}.

Cloud points were observed by optical transmittance of a light beam (λ = 670 nm) through a 1 cm sample quartz cell containing the polymer solution in deionized water (5 mg mL^{-1}), in dependence of the solution temperature. A *Jasco* V-630 photospectrometer with a *Jasco* ETC-717 Peltier element was used. The heating and cooling rate was 1 K min^{-1}, and values were recorded in 1 K steps.

In situ ^{1}H NMR kinetics

Copolymerization in the NMR tube was performed in DMSO-*d$_6$* following a procedure described in previous work. 4.0 mg (0.03 mmol, 1.0 eq.) 1,1,1-Tris(hydroxymethyl)propane (TMP) and 1.7 mg (0.01 mmol 0.3 eq.) cesium hydroxide monohydrate were dissolved in methanol. Benzene was added and volatiles were removed in high vacuum overnight. The following operations were performed under Argon atmosphere. The dried initiator salt was dissolved in 0.5 mL DMSO-*d$_6$*. The solution was transferred to an NMR tube equipped with a Teflon stopcock. 60 µL (0.9 mmol, 30 eq.) glycidol and 0.6 mmol (20 eq.) MTEGE were added and the solution was degassed subsequently. The tube was sealed under vacuum and then placed in the NMR spectrometer at 60 °C. Spectra were recorded with 16 scans at 2-minute intervals during the first hour, at 5-minute intervals during the following 2 hours, at 10-minute intervals within the next 15 hours and extended afterwards.

Oxidation of the thioether groups

Oxidation of the thioether groups was performed following a modified procedure of the protocol reported by Deming et al.[16] 100 mg hb(PG$_{32}$-co-PMTEGE$_{18}$) was dissolved in aqueous hydrogen peroxide solution (35%) and acidified with AcOH (1%). The mixture was stirred at room temperature for 30 min, quenched with 1 M aqueous sodium thiosulfate solution and dialyzed against deionized water (MWCO: 100 – 500 Da). Subsequently, the oxidized polymer was isolated by lyophilization in 80% yield.

Alkoxylation of the thioether groups

Alkoxylation of the thioether groups was performed following a modified procedure by Gharakhanian and Deming.[17] 100 mg hb(PG-co-PMTEGE) was dissolved in 6 mL glacial acetic acid. 3 Eq. (compared to the amount of thioether groups) propylene oxide, allyl glycidyl ether or furfuryl glycidyl ether were added and the mixture was stirred at room temperature for 24 h. Afterwards, the solvent and unreacted epoxide were removed in vacuum. The residue was dialyzed against 3 mM HCl$_{aq}$ (MWCO: 100 – 500 Da) and freeze-dried subsequently. Hence, the alkoxylated polymer was obtained in 90-95% yield.

Urethane formation

100 mg polymer was dried overnight in vacuum and dissolved in dry pyridine. Phenyl isocyanate (1.1 eq., compared to the amount of hydroxyl groups) was added and the mixture was stirred at room temperature for 4 hours. Then, pyridine and residual phenyl isocyanate were removed in vacuum. The residue was purified by preparative SEC and dried in vacuum subsequently, to yield the urethane-functionalized polymer.

Additional characterization data
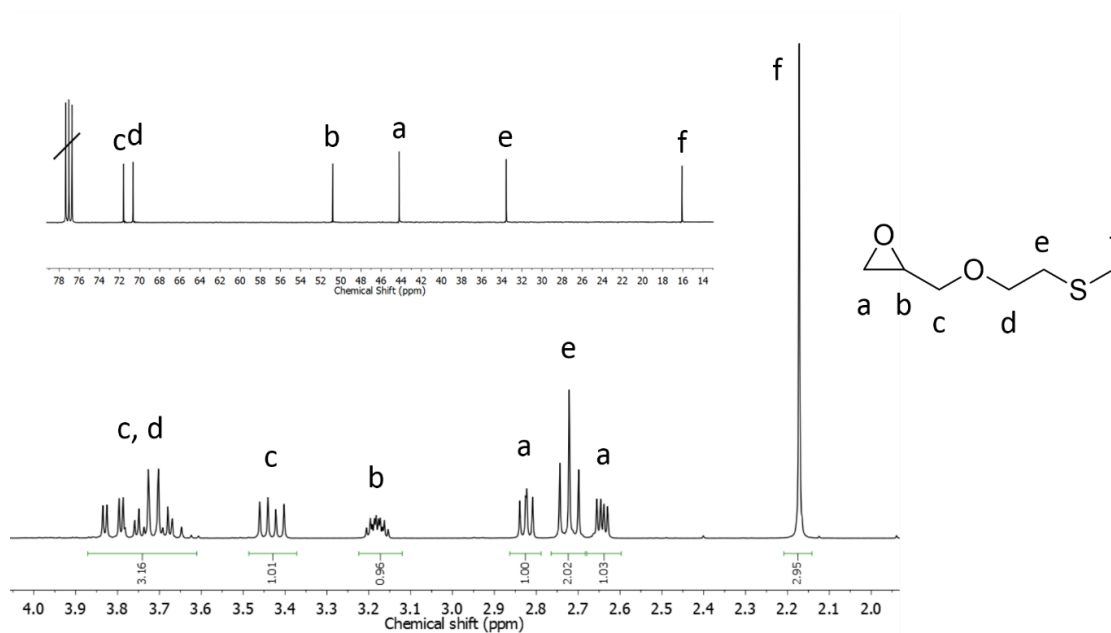
Figure S1. ^{1}H (bottom) and ^{13}C NMR (top) spectra of 2-(methylthio)ethyl glycidyl ether (MTEGE) (400/100 MHz, CDCl$_3$).
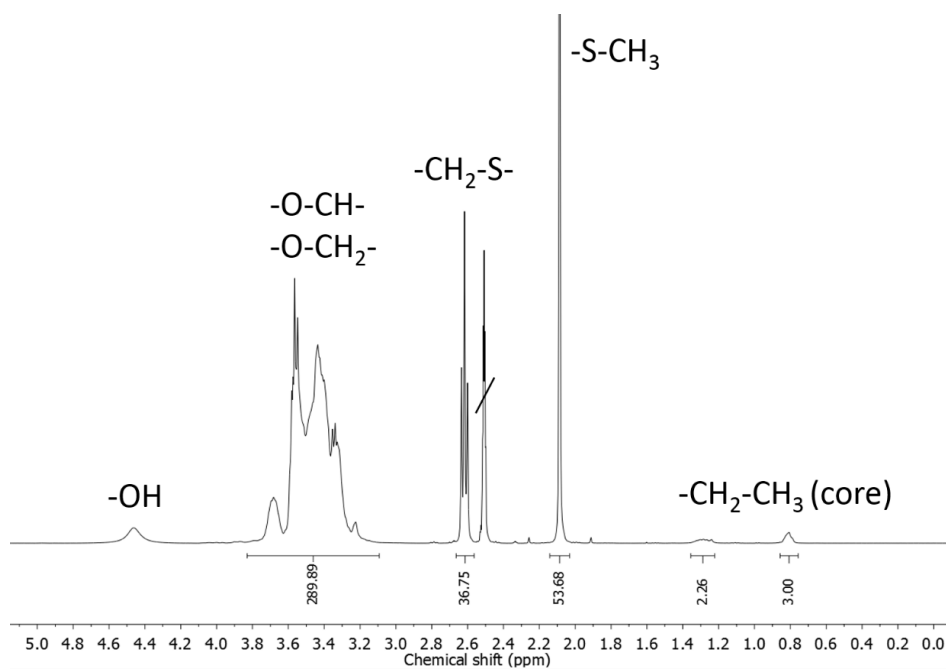
Figure S2. ^{1}H NMR spectrum of hb(PG$_{32}$-co-PMTEGE$_{18}$) (400 MHz, DMSO-d_6).
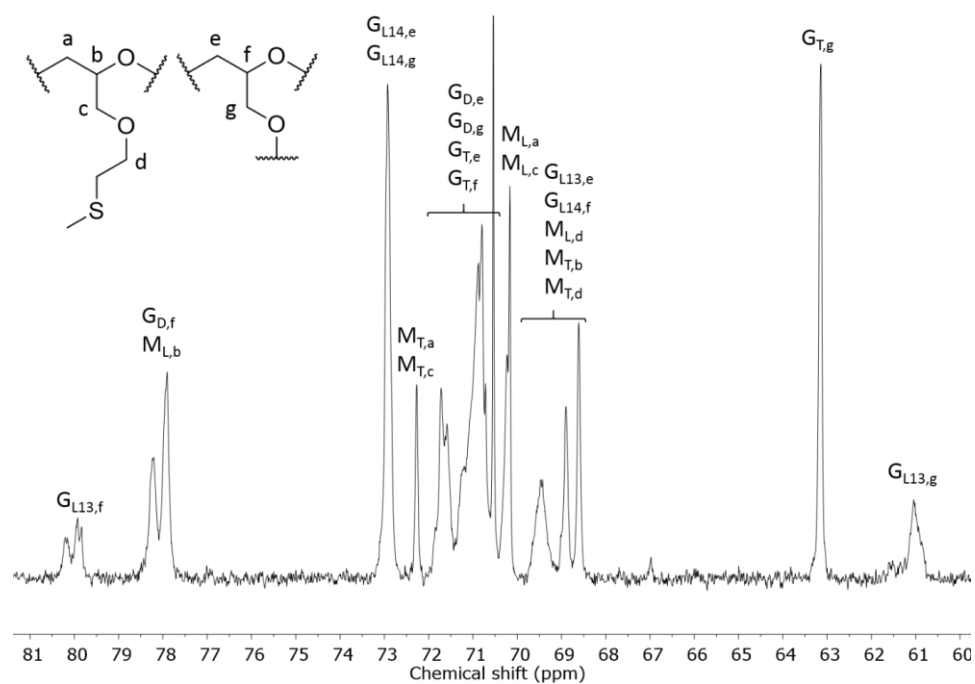
Figure S3. Signal assignment of dendritic (D), linear (L) and terminal (T) MTEGE (M) und glycerol (G) units of *hb*(PG-*co*-PMTEGE) in the ether region of the IG ^{13}C NMR spectrum (100 MHz, DMSO-*d6*).
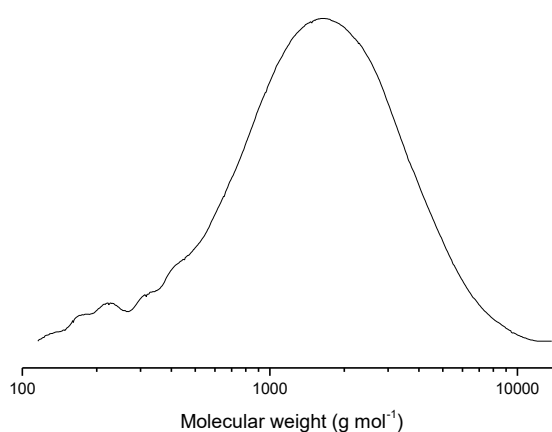
Figure S4. SEC trace (DMF, RI signal, PEG standard) of *hb*(PG$_{44}$-*co*-PMTEGE$_4$).
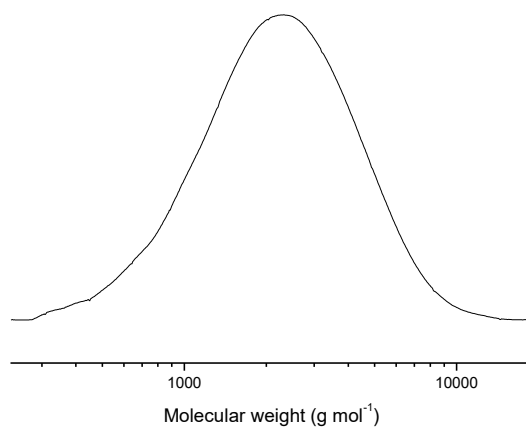
Figure S5. SEC trace (DMF, RI signal, PEG standard) of *hb*(PG$_{36}$-*co*-PMTEGE$_6$).
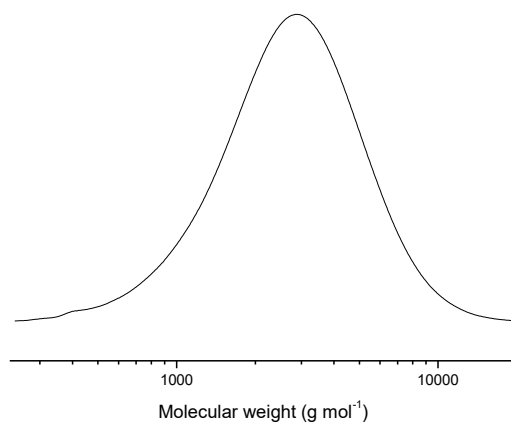
Figure S6. SEC trace (DMF, RI signal, PEG standard) of *hb*(PG$_{46}$-*co*-PMTEGE$_{13}$).
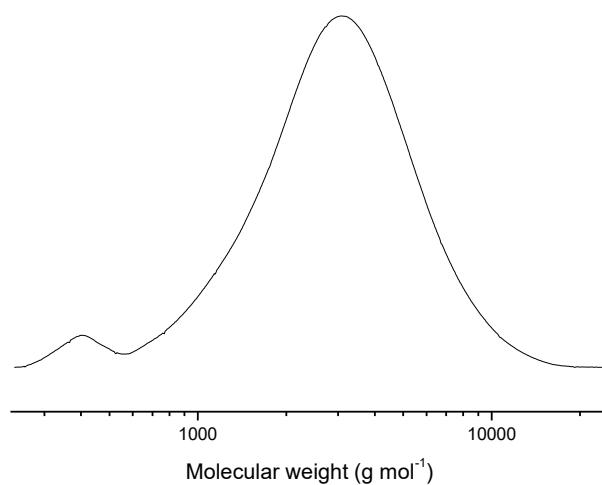
Figure S7. SEC trace (DMF, RI signal, PEG standard) of *hb*(PG$_{32}$-*co*-PMTEGE$_{18}$).
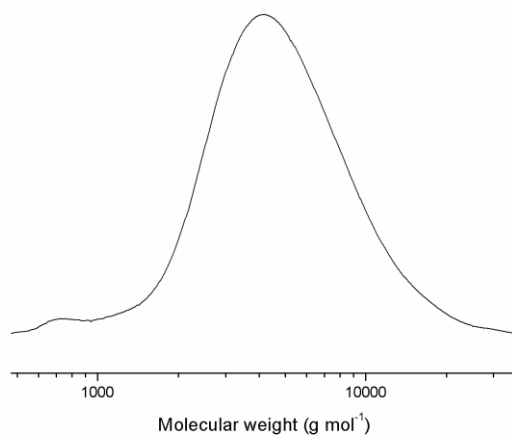
Figure S8. SEC trace (DMF, RI signal, PEG standard) of hb(PG$_{78}$-co-PMTEGE$_{7}$).
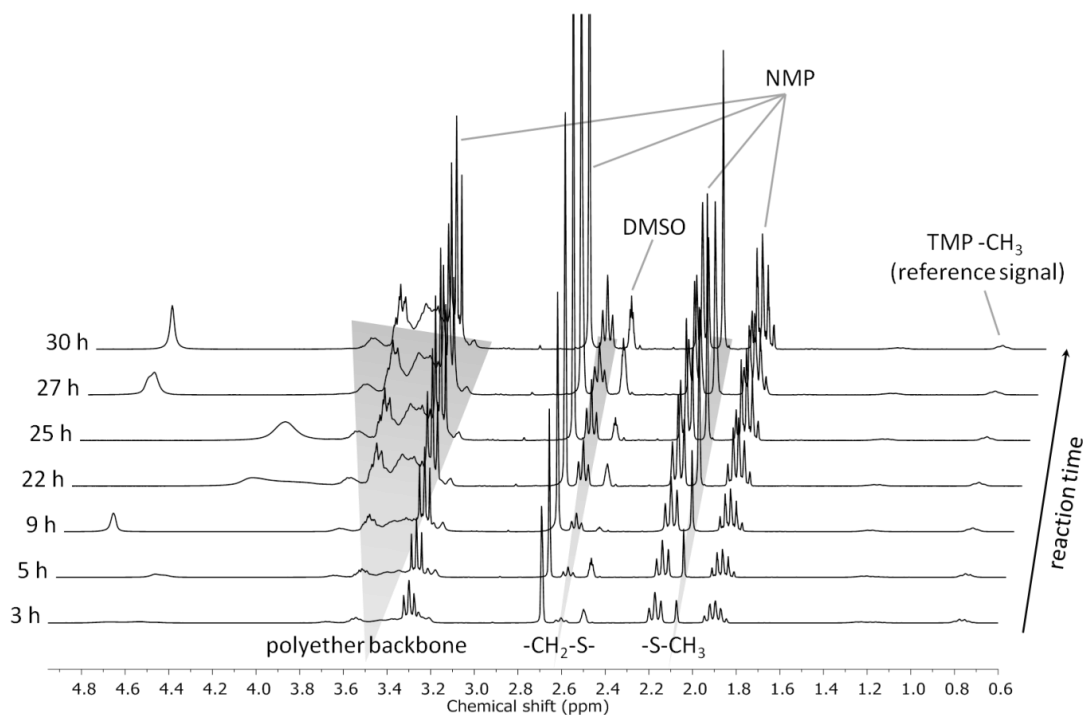
Figure S9. ^{1}H NMR spectra (DMSO-d_6, 300 MHz) of the copolymerization of MTEGE and glycidol under slow monomer addition conditions after different reaction times, normalized to the methyl signal of the TMP core.
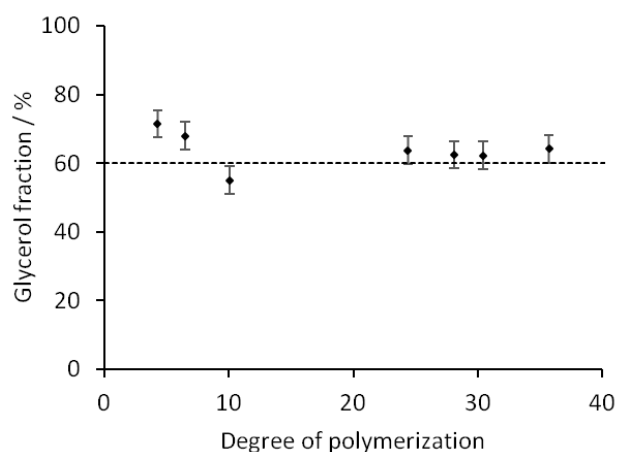
Figure S10. Copolymer composition over the course of a copolymerization of MTEGE and glycidol under slow monomer addition conditions. The dashed line represents the mole fraction in the monomer feed. (Errors estimated on the base of the inherent innacuracy of ^{1}H NMR spectroscopy).
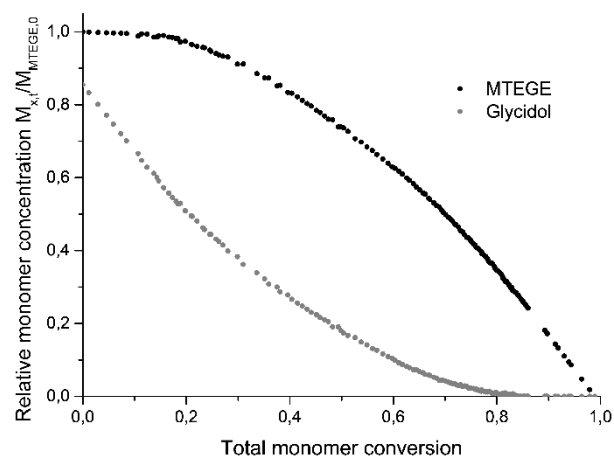
Figure S11. Relative single monomer conversion $M_x/M_{MTEGE,0}$ versus total monomer conversion.
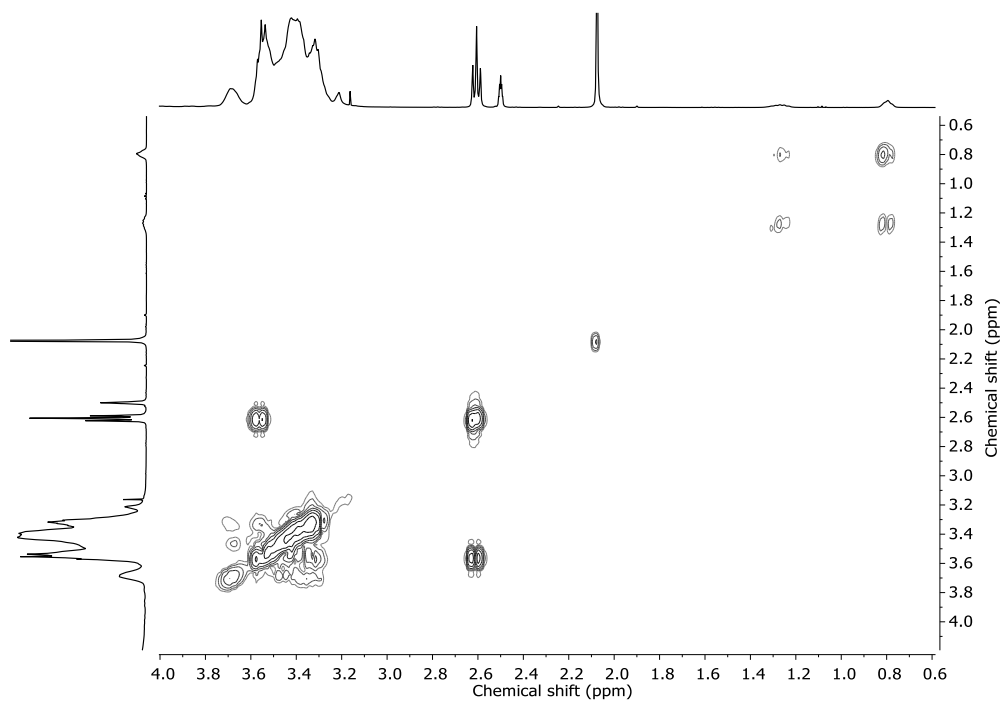
Figure S12. COSY NMR spectrum of *hb*(PG-*co*-PMTEGE) (400 MHz, DMSO-*d_6*).
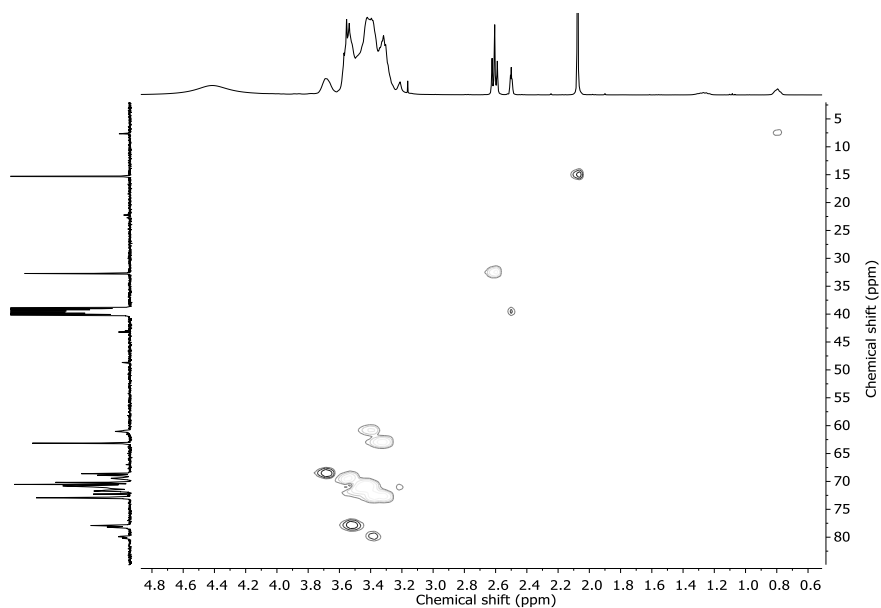
Figure S13. HSQC NMR spectrum of *hb*(PG-*co*-PMTEGE) (400/100 MHz, DMSO-*d₆*). Horizontal axis: ¹H NMR spectrum; vertical axis: ¹³C NMR spectrum. Phase correlation is given by correlation of cross peaks (dark grey: methyl, methine, light grey: methylene).
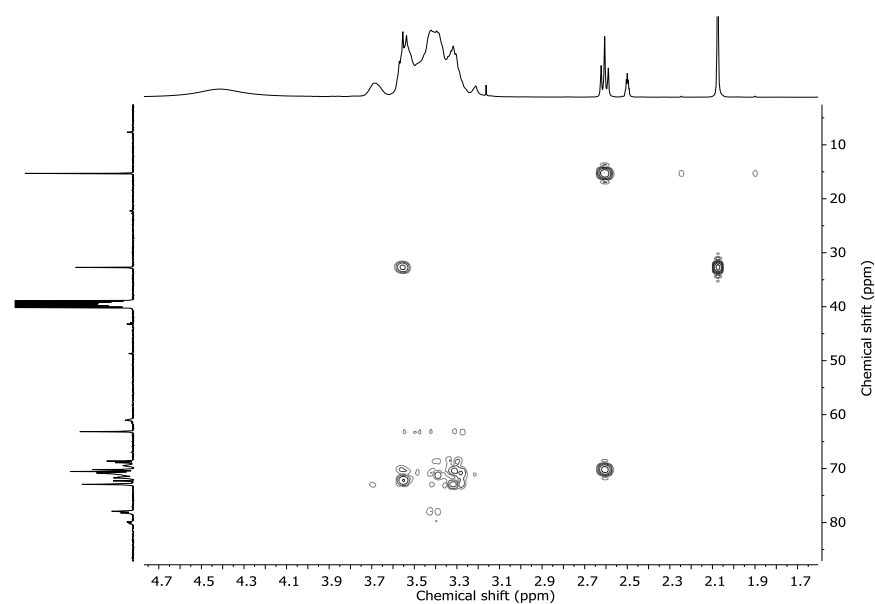
Figure S14. HMBC NMR spectrum of *hb*(PG-*co*-PMTEGE) (400/100 MHz, DMSO-*d₆*). Horizontal axis: ¹H NMR spectrum; vertical axis: ¹³C NMR spectrum.
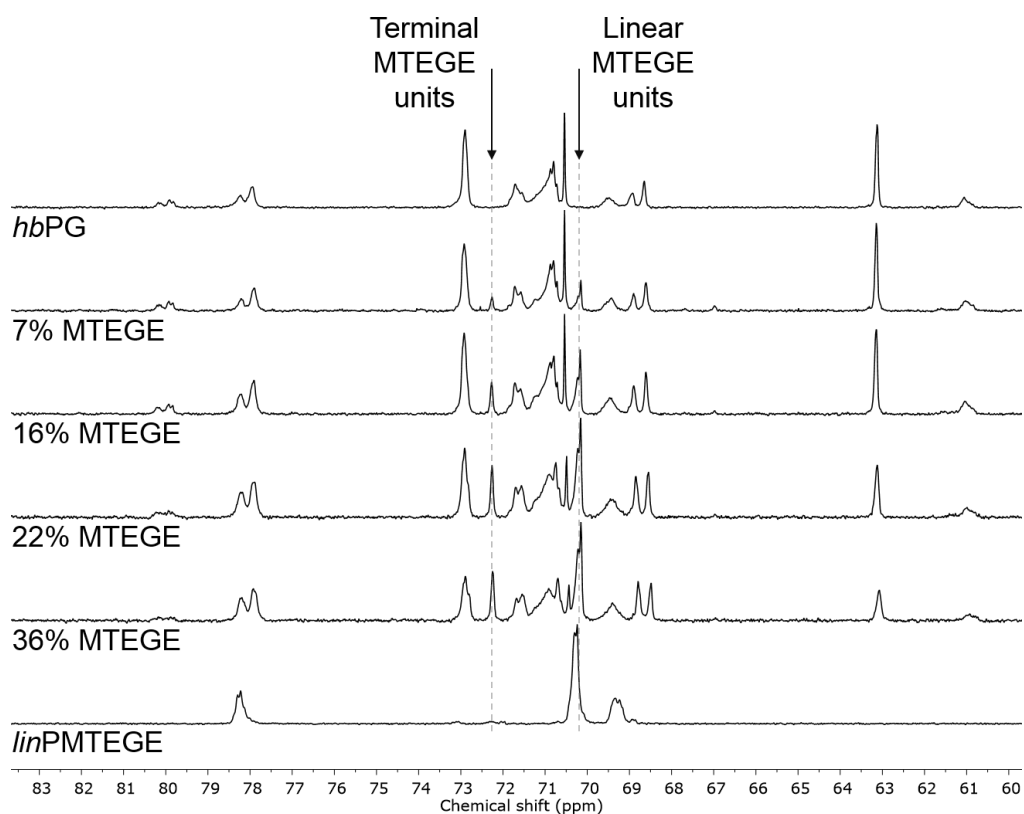
Figure S15. Inverse Gated ^{13}C NMR spectra of hb(PG-co-PMTEGE) copolymers with varying composition. Spectra of the two homopolymers for comparison (100 MHz, DMSO-d_6).
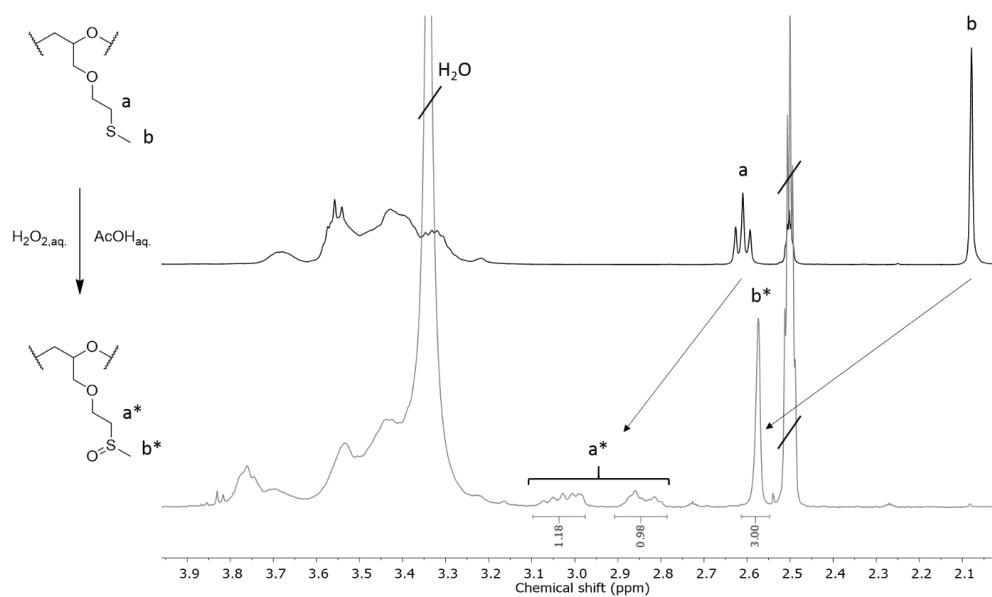
Figure S16. ^{1}H NMR spectra of hb(PG$_{32}$-co-PMTEGE$_{18}$) before (black, top) and after (grey, bottom) oxidation of the thioether groups (400 MHz, DMSO-d_6).
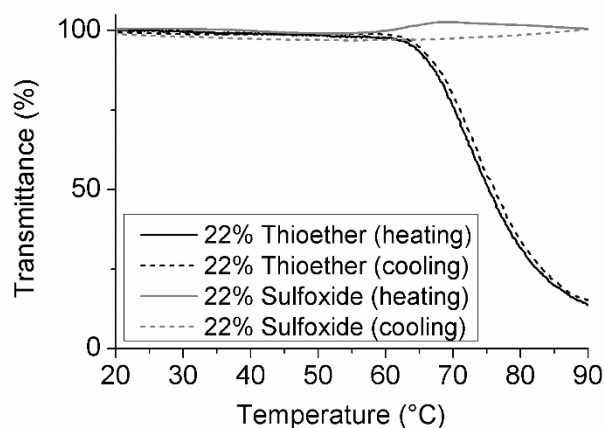
Figure S17. Intensity of transmitted laser light versus temperature for hb(PG$_{46}$-*co*-PMTEGE$_{13}$) in aqueous solution (c = 5 mg mL^{-1}) before and after oxidation of the thioether moieties.
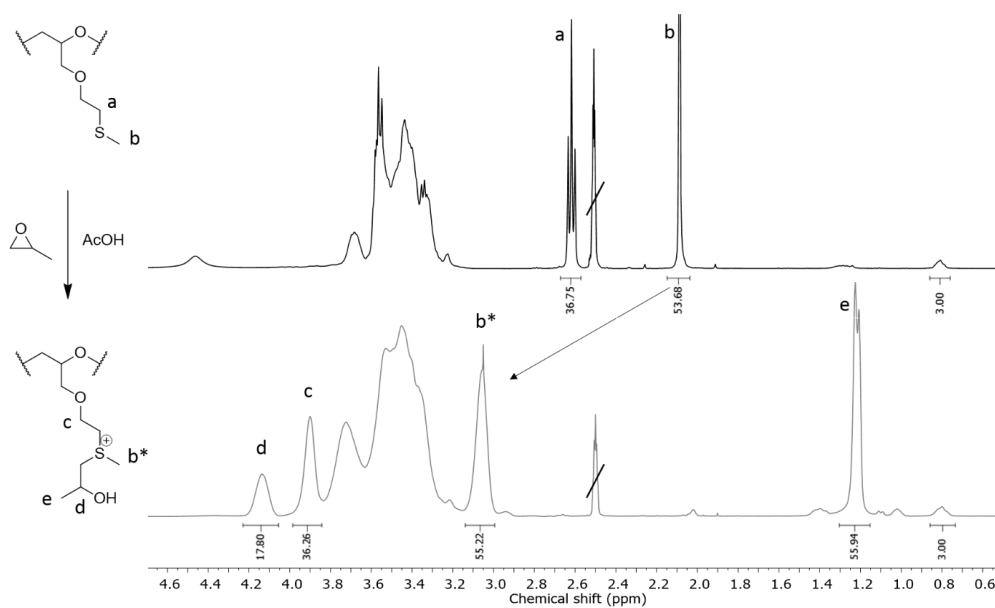
Figure S18. ^{1}H NMR spectra of hb(PG$_{32}$-*co*-PMTEGE$_{18}$) before (black, top) and after (grey, bottom) modification of the thioether groups with propylene oxide (400 MHz, DMSO-d_6).
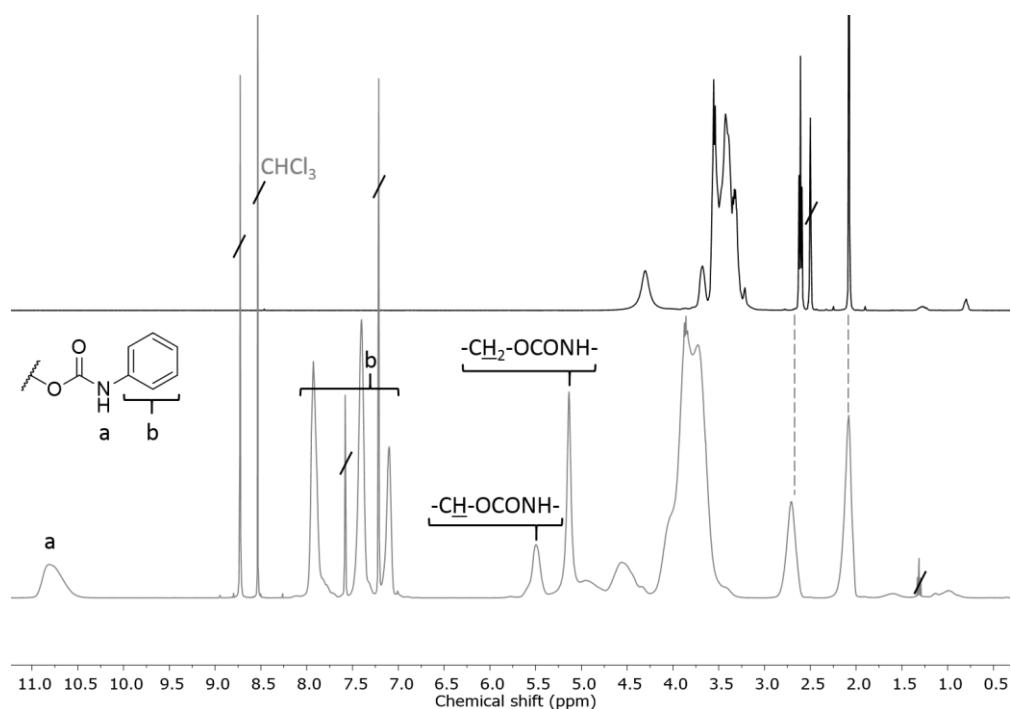
378
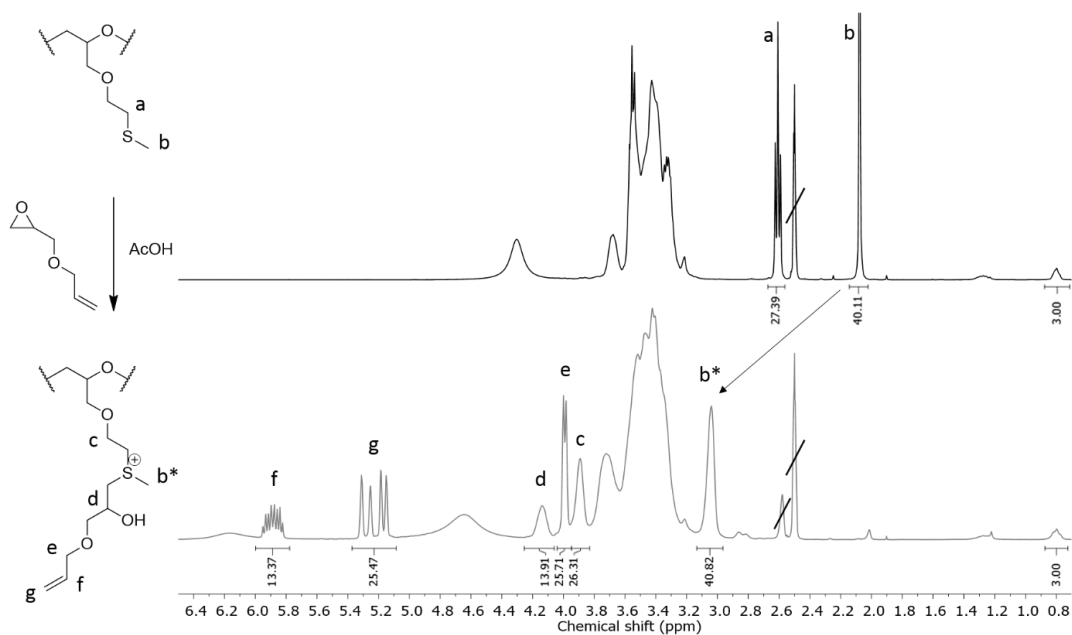
Figure S19. ^{1}H spectra of hb(PG$_{32}$-co-PMTEGE$_{18}$) before (black, top) and after (grey, bottom) modification of the thioether groups with allyl glycidyl ether (400 MHz, DMSO-d_6).

Figure S20. ^{1}H NMR spectra of hb(PG$_{46}$-co-PMTEGE$_{13}$) before (black, top) and after (grey, bottom) transforming the hydroxyl groups into urethane groups (400 MHz, top: DMSO-d_6, bottom: pyridine-d_5).
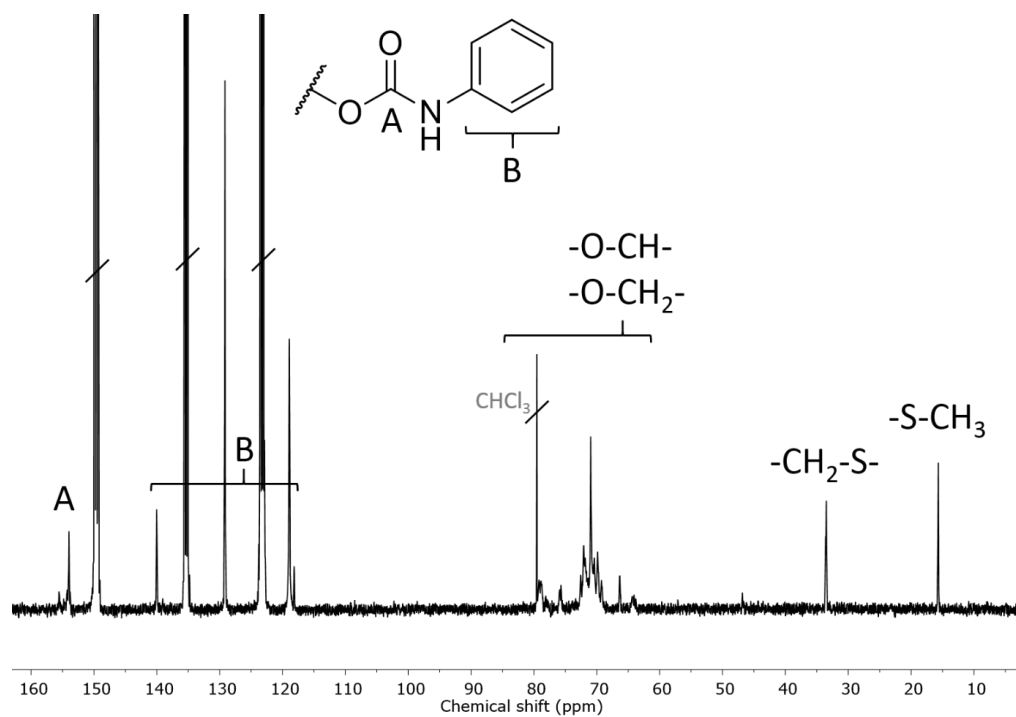
379

Figure S21. ^{13}C NMR spectrum of *hb*(PG$_{46}$-*co*-PMTEGE$_{13}$) after transforming the hydroxyl groups into urethane groups (100 MHz, pyridine-*d$_5$*).
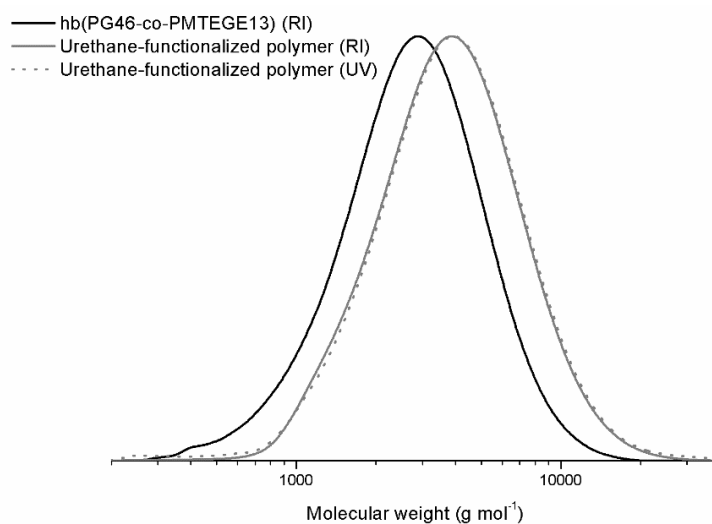

Figure S22. SEC traces (DMF, PEG standard) of *hb*(PG$_{46}$-*co*-PMTEGE$_{13}$) before and after modification with phenyl isocyanate.

Appendix A3

Reprinted with permission from Christ, E.-M.; Herzberger, J.; Montigny, M.; Tremel, W.; Frey, H. *Macromolecules*, **2016**, *49*, 3681-3695. Copyright 2016 American Chemical Society.

Poly(THF-*co*-cyano ethylene oxide): Cyano Ethylene Oxide (CEO) Copolymerization with THF Leading to Multifunctional and Water-Soluble PolyTHF Polyelectrolytes

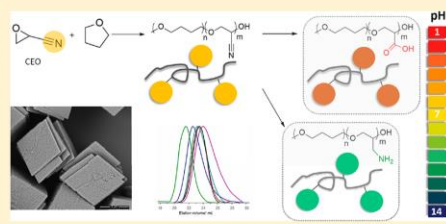Eva-Maria Christ,[†,‡] Jana Herzberger,[†,‡] Mirko Montigny,[§] Wolfgang Tremel,[§] and Holger Frey[*,†]

[†]Institute of Organic Chemistry, Johannes Gutenberg-University Mainz, Duesbergweg 10-14, D-55128 Mainz, Germany
[‡]Graduate School Materials Science in Mainz (MAINZ), Staudingerweg 9, D-55128 Mainz, Germany
[§]Institute of Inorganic Chemistry and Analytic Chemistry, Johannes Gutenberg-University, Duesbergweg 10-14, 55128 Mainz, Germany

S Supporting Information

ABSTRACT: Cyano-functional polyether copolymers based on THF were prepared via cationic ring-opening copolymerization of THF with cyano ethylene oxide (CEO). The CEO content of poly(tetrahydrofuran) (polyTHF) based copolymers varied from 3.3 to 29.3%, and molecular weights ranged from 5100 to 31900 g·mol^{-1} with M_w/M_n in the range of 1.31 to 1.74 (SEC in THF, PS standards). The polymerization was conducted with methyl trifluoromethanesulfonate (MeOTf) as an initiator. Kinetic studies concerning incorporation of both monomers were performed via NMR spectroscopy. The cyano groups at the poly(THF-*co*-CEO) copolymers enable direct access to amino (polyTHF−NH$_2$) and carboxyl groups (polyTHF−COOH) in facile one-step procedures, respectively. The modified copolymers were characterized via NMR, MALDI−ToF mass, and FT-IR spectroscopy. Thermal properties of the materials were studied via differential scanning calorimetry (DSC), demonstrating a gradual decrease of the melting points with increasing amount of CEO in the copolymers (from 30 °C for 3.3% CEO to 21 °C for 8.4% CEO). After postmodification to carboxylic acid groups the melting points decrease from 26 to 18 °C in the series of copolymers. Contact angles of water on thin films of the polymers can be tuned in a wide range from 72.7° to 17.8° by varying the CEO fraction as well as by postmodification. Crystallization studies of CaCO$_3$ with water-soluble polyTHF−COOH revealed the composition-dependent inhibition of calcite growth, with crystallite size in the mineralization process being controlled by the amount of carboxylic acid groups at the poly(THF) copolymers.

■ INTRODUCTION

Poly(tetrahydrofuran) (polyTHF) is an extremely versatile material that is characterized by its remarkably high chain flexibility and its apolar nature.[1] PolyTHF possesses a low melting point (28 °C), which contributes to its easy handling, besides excellent solubility in a wide range of rather hydrophobic solvents like chloroform or THF. This renders the material interesting for manifold applications, e.g., as soft component in the polyurethane production[2,3] (e.g., for Spandex), for the synthesis of fibers, adhesives, and sealants, and for coatings in the textile industry. Characteristic properties like the high hydrolytic stability in contrast to other polyester polyols, a high moisture vapor transmission, and high abrasion resistance as well as microbial resistance play a key role for these purposes. Furthermore, the resulting materials possess good visible light transparency.[4,5] Besides its applications in a wide industrial field, polyTHF is also favorable for manifold biomedical applications, such as a key component in contact lenses, due to its low solubility in water and its good biocompatibility.[4] Last but not least, polyTHF represents a straightforward "end-of-life polymer", since it can easily be degraded to THF in a facile and inexpensive way.[6,7]

The properties of polyTHF can be systematically expanded and manipulated by modification of the end-groups. Rowan et al. reported the synthesis of nucleobase-terminated polyTHF, which self-assembled to materials with film and fiber-forming capability.[8] By diversifying the initiator of the polymerization, the starting group of polyTHF can be varied as well[9,10] to create telechelic and heterobifunctional polyTHF.[11] The introduction of functional groups, such as alkyl, −OH, −NH$_2$, −COOH, and −COOR, is an attractive objective, because these moieties can be used to tune the hydrophilic/hydrophobic character, permeability, and mechanical properties, as demonstrated recently for polycarbonates.[12] Also for related hydrophilic polyethers, multifunctionality is generally an important target, as demonstrated in numerous publications in

recent years.[13−19] Amine-functional polyTHFs were presented in two works; however, the amino groups were positioned only as end-groups as well.[20,21] As a further end-group functionalized material, the group of Teixidor provided reversible, redox-active polyTHF by combining polyTHF with metallacarboranes.[22] The direct copolymerization of THF with ethylene oxide has been studied, e.g., by Bednarek and Kubisa[23] and later by Höcker et al.,[24] and was found to proceed in a random manner. The cationic copolymerization of THF with functional cyclic monomers has been presented in a few intriguing works. In this area, the group of Zhu reported the copolymerization of THF with glycidol to create branched copolymers with numerous hydroxyl groups[25] and the group of Pomposo et al. combined THF with glycidyl phenyl and glycidyl propargyl ether,[26] based on previous work of Du Prez and co-workers.[27] THF was also copolymerized with epichlorohydrin or bis(chloromethyl)-oxetane to create high-energy binders after postmodification, resulting in materials with high nitrogen content.[28,29]

In the current work we have studied the cationic random (co)polymerization of THF with the novel functional monomer cyano ethylene oxide (CEO) (Scheme 1).

Scheme 1. Copolymerization of CEO and THF, as Well as Post-Modification Reactions, Leading to PolyTHF Copolymers with Carboxylic Acid and Amine Moieties
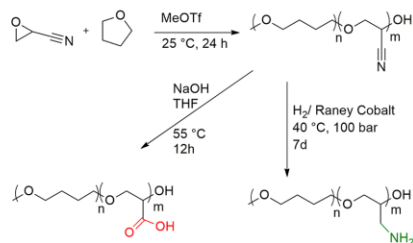
We demonstrate that the combination of these two monomers results in linear multifunctional polyTHF copolymers with a large number of functional cyano groups (from 3.3 to 29.3%, analyzed via NMR). Comprehensive characterization of all copolymers via MALDI−ToF mass spectrometry, NMR spectroscopy, size exclusion chromatography (SEC), FT-IR spectroscopy, and differential scanning calorimetry (DSC) has been carried out. We also demonstrate that the cyano groups can be postmodified to primary amine groups and carboxylic acid groups, resulting in water-soluble polyTHF at elevated pH. This material has been explored for the mineralization of calcium carbonate, as will be discussed in the final part of this work.

■ EXPERIMENTAL SECTION

Materials. All reagents were purchased from Acros Organics or Sigma-Aldrich and were used as received, unless otherwise stated. Anhydrous DMSO and o-dichlorobenzene were stored over molecular sieves prior to use. Column chromatography was performed on silica gel (particle size 63−200 μm, Merck, Darmstadt, Germany). Deuterated DMSO-d_6, pyridine-d_5, MeOD-d_3, CDCl$_3$, and HFIP-d_2 were purchased from Deutero GmbH. Tetrahydrofuran (THF) was purified by standard methods and was distillated over sodium in the presence of benzophenone. Dialysis membrane tubings were purchased from Sigma-Aldrich or Orange Scientific, respectively. For dialysis in chloroform, a membrane of regenerated cellulose

(benzoylated) was used. For dialysis in protic solvents, regular regenerated cellulose membranes were applied.

Instrumentation. ^{1}H NMR (300 and 400 MHz) and ^{13}C NMR spectra (75 and 100.6 MHz) were recorded on Bruker AC300, Bruker AC400, Avance III HD 300 (300 MHz, 5 mm BBFO-head with z-gradient and ATM, B-ACS 60 sample changer) spectrometers with Open-Access-Automation, Avance II 400 (400 MHz, 5 mm BBFO-head with z-gradient and ATM, SampleXPress 60 sample changer) with Open-Access-Automation or Avance III HD 400 (400 MHz, 5 mm BBFO-SmartProbe with z-gradient and ATM, SampleXPress 60 sample changer), respectively, and are referenced internally to residual proton signals of the deuterated solvents. ^{1}H NMR experiments for kinetic studies were acquired with a 5 mm BBFO z-gradient probe on the 500 MHz Bruker AVANCE III system. For the respective ^{1}H NMR spectra, 64 transients were used with a 10.6 μs long 90° pulse and 10000 Hz spectral width together with a recycling delay of 10 s. For the ^{13}C NMR kinetic measurements, 32 scans were used with a relaxation delay of 30 s (90° pulse, 13.2 μs, spectra width 30000 Hz). The temperature was kept at 298.3 K and calibrated with a standard ^{1}H methanol NMR sample using the topspin 3.2 software (Bruker). Control of the temperature was realized with a VTU (variable temperature unit) and an accuracy of ±0,1K.

For size exclusion chromatography (SEC) measurements in THF a PU 1580 pump, an auto sampler AS1555, a UV-detector UV 1575 (detection at 254 nm) and a RI-detector RI 1530 from JASCO were used. Columns (MZ-Gel SDplus 10^2 Å and MZ-Gel SDplus 10^6 Å) were obtained from MZ-Analysentechnik. Calibration was carried out with polystyrene (PS) standards purchased from Polymer Standard Services (PSS). MALDI−ToF MS measurements were performed on a Shimadzu Axima CFR MALDI-TOF mass spectrometer using dithranol (1,8,9-trishydroxyanthracene) or CHCA (α-Cyano-4-hydroxycinnamic acid) as a matrix. The samples were prepared from pyridine and ionized by adding lithium chloride or potassium trifluoro acetate.

DSC measurements were carried out on a PerkinElmer DSC 8500 in the temperature range of −80 to 50 °C, using heating rates of 10 K min^{-1} under nitrogen. Contact angle measurements were performed on a Dataphysics Contact Angle System OCA using water as an interface agent. SEM images were taken with a FEI Nova NanoSEM at acceleration voltage of 5 kV and a vC detector or a FEI Phenom SEM at 3 kV acceleration voltage, respectively.

TEM images were recorded using a FEI Technai T12 equipped with a 4K CCD camera and a LaB$_6$ cathode working on 120 kV acceleration voltage. Samples for TEM were prepared by dropcasting 20 μL of the sample dilution from crystallization beakers onto a carbon coated copper grid (Plano GmbH, Wetzlar, Germany).

Raman-spectroscopy measurements for phase identification were carried out using a confocal HR800 μ-Raman by Horiba Scientific. Raman stimulation was managed by exciting with λ = 633,318 nm He/Ne laser without using any filters. To get best signal-to-noise possible a pinhole with a 400 nm diameter has been used. The signal was collected with a CCD detector with a 1024 × 256 pixels open electrode chip.

Synthetic Procedures. *Synthesis of Cyano Ethylene Oxide (CEO).* CEO was synthesized as described in the literature.[30] Briefly, in the course of 3 h at 0 °C, 100 mL of sodium hypochlorite (13% active chlorine) was added with a dropping funnel to cold acrylonitrile (100 mL, 1.53 mol). The mixture was stirred vigorously with a mechanical stirrer at 0 °C for additional 21 h, leading to a yield of 39.5% (Lit.: 34.5%.[30]). Subsequently, residual acrylonitrile was recovered by distillation, and the product was purified by distillation *in vacuo* (60 °C, 10^{-2} mbar). ^{1}H NMR (300 MHz, CDCl$_3$): δ (ppm) = 2.95-3.25 (m, 2H, −CH$_2$−), 3.4−3.54 (m, 1H, −CH). ^{1}H and ^{13}C NMR spectra of CEO are shown in the Supporting Information, Figure S1. To avoid degradation to 3-cyanopropanal, the labile monomer CEO was stored under argon at −18 °C.

Representative Procedure for the Synthesis of Poly(THF-co-CEO) Copolymers. CEO (0.1 g, 1.45 mmol, 69.02 g mol^{-1}) and THF (1.05 g, 14.5 mmol, 72.06 g mol^{-1}) were mixed in a glass tube under argon atmosphere at room temperature. Methyl trifluoromethanesulfonate

Scheme 2. Hypothetic Reaction Mechanism of the (Co)polymerization of THF and CEO

Initiation

Propagation

Termination

P(CEO-*co*-THF)
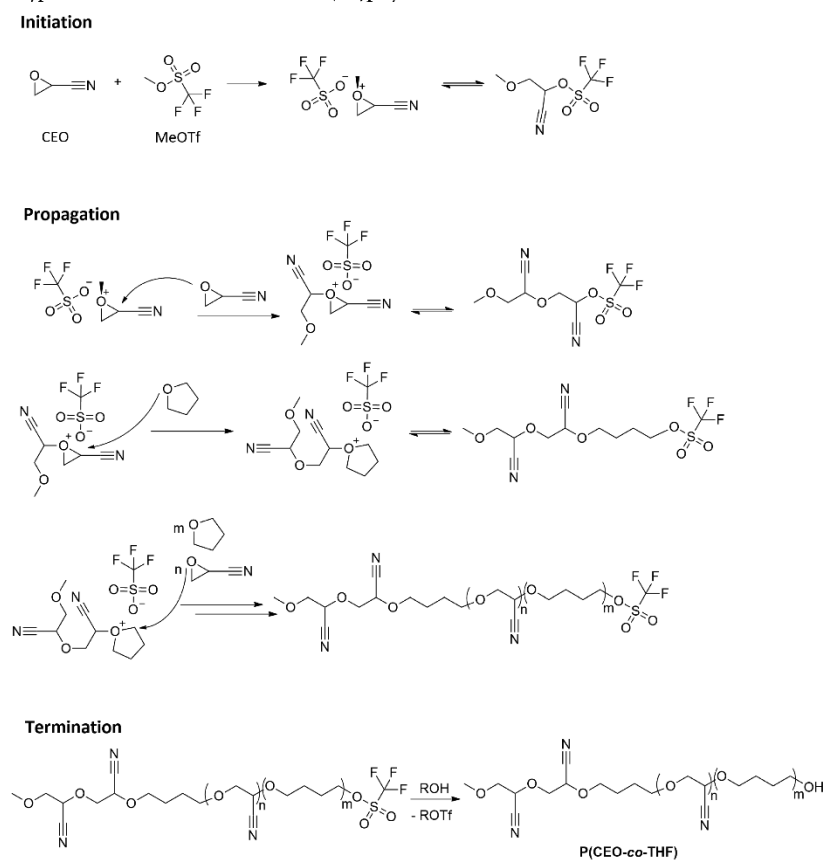
(MeOTf) (1 μL) was added via syringe. After 24 h, the polymerization was quenched with pyridine. The product was dissolved in 0.5 mL pyridine and purified via dialysis in THF for 4 days. After every 24 h, THF was renewed (yields: 53−84%). ^{1}H NMR (300 MHz, CDCl$_3$): δ (ppm) = 3.5−3.85 (m, −CH$_2$−), 4.14−4.66 (m, −CH−), 3.31−3.52 (m, −CH$_2$−), 1.47−1.74 (m, −CH$_2$−).

Postpolymerization Modification of Poly(THF-co-CEO) Copolymers to Polyether Polyacids. The procedure used for postpolymerization reaction of cyanide groups to carboxylic acid groups is comparable to literature for other cyano-functional structures.[31] 100 mg of the poly(THF-*co*-CEO)copolymer was dissolved in 2 mL of THF, sodium hydroxide (1 molar, 5 mL) was added and the reaction mixture was stirred overnight at 55 °C. Subsequently, the polymer was purified and the salts were removed via dialysis in THF/methanol (1:1) for 3 days. THF/methanol was renewed every 24 h. The product was dried under reduced pressure at 80 °C for 3 days (yield: 89%). ^{1}H NMR (300 MHz, THF-d_8): δ (ppm) = 5.37 (m, CH−O−), 3.48−3.32 (m, −CH$_2$O−), 3.28−3.25 (m, −CH$_3$), 2.53 (m, −OH), 1.56−1.54 (m, −CH$_2$−).

Postpolymerization Modification of Poly(THF-co-CEO) Copolymers to Polyether Polyamines. The postpolymerization reaction of cyanide groups to amine groups follows the description of Meijer et al. developed for poly(propyleneimine) dendrimers.[32] First, 100 mg of

the poly(THF-*co*-CEO)copolymer was dissolved in 2 mL of THF, then 200 mg of Raney cobalt catalyst (Cr promoted, Grace 2724, pretreated with hydroxide) in 2 mL of water was added and the mixture was stirred at 40 °C and 100 atm H$_2$ pressure, for 7 days. The cooled reaction mixture was then filtered and the solvents were evaporated under reduced pressure. Purification and further steps follow the procedure of the carboxylic acid functionalized copolymers. ^{1}H NMR (300 MHz, CDCl-d_3): δ (ppm) = 4.26−4.21 (m, −CH−), 3.73−3.28 (m, −CH$_2$O−), 3.19 (m, −CH$_3$), 2.19 (m, CH$_2$NH$_2$), 1.75−1.55 (m, −CH$_2$CH$_3$−).

Mineralization of CaCO$_3$. Crystallization experiments were carried out using the standard ammonia diffusion method reported elsewhere[33−35] on well-defined quarz-glass slides from Plano GmbH with a diameter of 13 mm and a thickness of about 1 mm. The glass-slides were placed on the bottom of 5 mL beakers filled with 2 mL of an aqueous dilution of polyether polyacid polymer with as mentioned concentration and a 5 M of calcium chloride. They were cleaned prior crystallization by washing in acidic piranha solution for 2 h, washing with ethanol and Millipore water until water reacted neutral. To make sure that the atmosphere of the desiccator was oversaturated permanently with ammonia and carbon dioxide, 7 g of ammonium carbonate was used for a small sized desiccator. After 15 h of crystallization, the glass slides were removed from solution, washed

383

Table 1. Characterization Data for the Series of Poly(THF-*co*-CEO) Copolymers Prepared

composition[a]	[CEO]/%	CEO fraction[a]/%	$M_n{}^a$/g mol^{-1}	$M_n{}^b$/g mol^{-1}	$M_w/M_n{}^b$
PTHF$_{586}$	0	0	42200	73000	1.83
P(THF$_{146.2}$-*co*-CEO$_5$)	5	3.3	10900	18800	1.59
P(THF$_{289}$-*co*- CEO$_{14}$)	5	4.6	21800	31900	1.42
P(THF$_{174.8}$-*co*-CEO$_{11.7}$)	6	6.3	13400	9800	1.31
P(THF$_{118.2}$-*co*-CEO$_{8.8}$)	7	6.9	9100	9700	1.34
P(THF$_{120.4}$-*co*-CEO$_{11.1}$)	9	8.4	9400	8600	1.49
P(THF$_{53}$-*co*-CEO $_{22}$)	25	29.3	5300	5100	1.74

[a]Obtained from ^{1}H NMR spectra. [b]Determined by SEC measurements (THF, PS standards, RI signal).

carefully on both sides with saturated CaCO$_3$ dilution and Millipore-water to ensure resolving ammonium carbonate crystals without inducing the resolving−recrystallization mechanism and to remove excessive unbound polymer followed by drying under airflow.

■ RESULTS AND DISCUSSION

A. Monomer Synthesis and Copolymerization of CEO with THF. *Monomer Synthesis.* Cyano ethylene oxide (CEO) can be synthesized in a one step-procedure, following a modified literature protocol.[30] Dropping sodium hypochlorite to acrylonitrile affords the desired product. The excess of acrylonitrile can be retrieved by distillation. In this way, the moderate to low yield of the product CEO (39.5%) can be enhanced by utilizing repetitive procedures. To avoid possible degradation of the monomer CEO to 3-cyano propanal, it was stored under argon at −18 °C. To date, CEO has not been employed successfully as a monomer for polymerizations to the best of our knowledge. First attempts to polymerize CEO were described by Wei and Butler in the 1970s, however no polymer could be obtained.[36]

Copolymerization of THF and CEO. The copolymerization of THF and CEO was carried out with methyl trifluorometha-nesulfonate (MeOTf) as an initiator, following recently reported results regarding cationic ROP of THF with MeOTf as an initiator.[37] We chose this initiator because of the high reactivity of MeOTf for the initiation of the "living" THF polymerization in a fast and quantitative way.[37] The polymerization mechanism of THF with this initiator is known to follow the so-called "active chain end" (ACE) mechanism (Scheme 2) regarding the polymerization of CEO, in accordance to literature describing the polymerization of THF.[38] The commonly very powerful methylating agent MeOTf[39] methylates the ring system either of THF or CEO to enable the following nucleophilic attack of the oxygen atom at another cyclic monomer. This step can be repeated either with CEO or THF monomers, leading to linear chains. The (co)polymerization can be terminated either with a base, e.g., pyridine or with a protic compound, e.g., methanol or water. Although the homopolymerization of THF is known to follow the ACE mechanism, this is not necessarily the case for the copolymerization of THF with other cyclic monomers.

As stated for the recently published copolymerization of THF and glycidyl phenyl ether with B(C$_6$F$_5$)$_3$ as a catalyst, the (co)polymerization can be controlled by synthesis conditions, such as reaction time, catalyst concentration, and monomer concentration.[40] However, a high THF content appears to be necessary to avoid cyclic products.[40] Furthermore, for the (co)polymerization of THF with other cyclic monomers as, e.g., ethylene oxide or the bisglycidyl ether of bisphenol A it appears to depend on reaction conditions, whether the ACE mechanism or the "Active Monomer" (AM) mechanism

occurs,[41] however this was observed only for other catalysts and not for MeOTf.[23,24,42−44] Finally, the polymerization of ethylene oxide is known to follow the AM mechanism with Broensted acids as a catalyst, in contrast to the polymerization of THF.[29] On the basis of this knowledge, we expected to observe coexistence of both mechanisms in the copolymerization of THF with CEO.

All copolymers prepared were characterized by SEC and MALDI−ToF MS, as well as ^{1}H NMR and ^{13}C NMR spectroscopy. For SEC measurements, the samples had to be dissolved in THF for 1 day to ensure complete solubility. The resulting molecular weights and PDIs of all samples obtained by SEC (measured in THF, PS standard) as well as the comonomer fractions (vide infra) by NMR are listed in Table 1. Molecular weights range from 5100 to 31900 g·mol^{-1} with low to moderate polydispersity (PDI) in comparison to comparable literature.[9,46−48] SEC elugrams with varied CEO monomer ratio (from 3.3 to 29.3% of CEO incorporation in the copolymer) are shown in Figure 1. With increasing CEO
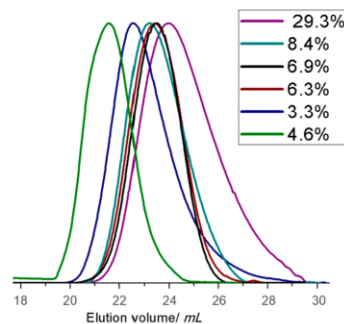

Figure 1. SEC elugrams (in THF, PS standard) of several poly(THF-*co*-CEO)copolymers with varied CEO incorporation ratio (from 3.3 to 29.3%).

fraction molecular weights clearly decrease, whereas the PDI remains unchanged. We attribute this to the coexistence of the ACE and AM mechanism. Hence, with increasing THF ratio the ACE mechanism occurs, in accordance to literature,[24,37,38] and with increasing CEO fraction coexistence of ACE and AM mechanism seems to take place, as expected.[24,40]

Figure 2 depicts a series of ^{1}H NMR spectra of copolymers with different monomer content, ranging from 3.3 to 29.3 mol % CEO. With increasing amount of CEO in the copolymers, the solubility of the materials in organic solvents decreased. Thus, in this work we aimed at materials with a minority
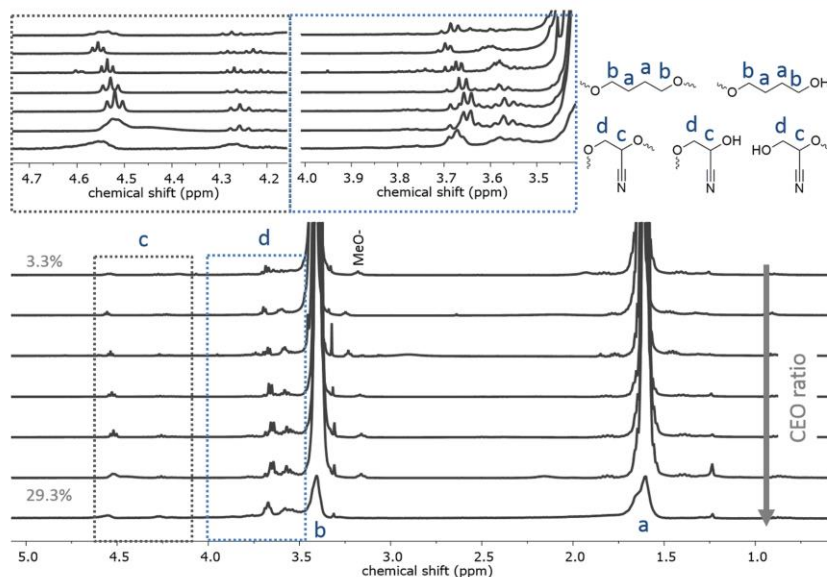
Figure 2. ¹H NMR spectra (CDCl₃, 300 MHz) of several poly(THF-*co*-CEO) copolymers with varied monomer ratio (from 3.3 to 29.3%). Bottom: magnification of the relevant signals c and d.
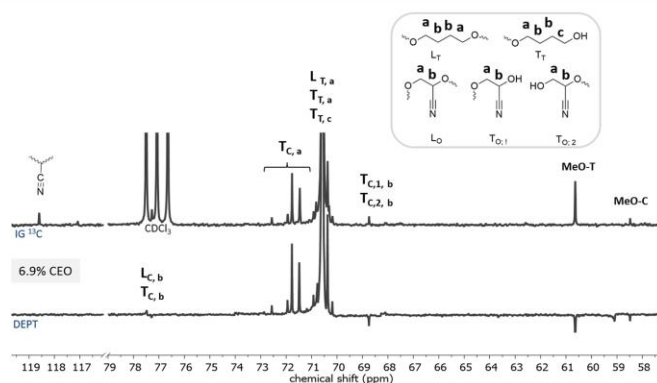

Figure 3. Top: *Inverse gated* ¹³C NMR spectra (CDCl₃, 100.6 MHz). Bottom: ¹³C DEPT NMR spectra of P(THF-*co*-CEO) with a fraction of 6.9% CEO (CDCl₃, 100.6 MHz) (C, CEO; T, THF).

fraction of CEO units. In the ¹H NMR spectra, the signals of the polyether backbone belonging to THF units appears at 1.47−1.74 ppm (Figure 2, a) and 3.31−3.52 ppm (Figure 2, b). The signals of the polyether backbone that stem from the CEO units are visible in the range of 4.14−4.66 ppm (Figure 2, C*H*) and 3.5−3.85 ppm (Figure 2, C*H*₂). On the basis of these assignments, the monomer incorporation rates of both THF and CEO were calculated, as listed in Table 1.

All relevant signals are found in the ¹³C NMR spectra as well (Figure S23). Here, the signals of the polyether backbone belonging to the THF units appears at 25.25−28.04 ppm

(Figure 23, a) and 69.85−71.10 ppm (Figure S23, b). The signals of CEO units are visible at 119.75−115.7 ppm (Figure S23, CN, blue framed), 73.27−71.10 ppm (Figure S23, C*H*₂, marked green) and 69.52−67.35 ppm (Figure S23, C*H*, marked red).

A detailed assignment of the signals in the ¹³C NMR spectrum is shown in Figure 3 for the spectrum of the copolymer with 6.9% CEO incorporation. The assignments are supported by the results of the ¹³C DEPT NMR (Figure 3) and are in good agreement with literature values for THF copolymers.[43,47]
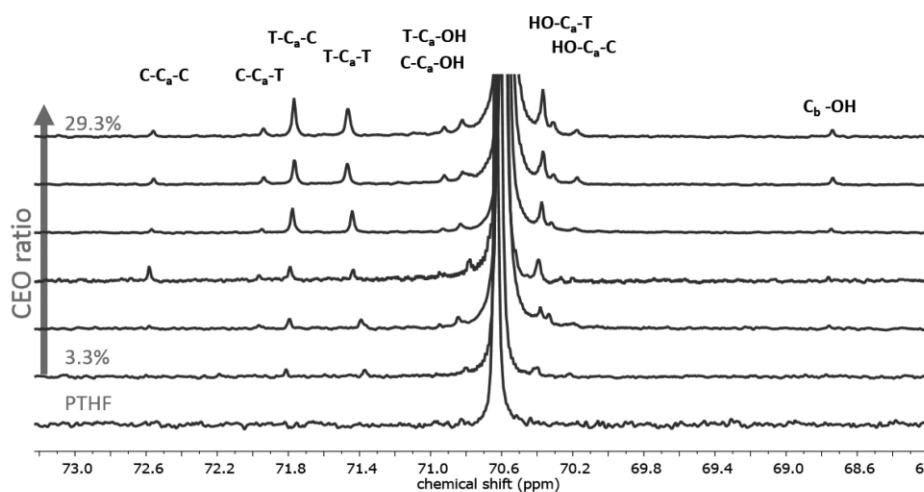
Figure 4. Relevant section of inverse gated (IG) ^{13}C NMR spectra (CDCl$_3$, 100.6 MHz) of several poly(THF-*co*-CEO) copolymers with varied monomer ratio from 3.3 to 29.3% CEO incorporation (C, CEO; T, THF).

^{13}C NMR Triad Analysis. To gain a deeper understanding of the microstructure of the poly(THF-*co*-CEO)copolymers, ^{13}C NMR spectroscopy based triad analysis was carried out. The analyzed triads (i.e., sequences of three subsequent monomer units) were labeled as recently described for EO/EPICH copolymers[48] and as established for EO/PO copolymers,[50,51] EO/DEGA copolymers[17] or other amine-functional PEGs.[18] Peak assignment was achieved by comparison with amine-functional PEGs[13,18,17,52] recently synthesized in our group, as well as by comparison with THF/glycidol copolymers[23,53] and other comparable spectra.[49] Figure 4 shows the relevant region of the *inverse gated* ^{13}C NMR spectra of several poly(THF-*co*-CEO) copolymers with varied CEO ratio (from 3.3 to 29.3% CEO incorporation).

With decreasing CEO content, the appropriate signals belonging to CEO at 72.58, 71.94, 72.77, 71.43, 70.93, 70.82, 70.36, 70.17, and 68.73 ppm disappear, while the CH$_2$ signal at 70.74−70.52 ppm, belonging to THF, is still visible, as expected. It is conspicuous that the signal belonging to the C−C−C triad does not increase with increasing CEO content, as well as the signal for the C−C−T triad. Furthermore, the triads T−C−C and T−C−T increase with increasing CEO content. We attribute this to a random or very slight gradient type microstructure, however, clearly not as a block-like structure. Besides the triad analysis of CEO units, a triad analysis of THF units was carried out as well, giving comparable results, as shown in the Supporting Information (Figure S.21).

Kinetic Studies via NMR Spectroscopy. To support the results of the triad analysis, kinetic studies have also been carried out. Different comonomer reactivity can lead to gradient type or block-like polymer chain structures, which determine the properties of the resulting materials. Hence, it is important to investigate the functional group distribution within the backbone. In the copolymerization of CEO and THF gradient copolymer structures might be expected due to the higher reactivity of oxiranes compared to oxolanes based on the respective ring strain. ^{1}H NMR kinetic studies were carried out by taking samples to compare the incorporation rates of THF and CEO in the copolymers. The (co)polymerization was

conducted in bulk under argon atmosphere with MeOTf as an initiator and at room temperature, following the procedure of the synthesis of the materials listed in Table 1. Figure 5 shows the ^{1}H NMR spectrum of a mixture of CEO and THF (1:5) before initiation and several ^{1}H NMR spectra after initiation in a time frame of 1 min to 58 h. The kinetic studies were carried out for 58 h due to the fact that the reaction mixture had still not solidified. Compared to the synthesis of the copolymers listed in Table 1 we expected solidification of the reaction mixture after 12 h. Hence, sampling of the reaction mixture seemed to impede the (co)polymerization process. However, the results show that the intensities of the signals of both monomers, CEO (3.08−2.92 ppm, green, a) and THF (1.8−1.68 ppm, blue, d), clearly decrease and signals belonging to the polymer backbone increase with increasing time. The signals of the CH$_2$−O− groups of the backbone overlay with a signal of CEO (3.33−3.29 ppm, b) and are visible at 3.47−3.24 ppm. Further signals belonging to the backbone are present at 1.61−1.39 ppm for CH$_2$ groups of THF units (blue framed, d′) and at 4.69−4.11 ppm for the CH groups of CEO units (green framed, b′).

To confirm that the signals stem from the copolymers and not from degradation products of the monomer, diffusion ordered ^{1}H NMR spectroscopy (DOSY) of the purified copolymer was carried out. The obtained spectrum is shown in the Supporting Information (Figure S7) and exhibits signals at 4.60 and 4.24 ppm, which are in agreement with the signals, visible in Figure 2 and with the signals obtained from the kinetic studies. However, the signals of the kinetic studies might be more precise and separated due to the good solubility of the growing oligomers. We attribute the presence of several signals for the CH groups to the fact that there might be different chemical shifts depending on whether the protons belong to terminal or linear units and whether CEO or THF is in the neighboring monomer unit. Finally, the signal at 4.6 ppm is visible via correlated spectroscopy (COSY) and correlates with the CH$_2$ signals of the CEO units at 3.69 ppm (please see Supporting Information, Figure S8).
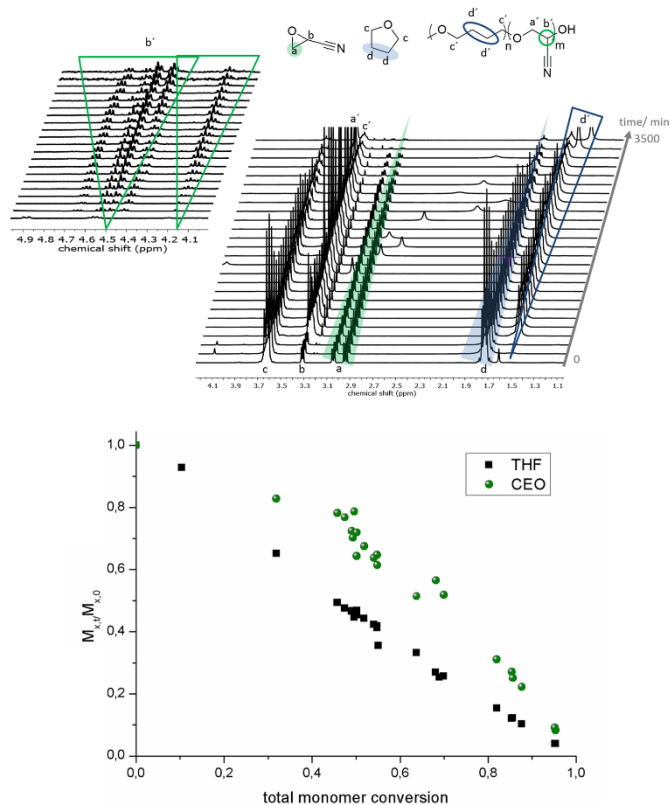
Figure 5. Kinetic studies via ^{1}H NMR spectroscopy (300 MHz, CDCl$_3$), green: CEO and blue: THF in a time frame of 1 min to 58 h, (1:5, CEO: THF), bottom: fraction of initial monomer concentration for both CEO and THF (M$_{x,t}$/M$_{x,0}$), normalized to 1(100%) for both monomers, respectively, vs total monomer conversion.

The results show that THF is incorporated faster than CEO (Figure 5, bottom). Thus, we expect a gradient type copolymer structure. We attribute the slower incorporation of CEO to the steric hindrance of the cyano group of the CEO comonomer, however the ring strain of oxiranes is clearly higher than for oxolanes (EO: 116 kJ mol^{-1}, THF: 23 kJ mol^{-1}).[54] Figure S3 in the Supporting Information shows a further plot of the respective monomer conversion vs total monomer conversion. In summary, the kinetic studies provide evidence for the successful incorporation of both monomers, as well as a faster incorporation of THF, leading to gradient type structures. Additionally, we conducted in situ ^{1}H and ^{13}C NMR kinetics in bulk, however the lack of stirring during the measurements impedes a detailed calculation of the reaction rates (Supporting Information, Figures S4–S6).

Homopolymerization of CEO was also carried out. However, as shown in the Supporting Information, the homopolymer PCEO shows very limited solubility in all solvents employed. Nevertheless, some results regarding the soluble fraction of the homopolymers are summarized in Table S3 and Figure S22 of

the Supporting Information. Molecular weights up to 2200 g·mol^{-1} were detected for the soluble fraction of the homopolymers.

B. Postpolymerization Modification of Poly(THF-*co*-CEO) Copolymers to Water-Soluble Polyether Polyacids and Polyetheramines. Linear polyacids with tunable number of functional groups as well as molecular weights are promising for various potential applications, e.g., as gelling agents, lubricants, or ion exchange resins or for thickening in pharmaceuticals, cosmetics, and paints. The most widely applied example of polyacids is poly(acrylic acid) (PAA).[55] Especially the facile one-step postpolymerization procedure renders the novel polyTHF copolymers interesting even for potential industrial applications, due to the commercially available chemicals like sodium hydroxide and THF, as well as low temperatures (55 °C) and short reaction times. To date, to the best of our knowledge no postpolymerization reaction of functional polyTHF has been reported for the synthesis of linear polyacids. In order to develop water-soluble polyTHF-based polyelectrolytes, five poly(THF-*co*-CEO) copolymer

387

samples used for the generation of poly(THF-*co*-carboxylic acid ethylene oxide) (P(THF-*co*-CAEO)) have been prepared and extensively characterized by NMR, MALDI−ToF MS, and FT-IR spectroscopy.

Postpolymerization modification was carried out following the procedure of Peng et al.[31] The poly(THF-*co*-CEO) copolymer was dissolved in THF, sodium hydroxide (1 molar) was added, and the reaction mixture was stirred overnight at 55 °C. Subsequently, the polymer was purified and the salts were removed via dialysis in THF/methanol (1:1) for 3 days. The THF/methanol mixture was renewed every 24 h. This reaction step is described in Scheme 1. All resulting polyether polyacids were soluble in water up to a concentration of 1 mg mL^{-1} and at a pH value of 10. However, polyether polyacids with a low CAEO fraction of 3.3 and 4.6% still yield slightly cloudy solutions, which did not become clear even at higher pH values. On the other hand, regarding the insoluble polyTHF backbone of the materials it is striking that even low amounts of hydrolyzed CEO units in the copolymers lead to a certain solubility of the polyTHF copolymers in water.

Because of the known interaction of carboxylic acids with the column material, no SEC measurements were carried out for the acid functional copolymers. However, molecular weights before and after modification were comparable according to ^{1}H NMR. Results are listed in Table 2 and show a trend

Table 2. Characterization Data of ^{1}H NMR Measurements for the Series of Poly(THF-*co*-CEO) Copolymers and the Post-Polymerization Modification to P(THF$_x$-*co*-CAEO$_{1-x}$)

CEO content^{a}/%	M_n(NMR)^{a}	
	P(THF$_x$-*co*-CEO$_{1-x}$)	P(THF$_x$-*co*-CAEO$_{1-x}$)
8.4	9400	12100
6.9	9100	7100
6.3	13400	10600
4.6	21800	25400
3.3	10900	9500

^{a}Calculated via ^{1}H NMR spectra in CDCl$_3$ (P(THF$_x$-*co*-CEO$_{1-x}$)) and in THF-d_8 (P(THF$_x$-*co*-CAEO$_{1-x}$)), 300 MHz.

concerning related molecular weights before and after postpolymerization. Some deviations occur (e.g., sample 1 in Table 2), which may be explained by utilizing different solvents for the ^{1}H NMR measurements (CDCl$_3$ for P(THF$_x$-*co*-CEO$_{1-x}$) and THF-d_8 for P(THF$_x$-*co*-CAEO$_{1-x}$)). This was necessary to ensure well dissolved materials, given that the polyether polyacids were not completely soluble in CDCl$_3$, which was the preferred solvent for the poly(THF-*co*-CEO) copolymers. Most notably, results show, that the average molecular weights do not decrease, which excludes degradation of the polymer backbone during the reaction step with sodium hydroxide. We suggest a possible steric hindrance of the functional nitrile groups belonging to the CEO units, which are closer to the polyether backbone in contrast to the alkaline labile PEG-*co*-PEPICH copolymers.[48]

^{1}H and ^{13}C NMR Spectroscopy. Figure S14 depicts a series of ^{1}H NMR spectra of polyether polyacids with varied CEO ratio (from 3.3 to 8.4%) and a spectrum of a poly(THF-*co*-CEO) copolymer with a fraction of 3.3% CEO for comparison. At the top of Figure S14, a zoom-in of the respective spectra is shown. At 3.48−3.32 ppm and 1.56−1.54 ppm the backbone of the THF units of the copolymer is visible, which overlap with the signals of the backbone of the functionalized CEO units. The signal belonging to the C*H* groups of CEO units at 4.42 ppm disappears and a signal for the C*H* groups of the carboxylic acids after transformation appears at 5.37 ppm, demonstrating the successful postpolymerization reaction.

The successful postpolymerization modification can be shown via ^{13}C NMR spectroscopy as well and even for the copolymer with a low fraction of 3.3% CEO (see Figure 6 and Figure S15). Unfortunately, it was not possible to find a solvent suitable for both copolymers before and after modification. However, the change of the solubility can be taken as a first indication for a successful postpolymerization reaction. As presented in the zoom-in in Figure 6, the signal concerning the cyanide group at 119.68−116.24 ppm disappears after conversion and a signal at 160.14 ppm appears, belonging to the carbon atoms of the carboxylic acid groups.

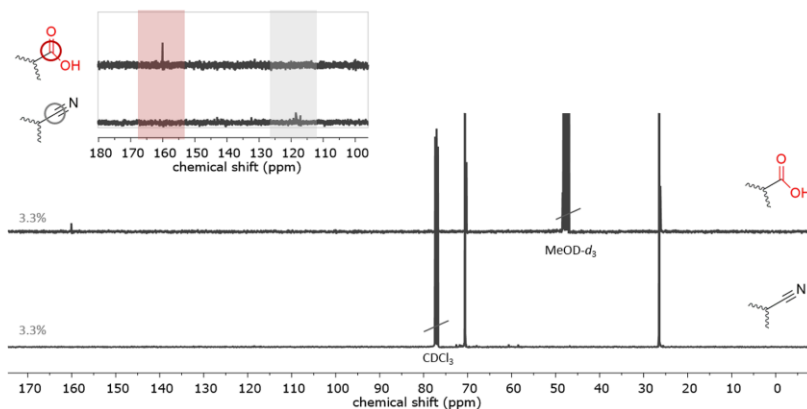*MALDI−ToF Mass Spectroscopy.* Besides NMR spectroscopy, MALDI−ToF mass spectroscopy (MS) was performed to

Figure 6. ^{13}C NMR spectra of the CEO-THF copolymer (300 MHz, CDCl$_3$) with a fraction of 3.3% CEO (bottom) and the same copolymer after postpolymerization reaction to carboxylic acid groups (300 MHz, MeOD-d_3). Top: magnification of the relevant section.
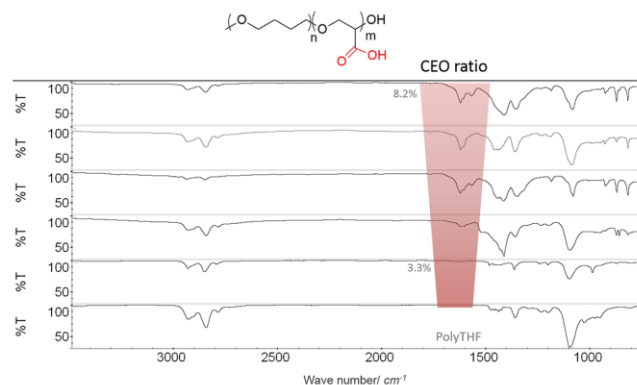
Figure 7. FT-IR spectra of several poly(THF-*co*-CAEO)copolymers with varied CEO content (3.3−8.4%) after transformation of the nitrile groups to carboxylic acid groups.

gain information on the successful copolymerization of CEO and THF, as well as to investigate the complete postpolymerization reaction of the cyanide groups. Furthermore, MALDI−ToF MS is a method to support molecular weights obtained via SEC or NMR spectroscopy, and to investigate possible degradation of the copolymers during the modification step.

Figure S9 (top) depicts the spectra of two exemplary poly(THF-*co*-CEO) copolymers with a fraction of 8.4 and 6.9% CEO, together with the spectra after postmodification to carboxylic acids of the same (blue), as well as the magnification of these spectra (bottom). A complete signal assignment is also given in Figure S9. The results show that the copolymerization of CEO and THF was successful, resulting in incorporation of both monomers. Furthermore, the postpolymerization reaction was complete, given that no residual signals of the poly(THF-*co*-CEO) copolymers were found. The average molecular weights did not vary significantly before and after postpolymerization modification (Figure S10). Molecular weights determined by MALDI−ToF were slightly smaller than observed via SEC or NMR. We attribute this to the so-called "mass discrimination effect", which underestimates higher molecular weight fractions.[56−58]

FT-IR Spectroscopy. As an additional method to investigate the successful copolymerization of CEO and THF, and to gather evidence for complete conversion to polyether polyacids, FT-IR spectroscopy was carried out. The normalized spectra of the five postpolymerized copolymers are depicted in Figure 7. With increasing CEO fraction, the bands at 1600−1700 cm^{-1} increase as well, which can be assigned to carboxylic salts, in accordance to literature for carboxylic acids.[31]

C. Postpolymerization Modification of Poly(THF-*co*-CEO) Copolymers: Polyetheramines. Amino-functional polyethers attract industrial as well as academic interest due to their pH-responsive behavior.[17,18,45,48,59−61] However, not only the well-established and water-soluble poly(ethylene glycol) has been applied for this purpose. The group of Tsvetanov introduced an even more hydrophobic glycidylamine derivative, glycidyl didodecylamine to provide high solubilizing power toward extremely hydrophobic drugs.[62]

The postpolymerization of poly(THF-*co*-CEO) copolymers to polyether polyamines permits access to amine-functionalized materials with moderate to high molecular weights. A

combination of polyTHF with functional amine groups was described in literature[11] with the aim to construct dendrimer containing hybrid networks.[63] An additional strategy to combine polyTHF with amine groups is the end-capping of polyTHF to obtain "ditopic" macromonomers.[8] Possible applications of these structures are envisaged especially in the polyurethane (PU) production, since polyTHF is a widely used material for the soft segments in PUs and since amines are typically added to catalyze urethane formation.

Postpolymerization modification to P(THF$_x$-*co*-CAmEO$_{1-x}$) was carried out following the hydrogenation procedure developed by Meijer et al. for polyamine dendrimers[32] and recently published routes of our group.[48] The poly(THF-*co*-CEO)copolymer was dissolved in THF, the Raney cobalt catalyst, dissolved in water, was added and the mixture was stirred under H$_2$ pressure for 7 days. A detailed description is given in the experimental section and the transformation is shown in Scheme 1. Molecular weight before and after the transformation determined via ^{1}H NMR is comparable as well. The results are listed in Table 3 and show similar molecular

Table 3. Characterization Data from ^{1}H NMR Measurements for the Series of Poly(THF-*co*-CEO) Copolymers and the Modification to P(THF$_x$-*co*-CAmEO$_{1-x}$)

| CEO content^a/% | M_n(NMR/g·mol^{-1})^a | |
	P(THF$_x$-*co*-CEO$_{1-x}$)	P(THF$_x$-*co*-CAmEO$_{1-x}$)
8.4	9400	9000
6.9	9100	7700
6.3	13400	8700
4.6	21800	9600
3.3	10900	10400

^{a}Calculated via ^{1}H NMR spectra in CDCl$_3$, 300 MHz.

weights before and after modification, with the exception of the sample with 4.6% CEO fraction. Here, the molecular weight after postmodification is lower after hydrogenation, which attribute this to solubilizing effects of the amine groups in the solvent.
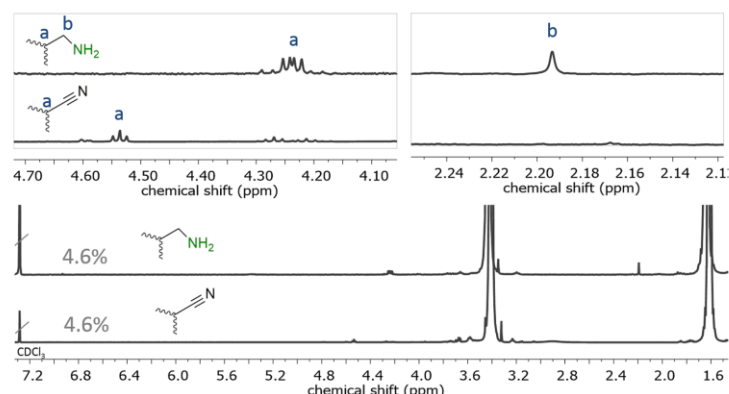
389

Figure 8. ^{1}H NMR (300 MHz, CDCl$_3$) of P(THF$_{0.95}$-*co*-CAmEO$_{0.05}$) (top) and the poly(THF-*co*-CEO) copolymer with a fraction of 4.6% CEO (bottom) and the magnification of the relevant signals, respectively.

^{1}H NMR Spectroscopy. Figure 8 shows the ^{1}H NMR spectra of the amine-functional polyTHF copolymers, together with a magnification of the relevant sections, of P(THF$_{0.95}$-*co*-CAmEO$_{0.05}$) (top) and of the poly(THF-*co*-CEO)copolymer with a fraction of 4.6% CEO (bottom), respectively. A detailed assignment of the signals stemming from the polymer backbone of poly(THF-*co*-CEO)copolymers was given in the context of the kinetic studies (Figure 5) and is comparable to the signal of the backbone of the postmodified copolymers. A clear transformation of the signals before and after postmodification is visible and depicted in the magnifications. The signal assigned to the CH groups at 4.54 ppm disappears completely and a new signal occurs at 4.26−4.21 ppm (Figure 8, top, on the left, a). Furthermore, a signal at 2.19 ppm appears, which can be assigned to the CH$_2$ groups next to the nitrogen atom. The chemical shift of this signal is in analogy to comparable structures in literature.[45,48]

It is interesting to note that above a concentration of 7 mg mL^{-1} of the amine-functionalized copolymers in suitable solvents gelation is observed. Suitable solvents for the formation of organogels are all solvents that dissolve the THF units in the backbone, as listed in the Supporting Information (Table SI 1). The copolymers can be redissolved after drying of the gels and used for the generation of organogels again reversibly. Further work on the nature of gelation in these materials is in progress. Unfortunately, this effect impedes ^{13}C NMR measurements, due to a higher attended amount of the material in comparison to ^{1}H NMR measurements. However, the successful postmodification of the CEO-THF copolymers to amine groups was confirmed via MALDI−ToF MS as well as with FT-IR spectroscopy.

Via MALDI−ToF MS the transformation of the cyanide groups to amine groups was investigated. Figure S12 in the Supporting Information presents the spectrum of the exemplary poly(THF-*co*-CEO) copolymer, modified to amine groups, with a fraction of 8.4% CEO. No residual signals for unmodified polymer chains were founded, as can be seen after overlaying both spectra (see Figure S13). Besides MALDI−ToF MS, FT-IR spectroscopy was carried out to investigate the formation of amine groups (Figures S17). Typical for amine groups two bands at 1603.41 and

1519.3 cm^{-1} appear, which can be assigned to primary amines.[64] At 1003.91 cm^{-1} the C−N stretch is visible, followed by the "out-of-plane NH bend" at 858.65 cm^{-1}.[64,65] The results confirm the successful transformation of the cyanide groups to carboxylic acid and amine groups, respectively.

D. Properties of the Polyether Copolymers. Differential scanning calorimetry (DSC) has been used to quantify the thermal properties of the materials. Table S2 lists the resulting melting points (T_m) of the poly(THF-*co*-CEO) copolymers with CEO fractions from 3.3 to 8.4%, as well as of the copolymers after postmodification to carboxylic acid and amine groups, respectively. With increasing amount of CEO in the copolymers the melting points decreased slightly from 30 (3.3% CEO) to 21 °C (8.4% CEO). The same trend can be seen for the carboxylic acid containing polymers, where the melting point decreased from 26 to 18 °C and for the amine containing polymers, where the melting point decreases from 28 to 23 °C (3.3 to 6.9% CEO). The melting points of the copolymers with carboxylic acid groups are slightly lower than before post-modification and lower than the melting points of the amine functionalized analogues (see Figure S18). This is in accordance with literature on related systems.[48] In one case no melting point of the amine functionalized copolymers could be obtained. This might be attributed to the functional amine groups, which seem to impede crystallization of the material. For the polyTHF homopolymer T_g values can be found in some publications and vary between −65[46] and −84 °C.[66]

Contact Angle Measurements. Besides the investigation of the thermal behavior, contact angle measurements of water on P(THF-*co*-CEO)-films have been carried out to assess surface properties of the materials. Furthermore, contact angles on films of P(THF-*co*-CEAO) as well as P(THF-*co*-CEAmO) were measured to investigate the different surface tensions of these materials, before and after postmodification. As expected, with decreasing CEO content in the copolymers, the materials showed increasing solubility in hydrophobic solvents. After postmodification, the carboxylic acid groups in the copolymer should contribute to lowered contact angles. Figure 9 shows the measured contact angles for the copolymers (Figure 9, black: P(THF-*co*-CEO), green: P(CEAmO-*co*-THF), red: P(CEAO-*co*-THF)). Silicon wafers were coated using copolymer
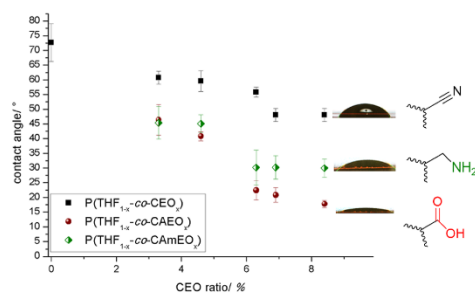
390

Figure 9. Contact angles of water at $P(CEO_x\text{-}co\text{-}THF_{1-x})$-films at different CEO/THF ratios (black), as well as contact angles of water on postmodified copolymer-films to carboxylic acids (red) and amines (green).

solutions in chloroform or THF. Subsequently, the solvent was evaporated under reduced pressure at 90 °C for 24 h. With increasing amount of CEO the contact angle decreased from 60.7° for 3.3% CEO units down to 48.0° for 8.4% CEO units. For the apolar polyTHF, we obtained a contact angle of 72.7°. The results mirror the content of CEO, as expected. After postmodification, contact angles decrease slightly for the carboxylic acids as well as for the amines, however the effect is more pronounced for the carboxylic acids. For instance, for the copolymer with 8.4% carboxylic acid groups the contact angle decreases to 17.8°, reflecting a highly polar film surface. With regard to the high contact angle of polyTHF (72.7°), even the low content of 8.4% carboxylic acid groups in the materials shows a strong effect on the contact angles.

E. Mineralization of Calcium Carbonate. To the best of our knowledge, polyethers with carboxylic acids have not been employed for mineralization experiments, mainly due to their very limited availability. In the case of the carboxylic acid functional polyTHF copolymers, the unusual combination of an apolar backbone with a controlled number of hydrophilic carboxylic acid groups is an intriguing precondition for such studies. $CaCO_3$ is a well-established inorganic model system for studying the effect of additives on the crystallization behavior.[33−35,67] Besides its industrial importance as a major source of water hardness,[68] as a mineral filler[69,70] or raw material for construction chemicals[71,72] $CaCO_3$ also represents the most common biomineral with complex morphologies and crystals exhibiting defined crystallographic orientations in shells[73] and exoskeletons.[74,75] A key feature of many biominerals is that they are composed of smaller crystals of similar size and shape, which are arranged in a regular periodic pattern. Cölfen and co-workers coined the term mesocrystal[67] to describe this oriented aggregation, where the smaller crystals have parallel crystallographic alignment.[76,77] Especially for potential use as antiscalant or as soft component in a $CaCO_3$ hybrid material the influence of polyether polyacids on the precipitation of $CaCO_3$ has to be understood.[78] In this context, the postmodified carboxylic acid functional poly(THF-co-CEO) copolymers have been used as additives to crystallize $CaCO_3$ on quartz glass slides.

As shown in Figure 10, without any additive $CaCO_3$ crystallizes in its thermodynamically most stable polymorph calcite with rhombohedral crystal morphology and crystal sizes between 10 and 20 μm and terminated by the [104] facets (the
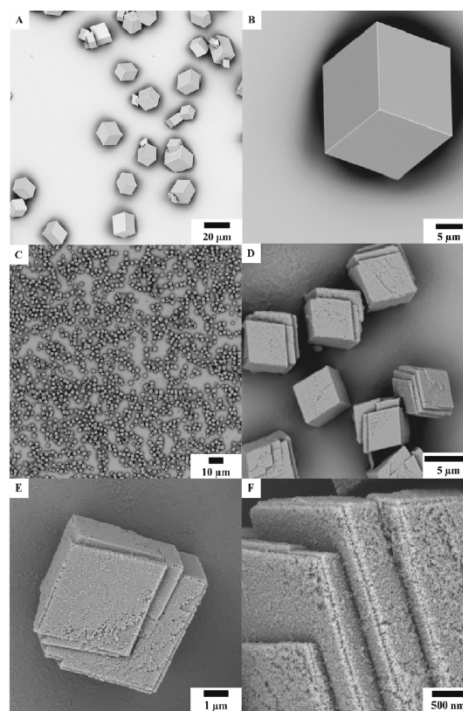

Figure 10. SEM images (A, B) calcite reference; (C−F) calcite crystals precipitated in the presence of 0.04 mmol·L^{-1} of postmodified copolymer with a fraction of 8.4% CEO (sample 1, listed in Table 2) to polyacids.

most stable and apolar surfaces). The most pronounced effect on crystal growth is observed on facets with highest polarity. These are the [010] and [012] facets, which are oriented parallel to the spatial (c axis) of the rhombohedra.[79] In the presence of polar additives polar steps are formed because of a stabilization of the polar edges.[79] If this occurs extensively, the crystals will be elongated along the c axis,[80] as shown in the SEM images in Figure 10D−F. In addition, the decrease of the crystal size from approximately 10−20 μm to 3−5 μm through the polyether-polyacid additive (Figure 10C) indicates either (i) an increase of the nucleation density or (ii) an inhibition of the crystal growth. The model of growth inhibition is supported by a statistical evaluation of the sizes of 100 mesocrystals (Figures S19 and S20, Supporting Information) formed after adding modified copolymers with increasing amounts of CEO. A plot of the number of carboxylate groups of the polymer versus the maxima of the Gaussian trend lines (Figure S19) clearly shows a linear decrease of the $CaCO_3$ crystal size with the content of carboxylate groups in the PTHF copolymers. This indicates that strong surface binding of the polymer to the crystal steps through Ca^{2+} surface complexation and a concomitant increase of the number of steps (Figure S21 C,D for 3.3% of CEO and Figure 10 for 8.4% of CEO). The polar steps are stabilized to a different extent by CEO groups,

3691

391

as illustrated in Scheme S1 (Supporting Information). We assume that for copolymers with a smaller amount of statistically distributed acidic groups a more flexible polymer chain is adsorbed on the surface. The loosely bound polymer does not provide full surface coverage, and $CaCO_3$ continues to precipitate, whereas an even higher amount of CEO groups forces stronger, less loopy and thus tighter binding of the polymer. This prevents ions from adsorbing on the edges, and new edges start to form. Surprisingly, the hydrophobic backbone appears to exert a stronger stabilizing effect than the acidic binding groups due to steric shielding.

The growth of calcite rhombohedra can be understood from Figure 10F showing a calcite mesocrystal with the characteristic calcite morphology composed of nanoscopic surface-functionalized building blocks. This is in agreement with the outcome of previous studies, where a polymer-induced liquid precursor phase (PILP)[80,81] stabilized by PAA[35,76,82−88] or Ca-binding proteins[75,89,90] played a leading role for the formation of mesocrystals.[67]

This hypothesis is also supported by TEM images (Figure 11) showing the formation of an amorphous (PILP) polymer-
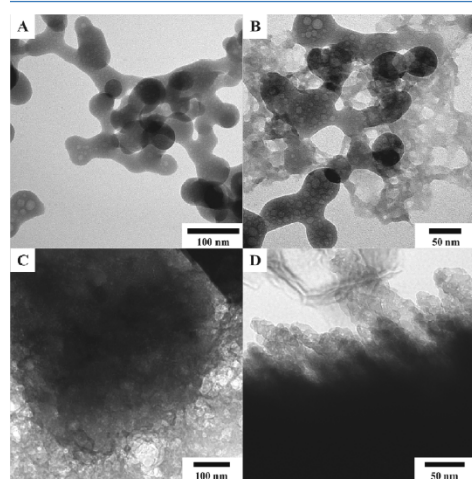

Figure 11. TEM images of polymer micelles before crystallization (A), polymer micelles and PILP after 1 h (B), agglomerated ACC from PILP after 2 h (C), microstructure of $CaCO_3$ particles agglomerated on calcite rhombohedra after 4 h of reaction time (D). All samples were prepared in the presence of 0.04 mmol/L of postmodified copolymer with 8.4% CEO fraction.

stabilized liquid-like phase. The solidification of the liquid droplets (Figure 11A) starts 1 h after initiating the ammonia diffusion in a desiccator (Figure 11B). Further increase of the CO_2 concentration leads to the formation of amorphous calcium carbonate (ACC) agglomerates from the PILP (Figure 11C) and $CaCO_3$ particles agglomerated on the surfaces of calcite rhombohedra.

The effect of the polymer is also visible in the Raman spectra (Figure S22, Supporting Information), where besides the calcite bands a background fluorescence signal of the polymer was observed. The lattice mode at 283 cm^{-1} is shifted to lower

wavenumbers (279 cm^{-1}). The broadening of all other signals indicates the presence of noncrystalline domains.[91,92] In essence, the strong surface binding properties make polyTHF polyacids an efficient crystallization inhibitor for the precipitation of $CaCO_3$ (in analogy to the more polar PAA).[83] The strong stabilization in spite of a smaller number of acidic groups is due to steric shielding of the polar edges by the more hydrophobic backbone of polyTHF.

■ CONCLUSIONS

PolyTHF is generally known as an apolar, flexible polymer. In this work, we demonstrate that copolymerization of minor amounts of a novel functional epoxide can be exploited to generate new polyTHF copolymers that are water-soluble at elevated pH and can even be used for mineralization studies in aqueous solution, despite the mainly apolar polyTHF backbone structure. To date copolymers consisting of THF and functional monomer units have hardly been investigated.[8−11] Here the random cationic ring-opening copolymerization of THF and cyano ethylene oxide (CEO) has been studied, using varied CEO fractions from 3.3 to 29.3% and molecular weights in the range of 5100 and 31900 $g \cdot mol^{-1}$ (molecular weight distributions: 1.31−1.74, SEC in THF, PS standards, RI detector). The polymerization was conducted with methyl trifluoromethanesulfonate (MeOTf), and kinetic studies concerning the reactivity of both monomers have been performed via NMR spectroscopy. Furthermore, we present postmodification reactions of the cyano groups to carboxylic acid groups as well as to amine groups in a one-step procedure. The copolymerization of CEO and THF and the postmodification reactions have been characterized via NMR, MALDI−ToF mass and FT-IR spectroscopy. The thermal properties of the materials have been examined via DSC. To investigate surface properties, contact angles have been measured, which can be tuned in the range of 72.7° to 17.8° by varying the CEO fraction as well as by postmodification. The effect of polyether polyacids with different amounts of carboxylic groups on the crystallization of $CaCO_3$ is not only dominated by the number of carboxylate groups but also by the steric shielding of the hydrophobic polyTHF backbone. The polyether polyols seem to play multiple roles during crystallization by (i) acting as nucleation sites, (ii) stabilizing liquid droplets of amorphous $CaCO_3$ (PILP) and (iii) inhibiting the growth of calcite by surface binding. Further studies on the materials properties of these unusual functional polyethers are under way.

■ ASSOCIATED CONTENT

ⓢ Supporting Information

The Supporting Information is available free of charge on the ACS Publications website at DOI: 10.1021/acs.macromol.6b00113.

> Additional ^1H, ^{13}C, DOSY, NMR kinetics, MALDI−ToF and IR spectra and other characterization data (PDF)

■ AUTHOR INFORMATION

Corresponding Author
*(H.F.) E-mail: hfrey@uni-mainz.de.

Notes
The authors declare no competing financial interest.

■ REFERENCES

(1) Dreyfuss, P.; Dreyfuss, M. P. Polytetrahydrofuran. *Adv. Polym. Sci.* **1967**, *4*, 528−590.

(2) Hwang, K. K. S.; Wu, G.; Lin, S. B.; Cooper, S. L. Cooper Synthesis and characterization of MDI-butanediol urethane model compounds. *J. Polym. Sci., Polym. Chem. Ed.* **1984**, *22*, 1677−1697.

(3) Odarchenko, Y. I.; Sijbrandi, N. J.; Rosenthal, M.; Kimenai, A. J.; Mes, E. P. C.; Broos, R.; Bar, G.; Dijkstra, P. J.; Feijen, J.; Ivanov, D. A. Structure formation and hydrogen bonding in all-aliphatic segmented copolymers with uniform hard segments. *Acta Biomater.* **2013**, *9*, 6143−6149.

(4) Guillaume, S. M.; Mespouille, L. Polycarbonates and green chemistry. *J. Appl. Polym. Sci.* **2014**, *131*, 40081.

(5) Kultys, A.; Puszka, A. Transparent poly(thiourethane-urethane)s based on dithiol chain extender. *J. Therm. Anal. Calorim.* **2014**, *117*, 1427−1439.

(6) Enthaler, S.; Trautner, A. Iron-catalyzed ring-closing depolymerization of poly(tetrahydrofuran). *ChemSusChem* **2013**, *6*, 1334−1336.

(7) Enthaler, S. Zinc(II)-triflate as catalyst precursor for ring-closing depolymerization of end-of-life polytetrahydrofuran to produce tetrahydrofuran. *J. Appl. Polym. Sci.* **2014**, *131*, 39791.

(8) Sivakova, S.; Bohnsack, D. A.; Mackay, M. E.; Suwanmala, P.; Rowan, S. J. Utilization of a combination of weak hydrogen-bonding interactions and phase segregation to yield highly thermosensitive supramolecular polymers. *J. Am. Chem. Soc.* **2005**, *127*, 18202−18211.

(9) Dubreuil, M. F.; Farcy, N. G.; Goethals, E. J. Influence of the alkyl group of triflate esters on their initiation ability for the cationic ring-opening polymerization of tetrahydrofuran. *Macromol. Rapid Commun.* **1999**, *20*, 383−386.

(10) Lim, S.-H.; Cha, E.-J.; Huh, J.; Ahn, C.-H. Micelle Behavior of Copolymers Composed of Linear and Hyperbranched Blocks in Aqueous Solution. *Macromol. Chem. Phys.* **2009**, *210*, 1734−1738.

(11) Tanghe, L. M.; Goethals, E. J.; Du Prez, F. Segmented polymer networks containing amino-dendrimers. *Polym. Int.* **2003**, *52*, 191−197.

(12) Liu, Y.; Huang, K.; Peng, D.; Wu, H. Synthesis, characterization and hydrolysis of an aliphatic polycarbonate by terpolymerization of carbon dioxide, propylene oxide and maleic anhydride. *Polymer* **2006**, *47*, 8453−8461.

(13) Obermeier, B.; Wurm, F.; Frey, H. Amino Functional Poly(ethylene glycol) Copolymers via Protected Amino Glycidol. *Macromolecules* **2010**, *43*, 2244−2251.

(14) Brocas, A.-L.; Mantzaridis, C.; Tunc, D.; Carlotti, S. Polyether synthesis: From activated or metal-free anionic ring-opening polymerization of epoxides to functionalization. *Prog. Polym. Sci.* **2013**, *38*, 845−873.

(15) Mangold, C.; Wurm, F.; Frey, H. Functional PEG-based polymers with reactive groups via anionic ROP of tailor-made epoxides. *Polym. Chem.* **2012**, *3*, 1714.

(16) Ye, L.; Feng, Z.-g.; Su, Y.-f.; Wu, F.; Chen, S.; Wang, G.-q. Synthesis and characterization of homo- and copolymers of 3-(2-cyano ethoxy)methyl- and 3-[methoxy(triethylenoxy)]methyl-3′-methyl-oxetane. *Polym. Int.* **2005**, *54*, 1440−1448.

(17) Reuss, V. S.; Werre, M.; Frey, H. Thermoresponsive copolymers of ethylene oxide and N,N-diethyl glycidyl amine: polyether polyelectrolytes and PEGylated gold nanoparticle formation. *Macromol. Rapid Commun.* **2012**, *33*, 1556−1561.

(18) Herzberger, J.; Kurzbach, D.; Werre, M.; Fischer, K.; Hinderberger, D.; Frey, H. Stimuli-Responsive Tertiary Amine Functional PEGs Based on N,N -Dialkylglycidylamines. *Macromolecules* **2014**, *47*, 7679−7690.

(19) Shintani, Y.; Tsutsumi, H. Ionic conducting behavior of solvent-free polymer electrolytes prepared from oxetane derivative with nitrile group. *J. Power Sources* **2010**, *195*, 2863−2869.

(20) Cohen, P.; Abadie, M.; Schué, F.; Richards, D. H. Reaction of living polyTHF with amines: 4. Primary amines. *Polymer* **1982**, *23*, 1350−1354.

(21) Rajendran, G. P.; Mahadevan, V.; Srinivasan, M. Synthesis of some low glass transition temperature polytetrahydrofuran polymers. *Eur. Polym. J.* **1989**, *25*, 461−463.

(22) Tarrés, M.; Viñas, C.; Cioran, A. M.; Hänninen, M. M.; Sillanpää, R.; Teixidor, F. Towards multifunctional materials incorporating elastomers and reversible redox-active fragments. *Chem. - Eur. J.* **2014**, *20*, 15808−15815.

(23) Bednarek, M.; Kubisa, P. Cationic copolymerization of tetrahydrofuran with ethylene oxide in the presence of diols. *J. Polym. Sci., Part A: Polym. Chem.* **1999**, *37* (17), 3455−3463.

(24) Hövetborn, T.; Hölscher, M.; Keul, H.; Höcker, H. poly-(ethylene oxide-*co*-tetrahydrofuran) and poly(propylene oxide-*co*-tetrahydrofurean): Synthesis and Thermal Degradation. *Rev. Roum. Chim.* **2006**, *7−8*, 781−793.

(25) Fan, W.-w.; Fan, X.-d.; Tian, W.; Zhang, X.; Wang, G.; Zhang, W.-b.; Bai, Y.; Zhu, X.-z. Phase transition dynamics and mechanism for backbone-thermoresponsive hyperbranched polyethers. *Polym. Chem.* **2014**, *5*, 4022.

(26) Rubio-Cervilla, J.; Barroso-Bujans, F.; Pomposo, J. A. Merging of Zwitterionic ROP and Photoactivated Thiol−Yne Coupling for the Synthesis of Polyether Single-Chain Nanoparticles. *Macromolecules* **2016**, *49*, 90−97.

(27) Basko, M.; Bednarek, M.; Billiet, L.; Kubisa, P.; Goethals, E.; Du Prez, F. J. Combining cationic ring-opening polymerization and click chemistry for the design of functionalized polyurethanes. *J. Polym. Sci., Part A: Polym. Chem.* **2011**, *49*, 1597−1604.

(28) Mohan, Y. M.; Raju, K. M. Synthesis and Characterization of GAP-THF Copolymers. *Int. J. Polym. Mater.* **2006**, *55*, 203−217.

(29) Penczek, I.; Penczek, S. Tetrahydrofuran−3,3-bis-(chloromethyl)-oxetane copolymerization catalyzed by (i-Bu)3Al. *J. Polym. Sci., Part B: Polym. Lett.* **1967**, *5*, 367−373.

(30) Kopecký, J.; Šmejkal, J. Einfache Darstellung von Acrylnitrilmetaboliten: Oxirancarbonitril und 2,3-Dihydroxy-propionitril. *Z. Chem.* **1984**, *24*, 211−212.

(31) Zhang, S.; Du, J.; Sun, R.; Li, X.; Yang, D.; Zhang, S.; Xiong, C.; Peng, Y. Synthesis of heterobifunctional poly(ethylene glycol) with a primary amino group at one end and a carboxylate group at the other end. *React. Funct. Polym.* **2003**, *56*, 17−25.

(32) de Brabander-van den Berg, E. M. M.; Meijer, E. W. Poly(propylene imine) Dendrimers: Large-Scale Synthesis by Hetereogeneously Catalyzed Hydrogenations. *Angew. Chem., Int. Ed. Engl.* **1993**, *32*, 1308−1311.

(33) Küther, J.; Seshadri, R.; Knoll, W.; Tremel, W. Templated growth of calcite, vaterite and aragonite crystals onself-assembled monolayers of substituted alkylthiols on gold. *J. Mater. Chem.* **1998**, *8*, 641−650.

(34) Küther, J.; Seshadri, R.; Tremel, W. Crystallization of Calcite Spherules around Designer Nuclei. *Angew. Chem., Int. Ed.* **1998**, *37*, 3044−3047.

(35) Gebauer, D.; Cölfen, H.; Verch, A.; Antonietti, M. The Multiple Roles of Additives in CaCO3 Crystallization: A Quantitative Case Study. *Adv. Mater.* **2009**, *21*, 435−439.

(36) Wei, P. E.; Butler, P. E. *J. Polym. Sci., Part A-1: Polym. Chem.* **1968**, *6*, 2461−2475.

(37) Guo, A.-r.; Yang, F.; Yu, R.; Wu, Y.-x. Real-time monitoring of living cationic ring-opening polymerization of THF and direct prediction of equilibrium molecular weight of polyTHF. *Chin. J. Polym. Sci.* **2015**, *33*, 23−35.

3693

393

(38) Kobayashi, S.; Danda, H.; Saegusa, T. Superacids and Their Derivatives. 1V.l Kinetic Studies on the Ring-Opening Polymerization of Tetrahydrofuran Initiated with Ethyl Trifluoromethanesulfonate by Means of ^{19}F and ^1H Nuclear Magnetic Resonance Spectroscopy. Evidence for the Oxonium- Ester Equilibrium of the Propagating Species. *Macromolecules* **1974**, *7*, 415−420.

(39) Alder, R. W.; Phillips, J. G. E.; Huang, L.; Huang, X. Methyltrifluoromethanesulfonate. *e-EROS Encyclopedia of Reagents for Organic Synthesis* **2005**, 1.

(40) Asenjo-Sanz, I.; Veloso, A.; Miranda, J. I.; Alegría, A.; Pomposo, J. A.; Barroso-Bujans, F. Zwitterionic Ring-Opening Copolymerization of Tetrahydrofuran and Glycidyl Phenyl Ether with $B(C_6F_5)_3$. *Macromolecules* **2015**, *48*, 1664−1672.

(41) Kubisa, P. *Polymer Science: A Comprehensive Reference*; Penczek, S., Grubbs, R. H., Eds.; Elsevier: Amsterdam, 2012; Vol. *4*, pp 141−163.

(42) Wu, Q.; Li, L.; Yu, Y.; Tang, X. The linear relations and living feature in cationic ring-opening copolymerization of epoxy/THF system. *Colloid Polym. Sci.* **2008**, *286*, 761−767.

(43) Vandenberg, E. J.; Mullis, J. C. Coordination copolymerization of tetrahydrofuran and oxepane with oxetanes and epoxides. *J. Polym. Sci., Part A: Polym. Chem.* **1991**, *29*, 1421−1438.

(44) Abe, S.; Ito, M.; Namba, K. *Makromol. Chem.* **1970**, *134*, 121−127.

(45) Meyer, J.; Keul, H.; Möller, M. Poly(glycidyl amine) and Copolymers with Glycidol and Glycidyl Amine Repeating Units: Synthesis and Characterization. *Macromolecules* **2011**, *44*, 4082−4091.

(46) Schüll, C.; Rabbel, H.; Schmid, F.; Frey, H. Polydispersity and Molecular Weight Distribution of Hyperbranched Graft Copolymers via "Hypergrafting" of ABm Monomers from Polydisperse Macroinitiator Cores: Theory Meets Synthesis. *Macromolecules* **2013**, *46*, 5823−5830.

(47) Van Caeter, P.; Goethals, E. J.; Gancheva, V.; Velichkova, R. Synthesis and bulk properties of poly(tetrahydrofuran)-poly(2-methyl-2-oxazoline) ABA triblock copolymers. *Polym. Bull.* **1997**, *39*, 589−596.

(48) Herzberger, J.; Frey, H. Epicyanohydrin: Polymerization by Monomer Activation Gives Access to Nitrile-, Amino-, and Carboxyl-Functional Poly(ethylene glycol). *Macromolecules* **2015**, *48*, 8144.

(49) Wilms, D.; Schömer, M.; Wurm, F.; Hermanns, M. I.; Kirkpatrick, C. J.; Frey, H. Hyperbranched PEG by random copolymerization of ethylene oxide and glycidol. *Macromol. Rapid Commun.* **2010**, *31*, 1811−1815.

(50) Hamaide, T.; Goux, A.; Llauro, M.-F.; Spitz, R.; Guyot, A. Stat-poly(ethy1ene oxide-*co*-propylene oxide). *Angew. Makromol. Chem.* **1996**, *237*, 55−77.

(51) Rejsek, V.; Sauvanier, D.; Billouard, C.; Desbois, P.; Deffieux, A.; Carlotti, S. Controlled Anionic Homo- and Copolymerization of Ethylene Oxide and Propylene Oxide by Monomer Activation. *Macromolecules* **2007**, *40*, 6510−6514.

(52) Reuss, V. S.; Obermeier, B.; Dingels, C.; Frey, H. N,N -Diallylglycidylamine: A Key Monomer for Amino-Functional Poly-(ethylene glycol) Architectures. *Macromolecules* **2012**, *45*, 4581−4589.

(53) Fan, X.-w.; Fan, X.-d.; Tian, W.; Zhang, X.; Wang, G.; Zhang, W.-b.; Bai, Y.; Zhu, X.-z. Phase transition dynamics and mechanism for backbone-thermoresponsive hyperbranched polyethers. *Polym. Chem.* **2014**, *5*, 4022.

(54) Dreyfuss, P. *Poly(tetrahydrofuran)*, 8th ed.; Gordon and Breach, Science Publishers, Inc.: New York, 1982.

(55) Orwoll, R. A.; Yong, C. S. *Polymer Data Handbook*; Oxford University Press, Inc.: 1999.

(56) Schüll, C.; Nuhn, L.; Mangold, C.; Christ, E.; Zentel, R.; Frey, H. Linear-Hyperbranched Graft-Copolymers via Grafting-to Strategy Based on Hyperbranched Dendron Analogues and Reactive Ester Polymers. *Macromolecules* **2012**, *45*, 5901−5910.

(57) Christ, E. M.; Hobernik, D.; Bros, M.; Wagner, M.; Frey, H. Cationic Copolymerization of 3,3-Bis(hydroxymethyl)oxetane and Glycidol: Biocompatible Hyperbranched Polyether Polyols with high Content of Primary Hydroxyl Groups. *Biomacromolecules* **2015**, *16*, 3297−3307.

(58) Magnusson, H.; Malmström, E.; Hult, A. Synthesis of hyperbranched aliphatic polyethers via cationic ring-opening polymerization of 3-ethyl-3-(hydroxymethyl)oxetane. *Macromol. Rapid Commun.* **1999**, *20*, 453−457.

(59) Wilms, V. S.; Frey, H. Aminofunctional polyethers: smart materials for applications in solution and on surfaces. *Polym. Int.* **2013**, *62*, 849−859.

(60) Kurzbach, D.; Wilms, V. S.; Frey, H.; Hinderberger, D. Impact of Amino-Functionalization on the Response of Poly(ethylene glycol) (PEG) to External Stimuli. *ACS Macro Lett.* **2013**, *2*, 128−131.

(61) Isono, T.; Asai, S.; Satoh, Y.; Takaoka, T.; Tajima, K.; Kakuchi, T.; Satoh, T. Controlled/Living Ring-Opening Polymerization of Glycidylamine Derivatives Using t -Bu-P 4 /Alcohol Initiating System Leading to Polyethers with Pendant Primary, Secondary, and Tertiary Amino Groups. *Macromolecules* **2015**, *48*, 3217−3229.

(62) Rangelov, S.; Tsvetanov, C. Towards the synthesis of amino-substituted epoxides: synthesis and characterization of glycidyldidodecylamine. *Des. Monomers Polym.* **2001**, *4* (1), 39−43.

(63) Tanghe, L. M.; Goethals, E. J. *e-Polym.* **2001**, *1*, 017.

(64) Smith, B. *Infrared Spectral Interpretation. A Systematic Approach*; CRC Press LLC: USA, 1999.

(65) Génin, F.; Quilès, F.; Burneau, A. Infrared and Raman spectroscopic study of carboxylic acids in heavy water. *Phys. Chem. Chem. Phys.* **2001**, *3*, 932−942.

(66) Gaur, U.; Wunderlich, B. Heat Capacitiy and Other Thermodynamic Properties of Linear Macromolecules. *J. Phys. Chem. Ref. Data* **1981**, *10*, 1001−1049.

(67) Cölfen, H.; Antonietti, M. *Mesocrystals and Nonclassical Crystallization*; John Wiley & Sons Ltd: Chichester, England, 2008.

(68) Schade, G. Water-dispersible ester resin containing a moiety of polyacid or bivalent alcohol containing a sulfo group. US 4,104,262, 1976.

(69) Zuiderduin, W.; Westzaan, C.; Huétink, J.; Gaymans, R. Toughening of polypropylene with calcium carbonate particles. *Polymer* **2003**, *44*, 261−275.

(70) Míhai, M.; Schwarz, S.; Doroftei, F.; Simionescu, B. C. Calcium Carbonate/Polymers Microparticles Tuned by Complementary Polyelectrolytes as Complex Macromolecular Templates. *Cryst. Growth Des.* **2014**, *14*, 6073−6083.

(71) Rieger, J.; Kellermeier, M.; Nicoleau, L. Die Bildung von Nanopartikeln und Nanostrukturen - CaCO₃, Zement und Polymere aus Sicht der Industrie. *Angew. Chem., Int. Ed.* **2014**, *53*, 12380−12396.

(72) Galván-Ruiz, M.; Hernández, J.; Baños, L.; Noriega-Montes, J.; Rodríguez-García, M. Characterization of Calcium Carbonate, Calcium Oxide, and Calcium Hydroxide as Starting Point to the Improvement of Lime for Their Use in Construction. *J. Mater. Civ. Eng.* **2009**, *21*, 694−698.

(73) Finnemore, A.; Cunha, P.; Shean, T.; Vignolini, S.; Guldin, S.; Oyen, M.; Steiner, U. Biomimetic layer-by-layer assembly of artificial nacre. *Nat. Commun.* **2012**, *3*, 966.

(74) Müller, W. E. G.; Neufurth, M.; Schlossmacher, U.; Schröder, H. C.; Pisignano, D.; Wang, X. The sponge silicatein-interacting protein silintaphin-2 blocks calcite formation of calcareous sponge spicules at the vaterite stage. *RSC Adv.* **2014**, *4*, 2577−2585.

(75) Natalio, F.; Corrales, T. P.; Panthöfer, M.; Schollmeyer, D.; Lieberwirth, I.; Müller, W. E. G.; Kappl, M.; Butt, H.-J.; Tremel, W. Flexible Minerals: Self-Assembled Calcite Spicules with Extreme Bending Strength. *Science* **2013**, *339*, 1298−1302.

(76) Balz, M.; Therese, H. A.; Li, J.; Gutmann, J. S.; Kappl, M.; Nasdala, L.; Hofmeister, W.; Butt, H.-J.; Tremel, W. Crystallization of Vaterite Nanowires by the Cooperative Interaction of Tailor-Made Nucleation Surfaces and Polyelectrolytes. *Adv. Funct. Mater.* **2005**, *15*, 683−688.

(77) Bergström, L.; Sturm, E. V.; Salazar-Alvarez, G.; Cölfen, H. Mesocrystals in Biominerals and Colloidal Arrays. *Acc. Chem. Res.* **2015**, *48*, 1391−1402.

394

(78) Dietzsch, M.; Barz, M.; Schüler, T.; Klassen, S.; Schreiber, M.; Susewind, M.; Loges, N.; Hellmann, N.; Fritz, M.; Theato, P.; Fischer, K.; Kühnle, A.; Schmidt, M.; Zentel, R.; Tremel, W.; Lang, M. PAA-PAMPS Copolymers as an Efficient Tool to Control CaCO3 Scale Formation. *Langmuir* **2013**, *29*, 3080−3088.

(79) Momper, R.; Nalbach, M.; Lichtenstein, K.; Bechstein, R.; Kühnle, A. Stabilization of Polar Step Edges on Calcite (10.4) by the Adsorption of Congo Red. *Langmuir* **2015**, *31*, 7283−7287.

(80) Wang, G.; Li, L.; Lan, J.; Chen, L.; You, J. Biomimetic crystallization of calcium carbonate spherules controlled by hyper-branched polyglycerols. *J. Mater. Chem.* **2008**, *18*, 2789.

(81) Gower, L. B.; Odom, D. J. J. Production and Mechanism of Formation of Monodispersed Hydrosols. *J. Cryst. Growth* **2000**, *210*, 719−734.

(82) Gower, L. B. Polymer-induced liquid precursor (PILP) phases of calcium carbonate formed in the presence of synthetic acidic polypeptides—relevance to biomineralization. *Chem. Rev.* **2008**, *108*, 4551−4627.

(83) Ihli, J.; Kim, Y.-Y.; Noel, E. H.; Meldrum, F. C. The Effect of Additives on Amorphous Calcium Carbonate (ACC): Janus Behavior in Solution and the Solid State. *Adv. Funct. Mater.* **2013**, *23*, 1575−1585.

(84) Ihli, J.; Bots, P.; Kulak, A.; Benning, L. G.; Meldrum, F. C. Elucidating Mechanisms of Diffusion-Based Calcium Carbonate Synthesis Leads to Controlled Mesocrystal Formation. *Adv. Funct. Mater.* **2013**, *23*, 1965−1973.

(85) Ouhenia, S.; Chateigner, D.; Belkhir, M. A.; Guilmeau, E.; Krauss, C. J. Synthesis of calcium carbonate polymorphs in the presence of polyacrylic acid. *J. Cryst. Growth* **2008**, *310*, 2832−281.

(86) Ren, D.; Feng, Q.; Bourrat, X. Effects of additives and templates on calcium carbonate mineralization in vitro. *Micron* **2011**, *42*, 228−245.

(87) Wei, H.; Shen, Q.; Wang, H.; Gao, Y.; Zhao, Y.; Xu, D.; Wang, D. Influence of segmented copolymers on the crystallization and aggregation of calcium carbonate. *J. Cryst. Growth* **2007**, *303*, 537−545.

(88) Yu, J.; Lei, M.; Cheng, B.; Zhao, X. Effects of PAA additive and temperature on morphology of calcium carbonate particles. *J. Solid State Chem.* **2004**, *177*, 681−689.

(89) Wolf, S. E.; Leiterer, J.; Pipich, V.; Barrea, R.; Emmerling, F.; Tremel, W. Strong Stabilization of Amorphous Calcium Carbonate Emulsion by Ovalbumin: Gaining Insight into the Mechanism of 'Polymer-Induced Liquid Precursor' Processes. *J. Am. Chem. Soc.* **2011**, *133*, 12642−12649.

(90) Pipich, V.; Balz, M.; Wolf, S.; Tremel, W.; Schwahn, D. Nucleation and Growth of CaCO$_3$ Mediated by the Egg-White Protein Ovalbumin: A Time-Resolved in situ Study Using Small-Angle Neutron Scattering. *J. Am. Chem. Soc.* **2008**, *130*, 6879−6892.

(91) Long, X.; Nasse, M. J.; Ma, Y.; Qi, L. From synthetic to biogenic Mg-containing calcites: a comparative study using FTIR micro-spectroscopy. *Phys. Chem. Chem. Phys.* **2012**, *14*, 2255−2263.

(92) Gouadec, G.; Colomban, P. Raman Spectroscopy of nanoma-terials: How spectra relate to disorder, particle size and mechanical properties. *Prog. Cryst. Growth Charact. Mater.* **2007**, *53*, 1−56.

395

Appendix A4

M. N. Tahir, J. Herzberger, F. Natalio, O. Köhler, R. Branscheid, E. Mugnaioli, V. Ksenofontov, M. Panthöfer, U. Kolb, H. Frey and W. Tremel, *Nanoscale*, **2016**, *8*, 9548-9555.

Published by The Royal Society of Chemistry.

Nanoscale

PAPER

Hierachical Ni@Fe₂O₃ superparticles through epitaxial growth of γ-Fe₂O₃ nanorods on *in situ* formed Ni nanoplates†

Muhammad Nawaz Tahir,*[a] Jana Herzberger,[b,c] Filipe Natalio,‡[a] Oskar Köhler,[a] Robert Branscheid,[d] Enrico Mugnaioli,[d] Vadim Ksenofontov,[a] Martin Panthöfer,[a] Ute Kolb,[d] Holger Frey[b] and Wolfgang Tremel*[a]

One endeavour of nanochemistry is the bottom-up synthesis of functional mesoscale structures from basic building blocks. We report a one-pot wet chemical synthesis of Ni@γ-Fe₂O₃ superparticles containing Ni cores densely covered with highly oriented γ-Fe₂O₃ (maghemite) nanorods (NRs) by controlled reduction/decomposition of nickel acetate (Ni(ac)₂) and Fe(CO)₅. Automated diffraction tomography (ADT) of the Ni–Fe₂O₃ interface in combination with Mössbauer spectroscopy showed that selective and oriented growth of the γ-Fe₂O₃ nanorods on the Ni core is facilitated through the formation of a $Fe_{0.05}Ni_{0.95}$ alloy and the appearance of superstructure features that may reduce strain at the Ni–Fe₂O₃ interface. The common orientation of the maghemite nanorods on the Ni core of the superparticles leads to a greatly enhanced magnetization. After functionalization with a catechol-functional polyethylene glycol (C-PEG) ligand the Ni@γ-Fe₂O₃ superparticles were dispersible in water.

Introduction

Nano-heterostructures containing chemically distinct components have great potential for advancing nanomaterial research by providing a means to define diverse functionalities within single nanoparticles.[1] Moreover, new properties that do not exist in the individual components may arise from strong interfacial interactions at the nanoscale. In recent years, some progress has been made concerning the fabrication of nano-composites with spherical,[2] coaxial core–shell,[3] or one- and two-dimensional (1D and 2D) heterojunction structures.[4–6] To explore potential applications, architecturally assembling of primary nano-building blocks into specific geometric forms is needed. However, despite a few reported hierarchical com complex structures[7–13] a general scheme for the controlled organization and the preferential crystallographic orientation of the secondary structure is lacking.

Therefore it would be desirable to obtain nanostructured materials, where the individual units, each of them characterized by its particular physical properties, surface chemistry and morphology, can be combined into a single nano-object. In the realm of nanostructures there are examples of architectures based on inorganic materials, such as nanowire superlattices,[14] or multi-layered nanowires.[15,16] A central target of colloidal nanocrystal research is to create similar – or even more complex – structures while leveraging the advantages of solution-phase fabrication, such as low-cost synthesis and compatibility in disparate environments. Important fundamental components could be catalytically active metals like Ni,[17] Pd[18] or Pt[19] and magnetic metal oxides like Fe₂O₃[20] or Fe₃O₄.[19]

The chemical functionality of the individual components allows studying the assembly of such hetero-nanostructures.[21]

[a] *Institut für Anorganische Chemie und Analytische Chemie der Johannes Gutenberg-Universität, Duesbergweg 10-14, D-55099 Mainz, Germany.*
E-mail: tahir@uni-mainz.de, tremel@uni-mainz.de
[b] *Institut für Organische Chemie, Johannes-Gutenberg-Universität, Duesbergweg 10-14, D-55099 Mainz, Germany*
[c] *Graduate School Materials Science in Mainz, Staudinger Weg 9, 55128 Mainz, Germany*
[d] *Institut für Physikalische Chemie, Johannes-Gutenberg-Universität, Welderweg 15, D-55099 Mainz, Germany*

Multicomponent core@shell,[22] yolk@shell[23] or phase-segregated heterodimer[24,25] particles or materials containing metal and magnetic metal oxide components with different compositions like Pt@Fe$_3$O$_4$,[26] Au@Fe$_3$O$_4$,[27–29] FePt@MnO,[30] Ag@Fe$_3$O$_4$,[31] Au@MnO[32] or Au@MnO@SiO$_2$ [33] have attracted particular attention. The synthesis of these hetero-nanoparticles is facilitated when the interfacial energy is reduced by epitaxial growth, *i.e.*, an extremely thin metallic interlayer forming at the interface, because the two components have similar lattice parameters.[34–37] The synthesis of nanoparticles by thermolysis of organometallic precursors in the presence of surfactants is a unique tool to control the kinetics of phase equilibria and particle aggregation, because phase formation and ordering of the components at the nanoscale are under molecular control. They depend on (i) the decomposition temperatures of the precursors, (ii) the relative activation energies for nucleation, and (iii) interfacial energies which are dictated by interactions of the surfactant and the solvents with the particle surfaces. Despite tremendous efforts to find a general synthetic access to such heterostructures, it still remains a challenge to prepare nanoparticles with complex structures *e.g.* superparticles having well-controlled sizes, shapes, compositions, and properties. To the best of our knowledge there is no report for the synthesis of superparticles using colloidal protocols. We have demonstrated the relevance of the precursor decomposition temperature by the selective synthesis of nanocrystals of the ternary compounds CoFe$_2$O$_4$, CuFe$_2$O$_4$ and phase segregated Co@Fe$_2$O$_3$ and Cu@Fe$_3$O$_4$ heteroparticles.[17,20,38] Based on these findings, we report here the controlled synthesis of colloidal hetero-superparticles consisting of nanoplates densely decorated with highly oriented maghemite (γ-Fe$_2$O$_3$, defect spinel) nanorods. Typically, particles in the size range of ~200 nm are difficult to solubilize (*e.g.* using low molecular weight C-PEGs). The catechol moiety is an excellent anchor group for high-valent metal oxide surfaces,[39–41] and in combination with PEG ensures excellent solubility of the superparticles in aqueous media. The commonly used established procedures to obtain catechol-functional PEGs are based on coupling chemistry, starting from a dopamine derivative and commercially available functional PEGs, *e.g.* NH$_2$-PEG or NHS-PEG,[42–44] but the palette of commercial PEGs with specific end-groups and different molecular weights is limited and can be high-priced. Therefore we use a new synthetic procedure for catechol-functional PEGs based on anionic ring opening polymerization of ethylene oxide (EO) starting from a protected catechol-initiator. This synthetic strategy allows precisely tailoring the chain-length of PEG through the initiator to monomer ratio and guarantees well-defined polymers through the living character of the polymerization. Further, additional functional groups could easily be introduced by various terminating agents or by incorporation of functional epoxides.[45,46] The as-synthesized superparticles could be solubilized after functionalization with a new catechol-polyethylene glycol (C-PEG) polymer ligand.[47] After functionalization the superparticles formed stable dispersions in a range of solvents including water.

Experimental

Materials

Iron(0) pentacarbonyl (Fe(CO)$_5$, 99.5%, Acros), nickel(ɪɪ) acetate tetrahydrate (Ni(ac)$_2$·4H$_2$O, 99%, Fluka), oleic acid (Aldrich), oleylamine (80–90%, Acros), trioctylphosphine ([CH$_3$(CH$_2$)$_7$]$_3$P, 99% Sigma-Aldrich), ethanol (99.8%, Roth), toluene (>99%, Aldrich), hexane (p.A. Fisher), dichloromethane DCM (p.A. Fisher), dimethylformamide (DMF) (extra dry, >99.8%, Acros), diethyl ether (p.A. Fisher) were used as received without further purification.

Polymer synthesis

Ethylene oxide (99.5%) was purchased from Aldrich and hydrochloric acid (37%) from VWR chemicals. Chloroform-*d* was purchased from Deutero GmbH. All other solvents and reagents were ordered from Acros Organics.

Synthesis of Ni@γ-Fe$_2$O$_3$ superparticles

Hierarchically decorated Ni@γ-Fe$_2$O$_3$ superparticles were synthesized by mixing 62.25 mg (0.25 mmol) of nickel acetate Ni(ac)$_2$, 7 mL of oleylamine, 1 mmol of trioctyl-phosphine, and 2 mmol of oleic acid and stirring them for 20 min under the inert condition before increasing the temperature. The mixture was heated to 120 °C for 20 min. Subsequently, 67.55 µL of Fe(CO)$_5$ were added and the solution was heated 180 °C for 30 min and cooled slowly to room temperature. A black product was precipitated from the solution by adding an excess of ethanol. The precipitate was separated by centrifugation (9000 rpm, 10 min, RT). Finally, the product was dissolved in toluene, flushed with argon (Ar) and stored at +4 °C.

Synthesis of catechol initiated PEG by anionic ring opening polymerization of ethylene oxide (CA-PEG)

The synthesis of catechol-initiated PEG (CA-PEG) was performed as described recently.[47] Under argon atmosphere, 2,2-dimethyl-1,3-benzodioxole-5-propanol (catechol-acetonide-OH, CA-OH) (1 eq., 136.9 mg, 0.66 mmol) and cesium hydroxide (CsOH·1H$_2$O) (0.8 eq., 87.9 mg, 0.53 mmol) were suspended in 10 mL of benzene and heated to 60 °C for 30 min. Subsequently, the partially deprotonated initiator was evacuated at 55 °C for 12 h. About 15 mL of dry THF (stored over sodium) were cryo-transferred into the flask followed by the addition of 5 mL of DMSO by a syringe. The mixture was stirred for 15 min at room temperature to ensure complete dissolution of the cesium alkoxide, followed by cooling the flask to −80 °C. 2 mL of ethylene oxide (67 eq., 44 mmol) were cryo-transferred into the flask *via* a graduated ampoule. The polymerization proceeded for 12 h (55 °C) and was stopped by addition of 0.5 mL methanol. The polymer was precipitated into ice cold diethyl ether and separated by a centrifuge, yielding CA-PEG in a quantitative yield.

^{1}H NMR (C*D*Cl$_3$, 400 MHz): δ (C*H*Cl$_3$ = 7.26 ppm) 6.63–6.56 (m, 3 H, H_{arom}), 3.82–3.41 (m, backbone and CH_2–O-PEG), 2.57 (t, 2 H, C$H_{2,benzyl}$), 1.88–1.79 (m, 2 H, CH_2), 1.65 (s, 6 H, CH_3).
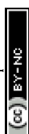
Deprotection of the acetonide group (C-PEG)

According to ref. 47, 100 mg of CA-PEG were dissolved in 5 mL of aqueous hydrochloric acid (1 mol L) and stirred for 12 h, letting the cleaved acetone escape. The solvent was removed under reduced pressure (10^{-3} mbar), and the polymer was dissolved in methanol, precipitated into ice cold diethyl ether and separated by a centrifuge. The yield was quantitative.

^{1}H NMR (methanol-d_4, 400 MHz): δ (MeOH = 3.31 ppm, 4.87 ppm) 6.67–6.62 (m, 2 H, HO–C–CH_{arom}), 6.51–6.48 (m, 1 H, CH_{arom}), 3.82–3.41 (m, backbone and CH_2–O-PEG), 2.53 (t, 2 H, C$H_{2,\text{benzyl}}$), 1.84–1.78 (m, 2 H, CH_2).

Surface functionalization of Ni@γ-Fe$_2$O$_3$ superparticles with CA-PEG

20 mg of Ni@γ-Fe$_2$O$_3$ superparticles dispersed in 20 mL of chloroform were dropped slowly over 1 h into the above synthesized polymer solution (40 mg/10 mL, of chloroform). The reaction was continuously stirred at room temperature for 5 h under inert conditions. The functionalized nanoparticles were precipitated by addition of hexane (90 mL) und separated from unbound polymer and surfactants by centrifugation. The Ni@γ-Fe$_2$O$_3$ superparticles were washed twice by dispersing them in a mixture of chloroform, hexane (1 : 3) and by phase transferring into water.

Physical characterization

Electron microscopy. The size and morphology of the as-synthesized Ni@γ-Fe$_2$O$_3$ NPs were investigated using transmission electron microscopy (TEM, Philips EM 420 with an acceleration voltage of 120 kV). Samples for TEM were prepared by placing a drop of dilute NP solution in hexane on a carbon coated copper grid. Low-resolution TEM images were recorded on a Philips EM420 microscope operating at an acceleration voltage of 120 kV. STEM data and ED patterns were obtained on a FEI Tecnai F30 S-TWIN with a 300 kV field emission gun.

X-Ray diffraction. XRD measurements were performed on a Bruker D8 Advance diffractometer equipped with a Sol-X energy-dispersive detector and operating with Mo Kα radiation. Crystalline phases were identified according to the PDF-2 database, using Bruker AXS EVA 10.0 software. Full profile fits on the basis of the crystal structural models[48,49] were performed with TOPAS Academic 4.1[50,51] applying the fundamental parameter approach.

Mössbauer spectroscopy and magnetic susceptibility measurements. Mössbauer spectra were obtained at room temperature, 150 K, 87.5 K and 4.2 K with a constant acceleration transmission Mössbauer spectrometer and a ^{57}Co (Rh) source. An α-Fe foil was used to calibrate the Mössbauer spectrometer in a velocity range of ±10 mm s^{-1}. Magnetic measurements were carried out using a Quantum Design MPMS-XL SQUID (superconducting quantum interference device) magnetometer.

### Automated electron diffraction tomography (ADT)

Automated electron diffraction tomography (ADT) is a method for *ab initio* structure analysis of nanocrystals. ADT allows fine sampling of the reciprocal space by sequential collection of electron diffraction patterns while tilting a nanocrystal in fixed tilt steps around an arbitrary axis. Electron diffraction is collected in nano diffraction mode (NED) with a semi-parallel beam with a diameter down to 50 nm. For crystal tracking micro-probe STEM imaging is used. Full automation of the acquisition procedure allowed optimization of the electron dose distribution and therefore analysis of highly beam sensitive samples. Cell parameters, space group and reflection intensities can be determined directly within a reconstructed 3d diffraction volume using a dedicated software package (ADT3D). Intensity data sets extracted from such a volume usually show a high coverage and significantly reduced dynamical effects due to "off-zone" acquisition. The use of this data for "*ab initio*" structure solution by direct methods implemented in standard programs for X-ray crystallography is demonstrated. NED, automated diffraction tomography (ADT) and HRTEM were used for crystallographically characterizing the superparticles. Automated electron diffraction tomography (ADT) is a method for *ab initio* structure analysis of nanocrystals,[52,53] which allows fine sampling of the reciprocal space by sequential collection of electron diffraction patterns while tilting a nanocrystal in fixed tilt steps around an arbitrary axis. Electron diffraction is collected in nano diffraction mode (NED) with a semi-parallel beam with a diameter down to 20–50 nm.[54]

^{1}H NMR. ^{1}H NMR spectra (400 MHz) were recorded using a Bruker Avance III HD 400 apparatus operated at 400 MHz with a 5 mm BBFO-SmartProbe (Z-gradient) and an ATM as well as a SampleXPress 60 auto sampler. GPC measurements were performed in DMF (containing 0.25 g L^{-1} lithium bromide as an additive). An Agilent 1100 Series was used as an integrated instrument, including a PSS HEMA column (106/105/104 g mol^{-1}), a UV (275 nm) and a RI detector. Calibration was carried out using poly(ethylene glycol) standards purchased from Polymer Standards Service.

Results and discussion

Synthesis of Ni@γ-Fe$_2$O$_3$ superparticles

The synthesis of the Ni@γ-Fe$_2$O$_3$ superparticles with a central Ni nanoplate core (~100 nm) and γ-Fe$_2$O$_3$ (~30 nm) nanorods domains is illustrated in Fig. 1. In the first step, Ni nanoparticles were nucleated homogeneously *via* co-reduction by heating nickel acetate, Ni(ac)$_2$, in the presence of iron pentacarbonyl, Fe(CO)$_5$, at 120 °C. The emerging Ni nuclei transformed to Ni nanoplates (confirmed by examining aliquots at 140 °C) still significantly below the decomposition temperature (T = 180 °C) of Fe(CO)$_5$. In the final heating step at 180 °C γ-Fe$_2$O$_3$ nanorods grew epitaxially on the preformed Ni nanoplates. The products were precipitated and separated by centrifugation (9000 rpm, 10 min, RT).
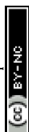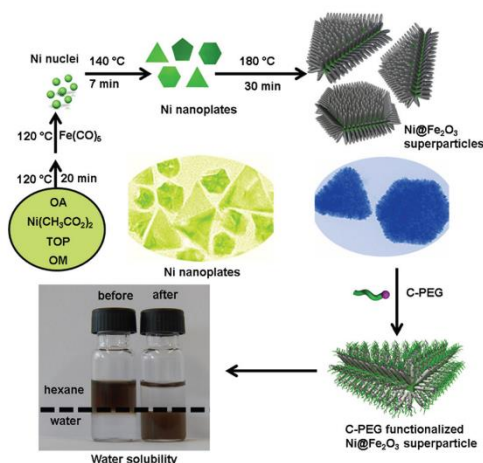
Fig. 1 Synthesis of Ni@γ-Fe$_2$O$_3$ superparticles. Initial Ni nuclei obtained by thermolysis of Ni(ac)$_2$ transform to Ni nanoplates with a N$_{i1-x}$Fe$_x$ interlayer in the presence of Fe(CO)$_5$, from which highly oriented γ-Fe$_2$O$_3$ rods grow epitaxially (OM stands for oleylamine, TOP for tri-octyl-phosphine, and OA for oleic acid). The resulting Ni@γ-Fe$_2$O$_3$ superparticles are functionalized with a catechol-polyethylene glycol (C-PEG) ligand to achieve water solubility.

Polymer synthesis

The as-synthesized superparticles were functionalized using catechol-polyethylene glycol (C-PEG) polymer ligands[47] (Scheme S1†), which were characterized by ^{1}H NMR spectroscopy and GPC (Fig. S1 and 2†). The C-PEG ligands were synthesized via anionic ring opening polymerization of ethylene oxide (EO) starting from a protected catechol-initiator. This synthetic strategy allows a precise tailoring of the chain-length of PEG through the initiator to monomer ratio and guarantees well-defined polymers because of the living character of the polymerization.[47] A cartoon of a C-PEG functionalized Ni@Fe$_2$O$_3$ superparticle is shown in Fig. 1. It is worth mentioning that particles of this size (~200 nm) cannot be solubilized using low molecular weight C-PEGs. After functionalization the superparticles were easily dispersible in water; the dispersions were stable for several weeks.

Superparticle growth mechanism

The growth of the Ni@γ-Fe$_2$O$_3$ superparticles was monitored by taking "snapshots" at given time intervals using transmission electron microscopy (TEM). After ~6 minutes plate-like structures were formed (Fig. 2a and b). High-resolution transmission electron microscopy (HRTEM) images revealed that the smallest particles (20–30 nm) were polycrystalline, often displaying penta-twinned structures (Fig. 2a), whereas larger plate-like particles (30–80 nm) had a well-defined triangular morphology. EDX showed the particles to have a com-
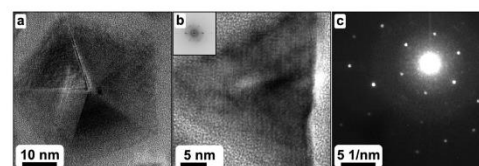

Fig. 2 Growth mechanism: Fe$_{0.05}$Ni$_{0.95}$ precursors after a reaction time of 5 minutes. (a) HRTEM of a pentagonally twinned particle. (b) HRTEM image and (c) NED of a single-crystal flat particle displaying a hexagonal pattern with d-distances of 2.2(1) Å.

position Fe$_{0.05}$Ni$_{0.95}$ (Fig. S3†). They were single crystalline (shown by HRTEM and nano-electron diffraction (NED)) with a hexagonal pattern and d-values of 2.2(1) Å (Fig. 2b and c). At this stage, all particles had a flat triangular or hexagonal habit in agreement with an earlier report by Leng et al.[55] and a composition of Fe$_{0.05}$Ni$_{0.95}$ as determined by NED, ADT and energy-dispersive X-ray spectroscopic EDX.

When heating slowly to 180 °C, γ-Fe$_2$O$_3$ nanorods started nucleating on the Fe$_{0.05}$Ni$_{0.95}$ cores. Their growth proceeded anisotropically (Fig. 3a). To show a better overview, an SEM image is provided Fig. S4.† The image further confirms hierarchical arrangements of nanodomains in three dimensional (3D) patterns. EDX line profiles taken across the superparticles showed the rods to consist of Fe$_2$O$_3$ nanorods decorating a core of metallic Ni plates containing a minor amount of Fe (Fig. 3b). The corresponding STEM image (Fig. 3c) confirms
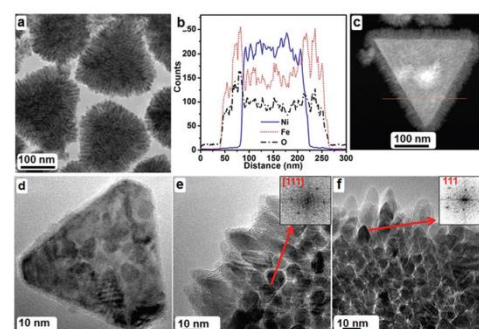

Fig. 3 Growth of Ni@γ-Fe$_2$O$_3$ superparticles. (a) Zoom of a superparticle showing preferential orientation of the rods growing on the large flat surfaces and the scattered orientation of the rods growing on the core side. (b) An EDX scan (along the red line) confirmed the elemental composition of the superparticle with the aid of a z-contrast image (STEM). (c) Corresponding Ni@γ-Fe$_2$O$_3$ superparticle. (d) HRTEM of a superparticle at an early stage with nucleated domains of [111] oriented Fe$_2$O$_3$. (e) HRTEM image of a superparticle showing rods growing on the main surface of the Ni plate and viewed along the main direction of growth, i.e. [111]. (f) HRTEM image showing rods growing on the side of the Ni plate with vector 111 pointing along out from the superparticle.

399

the presence of $Fe_{0.05}Ni_{0.95}$ cores and hierarchically grown Fe_2O_3 nanorods. Initially the rods covered only the flat surfaces of the $Fe_{0.05}Ni_{0.95}$ cores and grew perpendicular to the cores (Fig. 3d).

In Fig. S5† a *z*-contrast image from an upright standing plate gives a side view of the superparticles. The strong contrast difference between the Fe_2O_3 decoration and the very bright Ni plates was confirmed by energy-dispersive X-ray spectroscopic (EDX) line scan analysis. The average plate thickness was about 10 nm; this could be shown for many plates of different lateral size by tilting the sample. As the supercrystals kept growing, additional rods appeared on the side of the $Fe_{0.05}Ni_{0.95}$ cores with a less ordered orientation. The fully-grown nanorods were about 10 nm in diameter and about 30 nm in length (Fig. 3e). HRTEM images confirmed the main direction of the rod growth to be always [111]. Most nanorods developed orthogonally to the surface of the Ni plate, showing in projection a typical hexagonal base (Fig. 3e). Other rods grow on the lateral side of the Ni plate, with the [111] vector pointing out from the superparticle surface.

The size and density of the γ-Fe_2O_3 nanorods could be controlled by varying the concentration of the $Fe(CO)_5$ precursor in solution. The TEM images in Fig. 4a and b show that by reducing the concentration of $Fe(CO)_5$ the size and density of the γ-Fe_2O_3 nanorods decreased (Fig. 4a), whereas an increase of the $Fe(CO)_5$ concentration induced the formation of dense and almost 100 nm long γ-Fe_2O_3 nanorods (Fig. 4b). However, when $Fe(CO)_5$ was injected at 180 °C, *i.e.* the decomposition temperature of $Fe(CO)_5$, a mixture of Ni plates and iron oxide nanoparticles (Fig. S6a†) was obtained. Further increasing the injection temperature to 240 °C lead to the formation of core–shell nanoparticles, because the Ni cores had adopted already a spherical shape (Fig. S6b†). When the amount of $Fe(CO)_5$ was reduced to 10 μl, the reduction of the nickel precursor was incomplete, and agglomerated iron oxide nanostructures were formed (Fig. S6c†), whereas the injection of excess $Fe(CO)_5$ lead to the formation of Ni@γ-Fe_2O_3 superparticles with iron oxide nanorods ~100 nm long and also isolated iron oxide nanoparticles (Fig. S6d†). The reaction in the absence of $Fe(CO)_5$ did not allow a reduction of Ni as indicated by the
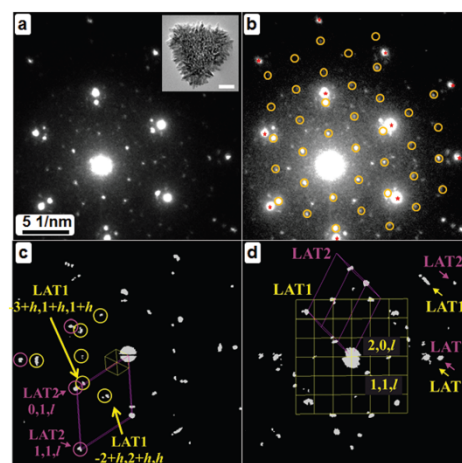
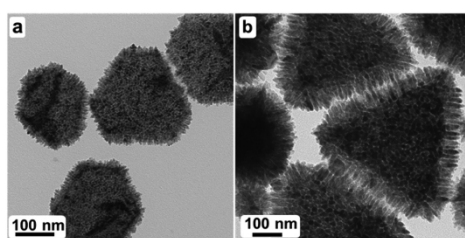**Fig. 5** NED and ADT characterization of mature $Fe_{0.05}Ni_{0.95}@\gamma$-$Fe_2O_3$ superparticles. (a) NED pattern from the particle inset (scale bar = 50 nm). (b) The pattern could be indexed with two hexagonal patterns with *d* values of 3.0(1) Å (in yellow) and 2.2(1) Å (in violet), respectively. (c) ADT 3D diffraction reconstruction viewed along the vertical and (d) along a lateral side. The two lattices identified by ADT are sketched in yellow (LAT1) and violet (LAT2).

color of solution even after heating to 180 °C for 30 min (Fig. S7†).

The superparticle formation is therefore clearly a hierarchical assembly, as the oxidation of Fe starts only after the Ni-based cores are fully developed. Selected area electron diffraction (SAED) patterns taken either from triangular or hexagonal superparticles could be fully described using two different lattices (Fig. 5a and b). One lattice is consistent with that already observed for the plate-like precursor, *i.e.* two *d* distances of 2.2(1) Å crossing at 60°. The second lattice is also hexagonal, with *d* values of 3.0(1) Å, and it is iso-oriented with respect to the first one.

Ni@γ-Fe_2O_3 superparticle structure

ADT[52,53] was used to obtain a three-dimensional diffraction reconstruction from four independent superparticles (Fig. 5c and d). The reconstructions were equivalent for triangular and hexagonal shapes. Besides diffuse scattering, presumably produced by randomly oriented γ-Fe_2O_3 rods, two single crystal lattices could be identified (Fig. 5). The first lattice (LAT1) corresponds to a face-centered cubic cell with $a = 8.4(1)$ Å, consistent with the maghemite (γ-Fe_2O_3) cell. The second lattice (LAT2) corresponds to a primitive hexagonal cell with $a = 2.55(5)$ Å and $c = 6.2(1)$ Å. The orientation of the two lattices is correlated, as $(111)^*$ and $(-211)^*$ reciprocal vectors of LAT1 are respectively parallel to the $(001)^*$ and $(100)^*$ vectors of LAT2. Vectors LAT1$(111)^*$ and LAT2$(001)^*$ are perpendicular to the

Fig. 4 (a, b) In order to control the density and size of the γ-Fe_2O_3 domains the concentration of the $Fe(CO)_5$ was reduced (a) and increased (b).

plane of the Ni core, while vectors LAT1(−211)* and LAT2(100)* point to the vertexes of the triangles and vectors LAT1(−110)* and LAT2(110)* point to the vertexes of the hexagons (Fig. S8†).

The cubic lattice LAT1 is associated with the γ-Fe$_2$O$_3$ nanorods growing perpendicular to the surface of the Fe$_{0.05}$Ni$_{0.95}$ cores. They produce a single crystal-type pattern, because they have the same orientation. HRTEM images confirm the main direction of the rod growth to be always [111] (Fig. 3f). The hexagonal pattern LAT2 is associated with the triangular (or hexagonal) Fe$_{0.05}$Ni$_{0.95}$ cores. This lattice is commensurate with the face-centered cubic lattice of metallic Ni, with a ~3.6 Å, but the cubic symmetry is reduced by additional reflections at (1/3, 1/3, 1/3) and (2/3, 2/3, 2) (Fig. S9†). These additional reflections may be rationalized by a superstructure induced by the insertion of Fe in the Ni structure, or by a 2-fold rotational twinning of the Ni structure along [111]. The precision of ADT precision does not allow resolving the small deviations between the cell dimensions of Ni and Fe$_{0.05}$Ni$_{0.95}$.

The presence of maghemite (γ-Fe$_2$O$_3$, defect spinel) in the samples was confirmed by powder X-ray diffraction (P-XRD). The XRD patterns of the Ni@γ-Fe$_2$O$_3$ superparticles displayed broad Bragg maxima indicative of small crystallite sizes (Fig. 6a). Due to reflection broadening, reflection overlap between the Ni and the γ-Fe$_2$O$_3$ phase and the high similarity of the corresponding line-patterns a quantitative phase analysis was performed by full pattern profile analysis ("Rietveld refinement") to distinguish between all possible phases (γ-Fe$_2$O$_3$, magnetite (Fe$_3$O$_4$) and nickel ferrite (NiFe$_2$O$_4$)).[56,57] For the Ni nanoplate domains of the Ni@Fe$_2$O$_3$ superparticles

the crystallite sizes of 8(1) nm from the Rietveld refinement are marginally larger for Ni and considerably larger for γ-Fe$_2$O$_3$ (21(1) nm). The extra reflections not captured by the Rietveld refinement are due to silicon used as substrate. The Mössbauer spectrum of the Ni@γ-Fe$_2$O$_3$ superparticles at 295 K (Fig. 6b) shows a superposition of wo magnetic sextetts with approximately equal intensities. The component with an isomer shift IS = 0.3(1) mm s^{-1} corresponds to maghemite with an average hyperfine magnetic field of 478 kOe.[58] A broad magnetic subspectrum with an average hyperfine magnetic field of 433 kOe and IS = 0.6(1) mm s^{-1} can be attributed to the interface region between the pure maghemite phase and the Ni substrate.

Physical properties

The magnetic properties of the Ni@γ-Fe$_2$O$_3$ superparticles extracted from the temperature-dependent magnetization and hysteresis curves are shown in Fig. 6c and d. The superparticles are ferrimagnetic at 5 K and superparamagnetic above room temperature. The magnetization curve in Fig. 6c exhibits saturation magnetization values of 2.96μ_B at 5 K, a value prevailing the expected one of 2.40μ_B for γ-Fe$_2$O$_3$ on a Ni substrate following from the estimation: 2/3 × 3.33μ_B + 1/3 × 0.62μ_B, where 3.33μ_B and 0.62μ_B are saturation magnetizations for γ-Fe$_2$O$_3$ [59] and metallic Ni.[60] This value is also much higher as compared to Ni@γ-Fe$_2$O$_3$ with heterodimer morphology (2.45μ_B at T = 5 K)[17] and core shell (1.53μ_B at T = 5 K) as shown in Fig. S10.† The ZFC magnetization increases monotonically with temperature and the FC magnetization shows no significant change. The splitting of the ZFC and FC curves reaches a crossing point around 302 K (Fig. 6d), indicating a blocking temperature above room temperature. The common orientation of the maghemite nanorods on the Ni core of the superparticles leads to a greatly enhanced magnetization because the anisotropy of the superparticles decreases the surface spin canting and disorder, thereby leading to enhanced magnetization. We do not consider inter-particle interactions to play a significant role, because the superparticles do not show aggregation (Fig. 3).

Fig. 6 Particle Characterization. (a) Quantitative phase analysis from the X-ray diffraction pattern of the Ni@γ-Fe$_2$O$_3$ superparticles (red dots: observed intensity, black line: calculated intensity, red line: difference curve; ticks mark the reflection positions of γ-Fe$_2$O$_3$ (upper) and elemental Ni (lower)), (b) ^{57}Fe Mössbauer spectra of Ni@γ-Fe$_2$O$_3$ superparticles at 295 K. (c, d) Magnetic hysteresis loops at 5 K and 300 K and temperature dependence of the magnetization in field-cooling (FC) and zero-field-cooling (ZFC) of Ni@γ-Fe$_2$O$_3$ superparticle heterodimers.

Conclusion

This work provides a general approach to a new type of magnetic nanocomposite with complex but well-defined mesoscopic architectures through "beaker epitaxy" of basic nano-objects, e.g. for probing the exchange coupling between magnetic particle components at the nanoscale. ADT analysis in combination with Mössbauer spectroscopy indicates that tailoring the interface between the metal and metal oxide components by "alloying" is a key step to the formation of this new kind of colloidal superparticles with multiple well-defined supercrystalline domains under kinetic control. Atom diffusion is eliminated here as rate-limiting step, and only reaction parameters such as interface or precursor structure control the nucleation event.[61] The formation of phase separ-
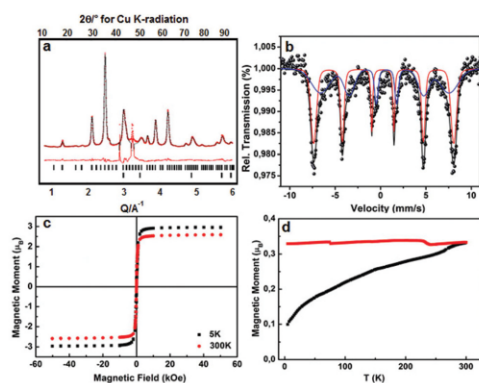
401

ated Ni@γ-Fe$_2$O$_3$ superparticles is highly unexpected, because Ni is not a noble metal and several stable ternary nickel oxides (e.g. nickel ferrite, NiFe$_2$O$_4$) are known, i.e. the nucleation temperature of these ternary phases is not reached under our experimental conditions.

The development of a controlled synthesis of nanocrystalline superparticles is relevant for several reasons: (i) The synthetic approach may be generalized for making nanocrystalline colloidal superparticles with other chemical compositions from organometallic precursors. (ii) The selective growth of the metal oxide nanorods is facilitated through the formation of Ni$_{1-x}$Fe$_x$ alloy and Fe$_{3-x}$Ni$_x$O$_4$ "buffer layers" (as shown by Mössbauer spectroscopy) at the interface between the Ni core and the γ-Fe$_2$O$_3$ rods within the Ni@γ-Fe$_2$O$_3$ superparticles that may serve to reduce strain in a regularly spaced arrangement on the Ni substrate as demonstrated by ADT. The miscibility of most d metals with each other in their elemental and oxide structures allows the fabrication of the buffer layer to be generalized. (iii) The properties of the nanocrystalline colloidal superparticles may be modified by "alloying" with other metals or by functionalization with organic molecules. Superparticles may be promising candidates for catalytic[17–19] or electrochemical[62] applications. Our functionalization strategy uses a well-defined catechol-functional PEG ligand with a tailored chain length and controlled molecular weight obtained from the living polymerization of EO.

We anticipate that our findings open many opportunities for assembling particles with complex, but well-defined mesoscopic architectures[63] and different magnetic, optical, or chemical properties. This could lead to new multifunctional materials or materials with enhanced performance for a wide range of potential (e.g. sensoric, catalytic) applications.[64,65]

Acknowledgements

Notes and references

1 H. C. Zeng, *Acc. Chem. Res.*, 2013, **46**, 226–235.
2 O. Chen, L. Riedemann, F. Etoc, H. Herrmann, M. Coppey, M. Barch, C. T. Farrar, J. Zhao, O. T. Bruns, H. Wei, P. Guo, J. Cui, R. Jensen, Y. Chen, D. K. Harris, J. M. Cordero, Z. Wang, A. Jasanoff, D. Fukumura, R. Reimer, M. Dahann, R. K. Jain and M. G. Bawendi, *Nat. Commun.*, 2014, **5**, 5093.
3 R. G. Chaudhuri and S. Paria, *Chem. Rev.*, 2012, **112**, 2373–2433.
4 M. Lattuada and T. A. Hatton, *Nano Today*, 2011, **6**, 286–308.
5 M. N. Tahir, F. Natalio, M. A. Cambaz, M. Panthöfer, R. Branscheid, U. Kolb and W. Tremel, *Nanoscale*, 2013, **5**, 9944–9949.
6 C. Huang, S. Wu, A. M. Sanchez, J. J. P. Peters, R. Beanland, J. S. Ross, P. Rivera, W. Yao, D. C. Cobden and X. Xu, *Nat. Mater.*, 2014, **13**, 1096–1101.
7 J. Y. Lao, J. G. Wen and Z. F. Ren, *Nano Lett.*, 2002, **2**, 1287–1291.
8 S. Park, S.-D. Seo, S. Lee, S. W. Seo, K.-S. Park, C. W. Lee, D.-W. Kim and K. S. Hong, *J. Phys. Chem. C*, 2012, **116**, 21717–21726.
9 D. F. Zhang, L. D. Sun, C. J. Jia, Z. G. Yan, L. P. You and C. H. Yan, *J. Am. Chem. Soc.*, 2005, **127**, 13492–13493.
10 Y. Chen, C. Zhu, X. Shi, M. Cao and H. Jin, *Nanotechnol.*, 2008, **19**, 205603.
11 W. Zhou, C. Cheng, J. Liu, Y. Y. Tay, J. Jiang, X. Jia, J. Zhang, H. Gong, H. H. Hong and T. Yu, *Adv. Funct. Mater.*, 2011, **21**, 2439–2445.
12 U. K. Gautam, X. Fang, Y. Bando, J. Zhan and D. Golberg, *ACS Nano*, 2008, **2**, 1015–1021.
13 M. Shang, W. Wang, W. Yin, J. Ren, S. Sun and L. Zhang, *Chem. – Eur. J.*, 2010, **16**, 11412–11419.
14 H. J. Fan, P. Werner and M. Zacharias, *Small*, 2006, **2**, 700–717.
15 B. R. Martin, D. J. Dermody, B. D. Reiss, M. Fang, L. A. Lyon, M. J. Natan and T. E. Mallouk, *Adv. Mater.*, 1999, **11**, 1021–1025.
16 R. D. Robinson, B. Sadtler, D. O. Demchenko, C. K. Erdonmez, L. W. Wang and A. P. Alivisatos, *Science*, 2007, **317**, 355–358.
17 B. Nakhjavan, M. N. Tahir, F. Natalio, M. Panthöfer, H. Gao, M. Dietzsch, R. Andre, T. Gasi, V. Ksenofontov, R. Branscheid, U. Kolb and W. Tremel, *Nanoscale*, 2012, **4**, 4571–4577.
18 J. Jang, J. Chung, S. Kim, S. W. Jun, B. H. Kim, D. W. Lee, B. M. Kim and T. Hyeon, *Phys. Chem. Chem. Phys.*, 2011, **13**, 2512–2516.
19 C. Wang, H. Daimon and S. Sun, *Nano Lett.*, 2009, **9**, 1493–1496.
20 B. Nakhjavan, M. N. Tahir, M. Panthöfer, H. Gao, T. Gasi, V. Ksenofontov, R. Branscheid, S. Weber, U. Kolb, L. M. Schreiber and W. Tremel, *Chem. Commun.*, 2011, **47**, 8898–8900.
21 H. Yu, M. Chen, P. M. Rice, S. X. Wang, R. L. White and S. Sun, *Nano Lett.*, 2005, **5**, 379–382.
22 J. Kim, J. E. Lee, J. Lee, J. H. Yu, B. C. Kim, K. An, Y. Hwang, C. H. Shin, J. G. Park and T. Hyeon, *J. Am. Chem. Soc.*, 2006, **128**, 688–689.
23 I. Lee, J. B. Joo, Y. Yin and F. Zaera, *Angew. Chem., Int. Ed.*, 2011, **50**, 10208–10211.
24 M. Casavola, R. Buonsanti, G. Caputo and P. D. Cozzoli, *Eur. J. Inorg. Chem.*, 2008, 837–854.
25 I. Schick, S. Lorenz, D. Gehrig, K. Fischer, S. Tenzer, H.-J. Schild, D. Strand, F. Laquai and W. Tremel, *Beilstein J. Nanotechnol.*, 2014, **5**, 2346–2362.
26 C. Wang, H. Daimon and S. Sun, *Nano Lett.*, 2009, **9**, 1493–1496.

402
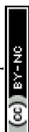
27 Y. Wei, R. Klajn, A. O. Pinchuk and B. A. Grzybowski, *Small*, 2008, **4**, 1635–1639.

28 C. Xu, J. Xie, D. Ho, C. Wang, N. Kohler, E. G. Walsh, J. R. Morgan, Y. E. Chin and S. Sun, *Angew. Chem., Int. Ed.*, 2008, **47**, 173–176.

29 I. Schick, S. Lorenz, D. Gehrig, A.-M. Schilmann, H. Bauer, M. Panthöfer, K. Fischer, M. Schmidt, D. Strand, F. Laquai and W. Tremel, *J. Am. Chem. Soc.*, 2014, **136**, 2473–2483.

30 T. D. Schladt, T. Graf, O. Köhler, H. Bauer, K. Schneider, C. Herold, J. Mertins and W. Tremel, *Chem. Mater.*, 2012, **24**, 525–535.

31 G. Lopes, J. M. Vargas, S. K. Sharma, F. Beron, K. R. Pirota, M. Knobel, C. Rettori and R. D. Zysler, *J. Phys. Chem. C*, 2010, **114**, 10148–10152.

32 T. D. Schladt, M. I. Shukoor, M. N. Tahir, F. Natalio, K. Schneider, I. Ament, J. Becker, F. Jochum, S. Weber, P. Theato, L. M. Schreiber, C. Sönnichsen, H. C. Schröder, W. E. G. Müller and W. Tremel, *Angew. Chem., Int. Ed.*, 2010, **49**, 3976–3980.

33 I. Schick, D. Gehrig, M. Montigny, B. Balke, M. Panthöfer, A. Henkel, F. Laquai and W. Tremel, *Chem. Mater.*, 2015, **27**, 4877–4884.

34 C. Wang, C. Xu, H. Zeng and S. Sun, *Adv. Mater.*, 2009, **21**, 3045–3052.

35 L. Carbone and P. D. Cozzoli, *Nano Today*, 2010, **5**, 449–493.

36 C. Wang, W. Tian, Y. Ding, Y.-Q. Ma, Z. L. Wang, N. M. Markovic, V. R. Stamenkovic, H. Daimon and S. Sun, *J. Am. Chem. Soc.*, 2010, **132**, 6524–6529.

37 M. R. Buck, J. F. Bondi and R. E. Schaak, *Nat. Chem.*, 2011, **4**, 37–44.

38 B. Nakhjavan, M. N. Tahir, H. Gao, T. Schladt, K. Schneider, F. Natalio, I. Ament, R. Branscheid, S. Weber, H.-C. Schröder, W. E. G. Müller, U. Kolb, C. Sönnichsen, L. M. Schreiber and W. Tremel, *J. Mater. Chem.*, 2011, **21**, 8605–8611.

39 C. Xu, K. Xu, G. Gu, R. Zheng, H. Liu, X. Zhang, Z. Guo and B. Xu, *J. Am. Chem. Soc.*, 2004, **126**, 9938–9939.

40 M. N. Tahir, M. Eberhardt, P. Theato, S. Faiß, A. Janshoff, T. Gorelik, U. Kolb and W. Tremel, *Angew. Chem., Int. Ed.*, 2006, **45**, 908–912.

41 J. Sedo, J. Saiz-Poseu, F. Busque and D. Ruiz-Molina, *Adv. Mater.*, 2013, **25**, 653–701.

42 E. Amstad, T. Gillich, I. Bilecka, M. Textor and E. Reimhult, *Nano Lett.*, 2009, **9**, 4042–4048.

43 B. P. Lee, J. L. Dalsin and P. B. Messersmith, *Biomacromolecules*, 2002, **3**, 1038–1047.

44 J. Su, F. Chen, V. L. Cryns and P. B. Messersmith, *J. Am. Chem. Soc.*, 2011, **133**, 11850–11853.

45 M. S. Thompson, T. P. Vadala, M. L. Vadala, Y. Lin and J. S. Riffle, *Polymer*, 2008, **49**, 345–373.

46 B. Obermeier, F. Wurm, C. Mangold and H. Frey, *Angew. Chem., Int. Ed.*, 2011, **50**, 7988–7997.

47 V. S. Wilms, H. Bauer, C. Tonhauser, A. M. Schilmann, M. C. Müller, W. Tremel and H. Frey, *Biomacromolecules*, 2013, **14**, 193–199.

48 A. Taylor, *J. Inst. Metals*, 1950, **77**, 585.

49 C. A. Greaves, *J. Solid State Chem.*, 1983, **49**, 325–333.

50 A. Coelho, *TOPAS Academic V 4.1*, Coelho Software, Brisbane, AUS, 2007.

51 R. W. Cheary and A. A. Coelho, *J. Appl. Crystallogr.*, 1992, **25**, 109–121.

52 U. Kolb, T. Gorelik, C. Kübel, M. T. Otten and D. Hubert, *Ultramicroscopy*, 2007, **107**, 507–513.

53 U. Kolb, T. Gorelik and M. T. Otten, *Ultramicroscopy*, 2008, **108**, 763–772.

54 E. Mugnaioli, I. Andrusenko, T. Schüler, N. Loges, R. E. Dinnebier, M. Panthöfer, W. Tremel and U. Kolb, *Angew. Chem., Int. Ed.*, 2012, **51**, 7041–7045.

55 Y. Leng, Y. Li, X. Li and S. Takahashi, *J. Phys. Chem. C*, 2007, **111**, 6630–6633.

56 W. Kelm and W. Mader, *Z. Naturforsch.*, 2006, **61b**, 665–671.

57 C. Cavelius, K. Moh and S. Mathur, *Cryst. Growth Des.*, 2012, **12**, 5948–5955.

58 N. N. Greenwood and T. G. Gibb, *Mössbauer Spectroscopy*, Chapman and Hall Ltd, London, 1971.

59 H. Lueken, *Magnetochemie, Teubner Studienbücher*, 2000.

60 H. Danan, A. Herr and A. J. P. Meyer, *J. Appl. Phys.*, 1968, **39**, 669–670.

61 D. C. Johnson, *Curr. Opin. Solid State Mater. Sci.*, 1998, **3**, 159–167.

62 B. Oschmann, M. N. Tahir, F. Mueller, D. Bresser, I. Lieberwirth, W. Tremel, S. Passerini and R. Zentel, *Macromol. Rapid Commun.*, 2015, **36**, 1075–1082.

63 C. Feldmann, *Angew. Chem., Int. Ed.*, 2013, **52**, 7610–7611.

64 C. Burda, X. Chen and M. A. El-Sayed, *Chem. Rev.*, 2005, **105**, 1025–1102.

65 H. Goesmann and C. Feldmann, *Angew. Chem., Int. Ed.*, 2010, **49**, 1362–1395.

403
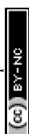
List of Publications

First Author

Herzberger, J; Leibig, D; Langhanki, J.; Moers, C.; Opatz, T.; Frey, H. "Clickable PEG via Anionic Copolymerization of Ethylene Oxide and Glycidyl Propargyl Ether." **2016**, *to be submitted*.

Herzberger, J*; Leibig, D*; Liermann, J. C.; Frey, H. "Conventional Oxyanionic versus Monomer-Activated Anionic Copolymerization of Ethylene Oxide with Glycidyl Ethers: Striking Differences in Reactivity Ratios." *ACS Macro Lett.* **2016***, 5,* 1206-1211.
*contributed equally

Herzberger, J.; Fischer, K.; Leibig, D; Bros, M.; Thiermann, R.; Frey, H. "Oxidation-Responsive and "Clickable" Poly(ethylene glycol) via Copolymerization of 2-(Methylthio)ethyl Glycidyl Ether.",
J. Am. Chem. Soc. **2016***, 138,* 9212-9223.

Herzberger, J.; Niederer, K.; Pohlit, H; Seiwert, J.; Worm, M.; Wurm, F.; Frey, H. "Polymerization of Ethylene Oxide, Propylene Oxide, and Other Alkylene Oxides: Synthesis, Novel Polymer Architectures, and Bioconjugation." *Chem. Rev.* **2016***, 116*, 2170–2243.

Herzberger, J.; Frey, H.; "Epicyanohydrin: Polymerization by Monomer Activation Gives Access to Nitrile-, Amino-, and Carboxyl-Functional Poly(ethylene glycol)." *Macromolecules* **2015***, 48*, 8144-8153.

Herzberger, J.; Kurzbach, D.; Werre, M.; Fischer, K.; Hinderberger, D.; Frey, H. "Stimuli-Responsive Tertiary Amine Functional PEGs Based on *N,N*-Dialkylglycidylamines." *Macromolecules* **2014***, 47*, 7679-7690.

Kluenker, M.; Tahir, M. N.; Ragg, R.; Korschelt, K.; Simon, P.; Gorelik, T. E.; Barton, B.; Shylin, S. I.; Panthöfer, M.; **Herzberger, J.**; Frey, H.; Ksenofontov1, V.; Möller, A.; Kolb, U.; Grin, J.; Tremel, W. "Pd@Fe_2O_3 Superparticles with Enhanced Peroxidase Activity by Solution Phase Epitaxial Growth." **2016**, *submitted*.

Ragg, R.; Schilmann, A. M.; Korschelt, K.; Wieseotte, C.; Kluenker, M; Viel, M.; Völker, L.; Preiß, S.; **Herzberger, J.**; Schreiber, L.; Frey, H.; Heinze, K.; Blümler, P.; Tahir, M. N.; Natalio, F.; Tremel, W. "Intrinsic Superoxide Dismutase Activity of MnO Nanoparticles Enhances Magnetic Resonance Imaging Contrast." **2016**, *submitted*.

Leibig, D.; Morsbach, J.; Grune, E.; **Herzberger, J.**; Müller, A. H. E., Frey, H. „Quicklebendig seit 60 Jahren: Die lebende anionische Polymerisation", **2016**, *submitted*.

Seiwert, J; **Herzberger, J**; Leibig, D; Frey, H. "Thioether-bearing Hyperbranched Polyether Polyols: A Versatile Platform for Orthogonal Functionalization." *Macromol. Rapid Commun.* **2016**, *accepted*.

Christ, M. E.; **Herzberger, J.**; Montigny, M.; Wagner, M.; Tremel, W.; Frey, H. "Poly(THF-*co*-cyano ethylene oxide): Cyano Ethylene Oxide (CEO) Copolymerization with THF Leading to Multifunctional and Water-Soluble PolyTHF Polyelectrolytes." *Macromolecules* **2016**, *49*, 3681-3695.

Tahir, M. N.; **Herzberger, J.**; Natalio, F.; Kohler, O.; Branscheid, R.; Mugnaioli, E.; Ksenofontov, V.; Panthofer, M.; Kolb, U.; Frey, H.; Tremel, W. "Hierachical Ni@Fe_2O_3 Superparticles through Epitaxial Growth of γ-Fe_2O_3 Nanorods on in situ Formed Ni Nanoplates." *Nanoscale* **2016**, *8*, 9548-9555.

Thioether-functional Poly(ethylene glycol) Copolymers: Oxidation-Responsive Micelles and "Click" Chemistry. Warwick Polymer Conference, Warwick, United Kingdom
(poster, **7/2016**)

Multi-functional Poly(ethylene glycol) via Epicyanohydrin. "Materials Science in Mainz" seminar, Lisbon, Portugal
(oral, **10/2015**)

Multi-functional Poly(ethylene glycol) via Epicyanohydrin. International Symposium on Ionic Polymerization, Bordeaux, France
(oral, **7/2015**)

Tertiary Amine-Functional Poly(ethylene glycols):Thermo- and pH-Responsive Behavior in Aqueous Solution. American Chemical Society poster session, San Francisco, CA
(poster, **8/2014**)

Tertiary Amine-Functional Poly(ethylene glycols):Thermo- and pH-Responsive Behavior in Aqueous Solution. "Materials Science in Mainz" seminar, Prague, Czech Republic
(poster, **7/2014**)